



South Texas Project Electric Generating Station P.O. Box 289 Wadsworth, Texas 77483

July 15, 2014
NOC-AE-14003105
10 CFR 50.12
10 CFR 50.90

U. S. Nuclear Regulatory Commission
Attention: Document Control Desk
Washington, DC 20555-0001

South Texas Project
Units 1 & 2
Docket Nos. STN 50-498, STN 50-499
Third Set of Responses to April, 2014, Requests for Additional Information
Regarding STP Risk-Informed GSI-191 Licensing Application
(TAC NOs MF2400 and MF2401)

References:

1. Letter, G. T. Powell, STPNOC, to NRC Document Control Desk, "Supplement 1 to Revised STP Pilot Submittal and Requests for Exemptions and License Amendment for Risk-Informed Approach to Resolving Generic Safety Issue (GSI)-191, " November 13, 2013, NOC-AE-13003043, ML13323A183
2. Letter, Balwant Singal, NRC, to Dennis Koehl, STPNOC, "South Texas Project, Units 1 and 2- Request for Additional Information Related to Request for Exemptions and License Amendment for Use of a Risk-Informed Approach to Resolve the Issue of Potential Impact of Debris Blockage on Emergency Recirculation During Design-Basis Accidents at Pressurized-Water Reactors", April 15, 2014, ML14087A075

This submittal responds to a portion of the requests for additional information (RAI) provided in Reference 2 with regard to the STP Nuclear Operating Company (STPNOC) risk-informed application to address GSI-191 (Reference 1). The responses provided are listed in the Attachments..

There are no regulatory commitments in this letter.

A001
KRR

If there are any questions, please contact Mr. Wayne Harrison at 361-972-8774.

I declare under penalty of perjury that the foregoing is true and correct.

Executed on: July 15, 2014



G. T. Powell

Site Vice President

awh

Attachments:

1. Response to APLAB Request for Additional Information
 - a. CASA Grande - General: RAI 1
 - b. CASA Grande – Plant Configuration: RAI 1, 2, 3
 - c. CASA Grande to PRA Interface - General: RAI 2
 - d. STP PRA Model – General: RAI 1, 3
 - e. STP PRA Model – Success Criteria: RAI 1, 2, 3
 - f. STP PRA Model – Human Reliability Analysis: RAI 3
 - g. STP PRA Model – PRA Scope: RAI 2
 - h. Results Interpretation – Uncertainty Analysis: RAI 1, 3, 4, 5, 6

Enclosures to Attachment 1

1. Response to APLAB, CASA Grande – Plant Configuration: RAI 3 Plant Configuration: Combinations of Pump Failures
 2. Attachment A to CR 07-1684 Resolution of PRA HRA Update Report Peer Review Fact/Observation (F&O) Comments
 3. Level B Observations Resolved
 4. Independent Review of Electric Power Recovery Analysis
 5. Response to APLAB 25 vs 40 Year Frequency Estimates: RAI 3
 6. Explanation of the Discrepancy in Mean LOCA Frequencies for Fitted Johnson Distribution versus NUREG-1829 Values
 7. Explanation of the Johnson Distribution Governing LOCA Frequency and Sensitivity of Summary Statistics to Scale Parameters
 8. Explanation of the Impact of Johnson Distribution Selection on CDF, LERF, Δ CDF, Δ LERF
2. Response to ARCB Request for Additional Information: RAI 1, 2, 3
 3. Response to EMCB Request for Additional Information: RAI 1 and June 2, 2014 Follow-up RAI
 4. Response to EPNB Request for Additional Information: RAI 1, 2, 3, 4, 5, 6

Enclosure to Attachment 4

1. Response to EPNB-Consistency of Weld Frequencies with RI-ISI Program: RAI 6

5. Response to ESGB Request for Additional Information:
 - a. Chemical Effects: RAI 1, 2, 4, 5, 6, 8, 9, 10, 14, 15, 16, 18, 21
 - b. Coatings: RAI 1, 6

Enclosure to Attachment 5

1. Leavitt, J.J. and Kee, E., ALION-REP-STP-8998-08 Rev. 0, Quantification of Chemical Head Loss Epistemic Uncertainty; Basis for Incremental Chemical Head Loss Correlation, May 2014.

6. Response to SNPB Request for Additional Information: RAI 4

7. Response to SRXB Request for Additional Information: RAI 1, 2, 3, 4

8. Response to SSIB Request for Additional Information:

- a. Debris Characteristics: RAI 3,
- b. Transport: RAI 4, 6, 7, 8, 10,
- c. Head Loss and Chemical Effects Bump Up: RAI 14, 15, 16, 17, 18, 19, 20, 21, 22, 23, 24, 27, 28
- d. NPSH and Degasification: RAI 33, 36
- e. Debris Bypass: RAI 38
- f. Defense in Depth and Mitigative Measures: RAI 40, 42

Enclosures to Attachment 8

1. Letellier, B.C., Macali, M.E., Kee, E.J., Viscous Inertial Shear-Transition-Adaptive (VISTA) Porous Media Head-Loss Formulation for Assessment of South Texas Project Licensing Amendment Request, ALION-REP-STP-8998-11, Rev. 1, July 2014.
2. Morton, D.P., Tejada, J.J., Zolan, A., South Texas Project Risk-Informed GSI-191 Evaluation, Volume 3, A Practical Guide to Sensitivity Analysis of Large-scale Computer Simulation

9. Definitions and Acronyms

cc:
(paper copy)

Regional Administrator, Region IV
U. S. Nuclear Regulatory Commission
1600 East Lamar Boulevard
Arlington, TX 76011-4511

Balwant K. Singal
Senior Project Manager
U.S. Nuclear Regulatory Commission
One White Flint North (MS 8 B1)
11555 Rockville Pike
Rockville, MD 20852

NRC Resident Inspector
U. S. Nuclear Regulatory Commission
P. O. Box 289, Mail Code: MN116
Wadsworth, TX 77483

Attention: Document Control Desk
U. S. Nuclear Regulatory Commission
Washington, DC 20555-0001

(electronic copy)

A. H. Gutterman, Esquire
Morgan, Lewis & Bockius LLP

Balwant K. Singal
U. S. Nuclear Regulatory Commission

John Ragan
Chris O'Hara
Jim von Suskil
NRG South Texas LP

Kevin Pollo
Cris Eugster
L. D. Blaylock
CPS Energy

Peter Nemeth
Crain Caton & James, P.C.

C. Mele
John Wester
City of Austin

Richard A. Ratliff
Texas Department of State Health
Services

Robert Free
Texas Department of State Health
Services

Attachment 1

Response to APLAB Request for Additional Information

- a. CASA Grande - General: RAI 1
- b. CASA Grande – Plant Configuration: RAI 1, 2, 3
- c. CASA Grande to PRA Interface - General: RAI 2
- d. STP PRA Model – General: RAI 1, 3
- e. STP PRA Model – Success Criteria: RAI 1, 2, 3
- f. STP PRA Model – Human Reliability Analysis: RAI 3
- g. STP PRA Model – PRA Scope: RAI 2
- h. Results Interpretation – Uncertainty Analysis: RAI 1, 3, 4, 5, 6

Enclosures to Attachment 1

- 1. Response to APLAB, CASA Grande – Plant Configuration: RAI 3
Plant Configuration: Combinations of Pump Failures
- 2. Attachment A to CR 07-1684 Resolution of PRA HRA Update
Report Peer Review Fact/Observation (F&O) Comments
- 3. Level B Observations Resolved
- 4. Independent Review of Electric Power Recovery Analysis
- 5. Response to APLAB 25 vs 40 Year Frequency Estimates: RAI 3
- 6. Response to APLAB-Results Interpretation-Uncertainty Analysis:
RAI 4a
- 7. Response to APLAB-Results Interpretation-Uncertainty Analysis:
RAI 4b
- 8. Response to APLAB-Results Interpretation-Uncertainty Analysis:
RAI 4c

APLAB, CASA Grande – General: RAI 1a

Regulatory Guide (RG) 1.174, Revision 2, “An Approach for Using Probabilistic Risk Assessment in Risk-Informed Decisions on Plant Specific Changes to the Licensing Basis,” May 2011 (ADAMS Accession No. ML100910006), Section 2.3.3, “Probabilistic Risk Assessment Technical Adequacy,” states that the PRA model should be technically adequate for the application. Volume 6.2 contains a list of input variables and describes whether each variable was modeled as a point estimate or a distribution in CASA Grande. According to item 5.d (page 158 of 179), the decision as to whether to use a point estimate or a distribution was based on the availability of data for uncertainty analysis and the available consensus on the values assigned to specific factors (e.g., for some values, there is a high level of confidence by industry and NRC). Please describe the process used to assign point estimates or distributions in more detail. For each input parameter, please provide:

(a) The basis for using a point estimate or a distribution.

STP Response:

The following Input parameter Summary Table provides:

- a. The basis for using a point estimate or a distribution.
- b. The source of the parameter value (e.g., licensing basis calculation).
- c. Whether the parameter is based on an NRC-accepted value (denoted by asterisk in the Input Parameter column)

The following categorizations differ from Volume 6.2, Table 2.5.65. The discrepancies have been entered in the STP corrective action program to be addressed in any future submittal of this information.

Input Parameter	Volume 6.2, Table 2.5.65	RAI Response Table
Time to secure containment Spray	Fixed Value	Distribution
Blowdown transport	Distribution	Fixed Value
Washdown transport	Distribution	Fixed Value
Fiberglass pool erosion	Distribution	Fixed Value
Conventional head loss bump-up	Fixed Value	Distribution
Unqualified Coatings (epoxy)	Not included	Distribution

Input Parameter	Distribution(s) or Fixed Value(s)	Dependencies	Basis	Reference(s) (from LAR Enc. 4-3)
Time to Recirculation	Fixed values	Break size	Switchover from the RWST to Recirculation is an automatic function. Time to recirculation as a function of break size is based upon system resistance (systems line-ups), RWST volume and pump performance. These values are finite and fixed. Therefore, "Time to Recirculation" is considered a fixed value	(5) Texas A&M University Department of Nuclear Engineering. Sump Temperature Sensitivity Analysis. Revision 2.0: January 2013
Time to secure containment Spray	Distribution	None	<p>Operator actions to secure one containment spray pump and operator actions to secure the containment spray system are dictated by STP Operating Procedures 0POP05-EO-EO10, and 0POP05-EO-ES11 respectively.</p> <p>Since this time is dependent on operator action, a window of performance time is defined for each action.</p>	<p>(32) 0POP05-EO-EO10. Loss of Reactor or Secondary Coolant.</p> <p>(34) 0POP05-EO-ES11. SI Termination.</p> <p>(35) Email from Tim Sande (Alion) to Kerry Howe (UNM) and Ernie Kee (STP). Best-Estimate Time for Spray Operation: February 23, 2012.</p>

Input Parameter	Distribution(s) or Fixed Value(s)	Dependencies	Basis	Reference(s) (from LAR Enc. 4-3)
Time to hot leg switchover	Distribution	None	<p>Time to the start of hot leg switchover is 5.5 hours after the event initiation as directed in STP Operation Procedures 0POP05-EO-EO10. Loss of Reactor or Secondary Coolant and 0POP05-EO-ES14. Transfer to Hot Leg Recirculation.</p> <p>Plant conditions will vary based upon break size and operating safety systems. Time to the start of hot leg switchover is 5.5 hours. It was assumed (LAR Encl. 4-3, Assumption 1.j.), from communication with plant personnel, that this action can be completed within 15 minutes. It was sampled as a distribution of equally likely times between 5.75 and 6 hours to account for variation in operator action times. Since the time to hot leg switchover may vary slightly and is based upon variable plant conditions it is modeled as a probability distribution.</p>	<p>(32) 0POP05-EO-EO10. Loss of Reactor or Secondary Coolant.</p> <p>(36) 0POP05-EO-ES14. Transfer to Hot Leg Recirculation.</p>
Containment Geometry	Fixed values	None	<p>The containment physical condition is fixed based upon as-built conditions as is therefore a fixed value input.</p>	<p>(4) ALION-SUM-WEST-2916-01. CAD Model Summary: South Texas Reactor Building CAD Model for Use in GSI-191 Analyses. Revision 3: November 27, 2012.</p>

Input Parameter	Distribution(s) or Fixed Value(s)	Dependencies	Basis	Reference(s) (from LAR Enc. 4-3)
Break size and frequency	Distributions	Break Location	<p>A probability distribution is used to model the LOCA frequency for breaks of different sizes at different locations within the plant.</p> <p>Break size and frequency are inherently variable and a probability distribution models this variability.</p> <p>Statistical sampling strategies ensure that the DEGB conditions for every pipe, discrete end points of frequency distributions, are explicitly included in the evaluation.</p>	<p>(4) ALION-SUM-WEST-2916-01. CAD Model Summary: South Texas Reactor Building CAD Model for Use in GSI-191 Analyses. Revision 3: November 27, 2012.</p> <p>(7) KNF Consulting Services LLC, and Scandpower Risk Management Inc. Development of LOCA Initiating Event Frequencies for South Texas Project GSI-191 Final Report for 2011 Work Scope. September 2011.</p> <p>(8) University of Texas at Austin. Modeling and Sampling LOCA Frequency and Break Size for STP GS1-191 Resolution. January 23, 2013.</p> <p>(9) Scandpower. Risk Informed GSI-191 Resolution LOCA Frequency Component Database. Revision 2: October 21, 2011.</p> <p>(37) NUREG-1829. Estimating Loss-of-Coolant Accident (LOCA) Frequencies Through the Elicitation Process: April 2008.</p>

Input Parameter	Distribution(s) or Fixed Value(s)	Dependencies	Basis	Reference(s) (from LAR Enc. 4-3)
Pool volume	Distributions	Break Size	<p>There are three sources of water for a loss of coolant accident (LOCA): the refueling water storage tank (RWST), the reactor coolant system (RCS) and the safety injection (SI) accumulators. Each of the sources are maintained within specific volume/mass ranges.</p> <p>Since there is a range of values, the use of a distribution rather than a point value was chosen.</p>	(14) ALION-CAL-STP-8511-01. STP Post LOCA Water Volume Analysis. Revision 1: September 20, 2012.
Pool area	Fixed value	None	This is a physical condition of the plant and not variable. Therefore a fixed value is appropriate.	(14) ALION-CAL-STP-8511-01. STP Post LOCA Water Volume Analysis. Revision 1: September 20, 2012.

Input Parameter	Distribution(s) or Fixed Value(s)	Dependencies	Basis	Reference(s) (from LAR Enc. 4-3)
Pool Temperature	Fixed Values	Break Size	<p>Pool temperature was selected to be a fixed value. One representative temperature history was chosen to represent small and medium breaks, and one representative temperature history was chosen to represent large breaks from a suite of thermal hydraulic calculations based on nominal conditions. Alternative temperatures under failure conditions would have successively lower probability of occurrence.</p> <p>Nominal profiles were chosen because it is not clear whether the minimum or maximum temperature profiles are conservative due to competing factors. It was also assumed that nominal temperature profiles are generally more conservative due to the shape of their transient behavior (LAR Encl. 4-3, Assumption 1.k.).</p>	(5) Texas A&M University Department of Nuclear Engineering. Sump Temperature Sensitivity Analysis. Revision 2.0: January 2013.

Input Parameter	Distribution(s) or Fixed Value(s)	Dependencies	Basis	Reference(s) (from LAR Enc. 4-3)
*Containment pressure	Fixed values	Pool Temperature	Fixed values were chosen based upon the ASME Steam Tables or assuming a fixed value of 14.7 psia. Saturation pressure at temperature is a constant. This is consistent with accident phenomenology and USNRC guidelines.	General Assumptions 1.c - Containment pressure was assumed to be 14.7 psia for all cases except when the pool temperature is higher than the boiling temperature. In cases where the pool temperature is above 212 °F, the containment pressure was assumed to be equal to the saturation pressure. This is a conservative assumption since neglecting containment overpressure reduces the ECCS pump NPSH margin and increases the amount of degasification at the strainer.
Operating pumps	Fixed values	None	The number of operating pumps is considered a fixed value and a specific design input as applicable to each plant failure state.	(38) STP-2699325-O-03. Subject: On the Frequency of Success States Involving Different Numbers of Pumps Operating. December 18, 2012.

Input Parameter	Distribution(s) or Fixed Value(s)	Dependencies	Basis	Reference(s) (from LAR Enc. 4-3)
Low head safety injection flow rate	Fixed values	Break Size, Pumps Running	<p>Flow rate is specific value determined by operating pumps (see above) and a specific design input as applicable to each plant failure state.</p> <p>These operating line-ups are fixed. Therefore, system flow rate is considered a fixed value that is determined by the number of operating pumps and break size.</p>	<p>(5) Texas A&M University Department of Nuclear Engineering. Sump Temperature Sensitivity Analysis. Revision 2.0: January 2013.</p> <p>(41) MC-6220. SI & CS Pump NPSH. Revision 4: February 5, 2002.</p>
High head safety injection flow rate	Fixed values	Break Size, Pumps running	<p>Flow rate is specific value determined by operating pumps (see above) and a specific design input as applicable to each plant failure state.</p> <p>These operating line-ups are fixed. Therefore, system flow rate is considered a fixed value that is determined by the number of operating pumps and break size.</p>	<p>(5) Texas A&M University Department of Nuclear Engineering. Sump Temperature Sensitivity Analysis. Revision 2.0: January 2013.</p> <p>(41) MC-6220. SI & CS Pump NPSH. Revision 4: February 5, 2002.</p>

Input Parameter	Distribution(s) or Fixed Value(s)	Dependencies	Basis	Reference(s) (from LAR Enc. 4-3)
Containment spray flow rate	Distributions	Pumps Running	<p>If containment sprays are initiated, the flow rate is not dependent on the size of the break. Flow rate varies depending on the number of trains in operation.</p> <p>The number of trains in operation is distributed over the range of break sizes and operating trains. Based on the distributed break sizes the containment spray flow rate is input as a distribution.</p>	<p>(41) MC-6220. SI & CS Pump NPSH. Revision 4: February 5, 2002.</p> <p>(42) 5N109MB01024. Design Basis Document Containment Spray. Revision 3: November 17, 2004.</p>
*Qualified coatings quantity	Fixed values	None	<p>The qualified coating quantities are based on a combination of plant configuration and NRC approved analysis methods.</p> <p>Qualified coatings quantities are considered fixed values as they are based on specific conservative break scenarios.</p>	<p>(11) ALION-CAL-STP-8511-03. STP Qualified Coatings Debris Generation. Revision 0: August 10, 2012.</p>

Input Parameter	Distribution(s) or Fixed Value(s)	Dependencies	Basis	Reference(s) (from LAR Enc. 4-3)
*Unqualified coatings quantity (non epoxy)	Fixed values	None	<p>The unqualified coating quantities (non-epoxy) are based on a combination of plant configuration and NRC approved analysis methods.</p> <p>Unqualified coatings quantities are considered fixed values as they are based on conservative assumptions regarding unqualified coating degradation.</p>	(12) ALION-CAL-STP-8511-06. STP Unqualified Coatings Debris Generation. Revision 2: November 26, 2012.
*Unqualified coatings quantity (epoxy)	Distribution	None	<p>The unqualified coating quantities are based on a combination of plant configuration and NRC approved analysis methods.</p> <p>Epoxy unqualified coatings quantities are considered a distribution and are based on the EPRI and Carboline analysis.</p>	(12) ALION-CAL-STP-8511-06. STP Unqualified Coatings Debris Generation. Revision 2: November 26, 2012.
*Unqualified coatings failure time	Fixed values	None	<p>The time after the start of the LOCA event that the unqualified coating fails is determined by analysis of data presented in the EPRI test report Design Basis Accident Testing of Pressurized Water Reactor Unqualified Original Equipment Manufacturer Coatings. Final Report September 2005.</p> <p>Timing is input as a fixed value as it is a given specific design parameter.</p>	(12) ALION-CAL-STP-8511-06. STP Unqualified Coatings Debris Generation. Revision 2: November 26, 2012.

Input Parameter	Distribution(s) or Fixed Value(s)	Dependencies	Basis	Reference(s) (from LAR Enc. 4-3)
Crud quantity	Fixed value	None	<p>This is a physical fixed value based on industry bounding estimates of the amount of crud available within the Reactor Coolant System and steam generator tubes. This amount does not vary with break selection and is therefore input as a fixed value. Acknowledged variations in this particulate source do not compete with dominant sources like failed unqualified coatings.</p>	<p>(13) ALION-CAL-STP-8511-07. STP Crud Debris Generation. Revision 0: November 12, 2012.</p>
*Latent debris quantity	Fixed values	None	<p>The latent debris quantities are based on a combination of plant configuration, conservative assumptions and NRC approved analysis methods.</p> <p>Latent debris quantities are considered fixed values as they are based on assumed plant conditions.</p>	<p>(43) ALION-CAL-STPEGS-2916-002. GSI 191 Containment Recirculation Sump Evaluation: Debris Generation. Revision 3: October 20, 2008.</p>

Input Parameter	Distribution(s) or Fixed Value(s)	Dependencies	Basis	Reference(s) (from LAR Enc. 4-3)
*Miscellaneous debris quantity	Fixed value	None	<p>Miscellaneous debris quantities are based on a combination of plant configuration, conservative assumptions and NRC approved analysis methods.</p> <p>Miscellaneous debris quantities are considered fixed values as they are based on assumed plant conditions.</p>	<p>(43) ALION-CAL-STPEGS-2916-002, GSI 191 Containment Recirculation Sump Evaluation, Debris Generation. Revision 3: October 20, 2008.</p>
Miscellaneous debris failure time	Fixed value	None	<p>Miscellaneous debris was assumed to fail at the beginning of the event. It is therefore considered a fixed value input. Miscellaneous debris failure time includes both crud and latent debris.</p>	<p>Debris Generation Assumptions, 4.b - It was assumed that 100% of the miscellaneous debris (tags, labels, etc.) would fail at the beginning of the event. This is a conservative assumption since the majority of the miscellaneous debris would be outside the ZOI and may not fail at all during the event.</p>

Input Parameter	Distribution(s) or Fixed Value(s)	Dependencies	Basis	Reference(s) (from LAR Enc. 4-3)
*Insulation ZOI size	Fixed values	Break Size, Insulation Location	Insulation-specific ZOI sizes have commonly accepted conservative definitions that are consistent with those used for strainer design. Plausible reductions in ZOI size have not been definitively demonstrated by testing, so deterministic ZOI sizes were adopted as fixed value inputs.	(44) NEI 04-07 Volume 1. Pressurized Water Reactor Sump Performance Evaluation Methodology. Revision 0: December 2004. (45) NEI 04-07 Volume 2. Safety Evaluation by the Office of Nuclear Reactor Regulation Related to NRC Generic Letter 2004-02, Nuclear Energy Institute Guidance Report "Pressurized Water Reactor Sump Performance Evaluation Methodology". Revision 0: December 2004.
*Fiberglass size distribution	Fixed values	Break Size, Insulation Location	The fiberglass size distribution is a specific design input to the analysis. The ZOI sizes do not change and therefore size distributions are also considered fixed value inputs.	(46) ALION-REP-ALION-2806-01. Insulation Debris Size Distribution for Use in GSI-191 Resolution. Revision 4: May 20, 2009.

Input Parameter	Distribution(s) or Fixed Value(s)	Dependencies	Basis	Reference(s) (from LAR Enc. 4-3)
Debris characteristics	Fixed values	None	The physical characteristics of debris, i.e. density, material composition, etc. are derived from manufacturer's data. As the physical characteristics do not vary with accident scenario, they are considered fixed values.	<p>(11) ALION-CAL-STP-8511-03. STP Qualified Coatings Debris Generation. Revision 0: August 10, 2012.</p> <p>(12) ALION-CAL-STP-8511-06. STP Unqualified Coatings Debris Generation. Revision 2: November 26, 2012.</p> <p>(13) ALION-CAL-STP-8511-07. STP Crud Debris Generation. Revision 0: November 12, 2012.</p> <p>(43) ALION-CAL-STPEGS-2916-002. GSI 191 Containment Recirculation Sump Evaluation: Debris Generation. Revision 3: October 20, 2008.</p>
*Chemical product formation time	Fixed values	None	Chemical product formation time is set to a fixed value, zero (0.0), so that opportunity for chemical product formation exists at all times during all scenarios. The parameter Chemical Precipitation Temperature controls the actual time when chemical induced head-loss effects are introduced.	(20) CHLE-016. Calculated Material Release. Revision 1: January 10, 2013.

Input Parameter	Distribution(s) or Fixed Value(s)	Dependencies	Basis	Reference(s) (from LAR Enc. 4-3)
*Blowdown transport	Fixed Values	Break Location, Debris Size	While blowdown transport is a function of the event and varies with each event, as described in ALION-CAL-STP-8511-08, conservative fixed values were adopted to aid understanding of complex transport logic sequences.	(23) ALION-CAL-STP-8511-08. Risk-Informed GSI-191 Debris Transport Calculation. Revision 2: January 21, 2013.
*Washdown transport	Fixed Values	Sprays initiated, Debris Size	While washdown transport is a function of the event and varies with each event, as described in ALION-CAL-STP-8511-08, conservative fixed values were adopted to aid understanding of complex transport logic sequences.	(23) ALION-CAL-STP-8511-08. Risk-Informed GSI-191 Debris Transport Calculation. Revision 2: January 21, 2013.
*Pool fill transport	Fixed values	Break Location, Debris Size	The analysis assumes that all latent debris and ZOI debris introduced at floor level is subject to transport to inactive cavities and to the strainers during pool fill. Although uncertainties exist in the accepted methodology, fixed values were adopted to aid understanding of complex transport logic sequences.	(23) ALION-CAL-STP-8511-08. Risk-Informed GSI-191 Debris Transport Calculation. Revision 2: January 21, 2013.

Input Parameter	Distribution(s) or Fixed Value(s)	Dependencies	Basis	Reference(s) (from LAR Enc. 4-3)
*Recirculation transport	Fixed values	Break Size, Break Location, Debris Type, Debris Size	<p>The various types and sizes of debris transport differently during the blowdown, washdown, and pool fill-up phases. The spatial distribution of this debris at the start of recirculation could vary widely because insulation debris on the pool floor would be scattered around by the break flow as the pool fills, and debris in upper containment would be washed down at various locations by the spray flow. To approximate this complexity, conservative fractions of fine and small debris (and all particulates) are assumed to be homogeneously mixed and available for transport by ECCS recirculation flow defined by the number of pumps operating.</p> <p>Therefore, recirculation transport is considered as fixed values.</p>	(23) ALION-CAL-STP-8511-08. Risk-Informed GSI-191 Debris Transport Calculation. Revision 2: January 21, 2013.
*Fiberglass spray erosion	Fixed value	Sprays initiated	Fiberglass spray erosion is based upon test data. Spray flow rate is approximately constant. Therefore Fiberglass spray erosion is considered a fixed value.	(23) ALION-CAL-STP-8511-08. Risk-Informed GSI-191 Debris Transport Calculation. Revision 2: January 21, 2013.

Input Parameter	Distribution(s) or Fixed Value(s)	Dependencies	Basis	Reference(s) (from LAR Enc. 4-3)
*Fiberglass pool erosion	Fixed value	None	Fiberglass spray erosion is based upon test data. Pool flow velocities vary based upon the physical configuration of the STP containment. To approximate this complexity, a single conservative value of spray erosion is assumed	(23) ALION-CAL-STP-8511-08. Risk-Informed GSI-191 Debris Transport Calculation. Revision 2: January 21, 2013. (new) ALION-REP-ALION-1006-04. Erosion Testing of Small Pieces of Low Density Fiberglass Debris – Test Report. Revision 1: November 7, 2011.
Fiberglass pool erosion time	Fixed values	None	Fiberglass pool erosion is a small additional fraction of the total fine fiber available for transport, so the total expected quantity of eroded fiber was introduced to the pool prior to recirculation as a fixed value.	(23) ALION-CAL-STP-8511-08. Risk-Informed GSI-191 Debris Transport Calculation. Revision 2: January 21, 2013. (new) ALION-REP-ALION-1006-04. Erosion Testing of Small Pieces of Low Density Fiberglass Debris – Test Report. Revision 1: November 7, 2011.

Input Parameter	Distribution(s) or Fixed Value(s)	Dependencies	Basis	Reference(s) (from LAR Enc. 4-3)
Transport time	Fixed values	Sump Flow Rate, Pool Volume, Failure Time	Transport time is based upon event timing and pump flow rates which have assigned distributions. Because transport time is calculated prescriptively, it is described here as a fixed value, even though transport time depends on random factors.	(23) ALION-CAL-STP-8511-08. Risk-Informed GSI-191 Debris Transport Calculation. Revision 2: January 21, 2013.

Input Parameter	Distribution(s) or Fixed Value(s)	Dependencies	Basis	Reference(s) (from LAR Enc. 4-3)
Strainer geometry	Fixed values	None	Strainer geometry is based upon the plant physical condition and is a direct numerical input. It was therefore input as fixed values.	<p>(47) SFS-STP-PA-7101. South Texas Project Units 1 & 2 Sure-Flow Strainer Module Details. Revision 5: September 5, 2006.</p> <p>(48) TDI-6005-01. SFS Surface Area, Flow and Volume Calculations. Revision 1: August 31, 2006.</p> <p>(49) SFS-STP-GA-00. South Texas Project Units 1 & 2 Sure-Flow Strainer General Arrangement. Revision 4: September 7, 2006.</p> <p>(50) SFS-STP-PA-7103. South Texas Project Units 1 & 2 Sure-Flow Strainer Sections and Details. Revision 2: August 4, 2006.</p> <p>(51) 2F369PS10572 Sheets 3, 4 & 6. Safety Injection 'SI'</p> <p>(52) 5L019PS0004. Specification for Criteria for Piping Design and Installation. Revision 23: s.n.</p>

Input Parameter	Distribution(s) or Fixed Value(s)	Dependencies	Basis	Reference(s) (from LAR Enc. 4-3)
Geometric strainer loading	Fixed values	Strainer geometry	<p>Geometric strainer loading is based upon the strainer physical geometry. It is a direct numerical input. It was therefore input as fixed values.</p>	<p>(47) SFS-STP-PA-7101. South Texas Project Units 1 & 2 Sure-Flow Strainer Module Details. Revision 5: September 5, 2006.</p> <p>(48) TDI-6005-01. SFS Surface Area, Flow and Volume Calculations. Revision 1: August 31, 2006.</p> <p>(49) SFS-STP-GA-00. South Texas Project Units 1 & 2 Sure-Flow Strainer General Arrangement. Revision 4: September 7, 2006.</p>
Clean strainer head loss	Fixed value	None	<p>Clean strainer head loss is a hydraulic attribute based upon the physical dimensions of the strainer. It is therefore a fixed value.</p>	<p>(53) 66-9088089-000. South Texas Project Test Report for ECCS Strainer Testing. Revision 0: August 29, 2008.</p>

Input Parameter	Distribution(s) or Fixed Value(s)	Dependencies	Basis	Reference(s) (from LAR Enc. 4-3)
Thin-bed thickness	Fixed value	None	<p>The thin-bed thickness is 1/16th of an inch. This is a physical fixed value assumption. Uncertainty regarding the exact value of this transition thickness is being addressed using parameter studies rather than direct propagation of a distribution.</p>	<p>Debris Generation Assumptions, 7.c - It was assumed that a fiber bed of at least 1/16th of an inch is necessary to capture chemical precipitates. This is a reasonable assumption since a thinner debris bed would not fully cover the strainer and would not support appreciable head losses due to chemical debris.</p>
Conventional head loss bump-up	Distribution	None	<p>Accuracy of the NUREG/CR-6224 correlation is known to vary with respect to debris composition. Also, known defects in the conventional implementation of the equation raise questions regarding general applicability. To account for the presence of extreme conditions in the scenario sample space, exponential probability distributions were defined and applied as direct multipliers to the estimated conventional head loss. Because consensus on these issues is difficult to establish, the conventional head loss bump-up is input as a distribution.</p>	<p>Section 5.6.2, Conventional Debris Head Loss Model - The NUREG/CR-6224 correlation was selected for the CASA computation of conventional debris head loss across the strainer. This correlation is a semi-theoretical head loss model and is described in detail in Appendix B of NUREG/CR-6224</p>

Input Parameter	Distribution(s) or Fixed Value(s)	Dependencies	Basis	Reference(s) (from LAR Enc. 4-3)
Chemical head loss bump-up	Distributions	Break Size	The corrosion and dissolution release model and the solubility model were not directly implemented in CASA Grande. Therefore, a set of chemical effects bump-up factor probability distributions were developed and applied for all breaks. To account for the presence of extreme conditions in the scenario sample space, exponential probability distributions were defined and applied as direct multipliers to the estimated conventional head loss. The probability distributions were developed based on the current results from the CHLE testing and on chemical head-loss effects observed during STP strainer testing.	(20) CHLE-016. Calculated Material Release. Revision 1: January 10, 2013.
Pump NPSH required	Fixed values	Void Fraction	This is a physical characteristic of the pump. Fixed values were defined by the pump vendor are therefore input as fixed values.	(25) ALION-CAL-STP-8511-05. STP Net Positive Suction Head Margin. Revision 0: November 19, 2012.
Pump NPSH available	Fixed values	Pool Temperature, Pump Flow Rate, Pool Level, Containment Pressure	Pump NPSH available is defined in ALION-CAL-STP-8511-05. They are therefore input as fixed values.	(25) ALION-CAL-STP-8511-05. STP Net Positive Suction Head Margin. Revision 0: November 19, 2012.

Input Parameter	Distribution(s) or Fixed Value(s)	Dependencies	Basis	Reference(s) (from LAR Enc. 4-3)
Strainer structural margin	Fixed value	None	<p>Strainer structural margin values are mechanical properties of the strainer material and code allowables. They are therefore input as fixed values.</p> <p>Also, see the response to EMCB-RAI-1 provided to the NRC Staff in STP letter NOC-AE-13003065, dated December 23, 2013 (ML14015A311).</p>	<p>(54) EC-PCI-STP-6005-1001. AES Document No. PCI-5473-SO1 Rev 2 "Structural Evaluation of Strainers for Containment Emergency Sumps". Revision 2: January 7, 2010.</p> <p>(55) EC-PCI-STP-6005-1004. AES Document No. PCI-5473-S03 Rev 0 "Structural Evaluation of Strainers for Containment Emergency Sumps for Long Term Post LOCA Case". Revision 0: January 7, 2010.</p>
Containment relative humidity	Fixed value	None	<p>Containment relative humidity was assumed to be 100%. This is a fixed value and does not change throughout the analysis.</p>	<p>Debris Generation Assumptions, 8.e - It was assumed that the relative humidity of the containment atmosphere is 100%.</p>
*Pump gas void limits	Fixed value	None	<p>Pump gas void limits are as defined in USNRC Regulatory Guide 1.82. Water Sources for Long-Term Recirculation Cooling Following a Loss-of- Coolant Accident. This is a fixed value.</p>	<p>(59) Regulatory Guide 1.82. Water Sources for Long-Term Recirculation Cooling Following a Loss-of- Coolant Accident. Revision 4: March 2012.</p>

Input Parameter	Distribution(s) or Fixed Value(s)	Dependencies	Basis	Reference(s) (from LAR Enc. 4-3)
Fiber filtration parameters	Distributions	None	Fiber filtration of a strainer is a function of the mass of debris on the strainer. STP-specific testing was used to derive parameters of the filtration model and their associated uncertainties. Therefore, the fiber filtration parameters are input as a distribution based on test data.	(60) University of Texas at Austin. Filtration as a Function of Debris Mass on the Strainer: Fitting a Parametric Physics-Based Model. s.l. June 5, 2013.
Fiber shedding parameters	Distributions	None	Fiber shedding is a function of the mass of debris on the strainer. STP-specific testing was used to derive parameters of the shedding model and their associated uncertainties. Therefore, the fiber shedding parameters are input as a distribution.	(60) University of Texas at Austin. Filtration as a Function of Debris Mass on the Strainer: Fitting a Parametric Physics-Based Model. s.l. June 5, 2013.
Boil off flow rate	Fixed values	None	Boil-off flow rates are a function of time and of core power and are based on the physical plant. Boil off flow rate were therefore input as fixed values.	(61) 5N079NB01000 (WCAP-12381). STPNOC Design Basis Document Accident Analysis. Revision 15: July 29, 2009. (62) Technical Specifications Section 1.27. Rated Thermal Power. Unit 1 Amendment No. 154; Unit 2 Amendment No. 142: s.n.

Input Parameter	Distribution(s) or Fixed Value(s)	Dependencies	Basis	Reference(s) (from LAR Enc. 4-3)
Number of fuel assemblies	Fixed value	None	The number of fuel assemblies is a physical plant parameter and does not vary. It was therefore input as a fixed value.	(61) 5N079NB01000 (WCAP-12381). STPNOC Design Basis Document Accident Analysis. Revision 15: July 29, 2009.
*Core blockage fiber limits	Fixed values	Break Location, Injection Path	Thermal hydraulic calculations of core blockage provided screening criteria that rendered the core blockage limits obsolete for the STP analysis. Core blockage fiber limits were therefore input as fixed values representing extreme limits of acceptable blockage.	(63) WCAP-16793-NP. Evaluation of Long-Term Cooling Considering Particulate, Fibrous and Chemical Debris in the Recirculating Fluid". Revision 2: October 2011.
Boron precipitation fiber limits	Fixed values	Break Location, Injection Path	The boron precipitation fiber limits are inherently uncertain because of both physical variability and lack of knowledge regarding associated phenomena. The boron precipitation fiber limit has been identified as a key factor controlling the risk of ECCS failure. It is difficult to achieve consensus regarding even a single value of this important threshold, let alone a statistical distribution, boron precipitation fiber limits were therefore input as fixed values and the impact has been emphasized via parameter studies.	(new) Letter from Sher Bahadur (NRC) to Anthony Nowinowski (PWROG). Final Safety Evaluation for Pressurized Water Reactor Owners Group Topical Report WCAP-16793-NP, Revision 2, "Evaluation of Long-Term Cooling Considering Particulate Fibrous and Chemical Debris in the Recirculating Fluid" (TAC No. ME1234): April 8, 2013.

* based on an NRC-accepted value or methodology

APLAB, CASA Grande – General: RAI 1b

(b) The source of the parameter value (e.g., licensing basis calculation).

STP Response:

See the response to APLAB, CASA Grande – General: RAI 1a.

APLAB, CASA Grande – General: RAI 1c

- (c) Whether the parameter is based on an NRC-accepted value (e.g., as documented in the safety evaluation (SE) for NEI-04-07, “Pressurized Water Reactor Sump Performance Evaluation Methodology” (Package ADAMS Accession No. ML043280641).**

STP Response:

See the response to APLAB, CASA Grande – General: RAI 1a.

APLAB, CASA Grande – Plant Configuration: RAI 1a

RG 1.200, Revision 2, “An Approach for Determining the Technical Adequacy of Probabilistic Risk Assessment Results for Risk-Informed Activities,” Revision 2 (ADAMS Accession No. ML090410014), Section 1.4, “PRA Development, Maintenance, and Upgrade,” states that plant information used in the PRA (e.g., expected thermal-hydraulic plant response to different states of equipment) should be as realistic as possible. Thermal-hydraulic simulations described in Volume 6.2 show that pool temperature is affected by parameters such as loss-of-coolant accident (LOCA) break size, component cooling water (CCW) temperature, and the status of containment spray, residual heat removal (RHR), and containment fan coolers. The simplified curves used by CASA Grande (Volume 3, Figure 2.2.13) assume “nominal” values for these parameters and an intact containment (Volume 6.2, page 6) yet are assumed to be bounding based on qualitative arguments stated by Volume 3, Assumption 1k, page 72.

- (a) Please state if varying the aforementioned (or other) parameters from their nominal values produce time-temperature curves that would yield higher conditional probabilities of sump or core blockage for any duration of time during the event. Please include consideration of all 15 pump state-LOCA size combinations (i.e., five pump cases 1, 9, 22, 26, and 43, and three LOCA categories (S/M/L [small/medium/large]) for both scenarios where containment is intact and not intact.

STP Response:

Yes, varying the aforementioned (or other) parameters from their nominal values will produce time-temperature curves yielding higher conditional probabilities of sump and core blockage

As an example, a summary of the Strainer Mapping for RCFCs is shown in Figure 1.

Fan Cooler Support Trains Available	CASA Case	Freq/yr LLOCA	Freq/yr MLOCA
3	1	4.15E-06	2.43E-04
2	1	3.25E-07	1.91E-05
1	1	3.32E-09	1.96E-07
0	1	0.00E+00	0.00E+00
3	9	3.76E-10	1.84E-08
2	9	2.76E-11	1.44E-09
1	9	0.00E+00	1.32E-11
0	9	0.00E+00	0.00E+00
3	22	2.19E-07	1.25E-05
2	22	1.65E-08	9.50E-07
1	22	2.89E-10	1.78E-08
0	22	0.00E+00	0.00E+00
3	26	2.49E-09	1.30E-07
2	26	1.58E-10	9.47E-09
1	26	1.67E-12	2.00E-10
0	26	0.00E+00	0.00E+00
3	43	4.60E-10	2.68E-08
2	43	6.94E-11	0.00E+00
1	43	5.52E-13	0.00E+00
0	43	0.00E+00	0.00E+00
3	99	1.48E-10	5.61E-09
2	99	4.41E-12	3.88E-10
1	99	0.00E+00	1.37E-12
0	99	0.00E+00	0.00E+00

Figure 1 - Strainer Mapping. Frequencies represent the plant configuration conditioned on LOCA Frequency. Frequencies <1E-14 (PRA truncation frequency) are reported as zero.

APLAB, CASA Grande – Plant Configuration: RAI 1b

- (b) Please provide a technical justification for using only nominal values or calculate core damage frequency (CDF), large early release frequency (LERF), delta-CDF (Δ CDF), and delta-LERF (Δ LERF) using time-temperature curves that maximize the probability of sump and core blockage for the entire assumed duration of the event.**

STP Response:

As stated previously, pool temperature has an effect on many aspects of the overall GSI-191 evaluation including chemical effects (material release rates and solubility limits), debris transport, strainer head loss, NPSH margin, degasification, and in-vessel effects. In some cases, a higher pool temperature profile is more conservative (e.g., NPSH margin and degasification), in other cases a lower pool temperature profile is more conservative (e.g., strainer head loss and debris transport).

With respect to pool temperature, due to its competing and complexity of effects on the overall evaluation, it is not possible to pre-determine whether a higher or lower pool temperature profile would be more limiting in the determination of CDF or LERF.

The premise of a risk-informed evaluation is to consider a holistic approach where competing effects collide. The use of nominal pool temperature profiles is consistent with a holistic risk-informed approach and provides a more realistic evaluation of risk.

APLAB, CASA Grande – Plant Configuration: RAI 2a

RG 1.174, Section 2.3.2, “Level of Detail Required to Support an Application,” states that the level of detail of the PRA model must be sufficient to model the impact of the proposed change. Section 2.2.8 of Volume 3 states that Table 2.2.14 safety injection (SI) flow rates are based on simulations using nominal operating conditions (i.e., all emergency core cooling system (ECCS) trains operating, all fan coolers operating, and nominal CCW heat exchanger temperatures). Furthermore, Volume 2, page 38 states that “to evaluate the potential for generic safety issue (GSI)-191 phenomena, the total pump flow from the sump is the most important consideration.”

- (a) Please state whether varying the aforementioned (or other) operating conditions from their nominal values could produce flow rates or other thermal-hydraulic conditions that would yield higher conditional probabilities of sump or core blockage for any duration of time during the event. Please include consideration of all 15 pump state-LOCA size combinations (i.e., five pump cases 1, 9, 22, 26, and 43, and three LOCA categories (S/M/L) for both scenarios where containment is intact and not intact.**

STP Response:

Yes, varying the aforementioned (or other) parameters from their nominal values will produce flow rates yielding higher conditional probabilities of sump and core blockage.

As an example, a summary of the Strainer Mapping for RCFCs is shown in Figure 1.

Fan Cooler Support Trains Available	CASA Case	Freq/yr LLOCA	Freq/yr MLOCA
3	1	4.15E-06	2.43E-04
2	1	3.25E-07	1.91E-05
1	1	3.32E-09	1.96E-07
0	1	0.00E+00	0.00E+00
3	9	3.76E-10	1.84E-08
2	9	2.76E-11	1.44E-09
1	9	0.00E+00	1.32E-11
0	9	0.00E+00	0.00E+00
3	22	2.19E-07	1.25E-05
2	22	1.65E-08	9.50E-07
1	22	2.89E-10	1.78E-08
0	22	0.00E+00	0.00E+00
3	26	2.49E-09	1.30E-07
2	26	1.58E-10	9.47E-09
1	26	1.67E-12	2.00E-10
0	26	0.00E+00	0.00E+00
3	43	4.60E-10	2.68E-08
2	43	6.94E-11	0.00E+00
1	43	5.52E-13	0.00E+00
0	43	0.00E+00	0.00E+00
3	99	1.48E-10	5.61E-09
2	99	4.41E-12	3.88E-10
1	99	0.00E+00	1.37E-12
0	99	0.00E+00	0.00E+00

Figure 1 - Strainer Mapping. Frequencies represent the plant configuration conditioned on LOCA Frequency. Frequencies <1E-14 (PRA truncation frequency) are reported as zero

APLAB, CASA Grande – Plant Configuration: RAI 2b

- (b) Please provide a technical justification for assuming only nominal operating conditions or calculate CDF, LERF, Δ CDF, and Δ LERF using flow rates or other thermal-hydraulic conditions that maximize the probability of sump and core blockage for the entire assumed duration of the event.**

STP Response:

The premise of a risk-informed evaluation is to consider a holistic approach where competing or widely varying effects provide overly conservative and competing results. The use of nominal flow rates provides a more realistic evaluation, is consistent with a holistic risk-informed approach and provides a more realistic evaluation of risk. The goal is to provide a reasonable probability, not necessarily a maximization of the probability of failure.

It is recognized and has been stated previously, that flow rate is one of the more important input parameters and has an effect on many aspects of the overall GSI-191 evaluation. In some cases, a higher flow in combination with other factors produces a more conservative result. In other cases a lower flow in combination with other factors produces a more conservative result. Using nominal values provides results that are reasonable, probable and that may be used in a holistic, risk-informed evaluation.

APLAB, CASA Grande – Plant Configuration: RAI 3a

RG 1.174, Section 2.3.2 states that the level of detail of the PRA model must be sufficient to model the impact of the proposed change. Volume 3 (page 71 of 248), Assumption 2b provides a qualitative argument for why a combination of pumps failing in the same train is “worse” than the same set of pumps failing in different trains. This qualitative argument includes a set of examples captured in Volume 3, Tables 3.1, 3.2, and 3.3.

(a) Please justify this assumption and clarify if an engineering analysis was performed in support of this assumption.

STP Response:

Pump state 22, the case when one high head, one low head and one spray pump is unavailable, was chosen to explore the impact of the assumption that all failed pumps are on the same train. Pump state 22 was chosen for detailed examination as it is the most likely pump state involving multiple pump failures.

Pump state 22 assumes that all three unavailable pumps are on the same train. To explore the impact of unavailable pumps being on different trains, four additional cases were evaluated.

The results of this analysis indicated that the configuration where all unavailable pumps are on the same train leads to the highest likelihood of failure at the sump. Three of the additional cases investigated that involved three unavailable pumps but on different trains did result in conditional failure likelihoods higher than pump state 22. In two of those cases, a higher core damage frequency due to in-vessel phenomena was predicted. The larger increase in core damage frequency resulting from these two cases was approximately 1.5%

Details documenting the rationale for selecting pump state 22 to demonstrate the impact of the assumption, the analysis approach and results are found in Enclosure 1.

APLAB, CASA Grande – Plant Configuration: RAI 3b

- (b) Please state if this assumption always increases the conditional probability of strainer failure (i.e., is this a conservative assumption?). In other words, please explain if there are any combinations of pumps failing in separate trains that would produce an equal or higher approach velocity and an equal or higher debris accumulation on any one strainer than the same combination of pumps failing in a single train. If so, please justify excluding them from the analysis.**

STP Response:

See the response to APLAB RAI 3a.

APLAB, CASA Grande – Plant Configuration: RAI 3c

- (c) Please state if this assumption always increases the conditional probability of in-vessel effects. Assumption 2b acknowledges that some combinations of pumps failing in separate trains may produce an equal or higher amount of debris accumulation in the core when compared to the same combination of pumps failing in a single train. Please provide a list of these combinations and justify excluding them from the analysis.**

STP Response:

See the response to APLAB RAI 3a.

APLAB, CASA Grande to PRA Interface-General: RAI 2a

RG 1.174, Section 2.3.2 states that the level of detail of the PRA model must be sufficient to model the impact of the proposed change. PRA models typically classify LOCA break sizes according to scenario differences and corresponding differences in structures, systems, and components (SSCs) available to mitigate the event and corresponding success criteria. For determining the effect of debris on the seven failure mechanisms defined in the submittal, a different set of break sizes might be more appropriate. For example, if there is a minimum size LOCA necessary to result in failure of recirculation due to debris, then including LOCAs below that size when determining failure probabilities may mask the true risk impact. Please provide the following information:

(a) The largest break size below which no failures were recorded during the CASA runs.

STP Response:

The largest break size below which no failures related to either the sump or vessel performance were recorded during the CASA Grande runs was a DEGB in a 5.189D inch pipe.

The “effective size” of the DEGB break in a 5.189D inch pipe is $5.189 * (2)^{1/2} = 7.338$ inch. The effective size was used to assign DEGB cases to a LOCA category. Therefore, this is the transition break size below which no failures were recorded and above which failures were observed in some cases. This specific break was characterized as a Large LOCA.

APLAB, CASA Grande to PRA Interface-General: RAI 2b

- (b) In addition, for the chosen LOCA sizes, please describe scenario timing differences for the debris model compared to the base PRA, changes in success criteria as a result of debris, and changes in operator response.**

STP Response:

There are no scenario timing differences for the debris model compared to the base PRA, changes in success criteria as a result of debris, and changes in operator response.

Figure 1.3, from LAR Enc. 4-3, reproduced below, shows the relationship between the STP PRA model and CASA Grande. With respect to timing and success criteria the two models are, of necessity, consistent.

APLAB, STP PRA Model-General: RAI 1

RG 1.200, Section 2.2, "Industry Peer Review Program," states that when the NRC staff's regulatory positions contained in its appendices are taken into account, use of a peer review can be used to demonstrate that the PRA is adequate to support a risk-informed application. It appears that the latest peer review of the STP PRA model was performed to support STP's application for risk-managed technical specifications and the results of this peer review were captured by STP in its letter dated February 28, 2007 (ADAMS Accession No. ML070670369). Please describe any significant changes to the plant or PRA model that have been made since that time. Please state if any of these changes represent "model upgrades" as discussed in the ASME/ANS PRA Standard. Please provide the results of any focused-scope or full peer reviews conducted since letter dated February 28, 2007.

STP Response:

An independent focused peer review followed an upgrade to the Human Reliability Analysis. The results of that review are found in Enclosure 2. No Significance Level A findings were found. All Level B observations (Enclosure 3) were resolved and incorporated into the PRA as appropriate.

A focused independent review of the electric power recovery analysis was performed with the resolution of the comments summarized in Enclosure 4. All comments have been resolved.

One significant level B finding and observation (F&O) indicted a lack of uncertainty analysis in electric power recovery for Station Blackout scenarios as summarized in Enclosure 4. Consequential loss of offsite power in a LOCA scenario followed by a loss of all 3 diesels is sufficiently unlikely that the consequential LOOPs are not included in the PRA model. Therefore the recovery analysis F&O is not relevant to the GSI-191 analysis.

APLAB, STP PRA Model-General: RAI 3

RG 1.200, Section 2.1, "Consensus PRA Standards," states that the capability category (CC) needed for each technical requirement is dependent on the specific application, although CC-II is generally acceptable. Please provide a list of the supporting requirements and corresponding CCs that were determined to be applicable to the risk-informed resolution of GSI-191. For any cases where the necessary CC was not found to have been met by the peer review process, please provide a technical justification.

STP Response:

It was determined that the requirements specified for internal events at-power PRA are applicable for this specific application at STP (please refer to the response to APLAB, STP PRA Model-RAI-2, NOC-AE-14003101, June 25, 2014, ML14178A481 and ML14178A485).

The PRA on which the GSI-191 RI application is based was developed from the STP PRA model of record (MOR). The STP PRA MOR has been peer reviewed and found to comply with capability category II for all internal event, level 1 and 2 requirements.

The GSI-191 PRA required focused modification of six of the eight internal event technical elements: Initiating Event Analysis (IE), Accident Sequence Analysis (AS), Success Criteria (SC), Systems Analysis (SY), and Quantification (QU). The Human Reliability Analysis (HR), Data Analysis (DA), and LERF Analysis (LE) were not impacted by the changes to the MOR to create the GSI 191 PRA.

The process of providing a reasonably complete identification of relevant initiating events (High Level Requirement IE-A) is discussed in the enclosure to the response to APLAB, STP PRA Model-RAI-2, NOC-AE-14003101, June 25, 2014, ML14178A481 and ML14178A485).

Modifications to the MOR did not impact this High Level Requirement so that the GSI 191 PRA meets all supporting requirements deriving from IE-A.

Likewise the grouping of the initiators (the focus of High Level Requirement IE-B) was not changed from the MOR so that the GSI-191 PRA meets all supporting requirements deriving from IE-B.

As explained in the LAR, the GSI-191 PRA did adapt an approach to the quantification of the LOCA frequencies (the focus of High Level Requirement IE-C) that is distinct from that adopted in the MOR. Supporting requirements IE-C1 through IE-C6, IE-C12, IE-C13 and IE-C15 are applicable. Time trend analysis (IE-C7) is not necessary to meet Capability Category II. Fault tree analysis was not used, so IE-C8 through IE-C11 are not applicable.

Supporting Requirements IE-D1 through IE-D3 (pertaining to Documentation) are applicable.

Modifications to the Accident Sequence model were made to explicitly include the impact of GSI-191 issues. Supporting requirements AS-A1 through AS-A11, AS-B1 through AS-B7, and AS-C1 through AS-C3 are applicable.

High Level Requirement SC-A specifies the requirements for success criteria. Supporting requirement SC-A2 is applicable as it provides guidance for acceptance requirements. SXC-A5 (pertaining to mission time) and SC-A6 (consistency with features, procedures and operating philosophy) are applicable. The definition of core damage (SC-A1), the success criteria for key safety functions (SC-A2) are not modified from the MOR and therefore remain Capability Category II and not applicable in the review of the GSI 191 PRA. The Medium and Large LOCA accident sequence models do not credit systems shared between the two units, so SC-A4 is not applicable.

SC-B1 through SC-B5 (which pertain to thermal-hydraulic and other supporting analyses) are applicable. SC-C1 through SC-C3 (pertaining to documentation) are applicable.

The changes to the Systems Models primarily involved providing logic to incorporate the results of the supporting phenomenological analyses (e.g., results from CASA Grande). Applicable Supporting Requirements associated with High Level Requirement SY-A (which seeks a reasonably complete treatment of causes for unavailability) are limited to SY-A1 through SY-A7, SY-A9 through SY-A14, and SY-A21 through SY-A24. SY-A8 refers to establishing component boundaries and is not applicable. SY-A15 through SY-A20 are otherwise not applicable. SY-A15 pertains to truncating the system model, which was not done in the system model. SY-A16 and SY-A17 pertain to human factors which are not included in the phenomenological models. SY-A18 through SY-A20 are otherwise not relevant.

High Level Requirement SY-B focuses on the reasonably complete treatment of common cause failures, intersystem and intersystem dependencies. Because the systems analyses are being used to introduce events of a phenomenological nature, only SY-B6 which addresses potential spatial or environmental impacts is applicable.

Supporting requirements SY-C1 through SY-C3 pertain to documentation and are applicable.

Most supporting requirements associated with the QU High Level Requirements are applicable. The one exception is QU-D4 which, for capability category II, calls for the comparison to the results from similar plants. As STP is a pilot plant, this is not practicable.

The applicable supporting requirements remain met at capability category II. The realistic plant-specific thermal-hydraulics and other supporting analysis are likely capability category III. These claims are not the result of a conventional peer review, but rather the conclusions of an in-depth independent review. This review was conducted by an independent technical oversight team from the University of Illinois Urbana-Champaign.

APLAB, STP PRA Model-Success Criteria: RAI 1

RG 1.174, Section 2.3.3 states that the PRA model should be technically adequate for the application. Volume 2, page 7, item 14, states:

One out of three each from HHSI [high head safety injection] and LHSI [low head safety injection] pumps is assumed required for mitigation of medium LOCAs.

Please provide the basis for this assumption including how debris effects on success criteria were considered.

STP Response:

Section 15.6.5.4.3 of the STP UFSAR notes that minimum safety injection capacity is adequate for all breaks between 2-10 inches; i.e., 1 train fails and 2 trains start, one of which goes out the break. The 2 inch break size is limiting for PCT. The analysis performed to justify this conclusion was performed in the absence of considering GSI-191 phenomena.

Analyses performed in support of the LAR included consideration of a 6 inch hot leg break with only one train of ECCS available. Note that in cases in which only a single train of ECCS is available, switchover to hot leg injection is not performed. The evaluation included consideration of debris effects. The analyses indicate that the core is reflooded, even if debris blocks the inlet to the fuel channels.

It is concluded that GSI-191 phenomena do not impact the success criteria used in the PRA.

APLAB, STP PRA Model-Success Criteria: RAI 2a

RG 1.174, Section 2.3.3 states that the PRA model should be technically adequate for the application. ASME/ANS Ra-Sa-2009 SC-B3 states:

When defining success criteria, USE thermal/hydraulic, structural, or other analyses/evaluations appropriate to the event being analyzed, and accounting for a level of detail consistent with the initiating event grouping (HLR-IE-B) and accident sequence modeling (HLR-AS-A and HLR-AS-B).

Volume 3, Section 5.10, “In-Vessel Downstream Effects” (page 222), and Volume 6.2, Item 5.a.14 describe a series of RELAP5 simulations used to assess small, medium, and large LOCAs on both the hot- and cold-leg side of the reactor coolant system (RCS) under full core blockage conditions. According to these sections, “only the medium and large cold leg breaks proceeded to core damage...”

- (a) Please discuss how these thermal-hydraulic analyses contained a level of detail consistent with the initiating event grouping and accident sequence modeling. In other words, explain whether the break sizes and locations assumed in the RELAP5 simulations were consistent with those used in the PRA and elsewhere in CASA Grande.**

STP Response:

The break sizes and locations assumed in the RELAP5 simulations were consistent with those used in the PRA and elsewhere in CASA Grande.

APLAB, STP PRA Model-Success Criteria: RAI 2b

- (b) Please explain whether the plant conditions assumed in the RELAP5 simulations (e.g., number of available ECCS trains) were consistent with each accident sequence in which the results from the RELAP5 simulations were used. For example, a sequence involving plant state 43 (single ECCS train) and a medium-break LOCA on the hot-leg side would appear to have assumed conditional probability of core blockage due to boron of zero. Please explain if the RELAP5 calculation showing adequate core cooling under this scenario accounts for the most limiting medium-break LOCA (break size/location) and if it is consistent with accident sequence modeling (i.e., models only one train of ECCS). The response should address all GSI-191 accident sequences that used RELAP5 simulations.**

STP Response:

The success criteria used in the PRA for medium LOCA are based on analyses reflected in the FSAR, namely that at least one train of ECCS is available. The analyses performed for the case where all trains of ECCS are available indicate that boron precipitation will not occur for medium hot leg breaks.

The supporting thermal hydraulic analyses performed in support of the LAR also included consideration of a 6 inch break in the hot leg with only one train of ECCS available. The assumed break represents the limiting case for a medium hot leg LOCA, and the condition of a single train of ECCS available represents pump state 43. The results of the RELAP5 analysis show that the core remains adequately cooled. In addition, the liquid level in the core is quickly recovered, so boron precipitation is not credible in medium LOCA scenarios with less than three ECCS trains available (assuming HLSO is successful).

APLAB, STP PRA Model-Success Criteria: RAI 2c

- (c) RELAP5 simulations are used to support the conclusion that adequate core cooling is achieved for some LOCAs even under the assumption of complete core blockage. Please describe how these simulations accounted for the reduction in cladding-to-coolant heat transfer that was calculated by the LOCADM computer code, as described in Volume 3, Section 5.10.1.**

STP Response:

LOCADM is a calculation tool that can be used to conservatively predict the build-up of chemicals deposits on fuel cladding after a LOCA and the effect on the cladding temperature due to the change (degradation) of the overall cladding conductivity.

RELAP5-3D does not have the capability to predict the build-up of chemicals deposits on the fuel but it is capable to predict the effect of the conductivity degradation on the surface cladding temperature, given that the thickness of the deposit and its thermal conductivity is specified as an input parameter in the core heat structure.

At the time the RELAP5-3D model was developed and the thermal-hydraulic calculations (specifically the core blockage analysis) were performed, the deposition layer was not included in the input model of the core heat structure. Nevertheless, if the following characteristics of the deposit layer are assumed:

Thickness = 13.64 mils (346.456 μm) (LAR: Volume 3 Paragraph 5.10.1)
Thermal Conductivity = 0.1 Btu/(F ft h) (WCAP-16793-NP)

the increase in ΔT is approximately 40°F. The conclusion is reached that the effect of the deposition layer on the cladding temperature does not change the outcome of the simulation results performed with the RELAP5-3D models for the core blockage scenarios.

APLAB, STP PRA Model-Success Criteria: RAI 3a

RG 1.174, Section 2.3.3 states that the PRA model should be technically adequate for the application. Volume 3, Section 4.2, "Structured Information Process Flow," describes the quantification of net positive suction head (NPSH) margin and core blockage as a function of time. According to this section, time-dependent values are compared against acceptance criteria from t=0 (i.e., time that the LOCA occurs) and t=30 days. This appears to conflict with Volume 3, assumption m, which states that "it was assumed that a 36-hr run time for the CASA Grande simulations is sufficient to predict the scenarios that would proceed to failure."

- (a) Please clarify the accident duration used by CASA Grande to calculate the conditional probability of sump and core blockage. Also, identify all other analyses performed outside of CASA Grande (e.g., time-dependent coatings failure) and their assumed accident duration.**

STP Response:

CASA Grande analyses for the STP LAR used a 36-hr period to evaluate failure modes arising from debris accumulation on the strainer and on the core.

CASA Grande computes the parameters that change significantly and/or have potential impact on post-LOCA operation within the 30 day mission time. However, STP parametric studies show that phenomena that occur within the first 18 hours essentially define the success or failure of post-LOCA ECCS operation. ECCS failure probability does not increase significantly after 18 hours.

A 36 hours (2 times 18) analysis time was chosen as a reasonable analysis period to ensure the tail end probabilities are considered and to keep CASA run times also within a reasonable duration.

Additionally, the conditions and mechanisms associated with debris effects are established within the first 18-36 hours from the start of the LOCA. Therefore a time range of 36 hours provides the key parameters and basis for concluding ECCS post-LOCA success or failure and therefore effectively addresses a 30 day mission time.

Other analyses performed outside of CASA Grande and their assumed accident durations are as follows:

Unqualified Coatings Failure Transport.

Containment transport of failed unqualified coatings is conservatively modeled as being introduced at a constant rate from 0 to 10 minutes. Essentially all debris is accumulated on the strainer within a few pool turn-over periods. Hence by 36 hours, all of the contribution from this parameter is considered. Note that the actual time range of Unqualified Coatings Failure and transport is 0 min – 30 days. (See Volume 3, Table 5.5.5)

Debris Transport.

100% of debris transports to the active sump strainers is considered to be completed within 10 hours, as verified by tracking accumulated inventory as a function of time.

Formation of Chemical Precipitants.

Formation of chemical precipitants is considered to occur within 10 to 20 hours from the start of the accident, based upon the temperature profiles used and the assumption of a forced precipitation temperature. (See Volume 3, Figure 2.2.1)

Chemical Effects.

Strainer head loss, including chemical effects, is assumed to approach an asymptotic value at approximately 2,000 minutes, i.e., 33.3 hours, after the LOCA. (See Volume 3, Figure 5.6.6)

Operator Actions.

Operator actions such as securing pumps or switching over to hot leg injection are modeled consistent with EOPs and SAMGs

Consequently, the effective accident duration used by CASA Grande to calculate the conditional probability of sump and core blockage is 30 days.

APLAB, STP PRA Model-Success Criteria: RAI 3b

- (b) Many of the simulations performed by CASA Grande concluded that none of the seven performance thresholds identified in Volume 1, Section 2.3.5, "LOCA Models," were exceeded. For these cases, please state if an analysis was performed to confirm that at the end of each simulation, the plant was in a safe, stable end state. For example, please explain if any cases were trending toward a performance threshold when the simulation was terminated. If so, please provide justification that the selected accident duration was appropriate to capture all physical phenomena (e.g., long-term chemical effects). If failures due to GSI-191 phenomena could occur after the CASA Grande analysis duration, please explain how this was considered in the PRA model (note Supporting Requirement SC-A5 in the ASME/ANS PRA Standard).**

STP Response:

Sensitivity studies were performed on the CASA Grande analysis duration. Decreasing the simulation time from 36 hours to 24 hours had only an incidental effect on ΔCDF indicating that success scenarios had reached a safe, stable end state. The full effect of chemical precipitates was included for any scenario meeting the bed-thickness and precipitation criteria within the duration of the simulation, so in effect, long-term chemical effects were forced to occur within the time-frame of interest regardless of the actual time needed for corrosion and precipitation phenomena to develop under realistic conditions.

APLAB, STP PRA Model-Success Criteria: RAI 3c

(c) Please state what plant conditions and configuration is assumed for the “safe, stable end state” in the PRA model. Please describe.

STP Response:

The safe, stable end state can be understood by referring to the medium and large LOCA event sequence diagram presented in Volume 2, Appendix A, Figure A.3-1. Only one stable condition is shown, and that is on the right side of sheet 2 of the figure. The stable condition results if core damage is avoided. Down branches in the figure indicate failures that may or may not lead to core damage end states depending on subsequent events. The core damage end states are shown as red symbols.

To reach the one, safe stable end state in response to a medium or large LOCA requires:

- Successful reactor trip,
- Successful safety injection actuation,
- MSIV closure or turbine trip or the reactor withstanding a potential PTS overcooling challenge,
- Sufficient accumulator injection,
- Low head pump injection to the RCS
- High head pump injection (not required if a large LOCA)
- Low head pumps in sump recirculation mode
- Sump available for recirculation considering GSI-191 issues
- No in-vessel flow blockage
- No boron precipitation leading to loss of core cooling, and
- Decay heat removal by either the RHR heat exchangers or the containment fan coolers

If the break is in the cold leg, then successful hot leg switchover is also required in order to avoid excessive boron precipitation. At the end of a safe, stable sequence, one or more low head pumps are aligned for sump recirculation, at least one train to an RCS loop via the cold leg, and 0, 1, or 2 the hot legs of the remaining loops. At least one low head pump must be aligned to an RCS loop that remains intact; i.e. to an RCS loop that is not where the break is located. The most likely safe, stable end state is that all containment fan coolers are operating and that cooling to the secondary side of each RHR heat exchanger aligned for low head pump sump recirculation is available. These are the only safe, stable end states credited in the STP PRA for medium and large LOCAs.

APLAB, STP PRA Model-Success Criteria: RAI 3d

(d) Please explain whether the conditional probabilities calculated by CASA Grande were adjusted in any way to match the PRA mission time of 24 hours.

STP Response:

No changes were made to the outputs from CASA Grande to adjust for the PRA mission time. They were judged suitable and used as is.

APLAB, STP PRA Model-Human Reliability Analysis: RAI 3a

RG 1.174, Sections 2.3.1 and 2.3.2 state that the scope and level of detail of the PRA model must be sufficient to model the impact of the proposed change. Volume 2 describes two top events that model operator actions used to secure containment spray. Top event "OSI" (page 77) represents a short-term action to secure one train of containment spray prior to recirculation, given that all three trains are available. Top event "OFFS" (page 83) represents a longer-term action to secure all trains of containment spray once containment pressure and iodine levels are suitably low, these are conditions that may occur after recirculation is established. According to their descriptions, these top events are "always assumed successful when determining the failure probabilities introduced by the GSI-191 phenomena." Please provide the following information:

- (a) Please state if the CASA Grande models the plant conditions (e.g., sump flow rates, washdown rates, refueling water storage tank (RWST) drain-down times, etc.) that would occur if three containment spray trains were running (i.e., if the manual actions modeled by top event OSI are unsuccessful.)**

STP Response:

CASA Grande samples the post-LOCA time at which one train of containment spray is secured from distributions defined by the user for small, medium and large breaks. For the STP LAR, these times were defined as normal distributions with the following mean and standard deviation: 0 ± 0 min. for SBLOCA (sprays never on), 20 ± 5 min. for MBLOCA, and 20 ± 5 min. for LBLOCA. Sump flow rates and sump flow rate dependent physical phenomena are the only plant conditions that the "time to secure one spray" input effects in the simulation. RWST drain down times are assigned point values for varying break sizes, calculated with two containment spray pumps running because these values result in the most probable recirculation switchover times (LAR Encl. 4-3, Pg. 33). Failed debris wash down rates are assigned point values taken from deterministic analysis where two containment spray pumps were assumed operational (LAR Encl. 4-3, Ref. 23). Descriptions of other inputs and their assignment in CASA Grande are listed in the response to APLAB, CASA Grande-General RAI 1.

It is noted that statistical sampling does not preclude selection of a very long task performance time that effectively represents failure of manual actions. However, no strategies are employed to ensure that this condition is always represented in the statistical design.

APLAB, STP PRA Model-Human Reliability Analysis: RAI 3b

- (b) Please state if the CASA Grande models the plant conditions (e.g., sump flow rates, washdown rates, RWST drain-down times, etc.) that would occur if the operators fail to secure containment spray long term once containment pressure and iodine levels are suitably low (i.e., the manual actions associated with OFFS are unsuccessful).**

STP Response:

No, CASA Grande does not model the plant conditions that would occur if the operators fail to secure containment spray long term once containment pressure and iodine levels are suitably low i.e., the manual actions associated with OFFS are unsuccessful.

Specifically, CASA Grande samples the post-LOCA time at which all trains of containment spray are secured from distributions defined by the user for small, medium and large breaks. For the STP LAR, these are defined as normal distributions with the following mean, standard deviation and truncation limits: 390 ± 5 min. between 390 and 420 min. for SBLOCA, 390 ± 10 min. between 390 and 420 min. for MBLOCA, and 390 ± 15 min. between 390 and 450 min. for LBLOCA. For these cases, the truncation limits preclude performance times beyond 450 min. (7.5 hr). Plant conditions (ie. sump flow rates, washdown rates, RWST drain-down times, etc.) are not modeled for the condition where operators fail to secure long-term containment spray.

APLAB, STP PRA Model-Human Reliability Analysis: RAI 3c

- (c) If the answer to either (a) or (b) is “no”, please provide a technical basis and explain how the PRA meets the ASME HLR-HR-G requirement to perform an assessment of post-initiator human failure events using a well-defined and self-consistent process that addresses scenario-specific influences on human performance.**

STP Response:

The PRA model does include logic to represent failure to trip one running containment spray pump as well as failure to trip all containment spray pumps late in the sequence. However, there are no results from CASA Grande that are representative of these failure conditions. Failure to trip one running containment spray pump early in the sequence would result in the debris being approximately evenly divided among the three sump strainers with a corresponding lower head loss than in the case of only two running containment spray pumps. Since failure of one strainer is assumed to result in failure of all strainers, this approach is conservative for strainer head loss. However, the approach may be slightly unconservative with respect to in-vessel effects as the additional debris on the strainer would provide more filtration.

APLAB, STP PRA Model-PRA Scope: RAI 2

Volume 2 (page 47 of 257) states, in part, that

...a medium LOCA on one primary loop would be assumed to be accompanied by medium LOCA on all other loops. The result is that seismically induced medium and large LOCAs are modeled as being excessive LOCAs-which have no success sequences by definition.

RG 1.174, Sections 2.3.1 and 2.3.2 state that the scope and level of detail of the PRA model must be sufficient to model the impact of the proposed change. While it is a common assumption that seismic failures among like components are 100 percent correlated, for this analysis this assumption leads to a lower calculated value of delta risk. That is, for cases where a single large pipe fails due to a seismic initiating event, or where multiple small bore pipes fail, it might be possible to mitigate the scenario to a greater extent if debris sources do not exist inside containment. Please justify not analyzing the additional risk of GSI-191 phenomena for seismic events without reliance on the conservative assumption of 100 percent correlation.

STP Response:

In the response to APLAB, STP PRA Model - PRA Scope: RAI 1 (STP letter provided to NRC Staff, NOC-AE-14003103, May 22, 2014, ML14149A434 page 24), it was established that the mean frequency of a seismically induced Medium LOCA is estimated to be 1.08×10^{-7} per year. The bounding assumption of a conditional likelihood of 0.1 for recirculation failure following a seismic event suggests the contribution to mean core damage frequency due to a seismically induced Medium LOCA is no greater than 1.1×10^{-8} per year.

APLAB, Results Interpretation-Uncertainty Analysis: RAI 1a

RG 1.200 defines model uncertainty as an issue where no consensus approach or model exists and where the choice of approach or model is known to have an effect on the PRA (e.g., introduction of a new basic event, changes to basic event probabilities, changes in success criteria, introduction of a new initiating event.). Volume 1 Section 2.5.3, "Model Uncertainty," contains a general discussion of model uncertainty (using chemical effects and debris filtration as examples) and broadly states that conservatism was used to address model uncertainty. This is inconsistent with RG 1.200, Section 3.3.2, "Assessment of Assumptions and Approximations" (and ASME HLR-QU-E) guidance that states that all sources of model uncertainty should be identified and their effects on the PRA (as identified above) should be determined as discussed in RG 1.174, Section 2.5.5. Uncertainty must be evaluated for this analysis, including the PRA model, CASA Grande, and any supporting analyses. Please provide the following information:

(a) Please identify all sources of key model uncertainty as defined by RG 1.200

STP Response:

Key sources of model uncertainty are:

- Success criteria for fuel blockage and boron precipitation
- Fiber penetration of the sump strainer
- Head loss correlation at sump strainer
- Debris generation, including size and shape of zone of influence
- Debris transport to the sump
- Ability of chemical precipitates to cause increased strainer head loss and fuel blockage

APLAB, Results Interpretation-Uncertainty Analysis: RAI 1b

(b) Please identify the key assumptions as defined by RG 1.200.

STP Response:

Key assumptions made are:

- A discrete set of operability states of the pumps taking suction from the containment sump was adopted. In a given scenario, the specific configuration of operating pumps was bounded by a one member of a set of five analyzed cases. If a specific pump configuration was not bounded by one of the five analyzed cases, core damage was assumed to occur.
- Failure conditions found at one or more of the three containment sumps was assumed to result in failure at all three sumps.
- For cold leg breaks, it was assumed that boron precipitation would be possible without hot leg injection switchover.
- A large zone of influence for jet induced debris generation was assumed.
- When increased by a factor of 5, the NUREG/CR-6224 is expected to bound conventional head loss.
- It was assumed that no core bypass capability is available for blockage exceeding 7.5 g per fuel assembly.
- No credit taken for core bypass.

APLAB, Results Interpretation-Uncertainty Analysis: RAI 1c

- (c) Please describe the potential effect of the key assumptions on the results of this study; that is, on the CDF and LERF attributable to GSI-191 phenomena. Describe the results of any related sensitivity analyses that were performed.**

STP Response:

The adaptation of discrete pump operability states likely had a modest conservative impact on the results for Large LOCA. However, this assumption had a more significant conservative impact in the assessment of Medium LOCAs. 100% of the reported contribution of sump failure for Medium LOCAs was due to sequences with pump operability combinations that were not bounded by the five analyzed pump states. If a finer more detailed set of pump states were chosen, then the calculated delta CDF would be lower.

The assumption that failure conditions at one sump would result in failure at all sumps is conservative.

The head loss correlation used, including 'bump up factors', is conservative based on the results of the STP-specific head loss tests.

The assumption that boron precipitation following Medium cold leg breaks is likely conservative. The large zone of influence for debris generation is bounding and possibly conservative.

The assumption that breaks occur on a leg equipped with SI yields a slightly conservative result, as there is only a ¼ likelihood that the break would be on the leg without SI.

Please see the response to APLAB, Results Interpretation-Uncertainty Analysis: RAI 6 for additional description of the sensitivity analyses conducted.

APLAB, Results Interpretation-Uncertainty Analysis: RAI 3

Volume 1, Section 1.3.1, "LOCA Frequency," states that LOCA frequencies were obtained from Table 7.19 of NUREG-1829 for 25 years' operation. Furthermore, assumption 3.b in Volume 3 (page 76) states that current-day LOCA frequencies are more appropriate to use for this evaluation than the end-of-plant-license frequencies. RG 1.174, Section 2.5.5 states that it is incumbent on the licensee to demonstrate that the choice of reasonable alternative hypotheses, adjustment factors, or modeling approximations or methods to those adopted in the PRA model would not significantly change the assessment. Also, it is assumed that the STP plants will continue to operate for more than 25 years; RG 1.174 Section 3, "Element 3: Define Implementation and Monitoring Program," states that the licensee should define an implementation and monitoring program to ensure that no unexpected adverse safety degradation occurs do to the change. Please justify the use of the 25-year frequency estimates rather than the 40-year estimates provided by NUREG-1829. Please provide CDF, LERF, Δ CDF, and Δ LERF using the 40-year estimates.

STP Response:

As described in the LAR Enclosure 4-1, Section 2.1.2, all STP large-bore piping PWSCC-susceptible welds (nozzle welds) have been replaced or otherwise mitigated, with the exception of the reactor vessel nozzle welds. As further described, the reactor vessel nozzle welds are less of a concern in the GSI-191 analysis than are other break locations because the reactor vessel is covered with RMI, and the primary shield wall would protect the majority of fiberglass insulation in the steam generator compartments. Finally, STPNOC is currently in compliance with ASME Section XI weld inspections.

Both STP plants are at approximately 25 years of service and therefore it is appropriate to expect that the 25-year LOCA frequency values would apply. It is further reasonable to "reset" the effective time of service to much less than 25 years when taking into account the most problematic welds have been mitigated or replaced.

The 40 year estimates for CDF, LERF, Δ CDF, and Δ LERF are provided in Enclosure 5. The following table summarizes the 40 year estimates.

Parameter	Value
CDF	2.20E-05
LERF	1.38E-06
Δ CDF	6.85E-08
Δ LERF	1.12E-10

APLAB, Results Interpretation-Uncertainty Analysis: RAI 4a

The acceptance guidelines of RG 1.174, Section 2.5.5 “are defined such that the appropriate measure for comparison is the mean value of the uncertainty distribution on the corresponding metric.” Typically, statistical sampling simulations will develop random variables that preserve the mean of the distribution from which the variables are sampled. STP has chosen to fit a Johnson bounded distribution that matches the expert-provided 5th, 50th, and 95th percentiles in NUREG-1829, but does not match the mean values. The properties of the distribution are such that, as fit, the mean of the fitted distribution is always less than the experts’ means from the distributions in NUREG-1829.

- (a) Please explain why the STP evaluation departs from the regulatory position in RG 1.174 regarding the use of mean values.

STP Response:

Quantiles were elicited in NUREG-1829 at the 5th, 50th, and 95th. The mean values were not elicited but instead, were derived from a split lognormal distribution for the elicited quantiles. The distributions used in the LAR were developed to most closely fit the values elicited in the expert elicitation process. As described in Enclosure 6, because the mean values are used by the PRA for the initiating event frequencies, Δ CDF and Δ LERF actually use the mean values from NUREG-1829.

APLAB, Results Interpretation-Uncertainty Analysis: RAI 4b

- (b) The Johnson fit to 5th, 50th, and 95th percentiles is not unique. Alternative accurate fits can be constructed with arbitrary values of the scale parameter λ . The scale parameter λ defines a bound on the maximal frequencies sampled in the Monte Carlo model. By increasing the value of λ , the relative proportion of large to medium to small breaks can be altered, especially in the extrapolation range beyond the 95th percentile. Please provide a technical justification for the selection of the scale parameter λ (other selections appear possible that could change the outputs by CASA Grande).**

STP Response:

The algorithm used to solve that model takes as input initial values for the Johnson parameters as a "starting point" for the optimization algorithm. For each category, the value of the lower bound, ξ , of the Johnson distribution was initialized to half of the 5th percentile given in NUREG-1829, and the range, λ , was initialized to twice the 95th percentile. This was done to produce additional spread of the distribution outside the NUREG-1829 percentiles and thereby capturing a reasonable range of uncertainty. Alternative Johnson distributions could be obtained by ranging the Johnson scale parameter, λ , that fit the three percentiles elicited from experts as part of NUREG-1829 as shown in Enclosure 7. Although Johnson fits can be obtained with higher mean frequencies, increasing the scale factor to a factor of 100 times the 95th percentile of the frequencies elicited from experts in NUREG-1829 produces less than a 2% increase in Δ CDF.

APLAB, Results Interpretation-Uncertainty Analysis: RAI 4c

- (c) Please provide the maximum expected difference between the CDF, LERF, Δ CDF, and Δ LERF developed from bounded Johnson distributions that consider alternative values of the scale parameter λ , and other distributions that would preserve mean values reported in NUREG-1829. Note, in particular, that alternative bounded Johnson distributions with large values of the scale parameter λ can be built to accurately fit the NUREG-1829 5th, 50th, and 95th percentiles, and produce mean estimates closer to the NUREG-1829 values than current fits used by STP.**

STP Response:

As shown in Enclosure 8 changes in CDF, Δ CDF, LERF, and Δ LERF are modest when the Johnson scale parameter, λ , is ranged from a factor of 1.25 up to a factor of 100 times the 95th percentile of the frequencies elicited from experts in NUREG-1829. (A factor of about 2.00 was used in STP's submittal.) More specifically, point estimates of Δ CDF and Δ LERF increase by no more than 2% for the specific values of λ considered in Enclosure 8. Estimates of CDF and LERF differ from Δ CDF and Δ LERF by values that do not depend on λ .

APLAB, Results Interpretation-Uncertainty Analysis: RAI 4d

- (d) In Table B.4-1 in Volume 2, LOCA exceedance frequencies are tabulated for different break sizes that are consistent with modified bounded Johnson distributions (the modified Johnson is a scaled bounded Johnson plus a uniform distribution) designed to match NUREG-1829 mean values. The fit to the 5th, 50th, and 95th NUREG-1829 percentiles of these modified Johnson distributions does not appear to be accurate. Therefore, these modified Johnson distributions inferred from Table B.4-1 appear to be different than the bounded Johnson distributions summarized in Table 2.2.2 in Volume 3. Please justify the apparent use of different bounded Johnson distributions in the PRA and CASA Grande.**

STP Response:

The distributions derived from the fitted bounded Johnson distributions were scaled for use in the PRA. This was done to match the resulting mean values with the means interpolated directly from NUREG-1829.

APLAB, Results Interpretation-Uncertainty Analysis: RAI 5

Volume 2, page 6 states, in part, that the “LOCA frequency uncertainties sampled in the PRA uncertainty analysis are assumed independent of the probabilities of failure from the uncertainty analysis of CASA GRANDE.” This assumption does not account for the state of knowledge correlation because the PRA and CASA Grande rely on the same parameter for their quantification (LOCA frequency derived from NUREG-1829). RG 1.174, Section 2.5.2, “Parameter Uncertainty,” states that the state of knowledge correlation should be accounted for unless it can be shown to be unimportant. Therefore, you are requested to either calculate CDF, LERF, Δ CDF, and Δ LERF accounting for the state-of-knowledge correlation or demonstrate that it is unimportant to this application.

STP Response:

The CASA Grande evaluation of GSI-191 failure phenomena is partly dependent on the LOCA frequency uncertainties, but not on the absolute LOCA Frequency estimates. The allocation of break sizes, within CASA Grande, is dependent on the downward slope of the LOCA exceedance frequencies within the break size range being investigated. The change in slope within the small, medium, or large LOCA break sizes dictates the weights given to the different break sizes only within the size being investigated. The break frequencies at every break size could be multiplied by a factor, and the estimates from CASA Grande would not change, because the relative allocation of break frequency to each sub-interval within, say the Large LOCA, break size range would not change.

For the PRA, the core damage frequency dependence is on the difference in frequency at two points on the LOCA frequency exceedance curve. Multiplying the LOCA frequency at the two points by a factor would change the break interval frequency by that same factor. There is no dependence on the varying slope within the two break sizes, only the on the overall frequency difference.

Both the PRA and CASA Grande use the same break size intervals and this is accounted for in both. We believe this dependence of the PRA and CASA Grande on different parameters of the LOCA break frequencies is sufficient so as to not warrant correlation between the PRA and CASA Grande.

APLAB, Results Interpretation-Uncertainty Analysis: RAI 6

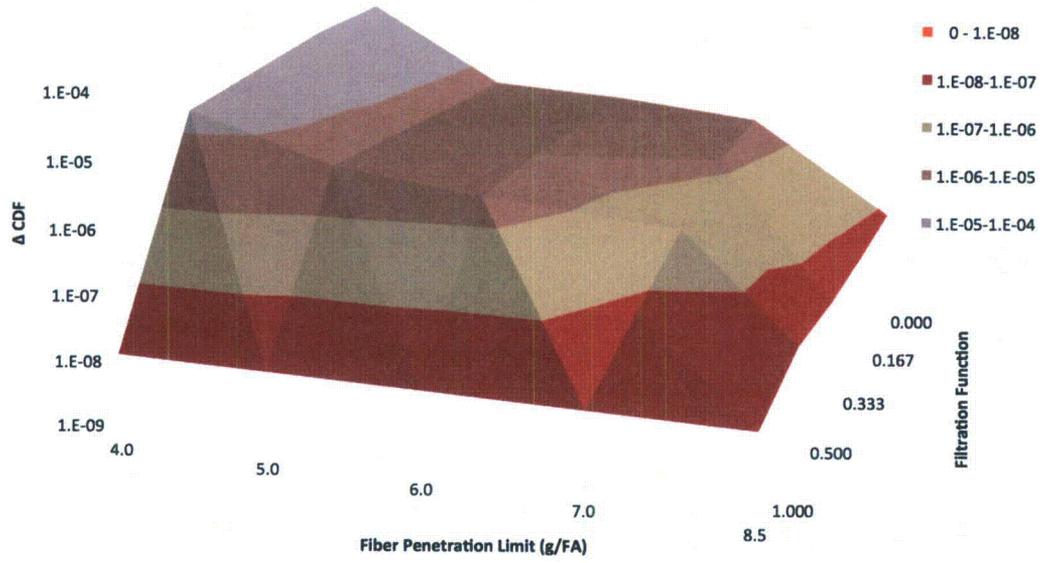
RG 1.174 Section 2.5.5 states that it is incumbent on the licensee to demonstrate that the choice of reasonable alternative hypotheses, adjustment factors, or modeling approximations or methods to those adopted in the PRA model would not significantly change the assessment. This demonstration can take the form of well-formulated sensitivity studies or qualitative arguments. In general, the results of the sensitivity studies should confirm that the risk acceptance guidelines are still met even under alternative assumptions.

Please provide the results of an aggregate analysis that quantifies the integrated impact on CDF, LERF, Δ CDF, and Δ LERF from all sensitivity studies that were performed. In this aggregate analysis, for those cases where individual assumptions have a synergistic effect on the results, a simultaneous analysis should be performed. For those cases where no synergy exists, a one-at-a-time analysis may be sufficient.

STP Response:

A sensitivity analysis was performed by 1) developing the scope of potentially important contributors to Δ CDF and then 2) analyzing their individual contributions in a one-way sensitivity study. The study was then expanded to include aggregate contributions from the two highest contributors, fiber penetration through the emergency core cooling system strainers and the success criteria for boron precipitation (boron fiber limit). The rest of the contributions were judged to be less important in the aggregate based on the one-way analysis. The Δ CDF estimate is most sensitive to three parameters that concern: 1) how much debris is required to trigger an in-vessel failure (boron fiber limit), 2) the fraction of debris that penetrates the sump strainer (fiber penetration function), and 3) the fraction of debris of different types that is transported from different locations during different operational phases (debris transport fractions in ZOI). The effect of the boron fiber limit exceeds that of the next most sensitive parameter by an order of magnitude. An analysis of the sensitivity to the aggregate effect of the bypass fraction and boron fiber limit is shown in the following figure.

Δ CDF (Total) as a Function of Fiber Penetration Limit and Filtration Function



Enclosures to Attachment 1

1. Response to APLAB, CASA Grande – Plant Configuration: RAI 3 Plant Configuration: Combinations of Pump Failures
2. Attachment A to CR 07-1684 Resolution of PRA HRA Update Report Peer Review Fact/Observation (F&O) Comments
3. Level B Observations Resolved
4. Independent Review of Electric Power Recovery Analysis
5. Response to APLAB 25 vs 40 Year Frequency Estimates: RAI 3
6. Response to APLAB-Results Interpretation-Uncertainty Analysis: RAI 4a
7. Response to APLAB-Results Interpretation-Uncertainty Analysis: RAI 4b
8. Response to APLAB-Results Interpretation-Uncertainty Analysis: RAI 4c



South Texas Project Risk-Informed GSI-191 Evaluation

Response to RAI APLA-II-3 Plant Configuration: Combinations of Pump Failures

Document: STP-RIGSI191- APLA-II-3

Revision: 1.0

Date: May 16, 2014

Prepared by:

Jeremy Tejada, The University of Texas at Austin
Alexander Zolan, The University of Texas at Austin
John Hasenbein, The University of Texas at Austin
David Morton, The University of Texas at Austin

Reviewed by:

Zahra Mohaghegh, University of Illinois at Urbana-Champaign
Seyed A. Reihani, University of Illinois at Urbana-Champaign

Approved by:

Ernie J. Kee, South Texas Project

Response to RAI APLA-II-3
Plant Configuration: Combinations of Pump Failures
Jeremy Tejada, Alexander Zolan, John Hasenbein, and David Morton
The University of Texas at Austin

Abstract

This document provides a statistical analysis of output of CASA Grande that can be used to inform a response to RAI APLA-II-3.

1 RAI APLA-II-3

The statement of the RAI APLA-II-3 is as follows:

RG 1.174, Section 2.3.2 states that the level of detail of the PRA model must be sufficient to model the impact of the proposed change. Volume 3, Assumption 2b provides a qualitative argument for why a combination of pumps failing in the same train is “worse” than the same set of pumps failing in different trains. This qualitative argument includes a set of examples captured in Volume 3, Tables 3.1, 3.2, and 3.3.

A) Please justify this assumption and clarify if an engineering analysis was performed in support of this assumption.

B) Please state if this assumption always increases the conditional probability of strainer failure (i.e., is this a conservative assumption?). In other words, please explain if there are any combinations of pumps failing in separate trains that would produce an equal or higher approach velocity and an equal or higher debris accumulation on any one strainer than the same combination of pumps failing in a single train. If so, please justify excluding them from the analysis.

C) Please state if this assumption always increases the conditional probability of in-vessel effects. Assumption 2b acknowledges that some combinations of pumps failing in separate trains may produce an equal or higher amount of debris accumulation in the core when compared to the same combination of pumps failing in a single train. Please provide a list of these combinations and justify excluding them from the analysis.

2 Selection of Case 22 as the Test Case

To quantitatively compare the effect of a combination of pumps failing in the same train and the same set of pumps failing in different trains, we selected a test case to analyze. For GSI-191 analysis, Table 1 presents both the frequency (PRA success frequency) and corresponding probability of being in each of 64 possible pump states in STP’s three-train design (Table 2.2.11 in [1]), where HHSI denotes a high head safety injection pump, LHSI denotes a low head safety injection pump, and SPRAY denotes a containment spray pump.

Table 1: Pump State Success Frequencies and Probabilities.

Case	HHSI	LHSI	SPRAY	Frequency	Probability
1	3	3	3	2.64E-04	9.35E-01
2	3	3	2	3.32E-06	1.18E-02
3	3	3	1	7.53E-08	2.67E-04
4	3	3	0	9.77E-09	3.46E-05
5	3	2	3	3.49E-06	1.24E-02
6	3	2	2	4.38E-08	1.55E-04
7	3	2	1	9.80E-10	3.47E-06
8	3	2	0	1.25E-10	4.43E-07
9	3	1	3	3.22E-08	1.14E-04
10	3	1	2	3.95E-10	1.40E-06
11	3	1	1	7.59E-12	2.69E-08
12	3	1	0	9.85E-13	3.49E-09
13	3	0	3	0	0
14	3	0	2	0	0
15	3	0	1	0	0
16	3	0	0	0	0
17	2	3	3	1.94E-06	6.87E-03
18	2	3	2	2.44E-08	8.64E-05
19	2	3	1	5.39E-10	1.91E-06
20	2	3	0	6.95E-11	2.46E-07
21	2	2	3	1.17E-07	4.14E-04
22	2	2	2	9.16E-06	3.24E-02
23	2	2	1	7.81E-08	2.76E-04
24	2	2	0	1.19E-09	4.21E-06
25	2	1	3	7.65E-10	2.71E-06
26	2	1	2	6.03E-08	2.13E-04
27	2	1	1	4.93E-10	1.75E-06
28	2	1	0	6.16E-12	2.18E-08
29	2	0	3	0	0
30	2	0	2	0	0
31	2	0	1	0	0
32	2	0	0	0	0
33	1	3	3	2.67E-08	9.45E-05
34	1	3	2	3.26E-10	1.15E-06
35	1	3	1	6.18E-12	2.19E-08
36	1	3	0	8.02E-13	2.84E-09
37	1	2	3	6.43E-10	2.28E-06
38	1	2	2	3.54E-08	1.25E-04
39	1	2	1	2.84E-10	1.01E-06
40	1	2	0	3.01E-12	1.07E-08
41	1	1	3	9.96E-12	3.53E-08
42	1	1	2	1.63E-09	5.77E-06
43	1	1	1	4.34E-08	1.54E-04
44	1	1	0	1.76E-10	6.23E-07
45	1	0	3	0	0
46	1	0	2	0	0
47	1	0	1	0	0
48	1	0	0	0	0
49	0	3	3	5.84E-11	2.07E-07
50	0	3	2	6.24E-13	2.21E-09
51	0	3	1	0	0
52	0	3	0	0	0
53	0	2	3	4.92E-13	1.74E-09
54	0	2	2	3.50E-11	1.24E-07
55	0	2	1	0	0
56	0	2	0	0	0
57	0	1	3	0	0
58	0	1	2	0	0
59	0	1	1	3.89E-11	1.38E-07
60	0	1	0	0	0
61	0	0	3	0	0
62	0	0	2	0	0
63	0	0	1	0	0
64	0	0	0	0	0

The probabilities in the right-most column of Table 1 are proportional to the frequencies in the table's penultimate column, and are normalized so that they sum to one. Table 2 repeats the top few cases from Table 1, sorted by their probability (Probability Mass), with the right-most column indicating the cumulative probability summing over the table's rows. Among the cases listed in Table 2, Cases 22 and 21 are the only

ones we can use to examine the phenomenon of interest in RAI APLA-II-3 (i.e., analyzing combinations of pumps failing on different trains) because in the other cases, at most one pump has failed. Case 22 is the second most likely case and has a probability mass larger than that of Case 21 by a factor of 78. Hence, we selected Case 22 for further analysis.

Table 2: Pump State Success Frequencies and Probabilities.

Case	HHSI	LHSI	SPRAY	Probability Mass	Cumulative Probability
1	3	3	3	9.35E-01	9.35E-01
22	2	2	2	3.24E-02	9.67E-01
5	3	2	3	1.24E-02	9.80E-01
2	3	3	2	1.18E-02	9.92E-01
17	2	3	3	6.87E-03	9.98E-01
21	2	2	3	4.14E-04	9.99E-01

3 Case 22 Analysis

As Tables 1 and 2 indicate, Case 22 represents the pump case in which one of each type of pump (HHSI, LHSI, and SPRAY) has failed. We investigate which combination of pump failures on the three trains leads to the largest expected frequencies for sump and vessel failures. Table 3 presents the default Case 22 (labeled Case 22-1 and analyzed in Volume 3), and the four other combinations in which each type of pump has failed. In CASA Grande, when debris reaches the pool, homogenous mixing is then assumed. As a result, there is a symmetry with respect to the trains so that the five cases in Table 3 are exhaustive sub-cases.

Table 3: Five Possible Pump State Combinations within Case 22.

Case 22-1				Case 22-2			
	HHSI	LHSI	SPRAY		HHSI	LHSI	SPRAY
Train 1	0	0	0	Train 1	1	0	0
Train 2	1	1	1	Train 2	0	1	1
Train 3	1	1	1	Train 3	1	1	1

Case 22-3				Case 22-4			
	HHSI	LHSI	SPRAY		HHSI	LHSI	SPRAY
Train 1	0	1	0	Train 1	0	0	1
Train 2	1	0	1	Train 2	1	1	0
Train 3	1	1	1	Train 3	1	1	1

Case 22-5			
	HHSI	LHSI	SPRAY
Train 1	0	1	1
Train 2	1	0	1
Train 3	1	1	0

Tables 4, 5, and 6 report results from CASA Grande for each of these five cases. We present the results separately for sump failure frequency, vessel failure frequency, and total core damage frequency (the sum of the previous two frequencies). The left-most column in Table 4 shows the five sub-cases, and the columns

in the upper half of the table labeled “Freps” and “Mreps” specify the sampling strategy within CASA Grande. “Mean Sump” gives the estimated frequency (events/year) of core damage due to sump failure. The next three columns report a 95% confidence interval halfwidth (CI HW), lower limit (CI LL), upper limit (CI UL), and the final column reports the confidence interval halfwidth as a percentage of the point estimate of the sump failure frequency. The “Ratio” column in the lower half of Table 4 reports the ratio of the estimate of sump failure frequency relative to Case 22-1. The “Mean Diff” column reports this same information as a difference. A ratio that is less than one, and a difference that is negative, indicate that the frequency under Case 22-1 is larger. The final five columns of the lower half of Table 4 provide information to indicate whether the difference is “statistically significant,” i.e., whether we can distinguish the mean failure frequency for each row’s case and the frequency for Case 22-1, given the Monte Carlo sampling error associated with the simulation output. We note that common random numbers were used to reduce the variance of the differences. (Note the CI values from the lower half, not the upper half, of the table are used in assessing these differences.) The results shown in Table 5 are analogous but for the vessel failure frequency, and the results in Table 6 are for the total core damage frequency due to both sump and vessel failures. With the exception of Case 22-4 for the vessel failure frequency, the positive and negative differences we report are statistically significant at a 0.05 level.

4 Discussion

Our analysis of Case 22 suggests the condition in which all pumps fail on the same train leads to the largest sump failure frequency. However, for vessel failure frequency, the three cases (Cases 22-2, 22-3, and 22-5) in which the HHSI and LHSI pumps fail on different trains result in larger frequencies than when these pumps fail on the same train. In two of these three cases (Cases 22-2 and 22-3), the resulting total core damage frequency is estimated to be larger than that when all three pumps fail on the same train.

The change in core damage frequency (Δ CDF) reported in Section 4 of Volume 2 [2] is $2.88\text{E-}08$ per year. The Δ CDF obtained by replacing Case 22-1 with Case 22-3 is $2.88\text{E-}08 + 3.24\text{E-}02 \cdot 1.17\text{E-}08 = 2.92\text{E-}8$ per year, where $3.24\text{E-}02$ is the probability mass associated with Case 22 (see Table 2) and $1.17\text{E-}08$ per year is the difference in frequencies between Case 22-3 and 22-1 (Case 22-3 row in lower half of Table 6), yielding an overall Δ CDF ratio of 1.015, i.e., a 1.5% increase. As Table 3 shows, the next case of interest has a probability mass of $4.14\text{E-}04$ rather than $3.24\text{E-}02$ meaning that a similar conditional change in CDF would lead to a significantly smaller change in Δ CDF.

References

- [1] Letellier, B., T. Sande, and G. Zigler (2013, November). South Texas Project Risk-Informed GSI-191 Evaluation, Volume 3, CASA Grande Analysis. Technical report, STP-RIGSI191-V03, Revision 2.
- [2] Wakefield, D. and D. Johnson (2013, January). South Texas Project Risk-Informed GSI-191 Evaluation, Volume 2, Probabilistic Risk Analysis: Determination of Change in Core Damage Frequency and Large Early Release Frequency Due to GSI-191 Issues. Technical report, STP-RIGSI191-VO2, Revision 0, ABSG Consulting Inc.

Table 4: Statistical Comparison of Sump Failure Frequency.

Case	Freps	Mreps	Mean Sump	95% CI HW	95% CI LL	95% CI UL	CI HW % of Mean
22-1	15	301	2.363E-08	2.709E-09	2.092E-08	2.634E-08	11.46%
22-2	15	301	2.231E-08	2.595E-09	1.971E-08	2.490E-08	11.63%
22-3	15	301	2.230E-08	2.595E-09	1.970E-08	2.489E-08	11.64%
22-4	15	301	2.256E-08	2.596E-09	1.996E-08	2.515E-08	11.51%
22-5	15	301	8.968E-09	1.591E-09	7.377E-09	1.056E-08	17.74%

Case	Ratio	Mean Diff	95% CI HW	95% CI LL	95% CI UL	p-value	Significant Difference?
22-1	1.00	0.00E+00	0.00E+00	0.00E+00	0.00E+00	-	-
22-2	0.94	-1.33E-09	7.96E-10	-2.12E-09	-5.32E-10	1.15E-03	Yes
22-3	0.94	-1.33E-09	7.96E-10	-2.13E-09	-5.38E-10	1.09E-03	Yes
22-4	0.95	-1.08E-09	7.87E-10	-1.86E-09	-2.91E-10	7.39E-03	Yes
22-5	0.38	-1.47E-08	2.35E-09	-1.70E-08	-1.23E-08	2.27E-28	Yes

Table 5: Statistical Comparison of Vessel Failure Frequency.

Case	Freps	Mreps	Mean Vessel	95% CI HW	95% CI LL	95% CI UL	CI HW % of Mean
22-1	15	301	1.789E-09	5.731E-10	1.216E-09	2.362E-09	32.04%
22-2	15	301	1.245E-08	3.257E-09	9.193E-09	1.571E-08	26.16%
22-3	15	301	1.482E-08	3.499E-09	1.132E-08	1.832E-08	23.62%
22-4	15	301	1.645E-09	5.243E-10	1.121E-09	2.169E-09	31.87%
22-5	15	301	1.192E-08	3.225E-09	8.698E-09	1.515E-08	27.05%

Case	Ratio	Mean Diff	95% CI HW	95% CI LL	95% CI UL	p-value	Significant Difference?
22-1	1.00	0.00E+00	0.00E+00	0.00E+00	0.00E+00	-	-
22-2	6.96	1.07E-08	3.25E-09	7.41E-09	1.39E-08	4.18E-10	Yes
22-3	8.28	1.30E-08	3.48E-09	9.55E-09	1.65E-08	1.59E-12	Yes
22-4	0.92	-1.44E-10	2.08E-10	-3.52E-10	6.46E-11	1.76E-01	No
22-5	6.67	1.01E-08	3.21E-09	6.92E-09	1.33E-08	1.79E-09	Yes

Table 6: Statistical Comparison of Total Core Damage Frequency.

Case	Freps	Mreps	Mean Total	95% CI HW	95% CI LL	95% CI UL	CI HW % of Mean
22-1	15	301	2.542E-08	2.808E-09	2.261E-08	2.823E-08	11.05%
22-2	15	301	3.476E-08	4.738E-09	3.002E-08	3.949E-08	13.63%
22-3	15	301	3.712E-08	4.879E-09	3.224E-08	4.200E-08	13.14%
22-4	15	301	2.420E-08	2.683E-09	2.152E-08	2.688E-08	11.09%
22-5	15	301	2.089E-08	3.955E-09	1.694E-08	2.485E-08	18.93%

Case	Ratio	Mean Diff	95% CI HW	95% CI LL	95% CI UL	p-value	Significant Difference?
22-1	1.00	0.00E+00	0.00E+00	0.00E+00	0.00E+00	-	-
22-2	1.37	9.33E-09	3.36E-09	5.98E-09	1.27E-08	9.51E-08	Yes
22-3	1.46	1.17E-08	3.58E-09	8.12E-09	1.53E-08	4.97E-10	Yes
22-4	0.95	-1.22E-09	8.11E-10	-2.03E-09	-4.11E-10	3.28E-03	Yes
22-5	0.82	-4.53E-09	3.74E-09	-8.27E-09	-7.88E-10	1.78E-02	Yes

ATTACHMENT A TO CR 07-1684

Resolution of PRA HRA Update Report

Peer Review Fact/Observation (F&O) Comments

FACT/OBSERVATION REGARDING PRA TECHNICAL ELEMENTS	
OBSERVATION ID: HR - 08	/ Element HR / Sub-element 26
(Related Sub-elements:)	
<p>The HRA update consideration of dependence analysis is documented in appendix D. The methodology described does not identify groups of actions that involve both dynamic actions modeled as part of the system initiator and subsequent dynamic actions in response to the initiator on the failure of actions considered in the system initiator. STP notes that reactor trip is a clear demarcation event that tends to decouple the operator actions before and after the trip and that hence the subsequent actions were assumed independent.</p> <p>The restriction of the sequences considered in the dependence analysis to only those involving two or more post-trip actions means that sequences involving actions evaluated in the system initiator and only one post-trip action were not considered for dependence. While it's true that some initiators are derived from data and information as to the cause of the trip (i.e. whether a human action failure contributed to the trip) is lost. For system initiators modeled using fault trees (e.g. LEB1L2), this information is available and the portion of the trip frequency that can be attributed to failure of time-sensitive actions can be determined.</p> <p>STP should consider further for dependence time-sensitive actions at the time of reactor trip and those after trip in the same sequence, especially those that address the same functional goal (e.g. response to loss of EAB). This may be handled using the "common cognitive" event in Figure D-1 of appendix D. If the action contributing to the system initiator contributes but a small part of the overall system initiator frequency, this would be a basis for assuming minimal dependence with subsequent actions in the sequence. Note that item 4 of Table 10-1 in NUREG/CR-1278 identifies the potential for dependence between actions due to functional relationships between events.</p>	
LEVEL OF SIGNIFICANCE: B	
The system initiator actions largely address loss of CCW, ECW, and either CR HVAC or EAB HVAC systems. Post-initiator actions that may be dependent on these are HEOS01 and HERCP1.	
POSSIBLE RESOLUTION	

FACT/OBSERVATION REGARDING PRA TECHNICAL ELEMENTS

OBSERVATION ID: HR - 08 / Element HR / Sub-element 26

(Related Sub-elements:)

Document that in the current analysis that independence is assumed between time-sensitive actions resulting in trip and those taking place after reactor trip.

Verify that no dynamic action pairs in the same sequence (counting those appearing in the system initiator model) are directed at the same functional goals. For example, we know that in dependency importance group 9 the initiator is LOECW3 which uses action HEECW1 and then involves failure of action HEOS01 to open doors for HVAC smoke purge mode. Some discussion of procedural guidance is needed to justify that these actions directed at the same functional goal are still independent. It seems difficult to rely solely on 2 hours time to justify ZD when simply aligning the off ECW train (HEECW1) would have been the easier action to avoid overheating. Clearly considering the actions imbedded in system initiators makes the dependence analysis more difficult. If action HEECW1 contributes only a small fraction of the total system initiator frequency this also could be a good basis for assuming no or small dependence between it and post-trip actions even though they are directed at the same functional goal.

PLANT RESPONSE OR RESOLUTION

In the HRA update performed for STP_REV5 PRA model, it is assumed that time-sensitive actions resulting in a reactor trip and those taking place subsequent to the reactor trip have no co-dependence (are independent).

The logic for this assumption is that initiator recoveries are performed prior to reactor trip (basically to prevent reactor trip). Once reactor trip occurs, the operators are guided into the EOPs and follow them until the plant is stabilized. Reactor trip is a clear demarcation event that decouples the operator actions before the event with those following the event, so operator actions following reactor trip were assumed to be independent of operator actions before reactor trip. This will be documented in the STP_REV6 HRA notebook as one of the ground rules for future HRA dependency analyses, tracked by CR Action 05-6218-21. Note also that the referenced system initiator HEPs contribute a small amount to the system initiating event frequency.

LEVELS OF SIGNIFICANCE FOR FACTS AND OBSERVATIONS

A.	Extremely important and necessary to address to ensure the technical adequacy of the PRA, the quality of the PRA, or the quality of the PRA update process. (Contingent Item for Grade Assignment.)
B.	Important & necessary to address, but may be deferred until next PRA update (Contingent Item for Grade Assignment.)
C.	Considered desirable to maintain maximum flexibility in PRA Applications and consistency in the Industry, but not likely to significantly affect results or conclusions.
D.	Editorial or Minor Technical Item, left to the discretion of the host utility.
S.	Superior treatment, exceeding requirements for anticipated applications & exceeding what would be found in most PRAs.

FACT/OBSERVATION REGARDING PRA TECHNICAL ELEMENTS

OBSERVATION ID: HR - 09 / Element HR / Sub-element 28

(Related Sub-elements:)

Table 7-1 (Post Initiator HEP Summary) of the report does not identify some dynamic actions (probably a portion of those which were not changed in this update) though they are used in the sequence model; i.e. ZHEDO8 and HEVSEQ. (It's understood that HEVSEQ is the new name and value for an action previously named ZHEDO5. Table 7-1 should be changed to the new name)

Some actions listed are not post-initiator actions but are actually actions used in the quantification of the system initiators; e.g. HEADJ1, HECCW1, HECRS1, HEEAB1, HECCW1. Other actions listed in Table 7-1 are quantified but not currently used in the study; e.g. HEOB02-CASEA, HEOB03, HEOB04, etc...

Table 7-1 also does not identify which actions are dependent on others or under what conditions. For some sequence groups in Table D-1, the explanation for the DL assigned is unclear; e.g. #68, the comment appears to be for the wrong sequence condition, and #96, the comment assigns LD for 2.5 hours whereas for the analysis of sequence group #9 it assumed ZD for 2 hours.

It is therefore questioned whether the results of the HRA dependence analysis could have been correctly interpreted for inclusion in the revised sequence models.

LEVEL OF SIGNIFICANCE: B

This may be significant depending on how diligent the sequence modeling team was in incorporating the new dynamic action dependence results or if the dependencies were previously identified in developing the sequence models.

POSSIBLE RESOLUTION

FACT/OBSERVATION REGARDING PRA TECHNICAL ELEMENTS

OBSERVATION ID: HR - 09 / Element HR / Sub-element 28

(Related Sub-elements:)

- Table 7-1 should be re-titled to note that it includes all dynamic actions, both concurrent with trip and those for post-trip. (editorial, no action required)
- Suggest adding a column to say whether the action is used in the sequence models and whether the actions are used for system initiators. (editorial, no action required)
- A new table summarizing the results of the inter-action dependence analysis should be prepared. Table 7-3 appears to only document intra-system dependencies. The findings in Table D-1 require too much interpretation for this purpose. The sequence modelers need to know clearly which actions are not viable (complete dependence; e.g. HEOR07 on selected fires; HERA7 on HEOT1 implying for ATWS) and under what conditions. Suggest creating a new summary table organized by action name to note the conditions when complete dependence should be assumed and when less than complete but not zero dependence should be assumed. Different values should be reported for the different conditions as appropriate. (Agree to summarize what we changed in the event trees to address dependency).
- The dependence analysis (sequences 18 and 19) seems to have uncovered a timing issue between actions HERC6 and HERCP1 which would point to a better way to model the top events involving these actions. (Agree – need to evaluate)
- The values in Table 7-1 are not adjusted for the dependence levels assigned in appendix D; e.g. for LD actions HEOB02 (on HEOR07), HEOB09 (on HEOR07), and HEOXB (on HERA5). (not a valid comment, Table 7-1 was not intended to include the CHEP values)
- The second sentence in section 4.2.3.1 seems in error. The annunciator model is not used for actions after the initiator. (clarify what we did)
- Explain why the values in Table 4-3 do not match those documented for action HEEAB1 where the annunciator model is used. Are median rather than mean values being used in the calculation? (EPRI HRA Calculator uses mean values, calculated from median values presented in Table 4-3).

PLANT RESPONSE OR RESOLUTION

Please see revised Table 7-1 below. Rev 6 Notebook was revised to incorporate all portions of the supporting documentation including T/H analysis.

LEVELS OF SIGNIFICANCE FOR FACTS AND OBSERVATIONS

A.	Extremely important and necessary to address to ensure the technical adequacy of the PRA, the quality of the PRA, or the quality of the PRA update process. (Contingent Item for Grade Assignment.)
B.	Important & necessary to address, but may be deferred until next PRA update (Contingent Item for Grade Assignment.)

FACT/OBSERVATION REGARDING PRA TECHNICAL ELEMENTS

OBSERVATION ID: HR - 09 / Element HR / Sub-element 28

(Related Sub-elements:)

C.	Considered desirable to maintain maximum flexibility in PRA Applications and consistency in the Industry, but not likely to significantly affect results or conclusions.
D.	Editorial or Minor Technical Item, left to the discretion of the host utility.
S.	Superior treatment, exceeding requirements for anticipated applications & exceeding what would be found in most PRAs.

Table 7-1: Dynamic Action HEP Summary (for Initiating Event Model and Post Initiator HEPs)

Event ID	Event Application (IE or PI*)	Basic Event Description	P _{cog}	P _{exe}	Total HEP	EF	Old HEP	Method or Comment
HEADJ1	IE	Operator Action to Align Spare Battery Charger - STP Rev. 4	2.70E-04	2.63E-05	2.96E-04	10	2.62E-05	Annunciator Response
HECCW1	IE	Align the Off CCW Train - STP Rev. 4			2.09E-03	5	2.09E-03	FLIM
HECH01	PI	Start Alternate CCP or PDP (GT IE)			1.48E-03	5	1.48E-03	FLIM
HECH03	PI	Seismic Event - Start TSC Diesel Generator and the PDP			9.41E-02	5	9.41E-02	FLIM
HECH04	PI	Seismic Event - Start the PD Pump			9.34E-03	5	9.34E-03	FLIM
HECRS1	IE	Start CR HVAC Train - STP Rev. 4	2.70E-04	4.32E-06	2.74E-04	10	7.16E-04	Annunciator Response
HECS01	PI	Manually Actuate Containment Spray			3.35E-02	5	3.35E-02	FLIM
HEEAB1	IE	Fail to Place Standby EAB HVAC Train Into Service - STP Rev.4	2.70E-04	3.67E-06	2.74E-04	10	6.98E-04	Annunciator Response
HEECW1	IE	Align the Off ECW Train - STP Rev. 4			1.60E-03	5	1.60E-03	FLIM
HEHLR	PI	Operator Fails To Initiate Hot Leg Recirculation, STP_REV4	1.80E-05	1.80E-05	3.60E-05	10	8.07E-05	CBDTM/THERP
HEOB02	PI	Bleed & Feed - No AFW (GT Tree) - STP Rev. 4	1.12E-03	7.96E-03	9.08E-03	5	6.07E-03	CBDTM/THERP

Table 7-1: Dynamic Action HEP Summary (for Initiating Event Model and Post Initiator HEPs)

Event ID	Event Application (IE or PI*)	Basic Event Description	P _{cog}	P _{exe}	Total HEP	EF	Old HEP	Method or Comment
HEOB02 - CASE A	PI	Bleed & Feed - No AFW (GT Tree) - STP Rev. 4	1.80E-02	2.60E-02	4.40E-02	5		CBDTM/THERP
HEOB03	PI	Bleed & Feed - No AFW, TT Fails (GT) - STP Rev. 4			8.62E-03	5	8.62E-03	FLIM
HEOB04	PI	Bleed & Feed - All SG PORVs Failed (SGTR) - STP Rev. 4				10	5.75E-03	Deleted from model
HEOB06	PI	Bleed & Feed - No AFW (SGTR) - STP Rev. 4	2.40E-04	8.50E-04	3.20E-04	5	6.43E-03	CBDTM/THERP
HEOB07	PI	Bleed & Feed - Turbine Trip Fails, No AFW (SGTR) - STP Rev.4			9.24E-03	5	9.24E-03	FLIM
HEOB09	PI	Bleed & Feed - No AFW (SLOCA) - STP Rev. 4			4.76E-03	5	4.76E-03	FLIM
HEOB10	PI	Seismic Event - Open PORVs for Bleed & Feed - STP Rev. 4			9.27E-03	5	9.27E-03	FLIM
HEOBA	PI	Bleed & Feed - No AFW, No TG Trip (SLOCA) - STP Rev. 4			6.57E-03	5	6.57E-03	FLIM
HEOC01	PI	Initiate Closed Loop RHR Cooling (SGTR) - STP Rev. 4	1.80E-05	7.57E-05	9.37E-05	10	2.01E-03	CBDTM/THERP
HEOD01	PI	Cool Down/Depress. with SG PORV/Pressurizer Spray/PORV - STP	1.00E-06	1.10E-04	1.10E-04	10	1.75E-03	CBDTM/THERP

Table 7-1: Dynamic Action HEP Summary (for Initiating Event Model and Post Initiator HEPs)

Event ID	Event Application (IE or PI*)	Basic Event Description	P _{cog}	P _{exe}	Total HEP	EF	Old HEP	Method or Comment
		Rev.4						
HEOD02	PI	Depressurize by Stopping HHSI Flow After B&F CD (SGTR) - STP Rev. 4	1.00E-03	1.30E-03	2.30E-03	5	2.93E-03	CBDTM/THERP
HEOD03	PI	Cool Down/Depressurize By Opening SG PORVs (SGTR) - STP Rev.4			2.93E-03	5	2.93E-03	FLIM
HEOD04	PI	RCS Cooldown/Depressurize using SG PORVs – SLOCA	9.00E-06	1.35E-05	2.25E-05	10		CBDTM/THERP
HEOD05	PI	Local Operation of SG PORV for RCS Cooldown	9.00E-04	1.21E-02	1.30E-02	5		CBDTM/THERP
HEOF01	PI	Start main FW to feed SG - No AFW	5.90E-05	4.30E-03	4.30E-03	5		CBDTM/THERP
HEOI01	PI	Recover PDS - LOSP			5.09E-02	5	5.09E-02	FLIM
HEOI02	PI	Recover PDS - LOEAB			4.09E-02	5	4.09E-02	FLIM
HEOI03	PI	Recover PDS - LOECW			4.53E-02	5	4.53E-02	FLIM
HEOL01	PI	Depressurize By Blowing Down SG (LT1)	3.00E-03	2.60E-03	5.60E-03	5	6.07E-03	CBDTM/THERP
HEOL02	PI	Depressurize By Blowing Down SG, SLOCA IE, No RCFCs			6.85E-03	5	6.85E-03	FLIM

Table 7-1: Dynamic Action HEP Summary (for Initiating Event Model and Post Initiator HEPs)

Event ID	Event Application (IE or PI*)	Basic Event Description	P _{cog}	P _{exe}	Total HEP	EF	Old HEP	Method or Comment
HEOR01	PI	Start Train with No Automatic Signal	1.76E-03	1.30E-03	3.06E-03	5	5.79E-03	HCR/ORE/THERP
HEOR02	PI	Start Train with No Auto Signal, Reactor Does Not Trip			6.13E-03	5	6.13E-03	FLIM
HEOR05	PI	Oper Starts Equipment After Sequencer Fails	9.00E-06	9.36E-04	9.45E-04	10	1.24E-01	CBDTM/THERP
HEOR07	PI	Manually Initiate ESFAS, No LOOP	9.00E-06	3.95E-04	4.04E-04	10	2.08E-02	CBDTM/THERP
HEOR08	PI	Manually Initiate ESFAS, LOCA IE	8.28E-02	2.15E-04	8.30E-02	5	3.35E-02	HCR/ORE/THERP
HEOR11	PI	Seismic Event - Start Equipment After Load Seq. Fails			1.37E-01	1	1.37E-01	FLIM
HEOS01	PI	Open Doors, 2 of 3 EAB HVAC Fan Trains Fail - STP Rev. 4	2.70E-04	5.95E-03	6.22E-03	5	2.84E-03	Annunciator Response
HEOS03	PI	Open Doors, LOOP, 2 of 3 ECH Trains Fail - STP Rev. 4			3.11E-03	5	3.11E-03	FLIM
HEOSL1	PI	Isolate Release Path from Ruptured SG (SGTR)	9.00E-06	3.03E-03	3.03E-03	5	2.13E-03	CBDTM/THERP
HEOT01	PI	Manually Trip Reactor, No MFW, ATWS	1.40E-02	2.16E-04	1.42E-02	5	1.18E-03	HCR/ORE/THERP
HEOT03	PI	Manually Trip Reactor, No MFW, No Turbine Trip, ATWS			1.16E-03	5	1.16E-03	FLIM

Table 7-1: Dynamic Action HEP Summary (for Initiating Event Model and Post Initiator HEPs)

Event ID	Event Application (IE or PI*)	Basic Event Description	P _{cog}	P _{exo}	Total HEP	EF	Old HEP	Method or Comment
HEOXA	PI	Recovery of 345kV Power - Grid Available			8.07E-03	5	8.07E-03	FLIM
HEOXB	PI	Align Emergency Transformer - No 345kV	2.60E-04	2.90E-03	3.16E-03	5	4.04E-02	CBDTM/THERP
HERA1	PI	Fail to Isolate Stuck Open PORV	9.00E-06	6.76E-06	1.58E-05	10	9.52E-03	CBDTM/THERP
HERA5	PI	Recovery Action 5			7.17E-02	5	7.17E-02	FLIM
HERA6	PI	Start PDP, No CCPs Operating - STP Rev. 4	1.16E-03	2.73E-04	1.43E-03	5	2.41E-03	CBDTM/THERP
HERA7	PI	Start Standby Trains after Loss of SSPS due to Fire - STP Rev. 4	1.60E-04	1.90E-03	2.06E-03	5	1.85E-02	CBDTM/THERP
HERC1	PI	Cooldown and Depressurize RCS to RHR Conditions	1.00E-06	1.35E-05	1.45E-05	10		CBDTM/THERP
HERC6	PI	Start PDP and Manually Trip RCP	1.43E-02	1.56E-02	2.99E-02	5	2.54E-02	HCR/ORE/THERP
HERCP1	PI	Trip RCP after Loss of CCW - STP Rev. 4	9.00E-04	6.16E-05	9.62E-04	10	3.79E-03	CBDTM/THERP
HESL02	PI	Locally Isolate Failed Open SG PORV - SGTR	9.00E-06	8.50E-05	9.40E-05	10		CBDTM/THERP
HESL03	PI	Locally Close Failed Open MSIV - SGTR	9.00E-06	1.96E-04	2.05E-04	10		CBDTM/THERP
ZHED05	PI	OPERATOR FAILS TO CLOSE MOV	7.50E-04	6.42E-04	1.39E-03	5	1.00E-01	CBDTM/THERP

Table 7-1: Dynamic Action HEP Summary (for Initiating Event Model and Post Initiator HEPs)

Event ID	Event Application (IE or PI*)	Basic Event Description	P _{cog}	P _{exe}	Total HEP	EF	Old HEP	Method or Comment
ZHEPR1	PI	Operator Fails to Close Block Valve			5.96E-03	5	5.96E-03	FLIM
*Note: IE – Action applied in the Initiating Event Model; PI – Action applied in the Post-Initiating Event Model.								

FACT/OBSERVATION REGARDING PRA TECHNICAL ELEMENTS	
OBSERVATION ID: HR - 10 / Element HR / Sub-element 28 <i>(Related Sub-elements:)</i>	
In one case, an HFE is modeled in a split fraction which is assigned equation (EQ) type; i.e. HERA6 in numerator of SF RE4A. The SF RAR is a BC type but it is used in SF RE4A as an EQ type. This means the importance of HERA6 will not be correctly reflected in the basic event importance report.	
LEVEL OF SIGNIFICANCE: B	
Will not affect quantification but may yield incorrect BE importance ranking of HERA6.	
POSSIBLE RESOLUTION	
Verify that all HFEs are modeled as basic events in fault trees AND that any split fractions that use these BC type SFs be defined as CSF type rather than EQ type SFs so that RISKMAN can substitute the intermediate SF for purposes of determining basic event importance. For RE4A, the SF type should have been CSF and an intermediate SF assigned. In the future, suggest that post trip actions be separated from the associated hardware so that each dynamic action appears as a separate top event. This will also simplify future dependence analyses.	
PLANT RESPONSE OR RESOLUTION	
There is no impact to Level 1 or Level 2 quantification or risk-informed applications used at STP. CR Action 08-15609-21-2 initiated to consider for STP_REV7 model update. Additional review of the cited split fractions shows that the HEP in question is HERA5, not HERA6.	
LEVELS OF SIGNIFICANCE FOR FACTS AND OBSERVATIONS	
A.	Extremely important and necessary to address to ensure the technical adequacy of the PRA, the quality of the PRA, or the quality of the PRA update process. (Contingent Item for Grade Assignment.)
B.	Important & necessary to address, but may be deferred until next PRA update (Contingent Item for Grade Assignment.)
C.	Considered desirable to maintain maximum flexibility in PRA Applications and consistency in the Industry, but not likely to significantly affect results or conclusions.
D.	Editorial or Minor Technical Item, left to the discretion of the host utility.
S.	Superior treatment, exceeding requirements for anticipated applications & exceeding what would be found in most PRAs.

FACT/OBSERVATION REGARDING PRA TECHNICAL ELEMENTS	
OBSERVATION ID: HR - 11 / Element HR / Sub-element 2 <i>(Related Sub-elements:)</i>	
Section 4.3 of the guidance document for HRA says to use an error factor of 1 for HFEs with values greater than 0.1, essentially saying there is no uncertainty. This is not defensible. Table A-1 of NUREG/CR-1278 provides a range of values for HFEs with probabilities greater than 0.1.	
LEVEL OF SIGNIFICANCE: C	
Not expected to affect the mean quantitative results. If uncertainties are reported, this will affect those results.	
POSSIBLE RESOLUTION	
Revise distribution formulas to better handle uncertainties for high HFE probability events.	
PLANT RESPONSE OR RESOLUTION	
While STPNOC may agree with this F&O comment in principle, it is our policy to follow the industry guidance document on this issue unless and until Section 4.3 of the industry guidance document is formally revised to accommodate NUREG/CR-1278 Table A-1 or other error factor values.	
LEVELS OF SIGNIFICANCE FOR FACTS AND OBSERVATIONS	
A.	Extremely important and necessary to address to ensure the technical adequacy of the PRA, the quality of the PRA, or the quality of the PRA update process. (Contingent Item for Grade Assignment.)
B.	Important & necessary to address, but may be deferred until next PRA update (Contingent Item for Grade Assignment.)
C.	Considered desirable to maintain maximum flexibility in PRA Applications and consistency in the Industry, but not likely to significantly affect results or conclusions.
D.	Editorial or Minor Technical Item, left to the discretion of the host utility.
S.	Superior treatment, exceeding requirements for anticipated applications & exceeding what would be found in most PRAs.

FACT/OBSERVATION REGARDING PRA TECHNICAL ELEMENTS

OBSERVATION ID: HR - 12 / Element HR / Sub-element 14

(Related Sub-elements:)

While it appears that many inputs have been obtained from the plant operating staff, suggesting that they did review the HRA, there is no text describing what was actually done for STP and what the analysis assumed. In short, the methodology write-up must be enhanced to ensure reproducible results.

LEVEL OF SIGNIFICANCE: C

It's believed that a review was performed so there is likely no impact on quantification.

POSSIBLE RESOLUTION

The HRA methodology should be revised to state what was done for STP rather than the apparent generic description given. The methodology section should be enhanced to better allow independent reviewers to understand exactly what was done. This may be accomplished by simply stating what role the operators had and what types of assumptions were made in lieu of judgments about each input. Also, clarify the following:

- Explain why the cognitive recovery matrix always uses a value of 0.1 for PCe
- Explain when HCR is used for an HFE rather than CBDTM.
- Present Table 20-7 from the HRA calculator since the values used do not match the corresponding values in NUREG/CR-1278 even after correcting for the factor 3 reduction for less verbose procedures and conversion from medians to means. Specifically explain when check-offs are assumed used because the values selected from Table 20-7 suggests that check-offs are being used but the specific procedures referenced for individual actions do not appear to require them. If general operator guidance dictates use of check-off procedures for all EOPs and OPs, suggest including these references in the methodology write-up.
- Report the sequence quantification cutoff (1E-12/year?) used as input to the HRA dependence analysis. Some more details about the generation of DI groups for the STP model would be useful. For example, if more than one action appears in a second failed SF are both set to 1.0 simultaneously?
- Document when credit for less verbose procedures is appropriate and short-lists are to be assumed; e.g. for alarm procedures over 90 pages long?

PLANT RESPONSE OR RESOLUTION

STPNOC PRA has reviewed the HRA notebook and determined the items in the proposed resolution are adequately documented either in the notebook or HRA Calculator database notes. No action is required.

FACT/OBSERVATION REGARDING PRA TECHNICAL ELEMENTS

OBSERVATION ID: HR - 12 / Element HR / Sub-element 14

(Related Sub-elements:)

LEVELS OF SIGNIFICANCE FOR FACTS AND OBSERVATIONS

A.	Extremely important and necessary to address to ensure the technical adequacy of the PRA, the quality of the PRA, or the quality of the PRA update process. (Contingent Item for Grade Assignment.)
B.	Important & necessary to address, but may be deferred until next PRA update (Contingent Item for Grade Assignment.)
C.	Considered desirable to maintain maximum flexibility in PRA Applications and consistency in the Industry, but not likely to significantly affect results or conclusions.
D.	Editorial or Minor Technical Item, left to the discretion of the host utility.
S.	Superior treatment, exceeding requirements for anticipated applications & exceeding what would be found in most PRAs.

FACT/OBSERVATION REGARDING PRA TECHNICAL ELEMENTS	
OBSERVATION ID: HR - 13 / Element HR / Sub-element 2	
<p>(Related Sub-elements:) The scenarios defined for evaluation of HERCP1 and HERC6 appear inconsistent with the sequence models for which they are used. HERCP1 is evaluated for a simple reactor trip followed by a loss of CCW to the RCP. Seal injection flow is however assumed available. HERC6 also is for a simple reactor trip followed by a loss of CCW, but this time seal injection is also lost, thereby shortening the time available for action. However, the sequences in which these actions appear involve loss of EAB HVAC or loss of ECW as per the dependence analysis; i.e. DI groups 18 and 19. These initiators impose much greater impacts on the plant response, potentially affecting the CR environment, the workload assumed, and the stress experienced. For HEP HERC6, it is also unclear if the PDP pump can run following the assumed loss of CCW.</p>	
LEVEL OF SIGNIFICANCE: B	
A re-analysis could be important since HERC6 and HERCP1 are risk significant events.	
POSSIBLE RESOLUTION	
<ul style="list-style-type: none"> • Revisit the HEP analysis for the sequence conditions for which these actions are evaluated. • Consider if failure of the second action in the sequence should be evaluated conditionally on the success of the first action. The first action is successful in DI groups 18 and 19 yet no credit for success is taken. 	
PLANT RESPONSE OR RESOLUTION	
The HEP for HERC6 has been completely redone to reconsider the timing in conjunction with information the Westinghouse Technical Bulletin regarding RCP purge volume and time to seal LOCA. The new success time is 6 minutes. This changed HERC6 and completely changes the dependency analysis as a result.	
LEVELS OF SIGNIFICANCE FOR FACTS AND OBSERVATIONS	
A.	Extremely important and necessary to address to ensure the technical adequacy of the PRA, the quality of the PRA, or the quality of the PRA update process. (Contingent Item for Grade Assignment.)
B.	Important & necessary to address, but may be deferred until next PRA update (Contingent Item for Grade Assignment.)
C.	Considered desirable to maintain maximum flexibility in PRA Applications and consistency in the Industry, but not likely to significantly affect results or conclusions.
D.	Editorial or Minor Technical Item, left to the discretion of the host utility.
S.	Superior treatment, exceeding requirements for anticipated applications & exceeding what would be found in most PRAs.

FACT/OBSERVATION REGARDING PRA TECHNICAL ELEMENTS
OBSERVATION ID: HR - 14 / Element HR / Sub-element 2 (Related Sub-elements:)
The annunciator response model is used for evaluation of HEEAB1. Some judgments made in the evaluation are questionable.
LEVEL OF SIGNIFICANCE: B
The action is borderline risk significant. Increasing the HEP would make the action risk significant.
POSSIBLE RESOLUTION
Resolve the following observations: <ul style="list-style-type: none"> • Although at least 2 alarms are mentioned for the scenario described, the diagnosis error assumes the value for 1 of 1 alarm applies instead of the average of the first 2. • The basis for the 1 hour time available for recovery is not adequately referenced. • For recovery from the execution error probability, an independent diagnosis of 1 of 1 annunciator is again assumed instead of 1 from 2 alarms; i.e. a higher failure rate. Within the first hour, many more alarms may be present for this sequence. • Justify not including an execution failure contribution for the recovery on the execution part of the action. • Justify assuming ZD for the recovery on the execution part of the action when it must be completed in less than 1 hour.
PLANT RESPONSE OR RESOLUTION
The HEEAB1 HEP was revised to account for the 2 alarms and in turn for the Low Dependency that is recommended instead of the Zero Dependency (ZD) originally chosen. The other items of concern are consistent with other HEPs in the model. A set of sensitivity studies was done to show that the HEP is not risk significant or borderline risk significant. By increasing the original failure rate by both one and two orders of magnitude, it was shown that the PRA model is mostly insensitive to this HEP. The results of the sensitivity are: Increase by 10x: Δ CDF = 4.00E-09, % increase in CDF = 0.06%; Δ LERF = 3.10E-10, % increase in LERF = 0.06% Increase by 100x: Δ CDF = 4.38E-08, % increase in CDF = 0.69%; Δ LERF = 3.38E-09, % increase in LERF = 0.67% PRA assessment PRA-12-005, Rev. 0, (STI 33426294), was written and approved to document the results of the sensitivity studies done.

FACT/OBSERVATION REGARDING PRA TECHNICAL ELEMENTS

OBSERVATION ID: HR - 14 / Element HR / Sub-element 2
(Related Sub-elements:)

LEVELS OF SIGNIFICANCE FOR FACTS AND OBSERVATIONS

A.	Extremely important and necessary to address to ensure the technical adequacy of the PRA, the quality of the PRA, or the quality of the PRA update process. (Contingent Item for Grade Assignment.)
B.	Important & necessary to address, but may be deferred until next PRA update (Contingent Item for Grade Assignment.)
C.	Considered desirable to maintain maximum flexibility in PRA Applications and consistency in the Industry, but not likely to significantly affect results or conclusions.
D.	Editorial or Minor Technical Item, left to the discretion of the host utility.
S.	Superior treatment, exceeding requirements for anticipated applications & exceeding what would be found in most PRAs.

FACT/OBSERVATION REGARDING PRA TECHNICAL ELEMENTS

OBSERVATION ID: HR-15 / Element HR / Sub-element **10**

(Related Sub-elements:)

Procedure OPGP04-ZA-0604, step 5.3.5, requires that the following;

“Every model update significant operator experience human performance trends SHOULD be reviewed. This review shall check for adverse trends and new information that could affect the way operator actions are currently modeled in the PRA Reference Model(Ref. 6.11.1)”

Also the final report in section 4.1.1.2 again refers to a review of historical plant data as a minimum.

“As a minimum, the plant-specific LERs that occurred during the preceding 10 years should be reviewed. LERs from similar plants could also provide useful insights, as can LERs from the industry in general.”

There was not obvious evidence that this review was accomplished for post-initiator HFEs. There also was no documentation of any issue or lack of any issues being found.

LEVEL OF SIGNIFICANCE: B

The significance of this observation is a procedural adherence issue and could affect the HRA. The intent of the step is to ensure that any human errors that could be plant specific or industry specific are addressed. Since there is no obvious documentation to show that the review was performed, it is assumed that this review was not performed. This could lead to risk significant HFEs not be analyzed or HFEs which were considered not to be risk significant now being risk significant but not being reanalyzed.

POSSIBLE RESOLUTION

Perform the review and document the results of the review for post-initiator HFEs.

PLANT RESPONSE OR RESOLUTION

FACT/OBSERVATION REGARDING PRA TECHNICAL ELEMENTS

OBSERVATION ID: HR-15 / Element HR / Sub-element 10

(Related Sub-elements:)

This step was performed and documented as part of our pre-initiator HEP update. Historical condition reports and LERs were reviewed and documented in Attachment B to the HRA notebook, Tables B-2 and B-3. This documentation is part of the STP_REV5 HRA notebook documentation files. We did not focus this review on post-initiators because our Rev. 5 PRA update plan included an HRA update of the most risk-significant operator actions

For the STP_REV 6 PRA model update, a review of plant CRs and LERs that relate to human performance was conducted and documented in Table HR-15-1 below. The events reviewed and documented in Table HR-15-1 were collected by merging three sets of plant information for the 1998-2007 time period, as follows: (1) a Brio query of the CAP database to return all CAQ-S and SCAQ CRs that were assigned to Plant Operations for ownership; (2) a Brio query of the CAP database to return all CAQ-S and SCAQ CRs that were assigned event codes of the form 2O% and 3B%; and (3) a general review of all LERs with event dates during the period with their associated CAP database CRs that have the Human Performance field encoded as "YES."

Based on this review, no new HEPs or update to existing HEPs are required.

LEVELS OF SIGNIFICANCE FOR FACTS AND OBSERVATIONS

A.	Extremely important and necessary to address to ensure the technical adequacy of the PRA, the quality of the PRA, or the quality of the PRA update process. (Contingent Item for Grade Assignment.)
B.	Important & necessary to address, but may be deferred until next PRA update (Contingent Item for Grade Assignment.)
C.	Considered desirable to maintain maximum flexibility in PRA Applications and consistency in the Industry, but not likely to significantly affect results or conclusions.
D.	Editorial or Minor Technical Item, left to the discretion of the host utility.
S.	Superior treatment, exceeding requirements for anticipated applications & exceeding what would be found in most PRAs.

TABLE HR-15-1. PLANT HUMAN PERFORMANCE CAQ-S AND SCAQ CR AND LER REVIEW (1998-2007)

CR #	CR Level	Cause Code	Associated LER(s)	Applicable HRA Event ID(s)	Remarks
98-777	CAQ-S	2O4	None noted in the CR description.	No direct impact on HRA events currently modeled in the PRA.	Poor management and supervisory control of processes. Inadequate adherence to established procedures/instructions. Possible weak supervision. Could impact EAB (CRE) HVAC reliability/availability.
98-1172	CAQ-S	2B5, A4E, L1C	None noted in the CR description.	No direct impact on HRA events currently modeled in the PRA.	Inadequate adherence to established procedures/instructions. Possible weak supervision. Could impact CVCS reliability/availability. Could impact general system misalignment errors implicitly included in the PRA.
98-1309	CAQ-S	2O4	None noted in the CR description.	No direct impact on HRA events currently modeled in the PRA.	Poor management and supervisory control of processes. Inadequate training. Inadequate procedures/instructions. Possible weak supervision.
98-1409	CAQ-S	R3B	None noted in the CR description.	No direct impact on HRA events currently modeled in the PRA.	Poor management and supervisory control of processes. Inadequate training.
98-2647	CAQ-S	3B8	None noted in the CR description.	No direct impact on HRA events currently modeled in the PRA.	Software problems causing employee/contractor data discrepancies.
98-3265	CAQ-S	2O4	None noted in the CR description.	No direct impact on HRA events currently modeled in the PRA.	Inadequate adherence to established procedures/instructions. Inadequate procedures/instructions. Possible weak supervision. Could impact EAB HVAC reliability/availability.
98-3502	CAQ-S	2U1, A4ZZ, H2D, L1C	None noted in the CR description.	No direct impact on HRA events currently modeled in the PRA.	Poor management and supervisory control of processes. Inadequate training.
98-4606	CAQ-S	2O4	None noted in the CR description.	No direct impact on HRA events currently modeled in the PRA.	Inadequate adherence to established procedures/instructions. Possible weak supervision. Could impact CVCS reliability/availability.
98-4983	CAQ-S	2B1, 2B5, 2U3, A4C7, A4E, L1C, L1D	None noted in the CR description.	No direct impact on HRA events currently modeled in the PRA.	Inadequate adherence to established procedures/instructions. Possible weak supervision. Could impact CW system reliability/availability. Could impact general system misalignment errors implicitly included in the PRA.

TABLE HR-15-1. PLANT HUMAN PERFORMANCE CAQ-S AND SCAQ CR AND LER REVIEW (1998-2007)

CR #	CR Level	Cause Code	Associated LER(s)	Applicable HRA Event ID(s)	Remarks
98-5095	CAQ-S	3B2	None noted in the CR description.	No direct impact on HRA events currently modeled in the PRA.	Inadequate adherence to established procedures/instructions. Possible weak supervision. Could impact PRA fire risk analysis.
98-5472	CAQ-S	2B5, A4A, L1N	None noted in the CR description.	No direct impact on HRA events currently modeled in the PRA.	Inadequate adherence to established procedures/instructions. Possible weak supervision. Could impact ECHS reliability/availability.
98-5780	CAQ-S	4K, 4N, 5276, A4C3	None noted in the CR description.	No direct impact on HRA events currently modeled in the PRA.	Inadequate adherence to established procedures/instructions. Possible weak supervision. Poor management and supervisory control of processes.
98-5800	CAQ-S	2O4	None noted in the CR description.	No direct impact on HRA events currently modeled in the PRA.	Inadequate adherence to established procedures/instructions. Possible weak supervision.
98-5801	CAQ-S	1C, L1N	None noted in the CR description.	No direct impact on HRA events currently modeled in the PRA.	Inadequate adherence to established procedures/instructions. Possible weak supervision. Could impact QDPS reliability/availability.
98-6190	CAQ-S	1D, 2U1, 3D, A11ZZ, H2D, H4I, L1C	None noted in the CR description.	No direct impact on HRA events currently modeled in the PRA.	Inadequate adherence to established procedures/instructions. Inadequate procedures/instructions. Possible weak supervision. Could impact BOP DG reliability/availability.
98-6283	CAQ-S	1D, H1C, L1C	None noted in the CR description.	No direct impact on HRA events currently modeled in the PRA.	Inadequate adherence to established procedures/instructions. Inadequate procedures/instructions. Possible weak supervision. Could impact CW system reliability/availability.
98-6468	CAQ-S	2O5	None noted in the CR description.	No direct impact on HRA events currently modeled in the PRA.	Inadequate adherence to established procedures/instructions. Possible weak supervision. Could impact CV system reliability/availability.
98-7681	CAQ-S	2I2, 4N, L1N	None noted in the CR description.	No direct impact on HRA events currently modeled in the PRA.	Personnel injury.
98-7889	CAQ-S	L3B	None noted in the CR description.	No direct impact on HRA events currently modeled in the PRA.	Software problems causing employee/contractor pay discrepancies.

TABLE HR-15-1. PLANT HUMAN PERFORMANCE CAQ-S AND SCAQ CR AND LER REVIEW (1998-2007)

CR #	CR Level	Cause Code	Associated LER(s)	Applicable HRA Event ID(s)	Remarks
98-7885	SCAQ	2O4	None noted in the CR description.	No direct impact on HRA events currently modeled in the PRA.	Inadequate adherence to established procedures/instructions. Inadequate procedures/instructions. Possible weak supervision. Could impact RHR and CCW system reliability/availability. Could impact general system misalignment errors implicitly included in the PRA.
98-7904	CAQ-S	L3B	None noted in the CR description.	No direct impact on HRA events currently modeled in the PRA.	Software problems causing employee/contractor pay discrepancies.
98-7985	CAQ-S	2B5, L1N	None noted in the CR description.	No direct impact on HRA events currently modeled in the PRA.	Inadequate adherence to established procedures/instructions. Possible weak supervision. Could impact general system misalignment errors implicitly included in the PRA.
98-9069	SCAQ	2O4	None noted in the CR description.	No direct impact on HRA events currently modeled in the PRA.	Inadequate adherence to established procedures/instructions. Inadequate procedures/instructions. Possible weak supervision. Could impact DJ and EE system reliability/availability.
98-9250	CAQ-S	2B5, L1N	None noted in the CR description.	No direct impact on HRA events currently modeled in the PRA.	Inadequate adherence to established procedures/instructions. Possible weak supervision. Could impact general system misalignment errors implicitly included in the PRA. Could impact CV system reliability/availability.
98-9646	CAQ-S	3B10, 3B2	None noted in the CR description.	No direct impact on HRA events currently modeled in the PRA.	Inadequate adherence to established procedures/instructions. Possible weak supervision. Could impact electric power system reliability/availability.
98-9651	CAQ-S	2C2, L1ZZ	None noted in the CR description.	No direct impact on HRA events currently modeled in the PRA.	Inadequate adherence to established procedures/instructions. Possible weak supervision. Could impact general system misalignment errors implicitly included in the PRA.

TABLE HR-15-1. PLANT HUMAN PERFORMANCE CAQ-S AND SCAQ CR AND LER REVIEW (1998-2007)

CR #	CR Level	Cause Code	Associated LER(s)	Applicable HRA Event ID(s)	Remarks
98-10229	CAQ-S	2B5, L1C	None noted in the CR description.	No direct impact on HRA events currently modeled in the PRA.	Improper installation. Could impact SW system reliability/availability.
98-11559	CAQ-S	2O5, 3B5	None noted in the CR description.	No direct impact on HRA events currently modeled in the PRA.	Inadequate adherence to established procedures/instructions. Inadequate procedures/instructions. Possible weak supervision. Could impact PRA internal flooding analysis.
98-12247	CAQ-S	2B1, 5273	None noted in the CR description.	No direct impact on HRA events currently modeled in the PRA.	Inadequate adherence to established procedures/instructions. Inadequate procedures/instructions. Possible weak supervision. Could impact FW system reliability/availability.
98-13928	CAQ-S	2B, 5273, 5276	None noted in the CR description.	No direct impact on HRA events currently modeled in the PRA.	Inadequate procedures/instructions. Possible weak supervision. Could impact FC system reliability/availability. Could impact LPSD PRA.
98-14202	SCAQ	2O4	LER 1-98-007	No direct impact on HRA events currently modeled in the PRA.	Inadequate adherence to established procedures/instructions. Inadequate procedures/instructions. Possible weak supervision. Could impact AFW system reliability/availability.
98-14592	SCAQ	2O4	LER 1-98-009	No direct impact on HRA events currently modeled in the PRA.	Inadequate adherence to established procedures/instructions. Inadequate procedures/instructions. Possible weak supervision. Could impact HC system (RCFC) reliability/availability.
98-15655	CAQ-S	3B5	None noted in the CR description.	No direct impact on HRA events currently modeled in the PRA.	Inadequate adherence to established procedures/instructions. Possible weak supervision. Could impact LPSD PRA.
98-15831	CAQ-S	3B9	None noted in the CR description.	No direct impact on HRA events currently modeled in the PRA.	Inadequate adherence to established procedures/instructions. Inadequate procedures/instructions. Possible weak supervision. Could impact MS system reliability/availability.

TABLE HR-15-1. PLANT HUMAN PERFORMANCE CAQ-S AND SCAQ CR AND LER REVIEW (1998-2007)

CR #	CR Level	Cause Code	Associated LER(s)	Applicable HRA Event ID(s)	Remarks
98-16047	CAQ-S	3B9	None noted in the CR description.	No direct impact on HRA events currently modeled in the PRA.	Inadequate adherence to established procedures/instructions. Inadequate procedures/instructions. Possible weak supervision. Could impact MS system reliability/availability.
98-16269	CAQ-S	3B9	None noted in the CR description.	No direct impact on HRA events currently modeled in the PRA.	Inadequate adherence to established procedures/instructions. Inadequate procedures/instructions. Possible weak supervision. Could impact MS system reliability/availability.
98-16360	CAQ-S	2B1, L1N	None noted in the CR description.	No direct impact on HRA events currently modeled in the PRA.	Inadequate adherence to established procedures/instructions. Inadequate procedures/instructions. Possible weak supervision. Could impact DP system reliability/availability.
98-16436	CAQ-S	3B9	None noted in the CR description.	No direct impact on HRA events currently modeled in the PRA.	Inadequate adherence to established procedures/instructions. Inadequate procedures/instructions. Possible weak supervision. Could impact MS system reliability/availability.
98-18279	CAQ-S	3B5	None noted in the CR description.	No direct impact on HRA events currently modeled in the PRA.	Inadequate adherence to established procedures/instructions. Possible weak supervision. Could impact AM and SI system reliability/availability.
98-20210	CAQ-S	2O1	None noted in the CR description.	No direct impact on HRA events currently modeled in the PRA.	Inadequate adherence to established procedures/instructions. Inadequate procedures/instructions. Possible weak supervision. Could impact CD system reliability/availability.
99-905	CAQ-S	3B2	None noted in the CR description.	No direct impact on HRA events currently modeled in the PRA.	Inadequate adherence to established procedures/instructions. Possible weak supervision. Could impact CP system reliability/availability.
99-935	CAQ-S	2O1	None noted in the CR description.	No direct impact on HRA events currently modeled in the PRA.	Inadequate adherence to established procedures/instructions. Possible weak supervision. Could impact general system misalignment errors implicitly included in the PRA.

TABLE HR-15-1. PLANT HUMAN PERFORMANCE CAQ-S AND SCAQ CR AND LER REVIEW (1998-2007)

CR #	CR Level	Cause Code	Associated LER(s)	Applicable HRA Event ID(s)	Remarks
99-1052	SCAQ	2B5, 5276	LER 2-99-002	No direct impact on HRA events currently modeled in the PRA.	Inadequate procedures/instructions. Possible weak supervision. Possible impact on DP system reliability/availability. Impacts RTRIP initiating event frequency determination.
99-3690	SCAQ	2O1	LER 2-99-003	No direct impact on HRA events currently modeled in the PRA.	Inadequate procedures/instructions. Possible weak supervision. Possible impact on electric power system reliability/availability. Could impact LOSP and LOSPX initiating event frequency determination (precursor).
99-3932	CAQ-S	1B1, 2B1, 2T1, 5165, 5185, 5273	None noted in the CR description.	No direct impact on HRA events currently modeled in the PRA.	Inadequate design documentation. Inadequate procedures/instructions. Possible weak supervision. Possible impact on MS system reliability/availability.
99-4632	SCAQ	2O4	LER 1-99-003	No direct impact on HRA events currently modeled in the PRA.	Inadequate adherence to established procedures/instructions. Possible weak supervision.
99-4899	CAQ-S	2E5, 2S3, 2U2, 5273	None noted in the CR description.	No direct impact on HRA events currently modeled in the PRA.	Inadequate adherence to established procedures/instructions. Inadequate procedures/instructions. Possible weak supervision. Possible impact on LPSD PRA.
99-5300	CAQ-S	2O2	None noted in the CR description.	No direct impact on HRA events currently modeled in the PRA.	Inadequate adherence to established procedures/instructions. Possible weak supervision.
99-6192	CAQ-S	2O5	None noted in the CR description.	No direct impact on HRA events currently modeled in the PRA.	Inadequate adherence to established procedures/instructions. Possible weak supervision.
99-6302	CAQ-S	2O2	None noted in the CR description.	No direct impact on HRA events currently modeled in the PRA.	Inadequate adherence to established procedures/instructions. Possible weak supervision. Possible impact on LPSD PRA.
99-7786	SCAQ	2O, 2O3	None noted in the CR description.	No direct impact on HRA events currently modeled in the PRA.	Inadequate adherence to established procedures/instructions. Possible weak supervision.
99-8375	SCAQ	2R9, 4R2, 5273	None noted in the CR description.	No direct impact on HRA events currently modeled in the PRA.	Inadequate adherence to established procedures/instructions. Inadequate training.

TABLE HR-15-1. PLANT HUMAN PERFORMANCE CAQ-S AND SCAQ CR AND LER REVIEW (1998-2007)

CR #	CR Level	Cause Code	Associated LER(s)	Applicable HRA Event ID(s)	Remarks
99-10645	CAQ-S	2U3, 5276	None noted in the CR description.	No direct impact on HRA events currently modeled in the PRA.	Inadequate adherence to established procedures/instructions. Possible weak supervision. Possible impact on LPSD PRA.
99-12426	SCAQ	2O4, 3B5	LER 2-99-006	No direct impact on HRA events currently modeled in the PRA.	Inadequate procedures/instructions. Possible weak supervision. Possible impact on FW system reliability/availability.
99-13387	CAQ-S	2O1, 2O3	None noted in the CR description.	No direct impact on HRA events currently modeled in the PRA.	Inadequate adherence to established procedures/instructions. Inadequate procedures/instructions. Possible weak supervision. Possible impact on MS system reliability/availability.
99-14116	CAQ-S	1A2, 2B6, 5276	None noted in the CR description.	No direct impact on HRA events currently modeled in the PRA.	Inadequate adherence to established procedures/instructions. Possible weak supervision. Possible impact on ECH system reliability/availability.
99-15787	CAQ-S	2I2, 5276	None noted in the CR description.	No direct impact on HRA events currently modeled in the PRA.	Inadequate adherence to established procedures/instructions. Possible weak supervision.
99-15906	CAQ-S	2O4	None noted in the CR description.	No direct impact on HRA events currently modeled in the PRA.	Inadequate adherence to established procedures/instructions. Possible weak supervision. Possible impact on AFW system reliability/availability.
99-17296	SCAQ	2O3, 2O5, 3B1, 3B3	None noted in the CR description.	No direct impact on HRA events currently modeled in the PRA.	Inadequate adherence to established procedures/instructions. Inadequate procedures/instructions. Possible weak supervision. Poor management and supervisory control of processes. Possible impact on HD system reliability/availability.
99-17481	CAQ-S	2U1, 5273, 5276	None noted in the CR description.	No direct impact on HRA events currently modeled in the PRA.	Inadequate adherence to established procedures/instructions. Inadequate procedures/instructions. Possible weak supervision. Poor management and supervisory control of processes.

TABLE HR-15-1. PLANT HUMAN PERFORMANCE CAQ-S AND SCAQ CR AND LER REVIEW (1998-2007)

CR #	CR Level	Cause Code	Associated LER(s)	Applicable HRA Event ID(s)	Remarks
99-17492	CAQ-S	2C1, 2C2, 5273, 5276	None noted in the CR description.	No direct impact on HRA events currently modeled in the PRA.	Poor management and supervisory control of processes.
99-17762	CAQ-S	2O3, 2O5	None noted in the CR description.	No direct impact on HRA events currently modeled in the PRA.	Inadequate adherence to established procedures/instructions. Inadequate procedures/instructions. Possible weak supervision. Could impact general system misalignment errors implicitly included in the PRA.
00-468	CAQ-S	2O	None noted in the CR description.	No direct impact on HRA events currently modeled in the PRA.	Inadequate adherence to established procedures/instructions. Possible weak supervision. Impacts actual plant risk profile.
00-1891	SCAQ	2B5, 2U1, 5273	None noted in the CR description.	ZHECH1 (Could also impact ZHECV1 and ZHESI2)	Inadequate adherence to established procedures/instructions. Inadequate procedures/instructions. Possible weak supervision. Could also impact CH system reliability/availability.
00-2281	CAQ-S	2O3	None noted in the CR description.	No direct impact on HRA events currently modeled in the PRA.	Inadequate adherence to established procedures/instructions. Inadequate procedures/instructions. Possible weak supervision. Could impact general transient initiating event frequency determination.
00-2406	SCAQ	2O3	None noted in the CR description.	No direct impact on HRA events currently modeled in the PRA.	Inadequate adherence to established procedures/instructions. Inadequate procedures/instructions. Possible weak supervision. Could impact general transient initiating event frequency determination.
00-2645	SCAQ	2O4	LER 1-00-001	No direct impact on HRA events currently modeled in the PRA.	Inadequate adherence to established procedures/instructions. Inadequate procedures/instructions. Possible weak supervision. Could impact SP system reliability/availability.

TABLE HR-15-1. PLANT HUMAN PERFORMANCE CAQ-S AND SCAQ CR AND LER REVIEW (1998-2007)

CR #	CR Level	Cause Code	Associated LER(s)	Applicable HRA Event ID(s)	Remarks
00-3341	SCAQ	2O4	LER 1-00-002	No direct impact on HRA events currently modeled in the PRA.	Inadequate adherence to established procedures/instructions. Inadequate procedures/instructions. Possible weak supervision. Could impact NI system reliability/availability. Could impact LPSD PRA.
00-3952	SCAQ	2O4	LER 1-00-004	No direct impact on HRA events currently modeled in the PRA.	Inadequate adherence to established procedures/instructions. Possible weak supervision. Could impact AE system (Load Center E1B) reliability/availability.
00-6348	SCAQ	2O3	LER 2-00-002	No direct impact on HRA events currently modeled in the PRA.	Inadequate adherence to established procedures/instructions. Inadequate procedures/instructions. Possible weak supervision. Could impact FW system reliability/availability and general transient (reactor trip) initiating event frequency determination (precursor).
00-10049	SCAQ	2O4	LER 1-00-003	No direct impact on HRA events currently modeled in the PRA.	Inadequate adherence to established procedures/instructions. Possible weak supervision. Could impact Class 1E 125 VDC battery reliability/availability.
00-10325	CAQ-S	1D, 2C2, 2U1, 5252	None noted in the CR description.	No direct impact on HRA events currently modeled in the PRA.	Poor management and supervisory control of processes.
00-11079	CAQ-S	2F1, 2U1, 5273	None noted in the CR description.	No direct impact on HRA events currently modeled in the PRA.	Inadequate adherence to established procedures/instructions. Possible weak supervision. Could impact general fire scenario suppression response.
00-11098	SCAQ	2O4	LER 2-00-003	No direct impact on HRA events currently modeled in the PRA.	Inadequate adherence to established procedures/instructions. Inadequate procedures/instructions. Possible weak supervision. Could impact containment isolation function and PS system reliability/availability.

TABLE HR-15-1. PLANT HUMAN PERFORMANCE CAQ-S AND SCAQ CR AND LER REVIEW (1998-2007)

CR #	CR Level	Cause Code	Associated LER(s)	Applicable HRA Event ID(s)	Remarks
00-11749	SCAQ	2O4	LER 1-00-005	No direct impact on HRA events currently modeled in the PRA.	Inadequate adherence to established procedures/instructions. Poor management and supervisory control of processes.
00-11924	CAQ-S	2B5, 2B8, 5273	None noted in the CR description.	No direct impact on HRA events currently modeled in the PRA.	Inadequate adherence to established procedures/instructions. Possible weak supervision. Could impact OC system reliability/availability.
00-16836	CAQ-S	2B1, 5855	None noted in the CR description.	No direct impact on HRA events currently modeled in the PRA.	Inadequate adherence to established procedures/instructions. Possible weak supervision. Could impact LPSD PRA.
00-17214	CAQ-S	2B1, 2B5, 2B8, 4Z, 5888	None noted in the CR description.	No direct impact on HRA events currently modeled in the PRA.	Inadequate adherence to established procedures/instructions. Possible weak supervision. Could impact diesel generator reliability/availability.
00-18510	CAQ-S	2C3, 5888	None noted in the CR description.	No direct impact on HRA events currently modeled in the PRA.	Poor management and supervisory control of processes.
01-2270	SCAQ	2O5	LER 2-01-001	No direct impact on HRA events currently modeled in the PRA.	Inadequate adherence to established procedures/instructions. Possible weak supervision. Impacts general transient initiating event (reactor trip) frequency.
01-5181	CAQ-S	2O2	None noted in the CR description.	No direct impact on HRA events currently modeled in the PRA.	Inadequate adherence to established procedures/instructions. Possible weak supervision. Could impact ECH system reliability/availability.
01-5375	CAQ-S	2O3	None noted in the CR description.	No direct impact on HRA events currently modeled in the PRA.	Inadequate adherence to established procedures/instructions. Possible weak supervision. Could impact SP system reliability/availability.
01-5454	CAQ-S	2B1, 2U1, 5276	None noted in the CR description.	No direct impact on HRA events currently modeled in the PRA.	Inadequate adherence to established procedures/instructions. Inadequate procedures/instructions. Possible weak supervision. Could impact SH system reliability/availability.

TABLE HR-15-1. PLANT HUMAN PERFORMANCE CAQ-S AND SCAQ CR AND LER REVIEW (1998-2007)

CR #	CR Level	Cause Code	Associated LER(s)	Applicable HRA Event ID(s)	Remarks
01-6327	CAQ-S	201	None noted in the CR description.	No direct impact on HRA events currently modeled in the PRA.	Inadequate adherence to established procedures/instructions. Inadequate procedures/instructions. Possible weak supervision. Could impact AFW Pump Train D (TDP) reliability/availability.
01-9310	CAQ-S	1D, 2C2, 5279	None noted in the CR description.	No direct impact on HRA events currently modeled in the PRA.	Inadequate procedures/instructions. Possible weak supervision. Could indirectly impact general transient initiating event (reactor trip) frequency.
01-12573	CAQ-S	20	None noted in the CR description.	No direct impact on HRA events currently modeled in the PRA.	Inadequate adherence to established procedures/instructions. Possible weak supervision. Could impact AFW Pump Train D (TDP) reliability/availability.
01-13799	CAQ-S	204, 205	None noted in the CR description.	No direct impact on HRA events currently modeled in the PRA.	Inadequate adherence to established procedures/instructions. Possible weak supervision. Could impact LPSD PRA.
01-14883	SCAQ	20	LER 1-01-001	No direct impact on HRA events currently modeled in the PRA.	Inadequate adherence to established procedures/instructions. Inadequate procedures/instructions. Possible weak supervision. Could impact ECW pump reliability/availability.
01-15822	CAQ-S	202	None noted in the CR description.	No direct impact on HRA events currently modeled in the PRA.	Inadequate adherence to established procedures/instructions. Inadequate procedures/instructions. Possible weak supervision. Could impact LPSD PRA. Could impact CCW system reliability/availability.
01-15888	CAQ-S	205	None noted in the CR description.	No direct impact on HRA events currently modeled in the PRA.	Inadequate adherence to established procedures/instructions. Inadequate procedures/instructions. Possible weak supervision. Could impact LPSD PRA.

TABLE HR-15-1. PLANT HUMAN PERFORMANCE CAQ-S AND SCAQ CR AND LER REVIEW (1998-2007)

CR #	CR Level	Cause Code	Associated LER(s)	Applicable HRA Event ID(s)	Remarks
01-16010	CAQ-S	2O1	None noted in the CR description.	No direct impact on HRA events currently modeled in the PRA.	Inadequate adherence to established procedures/instructions. Possible weak supervision. Could impact CVCS charging pump reliability/availability.
01-17865	CAQ-S	3B2	None noted in the CR description.	No direct impact on HRA events currently modeled in the PRA.	Inadequate adherence to established procedures/instructions. Possible weak supervision. Could impact HD system reliability/availability.
01-19256	CAQ-S	2B5, 2U, 2U1, 4I, 4Z10A	None noted in the CR description.	No direct impact on HRA events currently modeled in the PRA.	Inadequate adherence to established procedures/instructions. Possible weak supervision. Could impact diesel generator reliability/availability.
01-19735	CAQ-S	2B5, 5276	None noted in the CR description.	No direct impact on HRA events currently modeled in the PRA.	Inadequate adherence to established procedures/instructions. Possible weak supervision. Significant contamination issue.
01-20016	CAQ-S	2O5	None noted in the CR description.	No direct impact on HRA events currently modeled in the PRA.	Inadequate adherence to established procedures/instructions. Inadequate training. Inadequate follow-up on vehicle maintenance issue. Possible weak supervision.
02-1660	SCAQ	2K2, 5888	LER 2-02-001	No direct impact on HRA events currently modeled in the PRA.	Inadequate training. Could impact GWPS reliability/availability.
02-1839	CAQ-S	3B2	None noted in the CR description.	No direct impact on HRA events currently modeled in the PRA.	Inadequate adherence to established procedures/instructions. Possible weak supervision. Could impact EAB HVAC system reliability/availability.
02-2295	CAQ-S	2O4	None noted in the CR description.	No direct impact on HRA events currently modeled in the PRA.	Inadequate adherence to established procedures/instructions. Possible weak supervision. Could impact nuclear instrumentation reliability/availability.

TABLE HR-15-1. PLANT HUMAN PERFORMANCE CAQ-S AND SCAQ CR AND LER REVIEW (1998-2007)

CR #	CR Level	Cause Code	Associated LER(s)	Applicable HRA Event ID(s)	Remarks
02-2756	CAQ-S	2O4	None noted in the CR description.	No direct impact on HRA events currently modeled in the PRA.	Inadequate adherence to established procedures/instructions. Inadequate procedures/instructions. Possible weak supervision. Could impact nuclear instrumentation reliability/availability.
02-3183	SCAQ	2O4	LER 1-02-001	No direct impact on HRA events currently modeled in the PRA.	Inadequate adherence to established procedures/instructions. Possible weak supervision. Poor communication. Could impact EAB (CRE) HVAC reliability/availability.
02-5265	CAQ-S	3B, 3B3, 3B7	None noted in the CR description.	No direct impact on HRA events currently modeled in the PRA.	Inadequate adherence to established procedures/instructions. Inadequate procedures/instructions. Possible weak supervision. Could impact EDG reliability/availability.
02-6385	CAQ-S	3B8	None noted in the CR description.	No direct impact on HRA events currently modeled in the PRA.	Inadequate adherence to established procedures/instructions. Inadequate procedures/instructions. Possible weak supervision. Could impact SP system reliability/availability.
02-8373	CAQ-S	1D, 2U1, 2U3	None noted in the CR description.	No direct impact on HRA events currently modeled in the PRA.	Inadequate adherence to established procedures/instructions. Inadequate procedures/instructions. Possible weak supervision. Could impact AFW system reliability/availability.
02-8873	CAQ-S	2O5	None noted in the CR description.	No direct impact on HRA events currently modeled in the PRA.	Inadequate adherence to established procedures/instructions. Inadequate procedures/instructions. Possible weak supervision. Could impact LPSD PRA (possible schedule duration changes).
02-9857	CAQ-S	2B5	None noted in the CR description.	No direct impact on HRA events currently modeled in the PRA.	Inadequate adherence to established procedures/instructions. Inadequate procedures/instructions. Possible weak supervision. Could impact main generator reliability/availability.

TABLE HR-15-1. PLANT HUMAN PERFORMANCE CAQ-S AND SCAQ CR AND LER REVIEW (1998-2007)

CR #	CR Level	Cause Code	Associated LER(s)	Applicable HRA Event ID(s)	Remarks
02-10502	CAQ-S	3B1	None noted in the CR description.	No direct impact on HRA events currently modeled in the PRA.	Inadequate supervision and attention to detail.
02-11323	CAQ-S	2I1E, 2I1G, 2I2B, 2I4E	None noted in the CR description.	No direct impact on HRA events currently modeled in the PRA.	Inadequate supervision and attention to detail.
02-14656	CAQ-S	3B1, 3B3	None noted in the CR description.	No direct impact on HRA events currently modeled in the PRA.	Inadequate supervision and attention to detail. Could impact a Level 3 PRA.
02-14688	CAQ-S	2O2, 3B5	None noted in the CR description.	No direct impact on HRA events currently modeled in the PRA.	Inadequate adherence to established procedures/instructions. Inadequate procedures/instructions. Possible weak supervision. Could impact LPSD PRA.
02-15369	CAQ-S	3B4	None noted in the CR description.	No direct impact on HRA events currently modeled in the PRA.	Inadequate adherence to established procedures/instructions. Possible weak supervision. Could impact LPSD PRA (possible schedule duration changes).
02-17026	SCAQ	3B10	LER 1-02-003	No direct impact on HRA events currently modeled in the PRA.	Inadequate supervision and attention to detail. Impacts plant initiating event frequency analysis in the PRA (equipment failure resulted in reactor trip).
02-17405	CAQ-S	2B5	None noted in the CR description.	No direct impact on HRA events currently modeled in the PRA.	Inadequate adherence to established procedures/instructions. Inadequate procedures/instructions. Possible weak supervision.
02-18147	CAQ-S	2O4	None noted in the CR description.	No direct impact on HRA events currently modeled in the PRA.	Inadequate adherence to established procedures/instructions. Possible weak supervision. Could impact containment isolation and supplemental purge reliability/availability.
02-19519	CAQ-S	3B2	None noted in the CR description.	No direct impact on HRA events currently modeled in the PRA.	Inadequate adherence to established procedures/instructions. Impacts HHSI Pump Train B reliability/availability.
03-330	CAQ-S	3B10	None noted in the CR description.	No direct impact on HRA events currently modeled in the PRA.	Inadequate supervision and oversight.

TABLE HR-15-1. PLANT HUMAN PERFORMANCE CAQ-S AND SCAQ CR AND LER REVIEW (1998-2007)

CR #	CR Level	Cause Code	Associated LER(s)	Applicable HRA Event ID(s)	Remarks
03-1341	SCAQ	3B2	LER 2-03-001	No direct impact on HRA events currently modeled in the PRA.	Improper installation. Impacts RHR system reliability/availability.
03-2751	CAQ-S	2O2, 3B6	None noted in the CR description.	No direct impact on HRA events currently modeled in the PRA.	Inadequate design and operator training. Could impact LPSD PRA.
03-3929	CAQ-S	1D, 2K4, 2S3, 3D4, 4Z2A, 4Z3A	None noted in the CR description.	No direct impact on HRA events currently modeled in the PRA.	Inadequate adherence to established procedures/instructions. Inadequate procedures/instructions. Possible weak supervision. Impacts PZR PORV reliability/availability.
03-4704	SCAQ	2O2, 2O5	None noted in the CR description.	No direct impact on HRA events currently modeled in the PRA.	Inadequate adherence to established procedures/instructions. Inadequate procedures/instructions. Possible weak supervision. Impacts PZR PORV reliability/availability.
03-4794	SCAQ	2C4, 4Z2A, 4Z3A	None noted in the CR description.	No direct impact on HRA events currently modeled in the PRA.	Inadequate supervision and attention to detail. Impacts PZR PORV reliability/availability.
03-6128	CAQ-S	1D	None noted in the CR description.	No direct impact on HRA events currently modeled in the PRA.	Inadequate adherence to established procedures/instructions. Inadequate procedures/instructions. Possible weak supervision.
03-14590	CAQ-S	3B3	None noted in the CR description.	No direct impact on HRA events currently modeled in the PRA.	Inadequate adherence to established procedures/instructions. Possible weak supervision.
04-1257	CAQ-S	2A7	None noted in the CR description.	No direct impact on HRA events currently modeled in the PRA.	Inadequate adherence to established procedures/instructions. Possible weak supervision.
04-3110	CAQ-S	2B1	None noted in the CR description.	No direct impact on HRA events currently modeled in the PRA.	Negligence. Could impact LPSD PRA.
04-3148	SCAQ	2O4	LER 1-04-002	No direct impact on HRA events currently modeled in the PRA.	Inadequate supervision and attention to detail. Impacts CR HVAC reliability/availability.
04-4033	SCAQ	2B5, 2K4, 3C1W, 4Z3A	LER 1-04-003	No direct impact on HRA events currently modeled in the PRA.	Inadequate attention to detail. Could impact N2SIFV3964 reliability/availability.
04-4181	CAQ-S	2B10, 2U1	None noted in the CR description.	No direct impact on HRA events currently modeled in the PRA.	Inadequate adherence to established procedures/instructions. Possible weak supervision.

TABLE HR-15-1. PLANT HUMAN PERFORMANCE CAQ-S AND SCAQ CR AND LER REVIEW (1998-2007)

CR #	CR Level	Cause Code	Associated LER(s)	Applicable HRA Event ID(s)	Remarks
04-4239	CAQ-S	2O3	None noted in the CR description.	No direct impact on HRA events currently modeled in the PRA.	Inadequate design. Could impact steam dump valve reliability/availability.
04-4581	CAQ-S	2B1, 2U1	None noted in the CR description.	No direct impact on HRA events currently modeled in the PRA.	Inadequate adherence to established procedures/instructions. Possible weak supervision. Could impact RCB chill water pump reliability/availability.
04-4674	CAQ-S	2O2	None noted in the CR description.	No direct impact on HRA events currently modeled in the PRA.	This is a communications and quality issue with a possible impact on the LPSD PRA.
04-5264	CAQ-S	2B1, 2U1	None noted in the CR description.	No direct impact on HRA events currently modeled in the PRA.	Inadequate adherence to established procedures/instructions. Inadequate procedures/instructions. Possible weak supervision.
04-5895	CAQ-S	2O2	None noted in the CR description.	No direct impact on HRA events currently modeled in the PRA.	Inadequate adherence to established procedures/instructions. Inadequate procedures/instructions. Possible weak supervision.
04-6235	CAQ-S	3B5	None noted in the CR description.	No direct impact on HRA events currently modeled in the PRA.	Inadequate attention to detail. Could impact N2SIFV3964 reliability/availability.
04-6278	CAQ-S	3B3	None noted in the CR description.	No direct impact on HRA events currently modeled in the PRA.	Inadequate attention to detail. Could impact FWIV reliability/availability.
04-9088	CAQ-S	3B2	None noted in the CR description.	No direct impact on HRA events currently modeled in the PRA.	Inadequate adherence to established procedures/instructions. Possible weak supervision. Could impact CW system reliability/availability.
04-10012	CAQ-S	3B2	None noted in the CR description.	No direct impact on HRA events currently modeled in the PRA.	Inadequate procedures/instructions. Impacts essential chiller reliability/availability.
04-10584	CAQ-S	2B5, 2K3, 2U1	None noted in the CR description.	No direct impact on HRA events currently modeled in the PRA.	Inadequate attention to detail. Impacts essential chiller reliability/availability.
04-10854	CAQ-S	3B3	None noted in the CR description.	No direct impact on HRA events currently modeled in the PRA.	Managers/supervisors too tolerant of failures due to designed redundancy. Inadequate prior similar event cause determination.
04-11120	CAQ-S	2O5	None noted in the CR description.	No direct impact on HRA events currently modeled in the PRA.	Inadequate adherence to established procedures/instructions. Possible weak supervision.

TABLE HR-15-1. PLANT HUMAN PERFORMANCE CAQ-S AND SCAQ CR AND LER REVIEW (1998-2007)					
CR #	CR Level	Cause Code	Associated LER(s)	Applicable HRA Event ID(s)	Remarks
04-11428	SCAQ	2O4	LER 1-04-005	No direct impact on HRA events currently modeled in the PRA.	Inadequate adherence to established procedures/instructions. Inadequate procedures/instructions. Possible weak supervision. Affects EDG reliability/availability.
04-11518	CAQ-S	2O5, 3B5	None noted in the CR description.	No direct impact on HRA events currently modeled in the PRA.	Poor technician decision-making. Possible weak supervision.
04-11733	CAQ-S	3B2	None noted in the CR description.	No direct impact on HRA events currently modeled in the PRA.	Inadequate adherence to established procedures/instructions. Inadequate procedures/instructions. Possible weak supervision.
04-11874	CAQ-S	3B1, 3B2	None noted in the CR description.	No direct impact on the HRA events currently modeled in the PRA.	Could impact LPSD PRA.
04-13624	CAQ-S	1C, 2U1	None noted in the CR description.	No direct impact on HRA events currently modeled in the PRA.	Inadequate adherence to established procedures/instructions. Possible weak supervision.
04-15153	CAQ-S	2B5	None noted in the CR description.	No direct impact on HRA events currently modeled in the PRA. Possible low impact on pre-initiator misalignment HEPs.	Inadequate adherence to established procedures/instructions.
05-252	CAQ-S	2B1, 4GG1	None noted in the CR description.	No direct impact on HRA events currently modeled in the PRA.	Inadequate adherence to established procedures/instructions. Possible weak supervision.
05-721	CAQ-S	2O4	None noted in the CR description.	No direct impact on HRA events currently modeled in the PRA.	Inadequate adherence to established procedures/instructions. Possible weak supervision.
05-1197	CAQ-S	1D, 2C1, 2C2, 2K3, 2L2, 4GG2	None noted in the CR description.	No direct impact on HRA events currently modeled in the PRA.	Could impact fire, flood, and HVAC boundary bases and assumptions in the PRA. Inadequate procedures/instructions. Program weakness.
05-2079	CAQ-S	2B1, 4GG2	None noted in the CR description.	No direct impact on HRA events currently modeled in the PRA.	Inadequate adherence to established procedures/instructions. Possible weak supervision.
05-2710	SCAQ	2O4	LER 2-05-002	No direct impact on HRA events currently modeled in the PRA.	Inadequate procedures/instructions. Program weakness. Impacts CH system reliability/availability.

TABLE HR-15-1. PLANT HUMAN PERFORMANCE CAQ-S AND SCAQ CR AND LER REVIEW (1998-2007)

CR #	CR Level	Cause Code	Associated LER(s)	Applicable HRA Event ID(s)	Remarks
05-3071	SCAQ	2O2, 2O4	LER 2-05-003	No direct impact on HRA events currently modeled in the PRA.	Inadequate adherence to established procedures/instructions. Inadequate procedures/instructions. Possible weak supervision.
05-3779	CAQ-S	2K4, 2Q1A, 2Q1E, 2Q4B, 4GG1, 4Z, 4Z10A, 4Z5A	None noted in the CR description.	No direct impact on HRA events currently modeled in the PRA.	Inadequate adherence to established procedures/instructions. Possible weak supervision.
05-4573	CAQ-S	2B1, 2V13D, 4GG1	None noted in the CR description.	No direct impact on HRA events currently modeled in the PRA.	Inadequate adherence to established procedures/instructions. Possible weak supervision.
05-4915	CAQ-S	2O5	None noted in the CR description.	No direct impact on HRA events currently modeled in the PRA.	Inadequate adherence to established procedures/instructions. Inadequate procedures/instructions. Possible weak supervision. Could impact EDG reliability/availability.
05-6891	CAQ-S	2B1, 4GG1	None noted in the CR description.	No direct impact on HRA events currently modeled in the PRA. Possible low impact on pre-initiator misalignment HEPs.	Inadequate adherence to established procedures/instructions.
05-7068	CAQ-S	2O3D, 2O5	None noted in the CR description.	Could impact pre-initiator misalignment HEPs, such as ZHEAF1.	Inadequate adherence to established procedures/instructions. Inadequate procedures/instructions. Possible weak supervision.
05-11401	CAQ-S	2B5, 4EE, 4GG1	None noted in the CR description.	Could impact pre-initiator misalignment HEPs, such as ZHEAF1.	Inadequate adherence to established procedures/instructions. Inadequate procedures/instructions. Possible weak supervision.
05-12063	CAQ-S	2O2, 2O5	None noted in the CR description.	No direct impact on HRA events currently modeled in the PRA.	Inadequate adherence to established procedures/instructions. Possible weak supervision.
05-12736	CAQ-S	2O2, 2O3D	None noted in the CR description.	No direct impact on HRA events currently modeled in the PRA.	Inadequate adherence to established procedures/instructions.
05-12885	CAQ-S	2O3D, 2O5	None noted in the CR description.	No direct impact on HRA events currently modeled in the PRA.	Inadequate adherence to established procedures/instructions.

TABLE HR-15-1. PLANT HUMAN PERFORMANCE CAQ-S AND SCAQ CR AND LER REVIEW (1998-2007)

CR #	CR Level	Cause Code	Associated LER(s)	Applicable HRA Event ID(s)	Remarks
05-13349	CAQ-S	2O3D, 3B2	None noted in the CR description.	No direct impact on HRA events currently modeled in the PRA.	Inadequate adherence to established procedures/instructions. Inadequate procedures/instructions. Possible weak supervision.
05-13406	SCAQ	2O4, 3B2	LER 2-05-006	No direct impact on HRA events currently modeled in the PRA.	Inadequate adherence to established procedures/instructions. Inadequate procedures/instructions. Possible weak supervision.
05-13732	SCAQ	2O4	LER 2-05-005	No direct impact on HRA events currently modeled in the PRA.	Could impact LPSD PRA.
05-14103	CAQ-S	2O4	None noted in the CR description.	No direct impact on HRA events currently modeled in the PRA.	Inadequate adherence to established procedures/instructions. Inadequate procedures/instructions. Possible weak supervision.
05-14288	CAQ-S	2O3D	None noted in the CR description.	No direct impact on HRA events currently modeled in the PRA.	Inadequate adherence to established procedures/instructions. Possible weak supervision.
05-14545	CAQ-S	2O3B	None noted in the CR description.	No direct impact on HRA events currently modeled in the PRA.	Inadequate adherence to established procedures/instructions. Inadequate procedures/instructions. Possible weak supervision.
05-14771	CAQ-S	2O3D	None noted in the CR description.	No direct impact on HRA events currently modeled in the PRA, but could generally related to ZHERP1, ZHESI3, and other pre-initiator HEPs.	Inadequate adherence to established procedures/instructions. Possible weak supervision.
05-14884	CAQ-S	2I2D, 4GG1	None noted in the CR description.	No direct impact on HRA events currently modeled in the PRA.	Lost time injury. Shortcuts used.
05-16139	CAQ-S	2O1, 2O6	None noted in the CR description.	No direct impact on HRA events currently modeled in the PRA.	Inadequate adherence to established programs, processes, and procedures.
06-1073	CAQ-S	2O1, 3B7	None noted in the CR description.	No direct impact on HRA events currently modeled in the PRA.	Inadequate procedures/instructions.
06-1954	SCAQ	2O6	None noted in the CR description.	No direct impact on HRA events currently modeled in the PRA.	Could impact Level 3 PRA.

TABLE HR-15-1. PLANT HUMAN PERFORMANCE CAQ-S AND SCAQ CR AND LER REVIEW (1998-2007)

CR #	CR Level	Cause Code	Associated LER(s)	Applicable HRA Event ID(s)	Remarks
06-3132	CAQ-S	3B2	None noted in the CR description.	No direct impact on HRA events currently modeled in the PRA.	Poor pipe erosion monitoring and feedback program.
06-3408	CAQ-S	2B1A, 2B5	None noted in the CR description.	No direct impact on HRA events currently modeled in the PRA.	Inadequate procedures/instructions (ECO).
06-4091	CAQ-S	3C2	None noted in the CR description.	No direct impact on HRA events currently modeled in the PRA.	Inadequate procedures/instructions.
06-4207	SCAQ	2O4	LER 1-06-001	No direct impact on HRA events currently modeled in the PRA.	Inadequate procedures/instructions. Could impact EDG reliability/availability.
06-4494	CAQ-S	2O3D, 3B5	None noted in the CR description.	No direct impact on HRA events currently modeled in the PRA.	Inadequate evaluation of new/replacement repair parts.
06-6454	CAQ-S	3B4	None noted in the CR description.	No direct impact on HRA events currently modeled in the PRA.	Inadequate procedures/instructions.
06-6632	CAQ-S	2B1C, 4GG3	None noted in the CR description.	No direct impact on HRA events currently modeled in the PRA.	Operators not following procedures (ECO) closely enough. Possible weak supervision.
06-6802	CAQ-S	3B1	None noted in the CR description.	No direct impact on HRA events currently modeled in the PRA.	Operators not following procedures closely enough. Possible weak supervision.
06-7515	CAQ-S	2A3, 4LL	None noted in the CR description.	No direct impact on HRA events currently modeled in the PRA.	Could impact long-term condensate quality/purity.
06-8138	CAQ-S	3B2	None noted in the CR description.	No direct impact on HRA events currently modeled in the PRA.	Could impact fire, flood, and HVAC boundary bases and assumptions in the PRA.
06-8372	CAQ-S	2O6	None noted in the CR description.	No direct impact on HRA events currently modeled in the PRA.	Could impact AOV reliability/availability.
06-9139	CAQ-S	1D, 4II, 4Z10A, 4Z12A, 4Z3A	None noted in the CR description.	No direct impact on HRA events currently modeled in the PRA.	Could impact fire, flood, and HVAC boundary bases and assumptions in the PRA.
06-9513	CAQ-S	2O6	None noted in the CR description.	No direct impact on HRA events currently modeled in the PRA.	Impacts QDPS availability for a seismic event.
06-12274	CAQ-S	1D, 4EE, 4GG3	None noted in the CR description.	No direct impact on HRA events currently modeled in the PRA.	Impacts PZR PORV relief path availability.
06-12721	CAQ-S	2O5	None noted in the CR description.	No direct impact on HRA events currently modeled in the PRA.	Could impact LPSD PRA.

TABLE HR-15-1. PLANT HUMAN PERFORMANCE CAQ-S AND SCAQ CR AND LER REVIEW (1998-2007)

CR #	CR Level	Cause Code	Associated LER(s)	Applicable HRA Event ID(s)	Remarks
06-13920	CAQ-S	2O2	None noted in the CR description.	No direct impact on HRA events currently modeled in the PRA.	Could impact LPSD PRA.
06-14117	CAQ-S	2B5	None noted in the CR description.	No direct impact on the HRA events currently modeled in the PRA; could relate to all PRA human actions controlled by procedures, particularly those related to pre-initiator valve lineups.	Inadequate work practices. Inadequate procedures/instructions. Inadequate process coordination. Could impact LPSD PRA.
06-14249	CAQ-S	2O5, 3B4	None noted in the CR description.	No direct impact on HRA events currently modeled in the PRA.	Could be an IE (loss of MFW) contributor.
06-14509	CAQ-S	2B1C, 2B5	None noted in the CR description.	No direct impact on the HRA events currently modeled in the PRA; could relate to all PRA human actions controlled by procedures.	Resulted in mispositioned valve. Operators not following procedures closely enough.
06-14734	CAQ-S	2B5	None noted in the CR description.	No direct impact on the HRA events currently modeled in the PRA; could relate to all PRA human actions controlled by procedures.	Operators not following procedures closely enough. Possible weak supervision.
06-15295	CAQ-S	2O3E, 3B5	None noted in the CR description.	No direct impact on HRA events currently modeled in the PRA.	Impacts condensate flow stability.
06-15407	SCAQ	2O4	LER 1-06-005	No direct impact on HRA events currently modeled in the PRA.	Could impact LPSD PRA.
06-16239	CAQ-S	2O2	None noted in the CR description.	No direct impact on HRA events currently modeled in the PRA.	Could impact LPSD PRA.
06-16436	SCAQ	3B2	LER 2-06-001	Could impact ZHESI1.	Could impact HHSI pump reliability and availability.
06-17055	CAQ-S	3B1	None noted in the CR description.	No direct impact on HRA events currently modeled in the PRA.	Impacts steam dump failure to close on demand failure rate.
07-979	CAQ-S	3B10	None noted in the CR description.	No direct impact on HRA events currently modeled in the PRA.	Unclear on whether or not this would really constitute EAB HVAC unavailability.

TABLE HR-15-1. PLANT HUMAN PERFORMANCE CAQ-S AND SCAQ CR AND LER REVIEW (1998-2007)

CR #	CR Level	Cause Code	Associated LER(s)	Applicable HRA Event ID(s)	Remarks
07-1017	CAQ-S	2B1E, 2B5	None noted in the CR description.	No direct impact on the HRA events currently modeled in the PRA; could relate to all PRA human actions controlled by procedures.	Operator failed to acknowledge danger tag when operating equipment.
07-1632	CAQ-S	2B5	None noted in the CR description.	No direct impact on HRA events currently modeled in the PRA.	Could impact ECW availability. Poor operator adherence to intent of procedures.
07-1905	CAQ-S	2O4	None noted in the CR description.	No direct impact on HRA events currently modeled in the PRA.	Could impact fire propagation and HVAC effectiveness issues for some PRA scenarios.
07-2216	CAQ-S	2B1A, 2B5	None noted in the CR description.	No direct impact on the HRA events currently modeled in the PRA; could relate to all PRA human actions controlled by procedures.	Operator did not follow proper ECO procedure.
07-2369	CAQ-S	2O5	None noted in the CR description.	No direct impact on HRA events currently modeled in the PRA.	Inadequate operator self-checking.
07-2529	CAQ-S	3B2	None noted in the CR description.	No or low impact on actions involving manual AFW operation (e.g., HERA7, HEOR07, HEOR08, HEOSL1, etc.).	Could impact manual operation of the TDAFW pump train.
07-3189	CAQ-S	3B5	None noted in the CR description.	No direct impact on the HRA events currently modeled in the PRA.	Could impact LPSD PRA.
07-4371	SCAQ	2O3B, 2O5, 3B2	None noted in the CR description.	No direct impact on HRA events currently modeled in the PRA.	Poor man-machine interface design. Inadequate "skill of the craft" for target task.
07-5020	CAQ-S	3B4	None noted in the CR description.	No direct impact on the HRA events currently modeled in the PRA.	Could impact LPSD PRA.
07-5347	CAQ-S	3B10	None noted in the CR description.	No direct impact on the HRA events currently modeled in the PRA.	Could impact LPSD PRA.
07-5744	CAQ-S	1D, 2B1A, 2B1D, 4GG3	None noted in the CR description.	No direct impact on the HRA events currently modeled in the PRA; could relate to all PRA human actions controlled by procedures.	Inadequate procedures/instructions.

TABLE HR-15-1. PLANT HUMAN PERFORMANCE CAQ-S AND SCAQ CR AND LER REVIEW (1998-2007)

CR #	CR Level	Cause Code	Associated LER(s)	Applicable HRA Event ID(s)	Remarks
07-6515	CAQ-S	3B2	None noted in the CR description.	No direct impact on HRA events currently modeled in the PRA.	Polar crane issue; could impact LPSD PRA.
07-7055	CAQ-S	2B1C	None noted in the CR description.	ZHECH1, ZHECV1, ZHESI2	Inadequate attention to detail by ECO performer and checker. Possible poor labeling of equipment. Inadequate control of contractors.
07-7107	CAQ-S	2O4	None noted in the CR description.	No direct impact on the HRA events currently modeled in the PRA.	Could impact LPSD PRA.
07-7115	CAQ-S	2O2	None noted in the CR description.	No direct impact on the HRA events currently modeled in the PRA; could relate to all PRA human actions controlled by procedures.	Inadequate procedures/instructions.
07-7359	CAQ-S	2O5	None noted in the CR description.	No direct impact on the HRA events currently modeled in the PRA.	Inadequate valve design and inadequate pre-job briefing.
07-8374	SCAQ	3B10, 3B8	LER 1-07-002	No direct impact on the HRA events currently modeled in the PRA.	Could impact 4.16 KV EPS availability, but not HRA.
07-8454	CAQ-S	3B2	None noted in the CR description.	No direct impact on the HRA events currently modeled in the PRA.	This is a personal safety issue, but not a PRA issue.
07-9154	CAQ-S	2F5, 2V12B, 4II, 4Z8A	None noted in the CR description.	No direct impact on the HRA events currently modeled in the PRA.	Impacts DG fire protection. Human error resulted in simultaneously isolating fire protection to three trains of DGs.
07-9630	CAQ-S	3B2	None noted in the CR description.	No direct impact on the HRA events currently modeled in the PRA.	Could impact system piping failure rate, but not human actions modeled in the PRA.
07-12665	CAQ-S	2O5	None noted in the CR description.	No direct impact on the HRA events currently modeled in the PRA; could relate to all PRA human actions controlled by procedures.	Inadequate procedures/instructions.
07-15793	CAQ-S	2D3B	None noted in the CR description.	No direct impact on the HRA events currently modeled in the PRA.	Could impact TSC DG availability. Could add a pre-initiator for this type of event, but it should currently be included in the component demand failure rate.

TABLE HR-15-1. PLANT HUMAN PERFORMANCE CAQ-S AND SCAQ CR AND LER REVIEW (1998-2007)

CR #	CR Level	Cause Code	Associated LER(s)	Applicable HRA Event ID(s)	Remarks
07-16047	CAQ-S	3B2	None noted in the CR description.	No direct impact on the HRA events currently modeled in the PRA.	Weak procedure; inadequate procedure adherence. Could impact valve failure rates in BOP model and associated IE model.

FACT/OBSERVATION REGARDING PRA TECHNICAL ELEMENTS

OBSERVATION ID: HR-16 / Element HR / Sub-element 1
(Related Sub-elements: F)

Report STP HRA 082006 states:

Procedure OPGP04-ZA-0604, step 5.3.5, requires the following;

“The comprehensive data update incorporates changes to plant specific failure rate distributions and human reliability, and any other database distribution updates (examples would include equipment failure rates, recovery actions, and operator actions).”

There is no evidence that an analyst reviewed the changes to the PRA model incorporated since the IPE to decide if the current HFEs were adequate and that no new HFEs needed to be added. This is not a question of method but rather whether a review since the IPE has been done. The PRA model has been revised many times since the IPE and that would require that the HFEs be reviewed again.

LEVEL OF SIGNIFICANCE: A

The significance of this observation is there may be HFEs which because of plant changes and PRA model changes that to be created. If there are HFEs that need to be created, then they may be significant and could change the PRA results. The intent of the requirement is to ensure that any human error that could impact the PRA model is addressed.

POSSIBLE RESOLUTION

Reference a review of HFEs which would confirm that the HRA has been reviewed since the IPE for new HFEs This would ensure that all the operator actions that could impact the plant PRA have been addressed. This would include a review of all plant and PRA model changes made since the IPE was performed. This review should be documented in accordance with the site procedures.

PLANT RESPONSE OR RESOLUTION

FACT/OBSERVATION REGARDING PRA TECHNICAL ELEMENTS

OBSERVATION ID: HR-16 / Element HR / Sub-element 1

(Related Sub-elements: F)

The post-initiator HFE identification was performed for the original PSA and the IPEE. This was part of Event Sequence Diagram and front-line event tree development, as well as system model development. Documentation of task performance is contained in IPEE section 3.3.4.2 and our event tree notebooks. The HFE identification used steps 1 and 2 of the SHARP process, with results contained in the IPEE and current model notebooks. Subsequent updates to the PRA include review of design changes, procedure changes and LERs – these reviews identify the impact to modeled operator actions, or a need for new operator actions.

Also, documentation of any required changes to operator actions are contained in the PRA model notebooks.

LEVELS OF SIGNIFICANCE FOR FACTS AND OBSERVATIONS

A.	Extremely important and necessary to address to ensure the technical adequacy of the PRA, the quality of the PRA, or the quality of the PRA update process. (Contingent Item for Grade Assignment.)
B.	Important & necessary to address, but may be deferred until next PRA update (Contingent Item for Grade Assignment.)
C.	Considered desirable to maintain maximum flexibility in PRA Applications and consistency in the Industry, but not likely to significantly affect results or conclusions.
D.	Editorial or Minor Technical Item, left to the discretion of the host utility.
S.	Superior treatment, exceeding requirements for anticipated applications & exceeding what would be found in most PRAs.

FACT/OBSERVATION REGARDING PRA TECHNICAL ELEMENTS

OBSERVATION ID: HR-17 / Element HR / Sub-element 21

(Related Sub-elements:)

The following pertains to HRA basic event HEOC01.

The recovery of all the steps for this HRA is based on the monitoring of non-operating train of RHR. Verifying that a switch is in the correct position needs a better step than monitoring of non-operating train of RHR. An example would be the verification of flow on an operating system.

The following pertains to HRA basic event HEOSL1.

The recovery of all the steps for this HRA is based a caution step about isolating the rupture SG. Verifying that a controller is correctly set should be self checked with a better step. An example would be the verification that the controller does not actuate above the new setpoint.

All the recovery actions need to be reviewed to ensure that the step actually performs a self check of the step performed.

LEVEL OF SIGNIFICANCE: B

The significance of this observation is to document a step which actually can be used for recovery of the missed or incorrectly performed step. If recovery can not be credited the value for the HFE would change. This may be indicative of a problem in many HFE evaluations and the effect could be significant.

POSSIBLE RESOLUTION

Reference the correct steps.

PLANT RESPONSE OR RESOLUTION

FACT/OBSERVATION REGARDING PRA TECHNICAL ELEMENTS

OBSERVATION ID: HR-17 / Element HR / Sub-element 21

(Related Sub-elements:)

HEOC01

To address F&O, added the following text to the Cognitive Recovered window, "and the long time available in this scenario (71 hours)," so that the complete first sentence of the notes section now reads:

"Due to the iterative nature of ES33 and the long time available in this scenario (71 hours), self review can be credited as a recovery factor."

HEOSL1

To address F&O, revised the Cognitive Recovered window from, "Self review due to procedural verification in EO00 step 22 "Monitor SG Levels" to "Self review due to procedural verification in EO00 step 22 b or c will verify if the steam generator tubes are intact and redirect the operators to EO30, Steam Generator Tube Rupture, Step 1."

This statement more clearly defines the self check performed and that the step chosen will lead to recovery and identification of the SGTR.

LEVELS OF SIGNIFICANCE FOR FACTS AND OBSERVATIONS

A.	Extremely important and necessary to address to ensure the technical adequacy of the PRA, the quality of the PRA, or the quality of the PRA update process. (Contingent Item for Grade Assignment.)
B.	Important & necessary to address, but may be deferred until next PRA update (Contingent Item for Grade Assignment.)
C.	Considered desirable to maintain maximum flexibility in PRA Applications and consistency in the Industry, but not likely to significantly affect results or conclusions.
D.	Editorial or Minor Technical Item, left to the discretion of the host utility.
S.	Superior treatment, exceeding requirements for anticipated applications & exceeding what would be found in most PRAs.

FACT/OBSERVATION REGARDING PRA TECHNICAL ELEMENTS	
OBSERVATION ID: HR-18 / Element HR / Sub-element 3 <i>(Related Sub-elements:)</i>	
The following pertains to HRA basic event HEOB02. The unrecovered execution appears to be using EO00 instead of FRH1. The transition is from EO00 to FRH1 and the execution should all be done in FRH1. It appears that the wrong procedure is being referenced. The documentation should be rewritten so that it is clear that FRH1 is the procedure being used and not EO00 for the second and succeeding actions.	
LEVEL OF SIGNIFICANCE: B	
The significance of this observation is to correctly identify the procedure used for execution. This may be indicative of other HRA calculation sheets that are unclear in documenting which procedures are being used.	
POSSIBLE RESOLUTION	
Correctly identify the procedure used for execution.	
PLANT RESPONSE OR RESOLUTION	
In this conservative HFE scenario (loss of FW), EO00 Step 1 is listed to account for operators tripping the reactor early in response to loss of FW. The remaining unrecovered execution steps are from FRH1. The FRH1 procedure is referenced at the top portion of this table in the "Cognitive Procedure" and "Execution Procedure" fields. The dependency of these actions is purposeful and acknowledges that the operators will trip the plant early given this scenario to give them more time and more water for feed and bleed operations.	
LEVELS OF SIGNIFICANCE FOR FACTS AND OBSERVATIONS	
A.	Extremely important and necessary to address to ensure the technical adequacy of the PRA, the quality of the PRA, or the quality of the PRA update process. (Contingent Item for Grade Assignment.)
B.	Important & necessary to address, but may be deferred until next PRA update (Contingent Item for Grade Assignment.)
C.	Considered desirable to maintain maximum flexibility in PRA Applications and consistency in the Industry, but not likely to significantly affect results or conclusions.
D.	Editorial or Minor Technical Item, left to the discretion of the host utility.
S.	Superior treatment, exceeding requirements for anticipated applications & exceeding what would be found in most PRAs.

FACT/OBSERVATION REGARDING PRA TECHNICAL ELEMENTS	
OBSERVATION ID: HR-19 / Element HR / Sub-element 30 <i>(Related Sub-elements:)</i>	
The following pertains to HRA basic event HEOS01. The heat-up calculations need to be referenced by calculation number or document number. The cognitive failure could be failure of attention. The alarm is monitored and not checked. The only time the operator probably looks at the alarm is when it is in the alarm state. Therefore the alarm is monitored not checked.	
LEVEL OF SIGNIFICANCE: B	
The significance of this observation is to correctly identify the calculation used and the correct cognitive failures. These observations could be significant and may affect the results.	
POSSIBLE RESOLUTION	
Correctly identify the procedure used for execution.	
PLANT RESPONSE OR RESOLUTION	
The procedures are correct, but they have been updated since the peer review. The HRA has been updated accordingly.	
LEVELS OF SIGNIFICANCE FOR FACTS AND OBSERVATIONS	
A.	Extremely important and necessary to address to ensure the technical adequacy of the PRA, the quality of the PRA, or the quality of the PRA update process. (Contingent Item for Grade Assignment.)
B.	Important & necessary to address, but may be deferred until next PRA update (Contingent Item for Grade Assignment.)
C.	Considered desirable to maintain maximum flexibility in PRA Applications and consistency in the Industry, but not likely to significantly affect results or conclusions.
D.	Editorial or Minor Technical Item, left to the discretion of the host utility.
S.	Superior treatment, exceeding requirements for anticipated applications & exceeding what would be found in most PRAs.

FACT/OBSERVATION REGARDING PRA TECHNICAL ELEMENTS	
OBSERVATION ID: HR-20 / Element HR / Sub-element 26 <i>(Related Sub-elements:)</i>	
The dependency analysis process is well documented with references to the NEI guidance documents. The process itself is well laid out and is easy to follow. The documentation of the dependency analysis is good and provides an easy to follow path for the dependency decisions. This is considered to be a strong point in the HRA.	
LEVEL OF SIGNIFICANCE: S	
The significance of this observation is to credit the work done and the documentation of the dependency analysis.	
POSSIBLE RESOLUTION	
N/A.	
PLANT RESPONSE OR RESOLUTION	
No resolution is required for this observation.	
LEVELS OF SIGNIFICANCE FOR FACTS AND OBSERVATIONS	
A.	Extremely important and necessary to address to ensure the technical adequacy of the PRA, the quality of the PRA, or the quality of the PRA update process. (Contingent Item for Grade Assignment.)
B.	Important & necessary to address, but may be deferred until next PRA update (Contingent Item for Grade Assignment.)
C.	Considered desirable to maintain maximum flexibility in PRA Applications and consistency in the Industry, but not likely to significantly affect results or conclusions.
D.	Editorial or Minor Technical Item, left to the discretion of the host utility.
S.	Superior treatment, exceeding requirements for anticipated applications & exceeding what would be found in most PRAs.

FACT/OBSERVATION REGARDING PRA TECHNICAL ELEMENTS

OBSERVATION ID: HR-21 / Element HR / Sub-element 26

(Related Sub-elements:)

The recent update of the HRA addressed many of the post-trip HFEs including all those found to be risk significant. For other post-trip actions, the results from the original HRA analysis were retained. Conservative screening values were not used.

LEVEL OF SIGNIFICANCE: C

As the HFEs not assessed in the HRA update involve only low risk significant actions, the numerical impact of this is judged to be small.

POSSIBLE RESOLUTION

The methodology should describe the use of the original HRA values for those actions not reevaluated. SR HR-G1 appears to require conservative screening values be used when detailed analyses are unavailable. The values not reanalyzed cannot be considered conservative (6 of the recently assessed HFEs increased compared to the original analysis even before considering dependencies) nor fully satisfactory for detailed analysis because they do not separate cognitive and execution errors. Conservative screening values should be assigned to these remaining actions. If conservative values are assigned, it would then not be necessary to describe the original HRA analysis methodology.

PLANT RESPONSE OR RESOLUTION

The less important operator actions not updated in the PRA Rev.5 HRA update are not screening values; rather they were analyzed using the Failure Likelihood Index Methodology (FLIM), which is a refinement of the Success Likelihood Index Methodology (SLIM). The FLIM methodology is described in the original STPEGS PSA and in the IPE. SLIM is a detailed HRA analysis method, as documented in NUREG/CR-3518 and NUREG/CR-4016. There is no basis to change them to conservative screening values. Reference to the IPE and section 3.3.4.2 which describes this methodology has been added to the HRA notebook.

LEVELS OF SIGNIFICANCE FOR FACTS AND OBSERVATIONS

A.	Extremely important and necessary to address to ensure the technical adequacy of the PRA, the quality of the PRA, or the quality of the PRA update process. (Contingent Item for Grade Assignment.)
B.	Important & necessary to address, but may be deferred until next PRA update (Contingent Item for Grade Assignment.)
C.	Considered desirable to maintain maximum flexibility in PRA Applications and consistency in the Industry, but not likely to significantly affect results or conclusions.
D.	Editorial or Minor Technical Item, left to the discretion of the host utility.
S.	Superior treatment, exceeding requirements for anticipated applications & exceeding what would be found in most PRAs.

Level B Observations Resolved

Observation	Plant Response Summary
<p>A: (HR-16, Sub-element 1); There is no evidence that an analyst reviewed the changes to the PRA model incorporated since the IPE to decide if the current HFEs were adequate and that no new HFEs needed to be added. This is not a question of method but rather whether a review since the IPE has been done. The PRA model has been revised many times since the IPE and that would require that the HFEs be reviewed again.</p>	<p>Subsequent updates to the PRA include review of design changes, procedure changes and LERs – these reviews identify the impact to modeled operator actions, or a need for new operator actions.</p> <p>Also, documentation of any required changes to operator actions are contained in the PRA model notebooks.</p>
<p>B: (HR-08, Sub-element 26); The restriction of the sequences considered in the dependence analysis to only those involving two or more post-trip actions means that sequences involving actions evaluated in the system initiator and only one post-trip action were not considered for dependence.</p>	<p>The logic for this assumption is that initiator recoveries are performed prior to reactor trip (basically to prevent reactor trip). Once reactor trip occurs, the operators are guided into the EOPs and follow them until the plant is stabilized. Reactor trip is a clear demarcation event that decouples the operator actions before the event with those following the event, so operator actions following reactor trip were assumed to be independent of operator actions before reactor trip.</p>
<p>B: (HR-09, Sub-element 28); Table 7-1 (Post Initiator HEP Summary) of the report does not identify some dynamic actions (probably a portion of those which were not changed in this update) though they are used in the sequence model. Table 7-1 also does not identify which actions are dependent on others or under what conditions.</p>	<p>Table 7-1 was revised to identify event application. Rev 6 Notebook was revised to incorporate all portions of the supporting documentation including T/H analysis.</p>
<p>B: (HR-10, Sub-element 28); In one case, an HFE is modeled via an equation rather than a basic event. This means the importance will not be correctly reflected in the basic event importance report.</p>	<p>Starting in Rev 7 all HFEs were modeled in basic events to allow basic event importance to be calculated.</p>
<p>B: (HR-13, Sub-element 2); The scenarios defined for evaluation of HERCP1 and HERC6 appear inconsistent with the sequence models for which they are used. HERCP1 is evaluated for a simple reactor trip followed by a loss of CCW to the RCP. Seal injection flow is however assumed available. HERC6 also is for a simple reactor trip followed by a loss of CCW, but this time seal injection is also lost, thereby shortening the time available for action. However, the sequences in which these actions appear involve loss of EAB HVAC or loss of ECW as per the dependence analysis. These initiators impose much greater impacts on the plant response, potentially affecting the CR environment, the workload assumed, and the</p>	<p>The HEP for HERC6 has been completely redone to reconsider the timing in conjunction with information the Westinghouse Technical Bulletin regarding RCP purge volume and time to seal LOCA. The new success time is 6 minutes. This changed HERC6 and completely changes the dependency analysis as a result.</p>

Level B Observations Resolved

<p>stress experienced.</p> <p>B: (HR-14, Sub-element 2); The annunciator response model is used for evaluation of HEEAB1. Some judgments made in the evaluation are questionable.</p>	<p>The HEEAB1 HEP was revised to account for the 2 alarms and in turn for the Low Dependency that is recommended instead of the Zero Dependency (ZD) originally chosen. The other items of concern are consistent with other HEPs in the model. A set of sensitivity studies was done to show that the HEP is not risk significant or borderline risk significant. By increasing the original failure rate by both one and two orders of magnitude, it was shown that the PRA model is mostly insensitive to this HEP. The results of the sensitivity are:</p> <p>Increase by 10x: ΔCDF = 4.00E-09, % increase in CDF = 0.06%; ΔLERF = 3.10E-10, % increase in LERF = 0.06%</p> <p>Increase by 100x: ΔCDF = 4.38E-08, % increase in CDF = 0.69%; ΔLERF = 3.38E-09, % increase in LERF = 0.67%</p> <p>PRA assessment PRA-12-005, Rev. 0, (STI 33426294), was written and approved to document the results of the sensitivity studies done.</p>
<p>B: (HR-15, Sub-element 10); Procedure OPGP04-ZA-0604, step 5.3.5, requires that the following; "Every model update significant operator experience human performance trends SHOULD be reviewed. This review shall check for adverse trends and new information that could affect the way operator actions are currently modeled in the PRA Reference Model(Ref. 6.11.1)" There was not obvious evidence that this review was accomplished for post-initiator HFEs. There also was no documentation of any issue or lack of any issues being found.</p>	<p>We did not focus this review on post-initiators because our Rev. 5 PRA update plan included an HRA update of the most risk-significant operator actions.</p> <p>For the STP_REV 6 PRA model update, a review of plant CRs and LERs that relate to human performance was conducted and documented.</p> <p>Based on this review, no new HEPs or update to existing HEPs are required.</p>
<p>B: (HR-17, Sub-element 21); The following pertains to HRA basic event HEOC01.</p> <p>The recovery of all the steps for this HRA is based on the monitoring of non-operating train of RHR. Verifying that a switch is in the correct position needs a better step than monitoring of non-operating train of RHR. An example would be the verification of flow on an operating system.</p> <p>The following pertains to HRA basic event HEOSL1.</p>	<p>HEOC01 To address F&O, added the following text to the Cognitive Recovered window, "and the long time available in this scenario (71 hours)," so that the complete first sentence of the notes section now reads: "Due to the iterative nature of ES33 and the long time available in this scenario (71 hours), self-review can be credited as a recovery factor." HEOSL1 To address F&O, revised the Cognitive Recovered</p>

Level B Observations Resolved

<p>The recovery of all the steps for this HRA is based a caution step about isolating the rupture SG. Verifying that a controller is correctly set should be self-checked with a better step. An example would be the verification that the controller does not actuate above the new setpoint.</p> <p>All the recovery actions need to be reviewed to ensure that the step actually performs a self-check of the step performed.</p>	<p>window from, "Self review due to procedural verification in E000 step 22 "Monitor SG Levels" to "Self review due to procedural verification in E000 step 22 b or c will verify if the steam generator tubes are intact and redirect the operators to EO30, Steam Generator Tube Rupture, Step 1." This statement more clearly defines the self-check performed and that the step chosen will lead to <i>recovery and identification of the SGTR.</i></p>
<p>B: (HR-18, Sub-element 3);</p> <p>The unrecovered execution for HRA basic event HEOB02 appears to be using E000 instead of FRH1. The transition is from E000 to FRH1 and the execution should all be done in FRH1. It appears that the wrong procedure is being referenced. The documentation should be rewritten so that it is clear that FRH1 is the procedure being used and not E000 for the second and succeeding actions.</p>	<p>In this conservative HFE scenario (loss of FW), E000 Step 1 is listed to account for operators tripping the reactor early in response to loss of FW. The remaining unrecovered execution steps are from FRH1. The FRH1 procedure is referenced at the top portion of this table in the "Cognitive Procedure" and "Execution Procedure" fields. The dependency of these actions is purposeful and acknowledges that the operators will trip the plant early given this scenario to give them more time and more water for feed and bleed operations.</p>
<p>B: (HR-19, Sub-element 30); The following pertains to HRA basic event HEOB01.</p> <p>The heat-up calculations need to be referenced by calculation number or document number.</p> <p>The cognitive failure could be failure of attention. The alarm is monitored and not checked. The only time the operator probably looks at the alarm is when it is in the alarm state. Therefore the alarm is monitored not checked.</p>	<p>The procedures are correct, but they have been updated since the peer review. The HRA has been updated accordingly.</p>
<p>S: (HR-20, Sub-element 26); The dependency analysis process is well documented with references to the NEI guidance documents. The process itself is well laid out and is easy to follow. The documentation of the dependency analysis is good and provides an easy to follow path for the dependency decisions.</p> <p>This is considered to be a strong point in the HRA.</p>	<p>No resolution is required for this observation.</p>

Electric Power Recovery Peer Review

	Resolution
<p>HR – 01Sub-element 13 Significance B The evaluation of the recovery factors adopted a brand new approach which was developed under the documents reviewed. By comparison to the original method which uses the STADIC code to generate recovery factors for LOOP recovery, it's found that although there are some advantages of this new approach (e.g., like including distributions for DG repair/recovery), the part missing from this approach is the lack of an uncertainty analysis, which is required by most PRA applications.</p>	<p>This is being addressed in the next update</p>
<p>HR – 24 Significance Level BP The methodology developed for the LOOP and DG recovery is more flexible and precise in terms of recovering offsite power as well as the diesel generators that fail to run after the first hour. The integral forms developed for a particular cutset type represent the exact failure and recovery process, while allowing flexible analytical distributions for offsite power recovery and diesel generator repair/recovery. The methodology developed here is used to recover individual cutsets. The concept is to apply recovery to a number of cutsets that comprise a relatively high percentage of the total split fraction probability. A key feature of the current approach, not credited in the current analysis, is to identify the time of the first SDG fail to run so that the recovery can be considered from that time forward. Past methods only considered the recovery of SDG failures starting from the time of the last SDG failure; i.e., from the second or third SDG fail to run. In addition to implementing the approach for SDG recovery, the next item in the methodology is to consider the uncertainty of the model parameters throughout the model to the final model output. i.e., for factors in the recovery analysis.</p>	<p>Not required</p>



South Texas Project Risk-Informed GSI-191 Evaluation

Response to
APLAB 25– vs. 40–Year Frequency Estimates: RAI 3

Justification of the Use of 25–Year Frequency
Estimates

Document: STP-RIGSI191-RAI-APLA-X-3

Revision: 1.0

Date: July 2, 2014

Prepared by:

Jeremy Tejada, The University of Texas at Austin
John Hasenbein, The University of Texas at Austin
David Morton, The University of Texas at Austin

Reviewed by:

Zahra Mohaghegh, University of Illinois at Urbana-Champaign
Seyed A. Reihani, University of Illinois at Urbana-Champaign

Approved by:

Ernie J. Kee, South Texas Project

Response to APLAB 25- vs. 40-Year Frequency Estimates: RAI 3 Justification of the Use of 25-Year Frequency Estimates

Jeremy Tejada, John Hasenbein, and David Morton
The University of Texas at Austin

Abstract

We justify use of the 25-year frequency estimates, as opposed to the 40-year estimates, provided by NUREG-1829 [1]. We also estimate Δ CDF using 40-year frequency estimates, and we further provide results for 28.75, 32.5, and 36.25-year frequency estimates to better understand trends. Lastly, we discuss CDF, LERF, and Δ LERF estimation and the impact of using the 40-year frequency estimates on these values.

1 APLAB-25 vs. 40-Year Frequency Estimates: RAI 3

The statement of the APLAB-25 vs. 40-Year Frequency Estimates: RAI 3 is as follows:

Volume 1, Section 1.3.1 states that LOCA frequencies were obtained from Table 7.19 of NUREG-1829 for 25 years' operation. Furthermore, assumption 3.b in Volume 3 states that current-day LOCA frequencies are more appropriate to use for this evaluation than the end-of-plant-license frequencies. RG 1.174, Section 2.5.5 states that it is incumbent on the licensee to demonstrate that the choice of reasonable alternative hypotheses, adjustment factors, or modeling approximations or methods to those adopted in the PRA model would not significantly change the assessment. Also, it is assumed that the STP plants will continue to operate for more than 25 years; RG 1.174 Section 3 states that the licensee should define an implementation and monitoring program to ensure that no unexpected adverse safety degradation occurs do to the change. Please justify the use of the 25-year frequency estimates rather than the 40-year estimates provided by NUREG-1829. Provide CDF, LERF, Δ CDF, and Δ LERF using the 40-year estimates.

2 Justification of the Use of 25-year Frequency Estimates

STP's Unit 1 was commissioned on August 25, 1988, and Unit 2 was commissioned on June 19, 1989. Thus, STP has been operational for approximately 25 years, and so we see it as natural to use NUREG-1829 [1] current-day values to estimate the frequency of core damage, and large early release, due to GSI-191 issues at the current point in time. That said, we see use of the 40-year frequency estimates (and linearly interpolated estimates between 25 and 40 years meant to represent intermediate ages) as appropriate for a sensitivity analysis to attempt to answer questions like: How will the Δ CDF estimate at STP change over the next 15 years of operation?

We further note that, with the exception of the eight reactor vessel nozzle welds, STP's large-bore piping nozzle welds that are susceptible to degradation via the mechanism of "primary water stress corrosion cracking" have been replaced or mitigated. For these potentially problematic welds, these mitigation efforts arguably "reset" these welds to an age younger than 25 years. The analysis we present in the next section—for Δ CDF estimates based on 25, 28.75, 32.5, 36.25, and 40-year LOCA frequency estimates—does not take credit for replacement and mitigation of these welds.

3 Δ CDF Based on 25, 28.75, 32.5, 36.25, and 40-year Frequency Estimates

In this section, we present the results of a sensitivity analysis in which we estimate Δ CDF as a function of the number of years the plant has been in operation. NUREG-1829 [1] provides estimates of the 5th, 50th, and 95th percentiles of LOCA frequencies for 25 years of plant operation and for 40 years of plant operation. In an attempt to understand trends in between 25 and 40 years, we also estimate Δ CDF at 28.75, 32.5, and 36.25 years of operation, and we use linear interpolation of NUREG-1829 values to estimate the percentiles of LOCA frequencies associated with these intermediate years of operation. In Tables 1-5, we summarize LOCA exceedance frequency estimates for 25, 28.75, 32.5, 36.25, and 40 years of plant operation for each NUREG-1829 category. We include values for 2-inch and 6-inch breaks, obtained by linear interpolation between 1.625 inches and 3 inches and between 3 inches and 7 inches, and we provide the mean frequencies, because we use these means for small (0.5- to 2.0-inch), medium (2.0- to 6.0-inch), and large (6.0-inch and greater) breaks in estimating Δ CDF. In particular, we estimate Δ CDF via

$$\Delta CDF = f_{SL} \cdot \hat{P}(Failure|SL) + f_{ML} \cdot \hat{P}(Failure|ML) + f_{LL} \cdot \hat{P}(Failure|LL). \quad (1)$$

Here, SL , ML , and LL denote the events of a small, medium, and large break, and f_{SL} , f_{ML} , and f_{LL} denote corresponding mean frequencies in events per year. A GSI-191 failure event, whether in the sump or vessel, is denoted $Failure$, and the corresponding \hat{P} terms are conditional probabilities estimated using the CASA Grande simulation model.

The Δ CDF estimates we report here are based on output of the CASA Grande simulation model assuming all pumps on all three trains are available. We note that the conditional probability of the state of “all pumps operational” (Pump Case 1) is 0.935, given that we have a LOCA which does not cause a core damage event under non-GSI-191 issues.

After obtaining (via interpolation when necessary) the percentiles for the initiating frequencies for each of the five time points for number of years in operation and for each of the eight break sizes, we fit bounded Johnson distributions to these 5th, 50th, and 95th percentiles for each break size and time point. The process used for fitting the Johnson distribution is the same as was used for 25-year frequencies in the submittal, and this process is described in Pan et al. [2]. In Tables 6-10, we present the parameters of the fitted Johnson distributions for 25, 28.75, 32.5, 36.25, and 40 years of plant operation. Table 11 summarizes the mean LOCA frequencies used in computing Δ CDF for small, medium, and large breaks for 25, 28.75, 32.5, 36.25, and 40 years of plant operation. (Because the values of the Johnson parameters are fit in the same manner as that used in Pan et al. [2] for the submittal, the fit values for λ are close to being two times the 95th percentiles.)

The information in Tables 6-10 is used as input to CASA Grande, which produces estimates of failure probabilities, whether in the sump or vessel, for small, medium, and large breaks conditional on a break occurring. Those conditional failure probabilities are then multiplied by the frequency of small, medium, and large breaks in order to estimate Δ CDF. Using equation (1), we study the results of our sensitivity analysis in two contexts: (i) we obtain the conditional failure probabilities from CASA Grande using the Johnson parameters as input, and then multiply those conditional failure probabilities by the appropriate frequencies from a given column of Table 11 according the

number of years of plant operation; and, (ii) we obtain the conditional failure probabilities from CASA Grande using the Johnson parameters as input, and then multiply those conditional failure probabilities by the 25-year frequencies from the first column of Table 11 regardless of the years of operation associated with the Johnson parameters used as input. The first approach provides our best estimate of Δ CDF as a function of the number of years of plant operation. The second approach allows us to isolate the changes due to estimates of failure probabilities from CASA Grande, and still report them in the familiar Δ CDF manner. We emphasize that we do not see the latter Δ CDF estimates as being physically meaningful, per se, but as our results show, they provide valuable insight. In particular, we are able to assess the proportion of the change in Δ CDF that is attributable to changes in the conditional failure probabilities estimated by CASA Grande, and the proportion of the change in Δ CDF that is attributable to changes in f_{SL} , f_{ML} , and f_{LL} in equation (1), which rely on NUREG-1829 [1] mean frequencies. We use common random numbers (CRNs) between scenarios in CASA Grande in order to reduce variance of our estimates and allow us to statistically assess whether the changes in Δ CDF are due to changes in the initiating frequencies.

Tables 12 and 13 present the results in the first context described above (best estimates of Δ CDF). Table 12 provides estimates of Δ CDF for all five alternative years of plant operation, as well as a 95% confidence-interval (CI) half-width, and upper and lower confidence limits. Figure 1 is a sensitivity plot of Δ CDF versus years of plant operation using the information from Table 13, where Table 13 also shows the differences in Δ CDF between each of the years of operation and 25 years of operation. In addition to 95% confidence intervals on the difference between each of the scenarios and the 25-year base case, we present the ratio of each estimate to the 25-year estimate, and a p -value to assess the level at which each scenario is statistically significantly different from the 25-year case.

Tables 14 and 15 present information analogous to the previous two tables, but in the second context of only changing the Johnson parameters that serve as inputs to CASA Grande, while using the 25-year mean frequencies in the computation of Δ CDF in equation (1). Similarly, Figure 2 is a sensitivity plot of Δ CDF versus years of plant operation using the information from Table 15.

Examining Table 12 and Figure 1, we see that the estimates of Δ CDF increase roughly linearly from 25 years of operation to 40 years of operation, and at 40 years of operation the estimate of Δ CDF is greater than the value at 25 years by a factor of 2.38. Examining Table 14 and Figure 2, we see that the estimates of Δ CDF increase at a decreasing rate (i.e., in a concave fashion) from 25 years of operation to 40 years of operation, and at 40 years of operation the estimate of Δ CDF exceeds the value at 25 years by a factor of 1.06. We see from a comparison of Figure 1 and Figure 2 that the change in Δ CDF is dominated by changing the mean initiating frequencies as opposed to changing the Johnson distributions that serve as input to the CASA Grande simulation model. Note also that we can form the ratio of the 40-year to 25-year values of f_{SL} , f_{ML} , and f_{LL} values from Table 11, and that ratio for f_{LL} is 2.25.

4 Discussion

Our results indicate that Δ CDF increases by an estimated factor of 2.38 as we move from 25-year to 40-year frequency estimates. This increase can essentially be decomposed into a factor of 2.25 based on the growth of the mean frequency of a large LOCA, and a factor of 1.06 based on how changes in the Johnson distributions used in CASA Grande allocate breaks to break sizes. We emphasize that these numerical results assume that we are in "Pump Case 1," in which all pumps on all trains are available. This pump case occurs with probability 0.935. If the overall factor of 2.38 holds when we account for all pump cases then the Δ CDF of 2.88E-08 events per year from Volume 2 [3] for 25 years of operation would increase to 6.85E-08 events per year for 40 years of operation.

The estimate of Δ LERF is well approximated by using a fraction, say α , of our estimate of Δ CDF because there do not appear to be any GSI-191 effects that would amplify the conditional probability of a large-early-release event, given that we have a core damage event. From Volume 2 [3], Δ LERF based on 25-year frequency estimates is 4.70E-11 events per year (corresponding to $\alpha = 1.63\text{E-}03$). The factor of 2.38 then yields a 40-year Δ LERF estimate of 1.12E-10 events per year.

The estimate of CDF is simply Δ CDF plus the core damage frequency due to non-GSI 191 issues, and the estimate of LERF is simply Δ LERF plus the large early release frequency due to non-GSI 191 issues. PRA estimates are not typically made for 15 years in the future. In this context we use the same estimated aging factor of 2.38 of the CDF and LERF due to non-GSI 191 issues. The current estimates for total CDF and LERF that include GSI-191 issues are 9.23E-06 and 5.78E-07 events per year, respectively. With the aging factor of 2.38, these estimates for CDF and LERF become 2.20E-05 and 1.38E-06 events per year, respectively. We note that under these 40-year estimates of CDF, Δ CDF, LERF, and Δ LERF, STP remains within Region III per NRC Regulatory Guide 1.174.

Table 1: 25-year LOCA frequency estimates by break size. Break size is in inches and frequencies are in events per year. The same units in are used in subsequent tables.

Break Size	Category	5th %Tile	50th %Tile	Mean	95th %Tile
0.5	Small	6.8E-05	6.3E-04	1.9E-03	7.1E-03
1.625	2	5.0E-06	8.9E-05	4.2E-04	1.6E-03
2.0	Medium	3.6E-06	6.5E-05	3.1E-04	1.3E-03
3.0	3	2.1E-07	3.4E-06	1.6E-05	6.1E-05
6.0	Large	6.3E-08	1.1E-06	5.2E-06	2.0E-05
7.0	4	1.4E-08	3.1E-07	1.6E-06	6.1E-06
14.0	5	4.1E-10	1.2E-08	2.0E-07	5.8E-07
31.0	6	3.5E-11	1.2E-09	2.9E-08	8.1E-08

Table 2: 28.75-year LOCA frequency estimates by break size.

Break Size	Category	5th %Tile	50th %Tile	Mean	95th %Tile
0.5	Small	6.8E-05	6.5E-04	2.0E-03	7.3E-03
1.625	2	5.2E-06	9.7E-05	4.6E-04	1.8E-03
2.0	Medium	3.9E-06	7.2E-05	3.4E-04	1.3E-03
3.0	3	2.7E-07	4.5E-06	2.1E-05	8.1E-05
6.0	Large	8.2E-08	1.4E-06	6.8E-06	2.6E-05
7.0	4	1.7E-08	4.0E-07	2.1E-06	8.1E-06
14.0	5	5.5E-10	1.6E-08	2.7E-07	7.9E-07
31.0	6	4.8E-11	1.6E-09	4.0E-08	1.1E-07

Table 3: 32.5-year LOCA frequency estimates by break size.

Break Size	Category	5th %Tile	50th %Tile	Mean	95th %Tile
0.5	Small	6.9E-05	6.7E-04	2.0E-03	7.5E-03
1.625	2	5.6E-06	1.1E-04	5.0E-04	1.9E-03
2.0	Medium	4.1E-06	7.8E-05	3.7E-04	1.4E-03
3.0	3	3.5E-07	5.5E-06	2.6E-05	1.0E-04
6.0	Large	1.0E-07	1.7E-06	8.5E-06	3.3E-05
7.0	4	2.1E-08	4.9E-07	2.6E-06	1.0E-05
14.0	5	7.1E-10	2.0E-08	3.4E-07	9.9E-07
31.0	6	6.1E-11	2.1E-09	5.2E-08	1.5E-07

Table 4: 36.25-year LOCA frequency estimates by break size.

Break Size	Category	5th %Tile	50th %Tile	Mean	95th %Tile
0.5	Small	7.0E-05	7.0E-04	2.1E-03	7.7E-03
1.625	2	5.8E-06	1.1E-04	5.4E-04	2.1E-03
2.0	Medium	4.4E-06	8.3E-05	4.0E-04	1.5E-03
3.0	3	4.1E-07	6.6E-06	3.1E-05	1.2E-04
6.0	Large	1.2E-07	2.1E-06	1.0E-05	3.9E-05
7.0	4	2.5E-08	5.7E-07	3.1E-06	1.2E-05
14.0	5	8.5E-10	2.4E-08	4.1E-07	1.2E-06
31.0	6	7.4E-11	2.5E-09	6.4E-08	1.8E-07

Table 5: 40-year LOCA frequency estimates by break size.

Break Size	Category	5th %Tile	50th %Tile	Mean	95th %Tile
0.5	Small	7.0E-05	7.2E-04	2.1E-03	7.9E-03
1.625	2	6.1E-06	1.2E-04	5.8E-04	2.2E-03
2.0	Medium	4.6E-06	8.9E-05	4.3E-04	1.6E-03
3.0	3	4.8E-07	7.6E-06	3.6E-05	1.4E-04
6.0	Large	1.4E-07	2.4E-06	1.2E-05	4.6E-05
7.0	4	2.8E-08	6.6E-07	3.6E-06	1.4E-05
14.0	5	1.0E-09	2.8E-08	4.8E-07	1.4E-06
31.0	6	8.7E-11	2.9E-09	7.5E-08	2.1E-07

Table 6: Parameters for fitted Johnson distributions for 25-year LOCA frequency estimates by break size.

Break Size	γ	δ	ξ	λ
0.5	1.650950E+00	5.256964E-01	4.117000E-05	1.420000E-02
1.625	1.646304E+00	4.593913E-01	2.530000E-06	3.200000E-03
2.0	1.646308E+00	4.593851E-01	1.870000E-06	2.360550E-03
3.0	1.646605E+00	4.589467E-01	1.200000E-07	1.220000E-04
6.0	1.646403E+00	4.566256E-01	3.000000E-08	3.965000E-05
7.0	1.645739E+00	4.487957E-01	6.023625E-09	1.220000E-05
14.0	1.645211E+00	3.587840E-01	2.892430E-10	1.160000E-06
31.0	1.645072E+00	3.343493E-01	2.636770E-11	1.600000E-07

Table 7: Parameters for fitted Johnson distributions for 28.75-year LOCA frequency estimates by break size.

Break Size	γ	δ	ξ	λ
0.5	1.650176E+00	5.274187E-01	3.846250E-05	1.460000E-02
1.625	1.646090E+00	4.579137E-01	2.597500E-06	3.500000E-03
2.0	1.646101E+00	4.578737E-01	1.930000E-06	2.589503E-03
3.0	1.646616E+00	4.561455E-01	1.600000E-07	1.615000E-04
6.0	1.646407E+00	4.529135E-01	4.250000E-08	5.248750E-05
7.0	1.645653E+00	4.419307E-01	7.017719E-09	1.615000E-05
14.0	1.645215E+00	3.566764E-01	3.991523E-10	1.570000E-06
31.0	1.645070E+00	3.307249E-01	3.668238E-11	2.250000E-07

Table 8: Parameters for fitted Johnson distributions for 32.5-year LOCA frequency estimates by break size.

Break Size	γ	δ	ξ	λ
0.5	1.650434E+00	5.291410E-01	3.936500E-05	1.500000E-02
1.625	1.646161E+00	4.584063E-01	2.665000E-06	3.800000E-03
2.0	1.646170E+00	4.583775E-01	1.990000E-06	2.818455E-03
3.0	1.646628E+00	4.570793E-01	2.000000E-07	2.010000E-04
6.0	1.646410E+00	4.541509E-01	5.500000E-08	6.532500E-05
7.0	1.645682E+00	4.442191E-01	8.011813E-09	2.010000E-05
14.0	1.645218E+00	3.573789E-01	5.090615E-10	1.980000E-06
31.0	1.645071E+00	3.319330E-01	4.699705E-11	2.900000E-07

Table 9: Parameters for fitted Johnson distributions for 36.25-year LOCA frequency estimates by break size.

Break Size	γ	δ	ξ	λ
0.5	1.650692E+00	5.308633E-01	4.026750E-05	1.540000E-02
1.625	1.646233E+00	4.588988E-01	2.732500E-06	4.100000E-03
2.0	1.646239E+00	4.588813E-01	2.050000E-06	3.047408E-03
3.0	1.646639E+00	4.580130E-01	2.400000E-07	2.405000E-04
6.0	1.646414E+00	4.553882E-01	6.750000E-08	7.816250E-05
7.0	1.645710E+00	4.465074E-01	9.005906E-09	2.405000E-05
14.0	1.645222E+00	3.580815E-01	6.189708E-10	2.390000E-06
31.0	1.645071E+00	3.331412E-01	5.731173E-11	3.550000E-07

Table 10: Parameters for fitted Johnson distributions for 40-year LOCA frequency estimates by break size.

Break Size	γ	δ	ξ	λ
0.5	1.649918E+00	5.325856E-01	3.756000E-05	1.580000E-02
1.625	1.646018E+00	4.574212E-01	2.800000E-06	4.400000E-03
2.0	1.646032E+00	4.573699E-01	2.110000E-06	3.276360E-03
3.0	1.646650E+00	4.552118E-01	2.800000E-07	2.800000E-04
6.0	1.646417E+00	4.516761E-01	8.000000E-08	9.100000E-05
7.0	1.645624E+00	4.396424E-01	1.000000E-08	2.800000E-05
14.0	1.645225E+00	3.559738E-01	7.288800E-10	2.800000E-06
31.0	1.645069E+00	3.295167E-01	6.762640E-11	4.200000E-07

Table 11: Summary of mean LOCA frequencies used in estimating Δ CDF for 25, 28.75, 32.5, 36.25, and 40-year estimates.

Category	25.00	28.75	32.50	36.25	40.00
Small	1.59E-03	1.61E-03	1.63E-03	1.65E-03	1.67E-03
Medium	3.05E-04	3.33E-04	3.62E-04	3.91E-04	4.20E-04
Large	5.20E-06	6.83E-06	8.45E-06	1.01E-05	1.17E-05

Table 12: Δ CDF estimated using updated CASA conditional failure probabilities and updated mean frequencies for small, medium, and large breaks.

Case	Δ CDF	95% CI HW	95% CI LL	95% CI UL
25 Years	2.449E-08	2.520E-09	2.197E-08	2.701E-08
28.75 Years	3.287E-08	3.368E-09	2.951E-08	3.624E-08
32.5 Years	4.139E-08	4.241E-09	3.715E-08	4.563E-08
36.25 Years	4.988E-08	5.101E-09	4.478E-08	5.498E-08
40 Years	5.825E-08	5.950E-09	5.230E-08	6.420E-08

Table 13: Differences in Δ CDF compared with the base case of 25 years when using updated CASA conditional failure probabilities and updated mean frequencies for small, medium, and large breaks.

Case	Ratio	Mean Diff	95% CI HW	95% CI LL	95% CI UL	p-value	Sig Diff?
25 Years	1.00	0.00E+00	0.00E+00	0.00E+00	0.00E+00	-	-
28.75 Years	1.34	7.34E-10	1.54E-10	5.80E-10	8.88E-10	1.56E-18	Yes
32.5 Years	1.69	1.60E-09	1.65E-10	1.43E-09	1.76E-09	4.63E-54	Yes
36.25 Years	2.04	2.43E-09	2.54E-10	2.18E-09	2.69E-09	2.86E-53	Yes
40 Years	2.38	3.15E-09	3.32E-10	2.82E-09	3.48E-09	1.41E-52	Yes

Table 14: Δ CDF estimated using updated CASA conditional failure probabilities and 25-year mean frequencies for small, medium, and large breaks. These values show the results of only changing input to CASA Grande, while not changing the means frequencies used in computing Δ CDF via equation (1).

Case	Δ CDF	95% CI HW	95% CI LL	95% CI UL
25 Years	2.449E-08	2.520E-09	2.197E-08	2.701E-08
28.75 Years	2.505E-08	2.566E-09	2.248E-08	2.761E-08
32.5 Years	2.547E-08	2.610E-09	2.286E-08	2.808E-08
36.25 Years	2.574E-08	2.633E-09	2.311E-08	2.838E-08
40 Years	2.589E-08	2.645E-09	2.324E-08	2.853E-08

Table 15: Differences in Δ CDF compared with the base case of 25 years when using updated CASA conditional failure probabilities and 25-year mean frequencies for small, medium, and large breaks. These values show the results of only changing input to CASA Grande, while not changing the means frequencies used in computing Δ CDF via equation (1).

Case	Ratio	Mean Diff	95% CI HW	95% CI LL	95% CI UL	p-value	Sig Diff?
25 Years	1.00	0.00E+00	0.00E+00	0.00E+00	0.00E+00	-	-
28.75 Years	1.02	5.59E-10	1.17E-10	4.42E-10	6.77E-10	1.56E-18	Yes
32.5 Years	1.04	9.84E-10	1.01E-10	8.82E-10	1.09E-09	4.63E-54	Yes
36.25 Years	1.05	1.26E-09	1.31E-10	1.13E-09	1.39E-09	2.86E-53	Yes
40 Years	1.06	1.40E-09	1.47E-10	1.25E-09	1.55E-09	1.41E-52	Yes

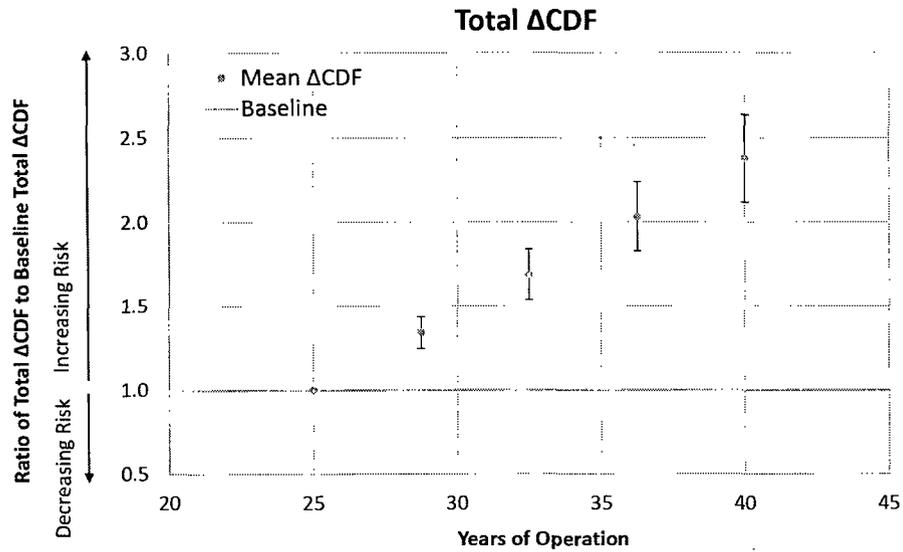


Figure 1: Sensitivity plot for Δ CDF using updated CASA conditional failure probabilities and the corresponding mean frequencies for small, medium, and large breaks used in computing Δ CDF via equation (1).

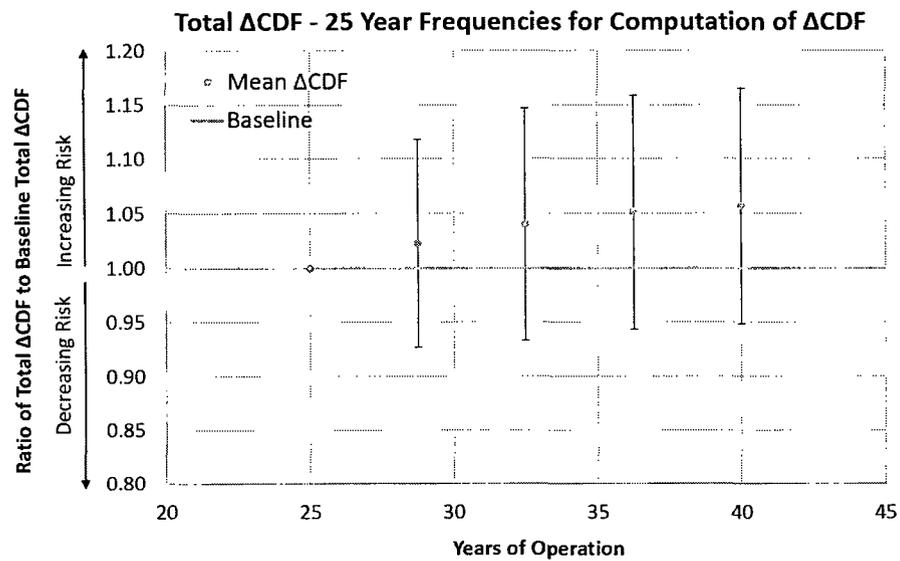


Figure 2: Sensitivity plot for Δ CDF using updated CASA conditional failure probabilities and the 25-year mean frequencies for small, medium, and large breaks used in computing Δ CDF via equation (1).

References

- [1] R. Tregoning, P. Scott, and A. Csontos (2008, April). Estimating Loss-of-Coolant Accident (LOCA) Frequencies Through the Elicitation Process: Main Report (NUREG-1829). NUREG 1829, NRC, Washington, DC.
- [2] Y.-A. Pan, E. Popova, and D. P. Morton (2013, January). Modeling and Sampling LOCA Frequency and Break Size. Technical report, STP-RIGSI191-V03.02, Revision 4, The University of Texas at Austin.
- [3] D. Wakefield and D. Johnson (2013, October). South Texas Project Risk-Informed GSI-191 Evaluation, Volume 2, Probabilistic Risk Analysis: Determination of Change in Core Damage Frequency and Large Early Release Frequency Due to GSI-191 Issues. Technical report, STP-RIGSI191-VO2, Revision 2, ABSG Consulting Inc.



South Texas Project Risk-Informed GSI-191 Evaluation

Response to
APLAB–Results Interpretation–Uncertainty Analysis:
RAI 4a

Explanation of the Discrepancy in Mean LOCA
Frequencies for Fitted Johnson Distribution versus
NUREG–1829 Values

Document: STP-RIGSI191-RAI-APLA-X-4a

Revision: 1.0

Date: July 8, 2014

Prepared by:

Alexander Zolan, The University of Texas at Austin

Jeremy Tejada, The University of Texas at Austin

David Morton, The University of Texas at Austin

John Hasenbein, The University of Texas at Austin

Reviewed by:

Zahra Mohaghegh, University of Illinois at Urbana-Champaign

Seyed A. Reihani, University of Illinois at Urbana-Champaign

Approved by:

Ernie J. Kee, South Texas Project

**Response to APLAB–Results Interpretation–Uncertainty Analysis: RAI 4a
Explanation of the Discrepancy in Mean LOCA Frequencies for
Fitted Johnson Distribution versus NUREG-1829 Values**

Alexander Zolan, Jeremy Tejada, David Morton, and John Hasenbein
The University of Texas at Austin

Abstract

We discuss selection of the Johnson distribution to model LOCA frequencies from NUREG-1829 [3], and we discuss why we do not pursue matching the means reported in NUREG-1829. We further investigate the discrepancy between the means of a family of Johnson distributions and NUREG-1829 means.

1 APLAB–Results Interpretation–Uncertainty Analysis: RAI 4a

The statement of the APLAB–Results Interpretation–Uncertainty Analysis: RAI 4a is as follows:

The acceptance guidelines of RG 1.174, Section 2.5.5 “are defined such that the appropriate measure for comparison is the mean value of the uncertainty distribution on the corresponding metric.” Typically, statistical sampling simulations will develop random variables that preserve the mean of the distribution from which the variables are sampled. STP has chosen to fit a Johnson bounded distribution that matches the expert-provided 5th, 50th, and 95th percentiles in NUREG-1829, but does not match the mean values. The properties of the distribution are such that, as fit, the mean of the fitted distribution is always less than the experts’ means from the distributions in NUREG-1829.

A) Please explain why the STP evaluation departs from the regulatory position in RG 1.174 regarding the use of mean values.

2 NUREG-1829 means

The means provided in NUREG-1829 [3] were not the result of expert elicitation, but rather were given by a split lognormal distribution fit to the percentiles (5th, 50th, and 95th) elicited from experts. Because they were not elicited, we did not feel compelled to match the NUREG-1829 means. Rather, we sought a smooth distribution that could match the elicited percentiles.

3 Use of the Johnson distribution

In Pan et al. [2] we present a hybrid method that combines NUREG-1829 frequencies and the bottom-up frequencies of Fleming et al. [1] for modeling LOCA frequencies and break sizes. This method fits a bounded Johnson distribution to the elicited 5th, 50th, and 95th percentiles of the LOCA frequencies for each of the six NUREG-1829 break-size categories.

The fit Johnson distributions and the hybrid approach specify how to probabilistically allocate a break to a weld in the CASA Grande simulation model. The simulation model, in turn, is used to estimate conditional failure probabilities given that the break is small, medium, or large. To estimate Δ CDF—the change in core damage frequency due to GSI-191 issues—the failure probabilities are then multiplied by the frequencies of small, medium, and large breaks and summed, with the break-size frequencies given in the “GSI-191 PRA column” of Table 4-1 in Volume 2 [4]. The frequencies of the small, medium, and large breaks in Table 4-1 of Volume 2 are obtained by: (i) linearly interpolating NUREG-1829 mean frequencies (current-day estimates from Table 7.19 of [3]), and (ii) taking differences of these exceedance frequencies to find mean frequencies within the small, medium, and large categories. So, while we do not aspire to fit NUREG-1829 means with our Johnson distributions, we essentially use NUREG-1829 mean frequencies when estimating Δ CDF.

4 Choice of the Johnson distribution to fit NUREG-1829 percentiles

We selected the bounded Johnson distribution because its four parameters allow us to match the three percentiles of NUREG-1829, and the bounded Johnson distribution allows us to capture the highly skewed nature these percentiles suggest. That said, we considered other possibilities including the semi-bounded distribution and the gamma distribution. The semi-bounded Johnson distribution also seems like a natural choice because it does not place an upper bound on frequency, and it has three parameters. The semi-bounded Johnson is a shifted lognormal distribution, i.e., a lognormal distribution with a possibly nonzero lower bound. However, fits of the semi-bounded Johnson distribution to NUREG-1829 percentiles yielded a negative lower bound, and so we rejected this distribution. Because it is conjugate to the Poisson distribution, the gamma distribution has also been used to model uncertain frequencies. However, fitting a gamma distribution to NUREG-1829 percentiles yields a poor fit.

5 Inconsistency of Johnson means and NUREG-1829 means

As we will explore more thoroughly in forthcoming responses to RAI APLAB 4b and 4c, for each of the six NUREG-1829 break-size categories, there is a family of Johnson distributions parameterized by the Johnson scale parameter λ . By ranging the scale parameter λ we can analyze the means of the Johnson distributions, as a function of λ . Figure 1 shows the results of this analysis. The x -axis in the figure depicts the ratio of λ to the elicited 95th percentile. As the figure indicates, the means tend to grow as λ grows, and they also appear to level off for large values of λ . Even at their maximum value, the Johnson means fall short of the NUREG-1829 means, particularly in categories 5 and 6.

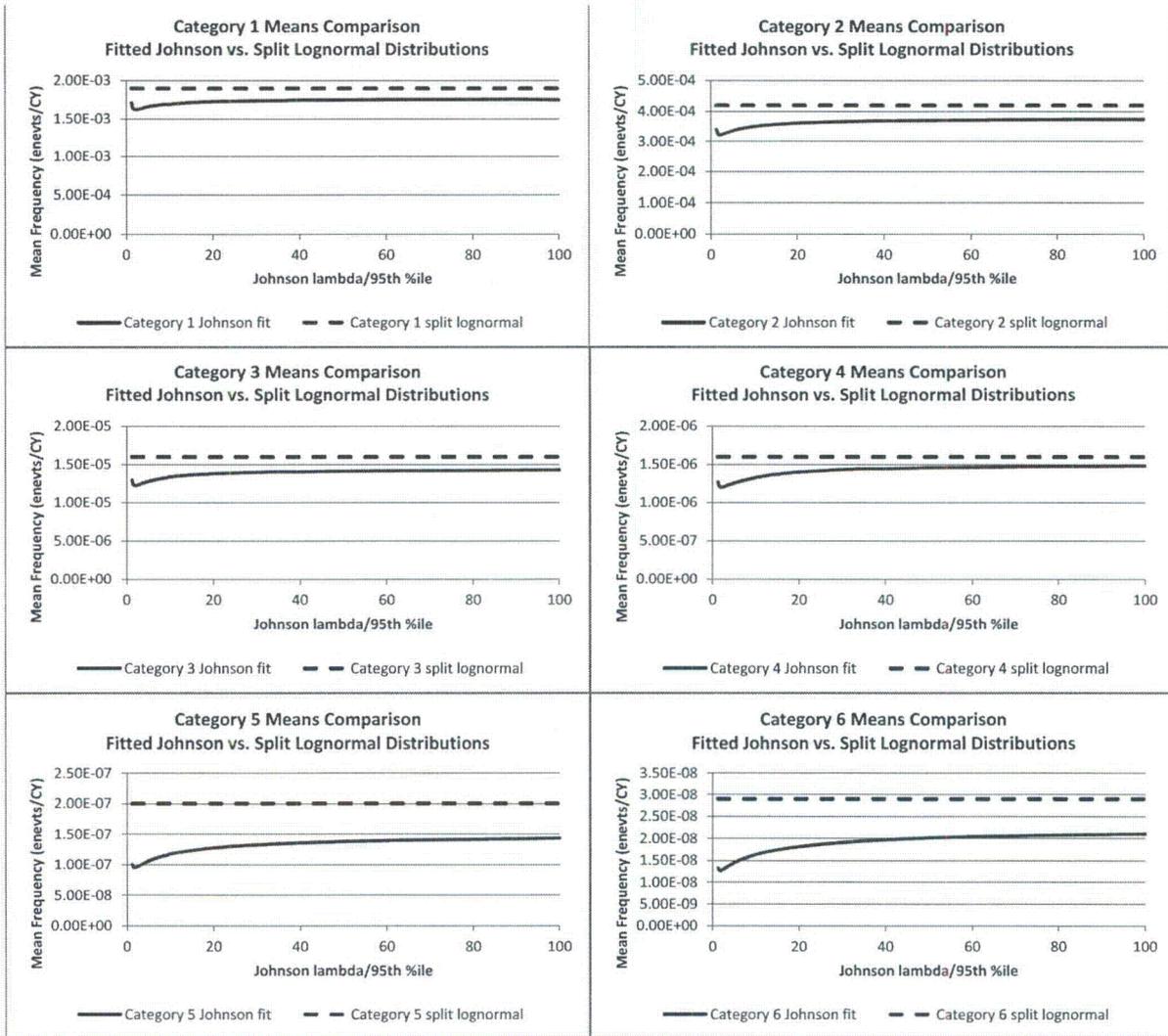


Figure 1: For current-day estimates and for each of the six NUREG-1829 break-size categories, the figure compares the means of the fitted Johnson distributions, as a function of the scale parameter λ , and the NUREG-1829 split lognormal mean.

References

- [1] Fleming, K. N., B. O. Lydell, and D. Chrun (2011, September). Development of LOCA Initiating Event Frequencies for South Texas Project GSI-191. Technical Report, KnF Consulting Services, LLC, Spokane, WA.
- [2] Pan, Y.-A., E. Popova, and D. P. Morton (2013, January). South Texas Project Risk-Informed GSI-191 Evaluation, Volume 3, Modeling and Sampling LOCA Frequency and Break Size. Technical report, STP-RIGSI191-V03.02, Revision 4, The University of Texas at Austin.
- [3] Tregoning, R., P. Scott, and A. Csontos (2008, April). Estimating Loss-of-Coolant Accident (LOCA) Frequencies Through the Elicitation Process: Main Report (NUREG-1829). NUREG 1829, NRC, Washington, DC.
- [4] Wakefield, D., T. Mikschl, and D. Johnson (2013, October). South Texas Project Risk-Informed GSI-191 Evaluation, Volume 2, Probabilistic Risk Analysis: Determination of Change in Core Damage Frequency and Large Early Release Frequency Due to GSI-191 Issues. Technical report, STP-RIGSI191-VO2, Revision 2, ABSG Consulting Inc.



South Texas Project Risk-Informed GSI-191 Evaluation

Response to
APLAB–Results Interpretation–Uncertainty Analysis:
RAI 4b
Explanation of the Johnson Distribution Governing
LOCA Frequency and Sensitivity of Summary
Statistics to Scale Parameters

Document: STP-RIGSI191-RAI-APLA-X-4b
Revision: 1.0
Date: July 8, 2014

Prepared by:
Alexander Zolan, The University of Texas at Austin
Jeremy Tejada, The University of Texas at Austin
David Morton, The University of Texas at Austin
John Hasenbein, The University of Texas at Austin

Reviewed by:
Zahra Mohaghegh, University of Illinois at Urbana-Champaign
Seyed A. Reihani, University of Illinois at Urbana-Champaign

Approved by:
Ernie J. Kee, South Texas Project

Response to APLAB–Results Interpretation–Uncertainty Analysis: RAI 4b Explanation of the Johnson Distribution Governing LOCA Frequency and Sensitivity of Summary Statistics to Scale Parameters

Alexander Zolan, Jeremy Tejada, David Morton, and John Hasenbein
The University of Texas at Austin

Abstract

We explain the reasoning behind the selection of the Johnson distribution parameters used to govern the LOCA frequencies from NUREG-1829, in particular the choice of the scale parameter λ . Furthermore, we investigate the effect of changing λ on summary statistics of the distribution including extreme percentiles, and the relative contribution of small, medium, and large breaks.

1 APLAB–Results Interpretation–Uncertainty Analysis: RAI 4b

The statement of APLAB–Results Interpretation–Uncertainty Analysis: RAI 4b is as follows:

The acceptance guidelines of RG 1.174, Section 2.5.5 “are defined such that the appropriate measure for comparison is the mean value of the uncertainty distribution on the corresponding metric.” Typically, statistical sampling simulations will develop random variables that preserve the mean of the distribution from which the variables are sampled. STP has chosen to fit a Johnson bounded distribution that matches the expert-provided 5th, 50th, and 95th percentiles in NUREG-1829, but does not match the mean values. The properties of the distribution are such that, as fit, the mean of the fitted distribution is always less than the experts’ means from the distributions in NUREG-1829.

B) The Johnson fit to 5th, 50th, and 95th percentiles is not unique. Alternative accurate fits can be constructed with arbitrary values of the scale parameter λ . The scale parameter λ defines a bound on the maximal frequencies sampled in the Monte Carlo model. By increasing the value of λ , the relative proportion of large to medium to small breaks can be altered, especially in the extrapolation range beyond the 95th percentile. Please provide a technical justification for the selection of the scale parameter λ (other selections appear possible that could change the outputs by CASA Grande).

2 Choice of λ in Johnson distributions used in CASA Grande

For each break size in NUREG-1829 [3], we fit a bounded Johnson distribution by matching the 5th, 50th, and 95th percentiles of the bounded Johnson distribution to the percentiles specified in NUREG-1829, as we describe in [2]. As the RAI indicates, the Johnson distribution has four parameters, and we fit three percentiles. Hence, we have one degree of freedom in performing this fit. Restated, there are infinitely many four-parameter bounded Johnson distributions that match the three percentiles elicited in NUREG-1829 for each category, and, as the RAI further indicates, we can represent that degree of freedom by the Johnson scale parameter, λ .

The analysis associated with STP’s submittal was based on performing the fit to NUREG-1829 current-day values by solving the nonlinear optimization model described in [2]. The algorithm used to solve that model takes as input initial values for the Johnson parameters as a “starting point” for the algorithm. For each category, we initialized the value of the lower bound, ξ , of the Johnson distribution to half of the 5th percentile given in NUREG-1829, and we initialized the range, λ , to twice the 95th percentile. The iterative optimization algorithm modifies these values when matching the desired percentiles, but the fit values for λ were strongly influenced by (i.e., the fit values were close to) the assigned initial values of half the 5th percentile and twice the 95th percentile. While we see these initial values as providing additional spread of the distribution outside the NUREG-1829 percentiles, the choice is arguably somewhat arbitrary. For this reason, we carry out further analysis to assess the sensitivity of the results we obtain to changes in λ . In particular, if we fix λ to a particular value, then the other three Johnson parameters (ξ, δ, γ) are uniquely determined by the three percentiles. In this response, we investigate the effect of parametrically varying λ on certain properties of the Johnson distribution, including the relative proportion of large to medium to small breaks. (Our response to APLAB-RAI 4a investigates the effect of parametrically varying λ on the mean of the Johnson distribution, and our response to APLAB-RAI 4c investigates the effect on Δ CDF based on output of CASA Grande.) In the numerical results we present here, we restrict attention to current-day values from NUREG-1829 [3].

Figure 1 displays the results of fixing the value λ to varying multiples of the 95th percentile for each category and solving for the other three Johnson parameters. The results in the figure confirm the RAI statement that there are alternative Johnson distributions that fit the three percentiles elicited from experts as part of NUREG-1829. As λ grows, the shape parameter γ has a nonlinear, monotonic, concave relationship with λ , while δ levels off in each category. As λ grows, the complementary scale parameter ξ drops and again levels off at a different value for each NUREG-1829 category.

3 Impact of increasing λ on extreme quantiles of the Johnson distribution and relative contribution by category

In our response to APLAB-RAI 4a, we study the Johnson distribution means with respect to the choice of the scale parameter λ , and we show that they tend to grow and then level off for large values of λ . Further, we show that the means, even at large values of λ , fall short of the means implied by the split lognormal distributions in NUREG-1829. As part of our analysis here, we evaluate the effect of the value of λ on extreme quantiles. A summary of the 99th and 99.9th percentiles of the fitted Johnson distributions, for each of the NUREG-1829 categories, is shown in Figure 2. In large part, the 99th percentiles appear to have leveled off for large values of λ , but the 99.9th percentiles continue to grow at such values of λ .

We calculate the relative contribution of each category as its summary statistic (mean, 99th percentile, 99.9th percentile) divided by the sum of the same summary statistic across all categories. The relative contribution to LOCA frequency by category, according to the NUREG-1829 mean, the Johnson mean, as well as the 99th, and 99.9th percentiles, is shown in Figure 3. Note that for each assessment of relative contribution, the x -axis shows the multiple of the 95th percentile to which λ was fixed for all categories. The results show that the relative contribution of category 1 dominates, but that at larger percentiles and as λ grows, the

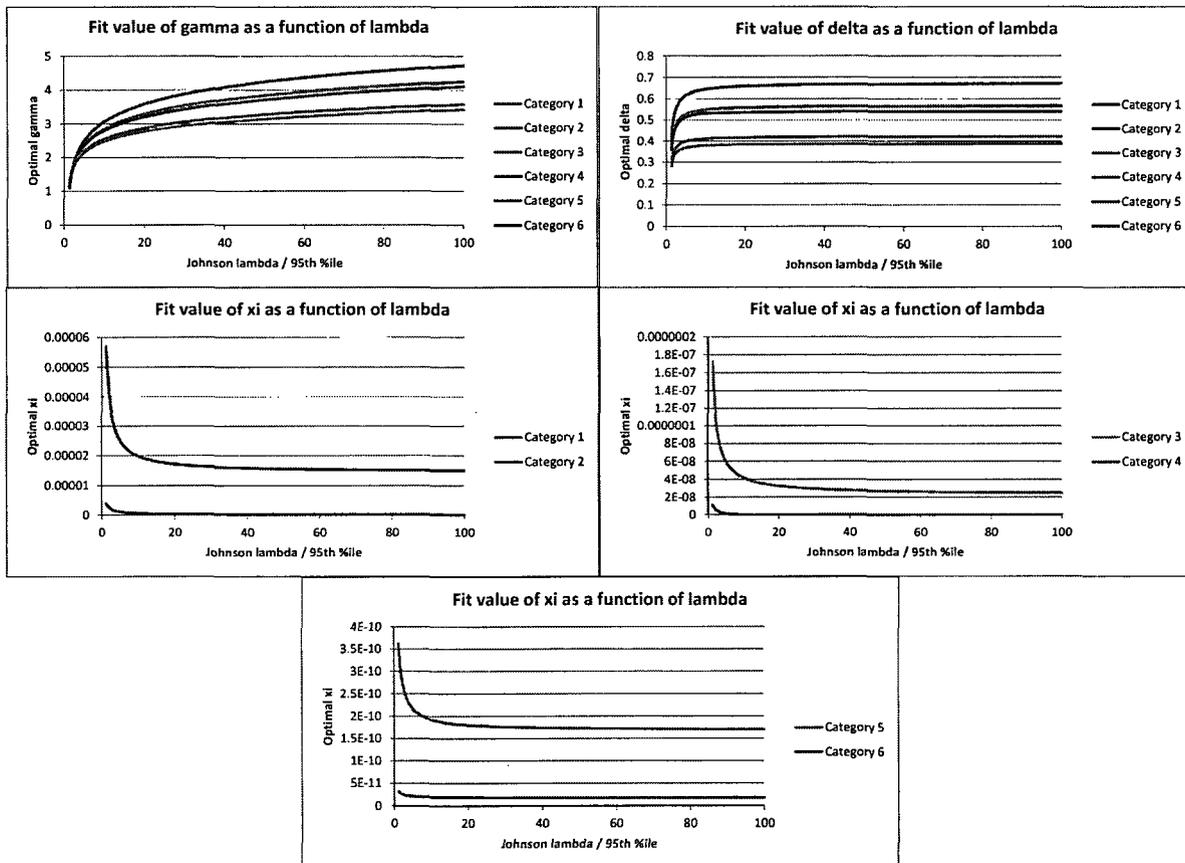


Figure 1: Comparison of parameters of different fitted Johnson distributions, as a function of fixed multiple of 95th percentile for λ for current-day values from NUREG-1829.

contribution of category 1 drops and the relative contribution of the other categories grows. If we use the means of the Johnson distributions as the metric for relative contribution of LOCA events by category, we somewhat underestimate the contribution of the larger break sizes of categories 5 and 6 as compared to using the implied means from NUREG-1829, while we overestimate the contribution of these categories versus the implied NUREG-1829 means if we use the 99th or 99.9th percentiles and a large value for λ . However, when we fix λ to twice the 95th percentile, we underestimate the contribution of categories 5 and 6 even using the 99th or 99.9th percentiles, relative to the NUREG-1829 means. The response to APLAB-RAI 4c shows the impact of these alternative Johnson distributions on Δ CDF estimates using CASA Grande results.

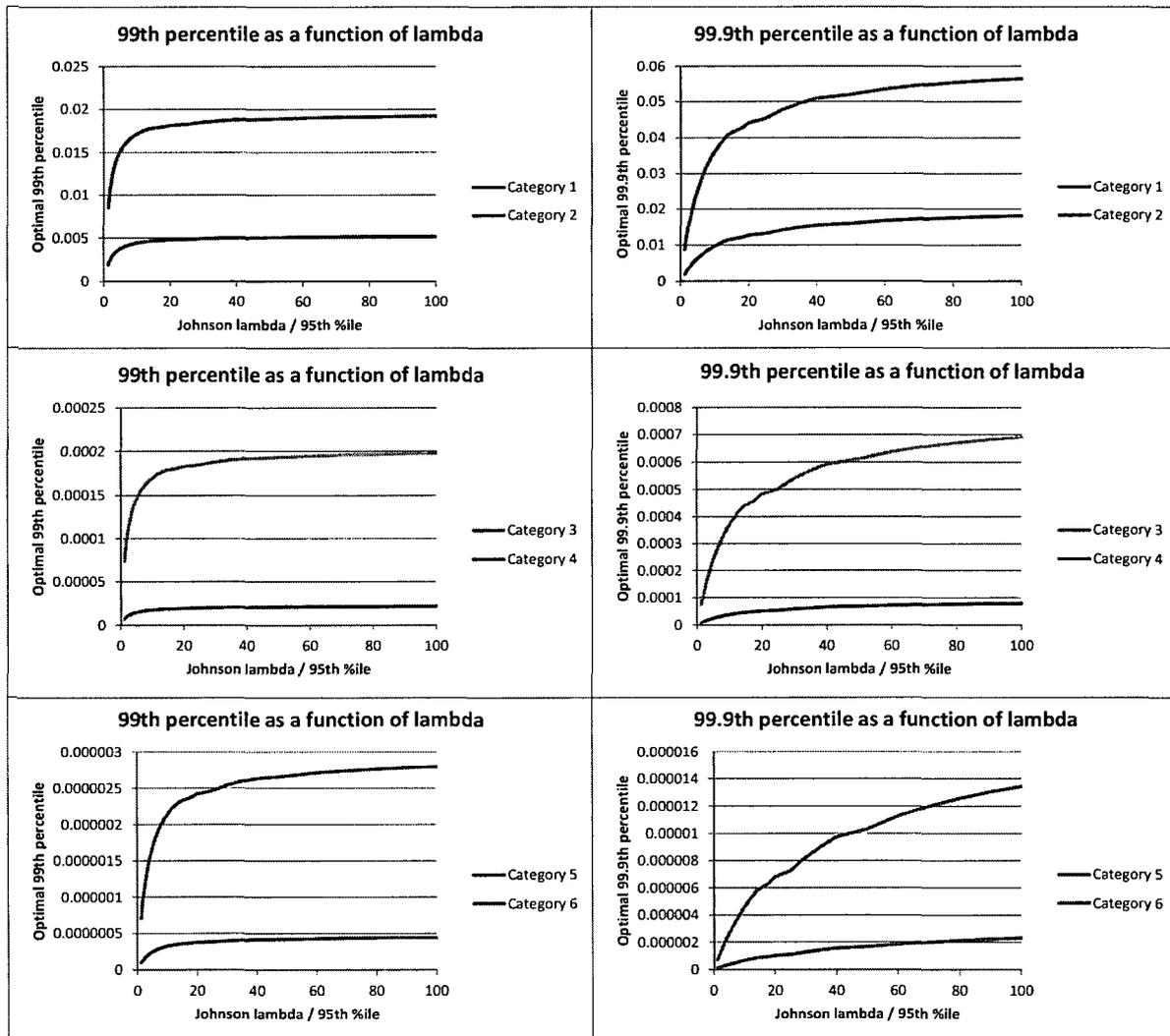


Figure 2: Comparison of extreme quantiles of different fitted Johnson distributions, by break size category for current-day values from NUREG-1829.

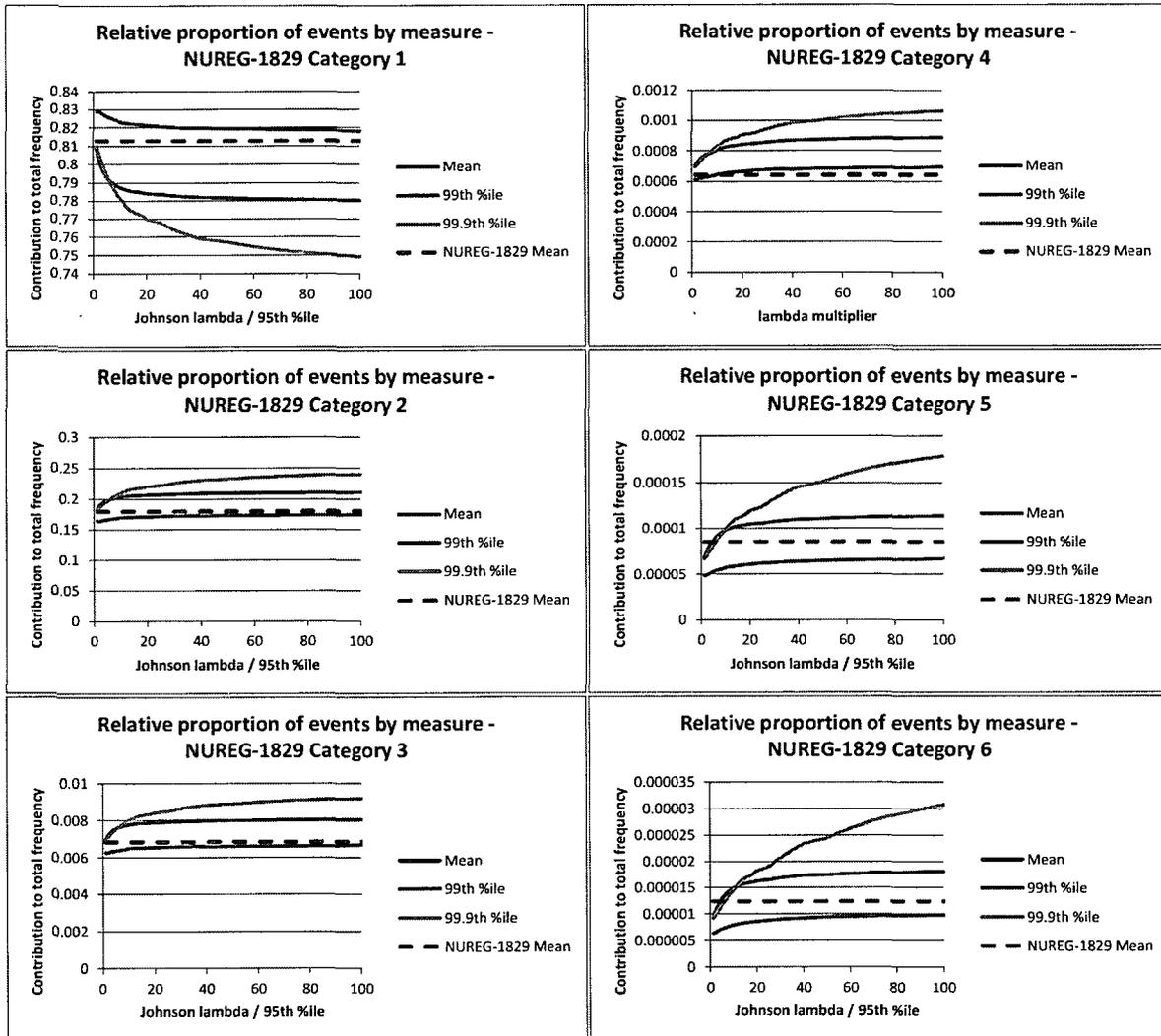


Figure 3: Comparison of relative contribution of different NUREG-1829 category break sizes to a fixed initiating frequency, based on initial solution parameter λ as a multiple of 95th percentile. The relative contribution using the implied means by category from NUREG-1829 mean is shown for comparison. Results are for current-day values from NUREG-1829.

References

- [1] Letellier, B., T. Sande, and G. Zigler (2013, October). South Texas Project Risk-Informed GSI-191 Evaluation, Volume 3, CASA Grande Analysis. Technical report, STP-RIGSI191-V03, Revision 2.
- [2] Popova, E., D. Morton, and Y. Pan (2013, January). Modeling and Sampling LOCA Frequency and Break Size for STP GSI-191 Resolution. Technical report, STP-RIGSI191-V03.02, Revision 4, The University of Texas at Austin.
- [3] Tregoning, R., P. Scott, and A. Csontos (2008, April). Estimating Loss-of-Coolant Accident (LOCA) Frequencies Through the Elicitation Process: Main Report (NUREG-1829). NUREG 1829, NRC, Washington, DC.
- [4] Wakefield, D. and D. Johnson (2013, October). South Texas Project Risk-Informed GSI-191 Evaluation, Volume 2, Probabilistic Risk Analysis: Determination of Change in Core Damage Frequency and Large Early Release Frequency Due to GSI-191 Issues. Technical report, STPRIGSI191-VO2, Revision 2, ABSG Consulting Inc.



South Texas Project Risk-Informed GSI-191 Evaluation

Response to
APLAB–Results Interpretation–Uncertainty Analysis:
RAI 4c
Explanation of the Impact of Johnson Distribution
Selection on CDF, LERF, Δ CDF, Δ LERF

Document: STP-RIGSI191-RAI-APLA-X-4c
Revision: 1.0
Date: July 8, 2014

Prepared by:
Alexander Zolan, The University of Texas at Austin
Jeremy Tejada, The University of Texas at Austin
David Morton, The University of Texas at Austin
John Hasenbein, The University of Texas at Austin

Reviewed by:
Zahra Mohaghegh, University of Illinois at Urbana-Champaign
Seyed A. Reihani, University of Illinois at Urbana-Champaign

Approved by:
Ernie J. Kee, South Texas Project

Response to APLAB–Results Interpretation–Uncertainty Analysis: RAI 4c Explanation of the Impact of Johnson Distribution Selection on CDF, LERF, Δ CDF, Δ LERF

Alexander Zolan, Jeremy Tejada, David Morton, and John Hasenbein
The University of Texas at Austin

Abstract

We show that using alternative Johnson distributions that match the 5th, 50th, and 95th percentiles given in NUREG-1829, and that have means closer to those in NUREG-1829, has a limited impact on the expected CDF, LERF, Δ CDF, and Δ LERF based on failure probability estimates from CASA Grande.

1 APLAB–Results Interpretation–Uncertainty Analysis: RAI 4c

The statement of APLAB–Results Interpretation–Uncertainty Analysis: RAI 4c is as follows:

The acceptance guidelines of RG 1.174, Section 2.5.5 “are defined such that the appropriate measure for comparison is the mean value of the uncertainty distribution on the corresponding metric.” Typically, statistical sampling simulations will develop random variables that preserve the mean of the distribution from which the variables are sampled. STP has chosen to fit a Johnson bounded distribution that matches the expert-provided 5th, 50th, and 95th percentiles in NUREG-1829, but does not match the mean values. The properties of the distribution are such that, as fit, the mean of the fitted distribution is always less than the experts’ means from the distributions in NUREG-1829.

C) Please provide the maximum expected difference between the CDF, LERF, Δ CDF, and Δ LERF developed from bounded Johnson distributions that consider alternative values of the scale parameter λ , and other distributions that would preserve mean values reported in NUREG-1829. Note, in particular, that alternative bounded Johnson distributions with large values of the scale parameter λ can be built to accurately fit the NUREG-1829 5th, 50th, and 95th percentiles, and produce mean estimates closer to the NUREG-1829 values than current fits used by STP.

2 Impact of alternative Johnson distributions on Δ CDF

For each break size in NUREG-1829 [4], we fit a bounded Johnson distribution by matching the 5th, 50th, and 95th percentiles of the bounded Johnson distribution to the percentiles specified in NUREG-1829, as we describe in [3]. As the RAI indicates, the Johnson distribution has four parameters, and we fit three percentiles. Hence, we have one degree of freedom in performing these fits. Restated, there are infinitely many four-parameter bounded Johnson distributions that match the three percentiles elicited in NUREG-1829 for each category, and, as the RAI further indicates, we can represent that degree of freedom by the Johnson scale parameter, λ . In our response to APLAB-RAI 4b, we investigate the effect of parametrically varying λ on certain properties of the Johnson distribution, including the relative proportion of large to medium to small breaks. In this section, we investigate the effect of parametrically varying λ on Δ CDF estimates.

We estimate ΔCDF as follows:

$$\Delta CDF = f_{SL} \cdot \hat{P}(Failure|SL) + f_{ML} \cdot \hat{P}(Failure|ML) + f_{LL} \cdot \hat{P}(Failure|LL). \quad (1)$$

Here, SL , ML , and LL denote the events of a small, medium, or large break, and f_{SL} , f_{ML} , and f_{LL} denote corresponding mean frequencies in events per year. A GSI-191 failure event, whether via sump or in-vessel, is denoted *Failure*, and the corresponding \hat{P} terms are conditional probabilities estimated using the CASA Grande simulation model. Throughout the analysis we report here, we use frequencies for small, medium, and large breaks (f_{SL} , f_{ML} , and f_{LL}) that match frequencies that are linearly interpolated from the mean current-day values in Table 7.19 from NUREG-1829 [4]. Thus, changes in λ for the Johnson distribution only change the joint probability distribution governing break size and weld case, which affects estimates of the \hat{P} terms in equation (1).

To assess whether these alternative distributions have a significant impact on expected ΔCDF , we analyzed output of the CASA Grande simulation model [1] with all pumps available for Johnson distributions with the scale parameter λ fixed at values ranging from 1.25 to 100 times the 95th percentile of the LOCA frequencies elicited from experts in NUREG-1829 (Table 7.19's current-day values [4]). We note that the conditional probability of the state of "all pumps operational" is 0.935, given that we have a LOCA which does not cause a core damage event under non-GSI-191 issues. Figure 1 displays ΔCDF estimates when using Johnson distributions with various values for the scale parameter λ , as compared to the base case. The actual multiplier for the base case varies slightly by category but all are close to 2.0.

Changing the Johnson distributions governing the frequency for each break size increases the point estimate of ΔCDF by at most a factor of 1.02. Furthermore, the largest values of λ we consider, where each Johnson mean is closest to the implied NUREG-1829 mean for that category, yield a ΔCDF estimate nearly equal to the base case when estimated using common random numbers (CRNs). The halfwidth of the error bars in Figure 1 are about 10% of the point estimates. (While we do not report them here, somewhat smaller errors are obtained for the differences in ΔCDF at different values of λ due to the use of CRNs.) Note that these error bars are based on sampling error associated with Monte Carlo simulation in CASA Grande. They differ from, say, the "uncertainty percentiles" reported in Tables 4-4 and 4-5 in Volume 2's [5] uncertainty analysis.

Viewing the estimate of ΔCDF as a function of λ as a sensitivity analysis, Figure 2 displays our results with the other factors, which we report in [2]. The results suggest the impact on ΔCDF is small compared to uncertainties on other input parameters in CASA Grande.

3 Impact of alternative Johnson distributions on CDF, LERF, and $\Delta LERF$

Our estimate of CDF is simply ΔCDF plus the core damage frequency due to non-GSI 191 issues. The estimate of the latter frequency depends on the distribution governing the initiating frequency only through its mean. Moreover, we use frequencies for small, medium, and large breaks (f_{SL} , f_{ML} , and f_{LL}) that match mean current-day frequencies from Table 7.19 of NUREG-1829 [4]. Thus the changes in CDF due to changes in the Johnson scale parameter λ are captured by our analysis for ΔCDF in Section 2.

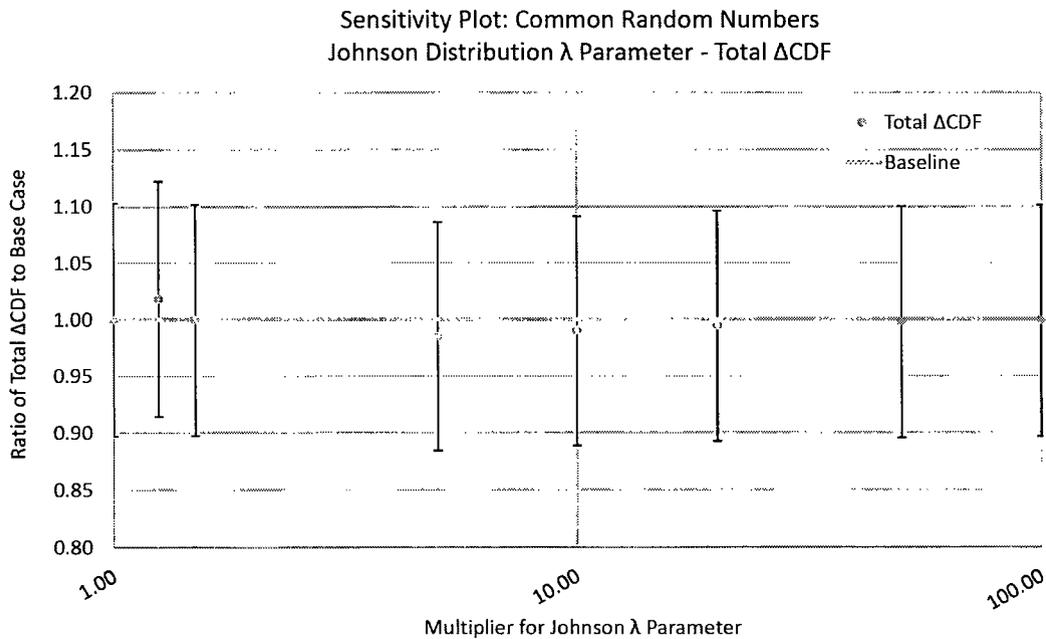


Figure 1: Comparison of Δ CDF estimates for Pump State 1 (all pumps available) using different fitted Johnson distributions, as a function of fixed multiples of the 95th percentiles for λ . Note that the value reported at “1.00” corresponds to the base case in STP’s submittal, rather than being a multiple of the 95th percentiles. The actual multiplier for the base case varies slightly by category but all are close to 2.0. Reading from left to right, the multipliers after the base case are 1.25, 1.5, 5, 10, 20, 50, and 100.

Our estimate of Δ LERF is well approximated by using a fraction, say α , of our estimate of Δ CDF because there do not appear to be any GSI-191 effects that would amplify the conditional probability of a large-early-release event, given that we have a core damage event. (From Volume 2 [5], $\alpha = 1.63\text{E-}03$.) Hence, we use the maximum 2% increase in Δ CDF as providing our estimate of the maximum percentage increase in Δ LERF due to changes in the Johnson scale parameter λ .

4 Summary

Our estimates of changes in CDF, Δ CDF, LERF, and Δ LERF are modest as we range the Johnson scale parameter, λ , from a factor of 1.25 up to a factor of 100 times the 95th percentile of the frequencies elicited from experts in NUREG-1829. (A factor of about 2.00 was used in STP’s submittal.) More specifically, point estimates of Δ CDF and Δ LERF increase by no more than 2% for the specific values of λ we consider here. Estimates of CDF and LERF differ from Δ CDF and Δ LERF by values that do not depend on λ .

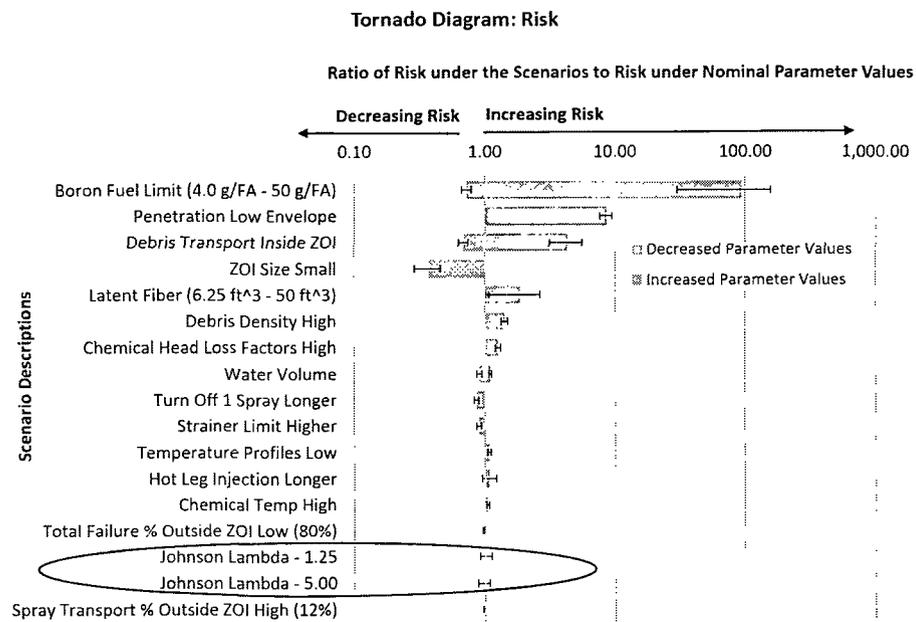


Figure 2: Tornado diagram comparing the ratio of Δ CDF attributable to varying Johnson distributions, as compared to the other key input parameters identified in the sensitivity report [2]. The two distributions with the largest changes in Δ CDF are circled for reference.

References

- [1] Letellier, B., T. Sande, and G. Zigler (2013, October). South Texas Project Risk-Informed GSI-191 Evaluation, Volume 3, CASA Grande Analysis. Technical report, STP-RIGSI-191-V03, Revision 2.
- [2] Morton, D., J. Tejada, and A. Zolan (2014, February). A Practical Guide to Sensitivity Analysis of a Large-scale Computer Simulation Model. Technical Report, STP-RIGSI191-ARAI.01, Revision 3.
- [3] Popova, E., D. Morton, and Y. Pan (2013, January). Modeling and Sampling LOCA Frequency and Break Size for STP GSI-191 Resolution. Technical report, STP-RIGSI191-V03.02, Revision 4, The University of Texas at Austin.
- [4] Tregoning, R., P. Scott, and A. Csontos (2008, April). Estimating Loss-of-Coolant Accident (LOCA) Frequencies Through the Elicitation Process: Main Report (NUREG-1829). NUREG 1829, NRC, Washington, DC.
- [5] Wakefield, D. and D. Johnson (2013, October). South Texas Project Risk-Informed GSI-191 Evaluation, Volume 2, Probabilistic Risk Analysis: Determination of Change in Core Damage Frequency and Large Early Release Frequency Due to GSI-191 Issues. Technical report, STP-RIGSI-191-V02, Revision 2, ABSG Consulting Inc.

Attachment 2

Response to ARCB Request for Additional Information: RAI 1, 2, 3

ARCB, Radiation Protection & Consequence Branch: RAI 1, 2, 3

In an effort to ensure a complete and accurate review of the dose consequence analyses, please provide additional information in tabular form describing, for each design basis accident affected by the proposed Risk Informed GSI-191 submittal, all the basic parameters used in the dose consequence analyses. For each parameter, please indicate the current licensing basis (CLB) value, the revised GSI-191 value where applicable, as well as the basis for any changes to the CLB. An example of the input/assumptions needed is provided in Table 4.3-11 "Dose Analysis Inputs for LOCA" provided in STP's alternate source term (AST) submittal dated March 22, 2007 (ADAMS Accession No. ML070890474). The NRC staff requests that the information include all of the basic parameters whether or not the individual parameter is being changed for the GSI-191 amendment. The NRC staff also requests that the information be presented in separate tables for each affected accident (i.e., LOCA, the fuel handing accident (FHA), the main steam line break accident (MSLB), the steam generator tube rupture accident (SGTR), the control rod ejection accident (CREA), and the locked rotor accident (LRA)).

STP Response:

The response to ARCB, RAI 1 was provided in the STP letter to NRC Staff, dated March 17, 2014 NOC-AE-14003082, ML14086A385, ML14086A386, ML14086A387.

ARCB, Radiation Protection & Consequence Branch: RAI 2

STP identified the following condition related to the AST submittal:

Westinghouse Electric Company Nuclear Safety Advisory Letter (NSAL)-06-15, dated December 13, 2006, advised operators of Westinghouse plants that the single-failure scenario for the SGTR analysis that licensees used in their accident analysis may not be limiting. As stated in the STP AST NRC Safety Evaluation dated March 6, 2008 (ADAMS Accession No. ML080160013), "The licensee has evaluated the applicability of NSAL-06-15 against the accident analysis assumptions and has determined that the current single-failure assumption for the STP SGTR analysis is not limiting. Therefore, the licensee is operating under compensatory measures to meet regulatory dose guidelines. The licensee plans to resolve this condition at the earliest opportunity so that the assumptions, including the limiting single failure, for the SGTR accident analysis described herein are consistent with the plant response to this event. To support the limiting single-failure assumptions in the SGTR analysis, STP will maintain an administrative limit for reactor coolant system (RCS) dose equivalent iodine 131 (DEI) so that the radiological dose reference values for the SGTR analysis remain bounding, and the licensee will continue to comply with GDC [General Design Criteria] 19."

Please state if this condition been resolved? If so, please describe how? Also, please provide justification that GDC 19 continues to be met.

STP Response:

The response to ARCB, RAI 2 was provided in the STP letter to NRC Staff, dated March 17, 2014 NOC-AE-14003082, ML14086A385, ML14086A386, ML14086A387.

ARCB, Radiation Protection & Consequence Branch: RAI 3

The LOCA analysis assumes that iodine will be removed from the containment atmosphere by containment spray and natural diffusion to the containment walls. As a result of these removal mechanisms a large fraction of the released activity will be deposited in the containment sump. The sump water will retain soluble gases and soluble fission products such as iodines and cesium, but not noble gases. The guidance from RG 1.183, "Alternate Radiological Source Terms for Evaluating Design Basis Accidents at Nuclear Power Reactors," July 2000 (ADAMS Accession No. ML003716792), specifies that the iodine deposited in the sump water can be assumed to remain in solution as long as the containment sump pH is maintained at or above 7.

The AST application indicates:

"After the first day, the containment sump pH will begin to decrease, reaching 6.8 by the end of the 30-day duration of the radiological consequence analysis for the Design Basis Accident (DBA) LOCA, and the impact of that decrease has been reflected in the Control Room and offsite doses."

It is noted that the AST application further indicates:

"The design inputs for calculating the containment sump pool pH were conservatively established by the licensee to maximize the acidic contribution to sump pH and minimize the basic contribution."

The GSI-191 application indicates the possibility that debris generated during a LOCA could clog the containment sump strainers in pressurized-water reactors (PWRs) and result in loss of NPSH for the ECCS and CSS [containment spray system] pumps, impeding the flow of water from the sump.

Please discuss the exemption justification as they relate to the effects on sump water pH, radiological consequences, and loss of the containment spray system (CSS).

STP Response:

The response to ARCB, RAI 3 was provided in the STP letter to NRC Staff, dated March 17, 2014 NOC-AE-14003082, ML14086A385, ML14086A386, ML14086A387.

Attachment 3

Response to EMCB Request for Additional Information: RAI 1
Response to EMCB Follow-up RAI dated June 2, 2014

EMCB, Mechanical and Civil Engineering Branch RAI 1

In the application, the licensee provided a qualitative response regarding the structural analysis without any supporting quantitative data. Without actual and allowable stresses and design margins for the various components of the sump strainer structural assembly, the NRC staff is unable to make a determination about the inherent level of conservatism employed in the design. This information was not provided in the licensee's recent submittals concerning Generic Letter (GL) 2004-02, "Potential Impact of Debris Blockage on Emergency Recirculation during Design Basis Accidents at Pressurized-Water Reactors," (ADAMS Accession No. ML042360586).

Please summarize the structural qualification results, including the actual and allowable stresses, and design margins for the various components of the sump strainer structural assembly.

STP Response:

The response to EMCB RAI 1 was provided in the STP letter to NRC Staff dated December 23, 2013, NOC-AE-13003065, ML14015A311.

**EMCB, Mechanical and Civil Engineering Branch RAI 1
(follow-up RAI dated June 2, 2014, ML14155A254)**

By letter dated December 23, 2013 (Agencywide Documents Access and management System (ADAMS) Accession No. ML14015A312, STP Nuclear Operating Company (STPNOC) provided response to the U.S. Nuclear Regulatory Commission (NRC) question

STP-GSI-191-EMCB RAI-1. In response to the NRC staff question, STPNOC provided interaction ratios (IRs) for various components of the strainer assembly for two load cases. All of the IRs were below one, indicating all applicable design code requirements were satisfied, by maintaining actual stresses and loads less than the allowable values. However, it is unclear to the NRC staff what differential pressures the analyzed load cases represent and how they relate to the 5.71 feet (ft.) and 9.35 ft. of equivalent head loss discussed in submittal dated November 13, 2013 ((ADAMS Accession No. ML13323A183). In addition, the risk-informed submittal noted that strainer structural failure was a possible failure mode. This appears to indicate that there are loading conditions where the IR values would be greater than 1 and the strainer could fail. However, Section 6.2.2.2.3 of Attachment 2 to Enclosure 3 of submittal dated November 13, 2013 states, "The sump structures are designed to withstand the maximum expected differential pressure imposed by the accumulation of debris."

Please identify the differential pressure or equivalent head loss associated with the two load cases provided in letter dated December 23, 2013, in response to the RAI question. Please explain if there are conditions which could load the strainers beyond the maximum differential pressure for which they are qualified. Revise the above statement from Section 6.2.2.2.3, as necessary, based on your response.

STP Response:

The two cases tabulated in NOC-AE-13003065 as Cases 1 and 2 used differential pressures of 2.47 psi and 4.00 psi, respectively. Case 1 is for the high temperature case of 267° F. Case 2 is for the low temperature case of 128° F.

The strainer load used for Case 1 is 5.71 ft which is equivalent to 2.47 psi using a density value of 62.4 lb per cubic feet (cold water density was conservatively used). The strainer load used for Case 2 is 9.35 ft which is equivalent to 4.0 psi using a density of 61.58 lb per cubic feet.

Deterministic analysis showed that the strainers do not fail under any design basis loading condition. Those results were provided in the tabulated IR values previously submitted. As noted in the question, all IR values were less than one. Unlike Deterministic analysis, Probabilistic analysis considers failure to be always possible and attempts to quantify the probability. For the Probabilistic analysis, "failure" is defined to be any scenario with a resulting differential pressure greater than 9.35 ft (the highest analyzed in the structural qualification calculation which uses Code allowables). Since Code allowables include considerable margin to actual physical failure, this definition of failure is conservative.

The proposed change to the UFSAR is:

6.2.2.2.3 Containment Emergency Sump Description

At the beginning of the recirculation phase, the minimum water level above the Containment floor is adequate to provide the required NPSH for the ECCS and CSS pumps. The sumps are designed to RG 1.82, proposed Revision 1, May 1983 and with consideration of the debris effects identified in Generic Letter 2004-02, as described in Appendix 6A. The sump structures are designed to limit approach flow velocities to less than 0.009 ft/sec permitting high-density particles to settle out on the floor and minimize the possibility of clogging the strainers. The sump structures are designed to withstand the maximum expected differential pressure imposed by the accumulation of debris. *The risk-informed methodology applied to evaluate the risk associated with effects of debris shows that the increase in risk associated with debris that would exceed the design limits of the sump structures is very small, in accordance with the acceptance criteria of Regulatory Guide 1.174.*

Attachment 4

Response to EPNB Request for Additional Information: RAI 1, 2, 3, 4, 5, 6

Enclosure to Attachment 4

1. Response to EPNB-Consistency of Weld Frequencies with RI-ISI Program: RAI 6

EPNB, Component Performance, NDE and Testing Branch: RAI 1

The NRC staff has reviewed the LOCA frequency estimates in Sections 2.2.3, "LOCA Frequencies," and 5.3, "LOCA Frequency," of Volume 3 and requests the following additional information.

Volume 3, Section 5.3.1, "Relative Weight of Breaks in Specific Weld Categories," page 125, specifies the degradation mechanisms that were considered in the LOCA frequency estimates. The risk-informed inservice inspection (RI-ISI) program at STP was based on EPRI TR-112657, "Revised Risk-Informed Inservice Inspection Evaluation Procedure (PWRMRP-05)," Revision B-A, Final Report, December 1999 (ADAMS Accession No. ML013470102). The NRC staff notes a discrepancy in the degradation mechanisms used between the RI-ISI program and the GSI-191 submittal. Several of the degradation mechanisms in Table 2-2 of EPRI TR-112657 report that are used in the RI-ISI program are not listed as the degradation mechanisms in the GSI-191 calculations. For example, erosion cavitation, corrosion fatigue, corrosion attack, and water hammer identified in Table 2-2 of the EPRI report are not considered in Section 5.3.1. Please discuss the discrepancy.

STP Response:

As described in several places in the LAR (for example, Enclosure 4-1, Section 2.3.5, Enclosure 4-2, Section 2, and Enclosure 4-3, Section 5.3) the EPRI RI-ISI frequencies are not used to directly develop LOCA frequencies. NUREG 1829 (Enclosure 4-3, Reference [37]), frequencies are used as the basis for LOCA frequencies and the EPRI RI-ISI frequencies are only used as weights to distribute the NUREG 1829 frequencies more heavily to locations where degradation mechanisms (DMs) are known to be present. The following summarizes the process used to identify the DMs used in the LAR.

The assessment of DM susceptibility is performed in three steps:

- 1) Independent review of the degradation mechanism evaluation performed for the STP RI-ISI Program [1,2,3,4]
- 2) Systematic review of the current worldwide service experience with Code Class 1 piping in Westinghouse PWR plants, and
- 3) Review of relevant industry reports on material degradation

DM susceptibility screening criteria are applied to determine applicable DM-susceptible locations as referenced in EPRI TR-112657. Only those DMs that apply to the environmental, stress/load conditions, and material types that are found in the STP reactor coolant pressure boundary piping are included.

References:

1. STP Nuclear Operating Company, Relief Request for Application of an Alternative to the ASME Boiler and Pressure Vessel Code Section XI Examination Requirements for Class 1 Piping Welds, RR-ENG-2-16, December 1999, ML003676903.
2. Structural Integrity Associates, Inc., Degradation Mechanism Evaluation for the South Texas Project Electric Generating Station (STPEGS) Units 1 and 2, EPRI-116-330, Rev. 0, December 1999.
3. STP Nuclear Operating Company, Relief Request for Application of an Alternative to the ASME Boiler and Pressure Vessel Code Section XI Requirements for Class 1 Socket Welded Piping and Class 2 Piping Welds, RR-ENG-2-23, February 2001, ML101650285.
4. STP Nuclear Operating Company, Relief Request for Application of an Alternative to the ASME Boiler and Pressure Vessel Code Section XI Requirements for Class 1 and Class 2 Piping Welds, RR-ENG-3-04, September 2011, ML11250A170.

EPNB, Component Performance, NDE and Testing Branch: RAI 2

Volume 3, Section 5.3.1, page 125, states that Table 5.3.1, Category 6B, contains two weld sizes (nominal 0.75-inch and 1-inch pipes). However, Table 2.2.6, Category 6B shows only 1-inch weld size. Please discuss how the LOCA frequency calculations handle this discrepancy. That is, please discuss whether the initiating frequency calculation includes the frequencies from the 0.75-inch and 1-inch pipe sizes or only the 1-inch pipe size is used. This discrepancy also applies to Categories 6A and 8C which also contain two weld sizes.

STP Response:

The initiating frequencies for the 1.5-inch and 2-inch pipe sizes for Category 6A were duplicated in the CASA Grande analysis.

The initiating frequencies for the 0.75-inch and 1-inch pipe sizes for Category 6B were duplicated in the CASA Grande analysis.

The initiating frequencies for the 1.5-inch and 2-inch pipe sizes for Category 8C were duplicated in the CASA Grande analysis.

The frequencies in Section 2.2.3 are used in conjunction with the weld counts in Section 5.3.1.

EPNB, Component Performance, NDE and Testing Branch: RAI 3

Please discuss whether welds evaluated in the GSI-191 analysis contain flaws while in service. If yes, please discuss whether the LOCA frequencies for these welds are increased from that of NUREG-1829 estimates. If the pipe failure probabilities for these welds are not increased, please provide justifications. Volume 3, Table 5.3.1, page 126 shows that four welds at the pressurizer were weld overlaid. Please discuss whether the pipe failure probability LOCA frequencies for these mitigated welds were reduced from the frequency estimates of NUREG-1829. If not, please provide justifications.

STP Response:

The LOCA frequencies associated with the welds in the LAR analysis are not specifically adjusted for flaws from the STP ISI program. LOCA frequencies are used in two ways in the analysis: 1) to form initiating event frequencies in the PRA and 2) to construct a joint probability distribution governing break size and weld in CASA Grande, conditional on a LOCA event. For 1), no adjustment is made relevant to flaws or mitigation; those frequencies are taken from NUREG 1829 directly. In the case of 2), within a break-size category the likelihood for a break at a particular weld is weighted to take into account degradation or mitigation, but the probability of having a break in each category matches the corresponding NUREG 1829 frequency.

Therefore, NUREG 1829 frequencies are preserved in the evaluation for any given break size in a weighting scheme. The method referred to as the 'LOCA-Hybrid method' (see the LOCA-Hybrid Final report, ML12145A466, 2012) as summarized in the LAR (for example, Enclosure 4-1, Section 2.3.5, Enclosure 4-2, Section 2, Enclosure 4-3, Section 5.3) weights the frequency more heavily on welds with higher potential for flaws. The weights are derived based on an industry-wide database of in-service inspection data for weld types, and larger weights are given to the problematic weld types relative to those with fewer flaws detected.

Welds that have been mitigated (replaced with robust weld material, for example Alloy 690, or mitigated with weld overlay) are weighted (again, based on industry-wide data) less heavily in the LOCA-Hybrid method. Both types of these welds are in service at STP, however only the welds that were overlaid on the pressurizer safe ends have been weighted accordingly in the analysis to account for the weld overlays. More definitive explanation of the detailed implementation of the LOCA-Hybrid method has been provided in the response to APLAB CASA Grande-LOCA Frequencies: RAI 4, STP letter to the NRC Staff dated May 22, 2014, ML14149A434.

EPNB, Component Performance, NDE and Testing Branch: RAI 4

Title 10 of the *Code of Federal Regulations* (10 CFR), Part 50, 50.55a(g)(6)(ii)(F) incorporates by reference American Society of Mechanical Engineers Boiler and Pressure Vessel Code (ASME Code) Case N-770-1, "Alternative Examination Requirements and Acceptance Standards for Class 1 PWR Piping and Vessel Nozzle Butt Welds Fabricated with UNS N06082 or UNS W86182 Weld Filler Material With or Without Application of Listed Mitigation Activities, Section XI, Division 1," with conditions. ASME Code Case N-770-1 requires licensees to perform augmented inspections beyond those that are required by the ASME Code, Section XI, for piping with Alloy 82/182 dissimilar butt welds. Please discuss whether periodic inspections per ASME Code Case N-770-1 would reduce the LOCA frequency estimation for the Alloy 82/182 dissimilar metal welds. If yes, please discuss how much LOCA frequency estimates were reduced for these welds.

STP Response:

The STP approach to estimating LOCA frequencies would not change as a result of Section XI inspection. LOCA frequencies are determined using the methodology described in the LOCA-Hybrid approach in the response to APLAB, CASA Grande LOCA Frequencies: RAI 1 provided in the STP letter to the NRC Staff, dated May 22, 2014, ML14149A434.

EPNB, Component Performance, NDE and Testing Branch: RAI 5

Volume 3, Section 5.3.5, "Sample Break Sizes at Each Weld Location," page 149, discusses how the break sizes are selected to derive the LOCA frequency estimates. Figure 5.3.4, page 151, provides the selected break sizes for weld case 1B as an example. (a) Figure 5.3.4 presents a total of 13 breaks being simulated at each weld belonging to Weld Case 1B (10 large breaks, two medium breaks and one small break). However, in Table 2.2.3, under weld case 1B, the NRC staff finds only 12 breaks. Please explain how 13 breaks were identified. (b) Please discuss how the break size distribution scheme in Figure 5.3.4 provides confidence and assurance that the break selection will result in appropriate debris generation as there are many possible scenarios for the break size distribution. The break sizes could be evenly distributed such that there are four small breaks, four medium breaks and four large breaks (assuming the total breaks are 12). The break sizes could be distributed skewed to the small size, such as 10 small breaks, one medium break and one large break. The break size could also be skewed toward medium breaks such as one small break, 10 medium breaks, and one large break. Please discuss how it was determined that the break size distribution in the CASA Grande analysis is appropriate (i.e., neither too conservative nor too non-conservative in terms of the debris generation) when examining the final probability result (the core melt frequency).

STP Response:

a) The entries in Table 2.2.3 define the distribution of annual frequency over break size for each weld case. The 12 break sizes identified in LAR Enclosure 4-3, Table 2.2.3 are not used for the same purpose as the 13 break size ranges plotted in Figure 5.3.4. Therefore, they cannot be compared directly.

The 12 break sizes with their respective frequencies listed in Table 2.2.3 are embedded in the complementary annual frequency distribution (blue curve) of Figure 5.3.4. The vertical dashed and solid lines in Figure 5.3.4 display the 13 sampling bins from which random break sizes are chosen for Case 1B. The number of sampling bins distributed in each break size category is calculated with Equation 25 and 26 (LAR Enclosure 4-3, Page 150). A complete explanation for how 13 sampling bins are identified for Case 1B is provided in Section 5.3.5 of LAR Enclosure 4-3.

Horizontal lines illustrate the annual frequency weights carried by each break size range. The weight for each break scenario is calculated as the difference of the upper and lower complementary annual frequencies that correspond to the bounds of each sampling bin (positive difference of the horizontal lines).

b) There are many possible scenarios for selecting a set of break sizes at each weld. The scenario illustrated in Figure 5.3.4 (Volume 3, Rev. 2, Pg. 151) is built on the complementary annual frequencies of Table 2.2.3 (Volume 3, Rev. 2, Pg. 35) and represents a nonuniform stratified sampling strategy. The break size distribution scheme in Figure 5.3.4 provides confidence and assurance that the break selection will result in appropriate debris generation by assigning a greater number of bins for larger break sizes. This practice ensures higher sampling resolution of the very-low-frequency tails where large breaks generate more debris and are more likely to challenge ECCS safety

systems. Although many more potential failure scenarios are examined by this strategy, no over-conservatism is introduced because the corresponding weighting factors (positive difference of horizontal lines) are proportionally smaller where the sampling resolution is highest.

Rearranging the number of bins in each category may cause insufficient resolution of the tail, if the less probable region (Larger Breaks) has fewer bins than the other categories. Note in figure 5.3.4 that both the break size and the complementary annual frequencies are plotted on logarithmic scales. If a very coarse size resolution is chosen for the large-break range, there may be a vanishingly small chance that any breaks approaching the DEGB condition will be selected at random. The break size distribution in the CASA Grande analysis is neither too conservative nor is it non-conservative in terms of the debris generation because (1) a predominance of larger break scenarios are examined at every weld for possible failure and (2) stratified sampling with non-uniform weighting ensures a statistically unbiased estimate of failure probability. Non-uniform sampling is a common variance reduction technique for estimating low probability events where it is better to have at least a few failure events with small weighting factors than to have no failure events at all.

EPNB, Component Performance, NDE and Testing Branch: RAI 6a

By letter dated September 10, 2012, the NRC approved the risk-informed inservice inspection (RI-ISI) program for the third 10-year inservice inspection interval at STP, Units 1 and 2 (ADAMS Accession No. ML12243A343). Please discuss the following:

- (a) Please state if the LOCA frequency estimates used for welds in the GSI-191 submittal are consistent with the LOCA frequency estimates used in the RI-ISI program. If the comparison is appropriate, please provide numerical examples of the comparison. If the comparison is not appropriate, please provide explanation.**

STP Response:

The LOCA frequency estimates are consistent with NUREG-1829 as described in the response to APLAB, CASA Grande LOCA Frequencies: RAI 1 provided in the STP letter to the NRC Staff, dated May 22, 2014, ML14149A434. These estimates are different than those that would be provided by the EPRI RI-ISI program. Additional explanations are provided in response to EPNB RAI 6b.

EPNB, Component Performance, NDE and Testing Branch: RAI 6b

- (b) If the LOCA frequencies for welds are not consistent between the two analyses, (1) please identify the differences and explain why there are differences, and (2) please discuss why the LOCA frequencies proposed in the GSI-191 submittal are acceptable if they are not consistent with that of the RI-ISI program.**

STP Response:

NUREG-1829 LOCA frequencies are used in the PRA as the basis for LOCA frequency. The Risk-Informed ISI program has, as its purpose, scheduling inspections based on the expectation for finding a flaw for the purpose of mitigation. The statistical basis is therefore inappropriate for LOCA frequency estimates.

The differences in the frequency estimates between the GSI-191 submittal and the RI-ISI program are discussed in more detail in the attached report entitled EPNB-Consistency of Weld Frequencies with RI-ISI Program, Revision 1 (Enclosure 1).

Enclosure to Attachment 4

Enclosure 1 - Response to EPNB-Consistency of Weld Frequencies with RI-ISI Program: RAI 6



NOC-AE-14003105
Attachment 4
Enclosure 1

South Texas Project Risk-Informed GSI-191 Evaluation

Response to
EPNB–Consistency of Weld Frequencies with
RI–ISI Program: RAI 6

Document: STP-RIGSI191-RAI-EPNB-6

Revision: 1.0

Date: June 9, 2014

Prepared by:

Jeremy Tejada, The University of Texas at Austin
John Hasenbein, The University of Texas at Austin
David Morton, The University of Texas at Austin

Reviewed by:

Zahra Mohaghegh, University of Illinois at Urbana-Champaign
Seyed A. Reihani, University of Illinois at Urbana-Champaign

Approved by:

Ernie J. Kee, South Texas Project

Response to EPNB—Consistency of Weld Frequencies with RI-ISI Program: RAI 6

Jeremy Tejada, John Hasenbein, and David Morton
The University of Texas at Austin

Abstract

We investigate the discrepancy in the frequencies of small, medium, and large breaks between: (i) NUREG-1829's [4] mean frequencies, which are used in STP's submittal, and (ii) the point estimates derived directly from RI-ISI values [1]. We further discuss the discrepancy in the conditional probability distribution (given that a break occurred) governing break size and weld case using: (i) the submittal's hybrid approach [3], which fits Johnson distributions to NUREG-1829 [4] percentiles and uses RI-ISI, and (ii) only the RI-ISI point estimates.

1 EPNB—Consistency of Weld Frequencies with RI-ISI Program: RAI 6

The statement of the EPNB—Consistency of Weld Frequencies with RI-ISI Program: RAI 6 is as follows:

By letter dated September 10, 2012, the NRC approved the risk-informed inservice inspection (RI-ISI) program for the third 10-year inservice inspection interval at STP, Units 1 and 2 (ADAMS Accession No. ML12243A343). Please discuss the following:

A) Please state if the LOCA frequency estimates used for welds in the GSI-191 submittal are consistent with the LOCA frequency estimates used in the RI-ISI program. If the comparison is appropriate, please provide numerical examples of the comparison. If the comparison is not appropriate, please provide explanation.

B) If the LOCA frequencies for welds are not consistent between the two analyses, (1) please identify the differences and explain why there are differences, and (2) please discuss why the LOCA frequencies proposed in the GSI-191 submittal are acceptable if they are not consistent with that of the RI-ISI program.

2 Consistency of LOCA Frequency Estimates: GSI-191 Submittal and RI-ISI

The LOCA frequency estimates used for welds in STP's GSI-191 submittal are not consistent with the LOCA frequency estimates used in the RI-ISI analysis. STP's GSI-191 submittal uses a "hybrid approach" detailed in Pan et al. [3], which combines information from the RI-ISI analysis [1] (plant-specific information) with the LOCA frequencies in NUREG-1829 [4] (fleet-wide information).

This lack of consistency in our analysis is by design. Specifically, we maintain consistency with NUREG-1829 frequencies for pipe ruptures at various break sizes, and at the same time, we use plant-specific information [1] to distribute these frequencies across weld cases within a break size. We see our approach as consistent with the NRC's comments [5] on the analysis of [2]. The analyses of [1] and [2] are similar in that they employ information regarding a "frequency of degradation" rather than a "frequency of pipe rupture." We see the RI-ISI analysis [1] as having value in

informing the conditional probability of pipe rupture within a break size, but we use the expert elicitation [4], which focused on pipe ruptures, to inform frequencies of breaks across break sizes.

For the reasons just discussed, we do not see a numerical comparison as necessarily appropriate. That said, in responding to B) we do provide a numerical comparison of the two approaches via: (i) the mean frequencies of small (0.5-inch to 2-inch), medium (2-inch to 6-inch), and large (6-inch and greater) breaks used in STP's PRA, and (ii) the joint probability of break size and weld case, given that there is a break.

3 Estimate of ΔCDF

Our point estimate of ΔCDF informs a two-part analysis in this document. We estimate ΔCDF as follows:

$$\Delta CDF = f_{SL} \cdot \hat{P}(Failure|SL) + f_{ML} \cdot \hat{P}(Failure|ML) + f_{LL} \cdot \hat{P}(Failure|LL). \quad (1)$$

Here, SL , ML , and LL denote the events of a small, medium, or large break, and f_{SL} , f_{ML} , and f_{LL} denote corresponding mean frequencies in events per year. A GSI-191 failure event, whether in the sump or vessel, is denoted $Failure$, and the corresponding \hat{P} terms are conditional probabilities estimated using the CASA Grande simulation model.

The respective frequencies of a small, medium, and large break (f_{SL} , f_{ML} , and f_{LL}) used in STP's submittal are reported in Volume 2's Table 4-1 [6], and match linearly interpolated mean frequencies from Table 7.19 (current-day values) of NUREG-1829 [4]. In Section 4, we compare the frequencies, f_{SL} , f_{ML} , and f_{LL} , based on NUREG-1829 means and based on point estimates from the RI-ISI analysis [1].

STP's submittal further uses a hybrid approach [3], which fits Johnson distributions to NUREG-1829 [4] percentiles and then uses point estimates from the RI-ISI analysis [1] to construct a joint probability distribution governing break size and weld case. Given that we have a LOCA event, this joint distribution is used in the CASA Grande simulation model to form the three estimates of the conditional failure probabilities, $\hat{P}(Failure|SL)$, $\hat{P}(Failure|ML)$, and $\hat{P}(Failure|LL)$, used in equation (1). In Section 5, we compare the joint distributions obtained using the hybrid approach [3] and those derived from the RI-ISI analysis [1].

4 Frequencies of Small, Medium, and Large Breaks

In Table 1 we present the frequencies used in equation (1) based on NUREG-1829 and RI-ISI. The table's "NUREG-1829 Mean" row reports current-day values from Table 7.19 of [4], using linear interpolation to obtain exceedance frequencies for 2-inch and 6-inch breaks, and forming differences to find within-category frequencies for 0.5-2.0-inch breaks and 2.0-6.0-inch breaks. Row "RI-ISI Point Estimate" contains analogous values based on the point estimates reported in [1]. The final row of the table shows the ratios of these frequencies using RI-ISI as the denominator. This row indicates that the NUREG-1829 mean frequencies used in STP's submittal are larger than those of RI-ISI by factors of 4.43, 15.18, and 2.27 for small, medium, and large breaks.

Table 1: Frequencies (events per year) for small, medium, and large breaks for NUREG-1829 and RI-ISI. Here, “Small,” “Medium,” and “Large” correspond to breaks in the 0.5-2.0-inch category, 2.0-6.0-inch category and 6.0-inch-or-greater category.

Method / Break Size	Small	Medium	Large
NUREG-1829 Mean	1.59E-03	3.05E-04	5.20E-06
RI-ISI Point Estimate	3.59E-04	2.01E-05	2.29E-06
Ratio (NUREG/RI-ISI)	4.43	15.18	2.27

5 Probability Distributions Governing Break Size and Weld Case

In Tables 2, 3, and 4 we show the probability distributions governing break size and weld case obtained using the hybrid approach for STP’s submittal and the RI-ISI analysis. The tables report probability distributions governing break size and weld case, conditional on the occurrence of a LOCA, all based on current-day estimates. Table 2 shows the probability of a break falling in the NUREG-1829 categories 1-6 for both methods. Here, the “Hybrid - Johnson Means” row is based on the means of the Johnson distributions fit to the percentiles elicited in NUREG-1829 [4]. The “RI-ISI - Point Estimate” row is based on the point estimates reported in the RI-ISI analysis [1]. The table’s final row shows the ratio of the probabilities for each of the six categories, using the hybrid method as the denominator. The table shows that the RI-ISI analysis has similar probability mass as NUREG-1829 in category 1 and a smaller probability mass in category 2. This decrease in category 2, coupled with the smaller frequency at a 0.5-inch break (normalization by this frequency yields exceedance probabilities) leads to increased probability mass, under RI-ISI, being distributed to categories 3-6 by factors of 2.70, 5.03, 20.38, and 15.68.

Table 3 shows the joint probability distribution across 45 weld cases, again based on current-day estimates for the hybrid approach using the means of the fitted Johnson distributions. The bottom row of Table 3 corresponds to the top row of Table 2. The right-most column of Table 3 shows the conditional probability of a break occurring in each weld case, given that a break occurred. Table 4 presents the same information when using the RI-ISI LOCA frequency point estimates.

Table 2: Conditional LOCA probabilities by category using both the hybrid method with the Johnson means and RI-ISI point estimates. The ratios of the probabilities (latter divided by former) for the two methods are shown in the bottom row. These values are based on current-day estimates.

Method / Category	Cat 1	Cat 2	Cat 3	Cat 4	Cat 5	Cat 6
Hybrid - Johnson Means	8.02E-01	1.91E-01	6.85E-03	6.82E-04	5.12E-05	7.72E-06
RI-ISI - Point Estimate	9.08E-01	6.84E-02	1.85E-02	3.43E-03	1.04E-03	1.21E-04
Ratio (RI-ISI/Hybrid)	1.13	0.36	2.70	5.03	20.38	15.68

Table 3: LOCA probabilities for the 45 weld cases for current-day estimates using the means of the fitted Johnson distributions for current-day estimates.

Weld Case	Cat 1	Cat 2	Cat 3	Cat 4	Cat 5	Cat 6	P(Break)
Weld 1 - 1A	2.92E-03	1.18E-03	1.18E-04	1.83E-05	2.73E-06	1.13E-06	4.24E-03
Weld 2 - 1B	3.90E-05	1.58E-05	1.57E-06	2.45E-07	3.65E-08	1.51E-08	5.66E-05
Weld 3 - 1C	2.27E-05	9.20E-06	9.15E-07	1.42E-07	2.12E-08	8.81E-09	3.30E-05
Weld 4 - 2	1.43E-02	5.84E-03	5.87E-04	9.60E-05	1.28E-05	5.72E-06	2.09E-02
Weld 5 - 3A	1.11E-03	5.10E-04	3.79E-05	5.07E-06	7.34E-07	3.87E-07	1.66E-03
Weld 6 - 3B	1.11E-03	5.10E-04	3.79E-05	5.07E-06	7.34E-07	3.87E-07	1.66E-03
Weld 7 - 3C	6.12E-05	2.82E-05	2.10E-06	2.81E-07	4.06E-08	2.14E-08	9.19E-05
Weld 8 - 3D	1.22E-04	5.65E-05	4.20E-06	5.62E-07	8.13E-08	4.29E-08	1.84E-04
Weld 9 - 4A	1.54E-02	1.10E-02	1.09E-03	1.76E-04	1.52E-05	X	2.77E-02
Weld 10 - 4B	8.24E-04	5.86E-04	5.83E-05	9.37E-06	8.13E-07	X	1.48E-03
Weld 11 - 4C	3.84E-04	2.73E-04	2.72E-05	4.37E-06	3.79E-07	X	6.89E-04
Weld 12 - 4D	7.06E-04	5.02E-04	7.03E-05	X	X	X	1.28E-03
Weld 13 - 5A	2.34E-03	1.74E-03	6.65E-05	5.95E-06	X	X	4.15E-03
Weld 14 - 5B	1.13E-03	8.39E-04	3.75E-05	X	X	X	2.01E-03
Weld 15 - 5C	1.60E-03	1.19E-03	5.31E-05	X	X	X	2.84E-03
Weld 16 - 5D	1.21E-04	8.97E-05	4.01E-06	X	X	X	2.15E-04
Weld 17 - 5E	8.77E-04	6.50E-04	2.49E-05	2.23E-06	X	X	1.55E-03
Weld 18 - 5F	0.00E+00	0.00E+00	0.00E+00	0.00E+00	X	X	0.00E+00
Weld 19 - 5G	1.23E-04	9.09E-05	3.48E-06	3.11E-07	X	X	2.17E-04
Weld 20 - 5H	6.05E-05	4.48E-05	2.00E-06	X	X	X	1.07E-04
Weld 21 - 5I	1.62E-04	1.60E-04	X	X	X	X	3.22E-04
Weld 22 - 5J	0.00E+00	0.00E+00	0.00E+00	0.00E+00	X	X	0.00E+00
Weld 23 - 6A	3.52E-02	3.20E-02	X	X	X	X	6.72E-02
Weld 24 - 6B	5.47E-01	X	X	X	X	X	5.47E-01
Weld 25 - 7A	1.03E-01	7.76E-02	2.68E-03	1.91E-04	1.64E-05	X	1.83E-01
Weld 26 - 7B	4.40E-02	3.33E-02	1.15E-03	1.10E-04	X	X	7.85E-02
Weld 27 - 7C	1.64E-02	1.24E-02	4.27E-04	4.10E-05	X	X	2.92E-02
Weld 28 - 7D	1.87E-03	1.41E-03	4.88E-05	3.48E-06	3.00E-07	X	3.34E-03
Weld 29 - 7E	1.15E-03	8.65E-04	2.99E-05	2.13E-06	1.83E-07	X	2.04E-03
Weld 30 - 7F	6.03E-04	4.55E-04	1.57E-05	1.12E-06	9.65E-08	X	1.08E-03
Weld 31 - 7G	8.44E-04	6.38E-04	2.20E-05	2.11E-06	X	X	1.51E-03
Weld 32 - 7H	4.62E-04	3.49E-04	1.21E-05	1.16E-06	X	X	8.24E-04
Weld 33 - 7I	1.00E-04	7.59E-05	3.09E-06	X	X	X	1.79E-04
Weld 34 - 7J	1.81E-04	1.37E-04	5.56E-06	X	X	X	3.23E-04
Weld 35 - 7K	2.01E-04	1.98E-04	X	X	X	X	3.99E-04
Weld 36 - 7L	0.00E+00	0.00E+00	X	X	X	X	0.00E+00
Weld 37 - 7M	0.00E+00	0.00E+00	0.00E+00	0.00E+00	0.00E+00	X	0.00E+00
Weld 38 - 7N	3.20E-03	2.41E-03	8.37E-05	5.98E-06	5.15E-07	X	5.70E-03
Weld 39 - 7O	1.65E-04	1.25E-04	4.33E-06	3.10E-07	2.66E-08	X	2.95E-04
Weld 40 - 8A	7.55E-04	5.65E-04	2.35E-05	X	X	X	1.34E-03
Weld 41 - 8B	1.44E-03	1.07E-03	4.46E-05	X	X	X	2.55E-03
Weld 42 - 8C	1.55E-03	1.16E-03	4.83E-05	X	X	X	2.76E-03
Weld 43 - 8D	1.98E-04	1.48E-04	6.17E-06	X	X	X	3.53E-04
Weld 44 - 8E	5.63E-04	4.21E-04	1.75E-05	X	X	X	1.00E-03
Weld 45 - 8F	3.30E-05	2.47E-05	1.03E-06	X	X	X	5.88E-05
P(Break)	8.02E-01	1.91E-01	6.85E-03	6.82E-04	5.12E-05	7.72E-06	1.00E+00

Table 4: LOCA probabilities for the 45 weld cases for current-day estimates using the point estimates from RI-ISI [1] for current-day estimates.

Weld Case	Cat 1	Cat 2	Cat 3	Cat 4	Cat 5	Cat 6	P(Break)
Weld 1 - 1A	3.31E-03	4.25E-04	3.18E-04	9.23E-05	5.57E-05	1.78E-05	4.22E-03
Weld 2 - 1B	4.42E-05	5.67E-06	4.24E-06	1.23E-06	7.44E-07	2.37E-07	5.63E-05
Weld 3 - 1C	2.57E-05	3.30E-06	2.47E-06	7.17E-07	4.33E-07	1.38E-07	3.28E-05
Weld 4 - 2	1.62E-02	2.10E-03	1.58E-03	4.83E-04	2.61E-04	8.97E-05	2.07E-02
Weld 5 - 3A	1.25E-03	1.83E-04	1.02E-04	2.55E-05	1.50E-05	6.07E-06	1.58E-03
Weld 6 - 3B	1.25E-03	1.83E-04	1.02E-04	2.55E-05	1.50E-05	6.07E-06	1.58E-03
Weld 7 - 3C	6.94E-05	1.01E-05	5.66E-06	1.41E-06	8.28E-07	3.36E-07	8.77E-05
Weld 8 - 3D	1.39E-04	2.03E-05	1.13E-05	2.83E-06	1.66E-06	6.73E-07	1.75E-04
Weld 9 - 4A	1.75E-02	3.94E-03	2.95E-03	8.84E-04	3.10E-04	X	2.56E-02
Weld 10 - 4B	9.34E-04	2.10E-04	1.57E-04	4.72E-05	1.66E-05	X	1.37E-03
Weld 11 - 4C	4.35E-04	9.81E-05	7.33E-05	2.20E-05	7.72E-06	X	6.36E-04
Weld 12 - 4D	8.00E-04	1.80E-04	1.89E-04	X	X	X	1.17E-03
Weld 13 - 5A	2.65E-03	6.24E-04	1.79E-04	3.00E-05	X	X	3.49E-03
Weld 14 - 5B	1.28E-03	3.01E-04	1.01E-04	X	X	X	1.68E-03
Weld 15 - 5C	1.82E-03	4.27E-04	1.43E-04	X	X	X	2.39E-03
Weld 16 - 5D	1.37E-04	3.22E-05	1.08E-05	X	X	X	1.80E-04
Weld 17 - 5E	9.94E-04	2.33E-04	6.71E-05	1.12E-05	X	X	1.31E-03
Weld 18 - 5F	0.00E+00	0.00E+00	0.00E+00	0.00E+00	X	X	0.00E+00
Weld 19 - 5G	1.39E-04	3.26E-05	9.38E-06	1.57E-06	X	X	1.82E-04
Weld 20 - 5H	6.85E-05	1.61E-05	5.40E-06	X	X	X	9.00E-05
Weld 21 - 5I	1.83E-04	5.75E-05	X	X	X	X	2.41E-04
Weld 22 - 5J	0.00E+00	0.00E+00	0.00E+00	0.00E+00	X	X	0.00E+00
Weld 23 - 6A	3.99E-02	1.15E-02	X	X	X	X	5.14E-02
Weld 24 - 6B	6.20E-01	X	X	X	X	X	6.20E-01
Weld 25 - 7A	1.16E-01	2.79E-02	7.23E-03	9.60E-04	3.35E-04	X	1.53E-01
Weld 26 - 7B	4.99E-02	1.19E-02	3.10E-03	5.55E-04	X	X	6.55E-02
Weld 27 - 7C	1.85E-02	4.44E-03	1.15E-03	2.07E-04	X	X	2.43E-02
Weld 28 - 7D	2.12E-03	5.08E-04	1.32E-04	1.75E-05	6.11E-06	X	2.78E-03
Weld 29 - 7E	1.30E-03	3.11E-04	8.06E-05	1.07E-05	3.74E-06	X	1.70E-03
Weld 30 - 7F	6.83E-04	1.64E-04	4.24E-05	5.64E-06	1.97E-06	X	8.96E-04
Weld 31 - 7G	9.56E-04	2.29E-04	5.94E-05	1.06E-05	X	X	1.26E-03
Weld 32 - 7H	5.24E-04	1.25E-04	3.25E-05	5.83E-06	X	X	6.87E-04
Weld 33 - 7I	1.14E-04	2.73E-05	8.34E-06	X	X	X	1.49E-04
Weld 34 - 7J	2.05E-04	4.91E-05	1.50E-05	X	X	X	2.69E-04
Weld 35 - 7K	2.28E-04	7.12E-05	X	X	X	X	2.99E-04
Weld 36 - 7L	0.00E+00	0.00E+00	X	X	X	X	0.00E+00
Weld 37 - 7M	0.00E+00	0.00E+00	0.00E+00	0.00E+00	0.00E+00	X	0.00E+00
Weld 38 - 7N	3.62E-03	8.66E-04	2.26E-04	3.01E-05	1.05E-05	X	4.75E-03
Weld 39 - 7O	1.87E-04	4.48E-05	1.17E-05	1.56E-06	5.43E-07	X	2.46E-04
Weld 40 - 8A	8.56E-04	2.03E-04	6.34E-05	X	X	X	1.12E-03
Weld 41 - 8B	1.63E-03	3.85E-04	1.20E-04	X	X	X	2.13E-03
Weld 42 - 8C	1.76E-03	4.17E-04	1.30E-04	X	X	X	2.31E-03
Weld 43 - 8D	2.25E-04	5.32E-05	1.66E-05	X	X	X	2.94E-04
Weld 44 - 8E	6.38E-04	1.51E-04	4.72E-05	X	X	X	8.37E-04
Weld 45 - 8F	3.74E-05	8.87E-06	2.77E-06	X	X	X	4.91E-05
P(Break)	9.08E-01	6.84E-02	1.85E-02	3.43E-03	1.04E-03	1.21E-04	1.00E+00

6 Summary

Estimates of pipe rupture frequencies inform two key aspects of the analysis in STP's GSI-191 submittal. These two aspects are apparent in equation (1), which involves mean frequencies of small, medium, and large breaks and conditional failure probabilities. The former are precisely the frequencies that we discuss in Section 4, and estimates of the latter probabilities are formed using CASA Grande, based on the joint probability distributions that we discuss in Section 5. In both cases, we preserve characteristics of NUREG-1829, an expert elicitation concerning pipe rupture frequencies.

The mean frequencies reported in NUREG-1829 [4] are preserved in the mean frequencies denoted f_{SL} , f_{ML} , and f_{LL} in equation (1). In Section 4, we indicate that if we were to instead use RI-ISI, these three frequencies would decrease by factors of 4.43, 15.18, and 2.27 for small, medium, and large breaks.

The 5th, 50th, and 95th percentiles of NUREG-1829 frequencies are preserved in the Johnson distributions used in our hybrid approach [3], and we further use the relative frequencies in RI-ISI [1] to allocate failures within a break-size category across weld cases. If we instead use only RI-ISI frequencies to construct the distribution over break size and weld case, the probability mass increases by factors of 5.03, 20.38, and 15.68 in the respective categories 4, 5, and 6. This result occurs for three primary reasons: (i) the exceedance frequency at the smallest break size (0.5 inch) is smaller in RI-ISI [1] than NUREG-1829 by a factor of nearly five (compare current-day 0.5-inch exceedance frequencies in Table 5-6 in [1] and Table 7.19 in [4]); (ii) category 2 in RI-ISI has a smaller probability mass than that from NUREG-1829 by a factor of 0.36 (see Table 2 in Section 5); and, (iii) the degradation-based frequencies in RI-ISI [1] drop off more slowly than the pipe-rupture frequencies in NUREG-1829, particularly in categories 4-6.

We note that observation (iii) is consistent with the flatter trends at larger pipe sizes reported in the "degradation frequency" analysis of [2]. That said, the approach in STP's submittal instead matches the trends in NUREG-1829 at larger pipe sizes, consistent with comments in [5].

References

- [1] K. N. Fleming, B. O. Lydell, and D. Chrun (2013, January). Development of LOCA Initiating Event Frequencies for South Texas Project GSI-191. Technical Report, KnF Consulting Services, LLC, Spokane, WA.
- [2] L. E. Hochreiter (2005, December). Data Collection of Pipe Failures Occuring in Stainless Steel and Carbon Steel Piping. NucE 597D - Project 1, Pennsylvania State University.
- [3] Y.-A. Pan, E. Popova, and D. P. Morton (2013, January). Modeling and Sampling LOCA Frequency and Break Size. Technical report, STP-RIGSI191-V03.02, Revision 4, The University of Texas at Austin.
- [4] R. Tregoning, P. Scott, and A. Csontos (2008, April). Estimating Loss-of-Coolant Accident (LOCA) Frequencies Through the Elicitation Process: Main Report (NUREG-1829). NUREG 1829, NRC, Washington, DC.
- [5] J. L. Uhle (2005, December). NRC Comments on Pennsylvania State University Study of Pipe Failure Data. NRC, Washington, DC.
- [6] D. Wakefield and D. Johnson (2013, October). South Texas Project Risk-Informed GSI-191 Evaluation, Volume 2, Probabilistic Risk Analysis: Determination of Change in Core Damage Frequency and Large Early Release Frequency Due to GSI-191 Issues. Technical report, STP-RIGSI191-VO2, Revision 2, ABSG Consulting Inc.

Attachment 5

Response to ESGB Request for Additional Information:

- a. Chemical Effects: RAI 1, 2, 4, 5, 6, 8, 9, 10, 14, 15, 16, 18, 21
- b. Coatings: RAI 1, 6

Enclosure to Attachment 5

- 1. Leavitt, J.J. and Kee, E., ALION-REP-STP-8998-08 Rev. 0, Quantification of Chemical Head Loss Epistemic Uncertainty; Basis for Incremental Chemical Head Loss Correlation, May 2014.

ESGB, Chemical Effects: RAI 1a

The exponential probability density functions (PDF) for small-, medium-, and large-break LOCAs (e.g., Figure 5.6.4, Volume 3) are shown in terms of a chemical bump-up factor. The NRC staff has questions related to the conventional (non-chemical) head loss correlation. The review of a chemical bump-up factor is complicated by the fact that it is essentially a multiplier on a parameter that is concurrently being reviewed for adequacy. Please provide the following additional information.

- (a) **CASA Grande calculates the conventional head loss value for a given break and then applies a chemical bump-up factor independent of the conventional head loss. Please justify not correlating the chemical bump up factor to the conventional head loss since the same debris bed affects both values. Based on the NRC staff's experience observing testing, head loss for a given quantity of chemical precipitates should be related to both the type of precipitate and the filtering characteristics of the debris bed.**

STP Response:

Although chemical effects have not been found to be significant contributors to STP post-LOCA sump conditions, CASA Grande evaluates a chemical contribution based on break size to provide safety margin in the analysis. Two levels of possible correlation between conventional and chemical induced head loss can be defined: (1) the relationship between conventional debris head loss and the attributes of the chemical head-loss factor distributions applied across LOCA categories of SBLOCA, MBLOCA, and LBLOCA, and (2) the relationship between conventional debris head loss and values of the chemical head-loss factor sampled from within a LOCA category. The LAR analysis does include the first type of correlation by applying larger chemical head-loss factors to larger breaks where the conventional debris head loss is also expected to be higher. The LAR analysis does not enforce the second type of correlation (direct correlation between conventional debris head loss and chemical head-loss factors sampled for scenarios within a LOCA category). Uncorrelated sampling spreads the variance of the exponential chemical effect head-loss distributions across all break sizes and introduces an opportunity for small breaks to receive large chemical head-loss factors. Responses ESGB RAI 5 and ESGB RAI 1d discuss the possible effects of enforcing an inverse correlation between break size and chemical head-loss factor.

Although both type of precipitate and filtering characteristics of the debris bed do affect total head loss, head-loss factors described in LAR Enclosure 4-3, Table 5.6.4 were used in the CASA Grande analysis because the distributions apply values derived from the multiplicative response of a STP design-basis debris bed (DBA) to the maximum chemical load (LAR Enclosure 4-3, Reference [53], [1]) as described in the response to ESGB RAI 1c. However, total head loss assessed by the CASA Grande analysis may be underestimated for thin bed cases. Thin bed cases may have small conventional head loss but still have relatively large chemical head loss. Such head losses may be as high as those measured in STP DBA (bounding) conditions [Enclosure 1, Section 4.1 and 4.5].

Given this possible discrepancy, an alternative additive chemically-induced head loss calculation was performed [Enclosure 1]. The calculation method incorporates both the type of precipitate and STP DBA debris bed-per-surface area response to quantify total head loss. Results of this alternative calculation support the conclusion that the head-loss factor approach applied in the LAR is likely conservative for conditions with high conventional head loss [Enclosure 1, Section 4.5], but also demonstrates the suspected underestimation of total head loss for smaller breaks from application of smaller head-loss factors than the LBLOCA head-loss factor [Enclosure 1, Section 4.1 and Section 4.5]. However, this alternative calculation also demonstrates that addition of a maximum chemically-induced head loss response resulting from precipitate masses generated by WCAP-16530-NP release equations to conventional debris head loss may not increase failures [Enclosure 1, Section 4.5], and therefore, the risk estimate is largely unchanged.

References:

1. Westinghouse, "South Texas Project GSI-191 Chemistry Effects Evaluation CN-CSA-06-6," Westinghouse Electric Company, December 2006.

ESGB, Chemical Effects: RAI 1b

(b) In order to help the NRC staff judge the magnitude of the chemical head loss bump-up factor, please provide, by performing realizations for the existing CASA Grande model, a relative frequency plot of chemical effects for STP in terms of absolute units (e.g., feet of water) for the small-break LOCA (SBLOCA), medium-break LOCA (MBLOCA), and large-break LOCA (LBLOCA). For example, a histogram showing chemical head loss (feet) on the x-axis and number of occurrences on the y-axis would be very useful to the staff.

STP Response:

Histograms of chemical head loss vs frequency for CASA Grande Case 01 (all equipment operates) are presented by Figures 1 and 2. Of the large breaks analyzed in Case 01, only 77% formed a thin bed or larger and the resulting chemical head loss for all large breaks ranged between 0 and 154.9 ft as shown by Figure 1. Of the medium breaks analyzed in Case 01, 1.3% formed a thin bed or larger and the resulting chemical head loss for all medium breaks ranged between 0 and 0.14 ft as shown by Figure 2. Small break LOCA are not listed because none of the cases analyzed in CASA Grande Case 01 formed a thin bed or greater.

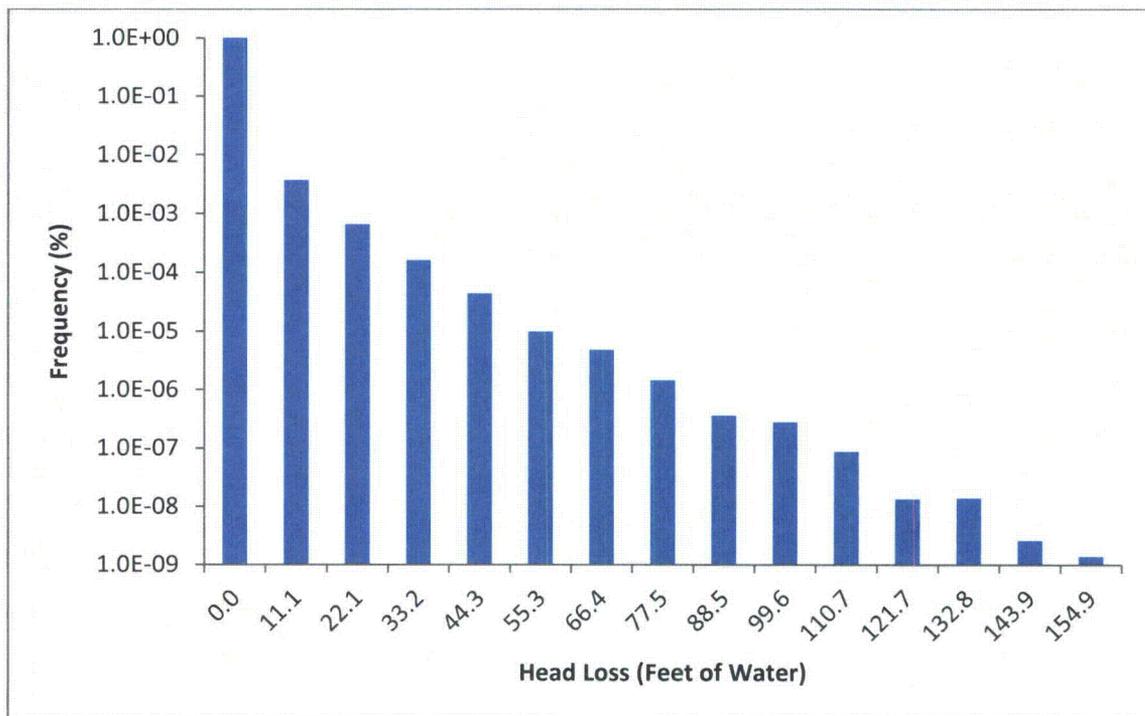


Figure 1: Large break chemical head loss as a function of relative frequency (log scale)

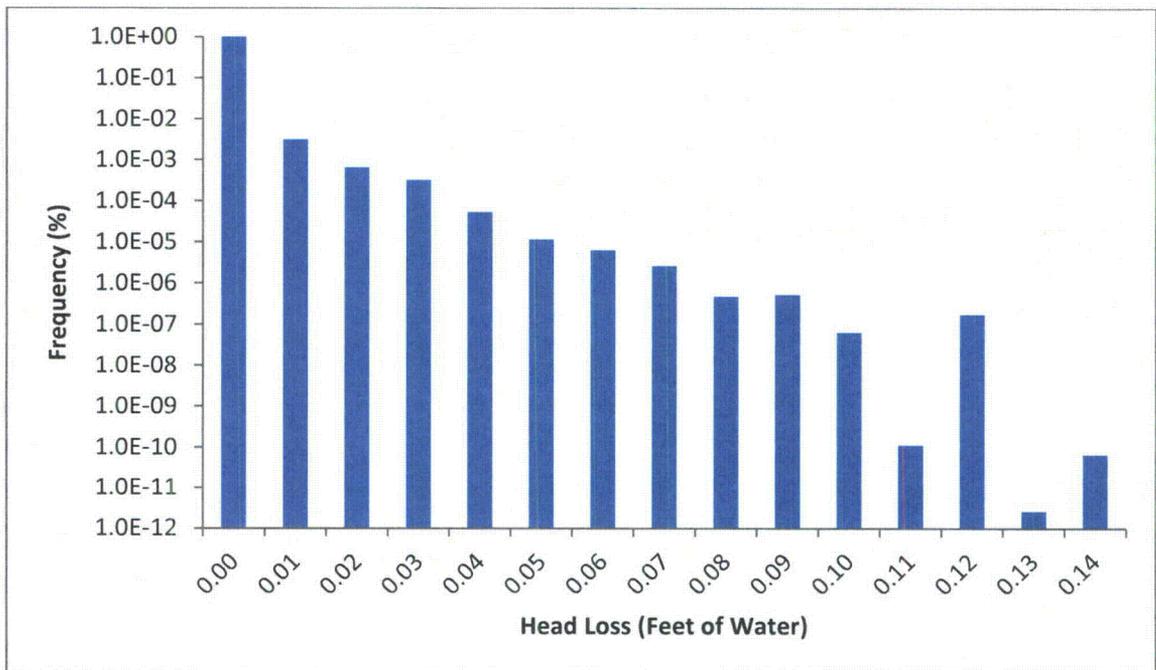


Figure 2: Medium break chemical head loss as a function of relative frequency (log scale)

ESGB, Chemical Effects: RAI 1c

- (c) Please provide additional details on how the results from the Chemical Head Loss Experiment (CHLE) testing, WCAP-16530-NP-A, "Evaluation of Post-Accident Chemical Effects in Containment Sump Fluids to Support GSI-191," March 2008 (ADAMS Accession No. ML081150379), calculations, and reasonable engineering judgment were used in the development of the exponential PDF. In addition, please supply the basis for choosing the exponential form of the PDF over others (e.g., Weibull).**

STP Response:

The single-parameter exponential PDF was chosen for shape and for convenience of fitting the desired statistics of the mean and a truncated tail probability. The exponential PDF was not selected to match an underlying physical process (exponential PDF is commonly used to describe time between failures) or to replicate a large body of data. In this application, the exponential PDF is applied as a subjective probability distribution that places the highest probability near the minimum chemical head-loss factor of 1.0 and rapidly declines across all positive values. Other PDFs including Weibull, gamma and beta that support unimodal, monotonically declining shapes could have been adapted for this purpose. The following discussion explains how the exponential statistics were specified.

The standard exponential PDF was adapted for use with the multiplicative (chemical "bump up") approach described in LAR Enclosure 4-3. First, addition of chemicals to a fiber bed should never reduce existing head loss associated with conventional debris accumulation at the ECCS strainer, so the PDF was shifted to a minimum factor of 1.0 (one). Also, STP CHLE tests with representative aluminum and fiberglass surface-area to water-volume ratios indicated that precipitation of chemical products was unlikely (LAR Enclosure 4-3 Reference [18-19]) While the STP CHLE test do not cover the full space of LOCA scenarios, the STP CHLE tests do simulate the most probable cases expected within the medium and large break categories. Therefore, a multiplier close to 1.0 (one) defined as the mode of the shifted exponential PDF represents the most probable cases.

The mean of the exponential PDF was determined from evaluation of STP ECCS strainer testing (LAR Enclosure 4-3, Reference [53]). The design-basis debris bed, having maximum debris volume and mass associated with a 7D ZOI, was determined to be the "bounding" scenario for STP because the quantity of debris observed on the strainer surface was significantly less than 1/8" thick; therefore the assessment of a thin bed was unnecessary (LAR Enclosure 4-3, Reference [53]). The applied chemical precipitate test load was representative of precipitate quantities generated from 30-day, continuous spray exposure of deterministically bounding materials (1, Table 6.3-7). Chemically-induced head loss attributable to the worst case precipitate load increased the design-basis conventional head loss by a factor of 2.25 (LAR Enclosure 4-3, Reference [53]). For added conservatism, the SBLOCA mean was set equal to this observation, while MBLOCA and LBOCA means were increased to 2.5 and 3.0, respectively. In this context, conservatism is applied because the assigned expectations (means) are higher than test data indicate.

The maxima of the exponential PDFs were confirmed to be values capable of producing a quantifiable number of chemically induced failures in combination with the spectrum of conventional head loss experienced within each break size. This approach is judged acceptable because the means for each break type already capture chemically induced head loss attributable to a bounding precipitate load observed across the bounding debris bed. The maximum factors for SBLOCA, MBLOCA, and LBLOCA chemical head loss were 6.8, 8.1, and 10.7 times larger, respectively, than the 2.25 factor increase of maximum head loss observed in testing under design-basis conditions.

Regarding development of the single-parameter exponential distributions, only the mean is needed to fully specify the distribution; so the maximum was manually confirmed as being reasonable to represent all larger factors with a cumulative tail probability of $1E-5$. The maximum was not imposed as an additional constraint on the distribution itself.

Reference:

1. Westinghouse, "South Texas Project GSI-191 Chemistry Effects Evaluation CN-CSA-06-6," Westinghouse Electric Company, December 2006.

ESGB, Chemical Effects: RAI 1d

- (d) Please provide a detailed technical basis for the mean bump up factors shown for the SBLOCA, MBLOCA, and LBLOCA. The NRC staff has observed head loss testing where the greatest chemical bump-up factors are associated with thinner beds. Please discuss why the mean bump up factor would be higher for a LBLOCA. Please explain if it is more probable that a debris bed for smaller and medium breaks (assuming the bed coverage criterion is met) would consist primarily of fiber fines that are the most readily transportable to the strainer. In general, finer fiber beds tend to lead to greater head loss.**

STP Response:

Means of the exponential PDFs were determined from evaluation of STP ECCS strainer testing (LAR Enclosure 4-3, Reference [53]) as discussed in the ESGB RAI 1c response. In summary, chemically-induced head loss observed in the STP ECCS strainer testing, attributable to the complete addition of the worst case precipitate load [1], increased the design-basis conventional head loss by a factor of 2.25 (LAR Enclosure 4-3, Reference [53]). The SBLOCA mean was set equal to this observation, while MBLOCA and LBLOCA means were increased to 2.5 and 3.0, respectively. Assigning LBLOCA and MBLOCA higher means and setting the SBLOCA mean equal to the test observation provides conservatism because the assigned expectations (means) are higher than STP design-basis strainer test data indicate. Tails of the exponential PDFs provide for even higher chemical effects consistent with staff observations of thin-bed strainer tests.

Analysis of chemically-induced head loss using an additive approach described in Enclosure 1 that calculates ECCS strainer head loss as a function of both precipitate type and STP design-basis-debris per strainer area indicates that the mean head loss factor used in the chemical model (LAR, Enclosure 4-3, Section 5.6.3) should likely increase with decreasing break size [Enclosure 1, Section 4.1 and 4.5]. The results obtained by Enclosure 1 are also in agreement with the cited observations where the greatest chemical head loss factors are associated with thinner beds as described in the response to ESGB RAI 1a. Although it is likely that means related to smaller breaks in the CASA Grande analysis should be larger than the mean of the LBLOCA, increasing the means for smaller breaks will not increase risk because the LBLOCA mean in CASA Case 01 (all equipment operates) is higher than the experimental observation and most failures occur for large breaks. A sensitivity study of smaller-break means indicated that a mean of 60 for smaller breaks does not increase risk. A mean of 60 for smaller breaks is a much larger chemical head loss factor than necessary to adequately assess the multiplicative effect on conventional head loss from precipitate loading [Enclosure 1, Section 4.1]. This conservatism is also demonstrated by the sensitivity analysis discussed in the response to ESGB RAI 5.

It is not more probable that a debris bed for small and medium breaks (compared to large breaks) would consist primarily of fiber fines. In the hypothetical case of breaks that occur inside of a containment building that is totally filled with LDFG (uniform fiberglass everywhere), every break generates the same volumetric proportion of fines, small pieces, large pieces and intact blankets (LAR Enclosure 4-3, Reference

[46], Table 3.1.3). Then, one set of debris-size dependent transport fractions is applied for every break (see debris transport logic diagrams in LAR Enclosure 4-3, Figure 5.5.2 – Figure 5.5.4, Pages 165 – 166). Finally, once debris arrives at the pool ALL fines and small pieces are assumed to transport. Thus, the composition of fiber arriving at the strainer is identical for all break sizes, but the volumes increase with increasing break size. At the strainer, all LDFG is treated with the properties of individual fibers for head loss calculation, regardless of its original destruction size.

References:

1. Westinghouse, "South Texas Project GSI-191 Chemistry Effects Evaluation CN-CSA-06-6," Westinghouse Electric Company, December 2006.

ESGB, Chemical Effects: RAI 2

Please explain how the highest head loss values (e.g., 90th, 95th percentile) obtained using CASA Grande compare with the head loss values obtained from the STP plant-specific strainer tests at Alden Laboratory. Please discuss both in terms of conventional head loss (i.e., before addition of chemical precipitates) and after chemical precipitates were added. Please discuss all strainer test results including the test that was terminated prior to addition of precipitates.

STP Response:

Table 1 displays the maximum conventional head loss and the maximum total head loss (i.e., after the addition of chemical precipitates) for all the relevant STP plant-specific strainer tests conducted at ARL. Table 1 also displays the corresponding LBLOCA head loss percentiles for CASA Grande Case 01 (all equipment operates).

Table 1: Head Loss Test Maximum and Corresponding Percentile

Test	Conventional Head Loss		Total Head Loss	
	Tested Maximum	Percentile for Case 01 LBLOCAs	Tested Maximum	Percentile for Case 01 LBLOCAs
Test 3, Feb.	> 15 ft	N/A	N/A	N/A
Test 4, Feb.	5.6 ft	99.96%	8.8 ft	99.51%
Test 5, Feb.	4.8 ft	99.81%	7.2 ft	99.34%
Test 2, Jul.	4.9 ft	99.83%	9.1 ft	99.53%

N/A, this result is not bounded by CASA Grande analysis.

(Test 1 in February and July were clean screen head loss tests. Test 2 in February was a fiber only test.)

Even though the February head loss tests were superseded by the July head loss tests, because the February tests used walnut flour as a particulate surrogate (determined to be non-representative with regard to walnut flour), the CASA Grande head loss population for Casa Grande Case 01 bounded all the results except for the conventional head loss of Test 3 in February. Test 3 was terminated after large head losses, greater than 15 ft, were observed following the addition of fine fibrous debris (2); as already stated, this test used walnut flour as a particulate surrogate and was superseded.

As expected the DBA tests occurred in the tails of the distribution.

The following maxima are for CASA Grande Case 01. The maximum conventional CASA Grande head loss was 8.2 ft. The maximum total CASA Grande head loss was 161.9 ft.

For the head loss comparisons cited above, the head losses were not corrected to a common flow rate and temperature, which is conservative as stated in the response to ESGB, Steam Generator Tube Integrity and Chemical Engineering – Chemical Effects:

RAI 20 in STP letter to NRC dated June 25, 2014, NOC-AE-14003101, ML14178A481 and ML14178A485).

References:

1. 0415-0100067WN / 0415-0200067WN. "South Texas Project Test Plan Feb 2008". Revision A. 11/24/2008
2. 0415-0100069WN / 0415-0200069WN. "South Texas Project Test Report for ECCS Strainer Performance Testing Feb 2008". Revision A. 11/24/2008
3. 0415-0100070WN / 0415-0200070WN. "South Texas Project Test Plan." Revision A. 8/14/2008.
4. 0415-0100071WN / 0415-0200071WN. "South Texas Project Test Report for ECCS Strainer Testing July 2008". Revision A. 11/24/2008.

ESGB, Chemical Effects: RAI 4

Please provide the results of a sensitivity study related to the assumption of the tail probability that shows how different assumptions (e.g., 1E-02, 1E-03, 1E-04) for the maximum chemical effects bump-up tail would affect the probability of exceeding the ECCS pumps NPSH criteria and the impact to the core damage frequency and large early release frequency. Please evaluate these tail probabilities assuming the conventional head loss is constant and equal to (a) 0.5 feet, (b) 1.0 feet, and (c) 2 feet.

STP Response:

A sensitivity study related to chemical head-loss factor tail probability was not performed concurrently with constant conventional head loss because this assumption would not generate meaningful risk-informed results that could be compared to the baseline. Baseline conventional head loss is computed as a function of water temperature, which complicates the requested comparison. However, a study was performed using CASA Grande Case 01 (all equipment operates) chemical head-loss factors with tail probabilities ranging from 1E-1 to 0.1E-9 to assess changes in ΔCDF referenced to the base case. As shown in Figure 1, decreasing the tail probability increases the ΔCDF ratio while increasing the tail probability decreases the ΔCDF ratio. It should be noted that because the exponential distribution is a single-parameter function, the concurrent maxima also decrease with increasing tail probability. All cases except the first (1E-1) were run with the same number of statistical samples to illustrate that the variance grows as expected when the same samples are spread over a wider span of the parameter.

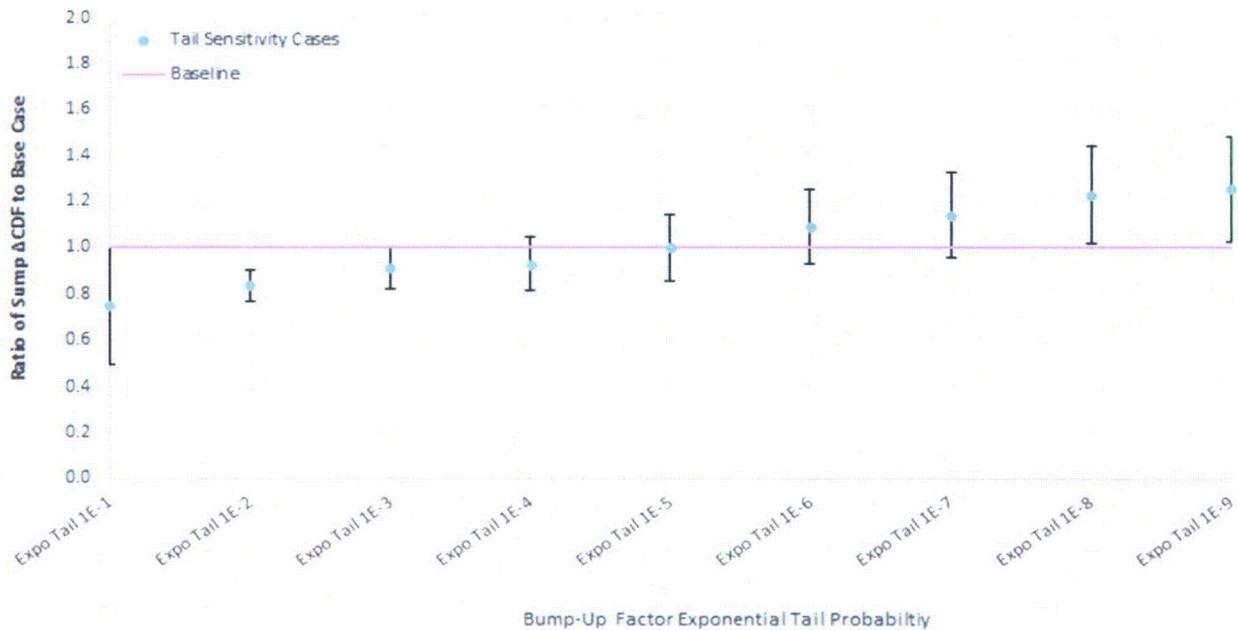


Figure 1: Sensitivity of ΔCDF to chemical effects tail probability for CASA Grande Case 01.

ESGB, Chemical Effects: RAI 5

Since the STP chemical effects evaluation is heavily dependent on engineering judgment, the NRC staff needs clarification regarding the sensitivity of various assumptions to the overall risk informed evaluation. In addition to the sensitivity study requests contained in other chemical effects RAIs (e.g., RAI#4), please evaluate the key chemical effects area assumptions (e.g., bump up factors, type of distribution, etc.) and provide sensitivity studies that will help the staff to evaluate how changes in those assumptions will alter the probability of failures. Please identify any assumptions that are correlated and explain how the correlation was considered in the analysis.

STP Response:

The CASA Grande model assesses head loss from possible chemical sources by applying a distribution of chemical head-loss factors as a function of break category (LAR Enclosure 4-3, Table 5.6.4) as described in LAR Enclosure 4-3, Section 5.6.3. Expected values (means) of the chemical head-loss factor distributions reflect the maximum observed conventional head loss increase of a design basis bed (LAR Enclosure 4-3, Reference [53]) from the complete addition of a precipitate load generated under the assumptions of 30-day, continuous spray exposure of deterministically bounding materials (LAR Enclosure 4-3, Reference [53], [1]). Although the distributions are correlated to each LOCA category by virtue of their separately defined means, magnitudes of the head-loss effects are not directly linked to estimated material release for each break condition assessed by CASA Grande; the conservative chemical inventory is assumed for all break scenarios.

Key parameters that may influence the chemical model performance are (1) use of the 140°F temperature criterion for application of the chemical head-loss factor, (2) selection of chemical head-loss factor mean values, (3) distribution type and (4) application of a thin-bed filtration criterion. Of the four key parameters listed, the type of the statistics distribution chosen for implementation of the chemical head-loss factors and the application of the thin-bed filtration criterion do not affect risk. Exponential distributions were chosen as a single parameter distribution with a shape controlled by the mean and an analytic probability integral for reporting maxima related to a fixed tail probability. Many choices of truncated distributions could be used with equal effect to preserve desired statistics. Sensitivity analysis of the thin bed criterion resulted in a ratio of one as shown by Figure 1 for contributions from sump-strainer failures computed when the thin bed criterion was removed divided by contributions from sump-strainer failures computed for the baseline, indicating a null effect of the thin bed criterion on risk.

To evaluate the effects of the remaining key parameters on CASA Grande results, sensitivity studies were performed. That showed no sensitivity to the temperature threshold. These sensitivity cases were run with the following assumptions: (1) with the 140°F temperature threshold applied (blue dots), and (2) without a temperature threshold applied (green dots). All calculations shown here do apply the thin-bed criterion for application of the chemical head-loss factors.

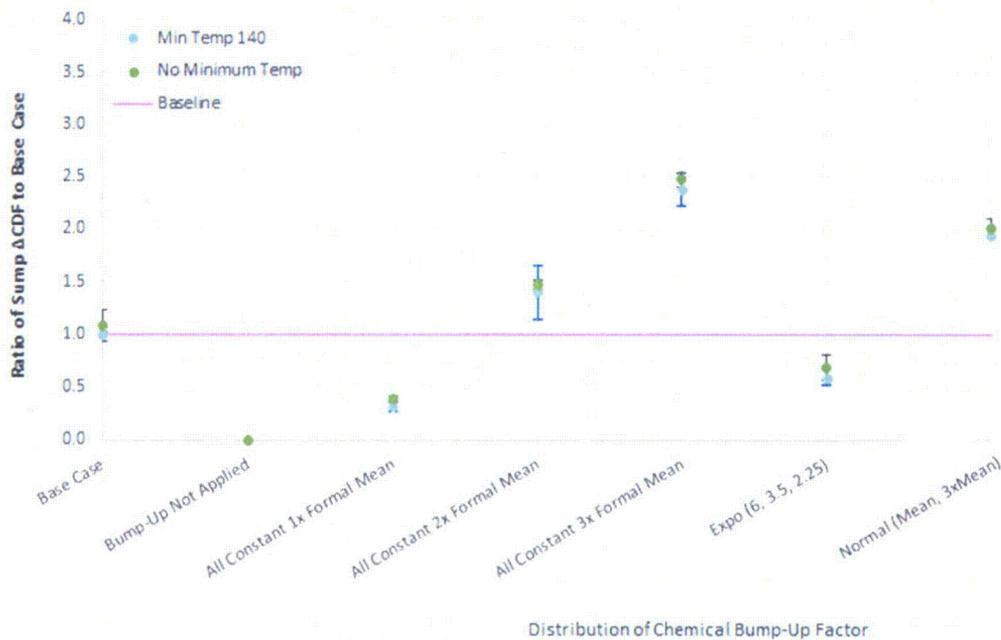


Figure 2: Summary of chemical head-loss key parameters sensitivity analysis and risk effects.

Clearly, some treatment of chemical head-loss is essential to evaluating risk as shown in Figure 2 by case “Bump-Up Not Applied,” because no failures in the sump were predicted to occur based on conventional head loss alone. Use of the 140°F temperature criterion for application of the chemical head-loss factor does not significantly affect any of the sensitivity results or the risk calculated by CASA Grande (see ESGB RAI 8 response).

Application of constant head-loss factors equal to the current formal means of the exponential distributions lowers the risk for the case “All Constant 1x Formal Mean”. However, application of constant multipliers (2X and 3X) on the formal mean increases the risk as shown by cases “All Constant 2X Formal Mean” and “All Constant 3X Formal Mean”. Use of a constant head-loss factor equal to the mean applies the experimentally-observed, worst case (or 2X to 3X the worst case) chemical head loss multiplicative response for all breaks.

Use of other distributions, while preserving the same interpretation of data, will result in nearly identical risk results. However, to show the effect of alternative probability distributions, risk ratios were assessed with a truncated normal distribution for each scenario (between 1 and the present maxima) with a standard deviation of three times the individual scenario mean shown as case "Normal (Mean, 3X Mean)" in Figure 2. Although the individual scenario means of the analysis were preserved in this distribution, the large standard deviation approximates a uniform distribution over the complete range, thus, changing the intended use of the data and producing a non-comparative result.

Effects of the exponential distribution mean values were also evaluated in this sensitivity analysis using a reverse correlation of increasing chemical head-loss factor with decreasing break size. Case "Expo (6, 3.5, 2.25)" assigned the SBLOCA mean to 6, the MBLOCA mean to 3.5 and the LBLOCA to 2.25. This reverse correlation preserves the STP experimentally observed multiplicative chemical head-loss response of the LBLOCA (LAR Enclosure 4-3, Reference [53]) and increases the other means as a function of decreasing break size. This reverse correlation reflects the observed "thin-bed effect" where the multiplicative response of precipitate loading on smaller break debris beds is greater than that observed from the same precipitate loading on large break debris beds [Enclosure 1, Section 4.1]. Although the means were larger for smaller breaks as compared to the mean of the large break, risk decreases because the conservatism associated with the LBLOCA mean was decreased and because the increase in means associated with the SBLOCA and MBLOCA breaks were not sufficient to induce failure. A further sensitivity study indicates that the multiplier on the MBLOCA condition must be higher than 60 to increase the risk assigned by CASA Grande Case 01(all equipment operates). The SBLOCA head loss factor in this sensitivity, although higher than assumed in the LAR, does not influence the risk because none of the SBLOCA scenarios form a thin bed.

References:

1. Westinghouse, "South Texas Project GSI-191 Chemistry Effects Evaluation CN-CSA-06-6," Westinghouse Electric Company, December 2006.

ESGB, Chemical Effects: RAI 6

Please describe the relative chemical contributions from the sprayed materials compared to the submerged materials. Please state if the chemical model input into CASA assumes a fixed, 6.5-hour spray duration. If so, please discuss the probability of containment spray operating at a time beyond 6.5 hours following a LOCA and how the chemical effects analysis would be changed. Please describe if any sensitivity study was performed on the spray time with respect to how it may affect the chemical source term, the probability of precipitation, and ultimately the GSI-191 failure modes.

STP Response:

The CASA Grande treatment of chemical effects does not distinguish the relative contributions from sprayed materials and submerged materials. The PDF mean values of the chemical head-loss factors used in the CASA Grande analysis (LAR Enclosure 4-3, Section 5.6.3) to induce a multiplicative increase in conventional head loss are based on STP testing of a worst-case precipitate load across a design basis bed [1]. The worst-case precipitate load was generated assuming 30-days of spray operation [2, Table 6.3-7], [1, Page 54]. While the CASA Grande analysis assumes that all sprays are secured at approximately 6.5 hours with respect to strainer flow rate, the chemical head-loss factors reflect chemical head loss attributable to 30 days of continuous spray on all exposed surfaces and 30-days of corrosion for all submerged materials.

Given the assumed 30-day inventory of chemical products, spray timing assumed in CASA Grande does not affect the chemical source term or the probability of precipitation, so no sensitivities were performed on the spray time to address this RAI.

References:

1. AREVA, "South Texas Project Test Report for ECCS Strainer Testing (66-9088089-000)," August 2008.
2. Westinghouse, "South Texas Project GSI-191 Chemistry Effects Evaluation CN-CSA-06-6," Westinghouse Electric Company, December 2006.

ESGB, Chemical Effects: RAI 8

The STP chemical effects analysis assumes no precipitation prior to the sump pool cooling to 140 degrees Fahrenheit (°F). It is possible, however, to precipitate a calcium phosphate precipitate at higher temperatures if sufficient dissolved calcium is present. Please explain if the CASA Grande model includes calcium sources such as concrete dust, concrete ablated by the jet, and other plant materials such as insulation. Please state if there is a potential for some pipe breaks to produce enough calcium such that formation of a precipitate at a greater than 140 °F temperature should be included. Since some precipitates can form at temperatures greater than 140 °F, please explain how increasing the temperature threshold in Casa Grande affects the outcomes.

STP Response:

The CASA Grande model does not explicitly include calcium sources such as concrete dust, concrete ablated by the jet, and other plant materials such as insulation, but rather, applies a separate chemical head-loss factor for each LOCA category to increase head loss for all anticipated chemical products. The head-loss factor means are based on the maximum head loss observed during STP ECCS strainer testing of a 30-day worst-case precipitate (including both calcium and aluminum) load (LAR Enclosure 4-3, Reference [53], [1]) across a design basis bed.

Some pipe breaks may produce enough calcium to form precipitates in the sump pool prior to bulk fluid temperatures reaching 140°F (approximately 17.8 hr for SBLOCA and MBLOCA, 5.0 hr for LBLOCA). In such cases, calcium leaching rates may be sufficient to exceed calcium phosphate solubility at pool temperatures and pH values within these time periods.

A higher temperature threshold that permits immediate chemical head-loss effects for CASA Grande Case 01(all equipment operates) increases the total risk by approximately 4%. All of the additional scenario failures are attributed to higher chemical induced head loss at the strainer. Core debris accumulation does not depend on the chemical head-loss factors.

An alternative chemically-induced head-loss calculation described in Section 4.5 of Enclosure 1 that is additive and incorporates both the type of precipitate and the debris bed area to quantify total head loss, also shows that possible precipitate formation prior to 140°F would induce little increase in total head loss.

References:

1. Westinghouse, "South Texas Project GSI-191 Chemistry Effects Evaluation CN-CSA-06-6," Westinghouse Electric Company, December 2006.

ESGB, Chemical Effects: RAI 9

Please describe the key sources of uncertainty (aleatory and epistemic) associated with the dissolution model and the solubility limits and how is this uncertainty factored into the probability density functions and the chemical bump up factors?

STP Response:

Although chemical effects have not been found to be significant contributors in STP post-LOCA sump conditions, CASA Grande includes uncertainty for chemical contribution to head loss as a random variable multiplier with a mean greater than 1. As such, no models of dissolution or solubility limits appear directly in the CASA Grande analysis, so uncertainties associated with a dissolution model and solubility limits were not examined explicitly. Exponential probability density functions (PDFs) defined for the chemical head-loss factors describe the magnitude of the head-loss effect that will be observed after chemical products form. The magnitude of head-loss effect is independent of dissolution processes and solubility limits, so these considerations are not factored into the PDFs defined for chemical bump-up factors.

As described in the response to ESGB RAI 1c, the chemical head-loss factor means reflect the maximum observed conventional head loss increase of a design basis bed [1] from the complete addition of a precipitate load generated under 30-day, continuous spray exposure of deterministically bounding materials [1, 2] and the single-parameter exponential PDF was chosen for shape and for convenience of fitting the desired statistics of the mean and a truncated tail probability. However, the criterion of 140 ± 5 °F for implementation of the bump-up approach was loosely derived from industry practice for delayed onset of precipitation based on aluminum solubility [3, 4] and does acknowledge that precipitation temperature depends on the products in question and on the chemical environment.

Application of the precipitation temperature is the only consideration of solubility present in the STP LAR analysis. As described in the response to ESGB RAI 10, acceptability of the 140 ± 5 °F temperature criterion was examined as a function of uncertainty in the expected range of STP post-LOCA pH, pool temperature, and variable inventory of material exposure (LAR Enclosure 4-3, Reference [20]). While LAR Enclosure 4-3, Reference [20] concluded that aluminum precipitation was unlikely to occur within the parameter ranges examined prior to 140 ± 5 °F, the reference did not examine potential of other uncertainties related to material release rates, chemical modeling (thermodynamic and kinetic) calculations used to assess solubility (equilibrium coefficients, enthalpy, specified reactions, and time) and calcium precipitation prior to 140 ± 5 °F.

Since all uncertainties associated with the criterion of 140 ± 5 °F that was loosely based on aluminum solubility were not fully addressed, the possible increase in risk that could occur through the use of a higher temperature criterion was examined as a sensitivity case. Use of a higher temperature threshold that permits immediate application of the chemical head-loss factors increases the risk of CASA Grande Case 01(all equipment operates) by approximately 4% as discussed in the response to ESGB RAI 8. This increase is not likely to pose a practical concern.

References:

1. AREVA, "South Texas Project Test Report for ECCS Strainer Testing (66-9088089-000)," August 2008.
2. Westinghouse, "South Texas Project GSI-191 Chemistry Effects Evaluation CN-CSA-06-6," Westinghouse Electric Company, December 2006.
3. Aluminum Solubility in Boron Containing Solution as a Function of pH and Temperature, Adams # ML091610696, September 2008.
4. Entergy, "GL 2004-02 Final Supplemental Responses Adams #ML082700499," 2008.

ESGB, Chemical Effects: RAI 10

The following parameters do not appear to be considered in the simplified approach used to quantify chemical effects for STP: pool chemistry, pool pH, and the amounts of aluminum, calcium, and zinc. If these items are not considered, please provide justification for acceptability of the analysis without their consideration.

STP Response:

Pool chemistry, pool pH and the amounts of aluminum and calcium were considered in the adoption of the chemical precipitation threshold temperature and in the definition of the chemical head-loss factors. However, these factors do not appear explicitly in CASA Grande input.

The conditions used to control application of chemical bump up approach in the CASA Grande analysis are a temperature of 140 ± 5 °F when a fiber bed greater than or equal to 1/16" forms, as indicated in LAR Enclosure 4-3. The choice of 140 °F as a chemical precipitation temperature is nominally based on industry practice for delayed onset of aluminum precipitation [1, 2], on review of CHLE tank test results (LAR Enclosure 4-3, Reference [18,19]) and on evaluation of multiple WCAP-16530-NP precipitate release calculations under STP post-loss-of-coolant accident (LOCA) scenarios (LAR Enclosure 4-3, Reference [20]). Multiple WCAP-16530-NP calculations were performed to confirm that the precipitation onset temperature adequately assesses uncertainty related to pH, pool chemistry and material exposure that affect precipitate generation (LAR Enclosure 4-3, Reference [20], Tables 1 – 3). The WCAP-16530-NP calculations show that the likelihood of aluminum precipitation above the temperature of 140 ± 5 °F with variable pool pH, pool chemistry and variable material inventories is low (LAR Enclosure 4-3, Reference [20], Table 4). The WCAP-16530-NP calculations of LAR Enclosure 4-3, Reference [20] did not explore spray durations longer than 6.5 hours and did not account for zinc release. However, chemical head-loss factor distributions were based on conservative chemical product inventories as described below.

Exponential probability density function (PDF) mean values applied as chemical head-loss factors provide a conservatively large chemical head loss response that accounts for exclusion of zinc-related chemical effects and bounds the realistic evaluation of 6.5 hours of spray exposure. Conservatism is ensured because the mean head loss values (LAR Enclosure 4-3, Table 5.6.4) reflect the multiplicative increase of conventional head loss caused by a worst case chemical precipitate test load applied to a design-basis debris bed (LAR Enclosure 4-3, Reference [53], [3]). This worst case precipitate load corresponds to 30-day spray exposure of deterministically bounding aluminum, silicon and calcium bearing material quantities [3]. The experimentally observed multiplier of 2.25 was assigned to small breaks and then increased for larger breaks. Also, the expected STP-post-LOCA material releases determined by calculations listed in LAR Enclosure 4-3, Reference [20] are much less than the 30-day chemical inventory used in strainer testing (LAR Enclosure 4-3, Reference [53], [3, Table 6.3-7]). Chemical effects head-loss factors based on a bounding chemical head loss response are dependent on break size regardless of realistic spray duration and materials exposed, which further enforces the conservative interpretation of the mean values.

References:

1. Bahn, C.B., Kasza, K.E., Shack, W.J., and Natesan, K. "Aluminum Solubility in Boron Containing Solutions and a Function of pH and Temperature", ADAMS #ML091610696, Argonne National Laboratory, September, 2008.
2. Entergy, "GL 2004-02 Final Supplemental Responses", Adams #ML082700499, September 2008.
3. Westinghouse, "South Texas Project GSI-191 Chemistry Effects Evaluation CN-CSA-06-6," Westinghouse Electric Company, December 2006.

ESGB, Chemical Effects: RAI 14a

Please discuss how uncertainties from the following items are considered in the STP chemical effects analysis:

(a) Radiation effects on precipitate formation.

STP Response:

Uncertainties from radiation effects on precipitate formation were not examined because in-situ corrosion and dissolution precipitates were not observed in prototypical test solutions (LAR Enclosure 4-3, Reference [18, 19]).

ESGB, Chemical Effects: RAI 14b

- (b) **Radiation effects on debris bed degradation. In addition, for this item, the submittal states (Volume 6.2, page 84) that breakdown of the fiber bed is not considered to be a significant issue due to similar materials being used for filtration media for high activity particulate. Please discuss how the filter service life in the referenced application compares to the ECCS mission time following a LOCA.**

STP Response:

Uncertainties from radiation effects on debris bed degradation were not examined because Tri Nuclear polyester and fiberglass filter cartridges used by STP have a specified maximum accumulated dose of 10^6 rads to avoid filter degradation [1,2]. These filters are used in the spent fuel pool and core to remove particulates and maintain water purity specifications. It was initially assumed that the dose limit was recommended to avoid degradation of fiberglass, when in fact, it is recommended to avoid degradation in models that contain polyester (hydrocarbon) filter media that is more susceptible to radiation damage than glass. The following order-of-magnitude argument demonstrates it is unlikely that fiberglass debris receives a dose greater than 10^6 rads from crud deposition alone.

The specific activity of crud present at STP is unknown, but health physics surveys of spent filters that collect crud are common practice. It is important to note that Co-58 and Co-60, significant dose contributors from crud, are highly soluble in the RCS solution and are not captured in the filters. Similarly, these isotopes would not remain resident in the debris bed. Crud constituent solubility does not affect the accuracy of this analysis, but it is an important consideration before adopting crud activity values reported in the literature.

The mass of crud collected in filters can be related to the threshold of 10^6 rad to judge whether fiberglass debris can receive a higher dose. It is assumed that the physical form of crud captured in the bed is identical to the form captured in the filters. The dose to fiberglass debris can be approximated as

$$D_{bed} = M_{bed}^{crud} (\Gamma A)_{crud} \epsilon_{bed} T_{bed} / M_{bed}^{fiber} \quad \text{Equation A}$$

where:

M_{bed}^{fiber} = mass of fiberglass in the debris bed

M_{bed}^{crud} = mass of crud in the debris bed

$(\Gamma A)_{crud}$ = energy release rate per unit mass for specific activity A and average gamma energy Γ

ϵ_{bed} = effective absorption efficiency in the fiber mat
 T_{bed} = bed exposure time

The dose rate measured by a health physics survey meter can be approximated as

$$\dot{D}_{filt} = M_{filt}^{crud} (\Gamma A)_{crud} \epsilon_{detect} / M_{detect} \quad \text{Equation B}$$

where:

M_{filt}^{crud} = mass of crud in the filter
 $(\Gamma A)_{crud}$ = energy release rate per unit mass for specific activity A and average gamma energy Γ
 ϵ_{detect} = effective capture efficiency of the survey meter
 M_{detect} = effective mass of the detector

Solving Equation A and B for the common energy release rate per unit mass $(\Gamma A)_{crud}$ and isolating crud mass in the filter gives

$$M_{filt}^{crud} = \frac{\dot{D}_{filt} M_{bed}^{crud} \epsilon_{bed} T_{bed} M_{detect}}{D_{bed} \epsilon_{detect} M_{bed}^{fiber}} \quad \text{Equation C}$$

Numeric parameters used to evaluate Equation C are shown in Table 1. A constant maximum crud inventory is assumed in the STP LAR analysis, but the debris quantity can vary. Concentrating the associated energy release in minimum debris mass represents a maximum exposure to radiation, so a 1/16-in. equivalent thin bed was assessed for comparison purposes. Assuming low bed compaction equal to the manufactured density further concentrates the radiation dose. Relatively thin porous media are not well coupled to the particulate radiation source for efficient gamma energy absorption, so an effective absorption fraction of 0.1 was assigned. Similarly, a hand-held gamma survey meter has poor collection efficiency for a 30-in. long, 6-in. diameter stainless steel filter cartridge containing an annular, cylindrical radiation source, so a value of 0.15 was assigned.

Table 1. Parameters for fiberglass dose assessment.

bed packing density	2.4 lb _m /ft ³
max dose	10 ⁶ rad(J/kg)
bed absorbtion fraction	0.1
bed thick	1/16 th in
one strainer area	1818.5 ft ²
# strainers	3
debris exposure time	30 days
crud mass in bed	24 lb _m
effective detector mass	100 g
detector efficiency	0.15
max filter dose rate	20 rad/hr

Under the assumptions listed in Table 1, the mass of fiberglass distributed on all 3 strainers is approximately 31 kg and the crud mass estimated to be on the filter is less than 1 gram. For crud burst cleaning procedures to be effective relative to the 24 lbm maximum inventory, filters must collect up to 1-pound quantities. Therefore, it is not likely that fiberglass in the debris bed can receive a dose from accumulated crud that meets or exceeds 10⁶ rad. A predicted filter mass of 1 pound (450 g) corresponds to a debris-bed dose of only 750 rad. RCS filters at STP are not commonly weighed for mass increase, so quantitative confirmation of these observations is not available.

References:

1. Tri Nuclear Corp. Underwater Filter/Vacuum Units Assembly & Operating Instructions. December 2012.
2. Tri Nuclear Corp. TNC-019-02 standard filter drawing and product description.

ESGB, Chemical Effects: RAI 14c

Effects of unqualified coatings degradation. For example, please explain if leached chemicals from the coatings at STP contribute to potential chemical effects. Please explain if the coatings themselves become a debris source that is more problematic than particulates (e.g., gelatinous). As part of the response, please compare the coatings tested in the report referenced in the LAR to the STP plant-specific unqualified coatings.

STP Response:

Uncertainties from chemicals leached from unqualified coatings at STP were not considered explicitly in the assessment of potential chemical effects. However, exponential distributions of chemical head-loss factors applied in the analysis do permit chemical head-loss effects that exceed levels that are expected from 30-day inventories of aluminum and calcium compounds. Some of this margin can be interpreted as variability introduced by any chemicals leached from unqualified coatings. The phenomena of unqualified coatings degradation into a gelatinous debris source was not considered in the chemical effects analysis that supported the STP CASA Grande evaluation. It is generally assumed (LAR Enclosure 5, Reference [3]) that unqualified coatings fail into constituent solids without further contribution to the chemical environment.

Coatings tested in LAR Enclosure 5, Reference [3] are assumed to be similar to those documented in STP unqualified coatings documentation (LAR Enclosure 4-3, Reference [12]). However, since detailed product information associated with each type of coating was not available, only general comparisons were made between coating categories of those at STP and those listed in LAR Enclosure 5, Reference [3].

ESGB, Chemical Effects: RAI 15

The CHLE tests simulated a 15-inch LBLOCA. Please describe how the CASA Grande chemical model determines the chemical source term for different size breaks, such as a smaller than 15-inch LBLOCA or a larger than 15-inch LBLOCA. In addition, please explain if CASA Grande considers how a smaller but potentially more focused jet that takes longer to blow down may affect the calcium and aluminum concentrations.

STP Response:

The CASA Grande model does not determine a chemical source term for different break sizes, and it does not assess smaller break conditions that may affect the calcium and aluminum concentrations within the analysis. Rather, the CASA Grande model assesses head loss from possible chemical sources by applying a range of chemical head-loss factors as a function of break category (LAR Enclosure 4-3, Table 5.6.4) that account for chemically-induced head loss (LAR Enclosure 4-3, Section 5.6.3). The ranges of applied chemical head-loss factors are based on strainer testing conducted using a design-basis debris bed as described below, adequately bound chemically induced head loss from a spectrum of chemical source terms. Deterministic analyses also do not typically consider how a smaller but potentially more focused jet may affect the calcium and aluminum concentrations.

The chemical head-loss factors range from representative to highly conservative multipliers and are used in break-specific exponential probability distributions that were adapted for use with the chemical "bump up" approach described in LAR Encl. 4-3, Section 5.6.3. As described in the response to ESGB RAI 1c, the most probable head-loss factors, based on experimental observation (LAR Enclosure 4-3, Reference [18, 19]), correspond to the mode of 1.0 (one) for all breaks. The chemical head-loss factor means reflect the maximum observed conventional head loss increase of a design basis bed [1] from the complete addition of a precipitate load generated under 30-day and continuous spray exposure of deterministically bounding materials (LAR Enclosure 4-3, Reference [53], [1]). The maxima of the exponential PDFs were confirmed to be values capable of producing a quantifiable number of chemically induced failures in combination with the spectrum of conventional head loss experienced within each break size and were at least 6.8 times larger, than the mean factor of a given break size PDF. The exponential distributions were not adjusted for lower chemical inventories that might be evolved during shorter accident periods or for the absence of sprays in small break scenarios.

Reference:

1. Westinghouse, "South Texas Project GSI-191 Chemistry Effects Evaluation CN-CSA-06-6," Westinghouse Electric Company, December 2006.

ESGB, Chemical Effects: RAI 16

Volume 1, Section 1.2.6, “Chemical Release and Precipitation Model,” states that several scenarios were investigated using the WCAP-16530-NP-A formula for chemical release. The scenarios used different combinations of liquid temperature, pH, water volume, and fiber quantity for several different break sizes up to a double ended guillotine break. Please clarify if Tables 2.5.34 and 2.5.35 in Volume 6.2 summarize the results of these investigations. Please provide the minimum and maximum values for the pH, fiber quantity, and water volume in the tables. Also please discuss if post-LOCA values could reasonably exceed the minimum and maximum values used in the evaluations. For example, please explain if it is plausible for the pH to be greater than was assumed to be the maximum pH.

STP Response:

Yes, Tables 2.5.34 and 2.5.35 in Volume 6.2 summarize the results of the 30-day released material concentrations and the evaluation of precipitate occurrence under specified conditions (LAR Enclosure 4-3, Reference [20], Table 4 and 5). The pH profiles used in the simulations supporting the tables were a linear response in TSP dissolution time that started at a pH of 4.5 and rose to the steady-state minimum (pH 7.0) or maximum (pH 7.3) over 80 minutes (LAR Enclosure 4-3, Reference [20]). The steady state pH was determined from the range of TSP mass within containment [2] and the best estimate water mass for LBLOCA (LAR Enclosure 4-3, Reference [14], Table 6.2). The minimum and maximum fiber quantities and water volume for each break size that were used for WCAP-16530-NP-A calculations and the assumed plant condition is displayed in Table 1 (LAR Enclosure 4-3, Reference [20], Table 1). The amount of LDFG was determined from the Case 01(all equipment operates) CASA Grande simulation. Plant conditions for water volumes were determined from “STP Post-LOCA Water Volume Analysis” at 130°F (LAR Enclosure 4-3, Reference [14], Table 5.9).

Table 1 Table 1: WCAP-16530-NP-A Input and Plant Condition Comparison

	Min LDFG (ft ³)		Max LDFG (ft ³)		Min Water Vol. (ft ³)		Max Water Vol. (ft ³)	
	WCAP	Plant Conditions	WCAP	Plant Conditions	WCAP	Plant Conditions	WCAP	Plant Conditions
SBLOCA	0	0	10	12.8	62,700	63,314	75,921	76,665
MBLOCA	10	0	60	109.0	66,411	67,062	79,632	80,412
LBLOCA	60	0.7	2,385	2421.4	66,411	67,062	79,632	80,412

With the exception of the maximum fiberglass quantity for MBLOCA scenarios, the bounds of the analysis would not be significantly larger than those examined. The underestimated MBLOCA maximum fiberglass quantity may underestimate simulated calcium and aluminum release for MBLOCA cases. Another slight difference not accounted for in the simulation is associated with the pH. Complete buffer dissolution was assumed to occur within 80 minutes, but the pH profile for each break size may be slightly different because of variable RWST drain time. However, only the 1.5-inch break (LAR Enclosure 4-3, Page I-10) takes longer than 80 minutes to drain. Therefore, most breaks will reach the steady bounds sooner than indicated by the analysis. Also, the final steady state pH bounds were based on LBLOCA best estimate water mass, the final steady state pH bounds for a MBLOCA are correctly assessed since the best estimate

water mass for a MBLOCA and LBLOCA are the same ((LAR Enclosure 4-3, Reference [14], Table 6.2). However, there would be approximately 11% less solution in a SBLOCA than in a LBLOCA scenario. This fact suggests that the pH range examined may have been slightly underestimated in the simulation of small breaks. Therefore the pH range of a LOCA event could be slightly larger than the 0.3 pH units predicted.

The pH range may have been slightly underestimated in the simulation of SBLOCA, due to having about 11% less solution compared to LBLOCA scenarios. Because SBLOCAs do not challenge GSI-191 success criteria, and the 11% decrease in pool solution only results in a 5% relative increase in TSP concentration, the pH (and pH range) is valid and encompasses all scenarios of concern.

ESGB, Chemical Effects: RAI 18a

Volume 6.2, "Item 5.a.6: Corrosion and Dissolution Model," on page 72 states the following:

The determination of whether a chemical product would form was based on a combination of engineering judgment and limited thermodynamic modeling. The total quantity of material released was not assumed to fully precipitate into chemical products. Instead, solubility limits of chemical products expected to form ... were calculated as a function of temperature and pH using Visual MINTEQ to determine the lowest concentration of metal required for product formation from the range of selected conditions. Sodium aluminum silicate and aluminum oxyhydroxide are the aluminum products described as possible precipitates in WCAP-16530-NP-A; however only the aluminum hydroxide solubility limit (Log K of 10.8 ...) was considered in this analysis since it was determined as a suitable substitute for sodium aluminum silicate in head loss testing.... Calcium phosphate (Log K of -28.25) solubility limits were also evaluated.

The lowest concentration of metals required to form these chemical products were determined by identifying the lowest solubility over the pH range of 7.0 to 7.3 at a defined temperature.

Using this approach, the concentration of aluminum expected to result in formation of a chemical product is approximately 4.9 milligram per liter (mg/L). The calcium concentration expected to result in the formation of a chemical product was 0.8 mg/L. These values were used to assess the presence of chemical product formation from the calculated material release.

- (a) Please describe why the NRC staff's judgment that aluminum oxyhydroxide and sodium aluminum silicate precipitates prepared using the WCAP-16530-NP-A method can be substituted for each other in head loss testing is relevant to solubility when evaluating whether an aluminum based precipitate will form in a post-LOCA fluid containing dissolved aluminum.**

STP Response:

The supplementary information provided by Volume 6.2, "Item 5.a.6: corrosion and dissolution Model," only provides generalized information and was not directly applied in the CASA Grande analysis.

The staff's judgment that allows substituting aluminum oxyhydroxide for sodium aluminum silicate is not relevant to solubility when evaluating the formation of an aluminum based precipitate in post-LOCA fluids containing dissolved aluminum. The text did not convey the intended concept that the use of aluminum oxyhydroxide solubility to predict the formation of sodium aluminum silicate was assumed to be adequate for a general assessment of aluminum product formation or aluminum solubility since solubility limits of these two compounds were shown to be similar (i, Section 6, items 6 and 7).

ESGB, Chemical Effects: RAI 18b

- (b) Using Equation 4 in the Argonne National Laboratory Technical Letter Report “Aluminum Solubility in Boron Containing Solutions as a function of pH and Temperature,” dated September 19, 2008 (ADAMS Accession No. ML091610696), the lowest aluminum solubility in the pH range 7.0 to 7.3 is approximately 2.7 parts per million (ppm). Please discuss how the analysis results would be affected by assuming the aluminum solubility was 2.7 mg/L instead of 4.9 mg/L.**

STP Response:

LAR Enclosure 4-3, Reference [20] referenced an aluminum solubility determined from the use of VisualMINTEQ v 3.0 with STP specific solution chemistry at a pH of 7.0 and temperature of 140 °F. Using a solubility of 2.7 mg/L obtained from ANL’s equation would increase the likelihood of aluminum precipitation under conditions examined by LAR Enclosure 4-3, Reference [20] and would have likely resulted in a higher temperature criterion for onset of precipitation in the CASA Grande analysis. However, as discussed in the response to ESGB RAI 8, the use of a higher temperature threshold (or immediate implementation of the multiplicative head loss factors) does not significantly affect risk associated with CASA Grande Case 01 (all equipment operates).

ESGB, Chemical Effects: RAI 18c

- (c) The discussion states that calcium phosphate solubility limits were evaluated. Figure 2.5.34 (Volume 6.2) shows the calcium hydroxide solubility in borated-TSP [trisodium phosphate] solution. Please discuss the rationale for the 0.8 mg/L solubility for calcium and whether it was based on a calcium hydroxide solubility or calcium phosphate solubility.**

STP Response:

Figure 2.5.34 caption was mislabeled. The figure does reference calcium phosphate solubility (Log K of -28.25 and ΔH_{rxn} of -87 kJ/mol) at 185 °F ranging from pH 7.0 to 7.30.

Reference:

1. Westinghouse, WCAP-16785-NP, Rev 0 Evaluation of Additional Inputs to the WCAP-16530-NP Chemical Model, Westinghouse Electric Company, May 2007.

ESGB, Chemical Effects: RAI 21

The amount of crud released following a LOCA is estimated to be 5-24 pound-mass (lbm) (Volume 6.2, page 85). For the Casa Grande analysis, please discuss the quantity of crud or other activated debris that is assumed to reach the strainer and how it affects head loss. Please compare the total crud quantity estimated with the amount of crud collected during a controlled crud burst performed at the beginning of refueling outages.

STP Response:

As stated in Section 2.2.11, the quantity of crud assumed in the analysis is 24 lbm (LAR Enclosure 4-3, Reference [13]). Within CASA Grande, crud is considered to be a 15- μ m particulate fine with a 100% transport fraction under all LOCA scenarios. The full crud inventory is introduced during the first time step of each scenario, and crud transports to the strainers in proportion to their volumetric flow. Upon arrival at a strainer, crud is homogenized with all other particulates and fiber to form composite debris properties that are entered in the head-loss correlation.

STP does not quantify the amount of crud released during the crud burst evolution. The objective of the crud burst is to minimize radiation worker dose. The effectiveness of the crud burst evolution is measured by dose compared to previous evolutions. Unlike a momentum-driven process that may dislodge crud from RCS surfaces, hydrogen peroxide is used in a chemical process to maximize removal of crud.

An estimate of crud quantity available in an operating cycle is made for the purpose of core design using the EPRI BOA 3.1 software [1] to evaluate the impact of crud induced power shift. BOA estimates the crud deposit on the fuel and steam generators. 7 STP BOA estimates show that the STP Unit 1 predicted inventories are less than the industry nominal, so the 24 lbm crud assumed (LAR Enclosure 4-3, Reference [13]) in CASA Grande is appropriate and conservative.

Reference:

1. Boron-induced Offset Anomaly (BOA) Risk Assessment Tool: Version 2.0. EPRI, Palo Alto, CA, 1014961, December 2007.

ESGB, Coatings: RAI 1

Please provide the basis for the unqualified epoxy size distribution reported in Table 2.2.18 in Volume 3. The NRC staff has previously allowed licensees to assume that degraded qualified epoxy coatings fail in pieces larger than fines. This allowance was limited to epoxy coatings that were originally qualified and have become degraded. The same treatment has not been accepted for epoxy coatings that were unqualified, since these are typically less robust coating systems that would disintegrate into fines. Please specify the epoxy coating in question and provide a basis (i.e., testing) for assuming it fails in pieces larger than fines.

STP Response:

The unqualified coatings size distribution of Table 2.2.18 (LAR Enclosure 4-3) was taken from LAR Enclosure 4-3, Reference [12], Table 7, Page 32. This calculation references the epoxy size distributions from paint chip characterization of DBA coatings testing document "TXU Paint Chip Characterization," (1). Autoclave testing was conducted on TXU (Comanche Peak) supplied coating samples to determine size distribution characteristics of unqualified coatings debris, measured by failed mass, failed characteristic size, and qualitative failed shape (2). Results of the "TXU Paint Chip Characterization" (1) document included mass percentages for each of the size/qualitative shape categories of epoxy. These failed mass percentages and size/qualitative shape categories are representative of total failed inventory from the undocumented (assumed unqualified coated) autoclave tested samples. The results of the test were applied to estimate the size distribution of failed epoxy for a given volume of unqualified coatings.

References:

1. ALION-REP-LAB-TXU-4474-02. TXU Paint Chip Characterization. Revision 0: October 2007.
2. Keeler & Long PPG Report No. 06-0413, "Design Basis Accident Testing of Coating Samples from Unit 1 Containment TXU Comanche Peak SES", April 2006.

ESGB, Coatings: RAI 6a

The Volume 6.2 responses to request for supplemental information, indicate that the failure timing analysis relies heavily on filter data from the EPRI DBA testing of original equipment manufacturer (OEM) coatings. Please address the following questions regarding STP's use of this test data:

- (a) Please describe what STP has done in terms of documentation review or testing of plant materials in order to ensure that the plant-specific unqualified coatings at STP are the same as the coatings used in the EPRI testing.**

STP Response:

The generic type of each unqualified coating (i.e. epoxy, alkyd, etc.) is documented in the STP unqualified coatings inventory log (LAR Enclosure 4-3, Reference [12]). The specific product description, however, is unavailable for many unqualified coatings. Product descriptions are also unavailable for many of the coatings tested in the EPRI study (LAR Enclosure 5, Reference [3]), the extent of comparison is made to applicable generic coating types that are available.

ESGB, Coatings: RAI 6b

- (b) **The final proprietary EPRI report on OEM Coatings (EPRI 1011753, “Design Basis Accident Testing of Pressurized Water Reactor Unqualified Original Equipment Manufacturer Coatings. Final Report,” September 2005), states that, “Due to the prohibitive nature of the task, there was no attempt to quantify the amount of debris captured in the filters.” This testing included many different coating types with varying color, density, and constituent particle size. The autoclave was not opened and the tested components were not examined until the entire test was complete. The NRC staff could not determine if lighter coatings which would be less visible on a filter (and certainly less visible on a photo of a filter) failed at the same rate as darker coatings or if they may have been present on one or more of the filters removed early in the test. Given this information and the fact that the testers stated that they made no attempt to quantify debris on the filters, please provide additional justification for using this test data to assign a failure time to unqualified coatings.**

STP Response:

Estimated failure timing of unqualified coatings was based on visual analysis of filter discoloration. It is true that the colors of coatings tested affects filter discoloration. However, it is also seen from the EPRI testing that alkyds, the most colorful coatings group, experienced a higher average percentage of detachment than other coatings (LAR Enclosure 5, Tables 3-1, 4-2, Pages 3-2, 4-5). Because alkyd coatings experienced higher average failure over the 7-day test, they are also assumed to have the largest failure rate. This interpretation of the data implies that ranking filters by discoloration (visually dominated by heavily pigmented alkyds) may conservatively bias inferred failure timing to the maximum unqualified coatings failure rate of alkyds. A single estimated failure rate was applied for all upper-containment unqualified coatings types in the STP LAR Enclosure 4-3 analysis.

ESGB, Coatings: RAI 6c

(c) The EPRI OEM report also states that, "With regard to timing of the coating failures, the filters do not demonstrate a definitive time of failure, however in subjective terms, it appears that much of the failure occurred in the 24- to 48-hour timeframe." STP seeks to reduce the transported unqualified coating debris from upper containment by 94 percent compared to a deterministic approach (100 percent failure in a deterministic evaluation, 6 percent for STP). The NRC staff is not persuaded that a subjective review of photographs from a test performed in 2005 is adequate justification for the proposed failure timing. Please provide additional justification for the current analysis or provide a revised value for the failure timing.

STP Response:

Because alkyd coatings have the greatest influence on subjective interpretation of photographs (by virtue of distinctive coloration), and have the highest average substrate detachment, inferred failure rates can only be biased towards the maximum unqualified coatings failure rate of alkyds. See discussion in response to ESGB RAI 6b.

An alternative justification of the 6% failure fraction within the relevant mission time proceeds as outlined in Figure 1 below.

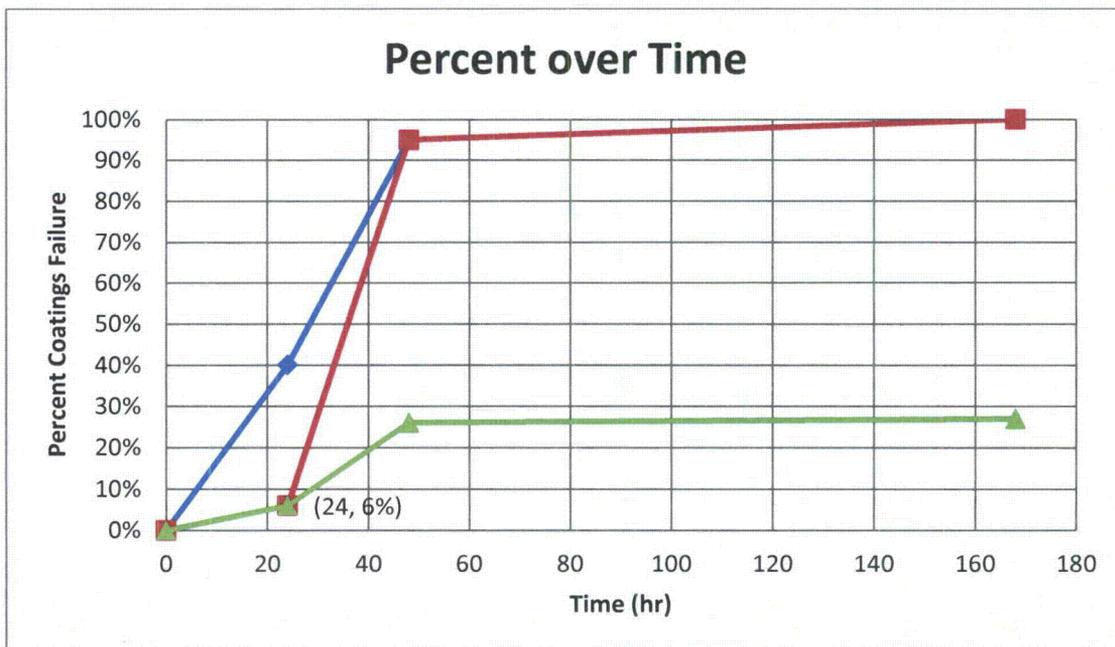


Figure 1- Failure Percentage as a Function of Time

The EPRI study (LAR Enclosure 5, Reference [3]), states "With regard to timing of the coating failures, the filters do not demonstrate a definitive time of failure, however in subjective terms, it appears that much of the failure occurred in the 24- to 48-hour timeframe." Although there is no definitive definition for the subjective observation "much of the failure," Figure 1 shows three different scenarios built on a variation in the amount of unqualified coatings that are estimated to detach between 24 and 48 hours. The green curve displays an ending detachment percentage equal to the total average

detachment of all STP analyzed coatings (epoxy, IOZ, alkyd) over the 7-day EPRI testing (27%). This curve sets the maximum percentage of failed unqualified coatings over 7 days to 27% and assumes that 21% of the total failure (from 6% to 27% total) occurs within the 24 to 48-hour period. If more than 21% of the coatings fail in the 24- to 48-hour time period, the percentage of coatings that fail at 24 hours will be shifted to less than the STP assumed 6% failure. If the definition of majority failure within 24 to 48 hours is changed to 55% of the available failure, then the assumed failure at 24 hrs would double to 12% (line not shown). Parametric evaluations have shown that total risk is insensitive to this range of added particulate.

If 100% failure is artificially assumed over the 7-day period and assume that "much of the failure" can be defined as 89% (from 6% to 95%) and 55% (from 40% to 95%), the results are the red and blue curves of Figure 1, respectively. Both curves assume a 5% residual failure after 48 hours. It can be seen that if 89% of the failure is assumed to occur between 24- and 48 hours, 6% will have to fail before 24 hours. However if it is postulated that 55% (one interpretation of majority) must fail in the 24- to 48-hour time frame (blue curve), the failure before 24 hours would be 40%, which would contradict the observed total average detachment of 27%.

Enclosure 1 to Attachment 5
Supporting Resolution of ESGB, Chemical Effects: RAI 1, 5, 8 and 9

1. Leavitt, J.J and Kee, E, ALION-REP-STP-8998-08 Rev 0, Quantification of Chemical Head Loss Epistemic Uncertainty; Basis for Incremental Chemical Head Loss Correlation," May 2014.

Document No: ALION-REP-STP-8998-08	Revision: 1	Page 1 of 46
Doc. Title: Quantification of Chemical Head Loss Epistemic Uncertainty; Basis for Incremental Chemical Head Loss Correlation		
Project No: STP-8998		
Project Name: STP: Risk Informed GSI-191 Support		
Client: STP Nuclear Operating Company		
<p>Document Purpose/Summary:</p> <p>The purpose of this document is both to describe Leavitt's Option 1 for quantifying CHL in light water reactor ECCS strainers and to demonstrate the implementation of a CHL correlation obtained from application of the modular approach (1) within a risk-informed framework.</p> <p>This test report is prepared as Non-Safety-related.</p> <p>Total Page Count: 46 pages including Appendices and Attachments.</p>		

Design Verification Method:		
<input checked="" type="checkbox"/>	Design Review	
<input type="checkbox"/>	Alternative Calculation	
<input type="checkbox"/>	Qualification Testing	
Professional Engineer (if required)	Approval: NA	Date: _____

Prepared By:	Janet Leavitt/Ernie Kee	<i>Janet Leavitt</i>	7/2/2014
	Printed/Typed Name	Signature	Date
Reviewed By:	Bruce Letellier	<i>Bruce C. Letellier</i>	7/10/14
	Printed/Typed Name	Signature	Date
Approved By:	Megan Stachowiak	<i>Lana Mitchell for M.S.</i>	07/10/2014
	Printed/Typed Name	Signature	Date



REVISION HISTORY LOG

Page 2 of 46

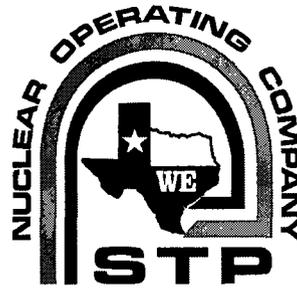
Document Number: ALION-REP-STP-8998-08 Revision: I

Document Title: Quantification of Chemical Head Loss Epistemic Uncertainty; Basis for Incremental Chemical Head Loss Correlation

Instructions:

Preparer to provide a brief description of each document revision, including rationale for the change and, if applicable, identification of source documents used for the change.

REVISION	DATE	DESCRIPTION
0	5/22/2014	Initial release
I	6/27/2014	Added new aluminum release data



Quantification of Chemical Head Loss Epistemic Uncertainty

Basis for Incremental Chemical Head Loss Correlation

June 27, 2014

Authors:

Janet Leavitt, PhD

Alion Science and Technology

Ernie Kee

South Texas Project Nuclear Operating Company

Reviewers:

Bruce Letellier, PhD

Alion Science and Technology

Seyed Reihani, PhD

University of Illinois Urbana-Champaign

Rodolfo Vaghetto, PhD

Texas A & M University

	Quantification of Chemical Head Loss Epistemic Uncertainty; Basis for Incremental Chemical Head Loss Correlation		
	Document No: ALION-REP-STP-8998-08	Rev: I	Page 4 of 46

Executive Summary

The effects of chemical precipitates in post-loss of coolant accident (LOCA) sump fluids on emergency core cooling system (ECCS) performance have been a concern in Generic Safety Issue (GSI) 191. Leavitt (1) proposed four options to a modular approach, derived from STP technical team discussions, for quantifying chemical head loss in a risk-informed frame work. Leavitt's four options are designed to produce chemically-induced head loss (CHL) correlations with increasing fidelity during development. The purpose of this document is to describe Leavitt's Option 1 for quantifying CHL in light water reactor ECCS strainers and to demonstrate the resulting CHL correlation implementation within a risk-informed analysis.

While the other options presented within the modular approach (1) would require additional experimental work to improve fidelity and further reduce uncertainty, Option 1 maintains a large degree of conservatism using best available data (2; 3; 4; 5; 6; 7; 8) to generate a representative CHL correlation. Option 1 derives a bounding CHL correlation (overestimated compared to best available data) that can be applied across a large spectrum of LOCA scenarios. When an Option 1, bounding (maximum) CHL correlation is used in a risk-informed setting, overestimation provides support for a safety margin and accounts for uncertainties as required by Regulatory Guide 1.174.

In this document, CHL is defined as the head loss arising strictly from chemical precipitates. Since risk-informed evaluations need all sources of head loss evaluated, the CHL correlation is developed to work with non-chemical head loss (NCHL) estimates (commonly referred to as "conventional head loss"). Total ECCS strainer head loss (THL) equals CHL obtained from use of the correlation added to NCHL calculated by Containment Accident Stochastic Analyses (CASA) as follows:

$$THL = NCHL + CHL.$$

Overestimation of CHL (per gram of available precipitate) is realized by modeling all post-LOCA precipitates in the containment sump fluid as aluminum oxyhydroxide (AIOOH). AIOOH was shown to produce the largest CHL per gram of the expected, transportable LOCA precipitates (2; 3; 4; 5; 6; 7; 8). South Texas Project (STP) ECCS strainer module AIOOH head loss test data (2) was fit in a bi-linear correlation with scaling parameter L^* ; the mass of available precipitate per surface area of the strainer module. The STP ECCS strainer module test data were collected at given temperature-dependent viscosity and face velocity. When the CHL correlation is applied to other conditions, the correlation results must be fit to the fluid conditions at which the estimates are desired.

Application of the derived correlation to the CASA framework is also summarized in this document. The correlation is then used to calculate CHL and the resulting THL for various LOCA scenarios and compared to THL results obtained from the "bump-up" approach (9). THL results obtained using the CHL correlation provide evidence that the original "bump-up" approach (9) likely overestimates THL when NCHL is high and may underestimate THL when NCHL is low. However, the differences are unlikely to change the risk calculated in the most likely plant state (all ECCS equipment starts and runs), CASA Case 01 (9).

	Quantification of Chemical Head Loss Epistemic Uncertainty; Basis for Incremental Chemical Head Loss Correlation		
	Document No: ALION-REP-STP-8998-08	Rev: I	Page 5 of 46

Table of Contents

Executive Summary	4
Definitions and Acronyms.....	8
1.0 Introduction.....	9
1.1 Background.....	9
2.0 Precipitate Evaluation	13
2.1 Chemical Precipitate Analysis.....	14
2.1.1 Zinc Phosphate	15
2.1.2 Evaluation of Transportable Precipitates	15
3.0 Head Loss Correlation	21
4.0 Results and Discussion	26
4.1 CHL Correlation Applied to Other TSP Plants’ Strainer Tests	27
4.2 CASA Incorporation of CHL Correlation.....	29
4.3 CHL Correlation Applied to Bounding STP LOCA Scenarios	30
4.4 CHL Correlation Applied Using CHLE Experimental Results	36
4.5 CHL Correlation Compared to the “Bump-Up” Method.....	37
5.0 Conclusion	44
6.0 References.....	45

List of Tables

Table 1: Parameters used to normalize results between test settings for comparison.....	12
Table 2: Debris used in strainer testing with location in CASA distributions.....	13
Table 3: Precipitates considered for CHL analysis.....	14
Table 4: Chemical precipitate addition to stable fiber/particulate debris bed.....	18
Table 5: DP resulting from individual additions within in each batch-precipitate added	19
Table 6: Variation in AIOOH response (in/g) observed during UNM vertical tests	20
Table 7: Head loss values obtained from SNC’s Vogtle strainer test referenced to test conditions (12) ..	29
Table 8: Parameters used in post-LOCA bounding scenario evaluation (14)	31
Table 9: Combination of parameters for STP post-LOCA bounding scenario evaluation (14).....	31
Table 10: Summary of CHL determined from post-LOCA bounding scenario evaluation (14)	32
Table 11: Experimental conditions ¹	35
Table 12: Reduction in 5 day release.....	36

	Quantification of Chemical Head Loss Epistemic Uncertainty; Basis for Incremental Chemical Head Loss Correlation		
	Document No: ALION-REP-STP-8998-08	Rev: I	Page 6 of 46

Table 13: Correlation applied to CHLE results assuming a 2,254,923 L pool volume (14) and three trains in operation..... 37

Table 14: Time and temperature when aluminum solubility was reached during post-LOCA bounding scenario analysis¹ 41

Table 15: Calcium phosphate CHL not accounted for prior to 140 °F 43

List of Figures

Figure 1: STP strainer testing (2) first day chemical load results (116.3 °F, 0.0086 ft/s, fiber and particulate debris) 10

Figure 2: Vertical loop test (3) response to AIOOH chemical loading (80 °F, 0.1 ft/s, blender processed fiber only)..... 11

Figure 3: Debris used in testing as compared to the weighted large break mean values..... 13

Figure 4: Option 1 of modular CHL quantification approach (1)..... 14

Figure 5: Cumulative CHL response to surrogate precipitate added in the STP strainer test (2) 16

Figure 6: Cumulative CHL response of each precipitate determined from first day of chemical addition of STP strainer test (2) 16

Figure 7: CHL per mass loading of each day-1 batch addition during STP strainer testing (2) 17

Figure 8: Trend of CHL response to precipitate addition to stabilized beds in columns 1 and 2 (Courtesy of UNM). 18

Figure 9: CHL vs. mass of Ca₃(PO₄)₂ and AIOOH precipitate added in different order 19

Figure 10: CHL vs. mass of precipitate (Ca₃(PO₄)₂ and AIOOH) added to particulate loaded fiber beds.... 20

Figure 11: Two day strainer response to added precipitate (AIOOH and Ca₃(PO₄)₂) in solution (2)..... 21

Figure 12: Strainer response to total AIOOH and first batch of Ca₃(PO₄)₂ precipitate (2). The last batches of aluminum that produce declining CHL have been removed..... 22

Figure 13: Non-declining AIOOH and first batch of Ca₃(PO₄)₂ CHL vs. precipitate availability normalized by strainer area..... 22

Figure 14: Bahn et al. (3) data, corrected to the STP strainer test conditions, compared to the STP data at low L* values. 23

Figure 15: Cumulative CHL determined from calculated and experimental values..... 24

Figure 16: ‘Corrected’ strainer data biased to provide conservative response as compared to experimental data 25

Figure 17: CHL correlation developed from shifted data 25

Figure 18: Strainer response to added mass of precipitate per strainer area (g/m²). STP test data is presented with a 25% uncertainty band..... 27

Figure 19: STP correlation prediction compared to St. Lucie’s experimentally observed CHL (13). 28

Figure 20: STP correlation prediction compared to Vogtle’s experimentally observed CHL (12)..... 28

Figure 21: CHL calculated for each time step evaluation by CASA. Green boxes are inputs at each time step (t) for the scenario evaluated (currently under development). 30

	Quantification of Chemical Head Loss Epistemic Uncertainty; Basis for Incremental Chemical Head Loss Correlation		
	Document No: ALION-REP-STP-8998-08	Rev: I	Page 7 of 46

Figure 22: L* generated from analysis of bounding LOCA conditions (3 trains operating) 33

Figure 23: Temperature corrected CHL generated from analysis of bounding post-LOCA conditions. 33

Figure 24: Raw data and predicted concentration; reproduced from UNM GSI-191 Telecon June 6, 2014
 "Aluminum Release Equation" presentation (18). 34

Figure 25: New release equation results obtained from altered WCAP-16530-NP calculator. Modeled
 data represented by line and experimental data represented by discrete markers..... 35

Figure 26: Aluminum release calculated using original WCAP-16530-NP release equations applied to
 series listed in Table 11..... 36

Figure 27: THL of Case 1 determined from CHL correlation (0.85 ft T1 CHL_{temp-corrected}) and from
 application of bump-up factor. Trains 1 and 2 overlay, CHL associated with bump-up occurs at
 140 ± 5 °F and HCHL includes clean strainer head loss. 38

Figure 28: THL for Case 43 determined from CHL correlation (2.56 ft T1 CHL_{temp corrected}) and from
 application of the bump-up factor. CHL associated with the bump-up occurs at 140 ± 5 °F and
 NCHL includes clean strainer head loss. 38

Figure 29: Probability of maximum THL (clean strainer + NCHL) as a function of break type (MBLOCA (A),
 LBLOCA (B)). SBLOCA THL not shown because bump-up approach is not applied since the thin
 bed criterion is not met 40

	Quantification of Chemical Head Loss Epistemic Uncertainty; Basis for Incremental Chemical Head Loss Correlation		
	Document No: ALION-REP-STP-8998-08	Rev: I.	Page 8 of 46

Definitions and Acronyms

AIOOH	Aluminum oxyhydroxide
Ca ₃ (PO ₄) ₂	Calcium phosphate
CASA	Containment Accident Stochastic Analysis
CHL	Chemical Head Loss
CHLE	Chemical Head Loss Experiment
DBA	Design Basis Accident
DEG	Double Ended Guillotine
ECCS	Emergency Core Cooling Systems
ft/s	feet per second
ft ²	square feet
ft ³	cubic feet
g	grams
GSI	Generic Safety Issue
hr	hour
L	Liter
LBLOCA	Large Break Loss of Coolant Accident
LOCA	Loss of Coolant Accident
MBLOCA	Medium Break Loss of Coolant Accident
mg/L	milligrams per liter
NCHL	Non-Chemical Head Loss
NEI	Nuclear Energy Institute
NPSH	Net Positive Suction Head
SAS	Sodium aluminum silicate
SBLOCA	Small Break Loss of Coolant Accident
SNC	Southern Nuclear Operating Company
STP	South Texas Project
THL	Total Head Loss
TSP	Tri-Sodium Phosphate
UNM	University of New Mexico
WCAP	Westinghouse Commercial Atomic Power
Zn ₃ (PO ₄) ₂ •4 H ₂ O	Zinc phosphate tetrahydrate
ZOI	Zone of influence

	Quantification of Chemical Head Loss Epistemic Uncertainty; Basis for Incremental Chemical Head Loss Correlation		
	Document No: ALION-REP-STP-8998-08	Rev: I	Page 9 of 46

1.0 Introduction

Leavitt's Option 1 of the Modular approach (1) was used to quantify CHL for a large spectrum of loss of coolant accident (LOCA) scenarios for the South Texas Project (STP) risk-informed analysis. As described by Leavitt, Option 1 maintains a large degree of conservatism and uses best available data to derive a correlation that quantifies conservatively high (that is, in this setting, overestimates) chemically-induced head loss (CHL) for risk-informed analyses. A conservatively high CHL correlation provides support for a safety margin and accounts for uncertainties as required by Regulatory Guide 1.174.

In this document, CHL is defined to be head loss arising strictly from chemical precipitates. Since risk-informed evaluations need all sources of head loss evaluated, the CHL correlation is added to non-chemical head loss (NCHL); commonly referred to as conventional head loss. Total emergency core cooling system (ECCS) strainer head loss (THL) equals CHL obtained from use of the correlation added to NCHL calculated by Containment Accident Stochastic Analyses (CASA) as shown in Equation 1.

$$THL = NCHL + CHL.$$

Equation 1

1.1 Background

Data related to CHL have been collected in two settings, (1) utility-specific ECCS strainer performance tests (strainer tests), and (2) vertical head loss loop tests (vertical tests) (3; 4). In these settings, chemical precipitates are added incrementally and the head loss across the debris bed is observed over time. Specifically, vertical tests commonly add a known quantity of precipitates to a loop containing a stable fiber-only bed, wait for CHL to stabilize and obtain a liquid sample to determine the mass of precipitate remaining in solution before more precipitate is added. Strainer tests generally add a known quantity of precipitates to a flume with a stable prototypical bed and wait a specific number of pool turnovers between precipitate additions (not necessarily head loss stabilization). Both settings, regardless of the differences in methodology, obtain very large CHL response to initial, small additions of chemical precipitates. However in strainer tests, increasingly greater amounts of precipitate additions tend to result in much lower incremental CHL responses; while vertical tests are many times terminated to protect test equipment soon after very high, initial precipitate CHL responses are measured. Quantitative CHL measurements obtained from each setting are a function of different strainer surface areas, bed morphology and chemical precipitate loading opportunities that result in different debris bed filtration efficiencies.

Between the two settings mentioned above, strainer tests are assessed to provide the most representative post-LOCA CHL response. This is because strainer testing is intended to represent utility-specific parameters of worst-case debris and maximum chemical precipitate quantities with maximum approach velocity across a representative strainer module. Further, THL results (NCHL+CHL) obtained from strainer testing are used to satisfy deterministic licensing requirements for utilities. Characteristic strainer test results are shown in

	Quantification of Chemical Head Loss Epistemic Uncertainty; Basis for Incremental Chemical Head Loss Correlation		
	Document No: ALION-REP-STP-8998-08	Rev: I	Page 10 of 46

Figure 1 [STP specific results (2)] where approximately 10% of the precipitate load determined in accordance with WCAP-16530-NP accounts for most of the total CHL response in a rapidly increasing head loss phase.

Figure 1 also indicates another characteristic of strainer tests whereby at extremely high precipitate loads, the head loss actually decreases. The subsequent decreasing head loss behavior, likely derived from debris bed response, is intentionally neglected in the Option 1 CHL correlation.

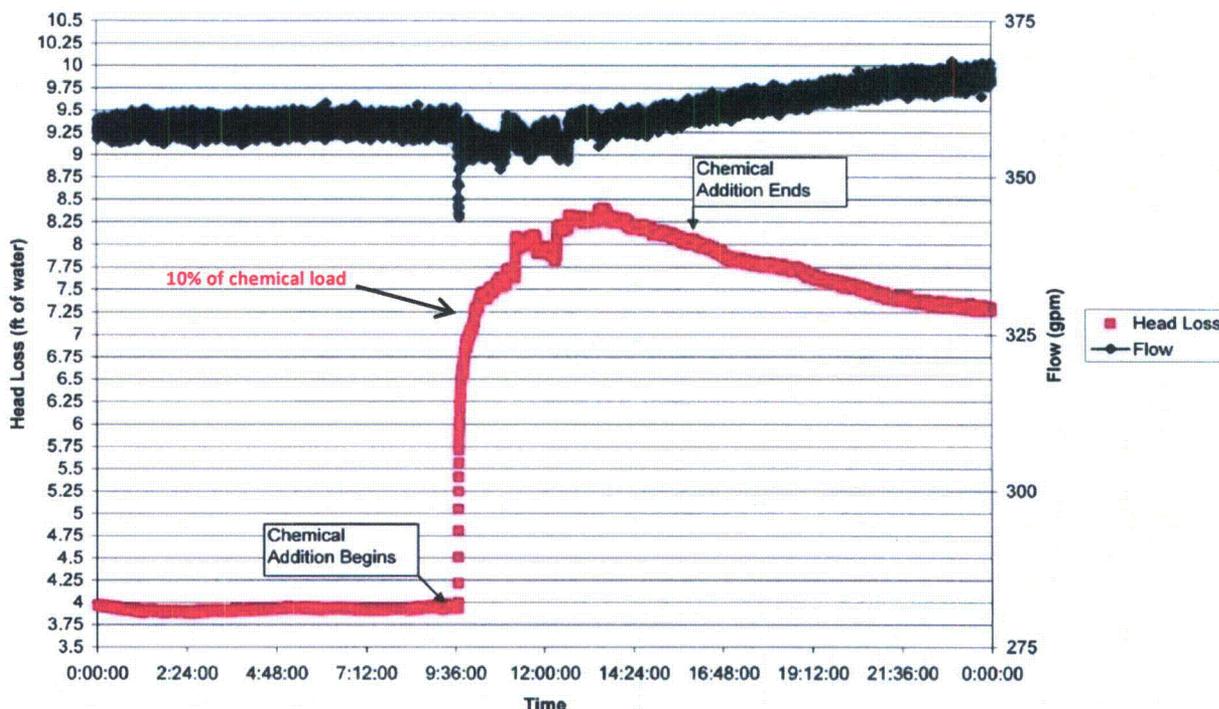


Figure 1: STP strainer testing (2) first day chemical load results (116.3 °F, 0.0086 ft/s, fiber and particulate debris)

As with strainer module test data, vertical loop test data tend to indicate a large CHL response to a relatively small chemical precipitate mass loading. As seen in

Figure 2, a small amount of WCAP-16530-NP precipitate (1.5 mg/L aluminum) produces a CHL response greater than the equipment limit of 38 kPa (13 ft of water at 39.2 °F) (3). While the magnitude of the measured response (approximately 13 ft) correlating to 1.5 mg/L aluminum is of concern, when the fluid conditions of the vertical test (80 °F and 0.1 ft/s) are scaled to the fluid conditions of STP strainer test (116.3 °F and 0.0086 ft/s) using Equation 2, the equivalent response is 0.4 ft:

$$CHL_{corrected} = \frac{v_t}{v_{ref}} \times \frac{U_t}{U_{ref}} \times CHL_t, \quad \text{Equation 2}$$

where:

- $CHL_{corrected}$ = the temperature and velocity corrected chemical head loss,

	Quantification of Chemical Head Loss Epistemic Uncertainty; Basis for Incremental Chemical Head Loss Correlation		
	Document No: ALION-REP-STP-8998-08	Rev: 1	Page 11 of 46

- v_t = viscosity at actual fluid conditions,
- v_{ref} = viscosity of fluid conditions during STP strainer testing,
- U_t = strainer approach velocity at actual fluid conditions,
- U_{ref} = strainer approach velocity during STP strainer testing, and
- CHL_t = Total chemical head loss.

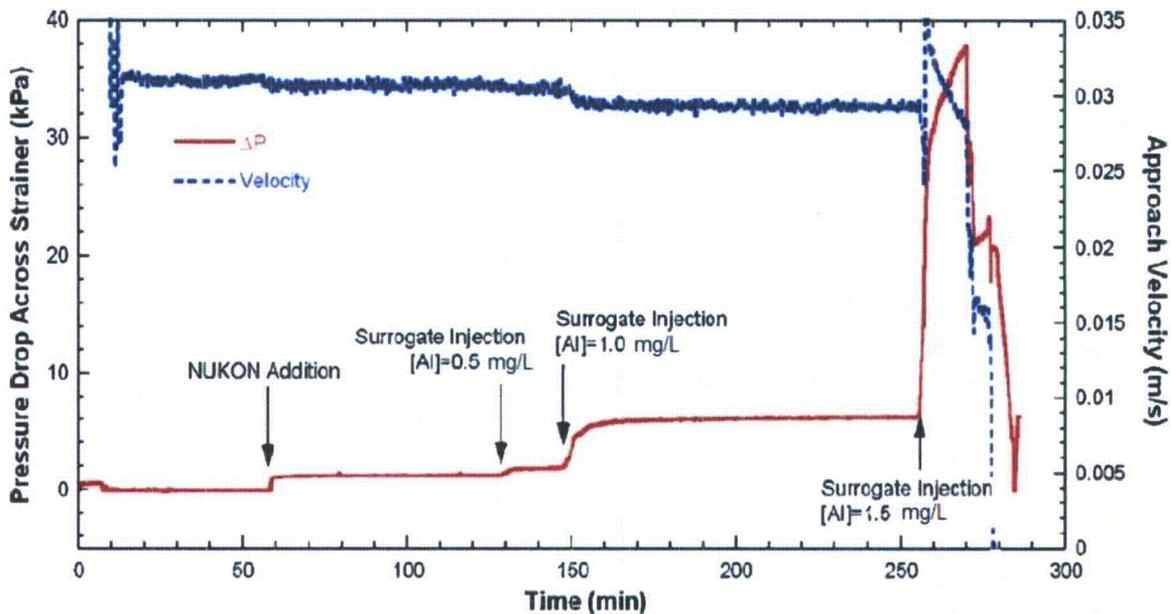


Figure 2: Vertical loop test (3) response to AIOOH chemical loading (80 °F, 0.1 ft/s, blender processed fiber only)

When scaled to the same conditions of the STP module test, the response from Bahn et al. data (3) indicate a lower CHL than the raw data. However, scaling between test fluid conditions is not enough for a direct comparison between the vertical and strainer test settings because the precipitate loading opportunity of the different debris beds must be taken into account. For this purpose, a superficial loading parameter (L^*) is defined as a third scaling parameter for CHL responses in different test settings:

$$L^* = \frac{\text{Total precipitate in solution (g)}}{\text{Total filter surface area (m}^2\text{)}} \tag{Equation 3}$$

Inclusion of the filtration area in L^* is empirically based on observed response to precipitate additions across different debris beds used in different test settings. That is, more total precipitates are required in large-scale tests to produce roughly the same head loss response as seen in smaller scale tests. Empirically, the total precipitate available for loading over any given filtration surface area, the velocity through the bed, and the fluid viscosity are taken to be first order for CHL. The L^* definition is

	Quantification of Chemical Head Loss Epistemic Uncertainty; Basis for Incremental Chemical Head Loss Correlation		
	Document No: ALION-REP-STP-8998-08	Rev: I	Page 12 of 46

convenient for use in risk-informed GSI-191 analyses because the number of strainers in service (and a known surface area for each strainer in service) provides a known filter area to calculate a CHL response.

Strainer and vertical CHL results obtained from aluminum oxyhydroxide (AIOOH) additions (2; 3) were compared using L*. As shown in Table 1, CHL response per L* of the vertical test is similar to that of the strainer test for conditions investigated. However, L* determined for the strainer test is approximately a factor of six times greater than that determined for the vertical tests. A similar CHL per L* response to such different L* values is likely attributable to the inherent and uncharacterized differences that affect filtration efficiency or loading opportunities between the test beds. Since the strainer test setting requires higher precipitate exposure in solution than that of the vertical test to produce similar CHL per L* responses, it is likely that vertical test settings overestimate CHL; while the strainer test setting more closely approximates expected CHL by inclusion of utility-specific parameters that may influence CHL.

Table 1: Parameters used to normalize results between test settings for comparison

Parameter	Vertical	Strainer ¹
Strainer area (m ²)	0.013	8.495
Aluminum concentration (mg/L)	1.500	94.383
Volume of apparatus (L)	118	6926
AIOOH (g)	0.393	1453
L* (g/m ²)	29.5	171.0
² CHL response (ft)	>0.4	2.6
² CHL response per L* (ft/g-m ⁻²)	>0.014	0.015

¹First batch of chemical addition (AIOOH) to debris bed

²Data normalized to 116.3 °F and 0.0086 ft/s

Results obtained from strainer and vertical test settings inadequately characterized parameters that could be used for the development of a comprehensive, theoretical CHL correlation. While opportunity exists to use both settings for development of such a correlation, as described in Leavitt's Options 3 and 4 (1), the STP strainer test represents a high, risk-informed bounding debris (fiber and particulate) bed response that includes all uncharacterized parameters for a CHL response to an upper range of chemical precipitate loading (that is, a bounding (high) risk-informed filtration efficiency and loading opportunity). The STP strainers test fiber quantities are described as high, risk-informed bounding debris responses because the fiber quantity used in testing was based on a 7D zone of influence (ZOI) as opposed to 17D ZOI as specified for deterministic analysis (10); However the 7D ZOI resulted in testing debris quantities that are larger than the weighted mean quantities determined for large breaks in CASA Case 01 as shown in Figure 3. Table 2 shows that the strainer testing fiber quantities, although generated from a 7D ZOI, lie in the tail of the analysis.

	Quantification of Chemical Head Loss Epistemic Uncertainty; Basis for Incremental Chemical Head Loss Correlation		
	Document No: ALION-REP-STP-8998-08	Rev: I	Page 13 of 46

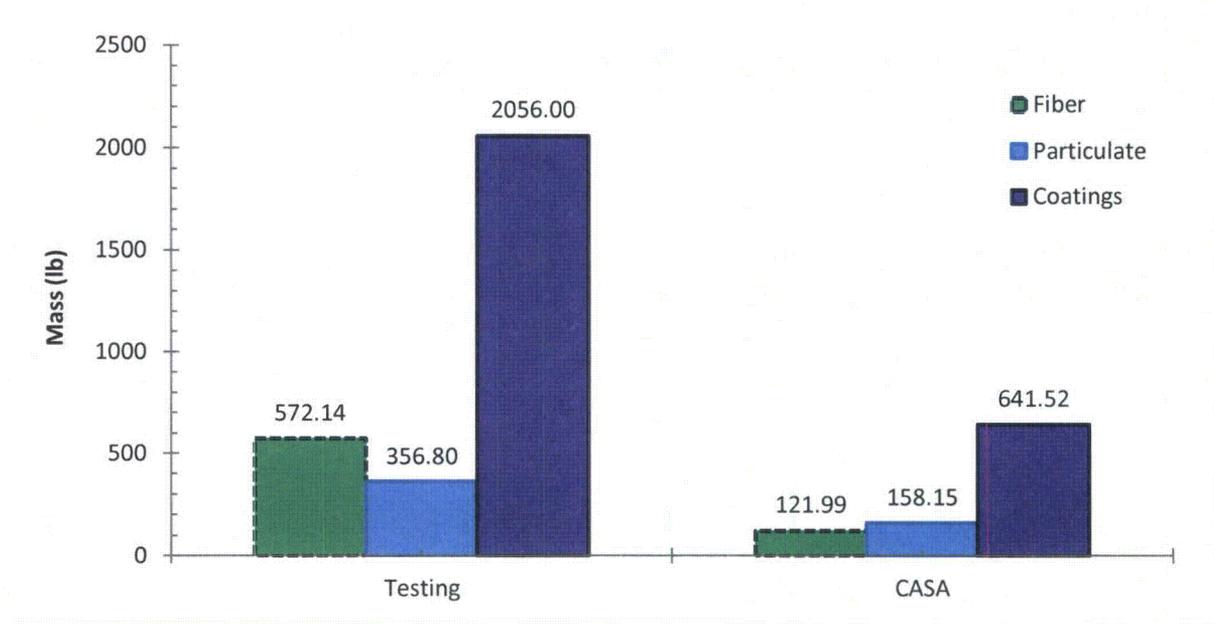


Figure 3: Debris used in testing as compared to the weighted large break mean values

Table 2: Debris used in strainer testing with location in CASA distributions

Debris Type	Strainer (lb _m)	Large Break Percentile in CASA
Fibers		
LDFG fines	163.01	0.9748
LDFG smalls	380.35	0.9852
LDFG large	3.82	N/A ²

¹ Result are related to quantity of smalls which consist of both fines from eroded smalls and non-eroded smalls

² Large LDFG does not transported in CASA, however eroded fines do transport and are accounted in CASA but not shown in this table

Since the strainer testing provides a risk-informed bounding amount of fibrous debris using quantities determined from a 7D ZOI, the strainer CHL responses obtained under STP conditions as a function of L* are useful for development of an empirical correlation that would quantify bounding (higher than expected) CHL responses for risk-informed analysis.

2.0 Precipitate Evaluation

An empirical correlation has been developed that would overestimate expected CHL based on STP strainer performance results (2). The correlation is applied using Option 1 of the modular chemical effects quantification approach shown in Figure 4 (1). Option 1 identifies precipitates to be included in the analysis and uses WCAP-16530-NP material release equations to predict precipitate formation. No

	Quantification of Chemical Head Loss Epistemic Uncertainty; Basis for Incremental Chemical Head Loss Correlation		
	Document No: ALION-REP-STP-8998-08	Rev: I	Page 14 of 46

credit for solubility is taken in order to arrive at a CHL correlation from best available data that would conservatively quantify (overestimate) CHL resulting from the appearance of precipitates (1).

In the following, Section 2.1 explains the identification (Module 1 (1)), quantification (Modules 2 and 3 (1)), and characterization (Module 4 (1)) of chemical precipitates used in the modular approach. Section 3.0 explains the derivation of the empirical correlation (Module 5 (1)).

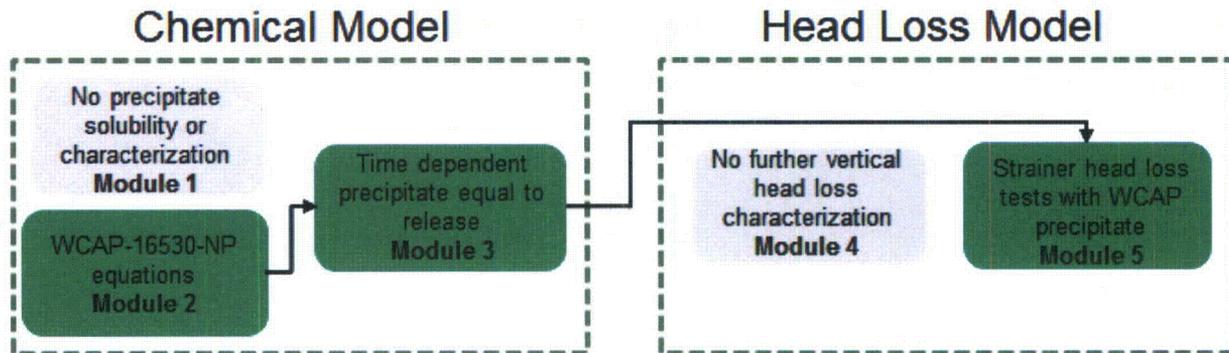


Figure 4: Option 1 of modular CHL quantification approach (1)

2.1 Chemical Precipitate Analysis

Table 3 summarizes the four common chemical precipitates that have been considered in CHL evaluations. Deterministic analysis includes formation of aluminum and calcium precipitates, regardless of buffer system used (11). Risk-informed analysis considered aluminum and calcium precipitate formation as well, but experimental investigations indicated an insoluble zinc product also formed in trisodium phosphate (TSP) systems (6; 7; 8). Identification of the products to be included in the analysis satisfies the requirement for Module 1 (1). Quantification of transportable precipitates (Module 2 and 3 (1)) can be accomplished using WCAP-16530-NP material release equations for Option 1. Analysis to identify transportable precipitates that produce the largest CHL response (Module 4 and 5 (1)) is described in Section 2.1.2.

Table 3: Precipitates considered for CHL analysis

Precipitate Type	Abbreviation	Application
Sodium aluminum silicate	SAS	Deterministic (11)
Aluminum oxyhydroxide	AlOOH	Deterministic (11)
Calcium phosphate	Ca ₃ (PO ₄) ₂	Deterministic (11)
Zinc phosphate	Zn ₃ (PO ₄) ₂ •4 H ₂ O	Risk-informed (6; 7; 8)

	Quantification of Chemical Head Loss Epistemic Uncertainty; Basis for Incremental Chemical Head Loss Correlation		
	Document No: ALION-REP-STP-8998-08	Rev: I	Page 15 of 46

2.1.1 Zinc Phosphate

While $Zn_3(PO_4)_2 \cdot 4 H_2O$ was observed to form in risk-informed tests (6; 7) it was observed to preferentially deposit on galvanized steel surfaces as opposed to forming in solution. Additional experiments indicate $Zn_3(PO_4)_2 \cdot 4 H_2O$ is unlikely to transport in solution (8). When zinc corrosion materials were included in the STP risk-informed tests, head loss response was observed during the initial hour of testing (6; 7); however, additional tests (8) indicated that the head loss response to the zinc product was likely the result of initial dissolution of a surface layer and not from transport of a continuously generated zinc corrosion product ($Zn_3(PO_4)_2 \cdot 4 H_2O$). Therefore, the initial zinc product release is treated as a particulate source and not considered a zinc chemical product. Since $Zn_3(PO_4)_2 \cdot 4 H_2O$ is unlikely to transport to the strainer and, given that Option 1 CHL is intended to produce conservative or overestimated CHL response to identified precipitate loads, $Zn_3(PO_4)_2 \cdot 4 H_2O$ generation is ignored in the CHL correlation development.

2.1.2 Evaluation of Transportable Precipitates

Traditional WCAP-16530-NP products (AIOOH, SAS, and $Ca_3(PO_4)_2$) expected to transport to the ECCS strainer were examined to identify the precipitate producing greatest CHL for use in the CHL correlation. Review of academic literature (3; 4), review of STP strainer results (2), and evaluation of unpublished University of New Mexico (UNM) head loss data were used to satisfy this analysis.

Bahn et al. (3; 4) investigated the WCAP-16530-NP aluminum surrogate CHL responses in a vertical loop. Although the investigation focused on large CHL response from small quantities of both types of aluminum precipitates, Bahn et al. concluded that the SAS surrogate did not appear to be quite as efficient as the AIOOH surrogate in increasing head loss (3; 4). Based on observations obtained by Bahn et al., AIOOH is assumed to produce greater CHL response than SAS.

Comparisons of AIOOH and $Ca_3(PO_4)_2$ CHL in equivalent settings were not found in the academic literature. Therefore, STP strainer test results (2) were used as a basis to assess and compare the CHL responses from $Ca_3(PO_4)_2$ and AIOOH additions. The STP strainer test spanned two days of chemical additions, but $Ca_3(PO_4)_2$ was only added during the first day of chemical addition; therefore only the first day's head loss results were reviewed. Both surrogates were added individually with one to two pool turnovers between additions, producing the CHL responses shown in Figure 5. Since the STP strainer test was an integral effects test that combines all contributors to a total head loss, the response from each surrogate addition, shown in Figure 5, is actually attributable to the specified surrogate addition and other effects, which include further filtration of chemicals remaining in circulation from previous addition. However, CHL is taken to be only attributable to the specified surrogate addition.

	Quantification of Chemical Head Loss Epistemic Uncertainty; Basis for Incremental Chemical Head Loss Correlation		
	Document No: ALION-REP-STP-8998-08	Rev: 1	Page 16 of 46

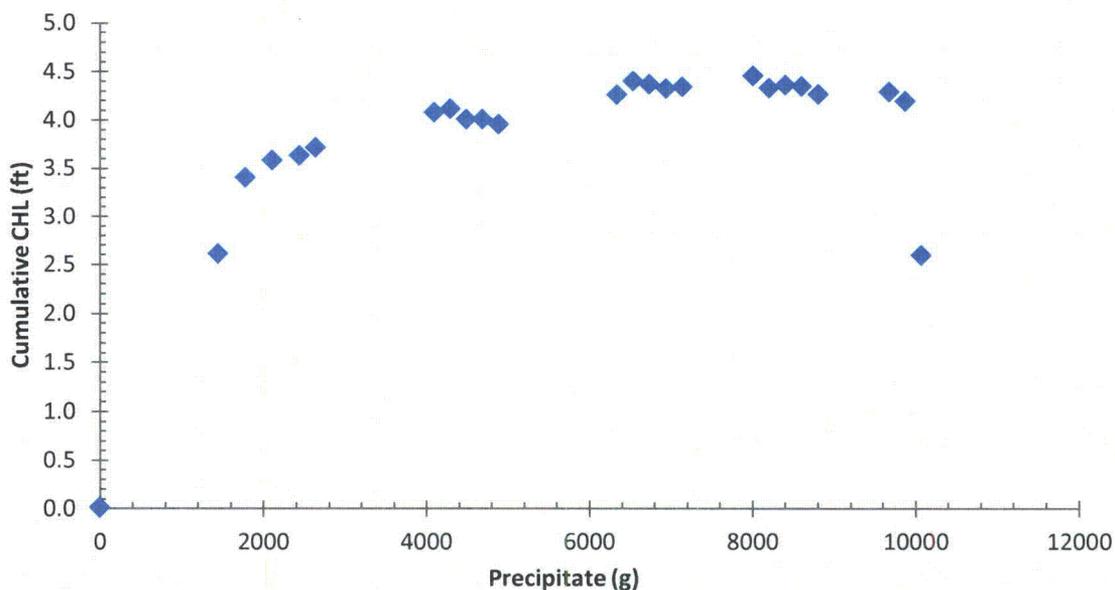


Figure 5: Cumulative CHL response to surrogate precipitate added in the STP strainer test (2)

As seen in Figure 5, the initial CHL response to chemical loading is steep and becomes less responsive as the chemical load increases. This transition in CHL response to precipitate loading of an STP design-basis debris bed occurs as the addition reaches 2,000 g of precipitate (combination of both surrogates). The measured CHL to each individual addition, shown in Figure 5, was consolidated in such a way that the cumulative pressure response could be determined for each surrogate type, as shown in Figure 6.

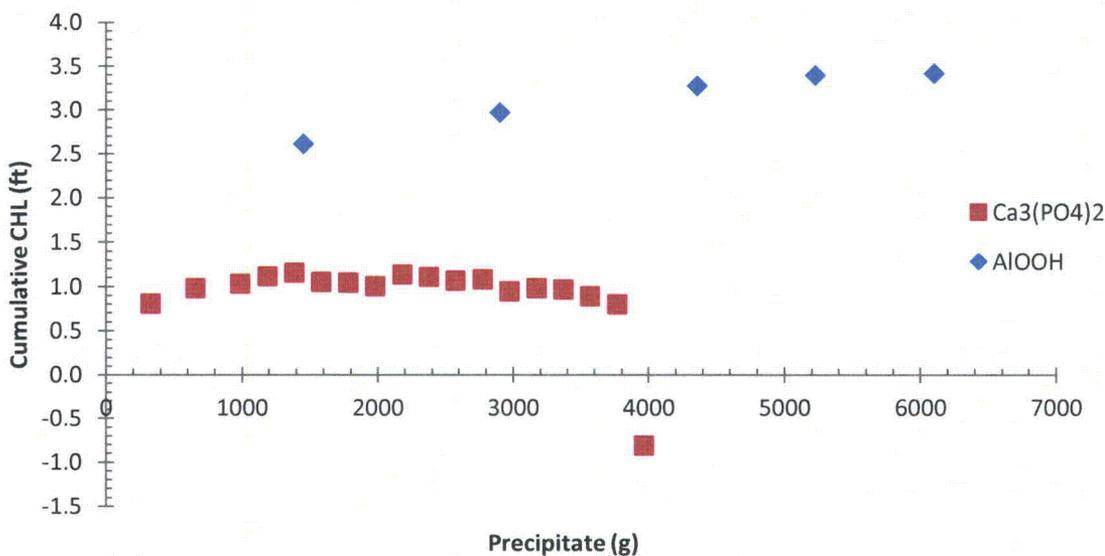


Figure 6: Cumulative CHL response of each precipitate determined from first day of chemical addition of STP strainer test (2)

	Quantification of Chemical Head Loss Epistemic Uncertainty; Basis for Incremental Chemical Head Loss Correlation		
	Document No: ALION-REP-STP-8998-08	Rev: I	Page 17 of 46

The cumulative AIOOH CHL response appears to be much larger than the cumulative $\text{Ca}_3(\text{PO}_4)_2$ response (Figure 6), since the addition of approximately 3000 g of $\text{Ca}_3(\text{PO}_4)_2$ produces less CHL than the same mass addition of AIOOH. However, given the transition in CHL response that occurs as a function of precipitate loading, further comparisons between AIOOH and $\text{Ca}_3(\text{PO}_4)_2$ CHL were necessary to ensure AIOOH CHL response adequately bounds the $\text{Ca}_3(\text{PO}_4)_2$ CHL response. Therefore, the AIOOH and $\text{Ca}_3(\text{PO}_4)_2$ CHL responses observed in the STP strainer test as a function of CHL response per mass of precipitate added, before and after the transition that occurs at 2000 g of total precipitate added, were evaluated. As shown in Figure 7, the CHL per mass of surrogate added with each batch appeared to be very similar regardless of surrogate types. However, given the variability in CHL per mass response that occurs after the transition point, the AIOOH and $\text{Ca}_3(\text{PO}_4)_2$ CHL responses indicated need for additional assessment.

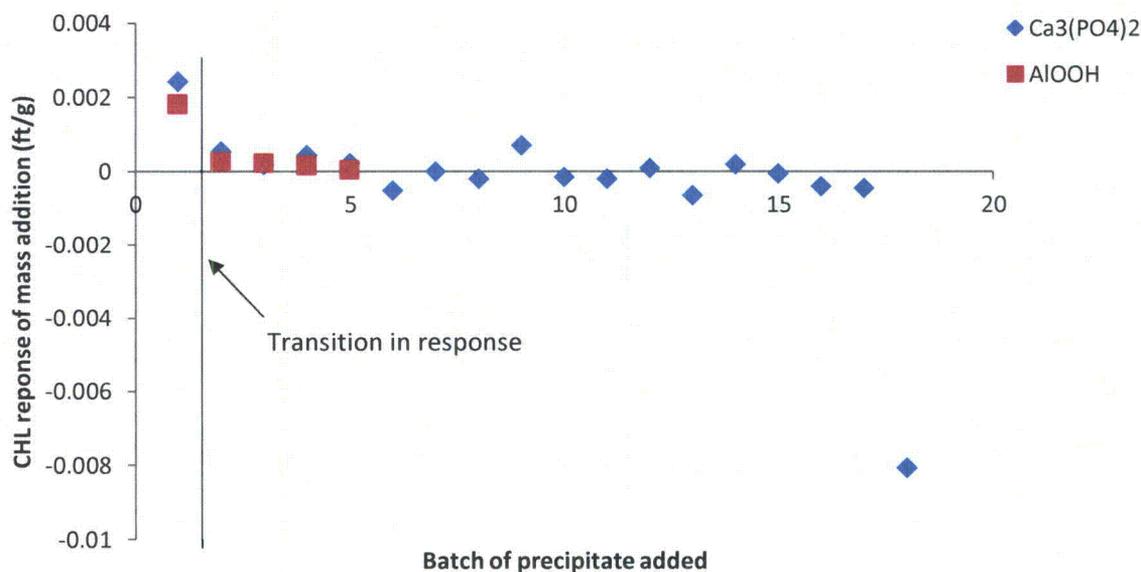


Figure 7: CHL per mass loading of each day-1 batch addition during STP strainer testing (2)

A comparative test to further evaluate CHL differences between $\text{Ca}_3(\text{PO}_4)_2$ and AIOOH was performed at UNM using the CHLE apparatus with the help of Dr. Amir Ali and debris beds developed for Southern Nuclear Company (SNC) Vogtle plant studies. The SNC Vogtle beds included particulate and fiber debris using the NEI protocol and had been at a stable head loss for several days. The CHL comparative test used two of the three UNM CHLE vertical head loss columns, both operated in isolation from each other and from the tank. Each column was loaded with 3.63 g of NEI prepared Nukon fiber and 50 g of 10 micron acrylic paint chips under approach velocity of 0.05 ft/s. The column approach velocity was decreased to Vogtle representative approach velocity of 0.013 ft/s. The debris beds were both shown to be stable over a period of two weeks of exposure to 0.013 ft/s approach velocity. Prior to chemical addition, the approach velocity was reduced to STP representative approach velocity of 0.0086 ft/s and

	Quantification of Chemical Head Loss Epistemic Uncertainty; Basis for Incremental Chemical Head Loss Correlation		
	Document No: ALION-REP-STP-8998-08	Rev: I	Page 18 of 46

the stabilized differential pressures (DP) of both columns measured 4.7 inches. Note that reported DP values are converted from pounds per square inch (PSI) to inches of water referenced to 39.2 °F prior to further temperature corrections. Equal masses of WCAP-16530-NP aluminum and calcium surrogates (prepared and tested per the WCAP-16530-NP protocol) were then added to the columns with stabilized debris beds as specified in Table 4. CHL responses obtained from the surrogate additions were allowed to stabilize prior to further additions as shown in Figure 8.

Table 4: Chemical precipitate addition to stable fiber/particulate debris bed

Time of Precipitate Addition (day)	Column 1		Column 2	
	Chemical Added	Mass (g)	Chemical Added	Mass (g)
0.3	Ca ₃ (PO ₄) ₂	0.05	AlOOH	0.05
1	AlOOH	0.05	Ca ₃ (PO ₄) ₂	0.05
2	Ca ₃ (PO ₄) ₂	0.05	AlOOH	0.05
2.3	AlOOH	0.05	Ca ₃ (PO ₄) ₂	0.05
3	Ca ₃ (PO ₄) ₂	0.05	AlOOH	0.025
4	AlOOH	0.025	Ca ₃ (PO ₄) ₂	0.05
Test termination	Complete mixture	0.275	Complete mixture	0.275

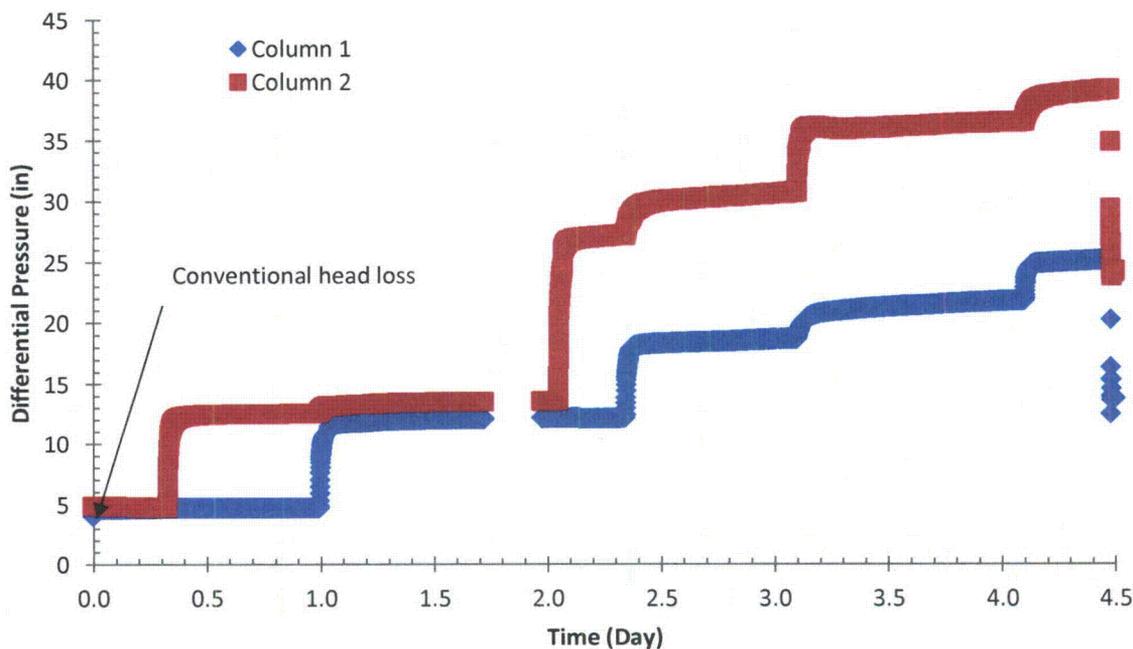


Figure 8: Trend of CHL response to precipitate addition to stabilized beds in columns 1 and 2 (Courtesy of UNM).

	Quantification of Chemical Head Loss Epistemic Uncertainty; Basis for Incremental Chemical Head Loss Correlation		
	Document No: ALION-REP-STP-8998-08	Rev: 1	Page 19 of 46

The first 0.05 g addition of $\text{Ca}_3(\text{PO}_4)_2$ to Column 1 did not significantly impact the existing conventional head loss as shown in Figure 9 below. Conversely, the first 0.05 g addition of AIOOH to Column 2 nearly tripled the conventional head loss. After the CHL response to the second chemical addition stabilized in both columns (on day 2), the resulting CHL mixture responses (0.05 g AIOOH + 0.05 $\text{Ca}_3(\text{PO}_4)_2$) of both columns were very similar with an approximate 11% relative difference. As additions of chemical precipitates continued, the AIOOH CHL was always much greater than the $\text{Ca}_3(\text{PO}_4)_2$ CHL on equivalent mass basis as shown in Table 5. However, the overall CHL response for equivalent precipitate mass loading ($\text{Ca}_3(\text{PO}_4)_2$ + AIOOH) deviated between the columns resulting in an approximate 41% relative difference between final CHL values.

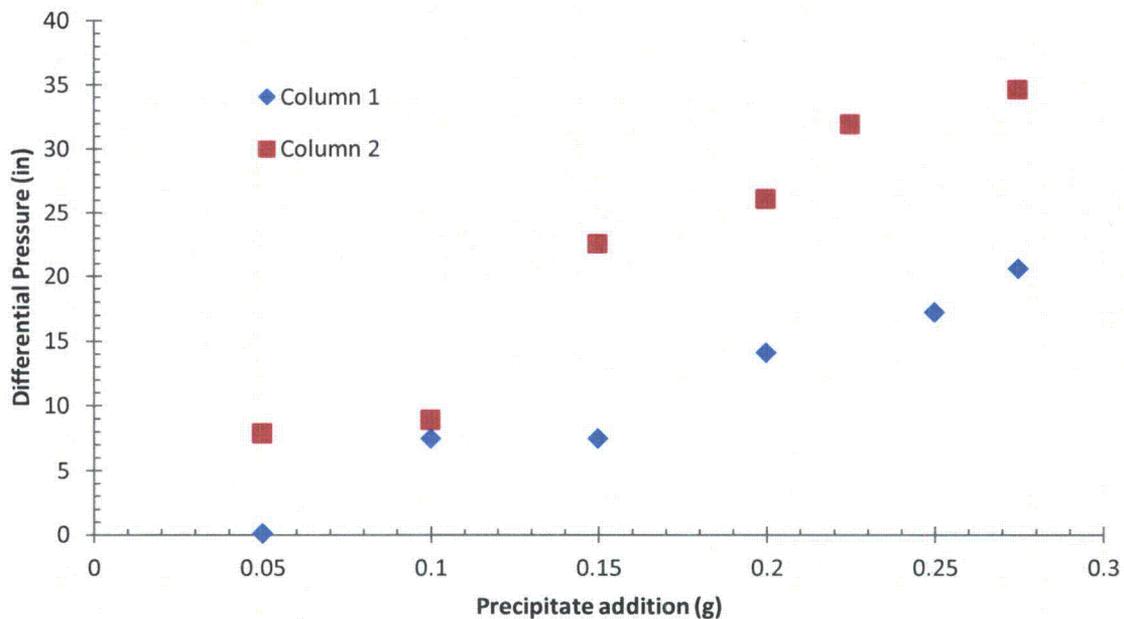


Figure 9: CHL vs. mass of $\text{Ca}_3(\text{PO}_4)_2$ and AIOOH precipitate added in different order

Table 5: DP resulting from individual additions within in each batch-precipitate added

Batch (Precipitate Added)	$\text{Ca}_3(\text{PO}_4)_2$ (in)		AIOOH (in)	
	Column 1	Column 2	Column 1	Column 2
1 (both types;0.50 g)	0.02	1.04	7.43	7.83
2(both types;0.50 g)	0	3.51	6.59	13.62
3 (AIOOH, 0.25 g) ¹	-	-	3.34	5.86
3 ($\text{Ca}_3(\text{PO}_4)_2$, 0.05g) ¹	3.14	2.67	-	-

¹AIOOH mass was reduced in the third batch to protect the differential pressure cell from expected large DP increase

	Quantification of Chemical Head Loss Epistemic Uncertainty; Basis for Incremental Chemical Head Loss Correlation		
	Document No: ALION-REP-STP-8998-08	Rev: I	Page 20 of 46

Although the AIOOH CHL was consistently greater than the $\text{Ca}_3(\text{PO}_4)_2$ CHL, a large difference in AIOOH CHL results between columns was observed and is summarized in Table 6. The variation in CHL due to AIOOH is likely attributable to inherent differences in bed morphology that exists within a given bed type and/or related to the order of addition with the different precipitate. However, substituting the minimum observed CHL response due to AIOOH (131.80 in/g) for all chemical precipitate mass additions (0.275 g) listed in Table 4 adequately bounds the total CHL response observed in both columns as shown in Figure 10 by "Prediction (minimum AIOOH response) series," despite the 41% relative difference in final CHL between the two columns. These results provide confidence that AIOOH CHL is greater than $\text{Ca}_3(\text{PO}_4)_2$ CHL for the same total mass added.

Table 6: Variation in AIOOH response (in/g) observed during UNM vertical tests

AIOOH Additions(g)	Column 1 (in/g)	Column 2 (in/g)
0.05	148.60	156.60
0.05	131.80	272.40
0.025	133.60	234.40

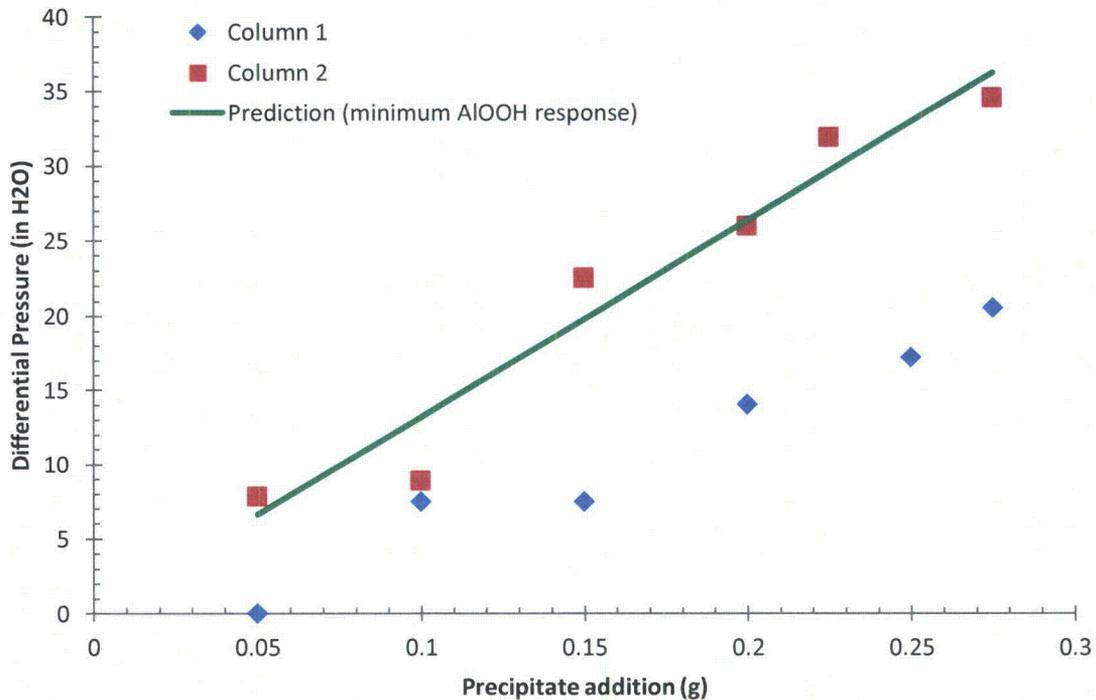


Figure 10: CHL vs. mass of precipitate ($\text{Ca}_3(\text{PO}_4)_2$ and AIOOH) added to particulate loaded fiber beds

	Quantification of Chemical Head Loss Epistemic Uncertainty; Basis for Incremental Chemical Head Loss Correlation		
	Document No: ALION-REP-STP-8998-08	Rev: I	Page 21 of 46

In summary, AIOOH CHL can be used to overestimate CHL expected to occur from the same mass addition of any individual transportable precipitates ($\text{Ca}_3(\text{PO}_4)_2$ and SAS) to a STP design-basis debris bed. Therefore, the Option 1 CHL correlation uses AIOOH as a basis for CHL response per mass of precipitate (for any precipitate assessed).

3.0 Head Loss Correlation

Identification of a precipitate (AIOOH) with a bounding CHL response simplified the correlation development (Module 5 (1)) by assuming any mass of precipitate generated produces the CHL response observed from AIOOH additions. Since the STP strainer test results (2), shown in Figure 11, included $\text{Ca}_3(\text{PO}_4)_2$ CHL, the data were processed to remove all but the first addition of $\text{Ca}_3(\text{PO}_4)_2$. Removal of these data supports conservative correlation development because UNM results show it is likely that $\text{Ca}_3(\text{PO}_4)_2$ additions produce a lower CHL per gram than AIOOH additions (Table 5). The first $\text{Ca}_3(\text{PO}_4)_2$ addition was included in the analysis since it occurred before the transition in CHL response of precipitate loading (around 2000 g of total precipitate added). Also, as indicated in Figure 11, declining data associated with high precipitate values were removed. After processing the data set as just described, the CHL data evaluated for correlation development, shown in Figure 12, are normalized by the test strainer surface area, as shown in Figure 13. The data was normalized to include the uncharacterized response of the STP design-basis bed per surface area as described in Section 1.1. The observed transition point that indicates a change in bed response occurs at 210 g/m^2 in the normalized data.

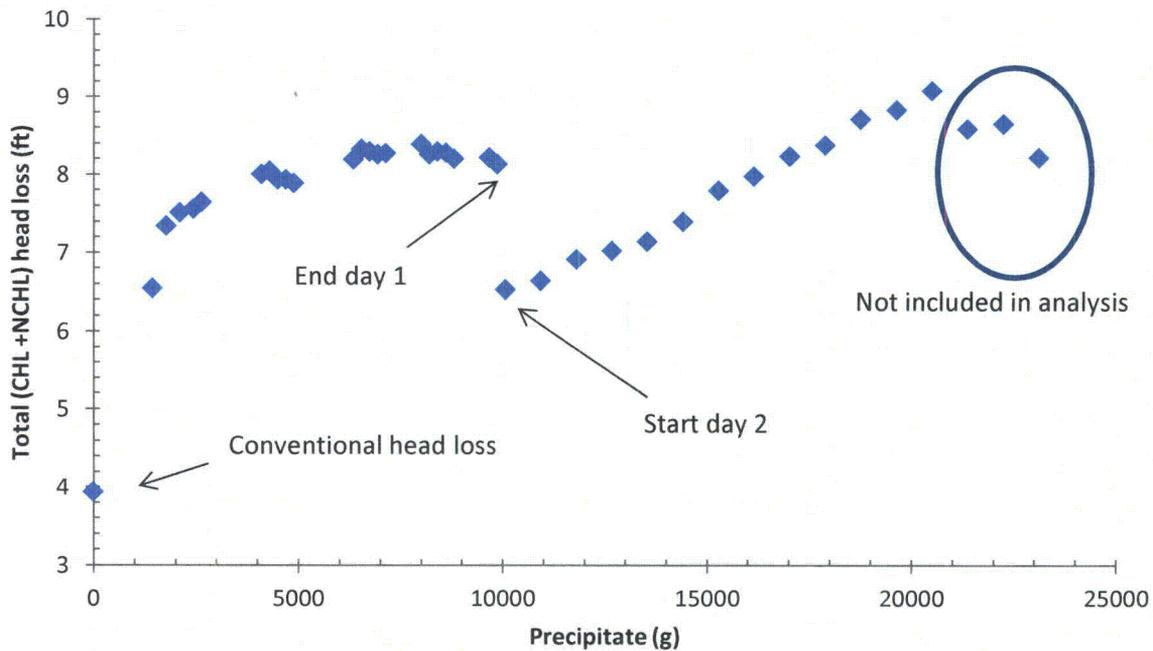


Figure 11: Two day strainer response to added precipitate (AIOOH and $\text{Ca}_3(\text{PO}_4)_2$) in solution (2).

	Quantification of Chemical Head Loss Epistemic Uncertainty; Basis for Incremental Chemical Head Loss Correlation		
	Document No: ALION-REP-STP-8998-08	Rev: I	Page 22 of 46

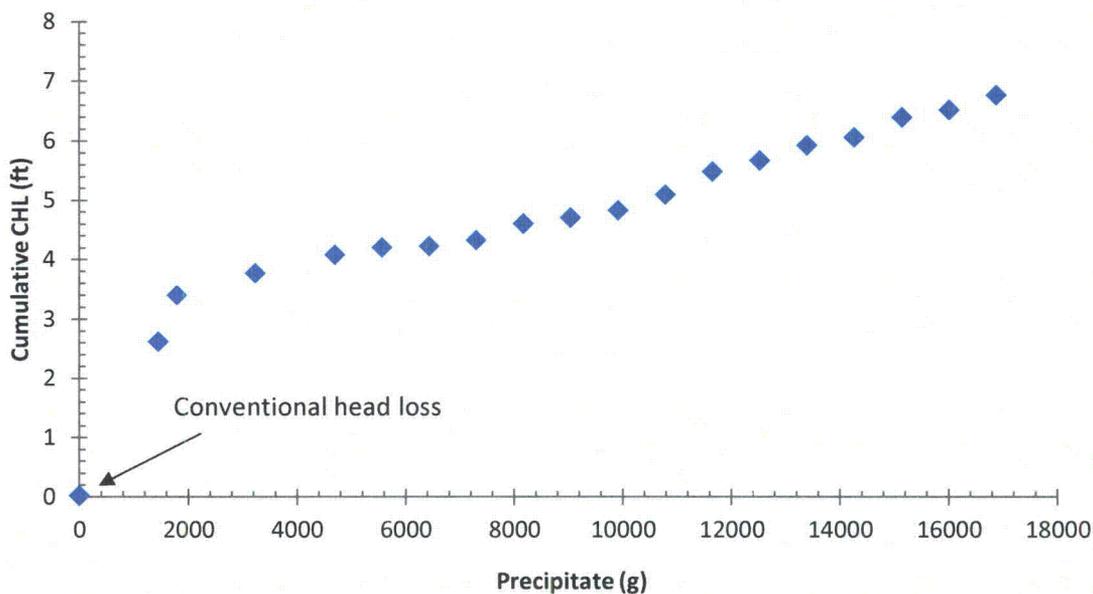


Figure 12: Strainer response to total AlOOH and first batch of $Ca_3(PO_4)_2$ precipitate (2). The last batches of aluminum that produce declining CHL have been removed.

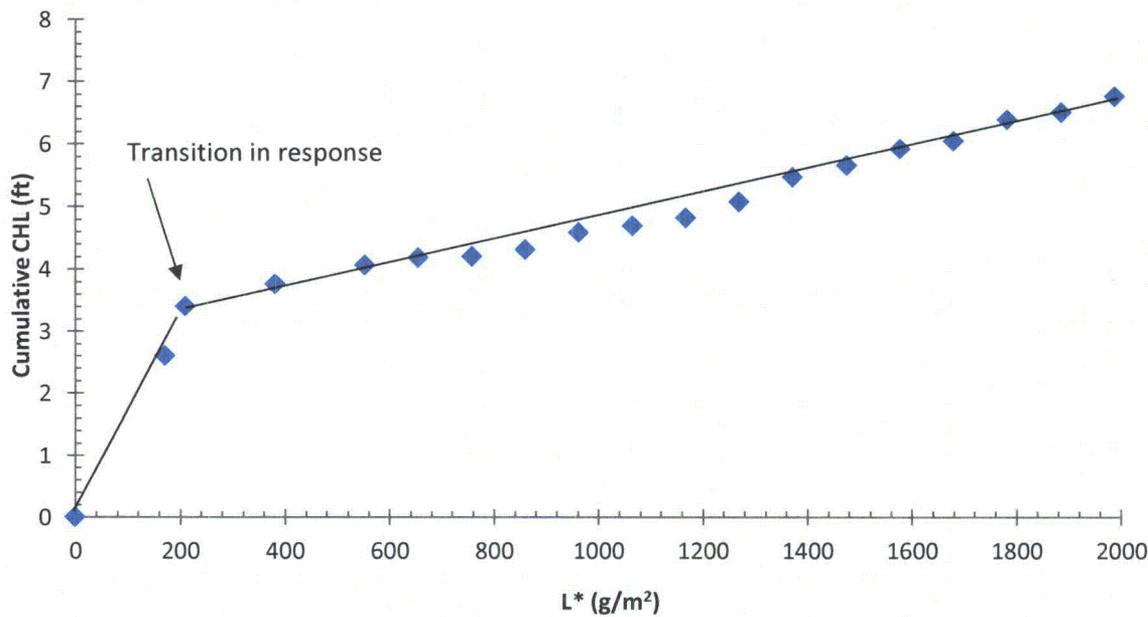


Figure 13: Non-declining AlOOH and first batch of $Ca_3(PO_4)_2$ CHL vs. precipitate availability normalized by strainer area.

	Quantification of Chemical Head Loss Epistemic Uncertainty; Basis for Incremental Chemical Head Loss Correlation		
	Document No: ALION-REP-STP-8998-08	Rev: I	Page 23 of 46

The correlated CHL response up to 210 g/m^2 shown in Figure 13 was studied carefully since the CHL response is steep and only two data points were used in that part of the fit. In particular, the Bahn et al. data (3) were studied at lower L^* values even though results are taken from a vertical loop test in which higher CHL responses are expected compared to strainer module tests. While the unpublished UNM vertical test results (Section 2.1.2) were taken at low L^* values, they were not added to this analysis because the UNM debris bed had a paint chip to fiber mass ratio of 13.8:1 whereas the STP strainer test debris bed had a paint to fiber ratio of approximately 1:1 and the Bahn et al. debris bed had no particulate. It is assumed the uncharacterized response of a very high particulate response bed is much higher than debris beds with low to no particulate loading, making comparison of CHL obtained from a very highly particulate-loaded fiber bed with a low to no particulate-loaded fiber bed irrelevant, even with the use of the L^* parameter.

To better assess the shape of the initial CHL response, CHL measurements from additions of AIOOH reported by Bahn (3) and the equipment limit CHL response for $1.5 \text{ mg aluminum/L}$ (13 ft) were corrected to STP strainer test conditions (2) using Equation 2. The corrected Bahn et al. CHL values and STP strainer test CHL results for L^* values below 210 g/m^2 were compared and are shown in Figure 14. Using the Bahn et al. data corrected to STP conditions to define the shape of the initial response would provide lower CHL response at lower chemical loads than the current model. This comparison also provides confidence the shape and slope of the initial response as defined by the STP strainer data adequately represents CHL at low L^* values (less than 210 g/m^2).

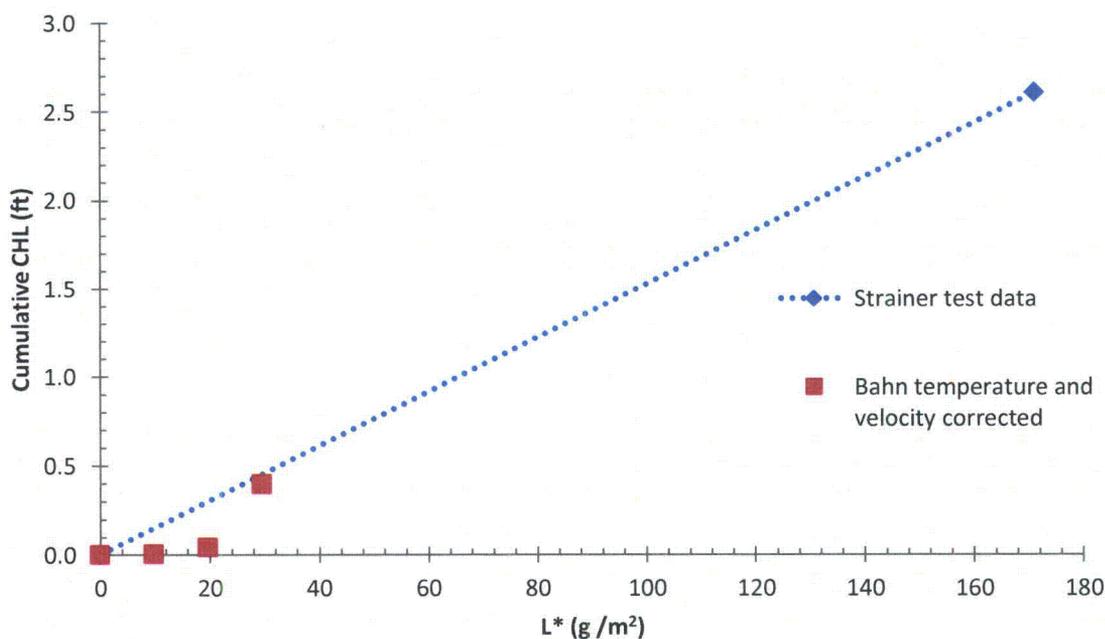


Figure 14: Bahn et al. (3) data, corrected to the STP strainer test conditions, compared to the STP data at low L^* values.

	Quantification of Chemical Head Loss Epistemic Uncertainty; Basis for Incremental Chemical Head Loss Correlation		
	Document No: ALION-REP-STP-8998-08	Rev: I	Page 24 of 46

The data at the transition point (210 g/m²) of the CHL response shown in Figure 13 were also re-assessed since only two data points are used to define the upper bound CHL response. While both initial surrogate additions produced an equivalent response of 0.002 ft/g, the highest raw value of 0.0024 ft/g was used to calculate CHL caused by both surrogate additions at L* values 171 and 210 g/m². This calculated CHL response for the chemical additions was slightly higher than the experimentally observed responses as shown in

Figure 15. To ensure that the conservative development of the CHL correlation, calculated responses were used up to the transition point of 210 g/m² and experimentally obtained incremental CHL which occurs after 210 g/m² was directly added to calculated CHL shown in

Figure 15. Shifted data, which increased the initial CHL response by 0.89 ft, was used to generate a new cumulative CHL response per L* as shown in Figure 16. The cumulative CHL as a function of L* shown in Figure 16 was evaluated to generate two linear equations to predict CHL. The final correlation equations and data used to generate these equations are shown in Figure 17.

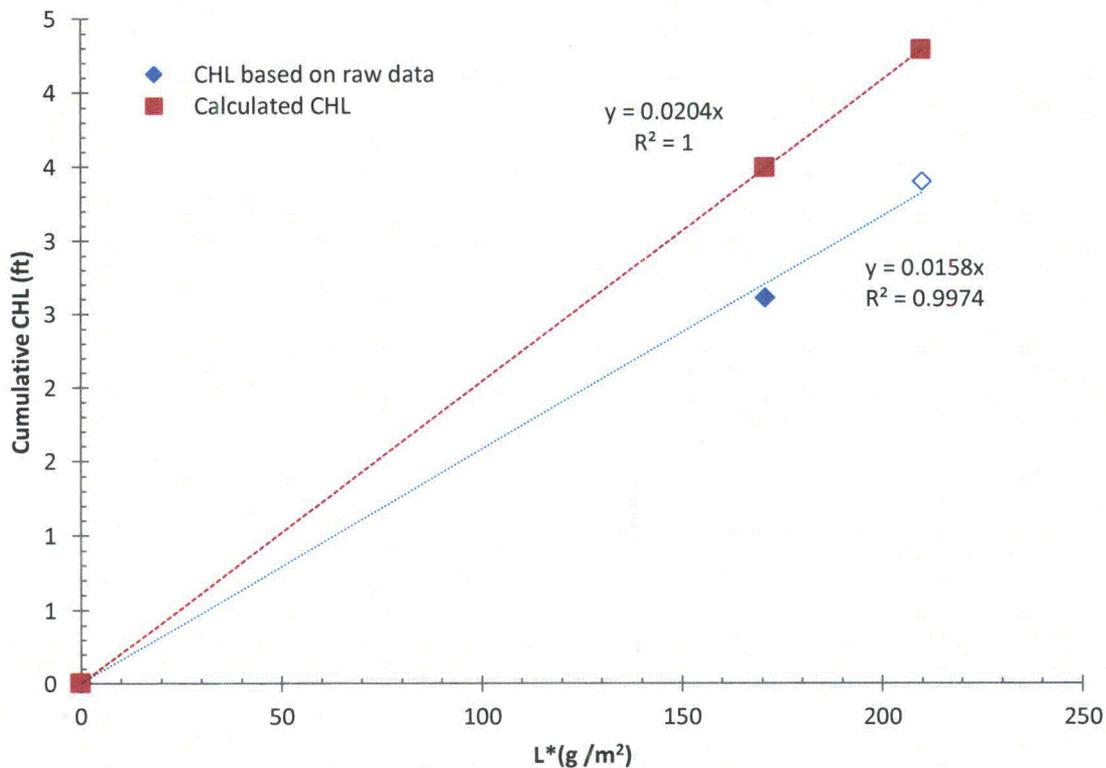


Figure 15: Cumulative CHL determined from calculated and experimental values

	Quantification of Chemical Head Loss Epistemic Uncertainty; Basis for Incremental Chemical Head Loss Correlation		
	Document No: ALION-REP-STP-8998-08	Rev: I	Page 25 of 46

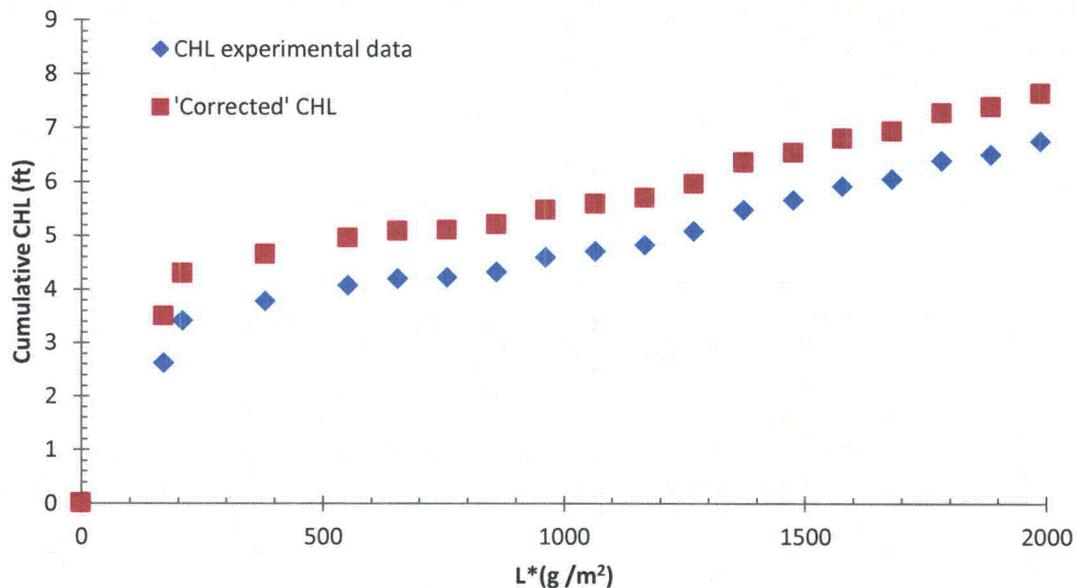


Figure 16: 'Corrected' strainer data biased to provide conservative response as compared to experimental data

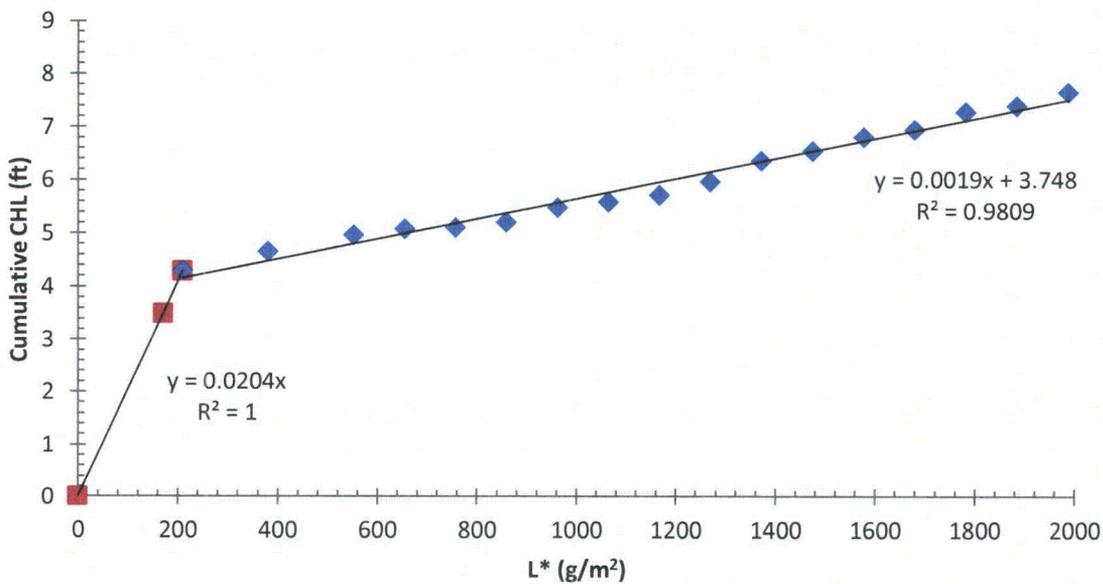


Figure 17: CHL correlation developed from shifted data

	Quantification of Chemical Head Loss Epistemic Uncertainty; Basis for Incremental Chemical Head Loss Correlation		
	Document No: ALION-REP-STP-8998-08	Rev: I	Page 26 of 46

While every effort was taken to ensure the correlation produces a conservative CHL response, the fact that the correlation is based on a single test report was not ignored. Review of other plant replicate strainer test data (12) and discussion with Alden laboratory concerning historical variability in tests with replicates lead to consideration of applying a 25% uncertainty band on the correlation. However, since the correlation has an inherent bias for conservative (overestimated) head-loss response built in by removing all negative or non-increasing pressure responses to surrogate addition and by assigning AIOOH CHL response to all surrogate additions, no further uncertainty was added to the correlation. By analogy to a one-tailed confidence interval, the conservative interpretation of test data increases the confidence level (for example from 95% to 99%) that replicate measurements would lie below the predictive correlation obtained from the data fit.

4.0 Results and Discussion

Two linear equations represent the correlation between CHL and L^* shown in Figure 17. The final form of the CHL correlation equations are represented by Equations 4 and 5.

$$THL(ft) = (NCHL(ft) + C_1 \left(\frac{ft}{g-m^2}\right) \times L^* \left(\frac{g}{m^2}\right)) \times \theta \quad \text{for } 0 < L^* \leq 210, \quad \text{Equation 4}$$

$$THL(ft) = (NCHL(ft) + C_2 \left(\frac{ft}{g-m^2}\right) \times L^* \left(\frac{g}{m^2}\right) + C_3(ft)) \times \theta \quad \text{for } 210 < L^* \leq 2723, \quad \text{Equation 5}$$

where,

- $C_1 = 0.0204$
- $C_2 = 0.0019$
- $C_3 = 3.748$
- $\theta = \frac{v}{v_{ref}} \times \frac{U}{U_{ref}}$
- v = fluid viscosity at the temperature condition
- v_{ref} = fluid viscosity used in the data fit
- U = fluid approach velocity at the strainer
- U_{ref} = fluid approach velocity used in the data fit

The manner in which the correlation was developed results in equations that over-estimate all the STP strainer data by equal to or greater than 25%. The correlation over-estimates the STP final strainer test result by approximately a factor of 2, as shown by Figure 18.

	Quantification of Chemical Head Loss Epistemic Uncertainty; Basis for Incremental Chemical Head Loss Correlation		
	Document No: ALION-REP-STP-8998-08	Rev: I	Page 27 of 46

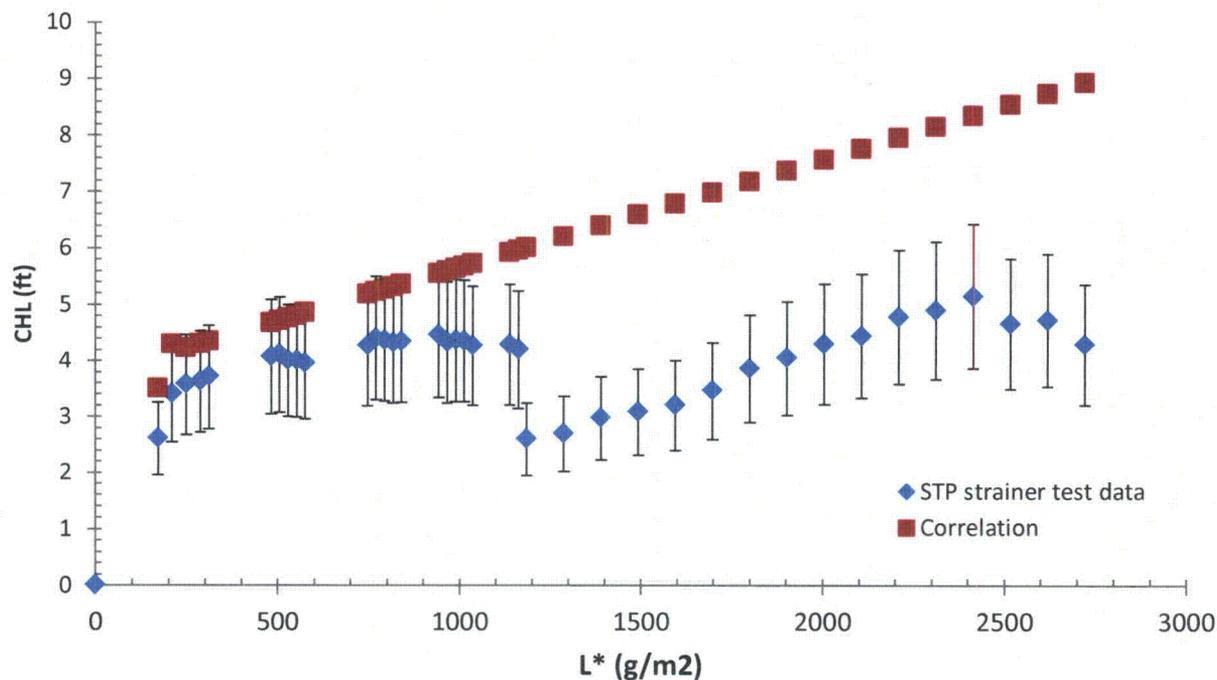


Figure 18: Strainer response to added mass of precipitate per strainer area (g/m^2). STP test data is presented with a 25% uncertainty band.

4.1 CHL Correlation Applied to Other TSP Plants' Strainer Tests

Although the correlation is specifically based on the CHL response from a STP design basis debris bed and strainer, the correlation was applied to strainer module CHL test data from other TSP plants to evaluate CHL performance for possible generic applicability of the equation. First, strainer test results (12; 13) were evaluated to determine L^* , reference temperature, and reference velocity required for the CHL calculation using the STP correlation (Equations 4 and 5). The calculated (temperature and velocity corrected) CHL values were then compared to the experimentally observed CHL values. As shown in Figure 19 and Figure 20, the STP correlation overestimates the final CHL for both plants evaluated by at least a factor of 2, providing further confidence of the conservative adequacy of the STP CHL correlation.



Quantification of Chemical Head Loss Epistemic Uncertainty; Basis for Incremental Chemical Head Loss Correlation

Document No: ALION-REP-STP-8998-08

Rev: I

Page 28 of 46

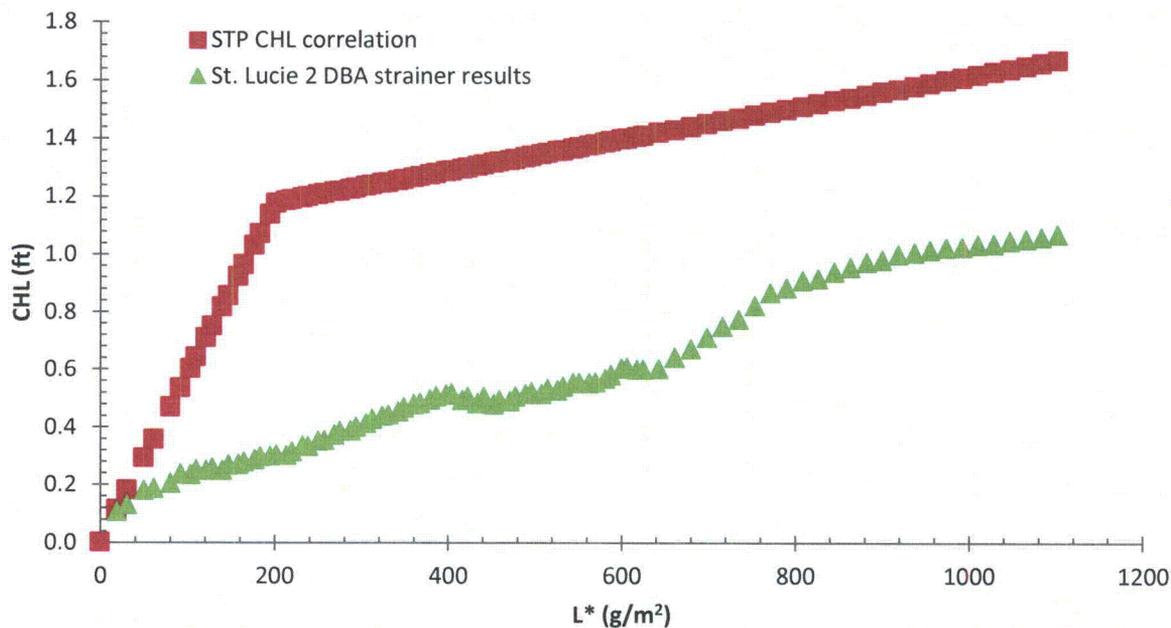


Figure 19: STP correlation prediction compared to St. Lucie's experimentally observed CHL (13).

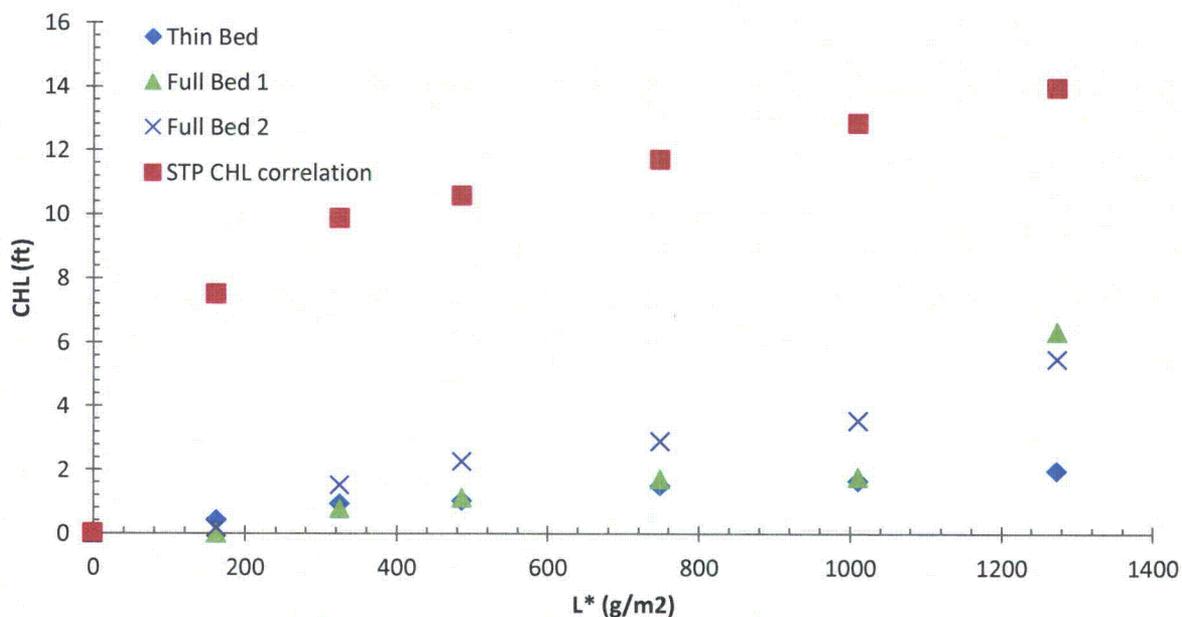


Figure 20: STP correlation prediction compared to Vogtle's experimentally observed CHL (12).

	Quantification of Chemical Head Loss Epistemic Uncertainty; Basis for Incremental Chemical Head Loss Correlation		
	Document No: ALION-REP-STP-8998-08	Rev: I	Page 29 of 46

In particular, evaluation of CHL correlation performance using Vogtle strainer test data also provides further evidence of the correlation applicability to all possible post-LOCA conditions. Although the CHL correlation is derived from CHL responses of a design-basis debris bed, it will conservatively bound (overestimate) the thin bed CHL response. Vogtle strainer test data shown in Figure 20 indicates that the thin bed CHL response, up to the fifth batch addition, was equivalent to the "Full Bed 1" (design-basis) CHL response and slightly lower than the "Full Bed 2" (design-basis) CHL response. However, the THL of a thin bed case is much less than the THL of the "Full Bed 1" and "Full Bed 2" cases as shown by Table 7. The difference in thin bed THL and design-basis bed THL with similar CHL responses (up to the fifth batch addition) was because the NCHL prior to chemical loading was much smaller for a thin bed as compared to the design-basis cases "Full Bed 1" and "Full Bed 2". Therefore, the additive method associated with the CHL correlation to determine THL adequately and conservatively bounds the higher CHL multiplicative response on the thin bed NCHL and the lower multiplicative response on the full bed (design-basis) NCHL.

Table 7: Head loss values obtained from SNC's Vogtle strainer test referenced to test conditions (12)

Condition	Stabilized NCHL (ft)	Final THL (ft)	CHL Multiplier	Final Additive CHL (ft)
Thin bed	0.63	2.60	4.16	1.98
Full bed 1	5.46	11.81	2.16	6.35
Full bed 2	3.50	8.99	2.57	5.49

4.2 CASA Incorporation of CHL Correlation

The correlation was developed using the worst case (largest possible) precipitate load (2) which is expected to exist in the tails of the risk-informed evaluation. This allows for correlation application across a wide range of risk-informed precipitate loads. As such, the correlation can be used in CASA to develop time-dependent THL for the many variable scenarios evaluated under that framework (i.e. any break size, any spray duration, etc.). The framework that can be utilized by CASA (after development is completed) is illustrated in Figure 21. In Figure 21, the process used to quantify CHL for one time step in a particular LOCA scenario is shown and it includes the physical and chemical processes that would be evaluated in the scenario.

In each LOCA scenario evaluated by CASA, the pool volume, pool pH, pool temperature, spray pH, spray temperature and surface area of materials exposed are used to determine the total, cumulative precipitate mass using an auxiliary precipitate calculator such as WCAP-16530-NP. The total precipitate mass will be used along with the total strainer surface area in use (number of trains operating) to determine L^* . The flow rate through the operating strainer(s) is used to establish the velocity through the applicable strainer(s). Because the CHL returned by the correlation (CHL_{std}) is at a specific fluid temperature (116.3 °F) and velocity (0.0086 ft/s), the scenario-specific temperature and velocity would

	Quantification of Chemical Head Loss Epistemic Uncertainty; Basis for Incremental Chemical Head Loss Correlation		
	Document No: ALION-REP-STP-8998-08	Rev: I	Page 30 of 46

be used to correct the CHL_{std} for temperature (fluid viscosity) and velocity effects. The CHL reflective of the time step conditions (CHL_t) will be added to the NCHL to determine THL at the time step. The uncertainty of CHL is determined from the input parameters sampled by CASA (represented by green boxes of Figure 21). However, further CHL uncertainty may be evaluated by application of new release equations (when completed) and WCAP-16530-NP equations to provide a range of total, cumulative precipitate mass.

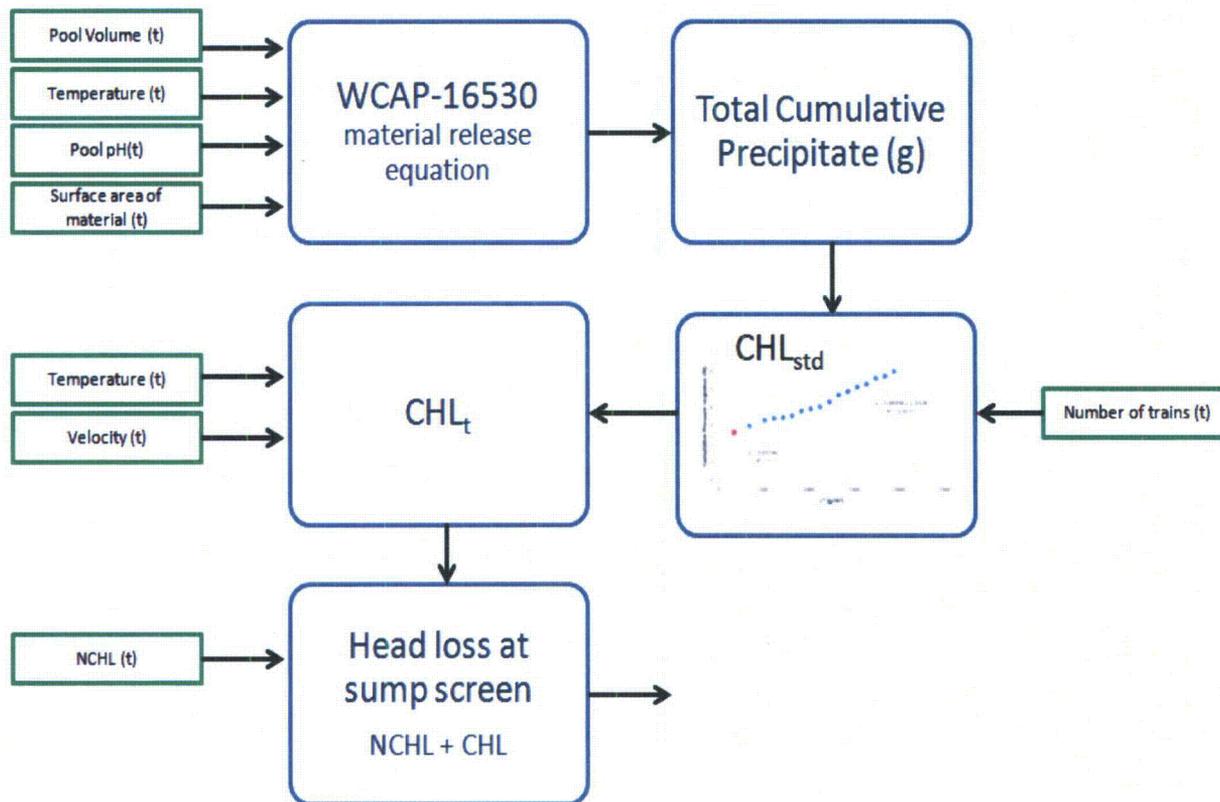


Figure 21: CHL calculated for each time step evaluation by CASA. Green boxes are inputs at each time step (t) for the scenario evaluated (currently under development).

4.3 CHL Correlation Applied to Bounding STP LOCA Scenarios

Since the CHL correlation was shown to adequately predict strainer test results, it was used to assess CHL as a function of probable bounding STP LOCA conditions (14). The parameters related to the LOCA conditions investigated in this analysis are summarized in Table 8. Input parameter combinations used to define LOCA scenarios are presented in Table 9. Quantities of aluminum (556.7 ft² submerged and 5010.3 ft² not submerged), miscellaneous fiberglass insulation (12.5 ft³), Microtherm insulation (1.8 ft³) and concrete (only submerged, 1447 ft²) were held constant for the entire analysis. Also, sprays were

	Quantification of Chemical Head Loss Epistemic Uncertainty; Basis for Incremental Chemical Head Loss Correlation		
	Document No: ALION-REP-STP-8998-08	Rev: I	Page 33 of 46

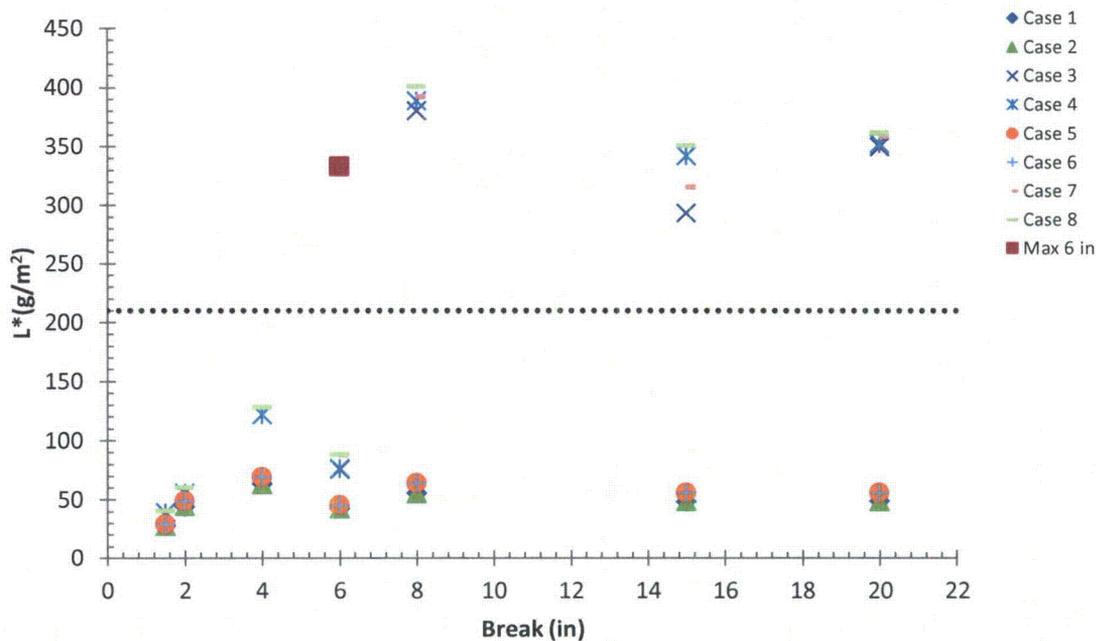


Figure 22: L* generated from analysis of bounding LOCA conditions (3 trains operating)

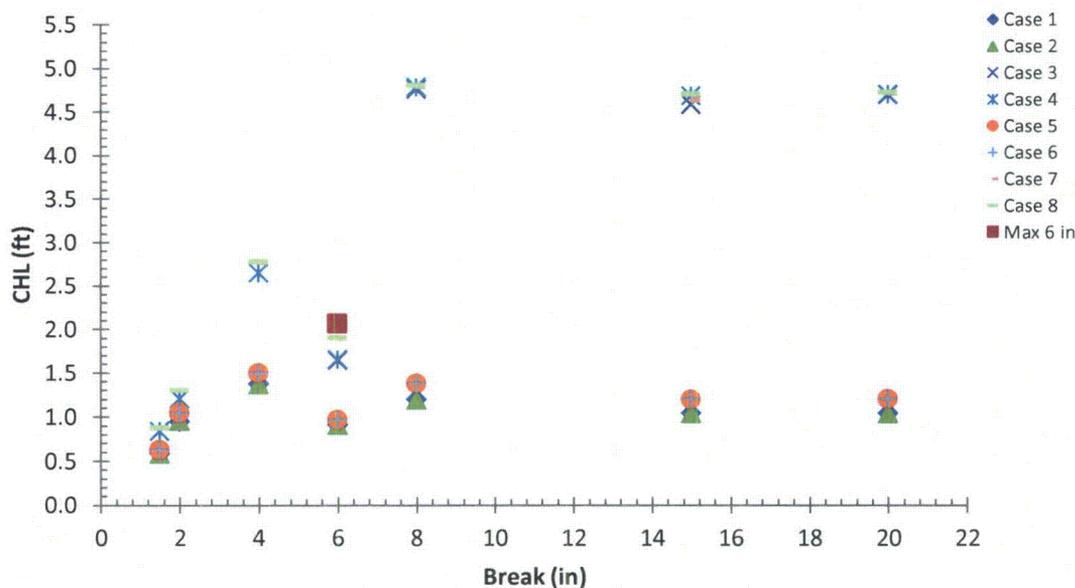


Figure 23: Temperature corrected CHL generated from analysis of bounding post-LOCA conditions.

	Quantification of Chemical Head Loss Epistemic Uncertainty; Basis for Incremental Chemical Head Loss Correlation		
	Document No: ALION-REP-STP-8998-08	Rev: I	Page 34 of 46

While 10% of the total chemicals (210 g/m^2) caused the majority of the CHL response in STP ECCS strainer testing (2), most of the scenarios evaluated are below this strainer loading. It is likely that more of the scenarios referred to above result in lower L^* values as implementation of the CHL correlation requires the use of WCAP-16530-NP equations, which have been shown to overestimate material release and precipitate generation. Particularly, recent testing (5; 6; 7; 16; 17) has proven the following for aluminum release from corrosion sources exposed to TSP -borated solution: 1) aluminum release approaches zero (passivation occurs) before the first 48 hours of exposure; 2) corrosion release of aluminum during the period prior to passivation has been shown to be less than predicted by the WCAP-16530-NP equation.

Results of aluminum release from corrosion sources as a function of temperature, pH and time (17) were used by Dr. Kerry Howe of UNM to generate a new aluminum release equation that reflects aluminum corrosion release and aluminum passivation of corrosion sources. A comparison of the new release equation results versus experimental results are shown in Figure 24. While details associated with experiments used to generate this new aluminum release equation are briefly summarized by Table 11, complete details can be found in SNC Series 1000 bench test report (17). It is important to note that although these experiments were performed for SNC, the phosphate concentration used in these tests, 10 mM, is approximately reflective of STP LOCA phosphate concentrations. The new aluminum release equation was adjusted for implementation into the WCAP-16530 precipitate calculator. Use of this new aluminum release equation, applied only to calculate aluminum release from corrosion sources in the WCAP-16530 precipitate calculator, provides a close fit to the experimental data as shown by Figure 25.

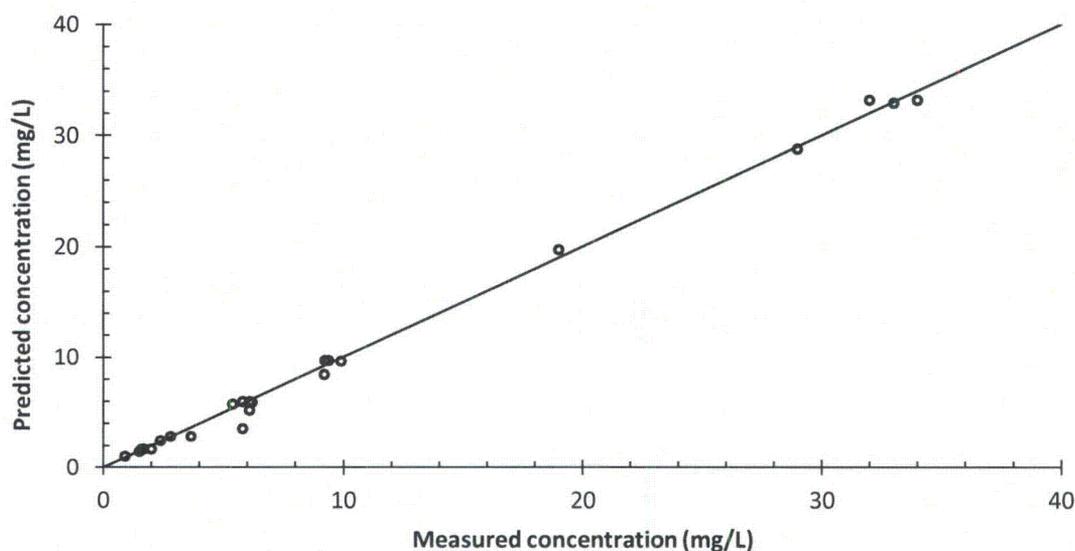


Figure 24: Raw data and predicted concentration; reproduced from UNM GSI-191 Telecon June 6, 2014 "Aluminum Release Equation" presentation (18).

	Quantification of Chemical Head Loss Epistemic Uncertainty; Basis for Incremental Chemical Head Loss Correlation		
	Document No: ALION-REP-STP-8998-08	Rev: I	Page 35 of 46

Table 11: Experimental conditions¹

Series	pH	Temperature, °C
1100	7.36	85
1300	6.86	85
1400	7.86	85
1500	7.34	70
1600	7.34	55

¹ Single material test; 1in² aluminum alloy 1100 coupons, exposed to 10 mM phosphate

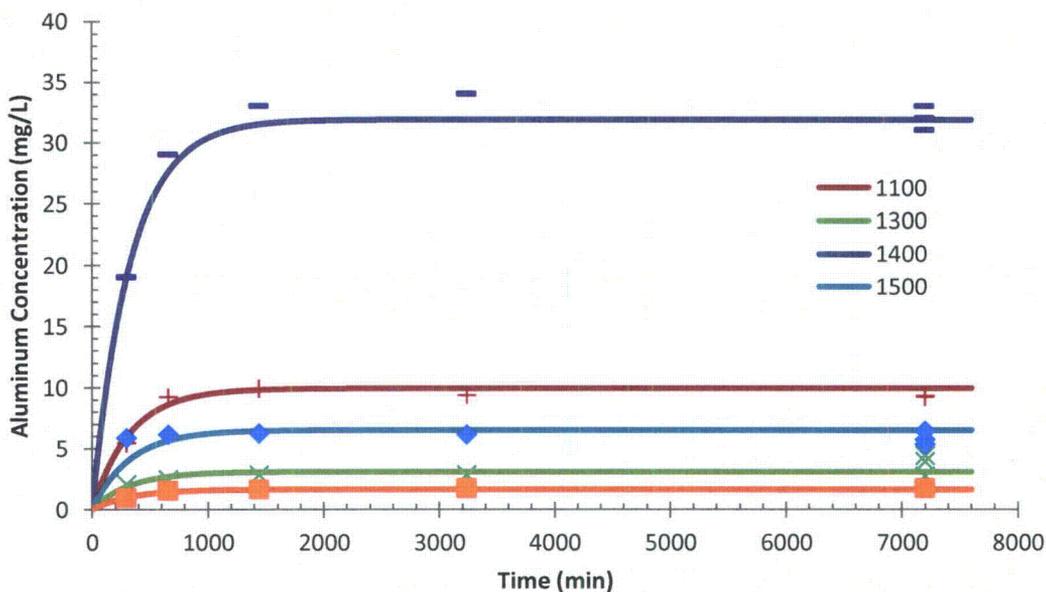


Figure 25: New release equation results obtained from altered WCAP-16530-NP calculator. Modeled data represented by line and experimental data represented by discrete markers.

Experimental conditions associated with results used to produce the new aluminum release equation were applied to the original WCAP calculator to predict aluminum release, Figure 26. As summarized by Table 12, use of the new aluminum release equation significantly reduces the predicted aluminum release when compared to release estimated using the original WCAP-16530-NP aluminum release equation.

	Quantification of Chemical Head Loss Epistemic Uncertainty; Basis for Incremental Chemical Head Loss Correlation		
	Document No: ALION-REP-STP-8998-08	Rev: I	Page 36 of 46

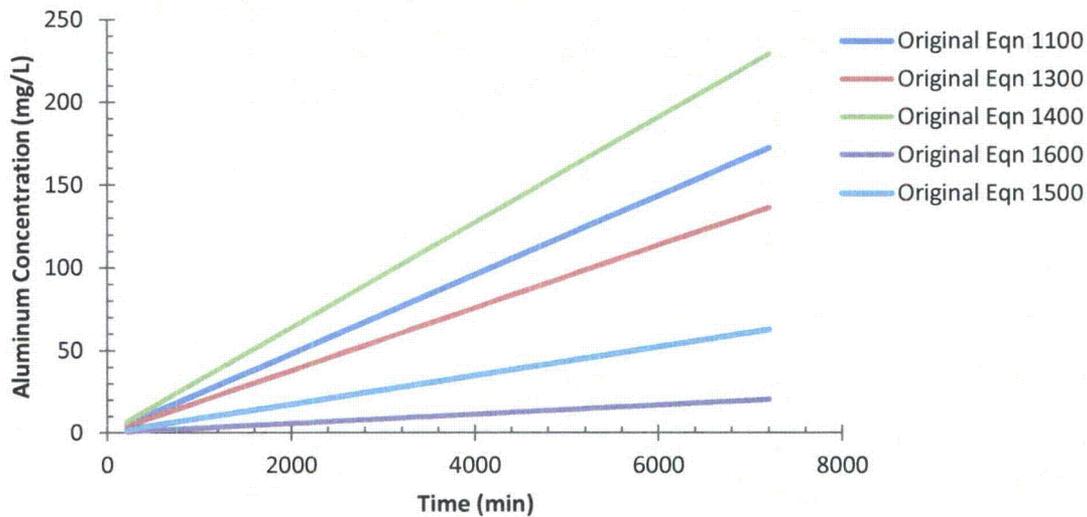


Figure 26: Aluminum release calculated using original WCAP-16530-NP release equations applied to series listed in Table 11.

Table 12: Reduction in 5 day release

Series	1100	1300	1400	1500	1600
New equation (mg/L)	9.98	3.12	31.90	6.53	1.67
Original equation(mg/L)	172.24	136.30	229.12	62.65	20.44
Reduction in predicted release	94%	98%	86%	90%	92%

Reduction of aluminum release through the use of a more representative aluminum release equation (Option 2 – 4 (1)) provides reference for conservatism (over-estimated CHL) associated with the Option 1 CHL correlation. An approximate 90% reduction in aluminum release will translate to a large reduction in L*. While replacing the aluminum release equation does demonstrate conservatism associated with the results of the CHL analysis, the reduction of aluminum release obtained by using the new equation still retains conservatism. The new release equation only reflects passivation and not the decreased release of aluminum (approximately 2X reduction) prior to passivation that is shown to occur in the presence of zinc sources (6; 7). Also, the application of calcium retrograde solubility and aluminum solubility (Option 4 (1)) would further reduce the precipitate mass generated.

4.4 CHL Correlation Applied Using CHLE Experimental Results

Results from experiments designed to more accurately assess prototypical material release can also be used to determine precipitate masses from materials released (taking no solubility credit, Option 2 (1)). CHLE test T1 (5), T2 (6), and T5 (19) provided experimentally obtained material release results from STP specific material to pool volume and temperature conditions. The obtained material releases represent probable releases expected to occur in STP post-LOCA conditions. CHLE tests T3 and T4 were not scaled

	Quantification of Chemical Head Loss Epistemic Uncertainty; Basis for Incremental Chemical Head Loss Correlation		
	Document No: ALION-REP-STP-8998-08	Rev: I	Page 37 of 46

to STP conditions and were designed to promote aluminum precipitation, containing 100 times more aluminum in solution than expected. The releases observed in tests T3 and T4 likely represent an improbable post-LOCA material release of sprays operating for 30-days.

The maximum soluble aluminum, calcium, and silicon concentrations observed at any time in CHLE T1-T5 were multiplied by the maximum STP pool volume listed in Table 8 to calculate the maximum total precipitate mass that could exist at STP under the conditions investigated. The precipitate masses, L* values determined from three trains operating (most probable configuration (Table 9-1 of Volume 2 (15)) and CHL for each test are listed in Table 13. For prototypical tests, the CHL was calculated to be less than 0.85 ft. For non-prototypical tests that have 100X more submerged aluminum surface area, the CHL was determined to be less than 4.20 ft. Adding the maximum non-prototypical test CHL results (4.20 ft) to design-basis strainer stabilized NCHL (3.93 ft) (2) produces a THL that is lower than the available net-positive suction head (NPSH) margin (20).

Table 13: Correlation applied to CHLE results assuming a 2,254,923 L pool volume (14) and three trains in operation

CHLE	Aluminum (mg/L)	Calcium (mg/L)	Silicon (mg/L)	AlOOH (g)	NaAlSi ₃ O ₈ (g)	Ca ₃ (PO ₄) ₂ (g)	Total (g)	L* (g/m ²)	CHL _{std} (ft)
T1	0.33	2.4	4.6	0	7227	13989	21216	41.86	0.85
T2	0.33	1.6	2.7	0	7227	9326	16553	32.66	0.67
T3	2.7	1.5	13	0	59129	8743	67872	133.91	2.73
T4	5.1	2.1	16	776	108295	12240	121312	239.35	4.20
T5	0.23	1.3	2.9	0	5037	7577	12614	24.89	0.51

4.5 CHL Correlation Compared to the “Bump-Up” Method

Incorporation of the CHL correlation within CASA software, as shown in Figure 21, is currently under development. Using the development software, an evaluation of THL as a function of CHL determined from the medium break (MB) LOCA condition, (T1 results), was performed. The MBLOCA CHL was chosen because it produced the largest experimental prototypical material release (6.5 hrs of spray exposure to risk-informed material quantities) as listed in Table 13. The 30-day MBLOCA CHL remained referenced to 0.0086 ft/s but was temperature corrected using the 27.5” temperature break profile. Temperature corrected CHL was added to the NCHL (determined by CASA) for a 31” double ended guillotine (DEG) break to calculate the THL of the two example cases shown in Figure 27 and Figure 28. The 31” DEG NCHL (includes clean strainer head loss) obtained was calculated as a function of three trains in operation (Case 1) and one train in operation (Case 43) (21). The THL determined from use of the CHL correlation was compared to the THL obtained from use of the bump-up factor as shown in Figure 27 and Figure 28.

	Quantification of Chemical Head Loss Epistemic Uncertainty; Basis for Incremental Chemical Head Loss Correlation		
	Document No: ALION-REP-STP-8998-08	Rev: I	Page 38 of 46

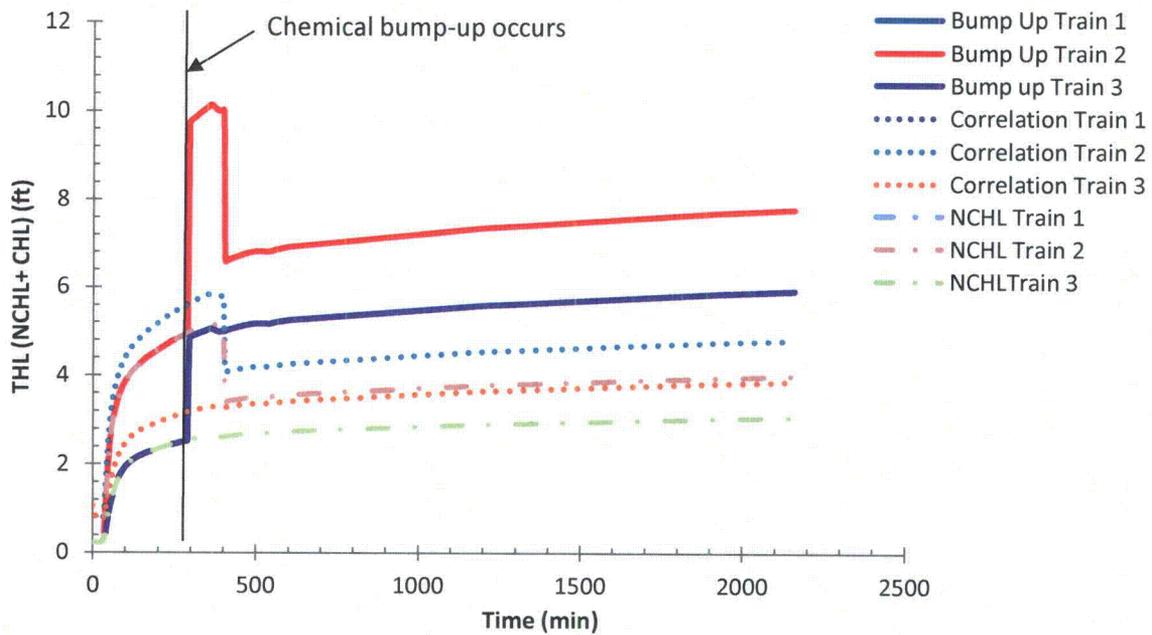


Figure 27: THL of Case 1 determined from CHL correlation (0.85 ft T1 CHL_{temp-corrected}) and from application of bum-up factor. Trains 1 and 2 overlay, CHL associated with bump-up occurs at 140 ± 5 °F and HCHL includes clean strainer head loss.

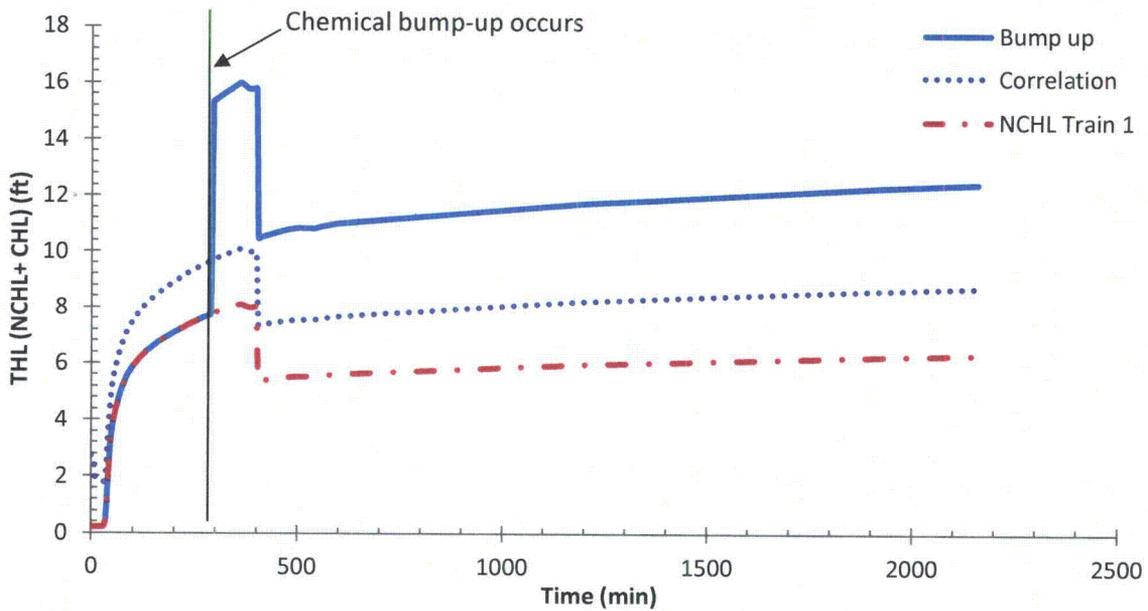


Figure 28: THL for Case 43 determined from CHL correlation (2.56 ft T1 CHL_{temp corrected}) and from application of the bump-up factor. CHL associated with the bump-up occurs at 140 ± 5 °F and NCHL includes clean strainer head loss.

	Quantification of Chemical Head Loss Epistemic Uncertainty; Basis for Incremental Chemical Head Loss Correlation		
	Document No: ALION-REP-STP-8998-08	Rev: I	Page 39 of 46

Comparison of THL obtained from immediate implementation of the CHL correlation and THL obtained from use of the bump-up approach was performed to demonstrate improved resolution obtained from use of the CHL correlation. Although the THL obtained from the CHL correlation is higher than that obtained from use of the bump-up approach prior to 300 minutes, if the same temperature threshold criterion for use was applied to the implementation of the CHL correlation, the bump-up approach would produce much higher THL than the CHL correlation for the entire analysis. Also, both cases indicated failure of the ECCS system using the bump-up approach. However, THL determined from CHL reflective of a prototypical chemical load (T1 result) indicates that Case 1 would not lead to failure. Addition of the maximum CHL response observed from STP ECCS strainer testing (approximately 5 ft as shown in Figure 11) will produce equivalent maximum THL values obtained from the bump-up approach when added to maximum calculated NCHL of 5.2 ft for Case 1 and NCHL 8.1 ft for Case 43. Therefore, using the CHL correlation for THL analysis of probable cases with large NCHL values (chemical loading obtained from 6.5 hours of spray exposure to risk-informed material quantities), reduces conservatism resulting from implementation of the bump-up approach. For THL analysis of less probable cases, chemical loading obtained from 30 days spray exposure of deterministically bounding material (22), the CHL correlation produces similar THL values as compared to those obtained from use of the bump-up approach.

Comparison of THL obtained from use of the CHL correlation with smaller break NCHL to THL obtained from use of the bump-up approach applied to smaller breaks was not done. However, review of Vogtle ECCS strainer data, Table 7, shows that the chemical head-loss multiplier for a smaller break or thin bed case may be approximately two times higher than that of a design basis bed. The bump-up approach uses a smaller chemical head loss multiplier for smaller breaks than for large breaks (9) which would likely produce non-conservative THL values within the current CASA analysis. Given that the CHL correlation was designed to provide an additive bounding response to chemical loading of a high filtration debris-bed, the CHL correlation will provide much higher THL results than experimental values as shown by Figure 20, and the calculated THL will be larger than the THL obtained from bump-up response for smaller breaks. While the likely underestimation of THL is of concern, the implementation of the CHL correlation for smaller breaks will merely improve the resolution of the THL value, since addition of the maximum CHL response observed from STP ECCS strainer testing (approximately 5 ft as shown in Figure 11) to the smaller break maximum NCHL values shown in Figure 29 would produce THL values less than the available NPSH margin (20).

	Quantification of Chemical Head Loss Epistemic Uncertainty; Basis for Incremental Chemical Head Loss Correlation		
	Document No: ALION-REP-STP-8998-08	Rev: I	Page 40 of 46

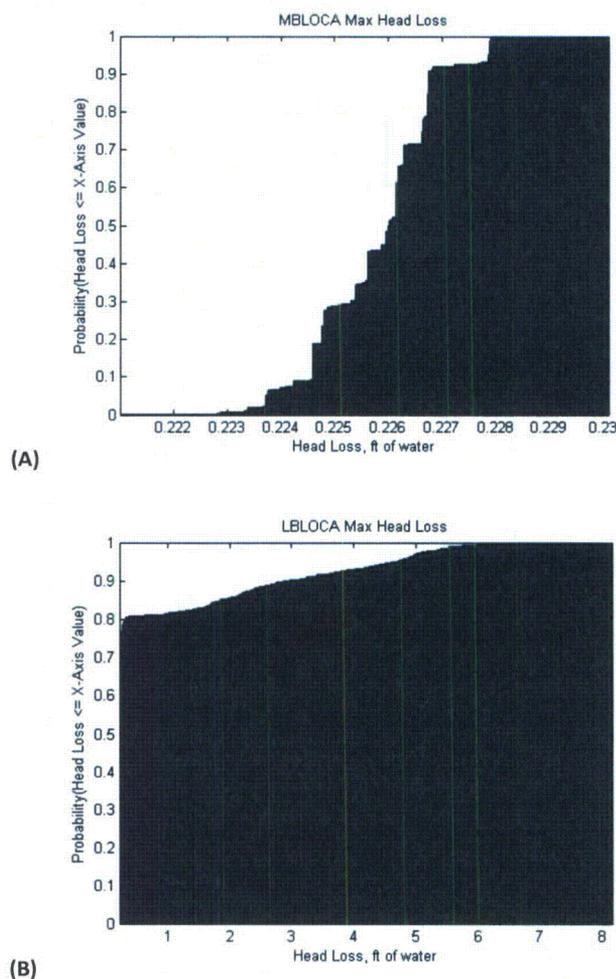


Figure 29: Probability of maximum THL (clean strainer + NCHL) as a function of break type (MBLOCA (A), LBLOCA (B)). SBLOCA THL not shown because bump-up approach is not applied since the thin bed criterion is not met

Use of the CHL correlation alleviates underestimations in THL derived from temperature criterion used to implement the bump-up approach. While the CHL correlation implementation occurs when material is released, the bump-up approach uses 140 ± 5 °F to implement chemical effects within the analysis. This temperature threshold is loosely derived from industry practice for delayed onset of chemical effects (23; 24). While the delayed onset temperature criterion conservatively assesses the onset of aluminum precipitation as shown in Table 14, use of 140 ± 5 °F neglects $\text{Ca}_3(\text{PO}_4)_2$ chemical effects.

	Quantification of Chemical Head Loss Epistemic Uncertainty; Basis for Incremental Chemical Head Loss Correlation		
	Document No: ALION-REP-STP-8998-08	Rev: I	Page 41 of 46

Table 14: Time and temperature when aluminum solubility was reached during post-LOCA bounding scenario analysis¹

Case	Break	Time (day)	Solubility Crossed (°F)	Case	Break	Time (day)	Solubility Crossed (°F)
1	1.5	12.1	102.2	5	1.5	25.7	95.7
	2	12.1	102.2		2	25.7	95.7
	4	13.1	101.6		4	27.3	95.0
	6	13.1	101.6		6	27.3	95.0
	8	10.3	97.1		8	20.8	89.8
	15	10.3	97.1		15	20.8	89.8
2	20	10.3	97.1	20	20.8	89.8	
	1.5	16.3	99.9	6	1.5	Not crossed	Not crossed
	2	16.3	99.9		2	Not crossed	Not crossed
	4	17.4	99.4		4	Not crossed	Not crossed
	6	17.4	99.4		6	Not crossed	Not crossed
	8	13.1	94.6		8	26.2	87.4
15	13.1	94.6	15		26.2	87.4	
3	20	13.1	94.6	20	26.2	87.4	
	1.5	12.0	102.3	7	1.5	25.5	95.7
	2	12.0	102.3		2	25.5	95.7
	4	12.4	102.0		4	26.2	95.5
	6	12.4	102.0		6	26.2	95.5
	8	6.3	102.1		8	14.1	93.8
15	6.3	102.1	15		14.1	93.8	
4	20	6.3	102.1	20	14.1	93.8	
	1.5	16.1	100.0	8	1.5	Not crossed	Not crossed
	2	16.1	100.0		2	Not crossed	Not crossed
	4	16.5	99.8		4	Not crossed	Not crossed
	6	16.5	99.8		6	Not crossed	Not crossed
	8	7.9	99.9		8	17.4	91.6
15	7.9	99.9	15		17.4	91.6	
	20	7.9	99.9	20	17.4	91.6	

¹Analysis performed with previously assessed STP post-LOCA scenarios described in section 4.3 and CASA temperature profiles (6" and 27.5")

An estimate of Ca₃(PO₄)₂ CHL ranges that were not accounted for prior to 140 ± 5 °F was obtained using a survey of previously assessed STP post-LOCA scenarios described in section 4.3. However, this survey was subjected to temperature profiles used in CASA, where breaks ≤ 6" were evaluated using the 6" temperature profile and breaks > 6" were evaluated using the 27.5" temperature profile. Also, this survey did not apply solubility rules; therefore any calcium leached produces Ca₃(PO₄)₂, which provides an upper bound of neglected CHL responses. Results obtained from this survey are listed in Table 15 and indicate that up to 19.73 kg of Ca₃(PO₄)₂ can be generated prior to 140 ± 5 °F. Ca₃(PO₄)₂ generated prior

	Quantification of Chemical Head Loss Epistemic Uncertainty; Basis for Incremental Chemical Head Loss Correlation		
	Document No: ALION-REP-STP-8998-08	Rev: I	Page 42 of 46

to 140 ± 5 °F determined from this analysis produced the following CHL ranges referenced to fluid conditions of 140 °F and 0.0086 ft/s; 0.02 ft to 0.04 ft for SBLOCA, 0.04 ft to 0.13 ft for MBLOCA, and 0.04 ft to 0.64 ft for LBLOCA . While the bump-up approach neglects up to 0.64 ft of CHL prior to 140 °F, when these values are included in the calculation of THL, they will merely change the absolute value of the THL and not likely influence CASA results since maximum THL (clean strainer + NCHL) without the bump-up factor for each case is very low, as previously shown in Figure 29.

	Quantification of Chemical Head Loss Epistemic Uncertainty; Basis for Incremental Chemical Head Loss Correlation		
	Document No: ALION-REP-STP-8998-08	Rev: I	Page 43 of 46

Table 15: Calcium phosphate CHL not accounted for prior to 140 °F

Case	Break	Ca ₃ (PO ₄) ₂ (Kg,140 °F)	L* (g/m ²)	CHL _{std} (ft)	CHL _{140 °F} (ft)	Case	Break	Ca ₃ (PO ₄) ₂ (Kg,140 °F)	L* (g/m ²)	CHL _{std} (ft)	CHL _{140 °F} (ft)
1	1.5	0.72	1.41	0.03	0.02	5	1.5	0.73	1.44	0.03	0.02
	2	0.72	1.41	0.03	0.02		2	0.73	1.44	0.03	0.02
	4	1.28	2.52	0.05	0.04		4	1.30	2.57	0.05	0.04
	6	1.28	2.52	0.05	0.04		6	1.30	2.57	0.05	0.04
	8	0.73	1.44	0.03	0.02		8	0.74	1.47	0.03	0.02
	15	0.73	1.44	0.03	0.02		15	0.74	1.47	0.03	0.02
	20	0.73	1.44	0.03	0.02		20	0.74	1.47	0.03	0.02
2	1.5	0.72	1.41	0.03	0.02	6	1.5	0.73	1.44	0.03	0.02
	2	0.72	1.41	0.03	0.02		2	0.73	1.44	0.03	0.02
	4	1.28	2.53	0.05	0.04		4	1.30	2.57	0.05	0.04
	6	1.28	2.53	0.05	0.04		6	1.30	2.57	0.05	0.04
	8	0.73	1.44	0.03	0.02		8	0.74	1.47	0.03	0.02
	15	0.73	1.44	0.03	0.02		15	0.74	1.47	0.03	0.02
	20	0.73	1.44	0.03	0.02		20	0.74	1.47	0.03	0.02
3	1.5	1.28	2.52	0.05	0.04	7	1.5	1.30	2.56	0.05	0.04
	2	1.28	2.52	0.05	0.04		2	1.30	2.56	0.05	0.04
	4	3.96	7.82	0.16	0.13		4	4.04	7.97	0.16	0.13
	6	3.96	7.82	0.16	0.13		6	4.04	7.97	0.16	0.13
	8	18.41	36.32	0.74	0.60		8	18.89	37.28	0.76	0.61
	15	18.41	36.32	0.74	0.60		15	18.89	37.28	0.76	0.61
	20	18.41	36.32	0.74	0.60		20	18.89	37.28	0.76	0.61
4	1.5	1.28	2.52	0.05	0.04	8	1.5	1.30	2.57	0.05	0.04
	2	1.28	2.52	0.05	0.04		2	1.30	2.57	0.05	0.04
	4	4.00	7.89	0.16	0.13		4	4.08	8.04	0.16	0.13
	6	4.00	7.89	0.16	0.13		6	4.08	8.04	0.16	0.13
	8	19.25	37.97	0.77	0.62		8	19.73	38.94	0.79	0.64
	15	19.25	37.97	0.77	0.62		15	19.73	38.94	0.79	0.64
	20	19.25	37.97	0.77	0.62		20	19.73	38.94	0.79	0.64

In summary, the CHL correlation provides a more detailed assessment of THL as a function of break size and conditions. While the CHL correlation provides more refined THL values for use in the CASA analysis, the THL obtained from use of these values likely would not affect final CASA results obtained from use of the bump-up approach because NCHL responses for the smaller breaks are not large enough (Figure 29, A and B) to cause failure when combined with the largest chemical response of approximately 5 ft, shown in Figure 11.

	Quantification of Chemical Head Loss Epistemic Uncertainty; Basis for Incremental Chemical Head Loss Correlation		
	Document No: ALION-REP-STP-8998-08	Rev: I	Page 44 of 46

5.0 Conclusion

An empirical CHL correlation was derived from past experiments (2; 3; 4; 5; 6; 7; 8) using Option 1 of the modular approach (1). The correlation was used to evaluate ECCS performance for a wide spectrum of LOCA conditions to help support the STP risk-informed analysis. CHL correlations with less conservatism can be obtained with the use of Options presented in the modular approach (1) before correlating the data, as described by the methodology presented within this document. Options defined in the modular approach include the following improvements: generation of new release equations for aluminum, calcium, zinc, and silicon (Option 2 -4 (1)); improvements of head loss calculations due to NCHL and CHL by using more representative surrogates for testing (Option 3-4 (1)) or by better characterization NCHL and filtration efficiency through use of vertical loop test and new strainer module testing (Option 3-4) and incorporation of thermodynamic modeling with support of kinetic assumptions to more accurately estimate the amount of precipitate formed (Option 4 (1)).

	Quantification of Chemical Head Loss Epistemic Uncertainty; Basis for Incremental Chemical Head Loss Correlation		
	Document No: ALION-REP-STP-8998-08	Rev: I	Page 45 of 46

6.0 References

1. **Leavitt, J J and Letellier, B.** *Modular Quantification of Chemical Effects. Rev. 1.* s.l. : Alion Science and Technology, May 2014.
2. **AREVA.** *63-9086408-001 South Texas Project Test Plan for ECCS Strainer Performance Testing. Rev. 1.* August 2008.
3. **Bahn, S B; Kasza, K E; Shack, W J; Natesan, K; Klein, P.** *Evaluation of precipitates used in strainer head loss testing. Part I Chemically generated precipitates.* s.l. : Nuclear Engineering and Design, Vol. 239, pp. 2981-2991, 2009.
4. —. *Evaluation of precipitates used in strainer head loss testing. Part II Precipitates by in situ aluminum alloy corrosion.* s.l. : Nuclear Engineering and Design, Vol. 241, pp. 1926-1936, 2011.
5. **University of New Mexico.** *CHLE-012 T1 MBLOCA Test Report. Rev. 3.* January 2013.
6. —. *CHLE-014 T2 LBLOCA Test Report. Rev. 2.* January 2013.
7. —. *CHLE-019 Test results for chemical effect tests stimulating corrosion and precipitation (T3 & T4).* Rev. 1. August 2013.
8. —. *CHLE-SNC-006 Bench Test Results for Series 2000 Tests for Vogtle Electric Generating Plant. Rev.2.* November 2013.
9. **South Texas Project Electric Generating Station.** *STP-RIGSI191-V03 South Texas Risk-Informed GSI-191 Evaluation Volume 3 CASA Grande Analysis. Rev. 2.* November 2013.
10. **NEI.** *Pressurized Water Reactor Sump Performance Evaluation Methodology, Rev. 0, Volume 2.* December 2004.
11. **Westinghouse.** *WCAP-16530-NP, Evaluation of Post-Accident Chemical Effects in Containment Sump Fluids to Support GSI-191. Rev. 0.* February 2006.
12. **Alion Science and Technology.** *ALION-CAL-SNC-7410-005 Head Loss Testing of a Prototypical Vogtle 1 and 2 Strainer Assembly. Rev. 0.* s.l. : Alion Science and Technology, December 2009.
13. **AREVA.** *66-69081735-001 SUMMARY TEST REPORT (STR) St. Lucie Unit 2 Strainer Test Report. Rev. 1.* June 2008.
14. **University of New Mexico.** *CHLE-016 Calculated Material Release. Rev. 2.* January 2013.
15. **South Texas Project Electric Generating Station.** *RI-GSI191-V02 South Texas Project Risk-Informed GSI-191 Evaluation Volume 2 Probablistic Risk Analysis Determination of Change in Core Damage Frequency and Large Early Release Frequency due to GSI-191 Issues. Rev. 2.* November 2013.
16. **University of New Mexico.** *CHLE-018 Results of Bench Test to Assess Corrosion of Aluminum in STP Containment Conditions. Rev. 1.* August 2013.

	Quantification of Chemical Head Loss Epistemic Uncertainty; Basis for Incremental Chemical Head Loss Correlation		
	Document No: ALION-REP-STP-8998-08	Rev: I	Page 46 of 46

17. —. *CHLE-SNC-005 Bench Test Results for Series 1000 Tests for Vogtle Electric Generating Plant. Rev. 1. s.l. : University of New Mexico, November 2013.*
18. *GSI-191 Telecon "Aluminum Release Equation". University of New Mexico Department of Chemical and Nuclear Engineering. June 6, 2014.*
19. **University of New Mexico.** *CHLE-020 Test results for 10-day chemical effect test stimulating LBLOCA condition (T5). Rev. 0. September 2013.*
20. **South Texas Project Electric Generating Station.** *MC-6220 SI & CHP Pump NPSH. Rev 4. February 2002.*
21. **South Texas Project Nuclear Operating Company.** *STP-RIGSI191-ARAI.01 A Practical Guide to Sensitivity Analysis of a Large-scale Computer Simulation Model. Rev. 3. February 2014.*
22. **Westinghouse.** *CN-CSA-06-6 South Texas Project GSI-191- Chemistry Effects Evaluation. Rev 1 . 2008.*
23. **Entergy.** *GL 2004-02 Final Supplemental Responses Adams # ML082700499. 2008.*
24. **Argonne National Laboratory.** *ML091610696 Aluminum Solubility in Boron Containing Solution as a function of pH and Temperature. September 2008.*

Attachment 6

Response to SNPB Request for Additional Information: RAI 4

SNPB, Nuclear Performance and Code Review Branch: RAI 4

Please provide the latest analysis or reference showing the timing for boric acid precipitation for the limiting large-break and small-break LOCAs.

STP Response:

The timing for boric acid precipitation is given in STPNOC Calculation NC-7136 (Reference 1). The calculation summary follows below:

OBJECTIVE

This calculation determines the effect of the increase in deliverable water volume from the Refueling Water Storage Tank (RWST) on the hot leg switchover time following a large break loss of coolant accident (LBLOCA). Hot leg switchover (HLSO) is required to ensure that boron precipitation does not occur in the reactor core.

1.4% Power Uprate:

The NRC approved a 1.4% increase in the reactor core power level from 3,800 MWt to 3,853 MWt. The effect of this increase is determined.

Replacement steam generators:

Delta-94 steam generators were installed. The effect of this change is determined.

INTENDED USE OF RESULTS

This calculation supports the HLSO time used in emergency operating procedure OPOP05-EO-EO10.

SUMMARY OF RESULTS

The increase in the RWST injected volume has negligible effect on the HLSO time following a LBLOCA. If the RCS volume is at a boron concentration of 2830 ppm, the mixed sump boron concentration is only about 3.3 ppm higher than previously analyzed which is well within measurement accuracy. If the RCS boron concentration is increased to 3500 ppm in Mode 3 one hour after exiting Modes 1 or 2, then an increase in RWST injected volume acts as a dilution source which is bounded by the analysis documented in ST-UB-HL-1680 previously performed. Therefore, the HLSO time of 6.0 hours is valid. However, to ensure adequate margin for time to HLSO is maintained, the plant emergency operating procedure OPOP05-EO-EO10 specify a HLSO time of 5.5 hours.

1.4% Power Uprate Results

The calculation is independent of reactor power level (to 3853 MWt), therefore the power uprate will not affect the results.

Delta-94 Steam Generator Results

The existing analysis of record is applicable to Units 1 and 2.

INTRODUCTION/BACKGROUND

As part of the requirement to maintain the core coolable geometry in the long term, Section 6.3 of NUREG-0800 required that steps be taken to preclude the precipitation of boron in the vessel. In the event of a cold leg break, while the ECCS is aligned to the RCS cold legs, boron concentration in the core region increases due to boil-off of the

water. To preclude boron precipitation, one train of SI is realigned to the RCS hot legs at the hot leg switch over (HLSO) time.

The design basis that requires HLSO is established by 10CFR 50.46 which requires that the reactor core maintain long term cooling after a LOCA event. During a double-ended break of the cold leg, most of the safety injection flow enters the unaffected cold leg(s), goes into the downcomer region of the reactor vessel and out the break in the broken cold leg. The safety injection flow that enters the reactor core for the purposes of cooling is attributable to the manometric pressure between the downcomer and the reactor vessel. This results in the safety injection flow boiling in the reactor core and leaving as steam. The boron concentration of the water in the reactor vessel increases until such a point that boron precipitation occurs. When boron precipitation occurs, the fuel rods can become coated and impede long term cooling of the fuel. Boron precipitation is assumed to occur when the boron concentration reaches 23.5 wt% (41,000 ppm), which is 4 wt% less than the boron solubility limit of a solution at 212° F. The 23.5 wt% is an NRC imposed limit.

The Refueling Water Storage Tank (RWST), SI accumulators, and the ECCS piping are sources of the highest concentration of borated water. An increase in the volume of any one of these sources will increase the boron concentration of the mixed sump water in containment, and therefore, decrease the time to boron precipitation in the core. The RCS, which is at a lower boron concentration, serves as a dilution source for the mixed sump water. Therefore, an increase in the primary side RCS volume will lead to an increase in the time to boron precipitation.

As part of the setpoint review effort, the calculation of the total deliverable RWST water volume has been revised. The new revision documents (Ref. 5) the maximum injection volume is 541,000 gallons. This new value is greater than the 453,400 gallons assumed in the safety analysis for the time to HLSO following a LOCA event. Since an increase in the RWST deliverable water volume will increase the mixed sump boron concentration, the HLSO time is expected to decrease.

Westinghouse has revised their methodology for calculating the time to HLSO to correct an error in the boron concentration density term. This correction resulted in a HLSO time that decreased from 6.5 to 6.0 hours. This was recommended by Westinghouse to be incorporated in the plant emergency operating procedures. However, per the Reportability Review for CR 98-5868 and USQE 98-0032, the HLSO time was reduced to 5.5 hours to ensure boron precipitation will not occur and reflected as such in procedure OPOP05-EO-EO10.

In support of the licensing application for the Delta-94 steam generators and the 1.4% uprate, various safety analyses are required to be performed for the new steam generators or reviewed to confirm the current applicability of the most recent analysis. This review shows that there is no effect on the results of NC-7136.

RESULTS/CONCLUSION

The increase in the RWST injected volume has negligible effect on the HLSO time following a LBLOCA. If the RCS volume is at a boron concentration of 2830 ppm, the mixed sump boron concentration is only about 3.3 ppm higher than previously analyzed which is well within measurement accuracy. If the RCS boron concentration is increased

to 3500 ppm in Mode 3 one hour after exiting Modes 1 or 2, then an increase in RWST injected volume acts as a dilution source which is bounded by the analysis documented in ST-UB-HL-1680 previously performed. Therefore, the HLSO time of 6.0 hours is valid. However, to ensure adequate margin for time to HLSO is maintained, the plant emergency operating procedures OPOP05-EO-EO10 has been changed to specify a HLSO time of 5.5 hours. This is documented in the Reportability Review for CR 98-5868.

For Mode 3, the HLSO time analysis with an increased RCS boron concentration to 3500 ppm following a one hour wait after exiting Modes 1 or 2 is bounded by the Mode 1 analysis as documented in ST-UB-HL-1680.

Reference:

1. STPNOC Calculation NC-7136 Rev. 1 "Hot Leg Switchover Time Following LOCA"

Attachment 7

Response to SRXB Request for Additional Information: RAI 1, 2, 3, 4

SRXB, Reactor Systems Branch: RAI 1,

The NRC staff requests the licensee to provide the following:

1. ***RELAP-3D input decks for these cases with a 3-D vessel and 1-D core:***
 - a. ***Steady state case in Cold Leg***
 - b. ***Medium Break LOCA (6") in Cold Leg***
 - c. ***Double-Ended Guillotine (DEG) Break in Cold Leg***
 - d. ***Core blockage input file***

2. ***RELAP-3D input decks for these cases with a 3-D vessel and 3-D core:***
 - a. ***Steady state case in Cold Leg***
 - b. ***Medium Break LOCA (6") in Cold Leg***
 - c. ***DEG Break in Cold Leg***
 - d. ***DEG Break in Cold Leg with maximum boron***
 - e. ***Core blockage input file***

3. ***Conversion tables between RETRAN and RELAP-3D ("South Texas Project Power Plant RETRAN-RELAP-3D Conversion Tables")***

4. ***Documentation describing model verification ("South Texas Project Power Plant RELAP-3D Steady-state model Verification")***

STP Response:

The response to SRXB RAI 1 was provided in the STP letter to NRC Staff dated January 9, 2014 NOC-AE-14003057, ML14029A533.

SRXB, Reactor Systems Branch: RAI 2,

RELAP-3D input decks for these cases with a 3-D vessel and 3-D core:

- a. Steady state case in Cold Leg*
- b. Medium Break LOCA (6") in Cold Leg*
- c. DEG Break in Cold Leg*
- d. DEG Break in Cold Leg with maximum boron*
- e. Core blockage input file*

STP Response:

The response to SRXB RAI 2 was provided in the STP letter to NRC Staff dated January 9, 2014 NOC-AE-14003057, ML14029A533.

SRXB, Reactor Systems Branch: RAI 3,

Conversion tables between RETRAN and RELAP-3D (“South Texas Project Power Plant RETRAN-RELAP-3D Conversion Tables”)

STP Response:

The response to SRXB RAI 3 was provided in the STP letter to NRC Staff dated January 9, 2014 NOC-AE-14003057, ML14029A533.

SRXB, Reactor Systems Branch: RAI 4

Documentation describing model verification ("South Texas Project Power Plant RELAP-3D Steady-state model Verification)

STP Response:

The response to SRXB RAI 4 was provided in the STP letter to NRC Staff dated January 9, 2014 NOC-AE-14003057, ML14029A533.

Attachment 8

Response to SSIB Request for Additional Information:

- a. Debris Characteristics: RAI 3,
- b. Transport: RAI 4, 6, 7, 8, 10,
- c. Head Loss and Chemical Effects Bump Up: RAI 14, 15, 16, 17, 18, 19,
20, 21, 22, 23, 24, 27, 28
- d. NPSH and Degasification: RAI 33
- e. Debris Bypass: RAI 38
- f. Defense in Depth and Mitigative Measures: RAI 40, 42

Enclosures to Attachment 8

- 1. Letellier, B.C., Macali, M.E., Kee, E.J., Viscous Inertial Shear-Transition-Adaptive (VISTA) Porous Media Head-Loss Formulation for Assessment of South Texas Project Licensing Amendment Request, ALION-REP-STP-8998-11, Rev. 0, July 2014.
- 2. Morton, D.P., Tejada, J.J., Zolan, A., South Texas Project Risk-Informed GSI-191 Evaluation, Volume 3, A Practical Guide to Sensitivity Analysis of Large-scale Computer Simulation

SSIB, Debris Characteristics: RAI 3

Please clarify if the material properties of debris listed in Table 2.2.21 of Volume 3 are used in the head loss correlation. If so, please state if varying the sizes of the particles to a more realistic distribution affect the results significantly. Explain how the particulate debris types that have size distributions are implemented in the correlation. Please explain whether the uncertainty of the size distribution of the materials can affect the permeability of the debris bed and therefore the head loss. Is this uncertainty significant, and if so, please state how is it accounted for in the STP model.

STP Response:

No, Table 2.2.21 of LAR Enclosure 4-3 is not directly implemented into the head-loss correlation. Table 2.2.21 of LAR Enclosure 4-3 lists the material properties of debris. As described in the LAR Enclosure 4-3, Page 178, some modifications were made to the values provided in Section 2.2.16. Tables 5.6.1 and 5.6.2 present the material properties as implemented into the head-loss correlation. Table 2.2.21 and Tables 5.6.1 and 5.6.2 are not identical due to assumptions related to the head-loss correlation and material debris size ranges. For example, all LDFG was assumed to be fines in the head loss correlation, which is noted as one difference between the tables. The effect of debris size on risk, selection of debris size for the head-loss correlation, and uncertainty of the size distribution are examined in the response to SSIB RAI 24. Uncertainty in material properties is accounted for in the factor of 5 uncertainty bound applied to all head-loss predictions.

SSIB, Transport: RAI 4

Please provide justification for assumption 6.h.i. of Volume 3 (page 78). According to Table 2.2.22 of Volume 3, line breaks below SG and surge line result in a greater percentage of small debris being blown directly to lower containment. This debris is considered to enter the pool directly while debris blown to upper containment may be held up. Please explain why the SG compartment transport fractions are considered to be conservative compared to these other break locations.

STP Response:

The steam generator compartment transport fractions were chosen for the following reasons.

- Transport fractions calculated from the Steam Generator Compartment are reasonably conservative and maximize transport for all considered breaks except those in the Below the Steam Generator Compartment location.
- The Steam Generator Compartment has a much larger Total Percentage of LDFG when compared to the other compartments.
- The Steam Generator Compartment has the second greatest Congestion to the Pressurizer Compartment which has non-conservative total transport fractions.

This response has three sub-parts, which consist of an explanation for assumption 6.h.i of LAR Encl. 4-3, Table 2.2.22 of LAR Encl. 4-3, and the implementation of SG compartment transport fraction.

Assumption 6.h.i of LAR Encl. 4-3

Assumption 6.h.i of LAR Encl. 4-3 states:

“I. Worst case values were selected from the transport fraction ranges for steam generator compartment blowdown and washdown”

Figure 1 illustrates that the values used to develop overall transport fraction logic trees were the maximum values of the ranges in the transport analysis and were selected in a way as to result in the maximum overall transport to the sump strainers, except for the error as noted in the response to SSIB RAI 7E.

In Figure 1, Table 2.2.22 and Table 2.2.23 are extracted from LAR Encl. 4-3. Figure 5.12.2 is taken from the debris transport calculation (LAR Encl. 4-3, Ref. [23]). (Reference 23 in LAR Encl. 4-3 has been revised to Revision 3 (1). However, the process illustrated in Figure 1 is the same in revision 3 as in revision 2.)

Table 2.2.22 – Blowdown transport fractions according to break location

Break Location	Debris Type and Size	Blowdown Transport Fractions		
		Upper Containment	Lower Containment	Remaining in Compartments
1. Steam Generator Compartments	Fines	70%	30%	0%
	Small LDFG	33-60%	11-25%	15-54%
	Large LDFG	0-22%	0%	78-100%

Table 2.2.23 – Washdown transport fractions according to spray initiation

Sprays Initiated?	Debris Type	Washdown Transport Fractions	
		Washed Down in Annulus	Washed Down inside Secondary Shield Wall
Yes	Fines	47%	53%
	Small LDFG	1-19%	21-27%
	Large LDFG	0%	0%
No	All	0%	0%

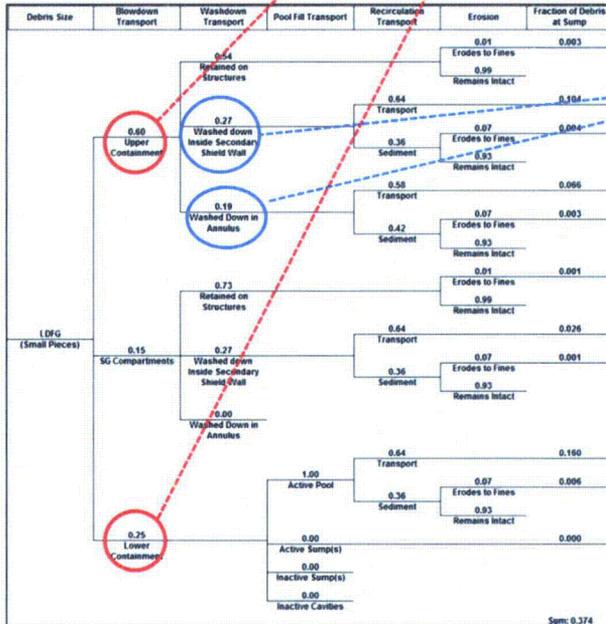


Figure 5.12.2 – Small piece fiberglass debris transport logic tree (SG compartment break)

Figure 1: Illustration of Process Described in Item I of Assumption 6.h

Table 2.2.22 of LAR Encl. 4-3

LAR Encl. 4-3, Table 2.2.22 summarizes transport fractions according to break location for only the blowdown portion of overall transport. The other processes that contribute to overall transport are washdown, pool fill, and recirculation, whose contributions are not reflected in Table 2.2.22.

Implementation of the SG Compartment Transport Fraction

The overall transport fractions computed in revision 3 of the debris transport calculation (1) are displayed in Table 1. For each debris category the maximum values are highlighted in the table.

Table 1: Overall Debris Transport Fractions

Break Location Region	Individual			
	LDFG	Small LDFG	Large LDFG	Latent
SG Compartment	99%	42%	1%	95%
Below SG Compartment	99%	60%	7%	95%
Pressurizer Compartment	97%	31%	1%	91%
Pressurizer Surge Line	97%	30%	1%	91%
RHR Compartment	97%	30%	2%	91%
Annulus	97%	33%	8%	91%

The total transport fraction for the steam generator compartment is conservative for individual LDFG and latent debris but is non-conservative for small and large LDFG.

A single break location's transport fractions were selected to model transport for all of the breaks CASA simulates. If below the steam generator compartment transport fractions (which generate the most conservative small total LDFG transport fraction) were implemented, the model would be accurate for the breaks below the steam generator compartment, but would over predict the transport for every other break. The steam generator transport fractions were implemented because they are reasonably conservative. The model is accurate for the breaks in the steam generator compartment, under predicts the LDFG transport for breaks below the steam generator compartment, and over predicts the LDFG transport for all other breaks.

Table 2 displays the total volume and percentage of LDFG in the break location regions. LDFG congestion (the ratio of insulation volume to the break location region volume) is a measure of the potential amount of LDFG that could be destroyed from a single break. This metric is also displayed in Table 2; the largest percentages are highlighted.

Table 2: Insulation in the Break Location Regions

Break Location Region	LDFG Vol. (ft ³)	Percentage of Total LDFG (%)	Region Volume (ft ³)	LDFG Congestion (%)
SG Compartment	5,529	55	201,552	2.7
Below SG Compartment	278	3	100,732	0.3
Pressurizer Compartment	553	6	10,933	5.1
Pressurizer Surge Line	50	1	3,013*	1.7
RHR Compartment	411	4	31,698	1.3
Annulus	3,166	32	637,708**	0.5
Reference	[i]	N/A	LAR Encl. 4-3, Ref. [23]	N/A

* The volume of the pressurizer surge line region was not stated in LAR Encl. 4-3 Ref. [23]; the pressurizer surge line region volume was included in the volume of the annulus region. The volume of the pressurizer surge line region was determined from the CAD Model Summary (2).

** The annulus region volume was determined by reducing the annulus region volume (LAR Encl. 4-3, Ref. [23]) by the pressurizer surge line region volume.

The values in Table 2 show the Steam Generator Compartment has the largest percentage of LDFG, ranging from approximately 2 to 50 times greater than all the other locations. The Steam Generator Compartment has the second greatest congestion. The congestion of the Pressurizer Compartment is approximately twice as much of the Steam Generator Compartment. However, the Steam Generator compartment has 10 times more LDFG than the Pressurizer Compartment.

References:

1. ALION-CAL-STP-8511-08. "Risk-Informed GSI-191 Debris Transport Calculation." Revision 3. 6/10/2014.
2. ALION-SUM-WEST-2916-01. "CAD Model Summary: South Texas Reactor Building CAD Model for Use in GSI-191 Analyses." Revision 4. 5/22/2014.

SSIB, Transport: RAI 6a

For the blowdown transport evaluation, it was not clear how the Drywell Debris Transport Study (DDTS), NUREG/CR-6369, "Drywell Debris Transport Study," Volumes 1, 2, and 3, September 1999 (ADAMS Accession Nos. ML003728226, ML003726871, and ML003728322, respectively), results were applied to the plant condition. (Reference: Volume 3, Section 2.2.17, "Blowdown Transport Fractions," and Volume 6.2, Item 5.a.2 (page 37). Please provide the following information:

- (a) The DDTS cautions that if gratings do not cover the entire transport path, they may not be as effective in debris capture. For transport paths where grating does not fully span the transport pathway, please state if the capture metrics was adjusted to account for this potential.**

STP Response:

The capture metrics are adjusted by a ratio of covered area to total area to account for situations where grating does not fully span the transport pathway, as described in the steam generator compartment blowdown section (LAR Encl. 4-3, Ref. [23], Pg. 39). Revision 3 of the debris transport calculation also adheres to this methodology (1, Pg. 47).

Reference:

1. ALION-CAL-STP-8511-08. "Risk-Informed GSI-191 Debris Transport Calculation". Revision 3. 6/10/2014.

SSIB, Transport: RAI 6b

(b) Please state if the calculational methodology account for depletion of debris, as it is captured on upstream objects. Please clarify if the amount reaching the second and third (etc.) objects reflects the debris lost on upstream objects. This was not apparent to the NRC staff upon inspection of the equations used to perform the calculation.

STP Response:

The computational methodology for blowdown did not always account for depletion of debris due to capture on upstream objects. An example of this is the equation on page 38 of LAR Encl. 5, which is presented below.

$$F_{BD} = \left(\frac{V_{upper}}{V_{total}} \right) (1.00 - F_{misc}) (1.00 - F_{90^\circ turns} \cdot N_{turns}) (1.00 - F_{grating} \cdot N_{gratings}) \quad (EQ-1)$$

where:

- F_{BD} = fraction of debris blown to upper containment
- V_{upper} = volume of upper containment
- V_{total} = total volume in containment
- F_{misc} = fraction of debris trapped by miscellaneous structures
- $F_{90^\circ turns}$ = fraction of debris trapped by changes in flow direction
- N_{turns} = number of turns or changes in flow direction debris would pass through
- $F_{grating}$ = fraction of debris trapped by grating
- $N_{gratings}$ = number of gratings debris would pass through

If N_{turns} or $N_{gratings}$ is greater than 1 (as is the case for numerous breaks in Item 5.a.2 of LAR Encl. 5) the model will not properly account for depletion on upstream objects.

However, Reference 23 of LAR. Encl. 4-3 has been revised to Revision 3 which correctly accounts for depletion of debris due to capture on upstream objects. The methodology used for the blowdown phase is based upon the equation below in the new revision (1, Pg. 47):

$$F_{UC/LCbd} = \left(\frac{V_{UC/LC}}{V_{total}} \right) \cdot (1.00 - F_{misc}) \cdot (1.00 - F_{90^\circ turns})^{N_{turns}} \cdot \prod_{i=0}^{n} (1.00 - F_{grating}^i \cdot A_{gratings}^i) \quad (EQ-2)$$

where:

- $F_{UC/LCbd}$ = fraction of debris blown to upper/lower containment
- $V_{UC/LC}$ = volume of upper/lower containment
- V_{total} = total volume in containment
- F_{misc} = fraction of debris trapped by miscellaneous structures
- $F_{90^\circ \text{ turns}}$ = fraction of debris trapped by changes in flow direction
- N_{turns} = number of turns or changes in flow direction debris would pass through
- $F_{grating}^i$ = fraction of debris trapped by i-th grating
- $A_{gratings}^i$ = ratio of i-th grating area versus total blowdown area (range from 0 – 1)
- $n = N_{gratings}$ = total number of gratings through which debris would pass

Since the overall amounts by which debris is accumulated on the different objects, e.g., grating, miscellaneous structures, etc., is determined by a product of the factors, the computational methodology accounts for depletion of debris as it is captured on upstream objects. For example, if the only mechanism of debris capture was miscellaneous structures, Equation 1 would yield:

$$F_{uc/lcbd} = (V_{UC/LC}/V_{total}) * (1.00 - F_{misc})$$

If further upstream debris capture occurs from 90° turns, its capture factor $(1.00 - F_{90^\circ \text{ turns}})^{N_{turns}}$ would be applied to an already reduced F_{BD} quantity based upon the upstream effect of miscellaneous structures; not on the entire debris quantity.

Likewise, if the additional effect of gratings is considered, its effect, $\prod_{i=0}^n (1.00 - F_{grating}^i * A_{grating}^i)$, is applied to a debris quantity that has already been depleted by the effects of miscellaneous structures and 90° turns.

Similarly, during the washdown transport phase, the effect of multiple gratings is taken into account with the implementation of $F_{washdown} = F_{CS} \cdot F_{WG} (1 - F_{AG})^{(N_{gratings}-1)}$ (LAR Encl. 4-3, Ref. [23], Equation 22 and i, Equation 24), where again, each successive holdup is applied to a quantity that has already been decreased.

Therefore, the new computational methodology accounts for depletion of debris as it is captured on upstream objects by applying the effect of the “nth” mechanism to an already depleted quantity from the 1st to (n-1)th mechanism.

Table B.1 displays the total transport fractions for both revisions of the debris transport calculations (LAR Encl. 4-3, Ref. [23] and 1). Transport fractions that changed in revision 3 are highlighted. Small and large LDFG were the only debris classifications whose transport fractions resulted in different values in revision 3. The discrepancy has been entered in the STP corrective action program for tracking for correction in future submittals.

Table B.1: Total Debris Transport Fractions

Break Location Region	Small LDFG		Large LDFG	
	Rev 2	Rev 3	Rev 2	Rev 3
SG Compartment	37%	42%	1%	1%
Below SG Compartment	59%	60%	7%	7%
Pressurizer Compartment	30%	31%	8%	1%
Pressurizer Surge Line	62%	30%	7%	1%
RHR Compartment	20%	30%	4%	2%
Annulus	27%	33%	1%	8%

A CASA Grande parameter study was performed where the debris transport fractions were modified to the Revision 3 SG Compartment values. This change resulted in a total Δ CDF decrease of 10%. The vessel Δ CDF decreased by 25% while the sump Δ CDF increased by 9%. The counterintuitive result, a decrease in total Δ CDF when the amount of debris reaching the strainer was increased, is attributed to competing phenomena. By increasing debris transport fractions, greater initial transport causes the filtration efficiency of the debris bed to increase, which in turn allows less debris to penetrate the strainer resulting in significantly lower in-vessel Δ CDF. Conversely, the additional debris at the strainer causes an increase in head loss and sump-related Δ CDF. However, the competing phenomena were dominated by the filtration efficiency and reduction of in-vessel Δ CDF. Similar instances were documented in Scenarios 1 and 2 of previous parameter studies (2, Appendix A) where a decrease in latent fiber resulted in an increase Δ CDF and an increase in latent fiber resulted in a decrease of Δ CDF.

Reference:

1. ALION-CAL-STP-8511-08. "Risk-Informed GSI-191 Debris Transport Calculation". Revision 3. 6/10/2014.
2. Morton, D. P., Tejada, J.J., Zolan, A., South Texas Project Risk-Informed GSI-191 Evaluation, Volume 3, A Practical Guide to Sensitivity Analysis of a Large-scale Computer Simulation Model., STP-RIGSI191-ARAI.01, Rev. 3.0, February 2014. The University of Texas at Austin.

SSIB, Transport: RAI 6c

- (c) Please explain what was considered to be a 90 degree turn in the plant and how this compared to the 90 degree turns modeled in the DDTs. Please explain how it was determined that the DDTs results are applicable to the STP conditions considered to be 90 degree turns.**

STP Response:

Reference 23 of LAR Encl. 4-3 included 90° turns that were not well represented by the DDTs. However, Reference 23 of LAR Encl. 4-3 was revised to Revision 3 (1) which only considered 90° turns comparable to the DDTs test set-up and expected resultant debris entrapment pattern as described below.

A review of NUREG/CR-6369, Drywell Debris Transport Study (DDTS), shows that the 90° bend in the test set-up was not designed to simulate any specific feature of a BWR; the 90° bend simply simulated a condition where debris-laden blowdown flow was forced to change its trajectory by 90° (0).

The subsequent three statements are quotes from the DDTs.

The debris was then carried by the airflow over 20-ft long structural congestion, a 90° bend, and a Mark I vent entrance, all of which were pre-wet fed by warm water to simulate surface wetness

In addition, the debris transport pathway passed through a 90° bend. The diameter of the test chamber was approximately 10 ft and the total transport path length was approximately 70 ft.

... make a 90° bend where the chamber wall had been wetted by mist drifting with the slight air draft through the chambers. A substantial amount of debris was deposited at this bend and this deposition expressed as a capture fraction is shown in Figure 3-35 as a function of the debris passing through the collar to the auxiliary chamber in term of mass flux based on the cross-sectional area of the chambers, not the collar. The mean value for the wet tests was 17%. Note that the cross-sectional area of the collar was about 60% of the main chamber area and that the mean capture fraction based on the collar cross-sectional area would be about 28%.

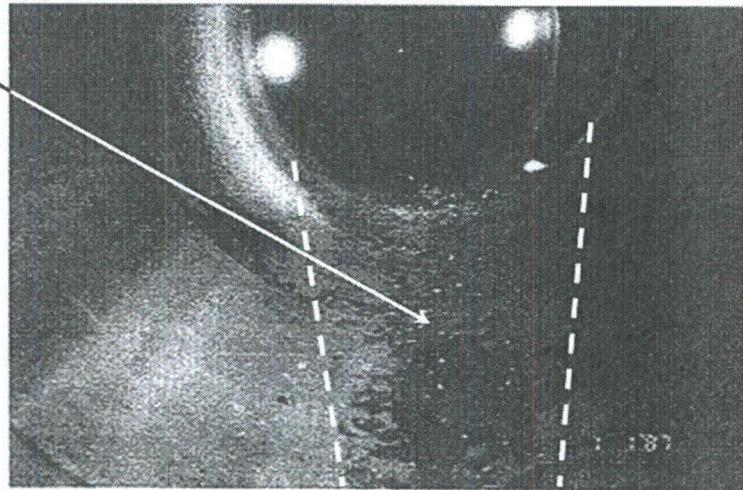
Hence, in the absence of any other factors, the test set-up and resulting debris entrapment associated with the 90° bend is equally applicable to a BWR, PWR or other similar industrial facility.

Application of the transport reduction factors associated with a 90° bend in the transport calculation was done with consideration of the DDTs test set-up and expected resulting debris entrapment pattern.

For example, blowdown up to upper containment from either a Steam Generator compartment break, or a break in piping in the annulus outside the Secondary Shield

Wall would result in some amount of change in trajectory from vertical. However such flowpaths were not considered 90° bends because the change in trajectory was judged to be less acute than that in the DDTS test set-up and would not result in the type of debris accumulation illustrated in Figure 3-25 *Deposition in auxiliary tank at bend (TestH2)* of the DDTS which is displayed below.

Trapezoidal
debris
accumulation
region



NUREG/CR-6369, Drywell Debris Transport Study, Figure 3-25 (0)

Conversely, relief of compartment pressurization through grated opening in corners of floors, which (a) required an acute 90° trajectory change, and (b) which would lead to a debris deposition pattern on the wall at the vertex of 90° bend which would be similar to the one illustrated in DDTS Figure 3-25, were considered to have debris entrapment similar to that described in the DDTS.

Compartments that forced the blowdown jet to go through a 180° "hairpin turn", such as the access ways to RHR Compartments, where debris entrapment patterns similar to the one illustrated in DDTS Figure 3-25 would be formed in one or more corners, and which clearly had acute trajectory changes, were considered to have debris entrapment similar to that described in the DDTS.

Table C1 summarizes the positions in the STP containment at which 90° turns were considered to produce a debris entrapment pattern similar to the ones observed in the DDTS (1).

Table CI: 90° Turn Positions in the STP Containment

Break Location	Flowpath to:	DT* Calc Equation Numbers	Discussion of 90-degree bends
Steam Generator Compartments	Upper Containment	2 and 3	No 90° bends were considered.
Steam Generator Compartments	Sump Elevation	4 and 5	One 90° bend was considered to model the change in flow path from the horizontal to downward trajectory through grating; the 90° bend is formed by floor/wall intersection.
Reactor Cavity	Upper Containment	2 and 3	No 90° bends were considered.
Reactor Cavity	Sump Elevation	4 and 5	One 90° bend was considered to model the change in flow path from the horizontal to downward trajectory through grating; the 90° bend is formed by floor/wall intersection.
Below the Steam Generator Compartment Floor	Upper Containment	6 and 7	One 90° bend was considered to model the change in flow path from the horizontal to upward trajectory through grating; the 90° bend is formed by floor/wall intersection.
Below the Steam Generator Compartment Floor	Sump Elevation	N/A	No 90° bends were considered.
Pressurizer Compartment	Upper Containment	8 and 9	One 90° bend modeled the turn to exit the openings at the top of the Pressurizer Compartment; the 90° bend is formed by ceiling/wall intersection.
Pressurizer Compartment	Sump Elevation	10 and 11	One 90° bend modeled the turn to exit the openings at the bottom of the Pressurizer Compartment enroute to gratings; the 90° bend is formed by floor/wall intersection.
Pressurizer Surge Line	Upper Containment	12 and 13	Two 90° bends modeled the exit at the bottom of the Pressurizer Compartment enroute to gratings; the 90° bend is formed by wall/wall intersection.
Pressurizer Surge Line	Sump Elevation	14 and 15	No 90° bends were considered
RHR Compartments	Upper Containment	16 and 17	Two 90° turns are required to exit the compartments (which effectively is a 180° hairpin turn turn); the 90° bend is formed by walls/walls intersections.
RHR Compartments	Sump Elevation	18 and 19	Two 90° turns are required to exit the compartments (which effectively is a 180° hairpin turn turn); the 90° bend is formed by walls/walls intersections.
Annulus	Upper Containment	20 and 21	No 90° bends were considered
Annulus	Sump Elevation	22 and 23	No 90° bends were considered

* DT refers to Revision 3 of Reference 23 of LAR. Encl. 4-3 (1)

In summary, the 90° bend in the DDTS test set-up is equally representative of a BWR, PWR or other similar industrial facility. The determination of the applicability of DDTS test 90° bend entrapment results was based upon the expected debris deposition pattern in STP 90° bend locations being similar to that shown in the DDTS.

Table C.2 displays the total transport fractions for both revisions of the debris transport calculations. Transport fractions that changed in revision 3 are highlighted. Small and large LDFG were the only debris classifications whose transport fractions were modified in revision 3.

Table C.2: Total Debris Transport Fractions

Break Location Region	Small LDFG		Large LDFG	
	Rev 2	Rev 3	Rev 2	Rev 3
SG Compartment	37%	42%	1%	1%
Below SG Compartment	59%	60%	7%	7%
Pressurizer Compartment	30%	31%	8%	1%
Pressurizer Surge Line	62%	30%	7%	1%
RHR Compartment	20%	30%	4%	2%
Annulus	27%	33%	1%	8%

In summary, the 90° bend in the DDTS test set-up is equally representative of a BWR, PWR or other similar industrial facility. The determination of the applicability of DDTS test 90° bend entrapment results was based upon the expected debris deposition pattern in STP 90° bend locations being similar to that shown in the DDTS.

Changes to total debris transport fractions are discussed in the response to SSIB RAI 6b, above.

References:

1. ALION-CAL-STP-8511-08. "Risk-Informed GSI-191 Debris Transport Calculation". Revision 3. 6/10//2014.
2. NUREG/CR-6369, Volume 2. "Drywell Debris Transport Study: Experimental Work". September 1999.
3. Morton, D. P., Tejada, J.J., Zolan, A., South Texas Project Risk-Informed GSI-191 Evaluation, Volume 3, A Practical Guide to Sensitivity Analysis of a Large-scale Computer Simulation Model., STP-RIGSI191-ARAI.01, Rev. 3.0, February 2014. The University of Texas at Austin.

SSIB, Transport: RAI 6d

(d) Please clarify if there are limits to the mass of debris that can be captured on structures or on specific surface areas of structures and, if applicable, how such limits would affect the calculations for holdup.

STP Response:

Specific limits have not been placed on the mass of debris that is computed to be caught on structures. However, a feasibility check has been performed and is discussed below.

The feasibility check focused on estimating the maximum credible quantities of Low Density Fiberglass (LDFG) debris that is considered to be caught on structures and comparing these quantities with the quantities that were observed in the DDTS. Results showed that the quantity of debris computed to be held up on STP structures was less than those observed in the DDTS test program, which confirms that DDTS test results are applicable to STP conditions.

The feasibility check consists of

- a. Determining the maximum quantities of LDFG generated for cases that resulted in successful ECCS operation and had probabilities of occurrence greater than $1.0E-15$,

It was determined that 100 cubic feet of LDFG was the maximum total STP LDFG quantity for cases that resulted in successful ECCS operation and had probabilities of occurrence greater than $1.0E-15$. Cases that resulted in failure were not of interest because if a limit on a structure allowed more debris to bypass, the case would still result in failure.

- b. Estimating the total quantities of LDFG debris computed to be held up on STP Structures and 90° bends during blowdown phase,
- c. Estimating the portion of the total quantities of STP LDFG debris computed to be held up that are "small pieces",
- d. Determining the area of structures on which the maximum quantities of STP LDFG "small pieces" were computed to be held up,
- e. Computing the quantity of STP LDFG "small piece" debris per unit area of STP structures,

The maximum quantities of debris accumulation on grating results from steam generator compartment break cases. It was determined that if the maximum quantity STP LDFG on grating was in the form of one inch cubes, approximately 11% of the grating considered would be covered. Likewise, it was determined that if the maximum quantity STP LDFG on grating was in the form of two inch

cubes, approximately 3% of the grating considered would be covered. Accumulation from breaks in other locations is an order of magnitude less.

The maximum quantities of debris accumulation on miscellaneous structures results from Steam Generator compartment break cases. It was also determined that if the maximum quantity STP LDFG on miscellaneous structures was in the form of one inch cubes, approximately 7% of the structures considered would be covered; and it was determined that if the maximum quantity STP LDFG on structures was in the form of two inch cubes, less than 2% of the miscellaneous structures considered would be covered. Accumulation from breaks in other locations are an order of magnitude less.

- f. Comparing the quantity of STP LDFG “small pieces” debris per unit area on STP structures versus DDTS results.

Based upon a visual comparison with test results shown in DDTS Figures 2-9, 2-10, 2-11, 3-21, 3-22 and 3-23, maximum grating coverage of 3% to 11% is comparable to was what observed in DDTS tests. Table D1 illustrates this comparison.

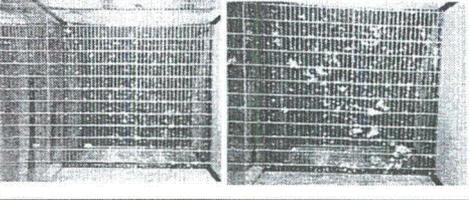
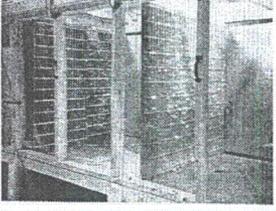
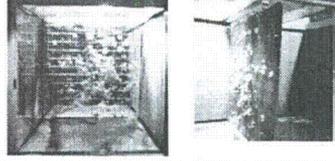
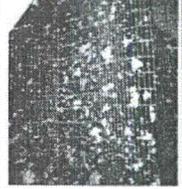
DDTS Figure Number	DDTS Figure	Observations
2-9		<p>Collectively, the photos in the DDTS Figures 2-9, 2-10, 2-11, 3-21, 3-22 and 3-23 illustrate that LDFG capture on grating is on the order of a few percent coverage to as much as (estimated) 20% (in Figure 2-11).</p>
2-10		<p>The photos show that relatively large debris pieces, on the order of 1" by 3" (Figure 3-21) are captured on grating.</p> <p>These observations are within the ranges of grating debris loading at STP.</p>
2-11		
3-21		
3-22		
3-23		

Table D1 – DDTS Grating Debris Accumulation

The maximum quantity of debris accumulation from Steam Generator compartment breaks on miscellaneous structures would result in coverage of 2% to 7% of the miscellaneous structures surface area. Based upon a visual comparison with test results shown in DDTS Figures 2-7 and 2-8, this is comparable or less than was what observed in DDTS tests. Table D2 illustrates this comparison.

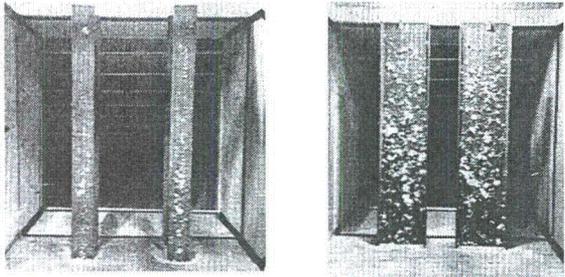
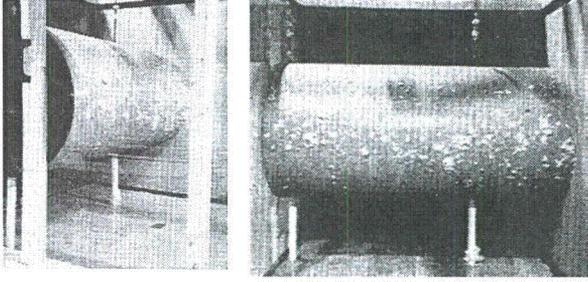
DDTS Figure Number	DDTS Figure	Observations
2-7		<p>Collectively, the photos in the DDTs Figures 2-7 and 2-8 illustrate that LDFG capture on structures is on the order of a few percent coverage to as much as (estimated) 30% (in Figure 2-7).</p> <p>This compares favorably with the 2% to 7% coverage expected at STP.</p>
2-8		

Table D2 – DDTs Miscellaneous Structures Debris Accumulation

However, since the minimum of the range (0%) of holdup on structures was used in the transport analysis for Steam Generator compartment breaks, the above results are theoretical. In practice, it is considered that no accumulation on miscellaneous structures would occur for Steam Generator compartment breaks.

For breaks below the Steam Generator compartment, the RHR Compartments and annulus, accumulation of debris per surface area of structures is less than what is reported in the DDTs test results (DDTS Table 2-2).

On the basis of these comparisons with DDTs results, it was concluded that the quantities of STP LDFG computed to be held up on grating and miscellaneous structures were feasible.

The DDTs did not furnish numerical quantities of debris collection at 90° bends. The maximum quantity of debris collection at a 90° bend in the assessment was equivalent to a 1.8-ft cube of LDFG. This maximum quantity is associated with steam generator compartment breaks. Debris quantities associated with breaks in other locations are an order of magnitude less. Given the plant geometries where such retention can be expected, there is no physical reason why such accumulation could not feasibly occur.

SSIB, Transport: RAI 6e

(e) Please explain how the ranges of values used in the DDTS were determined to be applicable to the STP conditions.

STP Response:

Several parameters were used to conclude that the values determined in the DDTS are applicable to STP. These are:

- a. debris type used in the DDTS versus debris type to which DDTS values were applied to STP,
- b. debris size for which capture fractions are reported in the DDTS versus the debris size for which DDTS capture fractions are used in STP debris transport calculations,
- c. the degree to which the wetted conditions that resulted in significant debris entrapment in the DDTS are similar to the conditions that can be expected at STP,
- d. the types of structural debris entrapments that were investigated in the DDTS versus the types of structural debris entrapments that are found at STP
- e. the congestion and jet velocity that were used in the DDTS versus what is expected at STP,
- f. orientation of the DDTS test set-up versus application for STP
- g. the manner in which the results of the DDTS were intended to be used versus the intended use for STP,
- h. consideration of overall debris quantities considered in the DDTS and expected to occur at STP.

Each item is discussed below. The discussion establishes the basis for concluding that the debris entrapment values reported in the DDTS, as used, are applicable to STP conditions.

Debris Type

The debris type investigated in the DDTS was Low Density Fiberglass (LDFG). NUKON was used as the test material. The results of the DDTS are applied to potential LDFG Post-LOCA generated debris at STP. This DDTS characteristic is directly applicable to STP.

Debris Size

Assumption 3.1.b (LAR Enclosure 4-3, Reference [23] and 1) states "It was assumed that small pieces of LDFG (smaller than 6") can be treated as 1"clumps, and large pieces of LDFG (larger than 6") can be treated as 6" pieces. Since the assumed sizes are on the low end of the size ranges described in the debris generation calculation (2), this is a conservative assumption."

The DDTS Separate Effects Test Program supplied ranges of numerical entrapment fractions for "small" debris. In the Separate Effects Test Program, small debris, called Class 2-4, was of the size shown in DDTS Figure 2-6. The DDTS Separate Effects Test

Program small pieces were generally 2 inches long; some were close to 4 inches, but none are as large as the 6 inch size that was included in the “small pieces of LDFG” (LAR Enclosure 4-3, Reference [23] and 1).

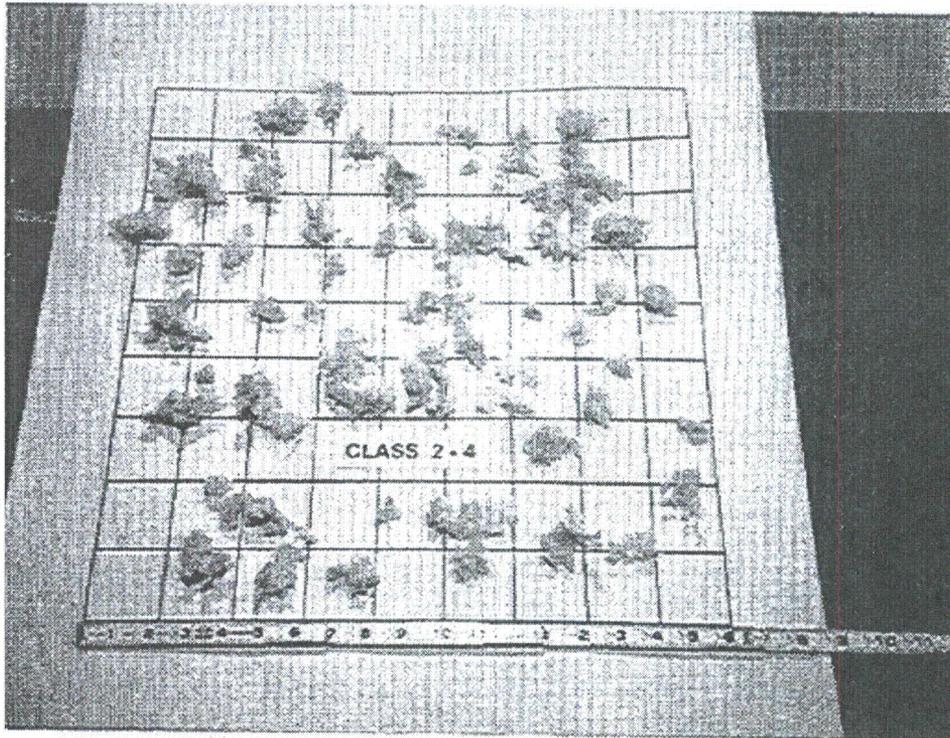
The debris size distribution used in the Integrated Effects program is shown in DDTS Table 3-7. Ranges of numerical entrapment fractions were developed for “small” debris; entrapment estimates for medium and large debris were qualitative. The DDTS Integrated Effects Small size, defined as being able to pass through a grating cell, is significantly smaller than the “small pieces of LDFG”, which were up to 6 inches (LAR Enclosure 4-3, Reference [23] and 1).

In summary, the size range of “small pieces of LDFG” in the debris transport calculation (LAR Enclosure 4-3, Reference [23] and 1) were substantially larger than the Class 2-4 and small sizes for which entrapment factors were reported in either the Separate Effects Test Program or the Integrated Effects program.

DDTS studies stated that entrapment increased with debris size, particularly for grating. Consequently, using DDTS entrapment factors based upon significantly smaller debris than considered in the debris transport calculation (LAR Enclosure 4-3, Reference [23] and 1) is a significant conservatism, particularly where grating entrapment is concerned.

While not stated in the DDTS, it is reasonable to conclude that at 90° bends, larger “small pieces of LDFG” (LAR Enclosure 4-3, Reference [23] and 1) debris would be equally or more likely to collect in corners than the relatively smaller Class 2-4 and Small debris considered in the DDTS.

On that basis, particularly grating and 90° bend entrapment estimates in the DDTS are applicable to STP and are a source of conservatism in the debris transport calculation (LAR Enclosure 4-3, Reference [23] and 1).



DDTS Figure 2-6

Debris classification	Relative size	Description
Large	> hand size	Large pieces were too large to pass through a grating and therefore were all located either upstream of the continuous grating or behind the target mount.
Medium	> grating cell but < hand size	Medium pieces sometimes were forced through a grating, although they were generally larger than a grating cell.
Small	< grating cell	Small pieces would generally pass through a grating cell unless the piece was to inertially impact on a grating bar. Small debris included fine particles such as individual fibers that could also pass through the catch screen of the exhaust flow.

DDTS Table 3-7

Wetted Conditions

The DDTS concluded that substantial debris entrapment on structures occurs when the structures are wetted, while less debris is caught on dry surfaces. Grating was less susceptible to entrapment differences between wetted and dry conditions. Given that a LOCA jet at STP, being a PWR, begins with a two-phase mixture, it is reasonable to conclude that the STP jet will sufficiently wet the surface in comparison to the artificially introduced wetting that was done in the DDTS test set-up. Consequently, this DDTS wetness characteristic is directly applicable to STP.

Structural Debris Entrapments Types

The structural debris entrapment structures used in the DDTs were pipe, structural (I) beams, grating, a 90° degree turn and a Mark II vent entrance. The DDTs investigated several combinations with upstream and downstream structural elements. In general, with the exception of the Mark II vent entrance, the types of entrapment structures used in the DDTs are similar to those which exist at STP. This DDTs test set-up characteristic is directly applicable to STP.

Congestion and Jet Velocity

Congestion. Given the size differences between BWR and PWR containments, it is recognized that BWR containments tend to be more congested. Intuitively, it would appear that increased congestion would result in increased debris entrapment. While generally true, the DDTs also states in section 2.4.7, Effect of Structural Combinations, for downstream obstructions in a heavily congested configuration, "the debris retention ability of the (downstream) beams is reduced when they are located in the turbulence of the wake region behind upstream members." Therefore, congestion, alone, is not a complete parameter on debris entrapment or applicability to a particular configuration.

Jet Velocity. Both for structural elements and grating, the DDTs reported in section 2.4.3, Effect of Approach Velocity, the general trend that increasing jet approach velocity tended to result in decreasing debris capture efficiency. Assuming that the DDTs was a reasonably scaled representation of a BWR containment, and given that PWRs in general and STP in particular would have a relatively larger volume, it is reasonable to expect that the generally larger volume would result in equal or lower approach velocities as the PWR/STP jet propagates through containment. As a result, it is not expected that based upon velocity, a generic PWR or STP would have capture efficiencies that are substantially lower than what was reported in the DDTs.

With the effect of congestion being somewhat moderated by the potential effects of local turbulence, and given that lower approach velocities tended to result in greater debris capture efficiency, it is reasonable to conclude that where these two parameters are concerned, the results of the DDTs are generally applicable to STP.

Orientation of the DDTs Test Set-up

The orientation of all the test jets in the DDTs was horizontal. However, results of DDTs test are used for analysis of horizontal and vertical jet propagations. It is noted in Item "vii" in section 2.5 (Conclusions) of the DDTs that the loss of fibrous debris by capture on the tunnel floor, was negligible for all tests except the MARK II vent geometry, the results of which were not used in the STP analyses. Therefore, results of the DDTs are acceptable for application of horizontal and vertical jet trajectories.

DDTS Results Usage

DDTS Figure 3-31 illustrates the fractional capture of small debris by I-beams and pipes. Values in DDTS Figure 3-31 for CEESI wetted tests range from approximately 7% to 14%. The minimum and maximum entrapment values used in the debris transport calculation (LAR Enclosure 4-3, Reference [23] and 1) are 0% to 13%, which are lower than those shown in DDTS Figure 3-31.

DDTS Figure 3-32 illustrates the fractional capture of small debris by V-grating. Values in DDTS Figure 3-32 for CEESI wetted tests range from approximately 21% to 36%. DDTS Figure 3-33 illustrates the fractional capture of small debris by split grating. Values in DDTS Figure 3-33 for CEESI wetted tests range from approximately 16% to 38%. DDTS Figure 3-34 illustrates the fractional capture of small debris by continuous grating. Values in DDTS Figure 3-34 for CEESI wetted and partially wetted tests range from approximately 3% to 29%. The minimum and maximum entrapment values used in debris transport calculation (1) are 5% to 35%, which are lower than those shown in DDTS Figures 3-32 and 3-33, and are similar to those in DDTS Figure 3-34 given that the low end of the range in DDTS Figure 3-34 is strongly influenced by partial versus significant wetting.

DDTS Figure 3-35 illustrates the fractional capture of small debris by the auxiliary tank bend, i.e., the 90° bend. Values in DDTS Figure 3-35 for CEESI wetted tests range from approximately 3% to 31%. The minimum and maximum entrapment values used in the debris transport calculation (LAR Enclosure 4-3, Reference [23] and 1) are 3% to 29%, which are within the range shown in DDTS Figure 3-35.

It is noted that in DDTS Figure 3-31 small debris capture fractions by I-beams and pipes represent individual obstructions. Therefore, for multiple structural elements, a formulation similar to that which was used for 90° bends and grating are appropriate, i.e., of the form

$$\prod_{i=1}^n (1.00 - F_{misc})$$

where F_{misc} is the capture fraction of one miscellaneous structural obstruction and n in the $n = N_{misc}$ which denotes the number of such obstructions to be multiplied in the Cartesian Product. Instead, the debris transport calculation (LAR Enclosure 4-3, Reference [23] and 1) uses, in effect, a single term in all cases, which is a conservative approach.

Overall Debris Quantities

In the STP CASA Grande analysis, over 640,000 break cases, ranging in location, break size and probability of occurrence, are considered. Of these, breaks resulting in total LDFG debris generated in excess of 100 cubic feet have a probability of occurrence in the 1.0E-15 range, hence they are of little practical interest. The quantities of LDFG debris considered held up on miscellaneous structures, grating and at 90-degree turns for break cases associated with total LDFG debris generated up to 100 cubic feet are relatively small when compared with the quantities of debris held up in the DDTS tests. Consequently, the results of the DDTS testing are applicable to STP conditions in terms

of quantities of debris considered to be held up on miscellaneous structures, grating and at 90-degree turns.

Summary

In summary, based upon similarity in debris type, debris sizes considered, the degree to which wetted conditions can be expected, similarity in types of structural debris entrapments, congestion and jet velocity comparison, the manner in which the results of the DDTS were used and overall debris quantities, it is concluded that, as used, the results of the DDTS were appropriately applied to STP conditions.

Reference:

1. ALION-CAL-STP-8511-08. "Risk-Informed GSI-191 Debris Transport Calculation". Revision 3, 6/10//2014.

SSIB, Transport: RAI 7a

For the washdown transport evaluation it was not clear to the NRC staff that the DDTS test results were applied realistically or conservatively to the STP plant condition as described in Volume 1, Section 1.2.3, "Washdown Transport," Volume 3, Section 2.2.18, "Washdown Transport Fractions," and Items 5.a.3 and 5.a.5 of Volume 6.2. Please provide the following information:

- (a) Please state if the washdown evaluation considered that it may be more likely for a piece of debris that has been blown through one or more gratings to subsequently wash down through gratings. It appears that the DDTS did not use debris that had been passed through gratings when studying washdown through gratings.**

STP Response:

Section 2.2.18, Washdown Transport Fractions, of LAR Enclosure 4-3 does not contain an explicit evaluation of the likelihood that a piece of debris that has been blown through one or more gratings will be more likely to subsequently wash down through gratings. NUREG/CR-6369, Vol. 2 Drywell Debris Transport Study: Experimental Work Final Report (DDTS) did not attach test debris to grating by impingement in a jet through gratings when studying washdown (1).

However, based on the following, it is concluded that the debris that was used in section 4 of the DDTS, Separate Effects Test Program to Evaluate Washdown of Insulation Debris by ECCS Flow, (hereafter referred to as "washdown") adequately represents the debris that was considered susceptible to washdown in the STP analysis, and the results of the DDTS can be applied to STP washdown calculations.

Section 5.4 of reference 23 in LAR Enclosure 4-3 states, "for this analysis, it was conservatively assumed that all debris would be washed to lower containment with the exception of any small and large piece debris held up on grating as it is washed down."

In the DDTS washdown discussion, "Small" washdown debris, is described as:

Insulation debris of a light, loose, and well-aerated texture with an average density lower than 0.25 lbm/ft^3 usually consisting of loose clusters of individual fibers. Typically these pieces were about 1.5" in size and possessed little of the original structure or the chemical binding. In CEESI tests, they were found to have been attached to the wet gratings. These debris pieces were obtained directly from blast-jet experiments conducted previously by SEA (see Section 3). These debris pieces were mainly used in spray tests.

Note the characterization of "a light, loose, and well-aerated texture with an average density lower than 0.25 lbm/ft^3 usually consisting of loose clusters of individual fibers." The DDTS washdown discussion states that compacted debris is less prone to erosion, while loose debris is more likely to erode. For example, DDTS washdown section 4.4.1, Confirmatory Tests, item 3 states "Pieces sufficiently larger than the grating (classified as M-O, M-J and L in Section 4.2.2) possess sufficient structure and are not susceptible

to being forced through the grating clearances in a short period of time. Erosion (if any) occurs over a longer period of time.”

The mechanism of debris generation, passage through a grating and subsequent capture on a grating is as follows:

- a. The process of debris generation destroys the initial compact form of debris.
- b. The process of debris, which is larger than the opening size of the grating, passing through a level of grating further disrupts the compactness of the debris.
- c. The process of inertial capture of debris on grating includes compaction as the debris collides with the grating, under the influence of jet forces. As more debris is caught on the grating, the debris is further compacted, both under the action of the jet forces acting on it and the effect of “additional layers” being compressed by jet forces.

Therefore, while the process of passing through a level of grating may loosen debris, the process of capture and retention has the opposite effect, compaction. For example, in section 2.4.10, Grating Debris Degradation Tests, of the DDTS, it was observed that debris caught on grating and subjected to jet forces tended to retain its structure, e.g., “No apparent breakdown of either the 1/2” or 1/4” insulation debris was seen, although the pieces bowed between the grating bars” and “the edges of the insulation pieces wrapped back around the grate bars to flap behind the grate ...”

In contrast, the debris used in the washdown tests had a “...a light, loose, and well-aerated texture ...”

It is therefore concluded that results obtained from washdown testing of “...light, loose, and well-aerated texture” debris is representative and may be conservative when compared to debris that has been compacted on grating by a combination of jet forces and potentially multiple layers of debris.

Reference:

1. NUREG/CR-6369, Vol. 2. “Drywell Debris Transport Study: Experimental Work Final Report”. September 1999.

SSIB, Transport: RAI 7b

- (b) The DDTS washdown tests were run for 30 minutes. The DDTS stated that most washdown occurred in the first 15 minutes. It was not clear to the NRC staff from the test results how washdown over a significantly longer period of time would occur. Please explain why the DDTS results are applicable to significantly longer washdown periods.**

STP Response:

The significantly longer washdown periods at STP than those considered in the DDTS are inconsequential to the STP analysis. Section VI.5, Blowdown/Washdown Conclusion, of NEI 04-07 Vol-2 (SER) (LAR Enclosure 4-3, Reference [45]) which is guidance that addresses the entire post-LOCA mission time on a deterministic basis, states: “the DDTS assessed the erosion of LDFG by CSs (i.e., spray) as less than 1 percent. In reality, the erosion may be significantly less than 1 percent. The 1 percent value was assumed to be conservative but not far from reality.” The basis of the washdown parameters used in the transport analysis was NEI 04-07 Vol-2 (SER), not the DDTS.

SSIB, Transport: RAI 7c

(c) Please state if debris is washed down through one level of grating, if it is more likely to wash through subsequent levels. If it washes through more than one grating, is it more likely to pass through subsequent levels? Please explain how the transport evaluation accounts for such a likely potential. What was considered when determining the retention fractions for debris on additional levels of grating in the washdown transport evaluation? It was stated that engineering judgment was used in this determination, but the NRC staff did not find an adequate basis documented for the engineering judgment.

STP Response:

The debris transport analysis takes into account the possibility that debris that is washed down through one level of grating may be more likely to wash through subsequent levels.

Section 5.4 of reference 23 in LAR Enclosure 4-3 states “The results of the DDTS testing showed that approximately 40-50% of small fiberglass debris landing on grating would be washed through the grating due to spray flows (14). Due to the fact that many of the flow paths to the containment pool would pass through multiple levels of grating, it was assumed that 0- 25% of small pieces would be held up on each additional grating level...”

In the transport calculation, the above ranges were implemented as follows:

- For the first grating, a 50% fraction was used, resulting in 50% hold-up and 50% wash through.
- For all subsequent gratings, a 0% fraction was used, thus resulting in no holdup of debris at subsequent grating(s).

This approach takes into account the possibility that debris washed down through one level of grating may be more likely to wash through subsequent levels.

It is noted that the DDTS does not include any discussion that it may be more likely for a piece of debris that has been blown through one level of gratings to be more likely to wash through subsequent levels. Nevertheless, it is concluded that the debris transport analysis takes into account the possibility that debris that is washed down through one level of grating may be more likely to wash through subsequent levels.

SSIB, Transport: RAI 7d

(d) Please state if the washdown transport evaluation accounted for the significantly higher velocities that may occur with sheeting flow at the beginning of washdown.

STP Response:

The response to SSIB, Transport, RAI 8 states “The response previously provided in Section 5.a.5 (LAR Enclosure 5) was not implemented. CASA Grande assumes no credit for hold up of partially submerged debris on the concrete of the operating deck as previously described.” This has been entered in the STP corrective action program for correction in future submittals.

The significantly higher velocities that may occur with sheeting flow at the beginning of washdown are inherently considered by the assumption that all debris landing on concrete would be washed to lower containment as described in the following quote.

Section 5.4 of reference 23 in LAR Enclosure 4-3 states “During the washdown phase of a LOCA, debris would be transported down to the containment pool by operation of the containment spray system. Significant amounts of debris could, however, be captured on the concrete floors and grated areas above the containment floor as containment spray water transporting the debris drains through grating to reach the pool... However, for this analysis, it was conservatively assumed that all debris would be washed to lower containment with the exception of any small and large piece debris held up on grating as it is washed down.”

SSIB, Transport: RAI 7e

- (e) The submittal provided the calculations for washdown percentages. Item 5.a.3 (Volume 6.2, page 43) uses values of 0.4 and 0.5 for F_{wg} , fraction of debris held up when washed through the first level of grating. The DDTS states that 40-50 percent pass through. Please clarify if 0.4 and 0.5 be reversed or if the 0.4 should be changed to 0.6. The terminology used is not clear and can be misunderstood.**

STP Response:

The observation is correct, incorrect values of F_{WG} were used in Section 5.a.3; the 0.40 and 0.50 should have been reversed. In other words, the 0.50 should have been implemented in the first equation (the equation which has a solution of 0.19), and the 0.40 should have been implemented in the other equation. Also, in accord with the equation, the correct definition of F_{WG} is fraction of debris washed through the first level of grating. If 40% of debris landing on grating is washed down through the grating, then 60% is held up.

Reference 23 of LAR Encl. 4-3 was revised to revision 3 and corrected this (1, Equation 25 and 26). The resulting changes to total debris transport fractions are discussed in the response to SSIB RAI 6b, above.

References:

1. ALION-CAL-STP-8511-08. "Risk-Informed GSI-191 Debris Transport Calculation." Revision 3. 6/10/2014.
2. Morton, D. P., Tejada, J.J., Zolan, A., South Texas Project Risk-Informed GSI-191 Evaluation, Volume 3, A Practical Guide to Sensitivity Analysis of a Large-scale Computer Simulation Model., STP-RIGSI191-ARAI.01, Rev. 3.0, February 2014. The University of Texas at Austin.

SSIB, Transport: RAI 7f

- (f) Table 2.5.24 of Volume 6.2 is titled, “Washdown transport fractions used in CASA Grande,” but the leading paragraph states that the table contains blowdown fractions. Please clarify whether it is blowdown transport fraction or washdown blowdown transport.**

STP Response:

The leading paragraph pertains only to washdown fractions. The discrepancy has been entered in the STP corrective action program for tracking for correction in future submittals.

SSIB, Transport: RAI 8a

The evaluation for transport of partially submerged debris on the operating deck makes several unsubstantiated assumptions (Item 5.a.5, Volume 6.2, page 54). Please provide the following information:

- (a) Please explain if the assumed size distribution considered that most of the debris blown to the operating deck would pass through grating thus likely reducing the size. Please clarify if the assumed size distribution was adjusted for this effect.**

STP Response:

The following response is for SSIB RAI 8a through SSIB RAI 8e.

The response previously provided in Section 5.a.5 (LAR Enclosure 5) was not implemented. CASA Grande assumes no credit for hold up of partially submerged debris on the concrete of the operating deck.

Section 5.a.5 of LAR Enclosure 5 was a response to NRC Staff Comment/Question 2.5.a.5 in the 2013 Submittal which states:

“The basis for the proposed change is that the residual risk from the remaining GSI-191 issues (e.g., those not already addressed in a deterministic manner) satisfies the criteria in Regulatory Guide (RG) 1.174, Revision 2, "An Approach For Using Probabilistic Risk Assessment In Risk-Informed Decisions on Plant- Specific Changes to the Licensing Basis," May 2011 (ADAMS Accession No. ML100910006). However, the application does not appear to provide sufficient detail for the NRC staff to determine whether the criteria in RG 1.174 have been met. Please describe in detail how the principles of RG 1.174 criteria regarding safety margin, defense-in-depth (DID), and change in risk are met. In particular, please include the following:

- a. Regarding the technical evaluation that supports the risk metrics, the Project Summary (Enclosure 4 to the application) describes numerous areas where the technical evaluation deviates from the approved guidance for addressing GS1 191. However, the application provides little or no information on how the issues were addressed. Please provide a discussion in sufficient detail to permit NRC staff review of the methods, bases, assumptions, acceptance criteria, and results. If test results are used to develop probability distributions, please describe how these distributions were determined and used in the overall risk evaluation. Please also provide the basis for the acceptance criteria chosen. The NRC staff requires additional information in the following areas:

5) Time dependent transport”

The correct response to question 5.a.5 is the only time dependent transport that occurs is the accumulation of debris on the strainers

SSIB, Transport: RAI 8b

- (b) Please state if the evaluation considered that the initial sheeting flow may be at a higher velocity than the steady state flow and that this may push debris across the floor before a steady state occurs.**

STP Response:

See response to SSIB RAI 8a

SSIB, Transport: RAI 8c

- (c) Please state the basis for the porosity equation. Please explain why the bulk density (as-fabricated) of the fiber relevant after it has been rendered into small pieces and then been blown through grating.**

STP Response:

See response to SSIB RAI 8a

SSIB, Transport: RAI 8d

(d) Please clarify if the evaluation considered that air may be trapped within the fiber and that it may pick up additional air as it tumbles across the floor.

STP Response:

See response to SSIB RAI 8a

SSIB, Transport: RAI 8e

(e) Please state if there is any experimental data available to validate the calculational methodology.

STP Response:

See response to SSIB RAI 8a

SSIB, Transport: RAI 10

The submittal states that unqualified coatings that fail after the sprays are secured cannot transport to the containment sump (Reference Volume 1, Section 1.2.3, "Washdown Transport," Volume 3, Section 2.2.10, "Unqualified Coatings Quantity," Volume 3, Section 5.4.5, "Unqualified Coatings Debris," Volume 3, Section 5.5.7, "Strainer Transport"). Please explain how it was determined that they would not transport. Please clarify if there are transport mechanisms besides washdown from containment spray that could cause some of the coatings to transport. For example, please explain if coatings are located in areas where they could fall directly into the sump or fall relatively freely to the sump. Explain if the flow of condensation on surfaces can carry particles of failed coatings to the sump, etc. (page 173, Section 1.2.3; page 571, Section 2.2.10, page 674, Section 5.4.5, page 680, Section 5.5.7)

STP Response:

The failure and subsequent transport of unqualified coatings is spray dependent (LAR Enclosure 4-3 Reference 12). If there is no spray (sprays are secured), there is no additional failed inventory available for transport. CASA Grande does not include a predictive model of debris transport, so consideration of additional transport mechanisms must be included in the assigned failure and transport factors.

There are other transport mechanisms besides washdown from containment sprays that could cause failed unqualified coatings inventory to transport, such as free fall and condensate flow. However, no additional unqualified coatings are assumed to fail after containment sprays are secured. The unqualified coatings inventory presumed failed, computed as the product of the total coatings inventory and the time-dependent failure fraction (unqualified washdown), was added to the containment pool within the first 10 minutes (See the response to ESGB, Coatings RAI 4 and 5 provided in the STP letter to the NRC Staff, NOC-AE-00143103, dated May 22, 2014, ML14149A434).

Condensate on surfaces could potentially carry particles of already failed unqualified coatings to the pool after containment sprays are secured. However, STP inputs to CASA Grande do not assume the additional failure of unqualified coatings once Containment Sprays are secured, and no time-dependent arrival was credited. The unqualified coatings inventory that failed, computed as the product of the total inventory and the failure timing (unqualified washdown) fraction, was added to the containment pool within the first 10 minutes (See response to ESGB, Coatings RAI 4).

SSIB, Head Loss and Chemical Effects Bump Up: RAI 14

The STPNOC submittal assumes that no chemical bump up occurs if the debris bed thickness is less than 1/16-inch (Reference: Volume 1, Section 1.1, Step 14; Volume 3, Assumption 7.c; Volume 6.2, Items 5.a.10 and 5.a.11). The NRC staff has previously concluded that a 1/16-inch debris bed is an adequate metric for this purpose for clean plants, where the worst analyzed break could result in 1/16-inch of fiber when conservative methods were used for estimating the amount of debris generated and transported to the strainer. The clean plant criteria also included other restrictions for the use of the metric, such as the lack of problematic debris within any ZOI. The staff has not determined that this limit is appropriate for a more realistic risk-informed evaluation. The staff has reviewed test results conducted with about 1/16-inch of fibrous debris that resulted in some head loss when chemical precipitates were added to the test. It also appears that the STP evaluation has not considered all aspects of the clean plant criteria. Whether or not the clean plant criteria are the basis for the 1/16-inch limit, please provide a justification for its use.

STP Response:

The clean plant criteria is not the basis for using 1/16th inch limit for chemical bump up.

Any fiber build-up less than 1/16th in. (thin bed) is unlikely to load contiguously, allowing chemical precipitants to pass through the strainer mesh without causing a significant head-loss increase. Conventional head loss for breaks that do not form a thin bed are calculated and evaluated in the analysis.

Debris beds of 1/16th in. or thicker are subjected to chemical head-loss factors as described in LAR Enclosure 4-3, Section 5.6.3. Each simulated break has its own time-dependent conventional head loss that is calculated based on debris accumulation and flow rate, which is then added to a baseline clean-strainer head loss of 0.220 ft-H₂O [1]. Chemical factors are applied to the conventional head loss when the temperature is less than 140±5 °F and the fiber load exceeds 1/16th in. equivalent thickness.

A sensitivity analysis was performed in CASA Grande by applying the chemical bump-up factor to a thin bed threshold value of 0 in. to assess the effects of that variable using the maximum amount of conservatism. This sensitivity analysis showed no effect on ΔCDF . Therefore, using a chemical multiplier on anything less than 1/16th in. would not influence risk.

A further sensitivity study indicates that the multiplier on the MBLOCA condition must be higher than 60 to increase the risk assigned by CASA Grande Case 01 (all equipment operates). The SBLOCA head loss factor in this sensitivity, although higher than assumed in the LAR, does not influence the risk because none of the SBLOCA scenarios form a thin bed.

References:

1. 66-9088089-000. *South Texas Project Test Report for ECCS Strainer Testing*.
Revision 0: August 29, 2008
2. Steam Generator Tube Integrity and Chemical Engineering Branch.
RAI ESGB-I-5 Revision 0

SSIB, Head Loss and Chemical Effects Bump Up: RAI 15a

The STPNOC submittal states that the strainer debris head loss is calculated using a correlation (References: Volume 3, Section 5.6.2, "Conventional Debris Head Loss Model," Volume 3, Assumption 7.e; Volume 1, Section 1.1, "Structured Information Process Flow.") The NRC staff has generally not accepted correlations for the qualification of PWR strainers for several reasons. Please explain why the following general concerns with the use of correlations are not an issue for the STP application:

- (a) Correlations have not been validated for the full range of debris loads and morphologies present under plant conditions.

STP Response:

Correlations are important for capturing subtle trends and interactions between physical variables including differing combinations of debris loads and morphologies. Strainer qualification tests, likewise, do not test all possible debris loads and morphologies present under plant conditions. However, in combination, correlations help identify combinations of concern, especially across the full spectrum of RI analysis, and strainer tests provide proof of performance for the most challenging conditions identified. Predictions of head loss and confirmatory strainer testing provide complementary and essential elements for full understanding of strainer-related ECCS failure. Other RAI responses address more directly the issue of validation over appropriate ranges of plant conditions.

SSIB, Head Loss and Chemical Effects Bump Up: RAI 15b

Please explain why the following general concerns with the use of correlations are not an issue for the STP application:

- (b) Correlations do not address non-homogeneous debris beds which are very likely to occur due to transport timing and non-homogeneous filtering of debris within the bed.

STP Response:

Lateral inhomogeneity (across the face of a strainer surface) is always presumed to cause less total head loss than a contiguous uniform bed of the same composition. Lateral inhomogeneity is commonly observed in strainer module testing where it can be difficult to form a contiguous bed that leads to maximum observed pressure drop. STP agrees that lateral inhomogeneity is likely to occur and will reduce the actual head loss that occurs compared to the maximum head loss predicted by correlation.

Inhomogeneous composition through the thickness of the bed may exist that elevate the observed head loss. Two examples of potential concern are (1) chemical products arriving in bulk at the top of a pre-established bed, and (2) impaction of finely divided debris in the holes of the strainer plate causing a local reduction in porosity. Both conditions are investigated in the supplementary report (Enclosure 1).

Although no evidence of bulk chemical precipitation potential has been observed for STP, simulations of a thin layer of low porosity, high- S_v debris at the top of the bed show a factor of 2 increase in head loss compared to the same mass of material distributed throughout the bed (Enclosure 1).

Local impaction of fiber in the strainer plate holes was observed in the CHLE-10 UNM test which used fiber preprocessed in a blender. The test started the introduction of chemicals at 6.75 days with a maximum 1400% increase in head loss compared to the 1-day steady state value (LAR Encl. 4-3, Ref. [17]). Calculations show comparable potential head-loss increase when porosity in the strainer plate orifice is greatly reduced. Large quantities of extremely small fiber shards (broken glass strands) are not expected to be produced in the LOCA ZOI environment, and are not included as part of the modified NEI debris-preparation protocol.

SSIB, Head Loss and Chemical Effects Bump Up: RAI 15c

Please explain why the following general concerns with the use of correlations are not an issue for the STP application:

- (c) Correlations have not been validated for the full range of potential flow conditions and strainer geometries that are present in plants.**

STP Response:

STP has only one strainer configuration that is consistent for all 3 trains. The PCI design was confirmed by testing to load uniformly across the face of the strainer surface area, so the potential for geometric variations at STP is greatly minimized.

Maximum flow velocities of 0.0086 ft/s at STP are not within the HTVL test range, but low velocities are represented in the ARL flume tests and in the UNM vertical column tests, which are available for validation of the NUREG/CR-6224 correlation that was implemented for the LAR. The supplementary report accompanying this response (Enclosure 1) provides a means for more robust correlation of flow conditions in terms of Reynolds number that encompasses velocity, water properties, and bed parameters of porosity and surface-to-volume ratio. The proposed correlation illustrates that existing tests used to validate NUREG/CR-6224 expose the bed to a much wider range of flow conditions (two orders of magnitude) than previously thought. The expanded range of conditions supports applicability for RI use of a correlation provided that acceptable comparisons to test data can be achieved.

Reynolds number for internal flow through a debris bed is defined as,

$$Re = \frac{\rho w_A}{\mu(1 - \epsilon_m) S_V}, \quad (1)$$

where ρ is fluid density, μ is fluid viscosity, w_A is strainer approach velocity, ϵ_m is mixture porosity, and S_V is surface-to-volume ratio for the solid debris.

These attributes can be determined independently of any presumed head-loss correlation for any homogeneous mixture of debris.

Distributions of Reynolds number were compiled from CASA Grande analysis conditioned on LOCA category for bed configurations and flow rates existing at the end of each break scenario. When the sludge compaction limit is not enforced, expected values (means) and maxima of Reynolds number for each LOCA category are

Break Size	Small	Medium	Large
Avg. Reynolds #	0.0237	0.0800	0.3105
Max Reynolds #	0.0748	0.2565	1.7480

The cumulative distribution of Reynolds number for large break scenarios is illustrated in Fig. A, which shows a very narrow range of interest. Many combinations of Eq. (1) parameters lead to similar flow regimes as defined by Reynolds number. The supplementary report (Enclosure 1) proposes a robust correlation based on an explicit representation of Reynolds number and demonstrates that typical HTVL testing does in fact span (and likely exceeds) the flow regimes of interest for STP flow conditions. Given the adequate overlap of flow conditions tested, discrepancies between blind predictions of a calibrated model and HTVL test data can be attributed to insufficient bed compression descriptions and to local stratification that affects the spatial distribution of porosity and surface area-to-volume ratio.

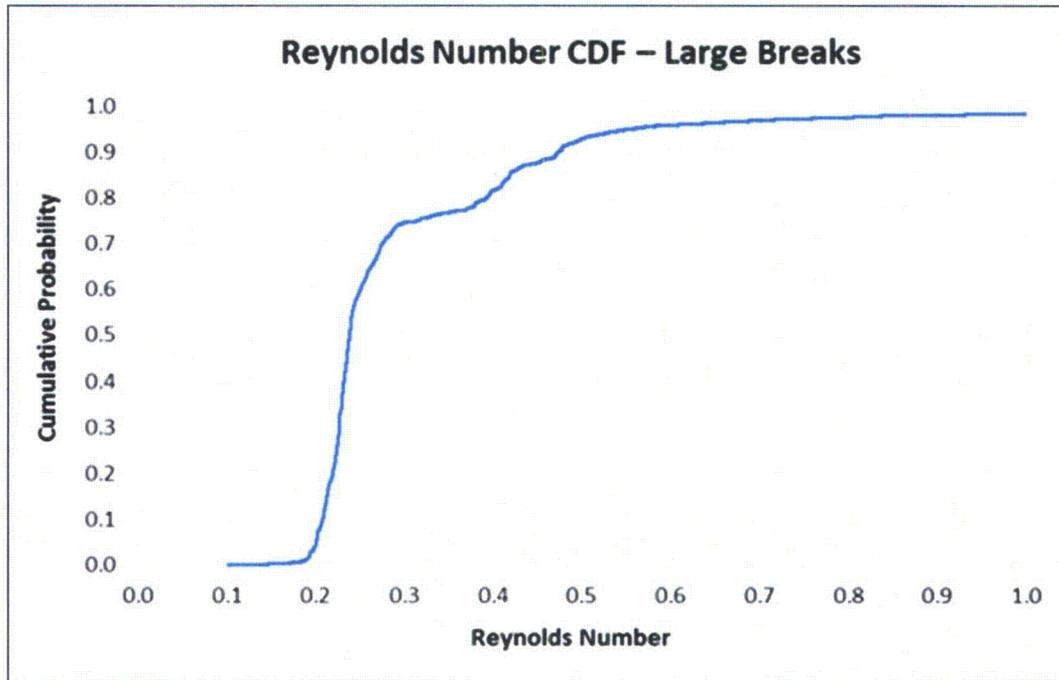


Figure A. Cumulative probability distribution for Reynolds number experienced under large-break scenarios.

In summary, velocity is only one factor that contributes to flow regime in a composite debris bed, but many factors interact as shown in Eq. (1). When all other factors are equal except velocity, conventional interpretations of head-loss correlations indicate that lower velocity leads to lower head loss, less bed compression, and slower migration of particulates. Therefore, since comparable Reynolds flow conditions have been achieved in the tests through a combination of factors, it is reasonable to expect that lower pressure drops would have been observed when testing at lower velocities identically matching plant conditions. Reynolds similitude extends to the plant configuration, so the current suite of test conditions can be considered adequate for validation.

SSIB, Head Loss and Chemical Effects Bump Up: RAI 15d

Please explain why the following general concerns with the use of correlations are not an issue for the STP application:

- (d) There is significant uncertainty in the model parameters used to describe the physical attributes of the debris bed constituents.**

STP Response:

Principal uncertainties exist in the drag area parameter S_v (solid surface-to-volume ratio) and in the bed porosity. Conclusions of the STP LAR are not affected because uncertainty in material properties is compensated by the factor of 5 uncertainty bound and because intended application of a bed compaction limit obviates concerns regarding local porosity.

The supplementary report (Enclosure 1) provided with the SSIB RAI responses uses direct measurement of surface-to-volume ratio to minimize uncertainties in debris properties. For the calibration test, measured values of S_v are approximately 250% less for acrylic paint debris, which is a surrogate for qualified epoxy, than the standard geometric approximation for qualified epoxy in LAR Enclosure 4-3. High-fidelity reproductions of the test data are obtained using measured S_v when bed compression is allowed to equilibrate with pressure drop and no credit is taken for relaxation (thickness recovery) after exposure to high differential pressure. By comparison, application of NUREG/CR-6224 with a factor of 5 uncertainty bound consistently overpredicts all test measurements.

Formulas for mixture porosity are well developed between the physical limits of sludge compaction and theoretical porosity of clean fiber. Uncertainties in bed porosity are therefore largely caused by uncertainties in potential local stratification, which is addressed in the response to SSIB RAI 15b, and by performance of the bed compression model. The STP analysis intended to apply the sludge compaction limit throughout the bed of homogeneously mixed composition to minimize the effect of these uncertainties. (Note: correct implementation of the sludge limit assumption will lead to an increase in ΔCDF . Responses to SSIB RAI 18b and 18c provide further detail.)

SSIB, Head Loss and Chemical Effects Bump Up: RAI 16a

Testing performed to validate the NUREG/CR-6224⁽¹⁾ correlation for specific STP conditions does not appear to accomplish the purpose (References: Volume 3, Section 5.6.2, "Conventional Debris Head Loss Model," and Volume 6.2, Item 5.a.10). Additionally, the NRC staff does not have complete information to conclude that the testing adequately represented the plant configuration and range of conditions that could occur at STP following a LOCA. Therefore, the staff was unable to determine that the plant specific vertical loop tests results were representative of head losses that could occur from a debris bed on a prototypical module. The correlation results and the single vertical loop test result that modeled the July 2008 Alden flume test under STP specific conditions were significantly different from each other, and from the results of the flume test. That is, all three results, although modeling similar conditions, had significantly different results. The submittal explained as to why the results were substantially different, but the explanation was not confirmed by testing or by use of accepted theories. Industry head loss tests using similar surrogates on prototypical strainer modules resulted in significantly higher head losses than those reported by STP for their vertical loop testing and those calculated by use of the correlation. The staff is concerned that vertical loop test and module test results from tests conducted under similar conditions may differ due to the differences between debris characteristics in vertical loop test and module test debris beds. These differences could be caused by differences in transport and deposition of the debris onto the perforated surfaces. Therefore, the staff is concerned that the validation testing is not representative of the plant. Please provide the following additional information:

- (a) If the vertical loop tests conducted by STP are important to the conclusions, please provide details as to why the STP vertical loop tests are valid considering that other module tests conducted in several different facilities under similar conditions, debris loads, and debris characteristics had significantly different results.

STP Response:

Vertical loop tests conducted by STP are important to demonstrate the conclusion that the STP LAR approach for predictive head-loss estimation, which includes an intended sludge compaction limit and a factor of 5 uncertainty bound applied to the NUREG/CR-6224 model, adequately envelopes variability noted by the staff between different facilities under similar conditions. It is noted, however, that important differences do exist between tests that are often described as "similar." For example, while HTVL Series 2 Test 8 emulates a strainer test with respect to debris quantity and flow conditions, debris preparation was substantially different; the HTVL test used NEI prepared debris and the ARL test used blender processed debris.

Vertical loop tests conducted by STP are valid to the extent that they reproduce flow conditions in representative debris configurations so that the aggregate head-loss approach can be demonstrated to bound prototypical conditions. The approach applied

⁽¹⁾ NUREG/CR-6224, "Parametric Study of the Potential for BWR ECCS Strainer Blockage Due to LOCA Generated Debris," Final Report," October 1995 (ADAMS Accession No. ML083290498).

in the STP LAR bounds all total head-loss measurements taken in prototypical test conditions. While it is desirable to have a predictive approach that can reproduce all test conditions with high fidelity, uncertainties in bed configuration and debris characteristics can dominate the comparison of replicate tests and numerical simulations. HTVL tests were designed to represent the most prevalent conditions expected, and successful comparison of the STP LAR calculation method to flume test data, as demonstrated in the response to ESGB, Chemical Effects RAI 2, provides high confidence that underprediction will not skew the risk quantification.

Deterministic perspectives related to the definition of a worst, or most challenging, set of conditions have long dominated assessment of test validity and acceptability. The risk-informed perspective combines that interest in challenging conditions with their frequency of occurrence, so that judgment of test validity can now include a broader interpretation of applicability to plant-specific conditions. The supplementary white paper provided with SSIB RAI responses (Enclosure 1) explains a new perspective on head-loss correlation based on Reynolds number for internal flow.

A distribution of Reynolds number was extracted from the CASA Grande analysis spectrum for all large break histories in a typical statistical replicate. As shown in the response to SSIB RAI 15c and 17c, typical internal Reynolds numbers for a LBLOCA vary between 0.1 and 1 when the sludge compaction limit is not enforced. STP vertical column tests were used to calibrate the new model over an adequate range of Reynolds number spanning from 0.2 to 4.5. The new correlation shows that existing vertical head-loss tests broadly represent the range needed for predictions in the RI application.

The supplementary report further demonstrates that the alternative head-loss correlation is consistent with test data and produces predicted head-loss values well below those produced by the NUREG/CR-6224 correlation as implemented in the LAR. Recall that the sludge limit for bed compaction is intended as a constraint on minimum bed porosity and that a factor of 5 is applied to cover uncertainties in bed properties, correlation fidelity, and testing variability between facilities.

SSIB, Head Loss and Chemical Effects Bump Up: RAI 16b

- (b) If the vertical loop tests conducted by STP are important to the conclusions, please provide evidence that vertical loop tests conducted under site specific conditions will correlate to flume tests conducted under similar conditions or to head losses that would occur in the plant. Please include information regarding how it was determined that the debris that transported to the horizontal strainer surface resulted in a debris bed of similar characteristics and morphology to that which would transport to the plant strainer. Please state how was it determined that the head losses would be comparable.**

STP Response:

Vertical loop tests are important to conclusions in the STP LAR only to the extent that they corroborate the conclusion that head-loss predictions made for uniform contiguous beds should bound actual strainer performance for similar total debris loads and flow conditions. Vertical test results alone are not intended as exclusive protection of this assumption. The factor of 5 uncertainty applied to the NUREG/CR-6224 head-loss predictions also helps to ensure this assumption. See the responses to SSIB RAI 16a and SSIB RAI 28 for additional discussion of this strategy.

Vertical loop tests conducted under site-specific conditions should correlate to flume tests conducted under similar conditions and to head losses that occur in the plant to the extent that more debris and/or higher velocity, and/or reduced porosity all produce higher head loss in all test configurations. However, HTVL Test 8, an intended replicate of the ARL flume test, resulted in a much lower head loss at a comparable temperature and a flow rate approximately 2.5 times higher than the flume test. Many disparities in the test conditions including debris preparation contributed to this discrepancy.

In this application, correlation does not imply a need for perfect agreement between model and tests. Conclusions in the application are constructed around limiting assumptions that compensate for known deficiencies in the NUREG/CR-6224 head-loss prediction, one of the most notable deficiencies being the bed compression response for mixed debris composition.

Debris transported by assumption to the horizontal strainer surface would result in a debris bed composed of fine and small fiber sizes loaded with 100% of particulate reaching the pool. All materials are assumed to be fully transportable with the ambient flow velocity, which offers further consistency with actual plant transport of small and fine material. The assumption of maximum compression should result in head-loss trends that are higher than measured in the vertical loop. Vertical head-loss tests in combination with assumptions implemented with the resulting correlation provide confidence that head-loss trends are reasonably (but not unduly) conservative with respect to actual plant strainer performance.

Head loss observed in vertical testing and in strainer testing is driven by flow conditions within the debris bed and not by the actual constituents of the debris. This similitude is the basis for substitution of particulates having similar size distributions. Therefore, head losses will be comparable for similar flow conditions defined by: velocity, fluid properties, porosity and drag area (S_v). The supplementary report (Enclosure 1) accompanying

these SSIB RAI responses further emphasizes the importance of robust correlation based on internal flow conditions. Responses to SSIB RAIs 15c, 17c, and 16a discuss ranges of Reynolds number covered by testing and by the spectrum of breaks covered in CASA Grande. Bed morphology in the form of alternate discrete stratification is addressed in the response to the SSIB RAI15b. In total, these comparisons demonstrate that the LAR approach to head-loss prediction will reproduce the proper behavior with respect to flow rate, debris load and temperature, while overestimating actual strainer performance under similar conditions.

SSIB, Head Loss and Chemical Effects Bump Up: RAI 16c

- (c) Please provide information that demonstrates that the correlation used by STP is valid for plant specific strainer geometries and plant specific conditions. Alternately, please provide a basis for using a correlation that has not been validated specifically for STP plant conditions and geometries.**

STP Response:

The purpose of using a predictive correlation in the STP LAR is to reproduce observed trends in head loss as a function of debris composition and flow conditions so that credible sensitivity studies can be performed to determine driving factors and subtle interactions that have not been anticipated prior to the RI closure pilot study. Implementation of the correlation, including sludge-limit compaction and a factor of 5 uncertainty bound, is designed to provide confidence that predictions bound realistic strainer performance for the majority of debris combinations and flow conditions that are experienced in the plant. None of these goals require exact agreement between test conditions and correlation. In fact, the correlation utilized in the vertical head-loss test report did not include the same head-loss assumptions used in the final implementation.

For example, the response to ESGB, Chemical Effects, RAI 2 cites comparisons of maximum head-loss values observed in flume testing placed in context as percentiles of all head-loss predictions obtained from the Case 01 (all equipment operates) CASA Grande analyses (which include the factor of 5 uncertainty, but not the full effect of sludge-limit compaction). Measured maxima lie within the envelope of computed maxima (even without the full effect of sludge-limit compaction), and predicted maxima lie well above the strainer-collapse threshold of 9.35 ft. None of the ARL flume tests measured head loss exceeding the strainer buckling limit. These comparisons provide assurance that the correlation as implemented serves its dual role of tracking the interaction of complex debris behavior and providing reasonably conservative bounds on actual strainer performance.

SSIB, Head Loss and Chemical Effects Bump Up: RAI 16d

- (d) Please discuss how the NUREG/CR-6224 correlation could be used to predict the head losses that would be expected under conditions similar to those in the two flume tests conducted by STP in February and July 2008.**

STP Response:

As implemented in the LAR with a code level error that reverted all cases to mixed-bed porosity without compression (described in the responses to SSIB-RAI 18b and 18c), and a factor of 5 uncertainty bound, the NUREG/CR-6224 correlation predictions bound the measured maximum head losses reported for the February (1) and July (2) 2008 tests. The one exception is February Test 3 that was determined to be non-representative. Response to ESGB, Chemical Effects, RAI 2 cites comparisons of maximum head-loss values observed in flume testing placed in context as percentiles of all head-loss predictions obtained from Case 01 (all equipment operates) CASA Grande analyses (which include the factor of 5 uncertainty, but not the full effect of sludge-limit compaction). DBA tests are well above the 95th percentile of all simulated breaks and yet well below predicted maxima that include chemical effects.

One criticism of the STP flume tests has been possible underestimation of fiber debris volume, and one possible deficiency of the predictive model is improper sludge compaction. Distributions of predicted head-loss include debris volumes consistent with 17D ZOI that are assumed for Nukon fiberglass, and at least one test included fiber volumes that are comparable to this inventory (February Test 4). Increased predicted head loss will be experienced when the sludge-compaction limit is properly implemented (possibly by a factor of 2), so predicted maxima will increase even as measured head loss would increase if fiber debris volumes were increased for strainer testing. Given the high percentiles of DBA testing with respect to the simulations, it is unlikely that more stringent test conditions would change the conclusion that current application of the NUREG/CR-6224 correlation provides an acceptable envelope for potential head loss across the ECCS strainer.

References:

1. 0415-0100069WN / 0415-0200069WN, "South Texas Project Test Report for ECCS Strainer Performance Testing Feb 2008", Revision A, 11/24/2008.
2. 0415-0100071WN / 0415-0200071WN, "South Texas Project Test Report for ECCS Strainer Performance Testing July 2008", Revision A, 11/24/2008.

SSIB, Head Loss and Chemical Effects Bump Up: RAI 17a

The submittal states that all testing performed to validate the NUREG/CR-6224 correlation was bounded by correlation predictions (References: Volume 1, Section 1.2.7, "Conventional Head Loss Model," and Volume 3, Section 5.6.2, "Conventional Debris Head Loss Model"). There have been numerous cases where the correlation severely under-predicted head losses that were carried out under carefully controlled conditions. NUREG-1862, "Development of Pressure Drop Calculation Method for Debris-Covered Sump Screens in Support of Generic Safety Issue 191," February 2007 (ADAMS Accession No. ML071520440), and NUREG/CR-6917, "Experimental Measurement of Pressure Drop Across Sump Screen Debris Beds in Support of Generic Safety Issue 191," February 2007 (ADAMS Accession No. ML071910180), contain data that show that the NUREG/CR-6224 correlation is not conservative in all cases. These NUREGs determined that correlation predictions are highly dependent on the parameters used to describe the physical attributes of the debris bed constituents and that these parameters have significant uncertainty. These NUREGs also determined that head losses are not well predicted by a correlation that assumes a homogenous debris bed. Some of the experimental data involved fine debris, microporous debris, non-homogeneous beds, and other conditions that the NUREG/CR-6224 correlation is not designed to account for. It is very likely that some conditions that NUREG/CR-6224 correlation does not account for, may be present under plant post-LOCA conditions. The submittal states that the head loss correlation from NUREG/CR-6224 has been extensively validated for various conditions. The NRC staff is of the opinion that there is little or no testing that has been conducted under conditions similar to those at STP. The staff is concerned with the validation issues listed below when using a correlation for qualification of strainers. Please state how the STP evaluation accounts for these uncertainties and lack of validation of the correlation under plant conditions.

(a) Debris constituents in validation testing are not plant-specific

STP Response:

The LAR is not attempting to apply the correlation alone to qualify performance of a particular strainer, but rather, is using the correlation to reveal trends in strainer performance that may challenge risk informed success criteria. The correlation alone is only one part of the application. The assumption of full bed compression and uncertainty factor of 5 must also be considered part of the head-loss prediction that compensates in part for some of the staff-noted complications with NUREG/CR-6224.

As noted in this RAI, the NUREG/CR-6224 correlation has not performed well for microporous debris. However, STP has a sparse amount of microporous debris that does not dominate the head loss behavior or the risk. The absence of microporous debris in validation testing is consistent with plant-specific conditions.

HTVL test series 2 (LAR Enclosure 4-3, Reference [24]) attempted to replicate ARL flume testing of STP strainers (1) using plant-specific debris combinations of fiberglass, tin, acrylic powder and chips, Microtherm, Marinade Board, and latent dirt/dust. At STP, fiberglass and unqualified epoxy coatings that are presumed to fail represent the dominant conventional debris types.

Other tests in the HTVL test series (LAR Enclosure 4-3, Reference [24]) employed a long-standing practice of using substitute particulates. For example, acrylic paint powder was used as a substitute for failed epoxy coatings and silicon carbide was used to represent latent debris.

Substitution of particulates should be acceptable as long as flow conditions internal to the bed can be established that are plant specific. An alternate head-loss model based on correlation of flow resistance to Reynolds number (Enclosure 1) was calibrated using existing HTVL test data. Comparison of Reynolds flow regimes achieved in the tests (0.2 to 4.5) to flow regimes extracted from the population of CASA Grande bed configurations shows very good agreement. Additional detail of this flow-regime comparison is provided in the responses to SSIB RAI 15c and 17c.

References:

1. 0415-0100071WN / 0415-0200071WN, South Texas Project Test Report for ECCS Strainer Testing July 2008, Rev A, 11/24/2008.

SSIB, Head Loss and Chemical Effects Bump Up: RAI 17b

Please state how the STP evaluation accounts for these uncertainties and lack of validation of the correlation under plant conditions.

(b) Debris sizes in validation testing are not plant-specific.

STP Response:

The UNM vertical loop testing is considered to be part of the NUREG/CR-6224 validation effort which included a wide range of debris sizes including blender-processed fiberglass. HTVL testing conducted at Alion Hydraulics Laboratory used a modified NEI debris preparation. Therefore, prototypical debris sizes are considered to be well represented.

As mentioned in the response to SSIB RAI15c examination of Reynolds flow conditions shows that regimes of interest identified in the CASA Grande analysis spectrum are well represented by existing test data.

SSIB, Head Loss and Chemical Effects Bump Up: RAI 17c

Please state how the STP evaluation accounts for these uncertainties and lack of validation of the correlation under plant conditions.

(c) Very little validation testing was conducted at STP velocities and none validated the correlation.

STP Response:

See the response to SSIB RAI 15c.

SSIB, Head Loss and Chemical Effects Bump Up: RAI 17d

Please state how the STP evaluation accounts for these uncertainties and lack of validation of the correlation under plant conditions.

(d) Validation testing did not include prototypical strainer geometries.

STP Response:

For the purpose of the risk-informed LAR, validation testing includes: (1) strainer testing, (2) HTVL testing, and (3) UNM vertical column testing. Strainer testing did include prototypical STP geometry, and one series of HTVL tests was patterned after the flume test conditions, debris types and debris loading (LAR Enclosure 4-3, Reference [24]).

SSIB, Head Loss and Chemical Effects Bump Up: RAI 17e

Please state how the STP evaluation accounts for these uncertainties and lack of validation of the correlation under plant conditions.

(e) Validation testing performed in vertical loops does not simulate potentially important aspects of debris bed formation under plant conditions

STP Response:

For the purpose of the risk-informed LAR, validation testing includes: (1) strainer testing, (2) HTVL testing, and (3) UNM vertical column testing. Strainer testing did include prototypical geometries used at STP. While true that vertical loop testing does not include all geometric effects, consistently uniform debris beds are difficult to form even under controlled test conditions. Occlusions and bridging often observed in strainer tests tend to admit more flow per unit area and reduce head loss. This is an important reason for conducting correlation testing under vertical loop conditions.

Current strainer test procedures emphasize 100% debris loading, so all debris sizes present in NEI-prepared test material is equally represented in both the strainer and vertical column test configurations. Small fiber material consistent with NEI debris preparation methods is similarly transportable as the fines.

In general, uniform beds constructed in vertical column configurations provide a more consistent basis for validation and more conservative results when all bed parameters are equal, so more validation analysis has been devoted to these test conditions.

SSIB, Head Loss and Chemical Effects Bump Up: RAI 17f

Please state how the STP evaluation accounts for these uncertainties and lack of validation of the correlation under plant conditions.

- (f) The records of early validation testing are not available or do not contain the information required to determine whether the tests were conducted to adequately represent plant conditions. Therefore, conclusions from early testing must be limited.**

STP Response:

Consistent with this observation, confirmatory analysis is primarily focused on recent data since 2010 with sufficient documentation to demonstrate applicability to plant conditions. The supplementary report accompanying this RAI response (Enclosure 1) presents an alternative head-loss correlation to provide perspective on the use of NUREG/CR-6224 as implemented in the LAR. The new model has been calibrated and verified using recent test data.

SSIB, Head Loss and Chemical Effects Bump Up: RAI 18a

The implementation of the correlation in the STP model makes specific assumptions and may potentially contain modeling errors that can significantly affect the results of the calculation (References: Volume 3, Assumptions 7.b, 7.e, and 7.f; Volume 3, Section 5.6.2, “Conventional Debris Head Loss Model”; Volume 6.2, Item 5.a.10; and Enclosure 6, Table 1). Please provide the following information to justify that the assumptions and use of the correlation is realistic or conservative for STP plant-specific conditions.

(a) Please provide justification that the beds are homogeneous representative of the plant (Volume 3, Assumption 7.e and Volume 6.2, Item 5.a.10).

STP Response:

The response to SSIB RAI 11c provides justification of a well-mixed containment pool and states, “1. For all breaks, the initial high floor velocities from sheeting flow caused by the pipe break and containment sprays are expected to scatter debris with no preferential direction throughout containment. 2. Fine debris will be further mixed after recirculation because of multidirectional velocity vectors and turbulent kinetic energy.” A homogeneously mixed containment pool supports formation of a homogenous debris bed. Also, the assumption of early and nearly simultaneous debris source introduction further supports formation of a homogenous debris bed.

Once debris arrives at the strainer, migration processes tend to homogenize any strata that might initially be formed by sequential arrival. Particulate migration is clearly evident in all test configurations as visible clouds of particulate or chemicals that pass through the debris. When visibility in a vertical column test improves through continued filtration, it is sometimes possible to observe particulate migration through the edges of the debris mat.

SSIB, Head Loss and Chemical Effects Bump Up: RAI 18b

(b) It is assumed that fiberglass debris would accumulate uniformly with a density of 2.4 pounds per cubic foot (lb/ft³). The NRC staff is of the opinion that assuming the debris bed density to be the same as the manufactured density may not be an accurate assumption and is based on the observation of debris beds formed in industry tests and NUREG-1862 testing. The NRC staff is further of the opinion that in the plant, only fine and small fiber will transport and collect at a much higher density. Please describe why the density assumption is valid and why it does not significantly affect the results. Alternately, re-perform the analysis with a density that has been shown to be appropriate. (Volume 3, Assumption 7.f and Section 5.6.2 and Volume 6.2, Item 5.a.10).

STP Response:

To clarify the implementation of manufactured density, the velocity and compression models must be explained in further detail. The time-dependent velocity used to evaluate the head-loss correlation was determined by dividing the volumetric flow rate by the surface area of an uncompressed bed with an assumed density of 2.4 lb/ft³. This assumption causes an earlier transition to the circumscribed area for large breaks having enough debris to fill interstitial strainer gaps that are most likely to challenge plant performance criteria. Transition to circumscribed area can cause a sudden increase in face velocity and a corresponding increase in head loss.

The intended treatment of bed compression was to evaluate all cases with a minimum porosity and minimum bed thickness defined by a maximum packing density of 65 lb/ft³. This approach is independent from the assumption used to calculate face velocity. The current quantification does not include effects of the intended compression limit. As suggested, a sensitivity test was performed using the sludge limit as a plausible compression condition that resulted in a ΔCDF increase by a factor of 1.8.

The bed compression calculation is being revised as shown below:

For very large pressure gradients, the compression has to be limited such that a maximum solidity is not exceeded. In NUREG/CR-6224, this maximum solidity is defined to be:

$$\alpha_m = \frac{65 \text{ lb}_m / \text{ft}^3}{\rho_p}$$

Equation 38a

This is equivalent to having a debris layer with a density of 65 lbm/ft³. Note that 65 lbm/ft³ is the macroscopic, or bulk density of a granular media such as sand or gravel and clay.

For mixed fiber and particulate beds, the sludge packing density is considered to be conservatively high and the analogous solidity limit is:

$$\alpha_m = \frac{V_f + V_p}{V_{bed}} = \left(\frac{m_f}{\rho_f} + \frac{m_p}{\rho_p} \right) \frac{65 \text{ lb}_m / \text{ft}^3}{m_f + m_p}$$

Equation 38b

where:

V_x = solid fiber volume (f), solid particulate volume (p), total bed volume (bed),

m_x = fiber mass (f), particulate mass (p),

ρ_x = average fiber density (f) or average particulate density (p).

To avoid iterative solutions implied by the fiber compression formulas that both affect and depend on the head loss, the high particle-to-fiber ratio limit for mixed bed solidity was applied to all head-loss calculations. The corresponding limiting bed thickness is found by substituting Eq. (36) into Eq. (35) and solving for bed thickness ΔL_m using Eq. (38b) as the limiting mixed-bed solidity;

$$\Delta L_m = \frac{1}{\alpha_m} \left(1 + \frac{\rho_f}{\rho_p} \eta \right) \alpha_0 \Delta L_0. \quad \text{Equation 38c}$$

SSIB, Head Loss and Chemical Effects Bump Up: RAI 18c

- (c) Please explain how the NUREG/CR-6224 correlation compression function is applied in the STP model. NUREG-1862 found that the compression relation from NUREG/CR-6224 does not accurately model the compression of the bed, especially at low flow velocities like those at STP. (Volume 3, Section 5.6.2).**

STP Response:

Present quantification of the STP LAR intended to impose sludge-limit packing density for all cases to avoid iterative requirements of the NUREG/CR-6224 compression model. However, a code-level logic error reverted all cases to mixed-bed porosity without compression. Implementation of the sludge limit as intended increases ΔCDF by a factor of 1.8 with all other inputs equivalent to the baseline. The response provided to RAI SSIB-RAI-18b describes how the sludge limit is calculated and applied.

The condition has been entered in the STP corrective action program and the Alion corrective action program.

SSIB, Head Loss and Chemical Effects Bump Up: RAI 18d

- (d) The submittal states that STP implemented a linear mass weighted average instead of the volumetric weighted average for implementation of composite surface to volume ratio (S_v) in the 6224 correlation. The submittal states that there are many possible composite weighting methods that could be used, but does not justify the method chosen in the application. NEI 04-07 and NUREG/CR-6371, "Blockage 2.5 Reference Manual," December 1996 (not publicly available), both recommended the volume weighting method. Please explain why mass weighting is acceptable. Please explain if both the methods result in significantly different results. (Volume 3, Section 5.6.2 and Enclosure 6).

STP Response:

The supplementary report prepared to accompany head-loss RAI responses (Enclosure 1) illustrates that linear volume weighting is the proper general treatment for composite averaging of surface-to-volume ratio. Mass and volume weighting give identical results in the ideal case where all debris densities are identical. Comparison calculations between the two methods show no significant increase in ΔCDF when linear volume weighting is applied with STP-specific inputs.

SSIB, Head Loss and Chemical Effects Bump Up: RAI 18e

- (e) Please provide a technical basis for Assumption 7.b regarding coating material packing fractions. Please discuss the effect of the assumption on results. Please provide the potential ranges of packing factors for coating materials. (Volume 3, Assumption 7.b and Volume 6.2, Item 5.a.10).**

STP Response:

Packing fraction is driven by the geometry of particles. The assumption that all coating materials have a similar packing fraction to acrylic coatings (0.39 as described in STP LAR Enclosure 4-3, Reference 24) is reasonable because the constituents are comparable in size, approximately 10 microns. Non-coating particulate debris was assumed to have a packing fraction similar to iron oxide sludge (0.20). NUREG/CR-6224 cites the packed density of iron oxide sludge as 65 lb/ft³. Per Mark's Engineering Handbook (1), a wet mixture of clay and soil also has a density of 65 lb/ft³.

Packing ratios for coatings materials are not used directly in the head-loss calculation, so there is no measurable effect of this assumption on results.

Limited information is available for packing ratios of pure coatings materials, which is why degraded coatings were assumed to have properties similar to acrylic coatings that are described in STP LAR Enclosure 4-3, Reference 24.

Reference:

1. Avallone, E. and Theodore, B. "Marks' Standard Handbook for Mechanical Engineers." McGraw-Hill Companies, Inc, 1999.

SSIB, Head Loss and Chemical Effects Bump Up: RAI 19

The application of a multiplier of five (5x) to the result of the head loss correlation used in the STP model appears to indicate uncertainty in the ability of the correlation to predict head losses correctly (References: Volume 1, Section 1.2.7 and Volume 3, Section 5.6.2). If the NUREG/CR-6224 correlation is a robust model as implied in the submittal, the NRC staff is of the opinion that it is unnecessary to use safety factors in the head loss calculations for achieving realistic results. The staff noted that some PNNL testing showed that the 6224 correlation under predicted head loss by more than a factor of 5X. Please provide justification for applying the multiplier to the results of the head loss correlation.

STP Response:

The staff has noted numerous sensitivities of the NUREG/CR-6224 head-loss correlation to material properties and debris configurations within the porous bed. Residual uncertainty also exists in data available to describe properties and bed configurations. Sensitivities and uncertainties may exist regardless of the fidelity of the predictive model, so it is appropriate to acknowledge the possibility of higher head-loss than indicated by the existing model. The factor of 5 (with a standard deviation of 1) is applied to represent propagation of uncertainty and modeling sensitivities. STP does not view this simply as a safety factor, but rather as a surrogate envelope on variability not fully resolved by the model.

STP application of the NUREG/CR-6224 correlation includes the assumption of sludge-limit compaction and the factor of 5 uncertainty envelope. While isolated conditions may exist that cause NUREG/CR-6224 alone to underestimate head loss by more than a factor of 5, it is not clear that those observations include the assumption of sludge compaction, nor the use of representative debris material. An alternative correlation based on Reynolds number in the viscous to inertial shear transition (VISTA) developed in a supplementary report (Enclosure 1) illustrates that the LAR assumptions are conservative for the predominant flow conditions of interest.

The strategy used to assure adequacy of STP LAR head-loss predictions includes three parts:

- 1) Supplementary report (Enclosure 1) demonstrates test results can be reproduced with good fidelity using an independent physical model that addresses known deficiencies of the NUREG/CR-6224 correlation,
- 2) Supplementary report (Enclosure 1) demonstrates available test conditions span flow regimes of interest for STP and that realistic models reproduce the most prevalent conditions with the highest accuracy,
- 3) Response to ESGB, Chemical Effects, RAI 2 demonstrates the LAR application reasonably bounds available test data.

SSIB, Head Loss and Chemical Effects Bump Up: RAI 20

The submittal assumes that paint chips or other relatively large debris that may reach the strainer can be accounted for in the correlation as spherical particles (Reference: Volume 3, Section 5.6.2). Large debris may fully or partially block strainer perforations and may deposit non-homogeneously on the strainer. Please provide an experimental basis to confirm that paint chips (or other large particles) may be accurately modeled in the correlation, including the assumption that they can be accurately modeled as spherical particles. In the absence of an experimental justification, please provide an alternate basis for the STP treatment of paint chips and other large particles in the head loss correlation.

STP Response:

Large miscellaneous debris (tags, labels, ties) is treated by standard methods as a direct reduction in strainer area.

In the LAR, paint chips are categorized by standard sizes and inventories for each size are determined by external analysis of bounding break conditions. Large chips and curls typical of failed unqualified coatings are not present during fill-up transport and have very low transport fractions under STP recirculation conditions, so they are not expected to obstruct flow through individual strainer openings.

When large particles (greater than 10 um largest dimension) are present in a composite debris bed, they affect fluid flow through their total drag area just like any other debris element. Although beds composed entirely of flakes and chips oriented perpendicular to the flow may have a unique behavior, there is no reason to suspect that randomly oriented chips and flakes cannot be modeled by standard correlations. In fact, because average surface-to-volume ratios for larger debris elements are small compared to very small particulates, the contribution of large particles and chips is often ignored in test configurations.

There is no intent in LAR Enclosure 4-3, Section 5.6.2 to treat chips and flakes as spherical particles. When the original quantification was performed, CASA Grande only included geometric surface-to-volume ratio formulas for spheres (particulate where $S_v^{sph} = 6/d$ for particle diameter d) and for cylinders (fibers where $S_v^{cyl} = 4/d$ for fiber diameter d). In the material properties table, artificial "spherical" diameters were introduced for paint chips to ensure that the desired surface-to-volume ratio for chips ($S_v^{chip} = 2/t$ for thickness t) were preserved. Equivalent spherical diameter is computed as $d = 2t$. This is an unnecessary complication originally introduced for expediency, but it does not change the fundamental treatment of paint chips in the head-loss evaluation.

SSIB, Head Loss and Chemical Effects Bump Up: RAI 21a

The STP correlation uses physical properties of materials predicted to be in the debris bed in order to calculate a head loss (References: Volume 3, Section 5.6.2, "Conventional Debris Head Loss Model," and Volume 6.2, Item 5.a.10). Results from the NUREG/CR-6224 correlation are heavily dependent upon the accurate representation of material physical properties. One of the most difficult parameters to accurately determine is the surface to volume ratio (S_v). Please provide the following information:

(a) Please state how S_v values were determined for each material.

STP Response:

As stated in Section 5.6.2 of LAR Enclosure 4-3, S_v values for each material were calculated by

Cylindrically-shaped debris: $S_v = 4/\text{diam}$

Spherically-shaped debris: $S_v = 6/\text{diam}$

Flakes (flat-plates): $S_v = 2/\text{thick}$

where diam is the diameter of the fiber or spherical particle and thick is the thickness of the flake/chip. The geometry, dimensions, and calculated S_v values are presented in Tables 5.6.1 and 5.6.2 of LAR Enclosure 4-3. The basis of these tables is described in the response to SSIB RAI 24.

Note that S_v values for chip debris were calculated in CASA Grande with the spherical formula using substitute diameters that produce values equivalent to the flake thickness formula (mentioned in the footnotes on Page 179 of LAR Enclosure 4-3).

SSIB, Head Loss and Chemical Effects Bump Up: RAI 21b

- (b) It is known that for some debris types, and possibly all debris types expected to be present in PWR debris beds, physical measurements cannot provide S_v values that allow accurate prediction of head loss in existing correlations. This was especially evident for microporous type materials and was shown to be true for other materials by NUREG-1862. Please explain the bases for the S_v values and other material properties used in the STP implementation of the correlation.**

STP Response:

The S_v values for individual materials were determined using characteristic diameters in standard geometric formulas as shown in the response to SSIB RAI 21a. The basis for the diameters used is displayed in the response to SSIB RAI 24. Bases for material densities (microscopic) are provided in references to LAR Enclosure 4-3 Table 2.2.21.

STP does not agree that physical measurements of material properties preclude accurate prediction of head loss. In general, independent measurements of properties and free parameters are essential to validate the theoretical basis of any predictive model. The supplemental report (Enclosure 1) illustrates how measured values can be used to calibrate an alternative head-loss model that reproduces differential pressure histories with good fidelity.

SSIB, Head Loss and Chemical Effects Bump Up: RAI 21c

- (c) Please state how the uncertainty, described on page 184 of Volume 3, is caused by the relationship between experimentally deduced S_v values and head loss, accounted for in the STP model.**

STP Response:

Uncertainty caused by the relationship between experimentally deduced S_v and head loss estimates is discussed in LAR Enclosure 4-3 as a cautionary note against indiscriminant application of debris properties measured in this manner. When a theoretical formulation is used to extract bed properties, the specific numeric values obtained are tied to the accuracy of the formula itself. An inherent part of physics models is that any inaccuracies in the explicit factors (or form) of a model are relegated to the values of free (or unknown) parameters in the model. It is better to determine material properties and other parameters independently if possible.

The example explained in LAR Enclosure 3 with respect to iron oxide S_v is a good example of confirmation by comparison. Surface-to-volume ratio was used like a free parameter to first achieve good agreement with the pressure drop measurements. The corresponding spherical particle size was then compared to descriptions of the bulk particulate to confirm that the nominal particle size was similar. All debris S_v used in the LAR are based on geometric approximations rather than on experimentally determined values. Thus, this form of propagated uncertainty is not a concern for the analysis. Inaccuracy in the geometric approximation is covered by the factor of 5 uncertainty bound as discussed in the response to SSIB RAI 19.

SSIB, Head Loss and Chemical Effects Bump Up: RAI 21d

- (d) The NRC staff does not agree with the statement, on page 185 of Volume 3, which states that the lack of agreement between the correlation and test results using green silicon carbide and tin do not affect the STP calculations. It appears that STP had difficulty determining parameters to input to the correlation to attain accurate results. Please provide basis for the conclusion that the lack of agreement between the correlation results and test results do not affect STP head loss calculations.**

STP Response:

One of the difficulties encountered in vertical head loss testing with NEI prepared fiberglass is achieving complete filtration of particulate that is introduced. The ratio of particulate to fiber resident in the bed affects calculation of the composite porosity. It is generally conservative to assume complete filtration so that the influence of debris on head loss is maximized. Assumption of complete filtration partially explains why measured head losses were overestimated by calculation. Although STP does not have the surrogate materials of silicon carbide and tin present in the debris inventory, if they were present, use of the correlation in its present form would lead to conservative estimates of head loss impact. Similar overestimation would be obtained for any particulates having similar material properties and being resident in similar quantities. In this sense, lack of precise agreement between test and calculation does not affect the conclusions of the risk quantification.

The supplementary white paper accompanying these RAI responses (Enclosure 1) provides visual SEM comparisons of prototypical debris types that were tested. Direct measurements of specific surface area for silicon carbide, acrylic coating, and fiberglass are used to demonstrate agreement of an alternate head-loss correlation with Tests 4 and 6 that were described as challenging in Reference 24 of LAR Encl. 4-3. Head-loss predicted by conventional implementation of 6224 consistently overestimated values measured for Tests 1 – 4 that contained low-density fiberglass and silicon carbide. Good predictive agreement with test data using an independent model provides confidence that the STP LAR application of NUREG/CR-6224 (including 5 times uncertainty factor and full bed compression) does not underpredict flow conditions of interest.

SSIB, Head Loss and Chemical Effects Bump Up: RAI 22

The NUREG/CR-6224 correlation, and other similar correlations, use specific surface areas (S_v) for cylindrical objects assuming that the fiber is oriented perpendicular to the flow and that the fibers have a uniform diameter. This assumption is used in the STP model (Reference: Volume 1, Section 1.2.7, "Conventional Head Loss Model," and Volume 3, Section 5.6.2, "Conventional Debris Head Loss Model"). NUREG-1862 calculated different specific surface areas for varying diameters of Nukon and noted a difference in S_v between fibers that had binder and those that did not. The NUREG also estimated the S_v of Nukon fiber to be around 250,000 to 300,000 ft^{-1} instead of 180,000 ft^{-1} when corrected for test data. (STP uses for the S_v of 571,429 m^{-1} (174,172 ft^{-1}) for Nukon fiber.) Please explain how the STP evaluation takes these findings into account. (Volume 3, Section 5.6.2).

STP Response:

STP does not agree that observations cited in this RAI are generally applicable to all correlations similar to NUREG/CR-6224. Independent confirmation of the surface-to-volume ratio for fiberglass suggests that no compensation is needed. Uncertainties in particulate properties that have not been confirmed are addressed by the factor of 5 uncertainty bound applied to all predictions of the model.

As explained in the white paper accompanying this response (Enclosure 1), the derivation of the Ergun equation and the NUREG/CR-6224 variant is based on a hydraulic scaling argument that depends on the total local drag area and not on the orientation of the debris elements. For example, the cylindrical surface-to-volume ratio is approximated as $S_v^{cyl} = (\pi dh) / (\pi d^2 h / 4) = 4/d$ for cylindrical diameter d and length h , where the very small face area of the cylinder ends is ignored. The possible interpretation of cylindrical surface-to-volume ratio as a ratio of perpendicular perimeter to perpendicular area is incomplete.

As a manufactured product, fiberglass does have a relatively uniform diameter compared to irregular particulate distributions. Direct measurement of specific surface area for clean fiberglass in combination with an assumed material density of 2.8 g/cm^3 (175 lb_m/ft^3) gives a surface-to-volume ratio of 594,282 m^{-1} , which is 4% higher than the standard assumption of 571,429 m^{-1} obtained by geometric approximation for a 7- μm cylinder. The slightly higher measured value can be attributed to the presence of binder as noted in the RAI statement. Independent confirmation of an important material property for one of the dominant debris types lends confidence to use of the geometric approximation for fiberglass in all applications of NUREG/CR-6224 found in the LAR.

As discussed in the response to SSIB RAI 21c, adjustments to free parameters based on agreement of a model with data inherently depend on the accuracy and form of the model itself. After long use, certain conventions become embedded in the quantification of important properties; for example, the factorization of $(1/2)\rho v^2$ in particulate drag coefficients. However, it is preferable to have independent measurements of key parameters that do not depend on the inherent accuracy of the theoretical model. The white paper supplement to this response (Enclosure 1) provides an example of model calibration using independently measured material properties.

SSIB, Head Loss and Chemical Effects Bump Up: RAI 23

The STPNOC submittal makes the assumption that Microtherm fibers will have properties similar to those of Nukon (bulk density = 2.4 lb/ft³, microscopic density = 165 lb/ft³ and $S_v = 666,667 \text{ m}^{-1}$) (Reference: Volume 3, Section 5.6.2). Please state the basis for this assumption. Also, please justify the use of the Nukon fiber bulk density as the debris bed density.

STP Response:

Material properties of Microtherm were primarily taken from LAR Enclosure 4-3, Reference [43, Attachment E]. The reference states that Microtherm fibers are glass filaments that are 6 microns ($6 \times 10^{-6} \text{ m}$) in diameter and have a specific gravity of 2.65.

Using the average surface to volume ratio equation ($S_v = 4/\text{diam}$), the surface-to-volume ratio was calculated to be $666,667 \text{ m}^{-1}$.

Using the density of water as 62.43 lb/ft³ and the equation $SG_{\text{microtherm}} = \text{Density}_{\text{Microtherm}} / \text{Density}_{\text{water}}$, the microscopic density of Microtherm was calculated to be 165 lb/ft³.

Microtherm was split up into its constituents (fiber, SiO₂ and TiO₂) to simplify characterization. LAR Enclosure 4-3 assumed that Microtherm fiber's bulk density is the same as low density fiber glass (LDFG) bulk density. 2.4 lb/ft³, the bulk density for LDFG, is a reasonable value for the bulk density of Microtherm fiber because Microtherm fiber has the same shape and a similar microscopic density and fiber diameter as LDFG.

Responses to SSIB RAIs 18b and 18c explain more completely the use of Nukon fiber bulk density for calculating the debris bed surface area. In general, a sludge compaction limit was intended for all debris packing densities so that minimum thickness is used in the head-loss calculations.

SSIB, Head Loss and Chemical Effects Bump Up: RAI 24

The physical characteristics used in the head loss correlation can have a significant effect on the results of the head loss calculations. Characteristic values that describe the assumed behavior of STP debris are provided in Tables 5.6.1 and 5.6.2 of Volume 3. NRC research conducted for NUREG-1862 has determined that some of the values that describe the physical characteristics of debris are not well understood. Please provide the bases for the values in Tables 5.6.1 and 5.6.2. Please provide reasonable uncertainty bands for the material properties. Also, please explain how compounded inaccuracies in assumed material properties would affect the head loss values predicted by the correlation.

STP Response:

As explained in response to SSIB RAI 21a, standard geometric formulas were used to calculate surface-to-volume ratios S_v using nominal representative debris sizes (radii for cylinders and spheres, thickness for chips). Characteristic values provided in STP LAR Enclosure 4-3, Tables 5.6.1 and 5.6.2 are based largely on manufacturer and supplier information data as well as on deterministic guidance referenced in explanation of STP LAR Enclosure 4-3, Table 2.2.21. The following excerpt cites relevant references from STP LAR Enclosure 4-3:

“Table 2.2.21 provides the material properties (size and density) for insulation (43; 46; 45), qualified coatings (11; 43), unqualified coatings (12), crud (13), and latent debris (43) at STP.”

Material densities based on manufacturer specifications should be accurate to better than $\pm 10\%$. Crud density was intentionally selected from the lower end of a range ($350 \text{ lb}_m/\text{ft}^3$ from a range of 325 to $556 \text{ lb}_m/\text{ft}^3$) leaving an asymmetric uncertainty band of -1% to $+60\%$. Lower material density is considered conservative because the particulate takes up more space inside of the debris bed reducing porosity for a given compaction ratio.

Definition of reasonable uncertainty bands for constituent surface-to-volume ratio equates to defining reasonable uncertainty bands on nominal size. In general, smaller particle sizes lead to higher head loss and increased risk, as demonstrated in the example below. It should be noted that fiberglass, being a manufactured product that forms the dominant substrate for all debris beds at STP, has a very regular geometry and density. The assumed $7\text{-}\mu\text{m}$ fiber diameter is confirmed by SEM images and by direct measurement of S_v (Enclosure 1), which agrees within 4% of the geometric approximation.

Uncertainty ranges on the nominal size of other constituents vary. A crud diameter of $15 \mu\text{m}$ was chosen from a range of 8 to $63 \mu\text{m}$, leaving an asymmetric uncertainty range of -47% and $+320\%$. Failed unqualified coatings were assigned a size of $10 \mu\text{m}$ from a range of 4 to $20 \mu\text{m}$, leaving an asymmetric uncertainty range of -60% to $+100\%$. Of course, there may be residual uncertainties present in the defined ranges and uncertainties in the distribution of particulates across the stated ranges, conservatism was introduced by selection of smaller sizes (point values that represent an entire distribution) than would be present using a complete well-defined distribution of particle sizes for each constituent. Particle size, and hence S_v , were intentionally not selected

as random variables in the CASA Grande sample matrix because a greater degree of consensus supports the adoption of point values than exists for other important parameters.

To investigate how compounded inaccuracies in assumed material properties might affect head-loss values predicted by the correlation, a parameter study was performed where all debris diameters were artificially increased by 30%, causing a 25% decrease in ΔCDF . A similar global 30% decrease in debris diameters caused a 40% increase in ΔCDF . The 30% degree of variation in this case study represents a substantial fraction of the reasonable uncertainty ranges defined above for important particulates, and impacts of less than 50% were experienced from variations in size compounded over all debris types.

SSIB, Head Loss and Chemical Effects Bump Up: RAI 27

The submittal states that the clean strainer head loss (CSHL) is 0.220 ft. based on a test (Reference: Volume 3, Sections 2.2.23, "Clean Strainer Head Loss," and 5.6.1, "Clean Strainer Head Loss"). It appears that the value was taken from a test that was conducted using a single module. The CSHL should be reflective of the entire strainer including all modules and connecting piping, fittings, etc. In the STPNOC letter dated December 11, 2008 (ADAMS Accession No. ML083520326), the CSHL was stated to be 1.95 ft. Please explain why the value provided in the risk-informed submittal is significantly different from the previously calculated value and verify that it includes all head losses associated with the entire clean strainer train.

STP Response:

The clean strainer head loss (CSHL) value used in the STP CASA Grande evaluation of 0.220 ft of H₂O was referenced from "South Texas Project Test Report for ECCS Strainer Performance Testing" (LAR Encl. 4-3, Ref. 53, Pg. 39). This CSHL value was measured directly from the single-module head loss testing performed with maximum flow at 116 °F, and did not include the calculated effect of increased head losses for the entire strainer assembly. The CSHL value of 1.952 ft of H₂O was calculated in Performance Contracting, INC calculation "Clean Head Loss – South Texas Project Units 1 & 2" (Enclosure 1) using conservative assumptions. The CSHL value of 1.952 ft of H₂O given in the clean strainer head loss calculation was calculated under the following assumptions:

- Total losses calculated for the bounding 6-module STP strainer assembly (all others have fewer modules),
- No credit taken for expansion losses (expansion factor = 1.0),
- 10% additional head loss added expansion factor,
- 6% conservatism added for core tube losses,
- Value calculated for maximum flow velocity and maximum (6) strainer string at a temperature of 128 °F.

The tested single-module CSHL value (LAR Encl. 4-3, Ref. 53, Pg. 39) of 0.22 ft of H₂O was inadvertently used as the CSHL value for the total assembly in STP CASA Grande evaluation. Using the PCI calculated value of 1.952 ft of H₂O would increase the total change in core damage frequency (Δ CDF) value by approximately 18% from the submittal calculated Δ CDF. This input error to the CASA Grande evaluation is being tracked under the STP corrective action program and the Alion corrective action program to assure that a more accurate CSHL is incorporated in the analysis and provided in future submittals.

References

1. South Texas Nuclear Operating Company, "Clean Head Loss – South Texas Project Units 1 & 2" (0415-0100055WN/ 0415-0200053WN), 2006

SSIB, Head Loss and Chemical Effects Bump Up: RAI 28

Considering the individual uncertainties that result from the issues described in the request for additional information on the subject of head loss, please provide justification that the use of a correlation is acceptable in the risk-informed model. Along with the justification, please provide an analysis of the overall uncertainty and state how this will be incorporated into the overall risk-informed evaluation.

STP Response:

Use of a head-loss correlation is essential to the risk-informed resolution process because it illuminates subtle interactions between debris types, source timing, operational flow rates, and temperature histories that would not otherwise be apparent using engineering judgment alone. Without a plausibly realistic correlation, it would be impossible to ask/answer questions about the implications of overall parameter and modelling uncertainty.

Three key uncertainties reside in the application of a head-loss model: (1) form of the model needed to capture relevant physics of hydraulic resistance, (2) material properties needed to describe contributions of individual debris constituents, and (3) bed compression (either uniform or non-uniform) that controls porosity. Responses to other RAIs have addressed each topic separately, but the aggregate approach to uncertainty in head-loss prediction includes the following elements:

- (1) Compare performance of NUREG/CR-6224 to an independently derived model and compare both to test data to demonstrate conservative performance of NUREG/CR-6224 as applied in the STP LAR;
- (2) Interpret the factor of 5 as an uncertainty bound that covers inaccuracies in individual material properties and chemical effects;
- (3) Apply a sludge compression limit to obviate concerns about non-uniform bed response. While this limit may ultimately prove to be overly restrictive, it establishes a bound on possible influence caused by bed mechanics.

Overall uncertainties have been addressed in the STP LAR by sensitivity studies that interrogate the degree of influence on ΔCDF introduced by changes in specific parameters (Enclosure 2). The interactions of material properties are complex because of their contributions to weighted average bed properties and can lead to non-intuitive results that both increase or decrease risk somewhat. The supplemental white paper accompanying this RAI response (Enclosure 1) discusses one such parameter study affecting the amount of epoxy fine material appearing in the pool. This perturbation decreased ΔCDF by no more than 10%. In one parameter study performed to support this response, all debris diameters were artificially increased by 30% causing a 25% decrease in ΔCDF . A similar global 30% decrease in debris diameters caused a 40% increase in ΔCDF . Note that changes in debris diameters imply direct changes in the assumed surface-to-volume ratios S_v . Parameter variation studies performed thus far lend confidence that the factor of 5 uncertainty bound applied to all pressure drop calculations is sufficiently, yet reasonably, conservative. In this application, the factor of

5 is analogous to a single-sided parameter variation that causes a uniform shift to higher head loss.

Because the x5 uncertainty bound represents an envelope of potential effects that are not fully resolved in the validation tests, a sensitivity study was run on this factor keeping all other inputs equal to the baseline. Being a simple multiple on conventional head loss, changes to this parameter can be viewed as shifting the entire distribution of predicted head loss up or down relative to the strainer-related performance criteria of NPSH, buckling and degasification. The effect of shifting the uncertainty bound along a range from 1 to 7, when applied as a precise value with no standard deviation, is illustrated in Fig. A. The influence of this parameter on ΔCDF is nearly linear in the region about 5.0. Note that the baseline quantification includes a standard deviation of 1 about a mean factor of 5 so the spread allows slightly more cases to fail than a sharp value of 5 so the ratio of risk at this value is less than 1.0.

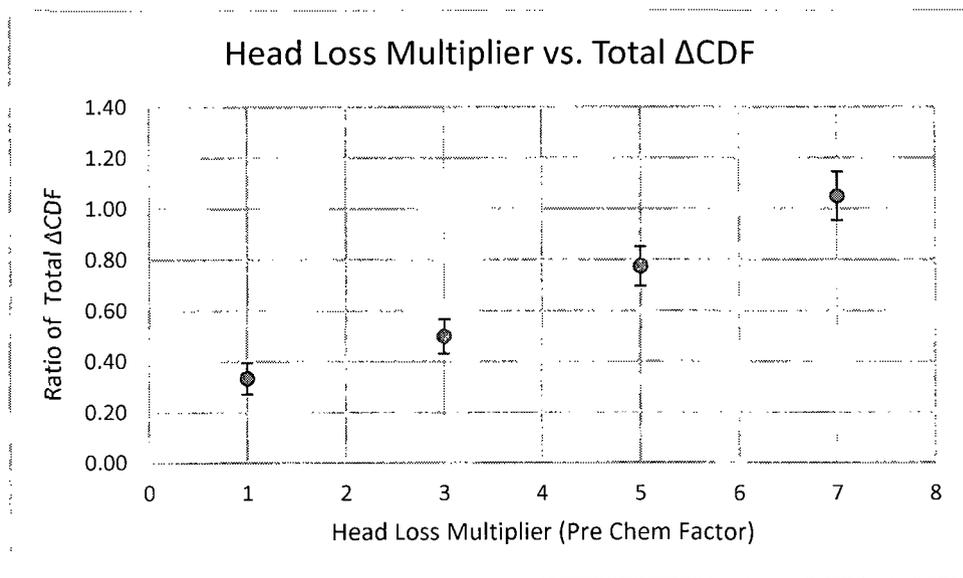


Fig. A. Sensitivity of ΔCDF to changes in head-loss uncertainty bound presented as a ratio to the baseline.

SSIB, NPSH and Degasification: RAI 33

The pool water level calculation provided in the STPNOC submittal does not appear to account for changes in pool area with elevation or changes in objects that may displace water (Reference: Volume 3, Section 2.2.5, "Pool Water Level"). Please state if there are significant changes in area or objects in the pool that could affect water level. If so, please demonstrate that the methodology used to calculate pool level is realistic or conservative.

STP Response:

The pool water level was calculated using Equation 1 of LAR Enclosure 4-3, Rev. 2 in Section 2.2.5 using the floor area at the bottom of the pool. This standard practice of using the floor area at the bottom of the pool does not account for changes in pool level with elevation or changes in objects that may displace water.

A CAD calculation was performed in support of this response to calculate pool levels as a function of water volume with displacement from equipment included. A comparison of the CAD and CASA Grande pool elevations are shown below. As pool levels increase, CASA Grande overestimates (is higher than) the pool level with respect to the CAD determined level.

The maximum and average differences between the higher CASA Grande elevations and the lower CAD elevations are 7.0 and 5.1 inches (10.6% and 9.8%) respectively. The elevations were evaluated between the minimum and maximum STP pool volumes (LAR Enclosure 4-3, Pg. 45).

There is an inconsistency between the levels calculated using the referenced pool area and the currently QA approved CAD model calculated levels. This error will be tracked in the STP corrective action program and changes will be made in any future submittals which will include using CAD elevations to determine pool levels.

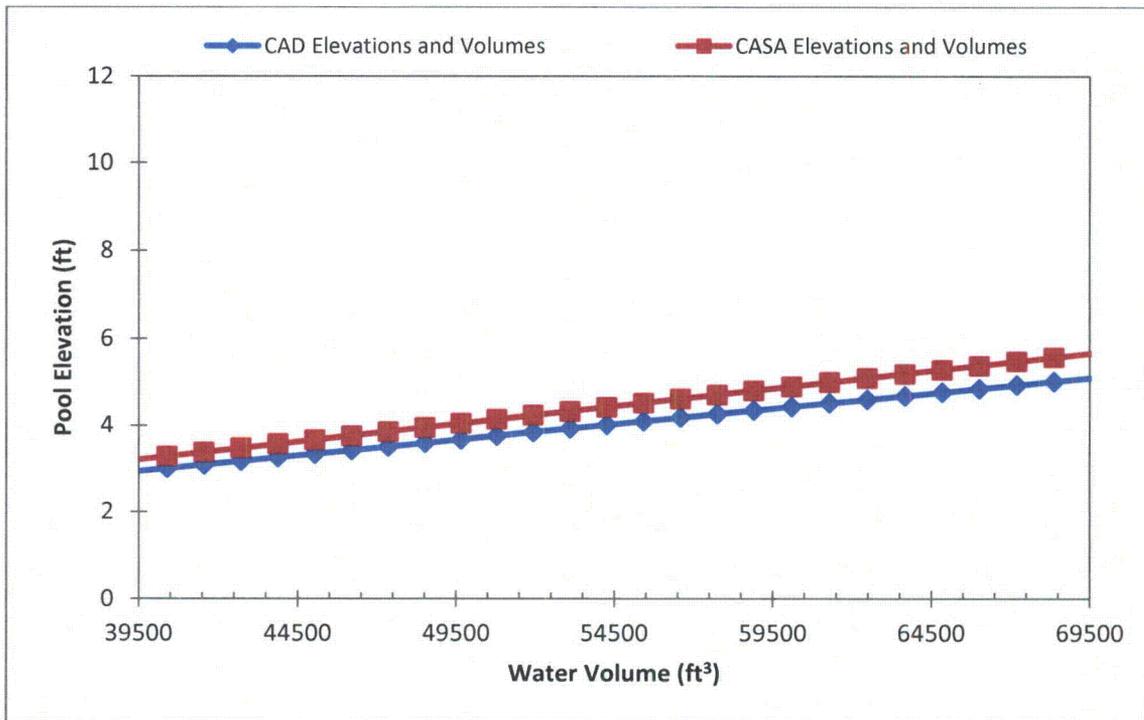


Figure 2: Comparison of CAD and CASA Grande pool elevations versus water volume

SSIB, NPSH and Degasification: RAI 36

The submittal states that the NPSHR for the ECCS and CSS pumps is 12 ft (Reference: Volume 3, Section 2.2.24, "Pump NPSH Margin," and Enclosure 6, Table 1). The proposed UFSAR revisions (pages 9 and 11 of Attachment 2 to Enclosure 3) state that the NPSHR for the pumps is between 16.1 and 16.5 ft. A previous STPNOC submittal dated December 11, 2008 (ADAMS Accession No. ML083520326), for response to Generic Letter (GL) 2004-02 stated that the NPSHR values for the LHSI, HHSI, and CS pumps are 16.5 ft., 16.1 ft., and 16.4 ft., respectively. Please provide the basis for the NPSHR values used in the current evaluation.

STP Response:

The basis for the values used in LAR Encl. 4-3 is the operation and maintenance manual (2 and 3) which provide the NPSH required at the pump first stage impeller. This was determined by pump testing and is met by the pump barrel design which has a height of 15 ft.

Table 1 displays the NPSH required at the pump impeller for each pump at the specified flow rate.

Table 1: NPSH Required at the Pump Impeller

Pump	Flow Rate, gpm	NPSH Required at the Pump Impeller, ft
LHSI	2,800	13
HHSI	1,620	11
CS	2,700	12

However, vertical centrifugal pumps have two independent NPSH required values: 1) at the first stage impeller (described above) and 2) at the pump suction nozzle located at the top of the pump barrel (1). While the NPSH required at the pump impeller is determined by testing, the NPSH required at the pump suction nozzle is equal to the velocity head at the top of the suction nozzle (1) as presented by Eq 1.

$$NPSH_{R@suct} = \frac{v^2}{2g} + \frac{1}{2}d \quad \text{Eq 1}$$

Table 2 displays the NPSH required at the pump suction nozzle for each pump at the specified flow rate.

Table 2: NPSH Required at the Pump Suction Nozzle

Pump	Flow Rate, gpm	NPSH Required at the Pump Suction Inlet, ft
LHSI	2,800	1.5
HHSI	1,620	1.1
CS	2,700	1.4

LAR Encl. 4-3 only determined the NPSH margin at the pump impeller. A CASA Grande parameter study was conducted where the NPSH margin was calculated at the pump suction nozzle. Although this input caused a net reduction in NPSH margin, the Δ CDF did not change because strainer buckling is the limiting failure criterion. In other words, the number of failures did not change because additional failures caused by the revised NPSH treatment were already failing the strainer buckling criterion in LAR Encl. 4-3. The response to ESGB RAI 17 in the STP letter provided to the NRC Staff dated June 25, 2014, NOC-AE-14003101, ML14178A481 and ML14178A485 further supports this observation by stating:

A chemical head-loss factor of 43 would lead to buckling failure of the strainer for all simulated breaks in Case 01, full train operation. A chemical head-loss factor of 209 would lead to the violation of the NPSH margin criterion and failure for all simulated breaks in Case 01, full train operation.

Even though the correction of the NPSH evaluation will have no effect on the conclusions in the LAR, it is still being tracked in the Alion corrective action program. The STP UFSAR also requires clarification and the condition has been logged into the STP Corrective Action Program.

References:

1. ST-WN-YB-1883. Westinghouse Electric Corporation Letter. 8/29/1985.
2. VTD-P025-0001. "Low Head Safety Injection and Containment Spray Pumps Operation and Maintenance Manual". Revision 4. 11/30/2004.
3. VTD-P025-0004. "High Head Safety Injection Pump Operation and Maintenance Manual". Revision 4. 1/10/2007.

SSIB, Debris Bypass: RAI 38

The submittal discusses the fraction of debris that is “sheddable” from a debris bed (Reference: Volume 3, Section 5.8, “Debris Penetration”). Please explain if V_n , (Fraction of debris that is “sheddable”), is a simple fraction or it is dependent on the amount of debris in the bed.

STP Response:

No. The fraction of debris that is sheddable is not dependent on the amount of debris on the bed. The fraction of debris that is sheddable is a constant for each scenario that is sampled from variations in observed data (LAR Enclosure 4-3, Reference [28], Page. 5).

SSIB, Defense In Depth and Mitigative Measures: RAI 40

Volume 1, Section 2.1.1, "Defense-in-Depth," states that the concerns raised in GSI-191 have no bearing on containment integrity or on the release of radiation (page 18 of Volume 1). Volume 1, Appendix C, page C6 states that the independence of barriers is not degraded. The NRC staff notes that barrier independence is a function of multiple factors (e.g., plant operations, maintenance, environmental conditions) that are not necessarily linked directly to SSC design. Appendix C presents a similar argument with respect to maintaining a balance among core damage prevention, containment, and consequence mitigation. It is not clear to the NRC staff that a lack of design/equipment changes can be equated unconditionally with a balanced approach to prevention, containment, and mitigation. The presence of debris may impact the effectiveness of core damage prevention and containment simultaneously. Implementation of a deterministic solution would result in zero predicted failures of the fuel or containment as a result of debris, following an assumed failure of the RCS barrier. STP's risk-informed solution predicts that some fuel or containment failures may occur. This implies that the independence of barriers may be degraded under the risk-informed approach. Consistent with RG 1.174, please provide discussion on defense in depth contained in Appendix C, using quantitative assessments to the extent practicable (to supplement the existing qualitative assessment), to demonstrate that the elements of defense in depth described by RG 1.174 are met. Where appropriate, provide a comparison between the hypothetical "clean plant" and the as-built, as-operated plant. Consistent with the RG, please also include an evaluation of the proposed change on affected equipment functionality, reliability, and availability.

STP Response:

Regarding failure that may occur

Quantitative evaluations of the defense in depth and safety margin as described in the LAR show that peak clad temperature remains below 800F with a single fuel channel unblocked or with flow through the core bypass that has large openings unlikely to retain debris. The quantitative thresholds of concern used for success criteria (for example, 7.5 g/FA for core blockage or boric acid precipitation strainer and no credit for containment overpressure) support assertions made regarding the requirements in RG1.174. Although chemical corrosion effects are included as part of the engineering support for the risk analysis, many experiments performed with realistic post-LOCA exposure to possible precipitate formation show that chemical precipitates are unlikely to cause the head losses included in the LAR supporting engineering analyses (LAR Enclosure 4-3). The RG1.174 analysis demonstrates the risk is very small and therefore the functionality, reliability, and availability of the ECCS and CSS remain acceptable.

Regarding defense in depth

Defense in depth is primarily focused on the ECCS functions as they relate to core cooling. The concerns related to GSI-191 in fact do not bear on containment integrity as containment cooling is by the reactor containment fan coolers, systems completely independent from the ECCS. In fact there is no increased likelihood for containment breach from the concerns related to GSI-191. This may seem counterintuitive in light of the (very small) increase in LERF from 8.6E-12/yr to 1.40E-11/yr documented in the LAR, page 2 of 5. This increase is related to the fact that the PRA analyzes cases when, for example, containment purge is in progress and can't be isolated when a core

damage event occurs. Since there is a very small increase in core damage frequency analyzed, this results in the small increase in LERF.

The LAR Enclosure 4-1, Part I, Procedures and Activities in the Licensing Basis (starting on page 1) describes effective changes in operation, processes, procedures, and design that have been either undertaken or strengthened, or identified as supporting a balanced approach to the concerns raised in GSI-191. The most important among these was the introduction of strainers capable of withstanding large debris loads that may result in the hypothetical LOCA scenarios analyzed in relation to GSI-191. In addition (described as well in Part I), the design process has been strengthened to prevent introduction of potentially harmful products in the containment building, large transition welds susceptible to PWSCC in areas where maximum target material is present have either been replaced or mitigated according modern industry standards. The steam generator nozzle welds were replaced with Alloy 690 when the steam generators were replaced, and the pressurizer safe-end welds have been overlaid. The reactor vessel nozzles are still Alloy 600, however, the reactor vessel uses stainless steel reflective metal insulation which is not a sump debris concern.

The regulatory framework for the STP licensing application is to apply a risk-informed analysis to demonstrate that the effects of debris on the systems that support the long-term cooling function (i.e., ECCS and CSS) are acceptably small and those systems remain reliable to perform their design function.

Even the deterministic approach involves the ECCS design meeting a "high level of probability" that ECCS performance criteria will not be exceeded. For example, 95% probability in Regulatory Guide 1.157 "Best Estimate Calculations of Emergency Core Cooling System Performance" addresses a relatively narrow scope of parameters that could affect ECCS performance. The risk-informed approach makes no unconditional assumptions related to success and quantifies a realistic confidence level. The realistic risk for loss of long term cooling is evaluated to be "very small" in the existing plant design in accordance with the guidance provided in RG 1.174, which could be considered equivalent to a "high level of probability".

Regarding the "hypothetical clean plant"

The "hypothetical clean plant" is described in Enclosure 1 to the LAR and is a plant that has no sources of debris that would result in the concerns related to GSI-191. The as-built, as-operated plant has fibrous insulation that is the source of the concerns related to GSI-191. There are materials included in the design that may interact with fibrous debris (including latent debris) to adversely affect head loss and flow to the core.

Regarding equipment changes

There are no proposed changes to how any equipment is operated or maintained in the STP application; consequently, no changes are proposed in the LAR to equipment availability, functionality, or reliability. As described in the LAR, Enclosure 2-1, Section 1, STPNOC requests an exemption in order to enable the use of a risk-informed method to demonstrate acceptable sump performance and to validate assumptions in the Emergency Core Cooling System (ECCS) evaluation model.

SSIB, Defense In Depth and Mitigative Measures:RAI 42

Volume 1, Appendix C, Section C.5.8, "Mitigation of Inadequate Reactor Core Flow," lists mitigative measures that can be taken if the flow to the core is not adequate to ensure core cooling. It is not clear to the NRC staff how the mitigative measures for inadequate reactor core flow will be effective. Most of the actions attempt to inject coolant through the flowpath that has already been identified as potentially blocked. Other actions do not appear to be effective if the core inlet is blocked. Please provide additional information showing that the mitigative measures are capable of providing coolant to the core.

STP Response

The effectiveness of mitigative measures as directed by the EOPs and SAMGs for inadequate reactor core flow has been evaluated as part of the development of the procedures and guidelines.

Not all actions listed in LAR Enclosure 4-1 Appendix C, Section 5.8 require use of blocked flowpaths. If the core and core bypass are both blocked during hypothesized medium or large cold leg break scenarios, transfer to hot leg recirculation would be effective in continuing to cool the core. For hypothesized hot leg break scenarios, or small cold leg break scenarios with core blockage, the cold leg injection path is all that is required as described in the LAR Enclosure 4.3, Section 5.10.2. In addition to transfer to hot leg recirculation for the medium and large cold leg break scenarios with full core and bypass blockage, the EOPs require running reactor coolant pumps in response to inadequate core cooling. The reactor coolant pump discharge pressure of approximately 76 psid (1) would be expected to clear debris or re-flood the core.

Alternatively, if the ECCS flow path is blocked, alternate success paths are provided independent of core blockage. Charging may be restored through either the normal charging flowpath (via the volume control tank) or through the positive displacement pump. The RWST may be used following refill above the EMPTY level. There is no procedure for backwashing the strainers at STP.

Reference:

1. STP letter to USNRC dated April 8, 2014 STP Power Plant RELAP5-3D Steady-State Model Verification. July 2013, ML14091A452

Enclosures to Attachment 8

1. Letellier, B.C., Macali, M.E., Kee, E.J., Viscous Inertial Shear-Transition-Adaptive (VISTA) Porous Media Head-Loss Formulation for Assessment of South Texas Project Licensing Amendment Request, ALION-REP-STP-8998-11, Rev. 1, July 2014.
2. Morton, D.P., Tejada, J.J., Zolan, A., South Texas Project Risk-Informed GSI-191 Evaluation, Volume 3, A Practical Guide to Sensitivity Analysis of Large-scale Computer Simulation

Document No: ALION-REP-STP-8998-11	Revision: 0	Page 1 of 52
Doc Title: Viscous Inertial Shear-Transition-Adaptive (VISTA) Porous Media Head-Loss Formulation for Assessment of the South Texas Project Licensing Amendment Request		
Project No: STP-8898		
Project Name: STP Risk-Informed GSI-191 Support		
Client: South Texas Nuclear Operating Company		
<p>Document Purpose/Summary:</p> <p>The South Texas Project Nuclear Operating Company (STPNOC) is responding to Nuclear Regulatory Commission (NRC) Requests for Additional Information (RAI) regarding their Licensing Amendment Request (LAR) to close Generic Safety Issue 191 (GSI-191) using a pilot risk-informed methodology. Several RAI focus on aspects of head loss (pressure drop) across debris beds of mixed composition that accumulate on emergency core cooling system (ECCS) strainers. This document provides additional theory, insights and example results needed to provide complete responses to those RAI. In particular, a robust head-loss correlation based on internal Reynolds flow transition is presented that provides insights regarding: (1) derivation of classic head-loss formulas and development of an innovative alternative, (2) mechanics of calculating weighted averages for mixed debris-bed constituents, (3) use of direct surface-to-volume ratio measurements for common debris types to aid independent calibration of a model, (4) sufficiency of test data defined in terms of Reynolds flow regime collected to validate STP application of the NUREG/CR-6224 head-loss correlation, and (5) effects of debris stratification within the bed. The Viscous Inertial Shear-Transition-Adaptive (VISTA) head-loss model naturally accommodates the transition between viscous and inertial flow regimes that is the primary cause of instability in conventional correlations like NUREG/CR-6224 that treat these phenomena as the sum of two independent terms.</p> <p>Total Page Count: 60 pages including Appendices and Attachments.</p> <p style="text-align: center;">© 2014 Alion Science and Technology Corporation. All rights reserved. Any distribution or unauthorized use of this content without the express written permission of Alion Science and Technology Corporation is strictly prohibited. This document shall only be used in conjunction with an Alion Project Report explicitly authorizing its use.</p>		

<p>Design Verification Method:</p> <p><input checked="" type="checkbox"/> Design Review</p> <p><input type="checkbox"/> Alternative Calculation</p> <p><input type="checkbox"/> Qualification Testing</p> <p>Professional Engineer (if required) Approval: _____ N/A _____ Date: _____</p>
--



TECHNICAL DOCUMENT COVER PAGE

Page 2 of 52

Prepared By:	Bruce C. Letellier	<i>Bruce C. Letellier</i>	7/10/2014
	Printed/Typed Name	Signature	Date
Prepared By:	Ernie Kee	<i>Ernie Kee</i>	7/10/2014
	Printed/Typed Name	Signature	Date
Reviewed By:	Mark E. Macali	<i>Mark E. Macali</i>	7/10/2014
	Printed/Typed Name	Signature	Date
Approved By:	Megan Stachowiak	<i>Lana Mitchell M. Stachowiak</i>	7/10/2014
	Printed/Typed Name	Signature	Date



REVISION HISTORY LOG

Page: 3 of 52

Document Number: ALON-REP-STP-8998-11 Revision: 0

Document Title: Viscous Inertial Shear-Transition-Adaptive (VISTA) Porous Media Head-Loss Formulation for Assessment of the South Texas Project Licensing Amendment Request

REVISION	DATE	DESCRIPTION
0	See Cover Page	Original preparation of white paper to accompany STP response to NRC requests for additional information related to head-loss prediction. Theory and applications presented to document origin of VISTA methodology.

	Viscous Inertial Shear-Transition-Adaptive (VISTA) Porous Media Head-Loss Formulation for Assessment of the South Texas Project Licensing Amendment Request		
	Document No: ALION-REP-STP-8998-11	Rev: 0	Page 4 of 52

Table of Contents

1.0 Abstract 8

2.0 Introduction..... 9

3.0 VISTA Head-Loss Formulation 10

 3.1 Differential Pressure Equation 10

 3.2 Bed Compression 17

4.0 Composite Properties..... 19

 4.1 Surface-to-Volume Ratio..... 19

 4.2 Mixture Porosity..... 28

 4.3 Fluid Viscosity 32

5.0 Calibration to Head-Loss Measurements..... 35

6.0 Iterative Head-Loss Prediction..... 41

7.0 Performance Comparison 45

 7.1 Blind Prediction of Silicon Carbide Test 45

 7.2 Sufficiency of NUREG/CR-6224 Correlation..... 48

 7.3 Stratified Debris Bed Case Studies..... 49

8.0 References..... 51

List of Figures

Figure 3.1.1 - Trend of measured drag coefficients typical for spheres, disks, and cylinders (patterned after Lapple, Ref. 8)..... 12

Figure 4.1.1 - Electron micrograph of common fiberglass with a nominal strand diameter of ~7 microns (Image provided courtesy of University of New Mexico)..... 20

Figure 4.1.2 - Electron micrograph of green silicon carbide abrasive (Image provided courtesy of University of New Mexico)..... 21

Figure 4.1.3 - Electron micrograph of pulverized acrylic paint particulates (Image provided courtesy of Texas A&M University)..... 21

Figure 4.1.4 - Electron micrograph of tin particulate (Image provided courtesy of Texas A&M University) 22

Figure 4.1.5 - Electron micrograph of iron oxide (Image provided courtesy of University of New Mexico) 22

Figure 4.1.6 - Electron micrograph of iron oxide (Image provided courtesy of University of New Mexico) 23

Figure 4.1.7 - Electron micrograph of zinc used in testing (left) and filtrate captured in-line membrane filter taken after 24 hours of testing (right). (Image provided courtesy of University of New Mexico)..... 23

Figure 4.3.1 - Kinematic viscosity measured for concentrations of aluminum oxyhydroxide precipitate suspended in boric acid/TSP solution..... 33

Figure 4.3.2 - Kinematic viscosity measured for concentrations of calcium phosphate precipitate suspended in boric acid/TSP solution..... 33

Figure 4.3.3 - Comparison over a common range of kinematic viscosity measured independently as a function of aluminum oxyhydroxide and calcium phosphate precipitate concentration. 34

Figure 4.3.4 - Kinematic viscosity for pure water over temperature range of interest for EECS applications. 35

	Viscous Inertial Shear-Transition-Adaptive (VISTA) Porous Media Head-Loss Formulation for Assessment of the South Texas Project Licensing Amendment Request		
	Document No: ALION-REP-STP-8998-11	Rev: 0	Page 5 of 52

Figure 6.1 - Prediction of differential pressure history (red) compared to measurement.44
 Figure 6.2 - Correlation of VISTA prediction to calibration data during initial bed formation and steady-flow operation.....44

List of Tables

Table 3.1.1 - Assumptions supporting VISTA head-loss formulation..... 11
 Table 4.1.1 - BET specific surface area for several debris types.26
 Table 4.1.2 - Simple example of composite surface-to-volume ratio for 2 spherical constituents.....28
 Table 4.3.1 - Kinematic viscosity measured for several concentrations of two surrogate chemical precipitates suspended in BA/TSP.....33
 Table 5.1 - STP HTVL data records available for analysis (Ref. 13)41
 Table 7.2.1 - VISTA, HLOSS (NUREG/CR-6224), and Test Head Loss Comparison.....48
 Table 7.3.1 - Stratified debris bed assumptions and findings.....50
 Table 7.3.2 – Stratified debris bed with piston load.....50

List of Appendices

Appendix I: Requests for Additional Information (RAI) Related to Head-Loss Prediction.....8 Pages

	Viscous Inertial Shear-Transition-Adaptive (VISTA) Porous Media Head-Loss Formulation for Assessment of the South Texas Project Licensing Amendment Request		
	Document No: ALION-REP-STP-8998-11	Rev: 0	Page 6 of 52

Acronyms and Definitions

Acronym	Definition
AIOOH	Aluminum Oxyhydroxide
ARL	Alden Research Laboratory
BA	Boric Acid
BET	Brunauer, Emmett, and Teller
CASA	Containment Accident Stochastic Analysis
$\text{Ca}_3(\text{PO}_4)_2$	Calcium Phosphate
ECCS	Emergency Core Cooling System
GSI-191	Generic Safety Issue 191
HTVL	High-Temperature Vertical Loop
LAR	Licensing Amendment Request
LOCA	Loss of Coolant Accident
NEI	Nuclear Energy Institute
NRC	Nuclear Regulatory Commission
PWR	Pressurized Water Reactor
RAI	Request for Additional Information
SiC	Silicon Carbide
STP	South Texas Project
STPNOC	South Texas Project Nuclear Operating Company
TSP	Trisodium Phosphate
UNM	University of New Mexico
VISTA	Viscous Inertial Shear-Transition-Adaptive

	Viscous Inertial Shear-Transition-Adaptive (VISTA) Porous Media Head-Loss Formulation for Assessment of the South Texas Project Licensing Amendment Request		
	Document No: ALION-REP-STP-8998-11	Rev: 0	Page 7 of 52

Viscous Inertial Shear-Transition-Adaptive (VISTA) Porous Media Head-Loss Formulation for Assessment of the South Texas Project Licensing Amendment Request

Bruce C. Letellier – Alion Science and Technology

Mark Macali – Alion Science and Technology

Ernie Kee – YK Risk

	Viscous Inertial Shear-Transition-Adaptive (VISTA) Porous Media Head-Loss Formulation for Assessment of the South Texas Project Licensing Amendment Request		
	Document No: ALION-REP-STP-8998-11	Rev: 0	Page 8 of 52

1.0 ABSTRACT

Classic head-loss formulas for pressure drop in porous media have two terms that are linearly and quadratically proportional to velocity, respectively. The first term $a\mu v$ preserves Stokes' limit for viscous shear, and the second term $b\rho v^2$ preserves Newton's limit for inertial drag. However, there is little theoretical justification for simple addition of the two terms, which individually dominate widely separated flow regimes. A new correlation method, Viscous Inertial Shear-Transition-Adaptive (VISTA) head loss is proposed that preserves the limits while accommodating the flow transition needed to best describe pressure drop through tested porous media. Theory is presented and the model is calibrated to head loss observed in compressible, fibrous, particulate-loaded media prototypical of composite debris beds found in nuclear safety applications. Strong correlation supports efficacy of the VISTA formulation and demonstrates how previously untapped constraints can be extracted from standard vertical column head-loss tests. Although a familiar parameterization of internal drag area (surface-to-volume ratio) is employed, laboratory measurements for fiberglass and representative particulate are applied rather than traditional geometric approximations based on shape and size. The predictive head-loss formula couples a simple model for uniform bed compression that requires iterative solutions between maximum and minimum compression limits. Under the assumption of uniform compression, factorized formulas isolate the effect of spatial variations in debris properties for convenient examination. The VISTA head-loss correlation does not address filtration and migration processes, so presumed or measured debris configurations must be introduced. Case studies explore predicted head-loss sensitivity to debris spatial distribution within the bed. Findings support comparison of the VISTA model to the well-known NUREG/CR-6224 head-loss correlation in the context of a licensing amendment request submitted to the Nuclear Regulatory Commission by South Texas Project Nuclear Operating Company.

	Viscous Inertial Shear-Transition-Adaptive (VISTA) Porous Media Head-Loss Formulation for Assessment of the South Texas Project Licensing Amendment Request		
	Document No: ALION-REP-STP-8998-11	Rev: 0	Page 9 of 52

2.0 INTRODUCTION

Semianalytic head-loss correlations have traditionally been used in nuclear safety applications to provide bounding estimates of pressure drop through composite debris beds accumulated on Emergency Core Cooling System (ECCS) strainers. It has further been assumed that one-dimensional formulas (where debris properties and flow fields vary principally with thickness only) provide a sufficient approximation to describe the performance of in-service strainers having very large total area and convoluted surfaces that commonly permit gaps and occlusions in the debris bed. Noncontiguous beds are presumed to allow more coolant flow and to suffer less head loss than predicted by the one-dimensional approximation with uniform strainer coverage. One additional, but less commonly discussed, advantage of semianalytic predictive models is that they enable investigation of head-loss trends caused by different debris combinations, bed compaction conditions, debris arrival times and bed-degradation mechanisms. This ability to compare subtle interactions across the spectrum of phenomena is necessary to support risk-informed resolution where propagation of uncertainty and a clear definition of sharp behavioral transitions are essential for high-fidelity risk quantification.

Perhaps the most familiar head-loss correlation in common use for nuclear safety applications is the formulation described in Appendix B of NUREG/CR-6224 (Ref. 1). The 6224 correlation has been the subject of extensive debate and study (Refs. 2, 3) regarding (1) fidelity of its derivation in published form, (2) appropriate treatment of composite debris properties, (3) nonphysical trends in bed compression, (4) applicability of the formula both within and beyond the range of available test data, and (5) use as an approximate differential pressure-drop formula for study of inhomogeneous layered debris beds. Despite the controversy, the 6224 correlation has inspired 15 years of research, design, and regulation related to reliable operation of ECCS recirculation strainers in both boiling water and pressurized water reactors. The 6624 correlation was also used in the recent South Texas Project (STP) pilot for risk-informed resolution of Generic Safety Issue 191 (GSI-191) (Ref. 4).

The objectives of this paper are:

1. provide an alternative formulation of debris bed head loss that addresses many of the criticisms levied against 6224,
2. calibrate and exercise the model against available data to demonstrate relevance to debris combinations and flow conditions of interest for STP ECCS performance, and
3. provide supplemental information needed to assess the adequacy of 6224 for use in the STP LAR including analysis of stratified bed conditions.

Many recent requests for additional information (RAI) received from Nuclear Regulatory Commission (NRC) staff (Ref. 5) question the adequacy and implementation of 6224 for the intended purpose of risk quantification. STP believes that providing responses based on the present 6224 correlation alone may represent a circular argument that does not offer sufficient comparative insight for final resolution. Relevant RAI statements are provided in Appendix I for convenient reference, but this paper does not represent a formal response to these questions. Itemized formal responses will be submitted under a separate communication using a standard format.

	Viscous Inertial Shear-Transition-Adaptive (VISTA) Porous Media Head-Loss Formulation for Assessment of the South Texas Project Licensing Amendment Request		
	Document No: ALION-REP-STP-8998-11	Rev: 0	Page 10 of 52

The following technical content represents a summary of a more extensive theoretical treatment of pressure loss prediction in porous media (Ref. 6). While the supporting document attempts to derive head-loss behavior from first principles starting with momentum and energy conservation in a complex flow field, the present discussion begins with the most general statement of head loss and then develops constitutive equations needed to define the principal parameters of porosity and surface-to-volume ratio for mixed bed compositions. The complete formulation is then calibrated using available data obtained in vertical column test configurations to demonstrate fitting the free parameters with uncertainty distributions that support risk-informed application. Theoretical formulation of the alternative method, calibration to data, and application to head-loss prediction is referred to as the Viscous Inertial Shear-Transition-Adaptive (VISTA) correlation for head-loss prediction in porous media. Finally, performance comparisons with the HLOSS version 1.1 (Ref. 7) implementation of 6224 are to illustrate principal differences in modeling behavior and to illustrate bounds on the STP LAR.

3.0 VISTA HEAD-LOSS FORMULATION

Two fundamental elements of head-loss prediction in compressible porous media are developed in the following subsections. Section 3.1 reviews the physical processes of viscous shear and inertial drag that cause pressure drop for fluid flow through a porous debris bed and develops the basic differential equation that preserves limiting behavior while adapting to the Reynolds flow regime of interest. Section 3.2 incorporates a uniform compression model with new constraints on maximum compression and presents an iteration scheme for efficient solution of bed thickness and its corresponding pressure drop. Section 4.0 to follow discusses constitutive formulas needed to describe composite debris properties and fluid viscosity.

3.1 Differential Pressure Equation

To facilitate explanation of the VISTA head-loss formulation, Table 3.1.1 lists fundamental assumptions that underpin the approach. Most of these assumptions are common to traditional derivations of 6224 and will not be discussed further.

	Viscous Inertial Shear-Transition-Adaptive (VISTA) Porous Media Head-Loss Formulation for Assessment of the South Texas Project Licensing Amendment Request		
	Document No: ALION-REP-STP-8998-11	Rev: 0	Page 11 of 52

Table 3.1.1 - Assumptions supporting VISTA head-loss formulation

	Alternate Formulation	Comparison to 6224
1	One-dimensional debris beds that vary only with thickness.	More general than original intended application of 6224, but substantially similar
2	Porosity used to factor local velocity in terms of approach strainer face velocity.	Same
3	Analytic basis in exact result for internal capillary flow.	Same
4	Hydraulic scaling to complex debris bed based on ratio of internal flow volume to internal surface area.	Same
5	Preserves Stokes flow limit (viscous shear) and Newton limit (inertial drag) continuously as a function of Reynolds number.	Same limits artificially added as two terms (linear and quadratic in velocity) with no basis for transition.
6	Temperature dependent fluid properties captured by explicit factors of viscosity and density.	Same
7	Same compression model as 6224 applied for proof of concept.	Power-law compression correlation based on observations of fibrous, particle-loaded beds.

Perhaps the most serious unrecognized deficiency of the 6224 correlation is the historical representation of viscous shear and inertial drag as two independent terms. Traditionally, viscous shear is introduced as a term linearly proportional to flow velocity, and inertial drag is introduced as a term quadratically proportional to flow velocity. Although, these two well-known limits both lead to larger pressure reductions, they individually dominate radically different flow regimes, and there is no theoretical basis for simple addition of the two effects. Furthermore, both effects are present to some degree in all flow regimes, since both viscous shear and momentum transfer via mass impingement arise from the same molecular dynamics. Thus, independent derivation of the limits with presumed additive effects must be acknowledged as an approximation. Proper representation of the transition between limiting behaviors is a common challenge in engineering physics. In the case of the traditional head-loss formulation, summation of the two terms causes 6224 to behave much like an over-fit polynomial that is not robust to extrapolation and often demands nonphysical negative quadratic coefficients to obtain best-fit agreement with measurements.

The following derivation offers a mechanism for combining the effects of viscous shear and inertial drag in proper proportion supported by data. A familiar formula for inertial drag is derived first, followed by substitution of a generalized drag coefficient that is also capable of preserving the viscous limit. Additional details and discussion are provided in Ref. (6).

The initial point of view for derivation of inertial drag (Newton limit) is one of external flow around a stationary sphere where the rate of mass displacement equals the cross sectional area of the body times the velocity times the fluid density within the displaced volume, i.e., $\dot{m} = \rho \frac{\pi}{4} d^2 \bar{w}$. The acceleration of the displaced fluid is proportional to the relative velocity between the body and the fluid, so when the fluid is at rest, $F_D = \frac{\text{change of momentum}}{\text{unit of time}} \propto \dot{m} \bar{w} = \rho \frac{\pi}{4} d^2 \bar{w}^2$. Thus, the force required

	Viscous Inertial Shear-Transition-Adaptive (VISTA) Porous Media Head-Loss Formulation for Assessment of the South Texas Project Licensing Amendment Request		
	Document No: ALION-REP-STP-8998-11	Rev: 0	Page 12 of 52

to move the body through the medium, or equivalently, the drag exerted on the body as the fluid passes around it, is given by $F_D = K\rho\frac{\pi}{4}d^2\bar{w}^2$ where K is a constant of proportionality.

Classic experiments show that the proportionality between drag force and momentum change is only approximately constant for spherical-particle Reynolds numbers $Re > 1000$, so a more general convention is adopted by introducing a drag coefficient that can be correlated as a function of Re . Thus, the standard convention is:

$$F_D = \frac{1}{2}C_D(Re)\frac{\pi}{4}\rho d^2\bar{w}^2. \tag{Eq. 1.0}$$

Figure 3.1.1 illustrates empirical behavior of the drag coefficient that is typical for several standard debris-element geometries (spheres, disks, cylinders) over a wide range of Reynolds number.

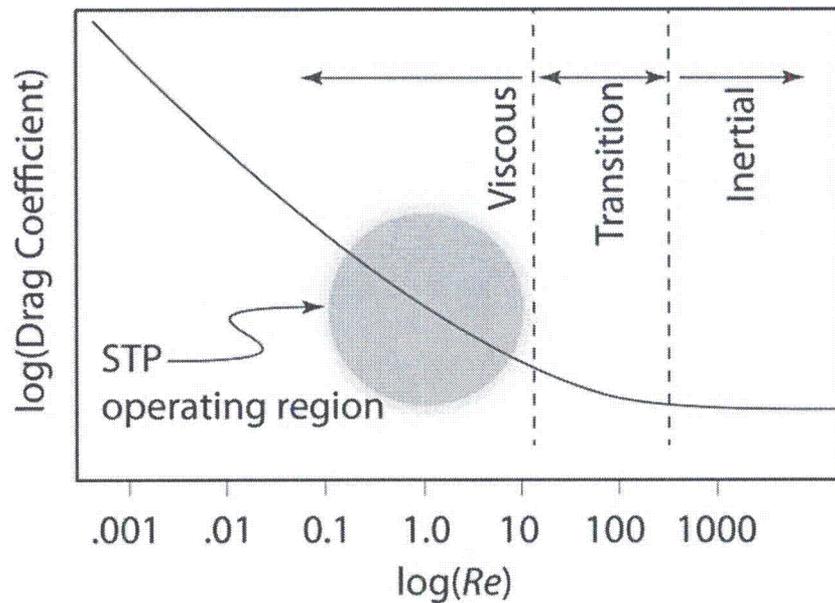


Figure 3.1.1 - Trend of measured drag coefficients typical for spheres, disks, and cylinders (patterned after Lapple, Ref. 9)

	Viscous Inertial Shear-Transition-Adaptive (VISTA) Porous Media Head-Loss Formulation for Assessment of the South Texas Project Licensing Amendment Request		
	Document No: ALION-REP-STP-8998-11	Rev: 0	Page 13 of 52

Eq. 1.0 describes the inertial drag force acting on individual debris elements by fluid moving through the bed. It is intuitively obvious that drag must be exerted along the surface of all debris that is in contact with moving fluid, so many similarities arise with the treatment of viscous shear coupled to the walls of a capillary flow channel. In fact, the standard treatment is to define an inertia-induced drag stress analogous to viscous stress such that:

$$\tau_{Drag} = \frac{F_D}{A_{particle}} = \frac{R}{2} \left(\frac{dP}{dz} \right)_{Drag}, \quad \text{Eq. 2.0}$$

where R is the effective radius of a typical flow path that will be related to a characteristic dimension called the hydraulic radius. One important question that arises immediately is, what area $A_{particle}$ should be used to distribute the drag force? Viscous shear, which should dominate flow regimes of interest, is generally assumed to affect the entire surface of the debris; so for now, it is reasonable to assume that inertial drag can also be distributed across the entire debris surface. However, it should be noted that conventional definitions of the drag coefficient like Eq. 1.0 have been scaled by the cross sectional area of obstacles presented to the flow. Distribution of drag force over the entire interior surface area will introduce different empirical factors that should be determined by fits to data.

Reversing the sign of Eq. 2.0 to account for inertial drag acting on a fluid element, substitution into Eq. 1.0, and solving for the pressure gradient leads to the relation:

$$-\left(\frac{dP}{dz} \right)_{Drag} = \frac{2}{A_{particle} R} \left[\frac{1}{2} C_D (Re) \frac{\pi}{4} \rho d^2 \bar{w}^2 \right]. \quad \text{Eq. 3.0}$$

The area of the spherical particle used as an illustration for drag force is $A_{particle} = \pi d^2$, which eliminates the same product from the brackets. Assuming that the total volumetric flow rate is constant throughout the bed (mass conservation) allows factoring the local average velocity in terms of the strainer face approach velocity, $\bar{w}^2 = w_A^2 / \varepsilon^2$, where ε is the local porosity. Finally, the characteristic length for internal flow (called the hydraulic radius) is defined as:

$$R_H = \frac{\text{fluid volume}}{\text{debris area}} = \frac{\varepsilon \nabla}{(1-\varepsilon) \nabla S_V} = \frac{\varepsilon}{(1-\varepsilon) S_V}, \quad \text{Eq. 4.0}$$

	Viscous Inertial Shear-Transition-Adaptive (VISTA) Porous Media Head-Loss Formulation for Assessment of the South Texas Project Licensing Amendment Request		
	Document No: ALION-REP-STP-8998-11	Rev: 0	Page 14 of 52

where \forall is an arbitrary debris volume, ε is the local porosity, $(1-\varepsilon)$ is the local solidity, and S_V is the ratio of debris surface area to debris solid volume. For a cylindrical capillary, the effective radius $R = 2R_H$. Substituting these relationships in Eq. 3.0 gives:

$$-\left(\frac{dP}{dz}\right)_{Drag} = \frac{1}{8} C_D (Re) \left(\frac{1-\varepsilon}{\varepsilon^3}\right) S_V \rho w_A^2. \quad \text{Eq. 5.0}$$

The discussion of composite debris properties in Section 4.1 proposes a further substitution for the surface-to-volume ratio $S_V = \rho^{mat} S_A$ where ρ^{mat} is the material density of a debris constituent and S_A is the specific surface area $\{area/mass\}$ of the constituent obtained by direct laboratory measurement. Note that in its most basic form, the hydraulic scaling stated by Eq. 4.0 assumes that the entire surface area of the debris participates in the flow, not just the surface area that is aligned perpendicular to the flow. Other scaling arguments have been proposed that introduce shape factors for high-porosity filter media (Ref. 8), but the present approximation is sufficient to demonstrate the methodology.

Only the form of the drag coefficient remains to be rationalized, and the empirical trend presented in Figure 1 suggests a deceptively simple opportunity for joint treatment of viscous shear and inertial drag. Note that the plots depict a smoothly behaved function of Reynolds number that spans 10 decades of magnitude. Reynolds number for internal flow relevant to debris beds vary between 0.1 and 10 where the dependence on Re is almost linear on the log-log scale. For this application, Reynolds number is defined as:

$$Re = \frac{\rho \bar{w} R_H}{\mu} = \frac{\rho w_A}{\mu(1-\varepsilon) S_V} \frac{\varepsilon}{\varepsilon}. \quad \text{Eq. 6.0}$$

The narrow range of Reynold's number internal to debris beds and regular variation of the drag coefficient with Reynold's number shown in Figure 1 suggest that a floating power-law fit of the drag coefficient vs. Reynold's number (linear plot in log-log space) might have sufficient flexibility to match the physical limits posed by both viscosity (low Reynolds) and inertia (high Reynolds). Thus, the drag coefficient is assumed to be a generalized power law such that:

$$C_D (Re) = \tilde{b} (Re) Re^{m(Re)} = \tilde{b} (Re) \left(\frac{\rho w_A}{\mu(1-\varepsilon) S_V} \right)^{m(Re)}, \quad \text{Eq. 7.0}$$

	Viscous Inertial Shear-Transition-Adaptive (VISTA) Porous Media Head-Loss Formulation for Assessment of the South Texas Project Licensing Amendment Request		
	Document No: ALION-REP-STP-8998-11	Rev: 0	Page 15 of 52

so that Eq. 5.0 becomes:

$$-\left(\frac{dP}{dz}\right) = b \left(\frac{\rho w_A}{\mu(1-\varepsilon)S_V}\right)^m \left(\frac{1-\varepsilon}{\varepsilon^3}\right) S_V \rho w_A^2, \tag{Eq. 8.0}$$

where the integer constant has been subsumed in the empirical parameter and the differential pressure is now understood to represent the total change caused by all phenomena. This form permits the slope of the log-log approximation to “float” along the composite drag coefficient by fitting local values of $b(Re)$ and $m(Re)$. In essence, a fully calibrated correlation would define for a complex debris bed the tangent of an underlying drag coefficient that would look very much like Figure 1 over a limited range of Re .

If sufficient data exist to infer additional parameters, it is possible to fit higher order polynomials to the drag coefficient. The simple generalization of the Eq. 7.0 power law is:

$$C_D(Re) = c_0 Re^{\sum_{i=1,N} ic_i} \tag{Eq. 9.0}$$

to achieve an N th-order polynomial in log-log space. After studying the role of the slope $m(Re)$ in the following formulas, there may be an opportunity to substitute $m(Re) = \sum_{i=1,N} ic_i$ and obtain a robust head-loss correlation within the range of interest that has stationary coefficients with respect to Reynolds number

The essential feature of this approach is that limiting formulas for viscous and inertial drag can be recovered separately when Eq. 8.0 is evaluated with appropriate exponents. When $m = -1$, Eq. 8.0 reduces to the Kozeny-Carman viscous limit (Ref. 10):

$$-\left(\frac{dP}{dz}\right) = b_{visc} \frac{(1-\varepsilon)^2}{\varepsilon^3} S_V^2 \mu w_A. \tag{Eq. 10.0}$$

When $m = 0$, Eq. 8.0 reduces to the inertial limit (Ref. 11):

$$-\left(\frac{dP}{dz}\right) = b_{drag} \left(\frac{1-\varepsilon}{\varepsilon^3}\right) S_V \rho w_A^2. \tag{Eq. 11.0}$$

	Viscous Inertial Shear-Transition-Adaptive (VISTA) Porous Media Head-Loss Formulation for Assessment of the South Texas Project Licensing Amendment Request		
	Document No: ALION-REP-STP-8998-11	Rev: 0	Page 16 of 52

Any correlation of a debris bed with $-1 < m < 0$ will include an appropriate mixture of both viscous and inertial effects. One major advantage of the composite correlation is that the fitting parameters b and m are themselves functions of the Reynolds number that includes factors of both porosity and surface-to-volume ratio. Dependence of the parameters on bed properties should permit additional collapse of the geometry dependence exhibited in Figure 3.1.1 (see Ref. 9). In this sense, the correlation can “adapt” to the local flow conditions presented by prototypical debris beds. By comparison, the parameters of 6224 are fixed at constant values. Test programs can easily span the desired range of Reynolds number by using any combinations of bed geometry, fluid velocity and fluid temperature. Confirmatory tests can then be conducted over the same span of Reynolds number using alternate factors that achieve the same hydraulic scaling to demonstrate that the Viscous Inertial Shear-Transition-Adaptive (VISTA) head-loss correlation is robust over debris compositions and flow conditions relevant to ECCS strainer performance. Residual variation present in the parameters b and m , which will be manifest as a variation in tangent lines, can then be propagated using uncertainty distributions for risk-informed applications.

It is very important to understand that all elements of Eq. 8.0 related to bed properties (namely, ε , S_V , b , m) are spatially dependent and can vary with position within the debris. Fluid properties defined by μ , ρ , w_A are constant throughout the bed. Because Reynolds number depends on both fluid properties and local flow geometry, Re is also a function of bed location. Spatial properties are important for addressing questions regarding time-ordered bed stratification, and for examining local flow restrictions such as debris impaction inside of perforation plate orifices (see Section 7.0).

A particularly useful form of Eq. 8.0 is:

$$-\left(\frac{dP}{dz}\right) = \frac{\rho^2 w_A^3}{\mu} \frac{b(z)}{\varepsilon(z)^3} Re(z)^{m(z)-1}, \quad \text{Eq. 12.0}$$

where all fluid properties are collected as a leading coefficient that can be assumed constant throughout a debris bed and spatial dependencies are explicitly noted. Given spatial profiles for porosity and surface-to-volume ratio that are either assumed, measured or predicted, Re is obtained from Eq. 6.0 and the drag coefficient parameters can be read from a calibration curve that is appropriate for the prototypical debris composition.

If bed properties are uniform with little to no evidence of compression, then the direct integral of Eq. 12.0 gives the total pressure drop across a bed of thickness ΔL :

$$\Delta P = \frac{\rho^2 w_A^3}{\mu} \frac{b}{\varepsilon^3} \Delta L Re^{m-1}. \quad \text{Eq. 13.0}$$

	Viscous Inertial Shear-Transition-Adaptive (VISTA) Porous Media Head-Loss Formulation for Assessment of the South Texas Project Licensing Amendment Request		
	Document No: ALION-REP-STP-8998-11	Rev: 0	Page 17 of 52

This result can be applied across any portion of a bed for which the stated assumptions are reasonable.

3.2 Bed Compression

Under hydraulic loads induced from moving fluid, thickness reduction observed in fibrous debris beds arises from two mechanisms: (1) compression, defined as fully recoverable tensile loading of the mechanical linkage between fibers; and (2) compaction, defined as irreversible relative motion of debris elements caused by local force imbalance that relieves tensile stress and results in internal reconfiguration. Both mechanisms reduce porosity. Under prolonged fluid flow, fibrous debris beds can settle via compaction mechanisms that prevent compressive recovery.

Internal hydraulic loads on the debris caused by viscous shear and inertial drag are transferred through physical contact between debris elements in a cumulative fashion very analogous to static hydrodynamic loads. Thus, debris elements near the bottom of the bed next to the strainer plate experience higher compression than debris elements near the top of the bed. In the theoretical limit of a perfect linear spring, the nonuniform spatial distribution of porosity can be calculated analytically knowing only the spring constant and the local drag force as a function of position, which in turn depends on local compression in a positive feedback loop that iterates to an equilibrium configuration. With high particulate loads, it is doubtful that nonuniform fiber compression competes with particulate migration as a dominant means of porosity reduction, so it is more common to apply uniform compression models that match total observed thickness reduction. Uniform compression is analogous to a spring loaded only from the top so that porosity reduction is constant throughout the bed.

NUREG/CR 6224 recommends a uniform compression model that describes the ratio between mixed bed thickness ΔL_m and the theoretical reference thickness ΔL_0 in terms of the ratio between the manufactured packing density c_0 and the actual bed packing density c ; $\Delta L_m / \Delta L_0 = c_0 / c$, where the manufactured density is approximately 2.4 lb_m/ft³ and the maximum recommended particulate-loaded packing density is approximately $c_{max} = 65$ lb_m/ft³. Although finely divided fiber beds are sometimes observed to have an effective thickness greater than the equivalent amount of manufactured insulation, it is reasonable to enforce the limits:

$$1 \leq \frac{\Delta L_0}{\Delta L_m} = \frac{c}{c_0} \leq \frac{65}{2.4} = 27. \quad \text{Eq. 14.0}$$

Based on work of Ingmanson (Ref. 8), NUREG/CR 6224 recommends a correlation for uniform bed compression of the form:

$$\frac{\Delta L_m}{\Delta L_0} = \frac{c_0}{c} = \frac{1}{\tilde{a}} \left(\Lambda \frac{\Delta P}{\Delta L_0} \right)^{-\gamma}, \quad \text{Eq. 15.0}$$

	Viscous Inertial Shear-Transition-Adaptive (VISTA) Porous Media Head-Loss Formulation for Assessment of the South Texas Project Licensing Amendment Request		
	Document No: ALION-REP-STP-8998-11	Rev: 0	Page 18 of 52

where $\tilde{a} \approx 1.3$ and $\gamma \approx 0.38$ are empirical constants, ΔP is the positive pressure drop, and $\Lambda = 8.5 \times 10^{-6}$ is the factor needed to convert from SI units of Pa/m to the correlation units of $ft-h_2O/inch$. Following formulas will factor the units conversion and substitute $a = \tilde{a}/\Lambda^{-\gamma}$ to simplify the notation.

Note that the ratio $\Delta P/\Delta L_0$ appearing in Eq. 15.0 represents the average pressure gradient that would be present if the same pressure drop were experienced across a bed with corresponding theoretical thickness. For the purpose of investigating non-uniform debris layers, we will further assume that the same compression formula holds in a differential sense such that $dL_m/dL_0 = (1/a)(dP/dL_0)^{-\gamma}$. The supplemental report (Ref. 6) proposes other differential compression formulas that could be considered as well.

Fiber beds that are repeatedly cycled between high- and low-velocity flow experience successive compaction events whereby the preceding bed thickness is never fully recovered when the flow is reduced. This behavior is analogous to hysteresis phenomena and could be modeled as a damped oscillation if there were a pressing need to predict debris bed thickness for cycled flow conditions. However, to simplify the following data analysis, Eq. 15.0 will be applied only while pressure drop is increasing and the bed is under compression. When measurements indicate a decrease in pressure drop, bed thickness will not be allowed to increase.

Total pressure reduction through a composite debris bed can be predicted by integrating Eq. 12.0 across the full bed thickness:

$$\Delta P = \frac{\rho^2 w_A^3}{\mu} \int_0^{\Delta L_m} \frac{b}{\epsilon^3} Re^{m-1} dz. \tag{Eq. 16.0}$$

When recast in the same terms as the compression correlation,

$$\left(\frac{\Delta P}{\Delta L_0} \right)^{-\gamma} = \left[\frac{\rho^2 w_A^3}{\mu \Delta L_0} \int_0^{\Delta L_m} \frac{b}{\epsilon^3} Re^{m-1} dz \right]^{-\gamma} = a \frac{\Delta L_m}{\Delta L_0},$$

$$\vdots$$

$$\int_0^{\Delta L_m} \frac{b}{\epsilon^3} Re^{m-1} dz = \frac{\mu \Delta L_0}{\rho^2 w_A^3} \left(a \frac{\Delta L_m}{\Delta L_0} \right)^{-\frac{1}{\gamma}}. \tag{Eq. 17.0}$$

	Viscous Inertial Shear-Transition-Adaptive (VISTA) Porous Media Head-Loss Formulation for Assessment of the South Texas Project Licensing Amendment Request		
	Document No: ALION-REP-STP-8998-11	Rev: 0	Page 19 of 52

Eq. 17.0 can only be true at the equilibrium bed thickness that will be established for a given debris arrangement having $\varepsilon(z)$ and $S_v(z)$, and distributed flow regime $Re(z)$. Eq. 17.0 is also true regardless of the pressure drop experienced. Iteration on composite bed thickness ΔL_m will yield the left-hand-side integral needed to evaluate final pressure drop using Eq. 16.0. Formulas given at the end of Section 4.2 should be substituted during iteration to ensure that compression effects on porosity are fully coupled.

4.0 COMPOSITE PROPERTIES

Having established a complete parameterization of head loss in composite debris beds, including a description of compression in fiber dominated conditions, attention now turns to a discussion of material properties and the averaging formulas needed to describe the media. Section 4.1 discusses the surface-to-volume ratio S_v and its relationship to specific surface area, which can be measured independently. Values of S_v are provided for fiberglass and several common particulates. Section 4.2 discusses mixture porosity and its relationship to bed thickness. Limiting conditions are described and the generalized VISTA head-loss formula is expressed for any spatial arrangement of debris properties. Finally, Section 4.3 emphasizes that fluid properties are explicitly factored in the VISTA formulation (and in 6224). Measurements of viscosity as a function of chemical concentration are presented for use in analysis of chemical loaded head-loss data.

4.1 Surface-to-Volume Ratio

Debris beds commonly encountered on recirculation strainers for nuclear safety applications are always composed of a variety of constituents that are broadly classified into groups by shape (morphology) including: (1) particulates, (2) fibers, and (3) chips. Theoretical treatments of flow resistance (pressure drop) through debris beds include parameters that describe physical attributes of the debris using locally homogeneous parameters. The term locally homogeneous means that average properties preserve the characteristics of the bed over a spatial scale comparable to the random (ergodic) variation of the flow field – typically layers on the order of 5 to 10 diameters of the debris elements (50 to 100 μm). Local homogeneity does not preclude one-dimensional spatial variations through the bed. The common challenge for implementation of theoretical equations is to use knowledge about the quantity of debris, either mass or volume, and form descriptions of composite properties that are consistent with the theory. This section discusses proper treatment of surface-to-volume ratio, S_v .

The practical challenges of calculating composite bed properties are made immediately obvious by examining electron micrographs of typical materials encountered in a debris bed. Figure 4.1.1 illustrates common fiberglass with a nominal strand diameter of ~7 microns. Figure 4.1.2 illustrates green silicon carbide with a nominal particle diameter of between 5 and 30 microns. Graded silicon carbide, used as an industrial abrasive, has commonly been used as a surrogate for failed coatings particulate. Figure 4.1.3 illustrates particulates from pulverized acrylic paint with a nominal particle diameter of 16 microns. Unqualified coatings are often assumed to degrade down to their constituent



pigment base of approximately 10 microns in size. Figure 4.1.4 illustrates tin particulates that are, in fact, nearly spherical. Tin particulates have been considered for introducing large surface areas of zinc into a chemical test environment. Figure 4.1.5 and Figure 4.1.6 illustrate iron oxide particulates that exhibit significant surface structure. Figure 4.1.7 illustrates an electron micrograph of zinc particulate used in chemical tank testing and compares similar material captured as a migrating filtrate on an in-line membrane filter.

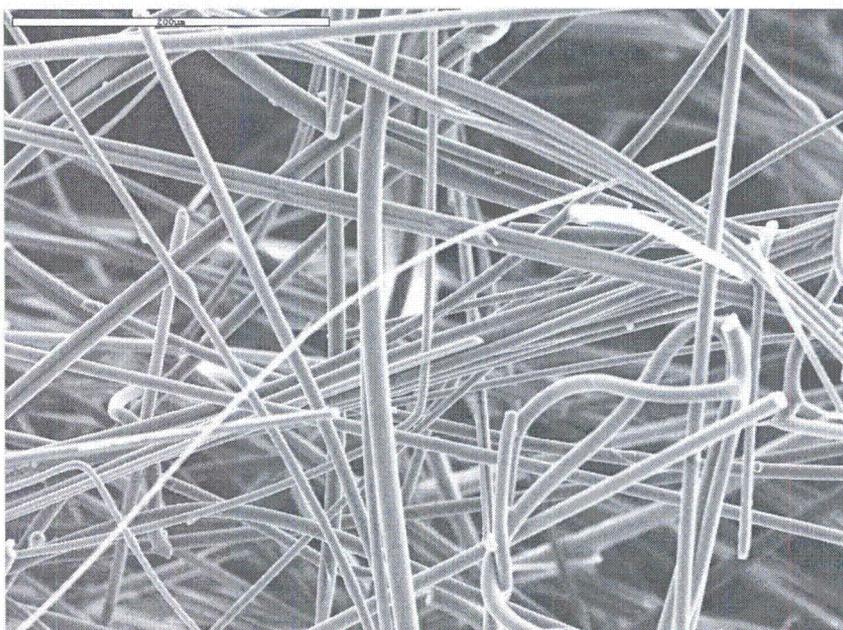


Figure 4.1.1 - Electron micrograph of common fiberglass with a nominal strand diameter of ~7 microns

(Image provided courtesy of University of New Mexico)

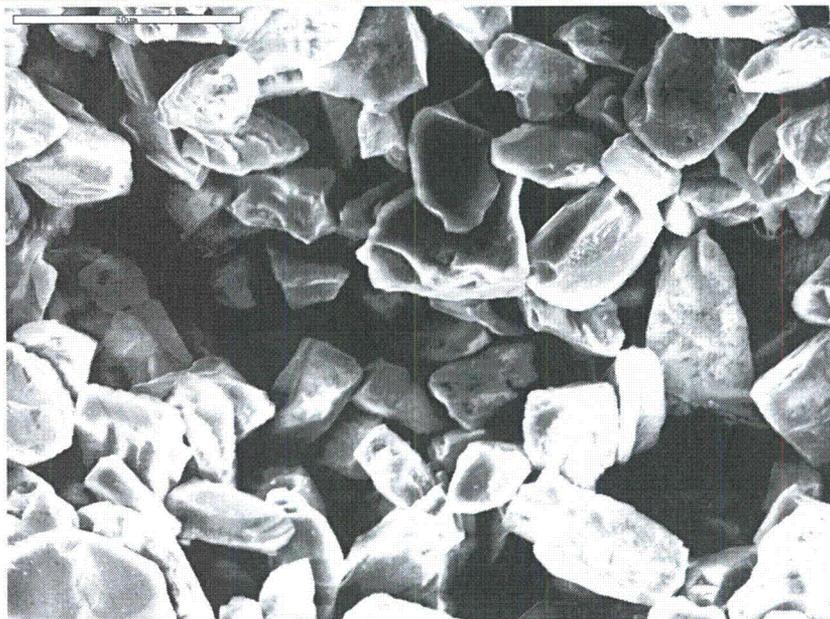


Figure 4.1.2 - Electron micrograph of green silicon carbide abrasive
(Image provided courtesy of University of New Mexico)

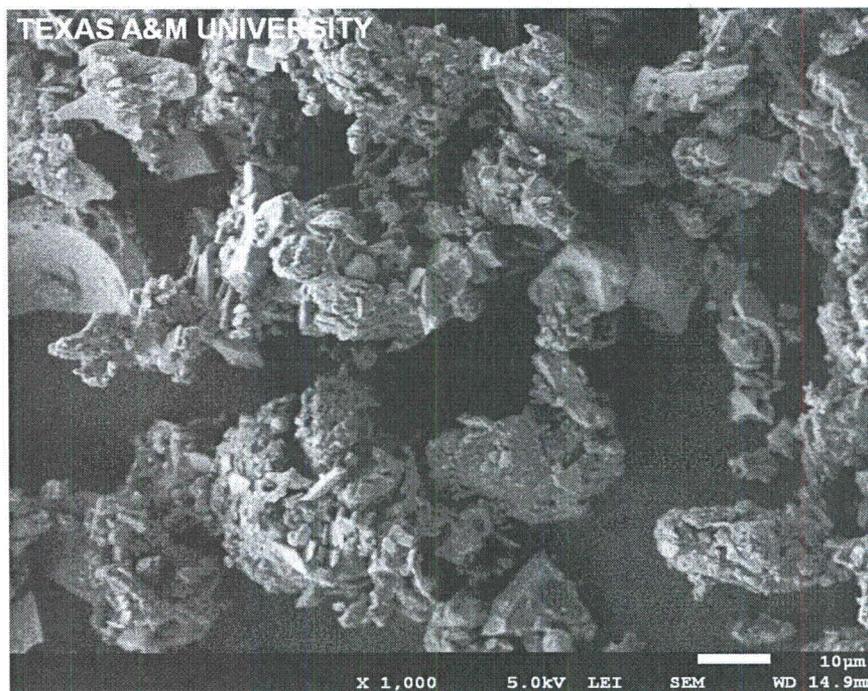


Figure 4.1.3 - Electron micrograph of pulverized acrylic paint particulates
(Image provided courtesy of Texas A&M University)

	Viscous Inertial Shear-Transition-Adaptive (VISTA) Porous Media Head-Loss Formulation for Assessment of the South Texas Project Licensing Amendment Request		
	Document No: ALION-REP-STP-8998-1 I	Rev: 0	Page 22 of 52

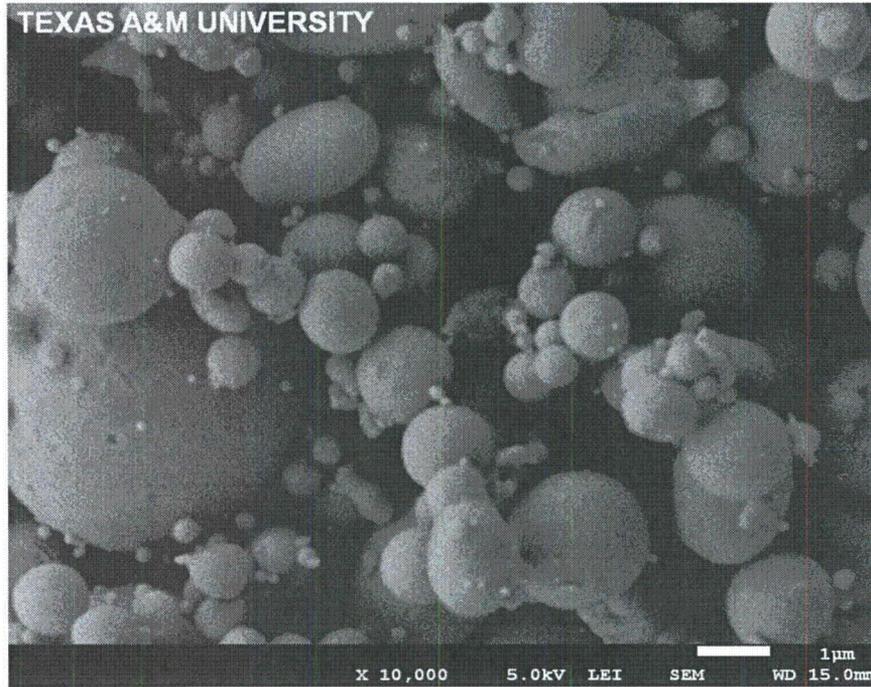


Figure 4.1.4 - Electron micrograph of tin particulate
(Image provided courtesy of Texas A&M University)

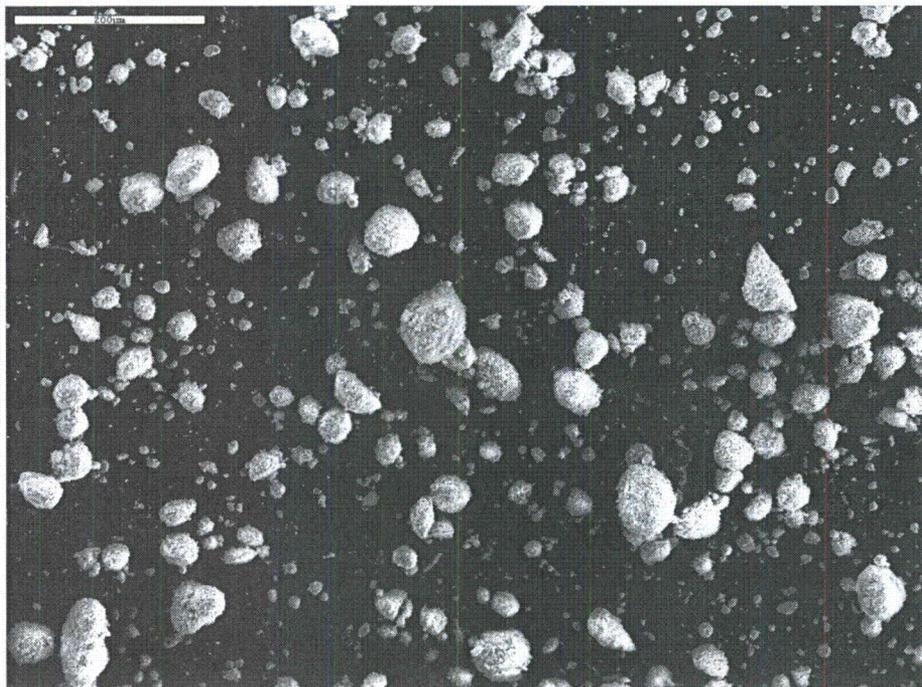


Figure 4.1.5 - Electron micrograph of iron oxide
(Image provided courtesy of University of New Mexico)

	Viscous Inertial Shear-Transition-Adaptive (VISTA) Porous Media Head-Loss Formulation for Assessment of the South Texas Project Licensing Amendment Request		
	Document No: ALION-REP-STP-8998-11	Rev: 0	Page 23 of 52

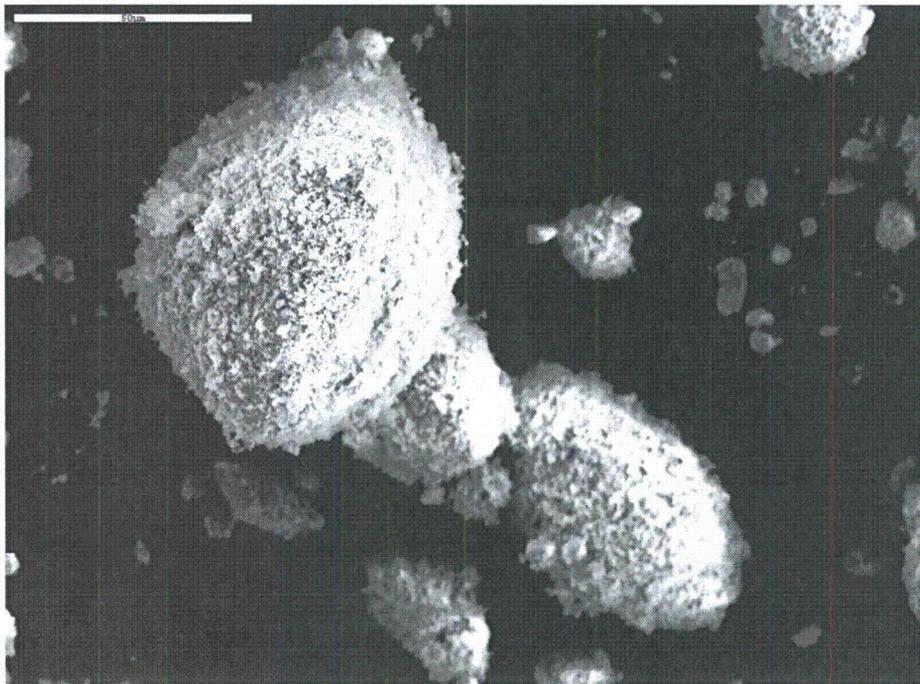


Figure 4.1.6 - Electron micrograph of iron oxide (center close up)
(Image provided courtesy of University of New Mexico)

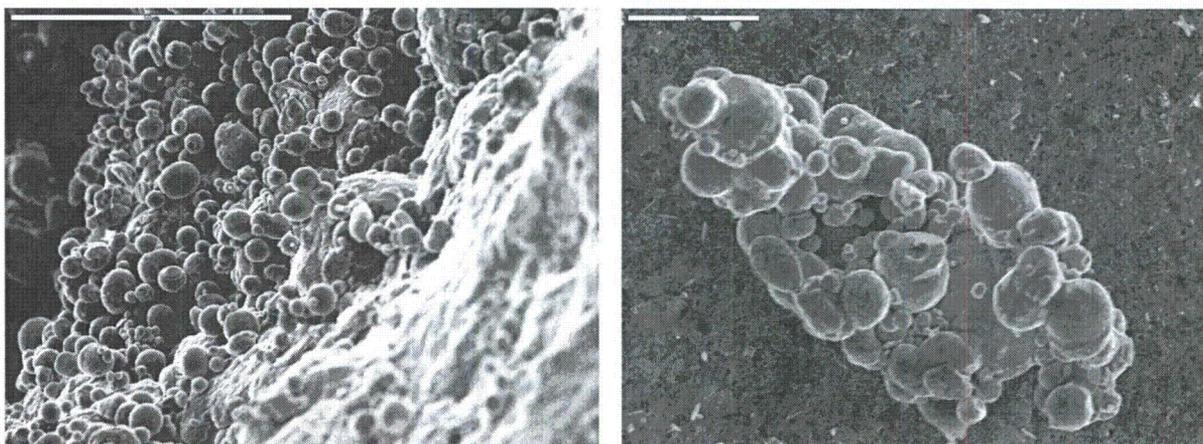


Figure 4.1.7 - Electron micrograph of zinc used in testing (left) and filtrate captured in-line
membrane filter taken after 24 hours of testing (right).
(Image provided courtesy of University of New Mexico)

Surface-to-volume ratio is sometimes improperly called “specific surface area,” which is not consistent with the usual description of “specific” properties that are expressed per unit of mass. The actual specific surface area is a very useful characteristic property that can be obtained from direct measurement of surface area within a sample of known mass. A direct application of specific surface area is provided below in Section: 5.0.

	Viscous Inertial Shear-Transition-Adaptive (VISTA) Porous Media Head-Loss Formulation for Assessment of the South Texas Project Licensing Amendment Request		
	Document No: ALION-REP-STP-8998-11	Rev: 0	Page 24 of 52

The Ergun equation (Ref. 11) and other derivations of flow in porous media based on microscopic phenomena are scaled to macroscopic flow conditions using a hydraulic radius defined in Eq. 4.0. Since the numerator $\varepsilon \nabla$ is obviously the fraction of the total volume occupied by fluid, the complement $(1 - \varepsilon) \nabla$ must be the solid volume of debris. The ratio of debris surface area to debris solid volume, S_v $\{m^2/m^3\}$, is purely a parameter of convenience that is introduced to obtain wetted area in the denominator. It is very important to understand that porosity ε and surface-to-volume ratio S_v are independent variables. This means that independently obtained values of each variable must be specified to fully describe flow conditions inside of a debris bed with fixed volume defined by ΔL_m . In essence, porosity describes the amount of empty space left in a bed and surface-to-volume ratio describes the area associated with solid that takes up space. The relationship between surface area and volume is determined by the shape and size of the debris elements, which can be extremely complex, as shown in the preceding micrographs.

The total solid volume of debris is easily computed if the material (microscopic) densities and masses are known for each constituent. Material density refers to the density of the most condensed physical elements of the debris material, which are much higher than the manufactured density of insulation composed of those materials. All insulation types contain a high fraction of void space to inhibit heat transfer. For example, the material density of the glass in fiberglass insulation is approximately 175 lbm/ft³, but the manufactured density of the insulation is only 2.4 lbm/ft³. Given the mass of constituents in the bed m_i and their respective material densities ρ_i^{mat} , the total solid debris volume is:

$$V_{debris} = \sum \frac{m_i}{\rho_i^{mat}} = \sum \left(\frac{m}{\rho^{mat}} \right)_i \quad \text{Eq. 18.0}$$

The reciprocal of density $v = 1/\rho$ is a measurable debris property called specific volume $\{m^3/kg\}$ that leads directly to the formula for solid debris volume based on measured characteristics of individual constituents. A similar measurable property for debris surface area would lead directly to a formula for solid-debris surface area:

$$A_{debris} = \sum m_i S_{Ai} \quad \text{Eq. 19.0}$$

where S_{Ai} is a legitimate specific surface area with units of $\{m^2/kg\}$. The solid area-to-volume ratio would then be

	Viscous Inertial Shear-Transition-Adaptive (VISTA) Porous Media Head-Loss Formulation for Assessment of the South Texas Project Licensing Amendment Request		
	Document No: ALION-REP-STP-8998-11	Rev: 0	Page 25 of 52

$$S_v = \frac{A_{debris}}{V_{debris}} = \frac{\sum m_i S_{Ai}}{\sum (m/\rho^{mat})_i} \quad \text{Eq. 20.0}$$

Both the numerator and denominator of Eq. 20.0 can be expressed in terms of mass-weighted average properties without changing the composite value by dividing both numerator and denominator by the total mass $M_{debris} = \sum m_i$:

$$S_v = \frac{A_{debris}}{V_{debris}} = \frac{\sum m_i S_{Ai} / M_{debris}}{\sum (m/\rho^{mat})_i / M_{debris}} = \frac{\sum w_i S_{Ai}}{\sum w_i (1/\rho^{mat})_i} = \frac{\bar{S}_A}{\bar{v}}, \quad \text{Eq. 21.0}$$

where w_i are the mass fractions of each constituent in the bed, \bar{S}_A is the mass-weighted-average specific surface area, and \bar{v} is the mass-weighted-average specific volume. Mass-weighted composite properties are commonly used in all branches of science and engineering as a matter of convenience because the mass of each constituent is so easily measured compared to any other physical property. The surface-to-volume ratio does not need to be factored or reduced any further than the expression of Eq. 21.0. The characteristic parameter S_v is simply the ratio of two summations over all debris in the bed for two different physical attributes.

Specific surface area S_A can be measured directly for various debris types like those shown in Figure 4.1.1 through Figure 4.1.7 and for composite mixtures using gas adsorption techniques attributed to Brunauer, Emmett, and Teller (BET). To determine the surface area, solid samples are pretreated by applying some combination of heat, vacuum, and/or flowing gas to remove adsorbed contaminants (typically water and carbon-dioxide) acquired from atmospheric exposure. The sample is then cooled under vacuum, usually to cryogenic temperature (77 K, -195 °C). An adsorptive (typically nitrogen or krypton) is then dosed to the solid in controlled increments. After each dose of adsorptive, the pressure is allowed to equilibrate and the quantity adsorbed is calculated. The quantity adsorbed at each pressure (and temperature) defines an adsorption isotherm, from which the quantity of gas required to form a monolayer over the external surface of the solid is determined. Theory predicts the area covered by each adsorbed gas molecule, so the total surface area can be calculated. BET analysis was used at UNM to measure specific surface areas for some of the debris types listed in Table 4.1.1. Surface-to-volume ratio is then determined using best-available material densities and the formula $S_v = \rho^{mat} S_A$.

	Viscous Inertial Shear-Transition-Adaptive (VISTA) Porous Media Head-Loss Formulation for Assessment of the South Texas Project Licensing Amendment Request		
	Document No: ALION-REP-STP-8998-11	Rev: 0	Page 26 of 52

Table 4.1.1 - BET specific surface area for several debris types.

Sample type	BET S_A (m^2/g)	assumed ρ^{mat} (g/cm^3)	S_V (m^{-1})
Clean fiberglass ^a	0.212	2.803 (175 lbm/ft ³)	594,282
NEI latent-particulate simulant ^b	19.725	2.650	52,272,000
Degraded acrylic paint ^c	0.1683	1.442	242,689
Iron Oxide ^d (red-brown)	13.2 ^f	5.03	66,396,000
Silicon Carbide ^e (green)	0.93	3.21	2,985,300

^aNominal cylindrical diameter $\sim 7 \mu m$

^bGraded silica (SiO₂) with size distribution to match prototypical latent particulate (dirt)

^cMechanically milled to $\sim 16\text{-}\mu m$ volume-median diameter

^dNominal size suggested by head-loss testing to be $\sim 11 \mu m$

^eNominal size between 5 and 30 μm

^fGood agreement with vendor catalog value of 11 m^2/g .

Direct measurements of specific surface area cannot be used indiscriminantly in pressure drop predictions, especially for microporous materials like calcium silicate insulation, because cryogenic adsorbers used in the measurement can access pore spaces much smaller (submicron) than water will freely flow through. Aqueous solutions attempting to enter submicron pore space are subject to surface tension forces at the occlusion boundary of gas (air) trapped in the pores. Internal pore pressure diverts fluid flow and creates an “effective porosity” that also limits total drag area. Effective porosity is a concept widely applied in geochemical fluid transport models. To fully understand the effective porosity of a microporous material, direct measurement of the specific surface area must be combined with concurrent measurement of the pore-size distribution (also typically provided by BET analysis) and a criterion for pore accessibility that is relevant to the rheology of the solutions and to the differential pressures expected across the debris. STP does not have any significant quantity of microporous insulation that can dominate the behavior of a composite debris bed.

Although specific surface area can be measured directly for various debris types like composite particulates, it is more common to use simple geometric approximations. The following example is illustrated using particulates that are assumed to be perfect spheres of known diameter d . Typical diameters of interest range from a few microns (10^{-6} m) up to a millimeter (10^{-3} m). The area and volume of a sphere are given as $a_{sphere} = 4\pi r^2 = \pi d^2$ and $v_{sphere} = \frac{4}{3}\pi r^3 = \frac{1}{6}\pi d^3$, so the surface-to-volume ratio of a sphere is $S_V^{sph} = 6/d$. By definition, the total area of monodimensioned spheres in a known mass would be $A_{spheres} = S_V^{sph} (m/\rho^{mat})$. For convenient reference, the surface-to-volume ratio of a cylinder (ignoring the ends) is $S_V^{cyl} = 4/d$, and the surface-to-volume ratio of a chip (ignoring the edges) is $S_V^{chip} = 2/t$ where t is the thickness.

The theoretical surface-to-volume ratio of fiberglass having a diameter of 7 μm is 571,429 m^{-1} , which matches the measured value to within 4%. This comparison for a sample with geometric regularity

	Viscous Inertial Shear-Transition-Adaptive (VISTA) Porous Media Head-Loss Formulation for Assessment of the South Texas Project Licensing Amendment Request		
	Document No: ALION-REP-STP-8998-11	Rev: 0	Page 27 of 52

builds confidence that the measurement method can be used for additive compositions of irregular elements described by Eq. 20.0 and Eq. 21.0.

The extension of geometric surface-to-volume formulas to a composite mixture of debris elements with different shapes, but known individual masses and material densities, is straightforward:

$$S_V = \frac{A_{solid}}{V_{solid}} = \frac{\sum S_{Vi} (m/\rho^{mat})_i}{\sum (m/\rho^{mat})_i} = \frac{\sum S_{Vi} (m/\rho^{mat})_i}{V_{debris}} = \sum v_i S_{Vi}, \quad \text{Eq. 22.0}$$

where v_i are the fractions of total solid volume contributed by each constituent. This formula demonstrates that when individual surface-to-volume ratios are known for each constituent debris element, the composite can be factored in the form of a linear volume-weighted average. If all specific volumes $v_i = 1/\rho_i$ are constant, Eq. 22.0 is equivalent to:

$$S_V = \frac{A_{solid}}{V_{solid}} = \frac{\sum S_{Vi} (m/\rho^{mat})_i}{\sum (m/\rho^{mat})_i} = \frac{v}{v} \frac{\sum m_i S_{Vi}}{M_{debris}} = \sum w_i S_{Vi}, \quad \text{Eq. 23.0}$$

where the w_i are mass fractions for each constituent in the bed.

The assumption of perfect geometric debris elements is a poor approximation at best and great care must be applied when a “distribution” of sizes is reported. There are many ways to report statistical distributions, for example, by mass, by diameter, by volume, and special factors must be applied to convert between them. To process a statistical distribution of debris elements like spherical particulates, the summations in the previous formulas become integrals.

It is instructive to examine a recent example of calculating composite S_V that seems to contradict intuition: when more debris is added, the composite value decreases. Recalling the definition from Eq. 20.0, the only way for S_V to decrease when debris composition changes is for the debris volume (denominator) to increase faster than the debris surface area (numerator). Consider the following table that describes a bed consisting of only 2 debris types. After the initial calculation of surface-to-volume ratio, more mass of type 2 is added to the mixture and the composite value decreases. Surface-to-volume ratio has a strong influence on predicted differential pressure drop, so a reduction in S_V will cause a reduction in ΔP unless there is a sufficiently strong reduction in porosity that compensates.

	Viscous Inertial Shear-Transition-Adaptive (VISTA) Porous Media Head-Loss Formulation for Assessment of the South Texas Project Licensing Amendment Request		
	Document No: ALION-REP-STP-8998-11	Rev: 0	Page 28 of 52

Table 4.1.2 - Simple example of composite surface-to-volume ratio for 2 spherical constituents.

	Spherical Diameter (μm)	Material Density (kg/m^3)	Initial Mass (kg)	Initial S_v (m^{-1})	Final Mass (kg)	Final S_v (m^{-1})
1	10	1490	100		100	
2	150	1986	25		30	
				512,000		1581

When more mass is added to a debris bed, every instinct says that head loss should also increase because there is more debris for fluid to pass through. While the instinct regarding overall effect may be sound, it is a mistake to believe that S_v alone must always increase with increasing debris mass in order to control ΔP . Though various approaches, like quadratic volumetric averaging, have been applied to force S_v into the desired trend for specific debris combinations, there is no reason that the homogeneous average surface-to-volume ratio cannot decrease when the relative contributions of the debris elements change. To correct any nonintuitive reduction in ΔP , one should examine the bed-averaged porosity to ensure that the added material reduces available flow volume within a bed of constant thickness.

As a final note for practical implementation of composite weighted surface-to-volume ratio, the preceding formulas apply equally well for any layer within a stratified bed as long as the basis for weighting (either mass or volume) is calculated specifically for the layer in question.

4.2 Mixture Porosity

Porous media composed of multiple constituents are typically treated as a homogeneous mixture with bulk averaged properties. Two of the most important properties are surface-to-volume ratio of the solid debris and porosity, or the amount of internal volume that permits fluid flow. Adding to the challenge is the fact that debris beds contain a variety of debris types, densities, shapes, sizes, and surface roughness factors, and the fact that fibrous debris beds compress under differential pressure. This section discusses the calculation of composite, or mixture, porosity.

The concept of composite porosity is easy to develop for a hypothetical example where there are only two debris types, like a single density of particulate and a single density of fiber. Debris of all types takes up space inside of a given volume of the porous bed, and the debris solid volume can be expressed in terms of both the “solidity”, or solid fraction of the total volume, and the ratio of mass to material density:

$$(1 - \varepsilon_m) \forall = \frac{m_f}{\rho_f^{mat}} + \frac{m_p}{\rho_p^{mat}} = \alpha_m \forall, \quad \text{Eq. 24.0}$$

	Viscous Inertial Shear-Transition-Adaptive (VISTA) Porous Media Head-Loss Formulation for Assessment of the South Texas Project Licensing Amendment Request		
	Document No: ALION-REP-STP-8998-1 I	Rev: 0	Page 29 of 52

where ε_m is the porosity, α_m is the solidity, $\forall = A\Delta L_m$ is the total bed volume of area A and thickness ΔL_m , and m_i and ρ_i^{mat} are the mass and material densities for particulate and fiber. Solving Eq. 24.0 for porosity gives:

$$\varepsilon_m = 1 - \frac{1}{A\Delta L_m} \left(\frac{m_f}{\rho_f^{mat}} + \frac{m_p}{\rho_p^{mat}} \right),$$

$$\varepsilon_m = 1 - \frac{1}{A\Delta L_m} \frac{m_f}{\rho_f^{mat}} \left(1 + \frac{m_p}{\rho_p^{mat}} \frac{\rho_f^{mat}}{m_f} \right), \quad \text{Eq. 25.0}$$

$$\varepsilon_m = 1 - \left(1 + \eta \frac{\rho_f^{mat}}{\rho_p^{mat}} \right) \frac{m_f}{\rho_f^{mat}} \frac{1}{A\Delta L_m},$$

where $\eta = m_p/m_f$ is the particle-to-fiber mass ratio.

The last two factors of Eq. 25.0 represent the ratio of fiber solid volume to total bed volume. If the fiber debris were considered as a debris bed by itself, it would have a characteristic solidity given by

$(1 - \varepsilon_0)\forall_0 = \frac{m_f}{\rho_f^{mat}} = (1 - \varepsilon_0)A\Delta L_0$. Here, the subscript 0 denotes a theoretical limit defined by the fiber-only bed response. Substituting this result in Eq. 25.0 gives:

$$\varepsilon_m = 1 - \left(1 + \eta \frac{\rho_f^{mat}}{\rho_p^{mat}} \right) (1 - \varepsilon_0) \frac{\Delta L_0}{\Delta L_m}. \quad \text{Eq. 26.0}$$

This is the form of composite porosity given as Eq. (B-22) in NUREG-CR 6224 (Ref. 1). The theoretical (manufactured) porosity of fiberglass insulation is generally assumed to be $\varepsilon_0 = 1 - \rho_f^{mfc} / \rho_f^{mat} = 0.986$.

Eq. 26.0 introduces two important concepts. First, the particle-to-fiber mass ratio η is easy to calculate from experimental data if filtration is complete and all of the material added to a test is resident in the debris bed. Second, the porosity is only well defined within a known volume. Eq. 28.0 is factored to express the finite volume as a comparison between a theoretical, fiber-only bed thickness ΔL_0 and the actual bed thickness ΔL_m , but regardless of the measure used, bed volume must be specified before porosity can be calculated.

The ratio of fiber density to particulate density requires additional thought for a composite bed of thickness ΔL_m that may contain many types of particulates and fibers. An averaging process is

	Viscous Inertial Shear-Transition-Adaptive (VISTA) Porous Media Head-Loss Formulation for Assessment of the South Texas Project Licensing Amendment Request		
	Document No: ALION-REP-STP-8998-11	Rev: 0	Page 30 of 52

required. Consider only the particulates that have a total mass of $M_p = \sum m_i$ and a total solid volume of $V_p = \sum (m/\rho^{mat})_i$. One estimate of “average” material density is:

$$\bar{\rho}_p^{mat} = \frac{M_p}{V_p} = \frac{\sum (m_p)_i}{\sum (m_p/\rho_p^{mat})_i} \text{ and } \bar{\rho}_f^{mat} = \frac{M_f}{V_f} = \frac{\sum (m_f)_i}{\sum (m_f/\rho_f^{mat})_i}.$$

The ratio needed for Eq. 26.0 is then:

$$\frac{\bar{\rho}_f^{mat}}{\bar{\rho}_p^{mat}} = \frac{\sum (m_f)_i}{\sum (m_f/\rho_f^{mat})_i} \frac{\sum (m_p/\rho_p^{mat})_i}{\sum (m_p)_i} = \frac{1}{\eta} \frac{\sum (m_p/\rho_p^{mat})_i}{\sum (m_f/\rho_f^{mat})_i},$$

which suggests that Eq. 26.0 can be written more concisely as:

$$\varepsilon_m = 1 - (1 + \xi)(1 - \varepsilon_0) \frac{\Delta L_0}{\Delta L_m}, \tag{Eq. 27.0}$$

where ξ is the particle-to-fiber volume ratio:

$$\xi = \frac{\sum (m_p/\rho_p^{mat})_i}{\sum (m_f/\rho_f^{mat})_i}. \tag{Eq. 28.0}$$

It is often common to write porosity in terms of the complement solidity $\alpha = 1 - \varepsilon$ so that:

$$\alpha_m = (1 + \xi) \alpha_0 \frac{\Delta L_0}{\Delta L_m}. \tag{Eq. 29.0}$$

The average particulate and fiber material densities can also be written as:

$$\bar{\rho}_p^{mat} = \frac{M_p}{V_p} = \frac{\sum \rho_{pi}^{mat} (m_p/\rho_p^{mat})_i}{\sum (m_p/\rho_p^{mat})_i} = \sum (v_p \rho_p^{mat})_i, \text{ and } \bar{\rho}_f^{mat} = \sum (v_f \rho_f^{mat})_i, \tag{Eq. 30.0}$$

	Viscous Inertial Shear-Transition-Adaptive (VISTA) Porous Media Head-Loss Formulation for Assessment of the South Texas Project Licensing Amendment Request		
	Document No: ALION-REP-STP-8998-11	Rev: 0	Page 31 of 52

where the v_i are constituent volume fractions. Eq. 30.0 is the standard usage for most implementations of composite density in head-loss formulas. Similarly, the average density of all solid materials in the bed can be calculated as:

$$\bar{\rho}^{mat} = \frac{M_p + M_f}{V_p + V_f} = \frac{\sum \rho_i^{mat} (m/\rho^{mat})_i}{\sum (m/\rho^{mat})_i} = \sum (v\rho^{mat})_i \tag{Eq. 31.0}$$

The final topic related to mixture porosity is bed compression, which clearly affects bed thickness through the last factor of Eq. 27.0 that in turn is defined by Eq. 15.0. In the limit of maximum compaction discussed in Section 3.2, the bed will have a maximum packing density of about $c_{max} = 65$ lb_m/ft³ (1041 kg/m³). From Eq. 24.0, it is noted that the solidity can be expressed as the ratio of debris solid volume to total bed volume, so under maximum compaction:

$$\alpha_{max} = (V_f + V_p)/V_{bed} = V_{debris} \frac{c_{max}}{M_{debris}} = \frac{c_{max}}{\bar{\rho}_{debris}^{mat}} \tag{Eq. 32.0}$$

where c_{max} is the maximum expected packing density (sometimes called the sludge limit) and $\bar{\rho}_{debris}^{mat}$ is the average material density of all debris elements. Given the maximum solidity, the minimum bed thickness can be obtained by solving Eq. 29.0:

$$\Delta L_{min} = (1 + \xi) \alpha_0 \frac{\Delta L_0}{\alpha_{max}} \tag{Eq. 33.0}$$

More problematic than the compression limit perhaps is the continuum of compression responses implied by Eq. 15.0. Eq. 17.0 stated the equilibrium condition that must exist between bed thickness and porosity given a parameterized correlation for fiber compression. The mixture porosity and complementary solidity from Eq. 27.0 and Eq. 29.0 are now substituted to obtain a statement of equilibrium that is explicit in ΔL_m and in the spatial arrangement of material properties:

$$\int_0^{\Delta L_m} \frac{bdz}{[1 - \alpha_0(1 + \xi)(\Delta L_0/\Delta L_m)]^3} \left[\frac{\rho w_A}{\mu S_v \alpha_0(1 + \xi)(\Delta L_0/\Delta L_m)} \right]^{m-1} = \frac{\mu \Delta L_0}{\rho^2 w_A^3} \left(a \frac{\Delta L_m}{\Delta L_0} \right)^{\frac{1}{\gamma}} \tag{Eq. 34.0}$$

	Viscous Inertial Shear-Transition-Adaptive (VISTA) Porous Media Head-Loss Formulation for Assessment of the South Texas Project Licensing Amendment Request		
	Document No: ALION-REP-STP-8998-11	Rev: 0	Page 32 of 52

Although the formula appears more complex, the essential nature of the iteration has not changed. Given spatial profiles of $S_v(z)$, $\xi(z)$, $b(z)$ and $m(z)$, iterate on ΔL_m until the equality is satisfied. This iteration is firmly bounded, so if no solutions are found within the range $\Delta L_{min} \leq \Delta L_m \leq \Delta L_0$, the limit having best agreement represents the desired equilibrium bed thickness.

4.3 Fluid Viscosity

To this point in the model development the word “water” has not been used to describe the liquid that passes through the debris bed. All head-loss formulas based on viscous and inertial shear factor fluid properties explicitly, and they are equally applicable to all Newtonian fluids for which shear stress is directly proportional to rate of deformation. Explicit factorization of fluid properties, including temperature-dependent viscosity and density and time-dependent velocity, enables inference of debris-bed properties from measured head-loss data because ρ , μ and w_A can be determined from direct measurement or from reference tables.

One outstanding question that often affects interpretation of head-loss predictions for ECCS applications is the potential effect of chemical loaded solutions and suspended chemical precipitates on fluid properties. Reference 12 reported <6% increase in viscosity at 22°C from background chemicals used at STP including boric acid (BA) and trisodium phosphate (TSP). Testing determined no appreciable difference in viscosity above temperatures approaching 50°C. Although measurable viscosity differences were noted as a function of shear rate, these differences were very small compared to the temperature effect across the range of shear rate tested. To support the present discussion, two common chemical precipitate surrogates, aluminum oxyhydroxide and calcium phosphate, were tested for their potential effect on fluid viscosity. Preliminary observations are that kinematic viscosity increases < 9% for the highest Al-product concentration (100 mg/L) and < 8% for the Ca-product up to 10 mg/L at the measurement temperature of 22°C.

Viscosity is a measure of a fluid’s resistance to deformation. For common aqueous liquids, dynamic viscosity (μ) is typically reported in cgs units of centipoise (cP, = 1 mPa·s, = 0.001 N·s/m²). Viscosity measurements reported here were determined using a Cannon Instruments Cannon-Fenske Routine viscometer. This instrument provides a determination of the kinematic viscosity (ν , in units of centistokes, cSt, = 1 mm² s⁻¹ = 10⁻⁶ m² s⁻¹), which is the ratio of the dynamic viscosity to the density of the fluid ($\nu = \mu/\rho$). The kinematic viscosity for water at 20°C is 1.002 cSt. The kinematic viscosity is equal to the dynamic viscosity when the density of the medium is equal to 1, as for water. For reference, the dynamic viscosity of water decreases significantly with temperature, down to ~0.8 cP at 30°C, ~0.4 at 70°C and below 0.3 cP at 100°C. Milk at 20°C is > 3 cP, while SAE 30 motor oil at the same temperature is about 200 cP.

Viscosities for various suspensions of aluminum oxyhydroxide (up to 100 mg/L) and calcium phosphate (up to 10 mg/L), both prepared from the WCAP-16530 recipe using deionized water and diluted in BA/TSP (250mM/10mM) solution at 22°C are given in Table 4.3.1 (Ref. 16). Graphic representations are provided in Figure 4.3.1 - Figure 4.3.3.

	Viscous Inertial Shear-Transition-Adaptive (VISTA) Porous Media Head-Loss Formulation for Assessment of the South Texas Project Licensing Amendment Request		
	Document No: ALION-REP-STP-8998-11	Rev: 0	Page 33 of 52

Table 4.3.1 - Kinematic viscosity measured for several concentrations of two surrogate chemical precipitates suspended in BA/TSP.

mg/L	AlOOH		Ca ₃ (PO ₄) ₂	
	ν (mm ² /s)	% change	ν (mm ² /s)	% change
0.25	1.040	1.96	0.964	-5.49
0.50	1.076	5.49	1.072	5.10
0.75	1.052	3.14	1.100	7.84
1.00	1.040	1.96	1.060	3.92
2.00	1.044	2.35	1.076	5.49
5.00	1.044	2.35	1.072	5.10
10.00	1.044	2.35	1.076	5.49
50.00	1.048	2.75	reference viscosity- BA/TSP only: 1.020	
75.00	1.056	3.53		
100.00	1.108	8.63		

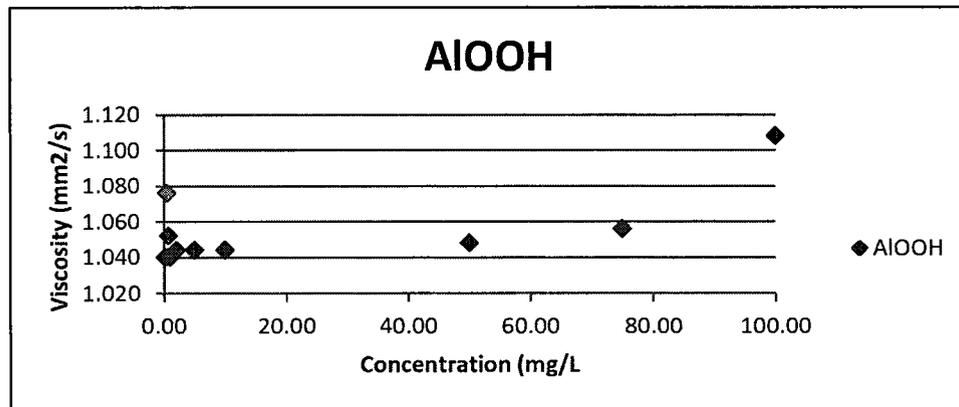


Figure 4.3.1 - Kinematic viscosity measured for concentrations of aluminum oxyhydroxide (AlOOH) precipitate suspended in boric acid/TSP solution.

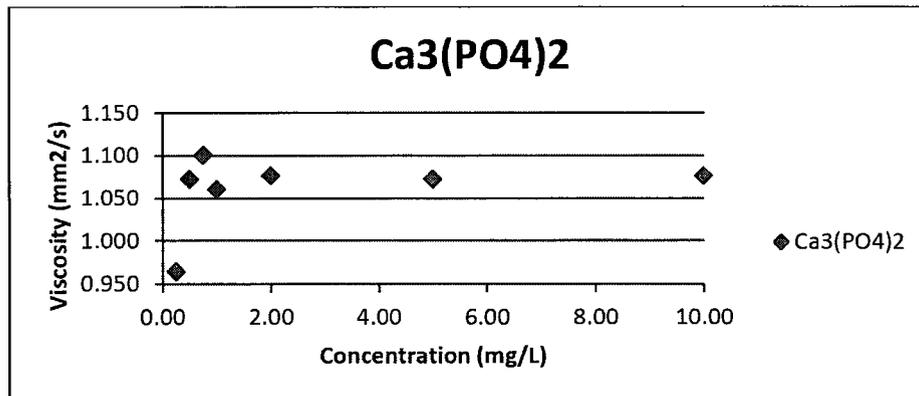


Figure 4.3.2 - Kinematic viscosity measured for concentrations of calcium phosphate (Ca₃(PO₄)₂) precipitate suspended in boric acid/TSP solution.

	Viscous Inertial Shear-Transition-Adaptive (VISTA) Porous Media Head-Loss Formulation for Assessment of the South Texas Project Licensing Amendment Request		
	Document No: ALION-REP-STP-8998-11	Rev: 0	Page 34 of 52

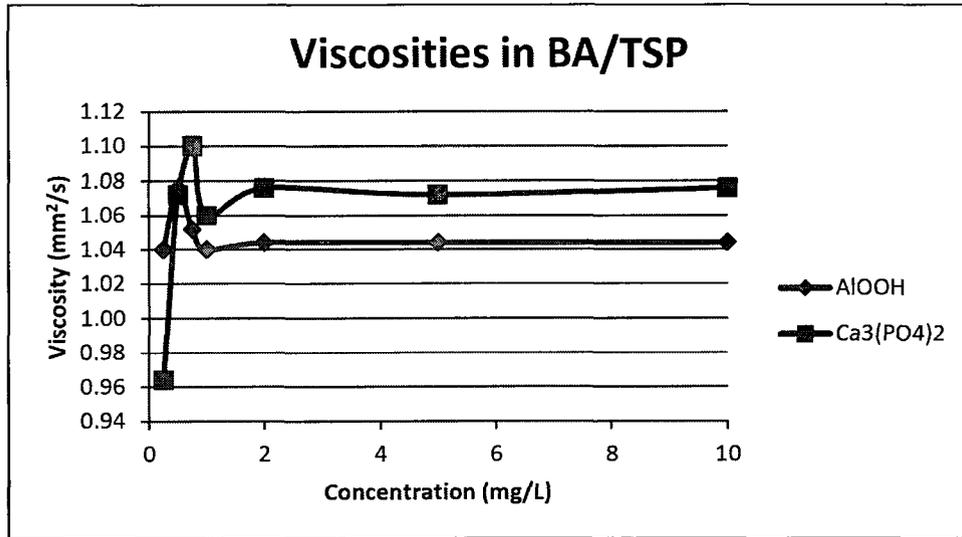


Figure 4.3.3 - Comparison over a common range of kinematic viscosity measured independently as a function of aluminum oxyhydroxide and calcium phosphate precipitate concentration.

All measurements reported in Table 4.3.1 were taken within a period of 3 hours following preparation of a single batch of WCAP-16530 chemical precipitate. Samples from the batch were extracted for dilution to the desired concentration in order of increasing concentration. At higher concentrations closer to the end of the series, it was noted that particle size and/or concentration began to interfere with the capillary viscosimeter, particularly for the calcium phosphate. A complete study of chemical product viscosity should consider use of rotational viscosimeters over a range of temperature and time histories to account for possible ripening of the suspension. Although the effect may be more pronounced for calcium phosphate, both flume testing and vertical column testing consistently report lower head-loss impacts for calcium phosphate addition than for aluminum oxyhydroxide addition. Also, note that these preliminary measurements were performed at 22°C where agglomeration may be more likely than at the lowest ECCS temperatures of interest.

Figure 4.3.4 illustrates the kinematic viscosity for pure water over the full range of temperature experienced at STP, and compares a 10% increase that is presumed to occur for chemical products under the assumption of common temperature dependence between pure water and chemical solution. Care must be exercised to use fluid property data that is specific to the problem at hand.

	Viscous Inertial Shear-Transition-Adaptive (VISTA) Porous Media Head-Loss Formulation for Assessment of the South Texas Project Licensing Amendment Request		
	Document No: ALION-REP-STP-8998-1 I	Rev: 0	Page 35 of 52

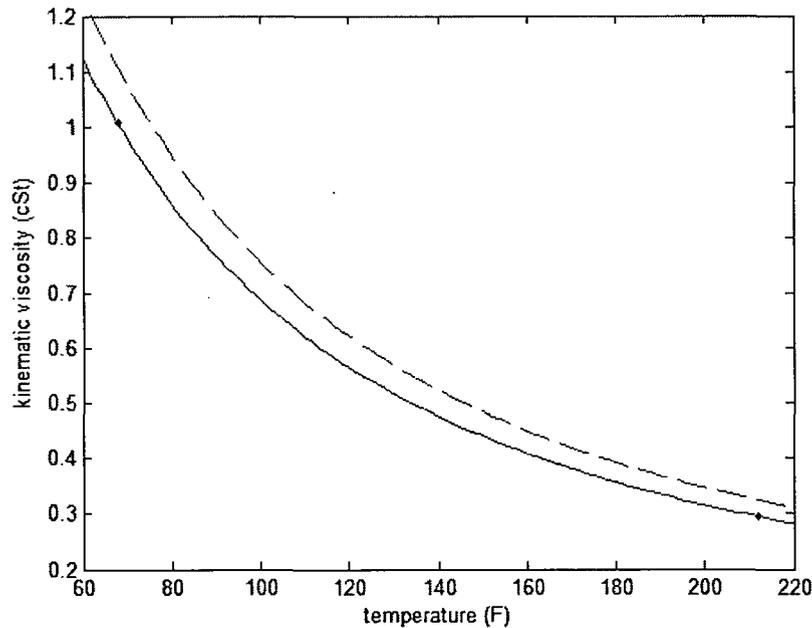


Figure 4.3.4 - Kinematic viscosity for pure water over temperature range of interest for EECS applications. (Ten percent increase shown as red dash for comparison).

5.0 CALIBRATION TO HEAD-LOSS MEASUREMENTS

Eq. 16.0 provides a general formula for head-loss prediction that accommodates spatial variations in bed properties, but the model can be calibrated to data collected under homogeneous bed conditions where there is no severe influence from stratification and the bed properties are relatively well known. For uniform beds under uniform compression described by Eq. 15.0:

$$\frac{\Delta P}{\Delta L_0} = \frac{\rho^2 w_A^3}{\mu \varepsilon^3} \frac{b}{\varepsilon^3} Re^{m-1} \frac{\Delta L_m}{\Delta L_0},$$

$$\vdots$$

$$\frac{\Delta P}{\Delta L_0} = \left[\frac{b}{a} \frac{\rho^2 w_A^3}{\mu \varepsilon^3} \left(\frac{\rho w_A}{\mu(1-\varepsilon)S_V} \right)^{m-1} \right]^{\frac{1}{1+\gamma}} \quad \text{Eq. 35.0}$$

Using high-temperature vertical loop (HTVL) test data for ΔP , Eq. 35.0 can be used to find least-squares, best-fit solutions for the unknown parameters b/a , $m-1$, and $1/(1+\gamma)$. Once these parameters are quantified over a range of Re , they can be applied in Eq. 16.0 to predict head-loss for postulated debris configurations.

	Viscous Inertial Shear-Transition-Adaptive (VISTA) Porous Media Head-Loss Formulation for Assessment of the South Texas Project Licensing Amendment Request		
	Document No: ALION-REP-STP-8998-11	Rev: 0	Page 36 of 52

Nonlinear optimization techniques are required to simultaneously infer the compression parameters, so for this exercise, the standard recommend values $\bar{a} = 1.3$ and $\gamma = 0.38$ are applied. It is further assumed that the fiber bed does not expand when the differential pressure decreases during the test. In other words, bed thickness is forced to be monotonically decreasing except when debris is being added.

Table 5.1 describes HTVL tests conducted for STP (Ref. 13) that have been identified for calibrating and exercising the alternative head-loss formulation. STP Test 6 – Series 2, was chosen for initial calibration of the VISTA drag parameters because a very uniform debris bed was formed by adding 12 small batches of fiber and particles in constant proportions to borated-buffered aqueous solutions. Figure 5.1 illustrates the relatively complex temperature, velocity, and head-loss history experienced during the test. Figure 5.2 illustrates the viscosity and density traces that existed during the test. Although borated-buffered solution was used for all tests, test temperatures were also elevated above 50°C, indicating no need for any additional viscosity increase above pure water to account for background chemicals. Figure 5.3 illustrates the internal flow Reynolds number that changes as a function of flow conditions through the static bed. No information was available regarding the thickness of the debris bed, so standard parameters were assumed for the 6224 compression function with no additional constraints from observation. Figure 5.4 illustrates the bed thickness as a function of time that was found to be consistent with measured pressure drops that were selected to be monotonically increasing to emulate continuous compression.

	Viscous Inertial Shear-Transition-Adaptive (VISTA) Porous Media Head-Loss Formulation for Assessment of the South Texas Project Licensing Amendment Request		
	Document No: ALION-REP-STP-8998-11	Rev: 0	Page 37 of 52

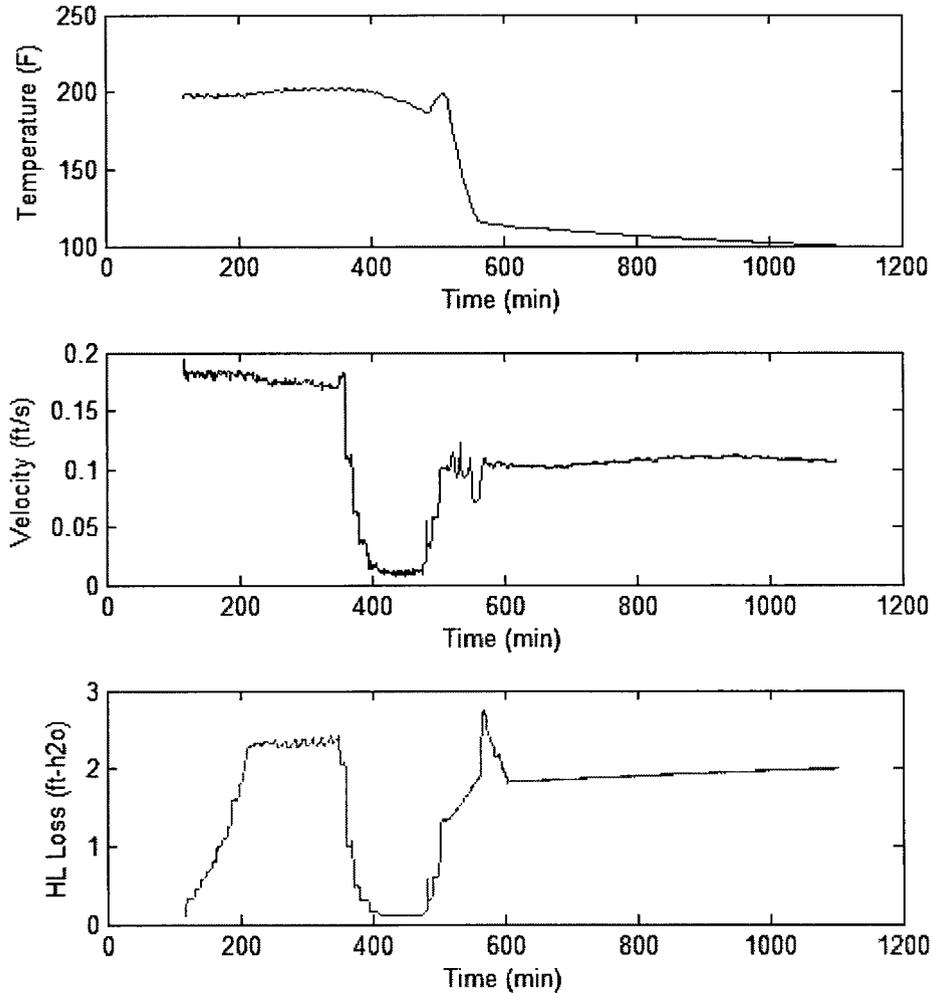


Figure 5.1 - Temperature, velocity and head-loss history experienced during test STP Test 6, Series 2 (Ref. 13).

	Viscous Inertial Shear-Transition-Adaptive (VISTA) Porous Media Head-Loss Formulation for Assessment of the South Texas Project Licensing Amendment Request		
	Document No: ALION-REP-STP-8998-11	Rev: 0	Page 38 of 52

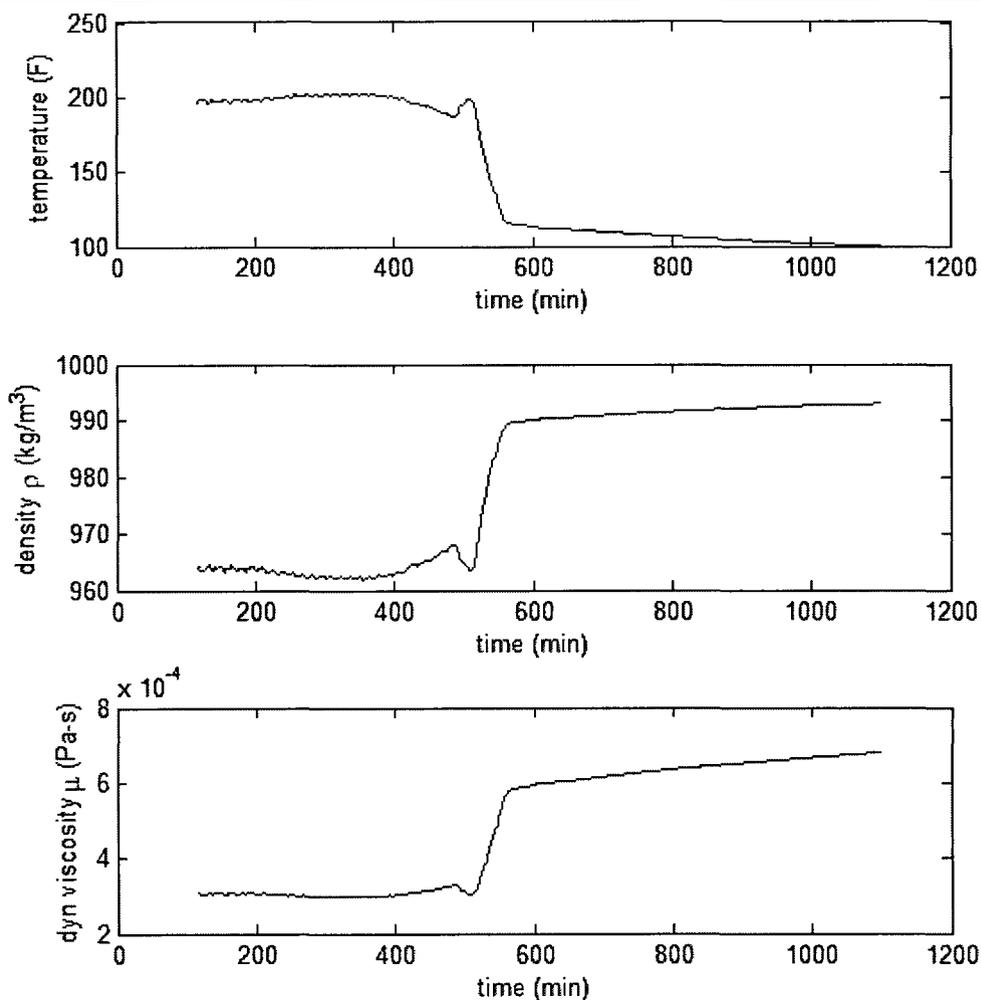


Figure 5.2 - Water properties that existed during STP Test 6 – Series 2.

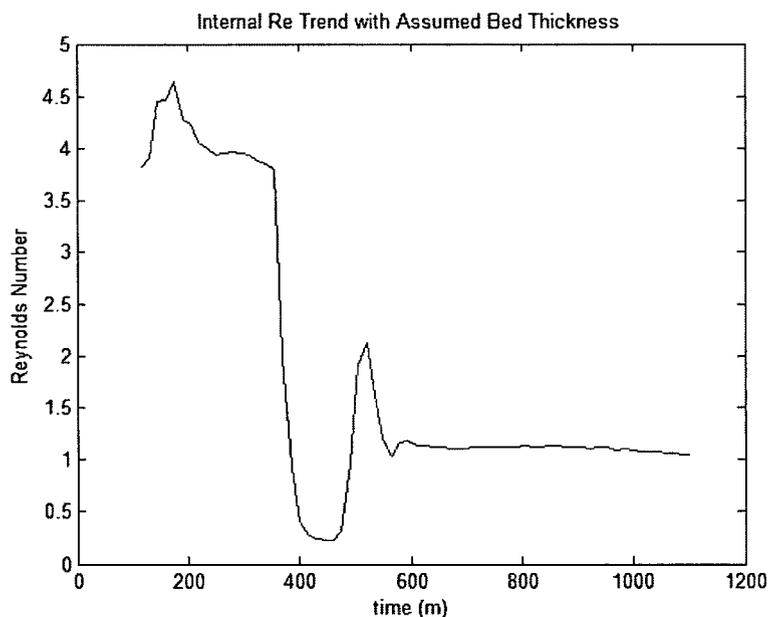


Figure 5.3 - Time-dependent internal flow Reynolds number during STP Test 6 – Series 2.

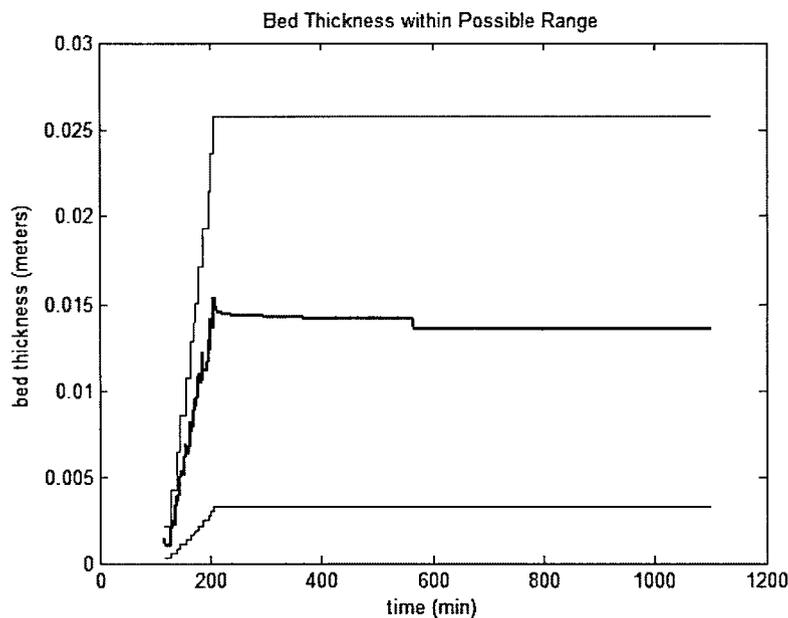


Figure 5.4 - Computed bed thickness (red) consistent with measured pressure between upper and lower theoretical limits.

Recall that the objective of the VISTA drag correlation is to collapse all factors of internal bed complexity onto the internal flow Reynolds number that is then used to index a low-order power law drag coefficient. A notional *a priori* trend for the drag law is shown in Figure 3.1.1 with a region of expected interest where the drag function is essentially a straight line in log-log space. Figure 5.5

	Viscous Inertial Shear-Transition-Adaptive (VISTA) Porous Media Head-Loss Formulation for Assessment of the South Texas Project Licensing Amendment Request		
	Document No: ALION-REP-STP-8998-11	Rev: 0	Page 40 of 52

illustrates the remarkable agreement with expectation that is obtained by correlating data from the preceding plots for STP Test 6. Nearly linear log-log drag coefficients computed as $C_{drag}(Re) = bRe^m$ are obtained within a factor of 2 over exactly the Reynolds range expected. Best-fit coefficients from the calibration test are $b = 3.14$ and $m = -0.49$. Presumably, agreement would improve with use of a higher fidelity compression model and observational evidence to use as a constraint on maximum compression.

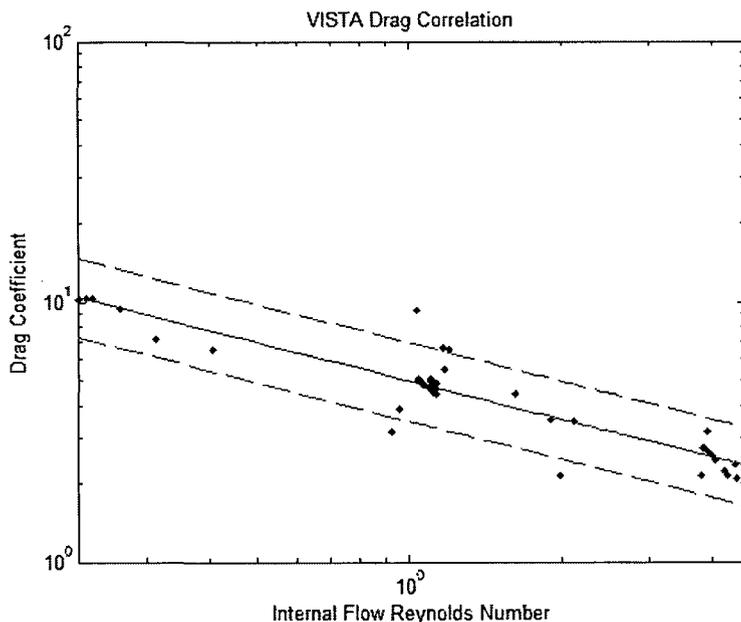


Figure 5.5 - VISTA drag correlation from single calibration test with uniform combination of fiber and acrylic paint particulate obtained using measured surface-to-volume ratios.

	Viscous Inertial Shear-Transition-Adaptive (VISTA) Porous Media Head-Loss Formulation for Assessment of the South Texas Project Licensing Amendment Request		
	Document No: ALION-REP-STP-8998-11	Rev: 0	Page 41 of 52

Table 5.1- STP HTVL data records available for analysis (Ref. 13)

#	Description	Assessment	Calibrate/Predict
Test 1	All Nukon added then all SiC	Possible initial strata with particulate infusion. Tends toward homogeneous over time	Prediction
Test 2	Discrepancy b/t graphs and text description	Data value is indeterminant	Not used
Test 3	SiC then all Nukon then SiC	Particulate infusion and low fiber tends toward homogeneous. Much higher particulate to fiber ratio than Test 1	Prediction
Test 4	Nukon and SiC added in constant proportion	12 small equal batches of fiber and SiC Should be homogeneous	Calibration or Prediction
Test 5	Nukon and Iron Oxide added together in constant proportion	12 small equal batches of fiber and iron oxide Should be homogeneous	Calibration or Prediction
Test 6	Nukon and Acrylic added together in constant proportion	12 small equal batches of fiber and acrylic Should be homogeneous	Calibration or Prediction
Test 7	Nukon and Tin added together in constant proportion	Should be homogeneous No measurements avail for tin Sv	Not used
Test 8	Mixed particles first, then Nukon – similar to ARL flume test (Ref. 15)	Should be homogeneous No meas'd Sv for tin, μ Therm, Marinite No dP response to flow spike? Suspect results for clean strainer calibration?	Not used
Test 9	Like Test 8 but different order - Tin and Microtherm last	May have strata No meas'd Sv for tin, μ Therm, Marinite Some Nukon+Acrylic only data available	Not used
Test 10	Nukon and Acrylic added together in constant proportion	Should be homogeneous	Calibration or Prediction
Test 11	Nukon and Acrylic added together in constant proportion	Should be homogeneous	Calibration or Prediction

6.0 ITERATIVE HEAD-LOSS PREDICTION

After all coefficients are determined for bed compression and for the VISTA drag correlation, spatial distributions must be assumed for debris properties within the bed so that predictive head-loss formulas can be evaluated to predict head-loss for a given fluid and flow regime. Head-loss prediction is complicated by the effect of iterative compression, which depends internally on the differential pressure. A two-step process requires that Eq. 17.0 be iterated to determine equilibrium bed thickness ΔL_m before Eq. (16) is integrated to obtain the desired prediction of ΔP . Bed thickness is determined by iterating the following formula on the ratio $r_m = \Delta L_0 / \Delta L_m$:

	Viscous Inertial Shear-Transition-Adaptive (VISTA) Porous Media Head-Loss Formulation for Assessment of the South Texas Project Licensing Amendment Request		
	Document No: ALION-REP-STP-8998-11	Rev: 0	Page 42 of 52

$$C_1 \int_0^1 \frac{[S_v(1+\xi)]^{1-m}}{[1-\alpha_0 r_m(1+\xi)]^3} dt = r_m^{1/\gamma}, \quad \text{Eq. 36.0}$$

where

$$C_1 = (r_m^{1-m} \Delta L_m) \alpha_0^{1-m} a^{1/\gamma} b \left[\frac{\rho^2 w_A^3}{\mu \Delta L_0} \right] \left[\frac{\rho w_A}{\mu} \right]^{m-1}. \quad \text{Eq. 37.0}$$

Note that the VISTA head-loss formulation allows explicit scaling of spatial bed variations to the total thickness so that convenient profiles of the bed properties $S_v(z)$ and $\xi(z)$ can be defined on a relative scale of proportional distance from top to bottom.

Corresponding pressure drop is then obtained for known ΔL_m using:

$$\Delta P = C_2 \int_0^1 \frac{[S_v(1+\xi)]^{1-m}}{[1-\alpha_0 r_m(1+\xi)]^3} dt, \quad \text{Eq. 38.0}$$

where

$$C_2 = \frac{1}{\mu} b \rho^2 w_A^3 \Delta L_m \left[\frac{\rho w_A}{\mu} \right]^{m-1} (\alpha_0 r_m)^{1-m}. \quad \text{Eq. 39.0}$$

Because the spatial integral is isolated, all questions regarding effects of bed orientation can be answered by examination of the spatial integral alone. Note that in the ratio of two pressure loss measurements taken in systems with identical fluid and flow conditions, the constant C_2 cancels leaving only the comparative effect of differing spatial distributions. Questions regarding the sensitivity of pressure drop to most other leading factors are easily answered by computing derivatives of ΔP with respect to the parameter of interest. However, the effects of ΔL_0 and ΔL_m cannot be isolated easily because of their appearance in the ratio r_m under the integral.

	Viscous Inertial Shear-Transition-Adaptive (VISTA) Porous Media Head-Loss Formulation for Assessment of the South Texas Project Licensing Amendment Request		
	Document No: ALION-REP-STP-8998-11	Rev: 0	Page 43 of 52

Any suitable integration scheme can be applied to evaluate the common integral appearing in Eq. 36.0 and Eq. 38.0. Under the simple assumption of uniform properties within N layers of finite width Δt_i , the equations can be expressed as:

$$C_1 \sum_{i=1}^N \frac{[S_v (1 + \xi_i)]^{1-m}}{[1 - \alpha_0 r_m (1 + \xi)]^3} \Delta t_i = r_m^{1/\gamma} \quad \text{Eq. 40.0}$$

and

$$C_2 \sum_{i=1}^N \frac{[S_v (1 + \xi_i)]^{1-m}}{[1 - \alpha_0 r_m (1 + \xi)]^3} \Delta t_i = \Delta P. \quad \text{Eq. 41.0}$$

Uniform bed properties were assumed to predict pressure drop for the calibration test using global VISTA parameters determined in the previous Section. Figure 6.1 compares the measured head loss to the head loss predicted using the two-step formulas given above for the calibration test. In this prediction, bed-thickness relaxation was not suppressed. Notice that after flow resumes at 500 min, the prediction underestimates the measurement because the standard compression formula has no awareness of prior compaction. During initial bed formation and pseudo steady-state flow (up to 400 min), the prediction shows good agreement with the measurement as illustrated in the Figure 6.2 correlation plot. Dashed bands indicate factors of 1.5 above and below the diagonal line that represents perfect correlation.

	Viscous Inertial Shear-Transition-Adaptive (VISTA) Porous Media Head-Loss Formulation for Assessment of the South Texas Project Licensing Amendment Request		
	Document No: ALION-REP-STP-8998-11	Rev: 0	Page 44 of 52

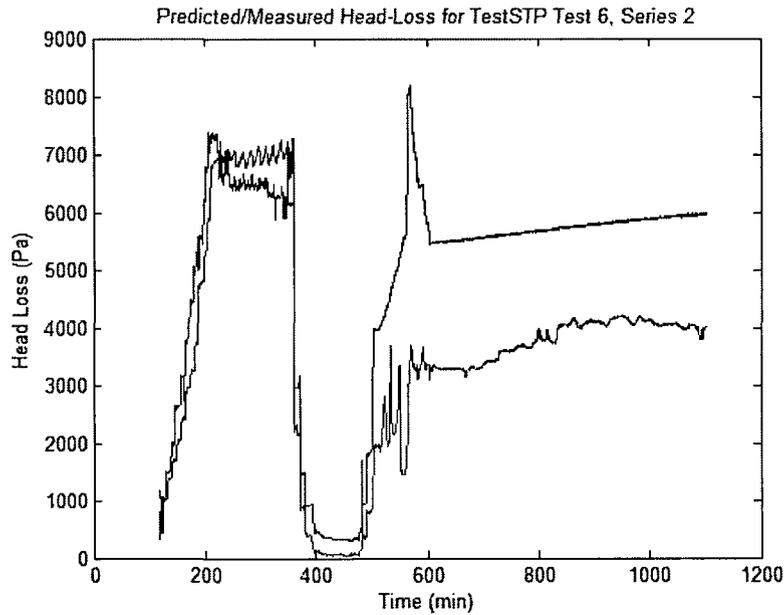


Figure 6.1 - Prediction of differential pressure history (red) compared to measurement.

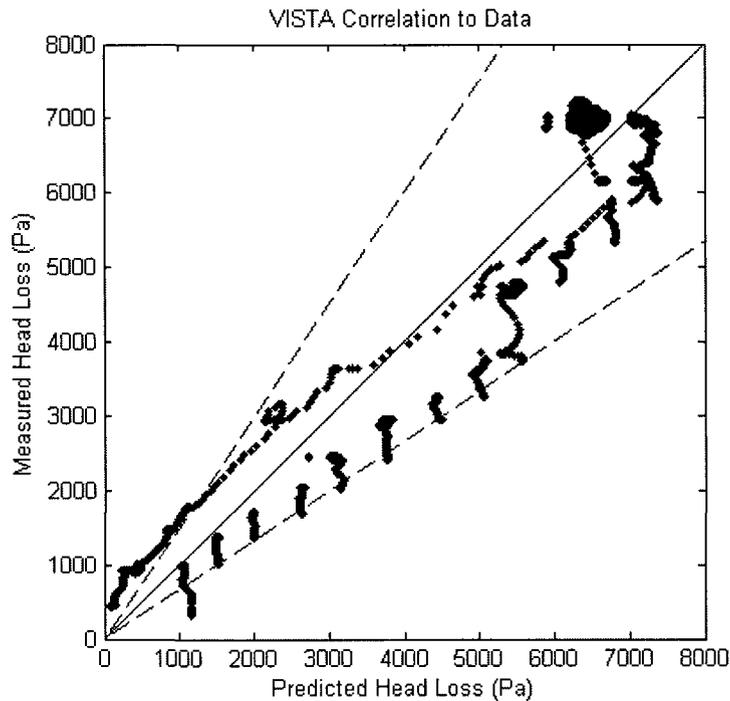


Figure 6.2 - Correlation of VISTA prediction to calibration data during initial bed formation and steady-flow operation.

	Viscous Inertial Shear-Transition-Adaptive (VISTA) Porous Media Head-Loss Formulation for Assessment of the South Texas Project Licensing Amendment Request		
	Document No: ALION-REP-STP-8998-11	Rev: 0	Page 45 of 52

7.0 PERFORMANCE COMPARISON

In this section the VISTA head-loss correlation is exercised against specific case studies to provide supplementary information for RAI responses. Subsection 7.1 uses model calibration data derived from an acrylic particulate test to predict pressure drop from a silicon carbide particulate test. Subsection 7.2 compares VISTA results for the selected validation test to the STP LAR implementation of NUREG/CR-6224. Subsection 7.3 examines two conditions of bed stratification that are of greatest potential concern: (1) low-porosity chemical loading on the top surface of a composite debris bed, and (2) low-porosity impaction of fiberglass in the strainer-plate orifices.

7.1 Blind Prediction of Silicon Carbide Test

One measure of robustness for a head-loss correlation is the ability to predict differential pressure drop under flow conditions and debris bed compositions that differ from the calibration data that were used to determine free parameters. HTVL Test 4 introduced silicon carbide (SiC) and Nukon fiber together in constant proportions under temperature and flow conditions that differ from the calibration Test 6. Pressure drop, temperature and flow rate data for Test 4 are shown in Figure 7.1.1. VISTA parameters determined from the Reynolds flow conditions presented in Test 6 were used to predict the differential pressure trace provided in Figure 7.1.2. A correlation plot of the measured vs. predicted pressure drop (Figure 7.1.3) shows good agreement over the full range of test conditions.

Visual comparison of Figure 5.1 and Figure 7.1.1 emphasizes that substantially different flow conditions can be characterized on a common basis using Reynolds similitude. This foundation of the VISTA model provides a more robust definition of applicable test conditions than the traditional view of minimum to maximum ranges on flow rate, temperature and debris ratios. In effect, similar Reynolds conditions can be established through many combinations of bed porosity, composite surface-to-volume ratio, temperature and velocity (see all factors of Eq. 6.0). The agreement achieved between the calibration and the blind comparison test illustrates the power of explicitly factoring as much independently measurable information as possible in a physically consistent theoretical basis. Consistency of theory with the phenomena reduces the burden placed on free parameters to maintain stable predictions over a wide range of conditions.

	Viscous Inertial Shear-Transition-Adaptive (VISTA) Porous Media Head-Loss Formulation for Assessment of the South Texas Project Licensing Amendment Request		
	Document No: ALION-REP-STP-8998-11	Rev: 0	Page 46 of 52

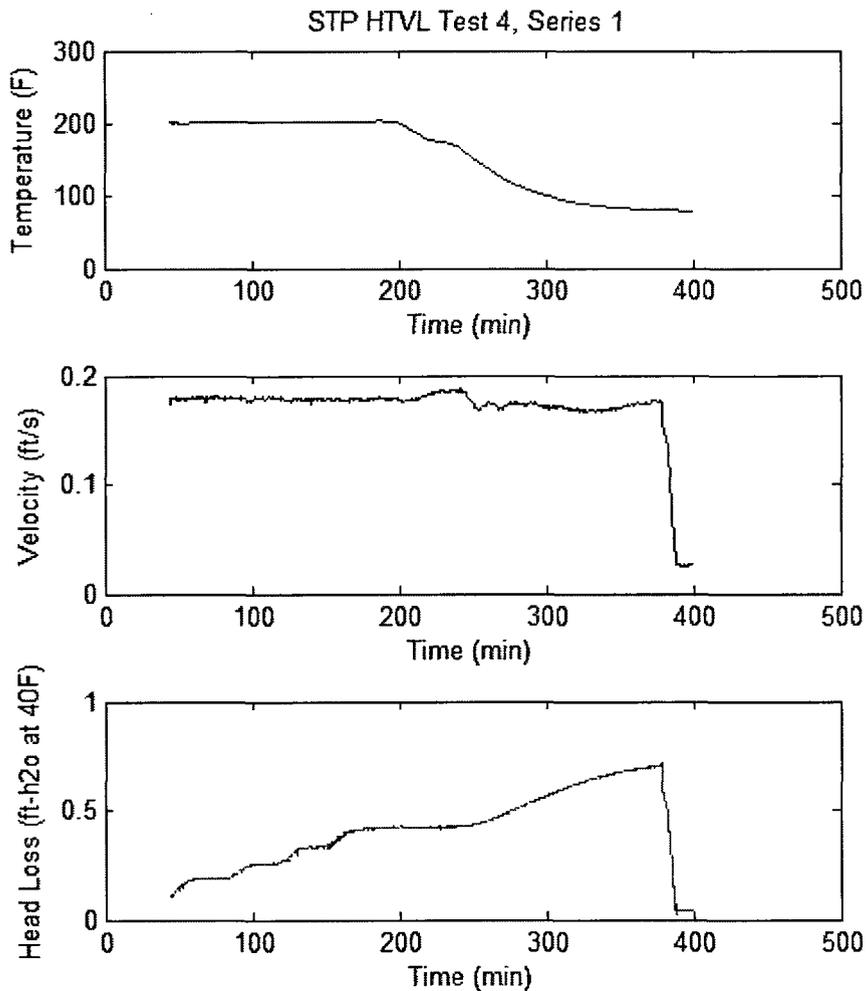


Figure 7.1.1 - Raw data history for STP Test 4 that included Nukon fiber and SiC particulate.

	Viscous Inertial Shear-Transition-Adaptive (VISTA) Porous Media Head-Loss Formulation for Assessment of the South Texas Project Licensing Amendment Request		
	Document No: ALION-REP-STP-8998-11	Rev: 0	Page 47 of 52

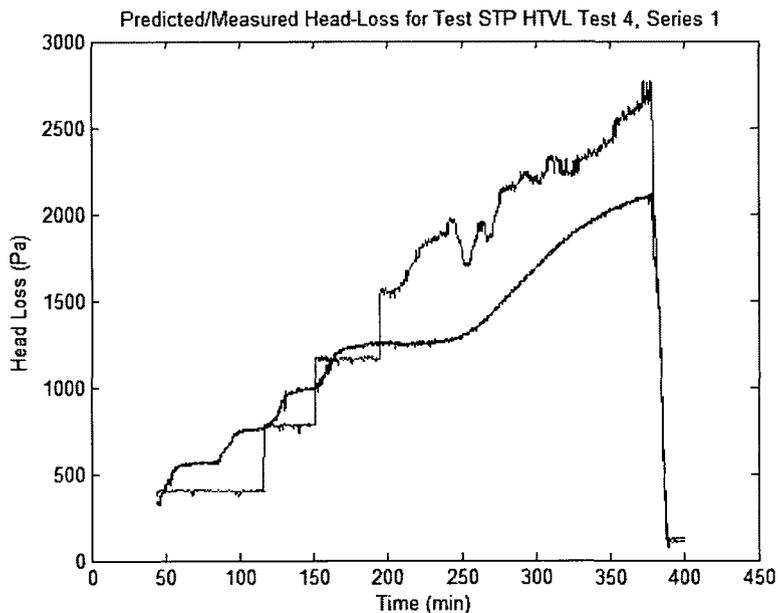


Figure 7.1.2 - VISTA blind prediction of head loss (red) compared to Test 4 measured head loss (black).

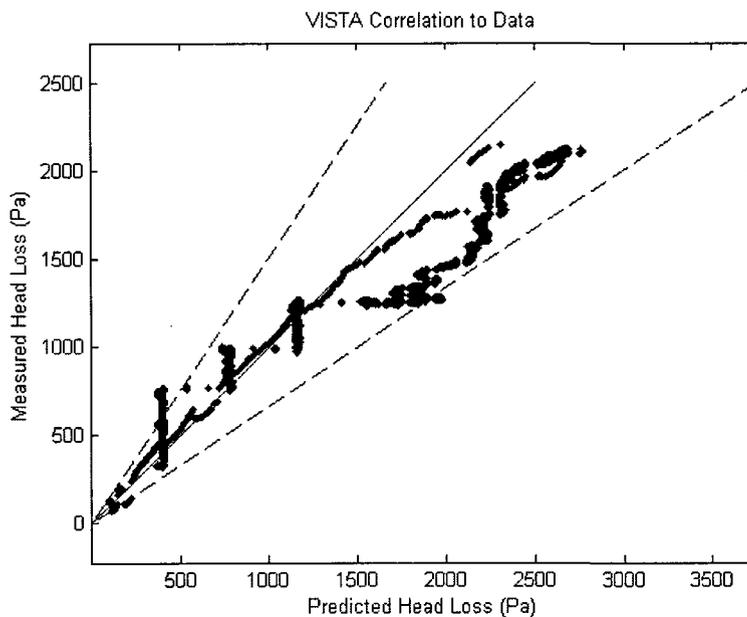


Figure 7.1.3 - Correlation plot of measured head loss (y axis) vs. predicted head loss (x axis) for Test 4 containing NUKON fiber and silicon carbide particulate.

	Viscous Inertial Shear-Transition-Adaptive (VISTA) Porous Media Head-Loss Formulation for Assessment of the South Texas Project Licensing Amendment Request		
	Document No: ALION-REP-STP-8998-11	Rev: 0	Page 48 of 52

Like any other head-loss correlation, VISTA depends on some knowledge or assumption about the distribution of porosity and drag area through the bed. Calibration tests can always be contrived to achieve homogeneous configurations, but alternative geometries including low-porosity strata and nonuniform compaction have been observed in practice. Like NUREG/CR-6224, VISTA predictions are sensitive to the degree of compression assumed for evaluation. This does not represent a deficiency of either model, but rather, is indicative of variability in the boundary conditions under which they are applied. Parameter studies of various configurations can be examined to help the degree of sensitivity, and test experience in combination with CASA Grande (Ref. 17) survey of debris and flow conditions can help judge the likelihood that extreme conditions will occur.

The greatest uncertainty encountered in this development so far has been the impact of the power-law compression model on the range of calculated Reynolds conditions. A suitable head-loss correlation will provide reasonably bounding predictions for all configurations given a definition of the spatial profile through the bed thickness. This is the primary rationale for evaluating the maximum compaction limit for the STP LAR, because the assumption reduces variability in the boundary conditions. However, the VISTA equations are amenable to iteration for any desired compression formula. Reference 6 suggests several theoretical treatments of bed compression, including analytic solutions for nonuniform compression under accumulated low-velocity hydraulic drag that can be used to guide an outer iteration on the discretized VISTA equations that will better match in situ conditions.

7.2 Sufficiency of NUREG/CR-6224 Correlation

HLOSS version 1.1 (Ref. 7) is an Alion proprietary software that estimates head loss by implementing the basic head-loss correlation presented in NUREG/CR-6224. This software was verified and validated under Alion's Quality Assurance Program.

HLOSS version 1.1 was run to simulate the same conditions as STP Series 2 Test 6 before the flow sweep and at the test conclusion. All the debris was assumed to be filtered by the debris bed at these instances. The maximum debris bed solidity within HLOSS was assumed to be 0.2. Table 6 compares head losses predicted by VISTA and HLOSS to the measured head loss.

Table 7.2.1 - VISTA, HLOSS (NUREG/CR-6224), and Test Head Loss Comparison

Instance	Test Head Loss (ft)	HLOSS Head Loss (ft)	VISTA Head Loss (ft)
Before Flow Sweep	2.1	2.3	2.3
Test Conclusion	2.0	2.8	1.3

The VISTA and HLOSS correlations over-predicted the head loss before the flow sweep. At the test conclusion HLOSS over-predicted the results, while VISTA under-predicted the result because the bed was allowed to fully recover porosity. In both cases the NUREG/CR-6224 correlation replicated or bounded the head loss predicted by VISTA.

This comparison demonstrates that the 6224 correlation is capable of reproducing realistic head-loss behavior for a composite debris test. VISTA development illustrates that the range of flow

	Viscous Inertial Shear-Transition-Adaptive (VISTA) Porous Media Head-Loss Formulation for Assessment of the South Texas Project Licensing Amendment Request		
	Document No: ALION-REP-STP-8998-11	Rev: 0	Page 49 of 52

conditions experienced in any single test is much broader than simply one flow and one bed condition. The VISTA correlation reproduces the entire test history with reasonable accuracy affected only by compressibility assumptions. Table 7.1.1 above illustrates that all conditions experienced during this test would have passed STP performance criteria and that two independent head-loss models are capable of reproducing realistic pressure drops. The STP LAR applies the 6224 correlation in combination with assumptions of maximum compressibility and a factor of x5 uncertainty bound. Under these assumptions, the test case would fail STP performance criteria and increase core damage frequency.

7.3 Stratified Debris Bed Case Studies

A stratified debris bed consists of finite layers with differing properties that may be modeled using the VISTA correlation. The following examples predict head losses of a debris bed with low-porosity strata in differing locations. Table 7.3.1 defines the geometry of a stratified debris bed with a normalized thickness. The thickness and properties of each region can be defined to emulate either (1) a low-porosity layer of chemicals at the top of the bed, or (2) a low-porosity layer of fibers impacted in strainer-plate holes. Recall that the compression model presently assumes independent uniform compression of each layer where the properties are defined to be different.

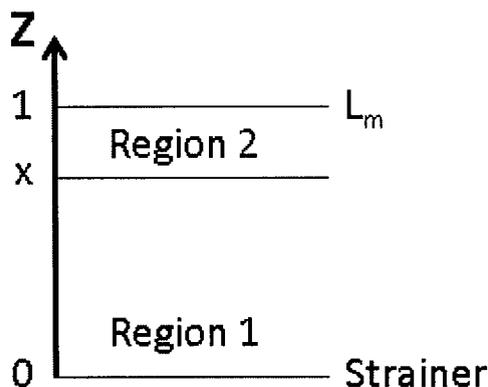


Figure 8.0

Figure 7.3.1 - Geometric definition of stratified debris bed

The strainer was assumed to be a flat plat with unit area and an approach velocity of 0.0026 m/s. See Table 7.2.1 for other assumed inputs and the results.

	Viscous Inertial Shear-Transition-Adaptive (VISTA) Porous Media Head-Loss Formulation for Assessment of the South Texas Project Licensing Amendment Request		
	Document No: ALION-REP-STP-8998-11	Rev: 0	Page 50 of 52

Table 7.3.1 - Stratified debris bed assumptions and findings.

Example	x	Region	ξ	Mean S_v (m^{-1})	Pressure Loss (Pa)	Total Pressure Loss (Pa)
A	0.9	1	0	594,282	257	1,746
		2	7.5	800,000	1,489	
B	0.1	1	7.5	800,000	1,489	1,746
		2	0	594,282	257	

Even though the location of the low-porosity layer is different, the head loss of each similar region and total head loss results are identical which is attributed to the commutative property of the sum and the assumption of a uniform pressure drop across each layer of the bed. However, recent experimental studies conducted at the University of New Mexico (UNM) have demonstrated differential pressure variations throughout a debris bed (Ref. 14). If a non-uniform pressure drop through the debris bed was applied, it is hypothesized the total predicted head losses of Example A and B would be different because the compression and thus porosity would be depend on the location of the low-porosity stratum.

Example C implements the exact inputs of Example A, except that Region 2 is assumed to introduce a piston load on Region 1 which results in a 15% reduction of bed thickness for Region 1.

Table 7.3.2 – Stratified debris bed with piston load

Example	x	Region	ξ	Mean S_v (m^{-1})	Pressure Loss (Pa)	Total Pressure Loss (Pa)
C	0.9	1	0	594,282	280	1,769
		2	7.5	800,000	1,489	

As expected, Example C has a greater pressure loss than Examples A and B. However, if this same scenario was conducted with the low porosity strata in Region 1, it would be unreasonable to assume the same reduction in debris bed thickness, and the resulting pressure loss would be different.

These examples demonstrate the functionality of VISTA to predict pressure losses for nonhomogeneous debris beds. Substituting a homogenous debris bed for either Example A or B using the same total constituents results in a pressure loss of 851 Pa, a reduction larger than 50% of the result obtained under stratification. To account for uncertainties in actual debris configuration in LAR Encl. 4-3, an uncertainty factor of approximately 5 was applied to the correlation.

	Viscous Inertial Shear-Transition-Adaptive (VISTA) Porous Media Head-Loss Formulation for Assessment of the South Texas Project Licensing Amendment Request		
	Document No: ALION-REP-STP-8998-11	Rev: 0	Page 51 of 52

8.0 REFERENCES

1. **Zigler, G., J. Brideau, D. V. Rao, C. Shaffer, F. Souto, and W. Thomas**, *Parametric Study of the Potential for BWR ECCS Strainer Blockage Due to LOCA Generated Debris*, NUREG/CR-6224, prepared for the U. S. Nuclear Regulatory Commission by Science and Engineering Associates, Inc., Albuquerque, NM, October 1995.
2. **Wallace, G.**, *The NUREG/CR-6224 HEAD LOSS CORRELATION*, Memorandum to the NRC, public document accession number ML051320323, September 3, 2004.
3. **Nuclear Regulatory Commission**, *Pressure Drop Calculation Method for Debris-Covered Sump Screens in Support of Generic Safety Issue 191*, NUREG-1862, Washington, DC, February 2007.
4. **Powell, G. T.**, *South Texas Project Units 1 and 2 Docket Nos. STN 50-498 and STN 50-499 Supplement 1 to Revised STP Pilot Submittal and Requests for Exemptions and License Amendment for a Risk-Informed Approach to Resolving Generic Safety Issue (GSI)-191 (TAC NOS. MF0613, MF0614, MF2400, MF2401, MF2402, MF2403, MF2404, MF2405, MF2406, MF2407, MF2408, AND MF2409)*. Letter from Gerald T. Powell to the NRC Control Desk, November 2013.
5. **Balwant Singal, NRC**, *South Texas Project, Units 1 and 2- Request for Additional Information Related to Request for Exemptions and License Amendment for Use of a risk-Informed Approach to Resolve the Issue of Potential Impact of Debris Blockage on Emergency Recirculation During Design-Basis Accidents at Pressurized-Water Reactors*, Letter to Dennis Koehl, STPNOC, AE-NOC-14002526 (MLI4087A075), April 15, 2014.
6. **Letellier, B. C.**, *Theoretical Treatment of Pressure Gradients in One-Dimensional, Inhomogeneous, Compressible Media*, ALION-REP-STP-8998-09, Rev. 0, July 2014.
7. **ITS-REP-QASW02001-01, HLOSS I.I: A Code for the Prediction of ECCS Strainer Head Loss**, Rev 0, January 2003.
8. **Ingmanson, W., B. D. Andrews, and R. C. Johnson**, *Internal Pressure Distribution in Compressible Mats Under Fluid Stress*, TAPI Journal 42(10), 840-849, 1959.
9. **Lapple, C.E., and C.B. Shepherd**, *Calculation of Particle Trajectories*, Ind. Eng. Chem. 35(5), 605-617, May 1940.
10. **Carman, P. C.**, (1997, reprint of original published in 1937, December, original published in May). *Fluid Flow Through Granular Beds. Trans IChemE 75* (reprint of original Vol. 15), S32-S48 (reprint of original 1937 pages 150-166).
11. **Ergun, S.**, *Fluid Flow through Packed Columns*, Chemical Engineering Progress, Vol. 48, No. 2, pp. 89-94, February 1952.
12. **Ozturk, S., X. Ma, and Y. A. Hassan**, *Rheological Characterization of Buffered Boric Acid Aqueous Solutions*. In ANS (Ed.), *Proceedings of the ANS National Meeting 2013 Winter Meeting and Technology Expo*, Washington, DC. November 10-14, 2013.
13. **ALION-REP-STP-8511-02**, *South Texas Vertical Loop Head Loss Testing Report*. Revision 1 January 24, 2013.
14. **Hammond, Kyle**, *A Study on the Mechanical Characteristics of a Fiberglass Bed Formed During a Loss-of-Coolant-Accident at a PWR Nuclear Facility*, Submitted in Partial Fulfillment of the Requirements for the Degree of Master of Science Mechanical Engineering, The University of New Mexico Albuquerque, New Mexico, December 2013.
15. **Alden Research Laboratory**, *Report 0415-0100071WN / 0415-0200071WN, South Texas Project Test Report for ECCS Strainer Testing July 2008*, Rev A, 11/24/2008.

	Viscous Inertial Shear-Transition-Adaptive (VISTA) Porous Media Head-Loss Formulation for Assessment of the South Texas Project Licensing Amendment Request		
	Document No: ALION-REP-STP-8998-11	Rev: 0	Page 52 of 52

16. **Corbett, Thomas**, *Aluminum Oxyhydroxide and Calcium Phosphate WCAP Precipitate Characterization*, ALION-REP-STP-8998-12, 2014.
17. **Munoz, D., J. Tejada, and B. Letellier**, *CASA Grande v1.6 User's Guide*, ALION-SPP-ALION-1009-05, February 2014.

	Viscous Inertial Shear-Transition-Adaptive (VISTA) Porous Media Head-Loss Formulation for Assessment of the South Texas Project Licensing Amendment Request		
	Document No: ALION-REP-STP-8998-11	Rev: 0	Page 1-1 of 1-8

Appendix I: Requests for Additional Information (RAI) Related to Head-Loss Prediction

SSIB - Head Loss and Chemical Effects Bump Up: RAI 15

The STPNOC submittal states that the strainer debris head loss is calculated using a correlation (References: Volume 3, Section 5.6.2, "Conventional Debris Head Loss Model," Volume 3, Assumption 7.e; Volume 1, Section 1.1, "Structured Information Process Flow.") The NRC staff has generally not accepted correlations for the qualification of PWR strainers for several reasons. Please explain why the following general concerns with the use of correlations are not an issue for the STP application:

- (a) Correlations have not been validated for the full range of debris loads and morphologies present under plant conditions.
- (b) Correlations do not address non-homogeneous debris beds which are very likely to occur due to transport timing and non-homogeneous filtering of debris within the bed.
- (c) Correlations have not been validated for the full range of potential flow conditions and strainer geometries that are present in plants.
- (d) There is significant uncertainty in the model parameters used to describe the physical attributes of the debris bed constituents.

	Viscous Inertial Shear-Transition-Adaptive (VISTA) Porous Media Head-Loss Formulation for Assessment of the South Texas Project Licensing Amendment Request		
	Document No: ALION-REP-STP-8998-11	Rev: 0	Page 1-2 of 1-8

SSIB - Head Loss and Chemical Effects Bump Up: RAI 16

Testing performed to validate the NUREG/CR-6224 (1 correlation for specific STP conditions does not appear to accomplish the purpose (References: Volume 3, Section 5.6.2, "Conventional Debris Head Loss Model," and Volume 6.2, Item 5.a.10). Additionally, the NRC staff does not have complete information to conclude that the testing adequately represented the plant configuration and range of conditions that could occur at STP following a LOCA. Therefore, the staff was unable to determine that the plant specific vertical loop tests results were representative of head losses that could occur from a debris bed on a prototypical module. The correlation results and the single vertical loop test result that modeled the July 2008 Alden flume test under STP specific conditions were significantly different from each other, and from the results of the flume test. That is, all three results, although modeling similar conditions, had significantly different results. The submittal explained as to why the results were substantially different, but the explanation was not confirmed by testing or by use of accepted theories. Industry head loss tests using similar surrogates on prototypical strainer modules resulted in significantly higher head losses than those reported by STP for their vertical loop testing and those calculated by use of the correlation. The staff is concerned that vertical loop test and module test results from tests conducted under similar conditions may differ due to the differences between debris characteristics in vertical loop test and module test debris beds. These differences could be caused by differences in transport and deposition of the debris onto the perforated surfaces. Therefore, the staff is concerned that the validation testing is not representative of the plant. Please provide the following additional information:

- (a) If the vertical loop tests conducted by STP are important to the conclusions, please provide details as to why the STP vertical loop tests are valid considering that other module tests conducted in several different facilities under similar conditions, debris loads, and debris characteristics had significantly different results.
- (b) If the vertical loop tests conducted by STP are important to the conclusions, please provide evidence that vertical loop tests conducted under site specific conditions will correlate to flume tests conducted under similar conditions or to head losses that would occur in the plant. Please include information regarding how it was determined that the debris that transported to the horizontal strainer surface resulted in a debris bed of similar characteristics and morphology to that which would transport to the plant strainer. Please state how was it determined that the head losses would be comparable.
- (c) Please provide information that demonstrates that the correlation used by STP is valid for plant specific strainer geometries and plant specific conditions. Alternately, please provide a basis for using a correlation that has not been validated specifically for STP plant conditions and geometries.
- (d) Please discuss how the NUREG/CR-6224 correlation could be used to predict the head losses that would be expected under conditions similar to those in the two flume tests conducted by STP in February and July 2008.

	Viscous Inertial Shear-Transition-Adaptive (VISTA) Porous Media Head-Loss Formulation for Assessment of the South Texas Project Licensing Amendment Request		
	Document No: ALION-REP-STP-8998-11	Rev: 0	Page 1-3 of 1-8

SSIB - Head Loss and Chemical Effects Bump Up: RAI 17

The submittal states that all testing performed to validate the NUREG/CR-6224 correlation was bounded by correlation predictions (References: Volume 1, Section 1.2.7, "Conventional Head Loss Model," and Volume 3, Section 5.6.2, "Conventional Debris Head Loss Model"). There have been numerous cases where the correlation severely under-predicted head losses that were carried out under carefully controlled conditions. NUREG-1862, "Development of Pressure Drop Calculation Method for Debris-Covered Sump Screens in Support of Generic Safety Issue 191," February 2007 (ADAMS Accession No. ML071520440), and NUREG/CR-6917, "Experimental Measurement of Pressure Drop Across Sump Screen Debris Beds in Support of Generic Safety Issue 191," February 2007 (ADAMS Accession No. ML071910180), contain data that show that the NUREG/CR-6224 correlation is not conservative in all cases. These NUREGs determined that correlation predictions are highly dependent on the parameters used to describe the physical attributes of the debris bed constituents and that these parameters have significant uncertainty. These NUREGs also determined that head losses are not well predicted by a correlation that assumes a homogenous debris bed. Some of the experimental data involved fine debris, microporous debris, non-homogeneous beds, and other conditions that the NUREG/CR-6224 correlation is not designed to account for. It is very likely that some conditions that NUREG/CR-6224 correlation does not account for, may be present under plant post-LOCA conditions. The submittal states that the head loss correlation from NUREG/CR-6224 has been extensively validated for various conditions. The NRC staff is of the opinion that there is little or no testing that has been conducted under conditions similar to those at STP. The staff is concerned with the validation issues listed below when using a correlation for qualification of strainers. Please state how the STP evaluation accounts for these uncertainties and lack of validation of the correlation under plant conditions.

- (a) Debris constituents in validation testing are not plant-specific.
- (b) Debris sizes in validation testing are not plant-specific.
- (c) Very little validation testing was conducted at STP velocities and none validated the correlation.
- (d) Validation testing did not include prototypical strainer geometries.
- (e) Validation testing performed in vertical loops does not simulate potentially important aspects of debris bed formation under plant conditions.
- (f) The records of early validation testing are not available or do not contain the information required to determine whether the tests were conducted to adequately represent plant conditions. Therefore, conclusions from early testing must be limited.

	Viscous Inertial Shear-Transition-Adaptive (VISTA) Porous Media Head-Loss Formulation for Assessment of the South Texas Project Licensing Amendment Request		
	Document No: ALION-REP-STP-8998-11	Rev: 0	Page 1-4 of 1-8

SSIB - Head Loss and Chemical Effects Bump Up: RAI 18

The implementation of the correlation in the STP model makes specific assumptions and may potentially contain modeling errors that can significantly affect the results of the calculation (References: Volume 3, Assumptions 7.b, 7.e, and 7.f; Volume 3, Section 5.6.2, "Conventional Debris Head Loss Model"; Volume 6.2, Item 5.a.10; and Enclosure 6, Table 1). Please provide the following information to justify that the assumptions and use of the correlation is realistic or conservative for STP plant-specific conditions.

- (a) Please provide justification that the beds are homogeneous representative of the plant (Volume 3, Assumption 7.e and Volume 6.2, Item 5.a.10).
- (b) It is assumed that fiberglass debris would accumulate uniformly with a density of 2.4 pounds per cubic foot (lb/ft³). The NRC staff is of the opinion that assuming the debris bed density to be the same as the manufactured density may not be an accurate assumption and is based on the observation of debris beds formed in industry tests and NUREG-1862 testing. The NRC staff is further of the opinion that in the plant, only fine and small fiber will transport and collect at a much higher density. Please describe why the density assumption is valid and why it does not significantly affect the results. Alternately, re-perform the analysis with a density that has been shown to be appropriate. (Volume 3, Assumption 7.f and Section 5.6.2 and Volume 6.2, Item 5.a.10).
- (c) Please explain how the NUREG/CR-6224 correlation compression function is applied in the STP model. NUREG-1862 found that the compression relation from NUREG/CR-6224 does not accurately model the compression of the bed, especially at low flow velocities like those at STP. (Volume 3, Section 5.6.2).
- (d) The submittal states that STP implemented a linear mass weighted average instead of the volumetric weighted average for implementation of composite surface to volume ratio (S_v) in the 6224 correlation. The submittal states that there are many possible composite weighting methods that could be used, but does not justify the method chosen in the application. NEI 04-07 and NUREG/CR-6371, "Blockage 2.5 Reference Manual," December 1996 (not publicly available), both recommended the volume weighting method. Please explain why mass weighting is acceptable. Please explain if both the methods result in significantly different results. (Volume 3, Section 5.6.2 and Enclosure 6).
- (e) Please provide a technical basis for Assumption 7.b regarding coating material packing fractions. Please discuss the effect of the assumption on results. Please provide the potential ranges of packing factors for coating materials. (Volume 3, Assumption 7.b and Volume 6.2, Item 5.a.10).

	Viscous Inertial Shear-Transition-Adaptive (VISTA) Porous Media Head-Loss Formulation for Assessment of the South Texas Project Licensing Amendment Request		
	Document No: ALION-REP-STP-8998-11	Rev: 0	Page 1-5 of 1-8

SSIB - Head Loss and Chemical Effects Bump Up: RAI 19

The application of a multiplier of five (5x) to the result of the head loss correlation used in the STP model appears to indicate uncertainty in the ability of the correlation to predict head losses correctly (References: Volume 1, Section 1.2.7 and Volume 3, Section 5.6.2). If the NUREG/CR-6224 correlation is a robust model as implied in the submittal, the NRC staff is of the opinion that it is unnecessary to use safety factors in the head loss calculations for achieving realistic results. The staff noted that some PNNL testing showed that the 6224 correlation under predicted head loss by more than a factor of 5X. Please provide justification for applying the multiplier to the results of the head loss correlation.

	Viscous Inertial Shear-Transition-Adaptive (VISTA) Porous Media Head-Loss Formulation for Assessment of the South Texas Project Licensing Amendment Request		
	Document No: ALION-REP-STP-8998-11	Rev: 0	Page 1-6 of 1-8

SSIB - Head Loss and Chemical Effects Bump Up: RAI 20

The submittal assumes that paint chips or other relatively large debris that may reach the strainer can be accounted for in the correlation as spherical particles (Reference: Volume 3, Section 5.6.2). Large debris may fully or partially block strainer perforations and may deposit non-homogeneously on the strainer. Please provide an experimental basis to confirm that paint chips (or other large particles) may be accurately modeled in the correlation, including the assumption that they can be accurately modeled as spherical particles. In the absence of an experimental justification, please provide an alternate basis for the STP treatment of paint chips and other large particles in the head loss correlation.

	Viscous Inertial Shear-Transition-Adaptive (VISTA) Porous Media Head-Loss Formulation for Assessment of the South Texas Project Licensing Amendment Request		
	Document No: ALION-REP-STP-8998-11	Rev: 0	Page 1-7 of 1-8

SSIB - Head Loss and Chemical Effects Bump Up: RAI 21

The STP correlation uses physical properties of materials predicted to be in the debris bed in order to calculate a head loss (References: Volume 3, Section 5.6.2, "Conventional Debris Head Loss Model," and Volume 6.2, Item 5.a.10). Results from the NUREG/CR-6224 correlation are heavily dependent upon the accurate representation of material physical properties. One of the most difficult parameters to accurately determine is the surface to volume ratio (Sv). Please provide the following information:

- (a) Please state how Sv values were determined for each material.
- (b) It is known that for some debris types, and possibly all debris types expected to be present in PWR debris beds, physical measurements cannot provide Sv values that allow accurate prediction of head loss in existing correlations. This was especially evident for microporous type materials and was shown to be true for other materials by NUREG-1862. Please explain the bases for the Sv values and other material properties used in the STP implementation of the correlation.
- (c) Please state how the uncertainty, described on page 184 of Volume 3, is caused by the relationship between experimentally deduced Sv values and head loss, accounted for in the STP model.
- (d) The NRC staff does not agree with the statement, on page 185 of Volume 3, which states that the lack of agreement between the correlation and test results using green silicon carbide and tin do not affect the STP calculations. It appears that STP had difficulty determining parameters to input to the correlation to attain accurate results. Please provide basis for the conclusion that the lack of agreement between the correlation results and test results do not affect STP head loss calculations.

	Viscous Inertial Shear-Transition-Adaptive (VISTA) Porous Media Head-Loss Formulation for Assessment of the South Texas Project Licensing Amendment Request		
	Document No: ALION-REP-STP-8998-11	Rev: 0	Page 1-8 of 1-8

SSIB - Head Loss and Chemical Effects Bump Up: RAI 22

The NUREG/CR-6224 correlation, and other similar correlations, use specific surface areas (Sv) for cylindrical objects assuming that the fiber is oriented perpendicular to the flow and that the fibers have a uniform diameter. This assumption is used in the STP model (Reference: Volume 1, Section 1.2.7, "Conventional Head Loss Model," and Volume 3, Section 5.6.2, "Conventional Debris Head Loss Model"). NUREG-1862 calculated different specific surface areas for varying diameters of Nukon and noted a difference in Sv between fibers that had binder and those that did not. The NUREG also estimated the Sv of Nukon fiber to be around 250,000 to 300,000 ft⁻¹ instead of 180,000 ft⁻¹ when corrected for test data. (STP uses for the Sv of 571,429 m⁻¹ (174,172 ft⁻¹ for Nukon fiber.) Please explain how the STP evaluation takes these findings into account. (Volume 3, Section 5.6.2).

SSIB - Head Loss and Chemical Effects Bump Up: RAI 23

The STPNOC submittal makes the assumption that Microtherm fibers will have properties similar to those of Nukon (bulk density= 2.4 lb/ft³ microscopic density= 165 lb/ft³ and Sv = 666,667 m⁻¹) (Reference: Volume 3, Section 5.6.2). Please state the basis for this assumption. Also, please justify the use of the Nukon fiber bulk density as the debris bed density.

SSIB - Head Loss and Chemical Effects Bump Up: RAI 24

The physical characteristics used in the head loss correlation can have a significant effect on the results of the head loss calculations. Characteristic values that describe the assumed behavior of STP debris are provided in Tables 5.6.1 and 5.6.2 of Volume 3. NRC research conducted for NUREG-1862 has determined that some of the values that describe the physical characteristics of debris are not well understood. Please provide the bases for the values in Tables 5.6.1 and 5.6.2. Please provide reasonable uncertainty bands for the material properties. Also, please explain how compounded inaccuracies in assumed material properties would affect the head loss values predicted by the correlation.

SSIB - Head Loss and Chemical Effects Bump Up: RAI 28

Considering the individual uncertainties that result from the issues described in the request for additional information on the subject of head loss, please provide justification that the use of a correlation is acceptable in the risk-informed model. Along with the justification, please provide an analysis of the overall uncertainty and state how this will be incorporated into the overall risk-informed evaluation



South Texas Project Risk-Informed GSI-191 Evaluation

A Practical Guide to Sensitivity Analysis of a Large-scale Computer Simulation Model

Document: STP-RIGSI191-ARAI.01

Revision: 3.0

Date: February 10, 2014

Prepared by:

David Morton, The University of Texas at Austin
Jeremy Tejada, The University of Texas at Austin
Alexander Zolan, The University of Texas at Austin

Reviewed by:

Ernie J. Kee, South Texas Project
Zahra Mohaghegh, University of Illinois at Urbana-Champaign
Seyed A. Reihani, University of Illinois at Urbana-Champaign
Don Wakefield, ABS Consulting

A Practical Guide to Sensitivity Analysis of a Large-scale Computer Simulation Model

David Morton, Jeremy Tejada, and Alexander Zolan
The University of Texas at Austin

Abstract

We describe a 10-step sensitivity analysis procedure that applies to a large-scale computer simulation model. We propose using tornado diagrams as the initial tool for identifying the input parameters to which the simulation's outputs are most sensitive. Sensitivity plots and spider plots complement tornado diagrams by capturing nonlinear responses in outputs to changes in inputs. Regression metamodels, and associated experimental design, help understand sensitivities to, and interactions between, input parameters. Our motivating model from GSI-191 has a number of distinguishing features: (i) The model is large in scale in that it has a high-dimensional vector of inputs; (ii) Some of the model's inputs are governed by probability distributions; (iii) A key output of the model is the probability of system failure—a rare event; (iv) The model's outputs require estimation by Monte Carlo sampling, including the use of variance reduction techniques associated with rare-event simulation; (v) It is computationally expensive to obtain precise estimates of the failure probability; (vi) We seek to propagate key uncertainties on model inputs to obtain distributional characteristics of the model's outputs; and, (vii) The overall model involves a loose coupling between a physics-based stochastic simulation sub-model and a logic-based PRA sub-model via multiple initiating events in the latter sub-model. We review a subset of a much larger literature, guided by the need to have a practical approach to sensitivity analysis for a computer simulation model with these characteristics. We illustrate our proposed 10-step procedure on a simple example of a simulation model for system reliability. Important themes repeat throughout our recommendations, including the use of common random numbers to reduce variability and smooth output analysis, a focus on assessing differences between two model configurations, and proper characterization of both sampling error and uncertainties on input parameters. In Appendix A we assess the sensitivity of core damage frequency (CDF) estimates to changes in input parameters for the South Texas Project Electric Generating Station GSI-191 risk-informed resolution project. In particular, we use output from the CASA Grande simulation model to construct a tornado diagram to assess which parameters, from a list of candidate parameters, CDF appears most sensitive, and we further construct a one-way sensitivity plot for one of the most sensitive parameters.

1 Background, Purpose, and Lexicon

Paraphrasing Kleijnen [9],

Sensitivity analysis, of a computer simulation model, estimates changes in the model's outputs with respect to changes in the model's inputs.

In this report, we review approaches to sensitivity analysis of a computer simulation model, focusing on specific approaches that we see as practically viable in the context of resolving GSI-191 through a risk-informed approach. And, we propose a 10-step sensitivity analysis procedure. Before proceeding, some remarks on our characterization of sensitivity analysis, adopted from Kleijnen, are in order.

1. We deliberately use the verb *estimates* because the “true” value of our model’s outputs (e.g., probability of system failure) cannot be computed. Rather this output must be estimated using Monte Carlo sampling in our implementation via a computer simulation model.
2. For the moment, we are purposefully vague about how to make *changes in the model’s inputs* because this is a key distinguisher of different approaches to sensitivity analysis. We explore this issue in some detail in this report.
3. Another key distinguisher of approaches to sensitivity analysis is the manner in which we quantitatively and qualitatively summarize changes in our estimates of the model’s outputs. We discuss some important and complementary approaches.
4. We use the plural *model’s inputs* because of our interest in being able to handle a high-dimensional vector of input parameters.
5. We again use *model’s outputs* recognizing that multiple performance measures are of simultaneous interest. For example, we may be interested in both the core damage frequency (CDF) and the change in core damage frequency relative to a base model (Δ CDF), where the latter model does not account for failure modes associated with GSI-191. Or, we may be interested in the four-tuple (CDF, Δ CDF, LERF, Δ LERF), where LERF denotes large early release frequency.
6. There is no redundancy in the term *computer simulation model*. Physical simulation models differ from models implemented on a computer. The notions of *to model* and *to simulate* both involve mimicking a real-world system. However, in our context *modeling* means the act of abstracting the real-world system into a set of mathematical equations and/or logic constituting an abstract model. While a *simulation model* is a mathematical model, it is usually taken as distinct from other classes of mathematical models that yield an analytical solution.
7. While a simulation model may be deterministic or stochastic, we focus on stochastic simulation models. The output of a stochastic simulation model may be deterministic or random. Consider the probability of system failure in the context of GSI-191. If we condition the input on a random initiating frequency, the output of the model is a conditional probability of system failure; i.e., the output is a random variable. On the other hand, if we integrate with respect to the distribution governing the random initiating frequency, the probability of failure is a deterministic output parameter. We consider both alternatives.
8. We cannot compute even a deterministic output measure exactly. Rather, we must estimate the output using Monte Carlo sampling. We have sampling-based errors associated with Monte Carlo methods, but these errors can be quantified. The errors can also be reduced by increasing the sample size, and they can be reduced by using so-called variance reduction

techniques. The latter methods are particularly important because of our interest in rare-event simulation in which failure probabilities are very small.

9. It is important to distinguish three sources of error: First, we have sampling-based errors associated with Monte Carlo methods discussed above. Second, we have errors due to uncertainties on some model inputs. Third, we have errors due to a lack of fidelity of the model itself. We can attempt to reduce the second type of error by gathering more data or eliciting (more) information from experts. We can also use data and elicitation to reduce the third type of error if we have competing hypothesized models, or sub-models. In all three cases, sensitivity analysis can help guide where such efforts should focus.

A second key notion regarding sensitivity analysis in the context of decision problems involves understanding which differences in inputs make a difference in the *decision* rather than simply differences in model outputs. In this context, Clemen and Reilly [3] characterize sensitivity analysis by saying:

*Sensitivity analysis answers the question, “What makes a difference in this decision?”
... Determining what matters and what does not requires incorporating sensitivity analysis throughout the modeling process.*

A similar sentiment is reflected in Eschenbach [6]:

This sensitivity analysis may be used (1) to make better decisions, (2) to decide which data estimates should be refined before making a decision, or (3) to focus managerial attention on the most critical elements during implementation.

Should some pipes that currently have fiberglass insulation be retrofitted to instead have reflective insulation to mitigate risk associated with a possible GSI-191 LOCA event? Such an action would incur significant cost and significant radiation exposure to workers. What differences in input parameters of a model lead to a “yes” versus “no” answer to this question? A surrogate question involves the notion of Regions I, II, and III from Regulatory Guide 1.174 [4]. Suppose nominal values of our model’s input parameters lead to an assessment that the plant is in Region III. Then, we may ask: What changes in the input parameters would lead us to conclude that the plant would instead be in Region I or Region II?

It is not the purpose of this report to directly answer the above pair of questions. Rather, we provide a framework that, when properly applied, can answer these questions. For concreteness, we apply our sensitivity analysis framework to a simple example of a parallel-series system with four components illustrated in Figure 1. Here, our analogous question will be, “Should we perform preventive maintenance on component 3 to decrease the probability the system fails prior to a pre-specified time, t_0 ?” We describe this illustrative example in more detail in Section 2.

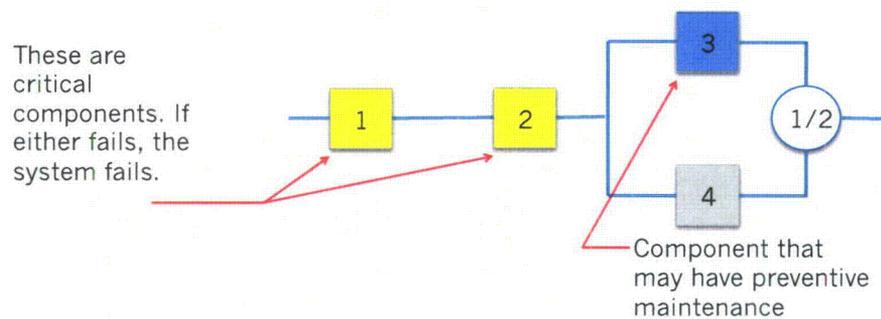


Figure 1: The figure depicts a series-parallel system in which the first two components (1 and 2) are in series with a subsystem that has two components (3 and 4) in parallel. One of the two parallel components must be “up” for the system to be up, along with both components 1 and 2.

2 Illustrative Example

Figure 1 depicts a simple model of system reliability we use to illustrate sensitivity analysis in this report. Our emphasis here is on having a concrete model that is rich enough to serve this purpose as opposed to having a high fidelity model of an actual system. The block diagram in the figure depicts four components with independent random failure times $T_1, T_2, T_3,$ and T_4 . If a component fails, it will not be repaired. We seek to understand the failure time of the system, given by $T = \min\{T_1, T_2, \max\{T_3, T_4\}\}$. While T is a random variable, we use two deterministic output measures $\mathbb{P}\{T > t_0\}$ and $\mathbb{E}[T]$, where the former output is our primary performance measure of *system reliability*; i.e., the probability the system fails after a pre-specified time, t_0 . A secondary output is the expected time until the system fails. We have oriented the measures so that we prefer larger values.

The parameters of the four random variables, T_1, \dots, T_4 , are inputs to our model of system reliability. We assume the four random variables have exponential distributions, and so we have as model inputs the failure rates of each of the components, $\lambda_1, \lambda_2, \lambda_3,$ and λ_4 (which have units of failures per unit time), along with the time threshold for which we desire the system to survive, which we denote t_0 . Usually, we suppress the dependency of T_1, \dots, T_4 on their rates but sometimes we write expressions such as $T_3(\lambda_3)$ to emphasize the rate associated with T_3 . The inverse of the failure rate is the mean time until a component fails, and often it is more natural to think in terms of these means: $\lambda_1^{-1}, \lambda_2^{-1}, \lambda_3^{-1},$ and λ_4^{-1} , which have units of time. In what follows we interchangeably speak of failure rates or mean times to failure, depending the context.

In our example, we have a decision to make for this system. We can operate the system as depicted in Figure 1 with failure rates $\lambda_1, \dots, \lambda_4$. We call this the *base option*. Or, at time 0 we can take component 3 off-line, and perform preventive maintenance on that component. Component 3 would then come back on-line at time $t = \Delta t$. Importantly, the system operates even when component 3 is off-line for preventive maintenance. So the system would operate as three

components in series with failure rates λ_1, λ_2 , and λ_4 during the time interval $(0, \Delta t)$ and as the system depicted in Figure 1 with failure rates $\lambda_1, \lambda_2, \lambda_3/k$, and λ_4 , on time interval $(\Delta t, t_0)$. Here, performing preventive maintenance on component 3 at time 0 reduces its failure rate from λ_3 to λ_3/k for $k \geq 1$. For brevity we call this latter option the *PM option*, although it arguably amounts to an “upgrade” of component 3 given the memoryless property of the exponential random variable. For the PM option, model inputs include $\lambda_1, \lambda_2, \lambda_3, \lambda_4, t_0, \Delta t$, and k .

System reliability under the base option is given by:

$$\mathbb{P}\{\min\{T_1, T_2, \max\{T_3(\lambda_3), T_4\}\} > t_0\}. \quad (1)$$

System reliability under the PM option is:

$$\mathbb{P}\{\min\{T_1, T_2, T_4\} > \Delta t\} \cdot \mathbb{P}\{\min\{T_1, T_2, \max\{T_3(\lambda_3/k), T_4\}\} > t_0 - \Delta t\}. \quad (2)$$

We are using the memoryless property of exponential random variables in equation (2), by writing the product and by writing the reliability of the system over time interval $[\Delta t, t_0]$ as the second term. Also, the rates associated with T_1, T_2 , and T_4 do not change under the base and PM options and hence we do not make them explicit in equations (1) and (2). That said, we investigate below changes in these rates in the course of our sensitivity analysis.

We may treat input parameters, such as λ_1 , as deterministic but vary the parameter for the purpose of understanding the sensitivity of system reliability to changes in λ_1 . Or, we may treat λ_1 as a random variable governed, e.g., by a gamma distribution or by a bounded Johnson distribution. In either case, we may compute, or estimate, the *conditional* output $\mathbb{P}\{T > t_0 \mid \lambda_1\}$ under the base option, where $T = \min\{T_1, T_2, \max\{T_3, T_4\}\}$. In the latter case, because $\mathbb{P}\{T > t_0 \mid \lambda_1\}$ is a random variable, we may compute, or estimate, the percentiles (e.g., the 5th, 50th, and 95th percentiles) of $\mathbb{P}\{T > t_0 \mid \lambda_1\}$ knowing the corresponding percentiles of λ_1 . Alternatively, we may integrate with respect to λ_1 's distribution and obtain $\mathbb{P}\{T > t_0\}$. Finally, if λ_1 is governed, e.g., by a bounded Johnson distribution, we could seek to understand the sensitivity of $\mathbb{P}\{T > t_0\}$ to the parameters of the Johnson distribution.

In the context of GSI-191, example input parameters include margins governing various failure modes such as the net positive suction head margin for pumps, the structural margin for pump strainers, air intrusion limits for pumps, in-vessel limits on debris penetration, and solubility limits on boron concentration in the core. Other key inputs include the temperature, pH, and water volume of the pool, parameters governing debris generation and debris transport, parameters governing strainer characteristics, and so on. Some parameters such as pool temperature change over time according to a specified input profile.

In a stochastic simulation model, random variables play a key role and their inputs can be characterized in one of two key ways, and we take the initiating LOCA frequencies as an example. We model a probability distribution as governing the frequency of breaks of various sizes. We can either take as input: (i) the parameters of that probability distribution, which in the case of STP's GSI-191 analysis are the parameters of the Johnson distributions governing the break sizes

for the six NUREG-1829 break-size categories or (ii) we can take as input a percentile (e.g., the median) associated with that distribution. This choice affects how we characterize model output. Similar choices can be made for random variables governing, e.g., the strainer safety margins. The discussion above regarding the treatment of $\mathbb{P}\{T > t_0 \mid \lambda_1\}$ is our analog for the illustrative example.

In terms of model outputs for GSI-191, we may be interested in both the core damage frequency (CDF) and the change in core damage frequency relative to a base-case model (Δ CDF). Or, we may be interested in the four-tuple (CDF, Δ CDF, LERF, Δ LERF). A detailed physics-based simulation model, such as CASA Grande, can help characterize the risk associated with a specific failure mode. However, proper assessment of overall risk requires propagating such failures through a coupled PRA model, and hence proper assessment of sensitivities to changes in underlying input parameters requires a similar propagation.

In the remainder of this report we do not discuss a GSI-191 example in detail, even though we are motivated by risk-informed GSI-191 analyses. Rather, we restrict attention to the example discussed in this section to illustrate ideas. This streamlines the discussion and allows us to provide simple and transparent insights on the relative merits of various approaches to sensitivity analysis.

3 A Practical Step-by-Step Guide to Sensitivity Analysis

Step 1: Define the Model

We let $f : \mathbb{R}^n \rightarrow \mathbb{R}^m$ denote our idealized model of the system. Here, our notation means that the model takes as input the values of n parameters and gives as output m performance measures. The vector of inputs is denoted $x = (x_1, x_2, \dots, x_n)$ and the vector of outputs is denoted $y = f(x_1, x_2, \dots, x_n)$, where $y = (y_1, y_2, \dots, y_m)$. We call the model *idealized* because we assume, for the moment, that the outputs are known exactly given the values of the estimates; i.e., for the moment we assume we do not need to perform a Monte Carlo simulation in order to estimate the values of the outputs.

Our illustrative example has two models rooted in the base and PM options. The base-option model has the following primitives: Four independent exponential random variables, T_1, \dots, T_4 , govern the failure times of four components with respective failure rates $\lambda_1, \dots, \lambda_4$, and the failure time of the system is given by $T = \min\{T_1, T_2, \max\{T_3, T_4\}\}$. With these constructs and $m = 2$ outputs we have the model f defined by

$$f(\lambda_1, \dots, \lambda_4, t_0) = (\mathbb{P}\{T > t_0\}, \mathbb{E}[T]),$$

where the equations for $\mathbb{P}\{T > t_0\}$ and $\mathbb{E}[T]$ could be further detailed using four-dimensional integrals. (We do not do so here as it does not further our discussion of sensitivity analysis.) An analogous idealized model can be written under the PM option using equation (2).

Step 2: Select Outputs of Interest

Our model f has m outputs (y_1, \dots, y_m) . In step 2 of the proposed process, we can restrict attention to a subset of these outputs. There are a number of possibilities for our illustrative example. We may have $m = 1$ with $(y_1) = (\mathbb{P}\{T \leq t_0\})$ or $(y_1) = (\mathbb{E}[T])$ as the single output of interest. Or, we have two outputs of interest: $m = 2$ and $(y_1, y_2) = (\mathbb{P}\{T \leq t_0\}, \mathbb{E}[T])$. We may have $m = 3$ outputs: $(y_1, y_2, y_3) = (\mathbb{P}\{T > t_0\}, \mathbb{E}[T], \mathbb{P}\{T > t_0 | \lambda_1\})$, and this can be extended to include additional outputs such as $\mathbb{P}\{T > t_0 | \lambda_i\}$ for all $i = 1, 2, \dots, 4$.

The notion of *attribution* is tied to our outputs of interest. Consider the base option in our example. Given that our system failed prior to time t_0 , we can assess whether this is due to a failure of component 1, component 2, or due to the failure of the parallel subsystem of components 3-4. Thus we can compute $\mathbb{P}\{T_1 = T | T < t_0\}$, $\mathbb{P}\{T_2 = T | T < t_0\}$, and $\mathbb{P}\{\max\{T_3, T_4\} = T | T < t_0\}$. When focusing on attribution, we could model $m = 3$ output parameters:

$$(y_1, y_2, y_3) = (\mathbb{P}\{T_1 = T | T < t_0\}, \mathbb{P}\{T_2 = T | T < t_0\}, \mathbb{P}\{\max\{T_3, T_4\} = T | T < t_0\}).$$

Of course, we could further assess whether component 3 or 4 caused the failure rather than taking their paired subsystem via $\mathbb{P}\{T_3 = T | T < t_0\}$ and $\mathbb{P}\{T_4 = T | T < t_0\}$.

Step 3: Select Inputs of Interest

Our model f has n inputs (x_1, x_2, \dots, x_n) . In step 2 of the process, we have already restricted attention to a subset of the model outputs. It may seem counterintuitive to choose the outputs before choosing the inputs, but this order is purposeful. Our choice of inputs hinges both on what the analyst sees as important and on the outputs of interest that the analyst selected in step 2. The notion of “important” here is driven by multiple considerations. In our example, the analyst may believe an input parameter may not change whether the “base option” versus “PM option” choice leads to higher system reliability until the parameter changes to some relatively extreme value, and the analyst may seek to understand the magnitude of that extreme. Or, the analyst may believe an output depends crucially on an input parameter, and the analyst seeks to understand the direction and magnitude of change in the output with respect to changes in the input.

For our example’s base option, if we have selected $m = 1$ with $(y_1) = (\mathbb{E}[T])$ then we may choose as the input vector $(x_1, \dots, x_4) = (\lambda_1, \dots, \lambda_4)$ and drop the time threshold t_0 because this is not relevant when estimating $\mathbb{E}[T]$. If the analyst believes that components 1 and 2 are identical and components 3 and 4 are identical then it may suffice to have the smaller dimensional input vector $(x_1, x_2) = (\lambda_1, \lambda_3)$, because changes in $\lambda_1 = \lambda_2$ apply to both components 1 and 2 and changes in $\lambda_3 = \lambda_4$ apply to both components 3 and 4.

If $\mathbb{P}\{T > t_0\}$ is one of our outputs of interest then we may seek to understand the sensitivity of the failure probability to choices of t_0 , and hence include t_0 as an input parameter. However, even if $\mathbb{P}\{T > t_0\}$ is one of our outputs of interest we may not seek to understand its sensitivity with respect to t_0 , if changes in t_0 are highly unlikely or the value of t_0 is fixed by mandate.

Step 4: Choose Nominal Values and Ranges for Inputs

In the previous step, we have selected n input parameters of interest, (x_1, x_2, \dots, x_n) . In step 4, we select nominal values for these parameters and lower and upper bounds for each of these input parameters. We denote the nominal values by $(x_1^0, x_2^0, \dots, x_n^0)$, the lower bounds by $(\underline{x}_1^0, \underline{x}_2^0, \dots, \underline{x}_n^0)$, and the upper bounds by $(\bar{x}_1^0, \bar{x}_2^0, \dots, \bar{x}_n^0)$.

The nominal value for an input parameter is typically based on the analyst's best point estimate for that input. That said, there are sometimes reasons for selecting an *appropriately conservative* nominal value. Consider our illustrative example. The threshold time, t_0 , may denote the lifetime for which we require the system to survive, but we may not know the value of t_0 with certainty. We could select a conservative (i.e., large but "reasonable") value of t_0 , and if $\mathbb{P}\{T > t_0\}$ is sufficiently close to 1, we may be satisfied that our system is of sufficiently high reliability. Sensitivity analysis explores this notion in a richer manner, seeking not just to understand the failure probability at a single, perhaps conservative, value of t_0 , but rather to understand the failure probability over a range of values of t_0 .

Table 1 gives the input parameters associated with our system reliability example. Lower and upper bounds are specified by what the analyst sees as how low or high these parameters might be, in an absolute sense. More typically, ranges are specified so that the interval contains values that are both reasonable and likely (e.g., we might exclude values that have less than a 10% chance of occurring). All seven parameters in Table 1 have absolute lower bounds of 0 and upper bounds of ∞ . However, we have no intention of exploring this entire interval. Even if PM might conceivably degrade a component, we will not explore $k < 1$. Similarly we will not explore $\Delta t > t_0$ because under such a large value for the PM time, it is clearly not worthwhile to pursue PM.

It is important to choose ranges for the input parameters that the analyst sees as reasonable and commensurate. This task can be difficult, and we do not mean to minimize that difficulty. That said, such choices are continually made during the process of modeling a system, and we see this difficulty as implicit in the intimate connection between modeling and sensitivity analysis.

Step 5: Estimating Model Outputs under Nominal Values of Input Parameters

So far we have referred to the idealized model, $f(x)$. So, with $m = 1$ model output, $\mathbb{P}\{T > t_0\}$, we can discuss the value of system reliability under the nominal values of the input parameters, $x = x^0$, given in Table 1. However, for the large-scale stochastic models in which we have interest, we cannot compute $f(x^0)$ exactly. Rather, we must estimate $f(x^0)$ using Monte Carlo sampling. Formally this means that we have another model, which we denote, $f_N(x^0)$, where this model is parameterized by a sample size, N . We can compute $f_N(x^0)$, but because its inputs involve sampling random variables—such as the failure times of the four components in Figure 1—the model output, $f_N(x^0)$, is also a random variable. The random sampling error associated with $f_N(x^0)$ can be quantified, provided the sample size, N , is sufficiently large, using $f_N(x^0)$'s standard deviation via the central limit theorem.

Table 1: Nominal values, lower bounds, and upper bounds for the input parameters in our system reliability example: $\lambda_1^{-1}, \dots, \lambda_4^{-1}$ denote mean time until failure for the four components depicted in Figure 1; t_0 specifies the desired lifetime of the system; Δt is the time required to perform PM on component 3; and, if PM is performed component 3's failure rate drops to λ_3/k where $k \geq 1$.

Input parameter (x)	Nominal value (x^0)	Lower bound (\underline{x})	Upper bound (\bar{x})
λ_1^{-1} (months)	200	150	250
λ_2^{-1} (months)	200	150	250
λ_3^{-1} (months)	50	25	75
λ_4^{-1} (months)	50	25	75
t_0 (months)	18	12	24
Δt (months)	1	0.5	3
k (unitless)	2	1	5

Using the nominal values for the input parameters from Table 1, estimates of the system reliability, expected time to failure, and failure attribution probabilities are reported in Table 2. The table contains point estimates, and estimates of sampling error in the form of 95% confidence interval halfwidths. For example, the point estimate of system reliability is 0.7520 under the base option and 0.7850 under the PM option, as reported in the " $\mathbb{P}\{T > t_0\}$ " row of Table 1. This suggests that the PM option leads to higher system reliability, however, we cannot ignore sampling error in coming to this conclusion. We also see from Table 2 that the mean lifetime of the system appears to be longer under the PM option. And, we get a sense of how the attribution probabilities change under the base and PM options, with the probability that the parallel subsystem 3-4 is the cause of system failure dropping under the PM option. The three probabilities in rows 3-5 of Table 2 sum to one because they are conditional on the system failing. Under the PM option the attribution to parallel subsystem 3-4 drops, and hence the likelihood of the failure being attributed to components 1 and 2 necessarily grows.

Based on Table 1, we are 95% confident that the true value for system reliability under the base option lies in the interval (0.7252, 0.7788), and we are similarly confident that the true value for system reliability under the PM option lies in the interval (0.7595, 0.8105). We may be tempted to use the two confidence intervals (0.7252, 0.7788) and (0.7595, 0.8105) to infer that the difference is not statistically significant (because the confidence intervals overlap), but this is not the proper way to analyze this difference. We describe the approach we recommend shortly.

Table 2: Estimates of output performance measures for the base-option model and the PM-option model under the nominal values of the input parameters from Table 1. For example, the point estimate for $\mathbb{P}\{T > t_0\}$ under the base option is 0.7520 and a 95% confidence interval halfwidth is 0.0268. All estimates in the table are based on a sample size of $N = 1000$.

Output Measure	Base-option Model	PM-option Model
$\mathbb{P}\{T > t_0\}$	0.7520 ± 0.0268	0.7850 ± 0.0255
$\mathbb{E}[T]$	44.0174 ± 2.3008	54.9770 ± 2.9976
$\mathbb{P}\{T_1 = T T < t_0\}$	0.2150 ± 0.0255	0.2520 ± 0.0270
$\mathbb{P}\{T_2 = T T < t_0\}$	0.2350 ± 0.0263	0.2940 ± 0.0283
$\mathbb{P}\{\max\{T_3, T_4\} = T T < t_0\}$	0.5500 ± 0.0309	0.4540 ± 0.0309

It is often significantly easier to estimate the difference of an output measure under two system configurations than it is to estimate the absolute values of that same output measure. When estimating differences we can take advantage of the simulation technique called *common random numbers* in which similar components in the two systems see similar inputs. We illustrate this by estimating

$$\Delta\mathbb{P}\{T > t_0\} \equiv \mathbb{P}\{T_{PM} > t_0\} - \mathbb{P}\{T_{base} > t_0\}$$

using both common random numbers and independent random numbers with the same sample size $N = 1000$, and we present the results in Table 3. The table rightly suggests that we can reduce the variance of estimates of such differences by using common random numbers.

Table 3: Estimates of the differences in output performance measures between the base-option model and the PM-option model under the nominal values of the input parameters from Table 1 using both common and independent random numbers. For example, the point estimate for $\Delta\mathbb{P}\{T > t_0\}$ under the base option is 0.0330 and a 95% confidence interval halfwidth is 0.0149, but the halfwidth for the same estimate using independent random numbers is larger by a factor of 2.5 at 0.0365.

Differences in Output Measures	Common Random Numbers	Independent Random Numbers
$\Delta\mathbb{P}\{T > t_0\}$	0.0330 ± 0.0149	0.0330 ± 0.0365
$\Delta\mathbb{E}[T]$	10.9597 ± 1.3985	13.1036 ± 3.8276
$\Delta\mathbb{P}\{T_1 = T T < t_0\}$	0.0370 ± 0.0124	0.0590 ± 0.0375
$\Delta\mathbb{P}\{T_2 = T T < t_0\}$	0.0590 ± 0.0159	0.0640 ± 0.0381
$\Delta\mathbb{P}\{\max\{T_3, T_4\} = T T < t_0\}$	-0.0960 ± 0.0197	-0.1230 ± 0.0424

Our point estimate of $\Delta\mathbb{P}\{T > t_0\}$ is 0.0330 and the sampling error is 0.0149 when using common random numbers. The point estimate indicates that the PM option appears to have higher reliability than the base option, and the fact that 0 is not included in the range $0.0330 \pm 0.0149 = (0.0181, 0.0479)$ indicates that this difference is statistically significant at a confidence level of 95%. Note that our point estimate of $\Delta\mathbb{P}\{T > t_0\}$ in Table 3 is *identical* to the difference of the point estimates in Table 2. However, the key difference is that the sampling error of 0.0149 under common random numbers is significantly smaller than the corresponding sampling errors reported in Table 3 for independent random numbers, and significantly smaller than the sampling error for the corresponding absolute performance measures in Table 2. Without hypothesizing *a priori* whether the base or PM option leads to higher reliability, the question of statistical significance hinges on whether the 95% confidence interval for $\Delta\mathbb{P}\{T > t_0\}$ includes 0. If it does not, the result is statistically significant with the sign of the point estimate of $\Delta\mathbb{P}\{T > t_0\}$ determining whether the base or PM option leads to a more reliable system. In this case, a positive difference indicates the PM option is preferred.

Step 6: One-Way Sensitivity Analysis: Sensitivity Plots and Tornado Diagrams

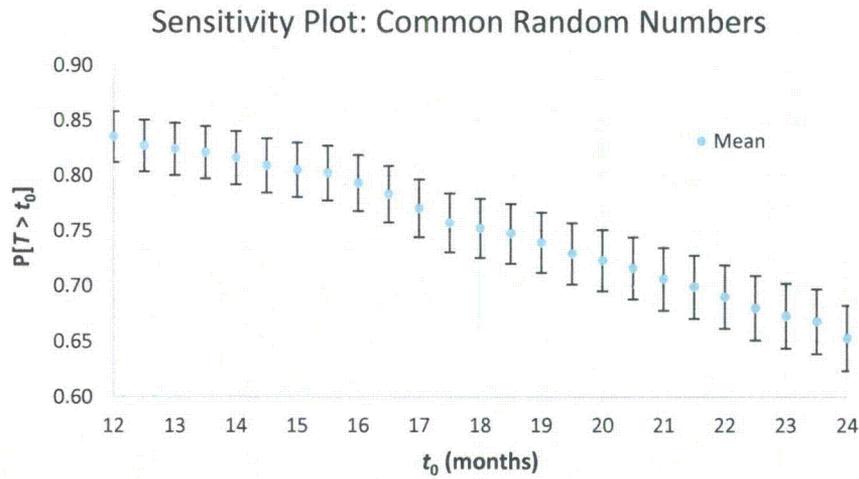
From steps 1-4, we have specified a model, restricted attention to key model outputs and inputs, and specified nominal values and ranges for the model inputs. From step 5, we have point estimates, and estimates of sampling error, associated with the model's outputs under the model's nominal input parameters.

Sensitivity plots restrict attention to one or two model outputs at a time and consider a single input parameter. *Tornado diagrams* restrict attention to one model output at a time and consider multiple inputs. We follow Clemen and Reilly [3] in referring to sensitivity plots and tornado diagrams as one-way sensitivity analysis because we vary one input parameter at a time, holding all other inputs at their nominal values.

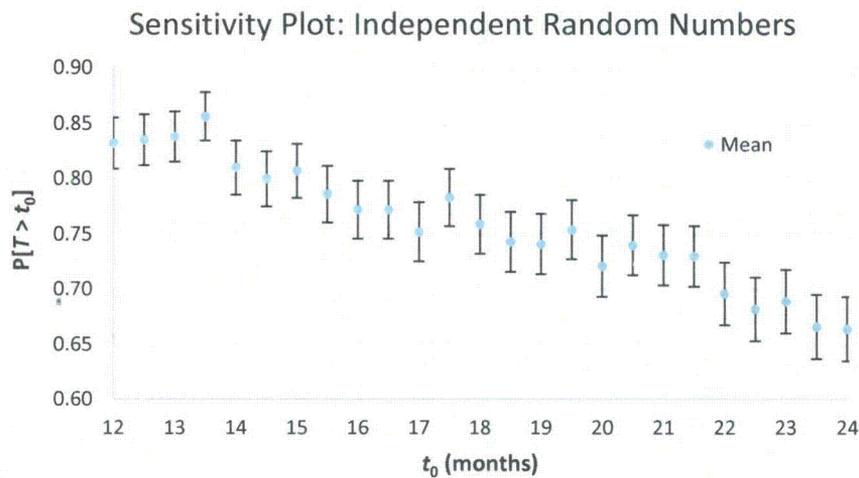
Figure 2 is a sensitivity plot, showing how system reliability $\mathbb{P}\{T > t_0\}$ changes for the base-option model (without PM) as t_0 varies. As t_0 grows the system reliability drops. The figure depicts point estimates along with 95% confidence intervals on $\mathbb{P}\{T > t_0\}$. Panel (a) of the figure shows the results when using *common random numbers*, and panel (b) shows the same results when using independent random numbers for estimating system reliability. The importance of using common random numbers is evident from the smoothness of the results in panel (a) versus the lack of smoothness in panel (b). Figure 3 is a similar sensitivity plot but for $\Delta\mathbb{P}\{T > t_0\}$, where positive values indicate that the PM option is preferable. The plot indicates a notion of dominance. That is, when other parameters are held at their nominal values, system reliability for the PM option exceeds that of the base option for all t_0 values of interest.

Figure 4 again shows a sensitivity plot for $\Delta\mathbb{P}\{T > t_0\}$, but now as a function of the reduction in the failure rate k . Here, we see that as k grows the PM option becomes increasingly preferable. We know that at $k = 1$ the base option should be preferred, but from our simulation results using a sample size of $N = 1000$, we cannot make this conclusion with statistical significance, as the figure

indicates. (This would change under a larger sample size.) Figures 5 and 6 concern attribution. Here, we suppress the confidence intervals to avoid clutter, but Tables 2 and 3 provide a sense of the respective 95% confidence interval halfwidths under common random numbers. These two figures quantify how the attribution probability of the parallel subsystem 3-4 drops as k grows. Note that sampling error accounts for the differences in attribution to components 1 and 2 because these components play identical roles and have identical failure rates.



(a) Common Random Numbers



(b) Independent Random Numbers

Figure 2: The y -axis in the figure is system reliability, $\mathbb{P}\{T > t_0\}$, and the x -axis is the value of t_0 in months for the base-option model. The figure depicts quantitatively how system reliability drops as the required lifetime of the system grows from its lower bound to its upper bound. The nominal value of t_0 is 18 months, and its lower and upper bounds are 12 and 24 months, respectively, as indicated in the figure. In addition to point estimates of $\mathbb{P}\{T > t_0\}$, 95% confidence intervals at each value of t_0 are displayed. Panel (a) versus panel (b) of the figure distinguishes the results when using common random numbers (recommended) versus the more naïve approach of using independent random numbers at different values of t_0 . All estimates are based on a sample size of $N = 1000$.

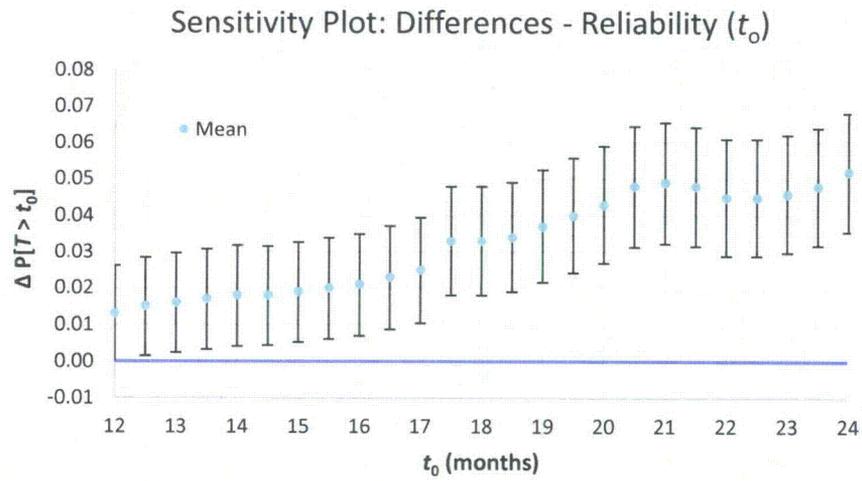


Figure 3: The figure is to be read in the same manner as Figure 2 except that $\Delta P\{T > t_0\}$ replaces $P\{T > t_0\}$ on the y -axis.

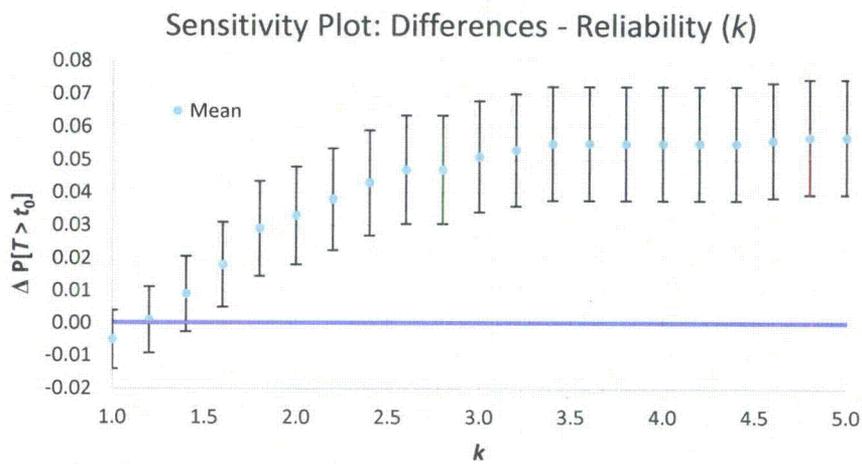


Figure 4: The figure is to be read in the same manner as Figure 2 except that $\Delta P\{T > t_0\}$ replaces $P\{T > t_0\}$ on the y -axis, and k replaces t_0 on the x -axis.

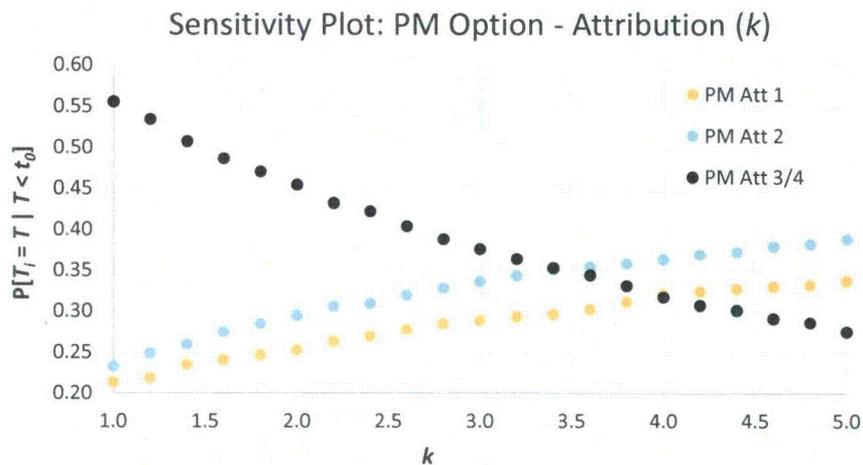


Figure 5: The figure is to be read in the same manner Figure 2 except that we are plotting the attribution probabilities such as $\mathbb{P}\{T_1 = T | T < t_0\}$. Note that at any vertical line drawn through the three series, the sum of the attribution probabilities is one.

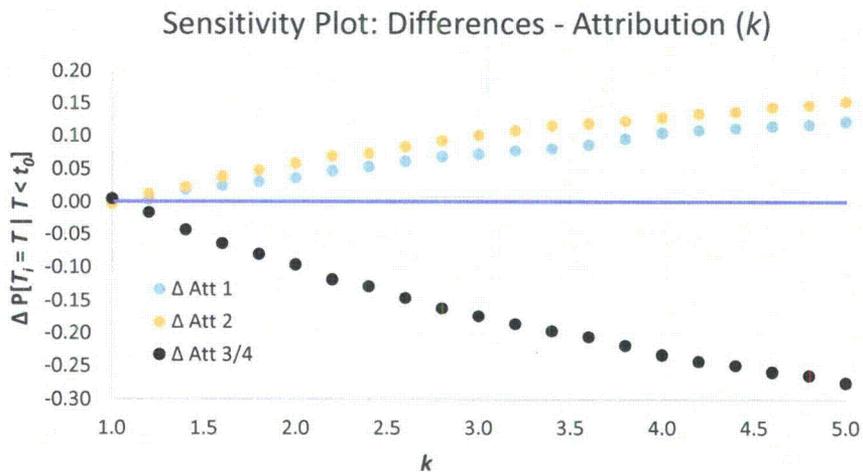


Figure 6: The figure is to be read in the same manner Figure 5 except that differences in attribution probabilities such as $\Delta\mathbb{P}\{T_1 = T | T < t_0\}$ replace $\mathbb{P}\{T_1 = T | T < t_0\}$ on the y -axis. In this case, at any vertical line drawn through the three series the sum of the differences in the attribution probabilities is zero.

A tornado diagram compares the effect of continuously decreasing each input parameter from its nominal value down to its lower bound and increasing the parameter up to its upper bound, and seeing the effect on the model's output. Often output measures change monotonically with respect to the inputs. For example, with all other input parameters held constant, increasing the mean time to failure of component 1, λ_1^{-1} , will increase system reliability ($\mathbb{P}\{T > t_0\}$), increase expected system lifetime ($\mathbb{E}[T]$), and decrease the probability that a failure is attributable to component 1 ($\mathbb{P}\{T_1 = T | T < t_0\}$). Decreases in λ_1^{-1} will have the opposite effect. However, in other cases monotonicity of output is not ensured, and hence we should exercise care that we obtain correct minimum and maximum values of the output as we vary an input over its range.

On the x -axis of a tornado diagram we plot the output measure of interest, in this case, system reliability, $\mathbb{P}\{T > t_0\}$, expected time to system failure, $\mathbb{E}[T]$, or their differences, $\Delta\mathbb{P}\{T > t_0\}$ and $\Delta\mathbb{E}[T]$. The y -axis stacks bars with the range of these outputs for each input parameter of interest. The output under the nominal values of the inputs is highlighted. The horizontal bars for the input parameters are ordered by sensitivity, with the longest bar, i.e., most sensitive input parameters on top. Note the importance of having selected commensurate ranges for the input variables in step 4, as these now affect which parameters are seen as most important. Panels (a) and (b) of Figure 7 display tornado diagrams for the base-option model for $\mathbb{P}\{T > t_0\}$ and $\mathbb{E}[T]$. Panels (a) and (b) of Figure 8 are analogous but for the PM option. Panels (a) and (b) of Figure 9 display $\Delta\mathbb{P}\{T > t_0\}$ and $\Delta\mathbb{E}[T]$, where positive values indicate the PM option has higher reliability and longer expected system lifetime.

Panel (a) of Figure 7 indicates that system reliability under the base option is most sensitive to the value of t_0 , followed by the mean failure times of components 3 and 4 and then the mean times for components 1 and 2. System reliability under the base option is not affected by input parameters k and Δt . For $\mathbb{E}[T]$, panel (b) of Figure 7 indicates the most sensitive parameters are the mean failure times of components 3 and 4 followed by the same times for components 1 and 2. Output $\mathbb{E}[T]$ is not affected by input parameters k , Δt , or t_0 . The results for the PM option in Figure 8 are similar except that we see the importance of parameter k . Interestingly, the results are relatively insensitive to the duration of the PM interval, Δt , although this changes slightly in Figure 9 when examining the results for $\Delta\mathbb{P}\{T > t_0\}$. For this reason, we do not show sensitivity plots with respect to Δt here, although we revisit sensitivity to Δt in step 8 (in spider plots) and step 9 (in a two-way sensitivity analysis with k).

Sampling errors are more easily displayed on sensitivity plots than on tornado diagrams. Still, in Figures 7-9 we display horizontal error bars at the two extremes. Sensitivity plots also have the advantage that multiple outputs can be plotted simultaneously. That said, tornado diagrams can display many input parameters simultaneously and are widely used to assess to which input parameters an output is most sensitive.

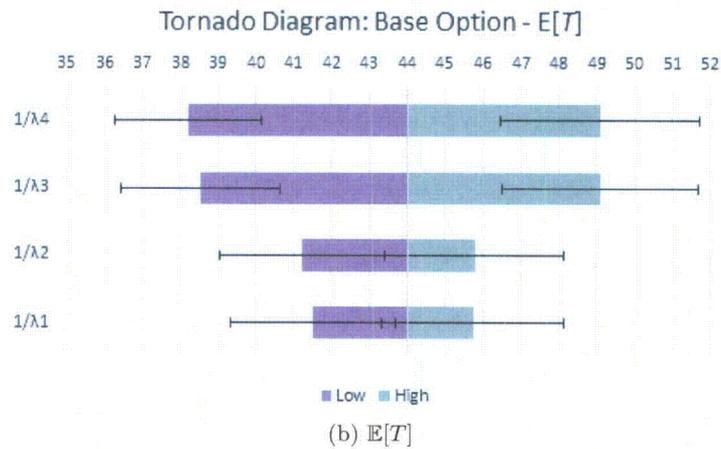
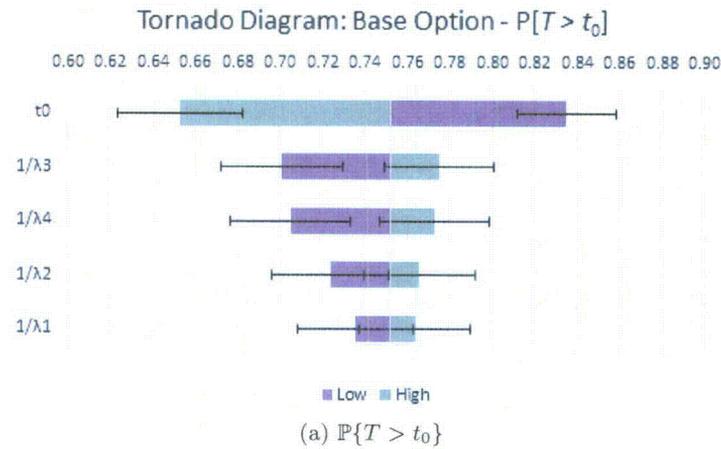


Figure 7: The figure depicts tornado diagrams for $\mathbb{P}\{T > t_0\}$ and $\mathbb{E}[T]$ for the base-option model. Point estimates along with 95% confidence intervals are displayed. The figure indicates that system reliability is most sensitive to the value of t_0 , followed by the mean failure times of λ_3^{-1} and λ_4^{-1} and then by the mean times λ_1^{-1} and λ_2^{-1} . Expected system lifetime is most sensitive to λ_3^{-1} and λ_4^{-1} and then λ_1^{-1} and λ_2^{-1} . Note that the color shading indicates whether a high or low value of the input parameter corresponds to the change in the output. Thus, higher values of t_0 lead to lower values of system reliability, but higher component mean lifetimes lead to higher system reliability. Again, estimates and error bars are calculated based on a sample size of $N = 1000$.

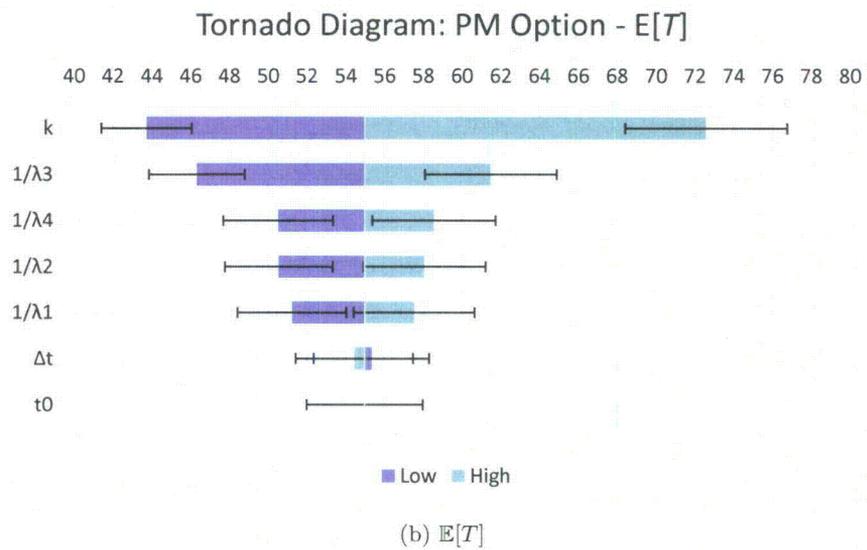
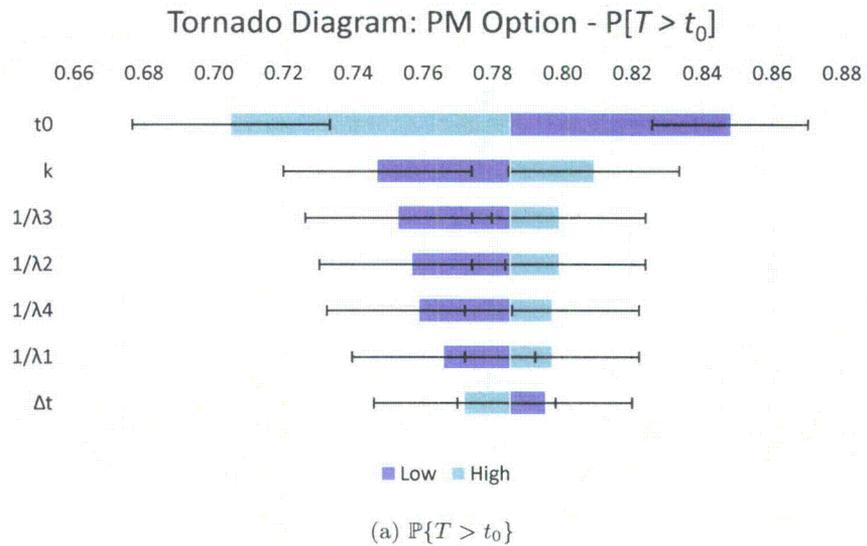


Figure 8: The figure depicts tornado diagrams for $P\{T > t_0\}$ and $E[T]$ for the PM option, and is to be read in the same manner as Figure 7.

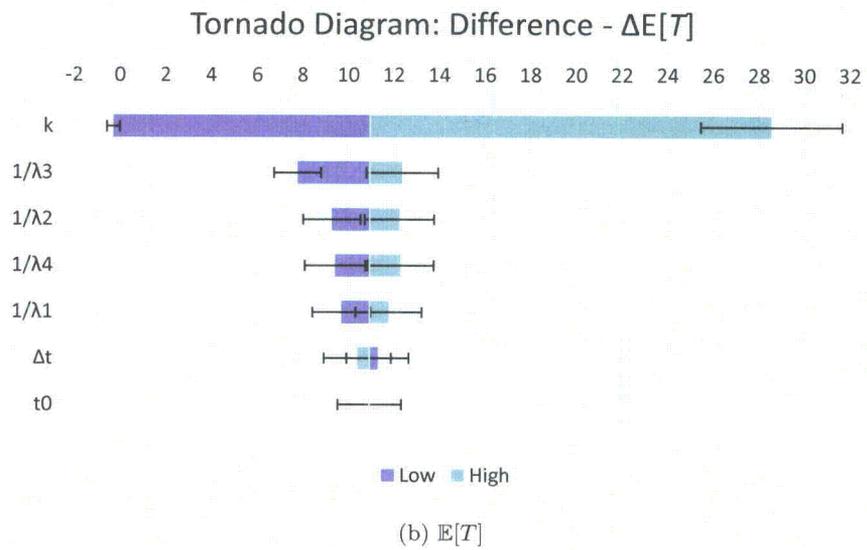
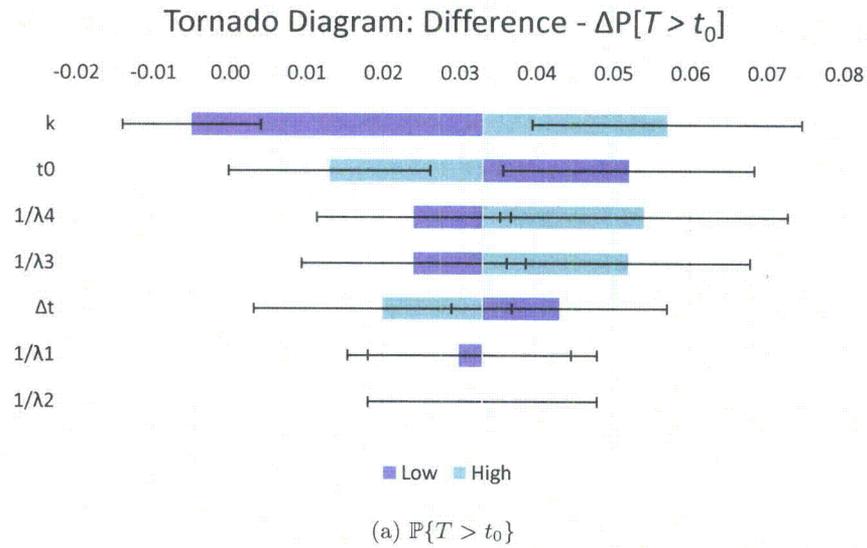


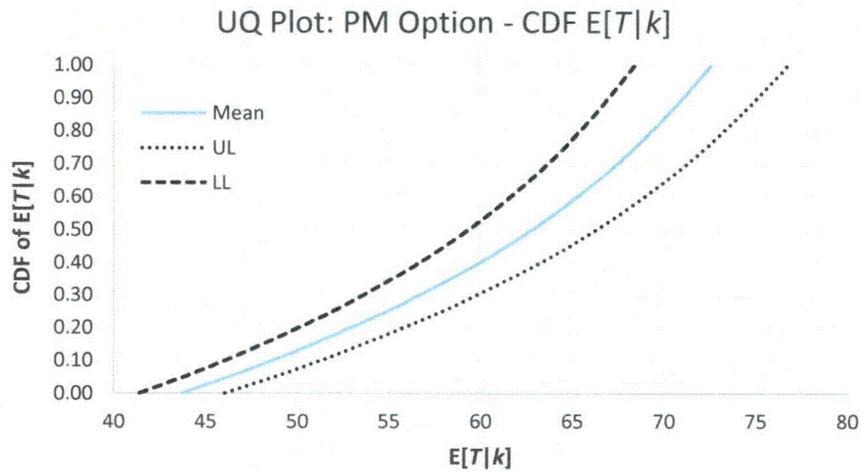
Figure 9: The figure depicts tornado diagrams for $\Delta P\{T > t_0\}$ and $\Delta E[T]$ where positive values favor the PM option.

Step 7: Uncertainty Quantification Plots

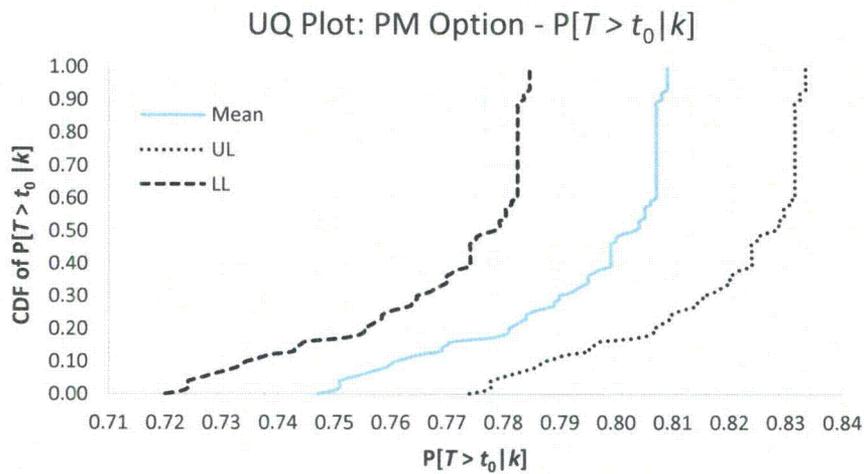
An important part of uncertainty quantification (UQ), and a part that distinguishes it from routine sensitivity analysis, concerns propagating a probability distribution placed on one or more input parameters through the nonlinear function represented by a simulation model and characterizing the resulting probability distribution on an output measure. We emphasize that the probability distribution we speak of here is a probability model that we place on input parameters and not the Monte Carlo sampling-based error we reference above. (That said, as elsewhere, we also capture sampling-based error here, too.) We call a graphical plot of the resulting probability distribution a *UQ plot*, regardless of whether it is expressed as a cumulative distribution function (cdf) or a probability density function (pdf). This idea is closely related to the sensitivity plots we form in step 6, except that we now embed information associated with the probability distribution placed on the input parameters. We begin by focusing on the case when a univariate distribution is placed on a single input parameter, and we then turn to UQ plots when multivariate distributions are placed on input parameters.

When constructing a sensitivity plot, the y -axis is the output parameter, and the x -axis is the input parameter. For a sensitivity plot we typically form a uniform grid over the range of the input parameter values, e.g., over the input ranges that Table 1 specifies. A cdf-based UQ plot is a plot of the cumulative distribution function of the output measure. We also form pdf-based UQ plots. In both cases we form estimates of these function based on sampling, where the sampling is done in a manner we make precise below. For a cdf UQ plot, the x -axis contains levels of the output measure, the y -axis contains probabilities, and the probability distribution on the input parameter is implicitly encoded in the result.

We again use our example to make this idea concrete. Suppose that the improvement factor, k , has a continuous uniform random variable on the interval $(1, 5)$ specified in Table 1. Figure 10 contains UQ plots of $\mathbb{E}[T | k]$ and $\mathbb{P}\{T > t_0 | k\}$ for the PM-option model. The two panels of the figure contain estimates of the cdf-based UQ plots for both these two outputs. As k grows the probability that a system failure is due to a failure of the parallel subsystem of components 3-4 drops. As a result, we see both cdfs grow quickly towards one for large values of $\mathbb{E}[T | k]$ and $\mathbb{P}\{T > t_0 | k\}$ because there is a large probability mass for k associated with little improvement in these values. Figure 11 is similar, except that we now show cdfs for $\Delta\mathbb{E}[T | k]$ and $\Delta\mathbb{P}\{T > t_0 | k\}$ rather than $\mathbb{E}[T | k]$ and $\mathbb{P}\{T > t_0 | k\}$. Finally, Figure 12 shows the pdfs for $\mathbb{E}[T | k]$ and $\Delta\mathbb{E}[T | k]$. We do not show analogous pdfs for $\mathbb{P}\{T > t_0 | k\}$ and $\Delta\mathbb{P}\{T > t_0 | k\}$ because the estimates have excessive sampling error. Developing good pdf estimates for $\mathbb{P}\{T > t_0 | k\}$ and $\Delta\mathbb{P}\{T > t_0 | k\}$ would require a larger sample size.

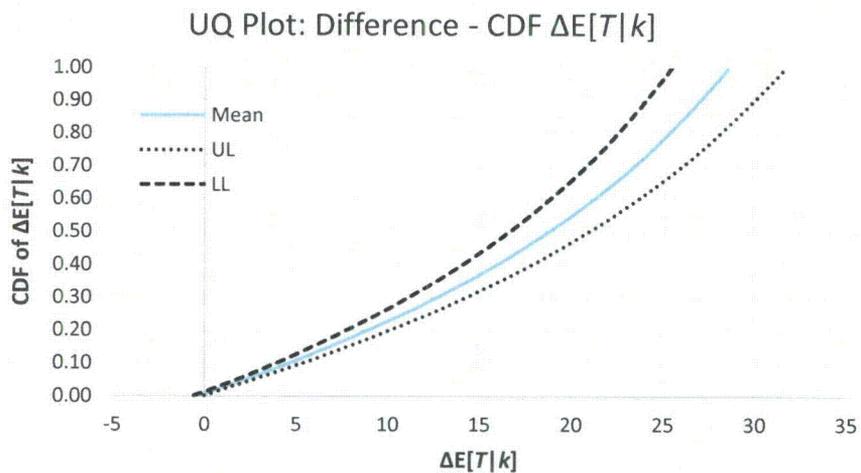


(a) $\mathbb{E}[T | k]$ cdf

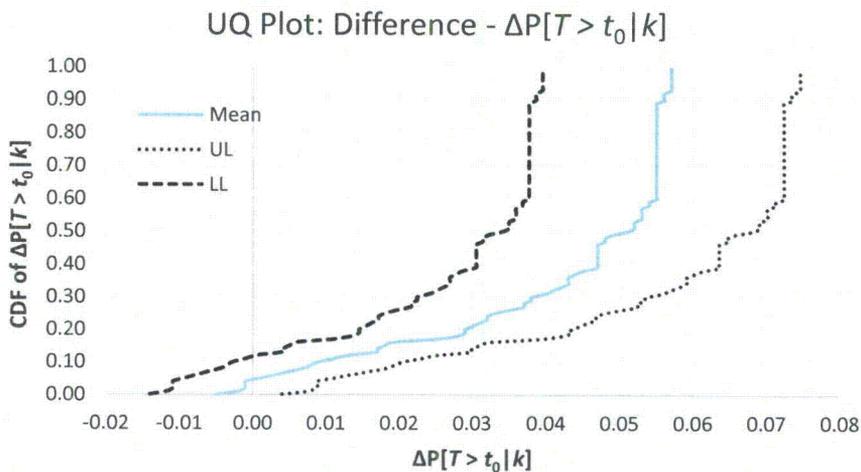


(b) $\mathbb{P}\{T > t_0 | k\}$ cdf

Figure 10: The figure depicts UQ plots which consist of estimates of the cdf of the corresponding output measures when the improvement factor, k , is a uniform random variable on the interval $(1, 5)$. Point estimates as well as a 95% confidence envelope are plotted. As k grows the probability that a system failure is due to the parallel subsystem of components 3-4 shrinks. As a result, we see both cdfs grow quickly towards one for large values of $\mathbb{E}[T | k]$ and $\mathbb{P}\{T > t_0 | k\}$.

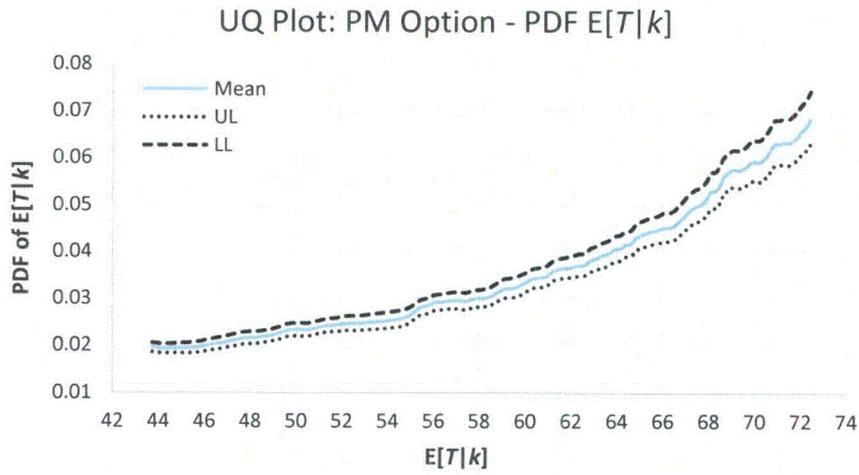


(a) $\Delta\mathbb{E}[T|k]$ cdf

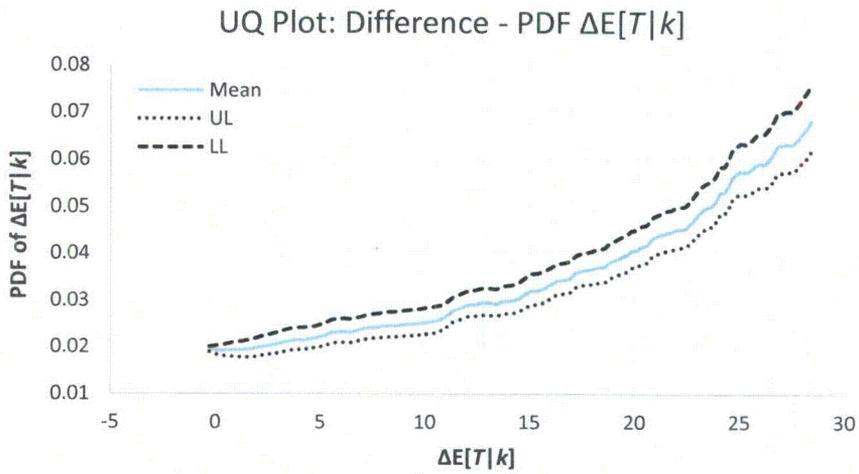


(b) $\Delta\mathbb{P}\{T > t_0|k\}$ cdf

Figure 11: The figure is to be read as Figure 10 except that we now show cdfs for $\Delta\mathbb{E}[T|k]$ and $\Delta\mathbb{P}\{T > t_0|k\}$ rather than $\mathbb{E}[T|k]$ and $\mathbb{P}\{T > t_0|k\}$.



(a) $\mathbb{E}[T|k]$ pdf



(b) $\Delta\mathbb{E}[T|k]$ pdf

Figure 12: The figure depicts UQ plots which consist of estimates of the pdf of $\mathbb{E}[T|k]$ and $\Delta\mathbb{E}[T|k]$ when the improvement factor, k , is a uniform random variable on the interval $(1, 5)$.

In our example, when forming UQ plots of $\mathbb{E}[T|k]$ and $\mathbb{P}\{T > t_0|k\}$ we regard the other six input parameters, $\lambda_1, \dots, \lambda_4, \Delta t$, and t_0 , as deterministic parameters, and the failure times of the four components, T_1, \dots, T_4 as random variables. Our sampling consists of drawing $N = 1000$ independent and identically distributed (i.i.d.) observations of the four-tuple (T_1, \dots, T_4) . In this one-dimensional setting we form the 1%, 2%, 3%, \dots , 99% percentiles of the distribution of k , using its distribution, and we then use our $N = 1000$ i.i.d. observations of (T_1, \dots, T_4) to estimate $\mathbb{E}[T|k = k_\alpha]$, for $\alpha = 0.01, 0.02, \dots, 0.99$, where k_α denotes these percentiles. Although we describe conditioning on evenly-spaced quantiles—evenly spaced in terms of probability—it may be desirable to have a finer grid in regions where the function changes most rapidly. Again, we emphasize the importance of using common random numbers in forming UQ plots such as those in Figures 10-12.

Obvious alternatives to what we have just sketched are also possible, appropriate, and even necessary. (It also important to recognize what is inappropriate and we point to that, too, below.) For example, we could regard the other six parameters as random variables instead of fixing them at their nominal values and sample them in the same way we sample (T_1, \dots, T_4) , while still conditioning on $k = k_\alpha$ to form estimates of $\mathbb{E}[T|k = k_\alpha]$. Clarity in exposition should indicate what precisely the expected-value operator is averaging over.

In another alternative, we could also sample from k 's distribution instead of conditioning on its quantiles in order to form a UQ plot. When sampling k , it is important to distinguish this sampling from that for (T_1, \dots, T_4) . Specifically, we could use one sample size N_{uq} for k and form $k^i, i = 1, \dots, N_{uq}$ from k 's distribution. For each of these samples we then compute, or rather estimate $\mathbb{E}[T|k = k^i], i = 1, \dots, N_{uq}$, where each estimate averages over the N sampled realizations of (T_1, \dots, T_4) . We then use the estimates of $\mathbb{E}[T|k = k^i], i = 1, \dots, N_{uq}$, to form the types of plots in Figure 10.

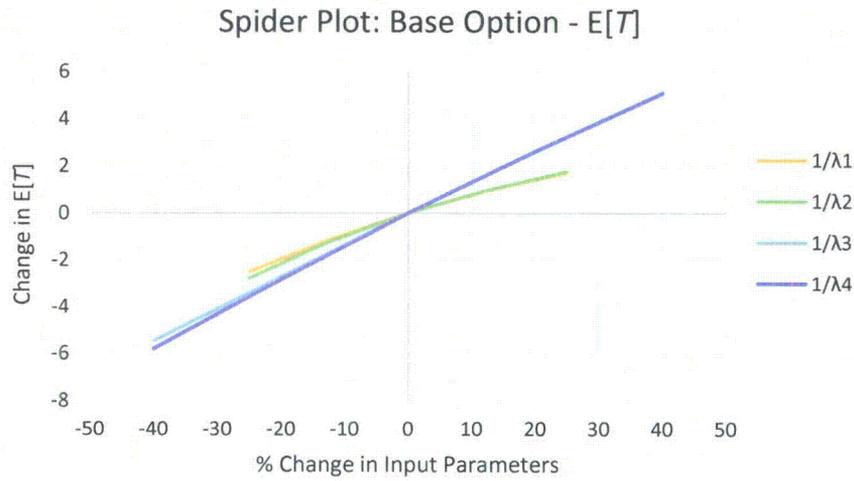
We did not use this sampling-based method in forming the UQ plots of Figure 10 because it is more efficient in the one-dimensional setting to condition on the quantiles as we describe above. However, this sampling-based approach is necessary to form a UQ plot when bivariate, or higher dimensional multivariate, distributions are placed on input parameters. For example, if we place a bivariate distribution on the PM time–reduction factor pair, $(\Delta t, k)$, then such a bivariate distribution has no notion of quantiles, and so the one-dimensional procedure does not have a bivariate analog. We must sample. Importantly, we do not have to sample (T_1, \dots, T_4) from its underlying distribution. If we have a variance reduction scheme that forms, e.g., unbiased estimates of $\mathbb{E}[T|k = k^i]$ then that sampling scheme can be used. However, it is important to recognize that we must sample from the “true” underlying distribution of $(\Delta t, k)$. If we use a distribution-altering variance reduction scheme to sample from $(\Delta t, k)$ when averaging out those parameters, that scheme cannot be used when forming a UQ plot. Such altered schemes are designed to reduce variance and hence would yield misleading plots, indicating, e.g., a pdf that is too narrow about the mean value of the output measure.

Step 8: One-Way Sensitivity Analysis: Spider Plots

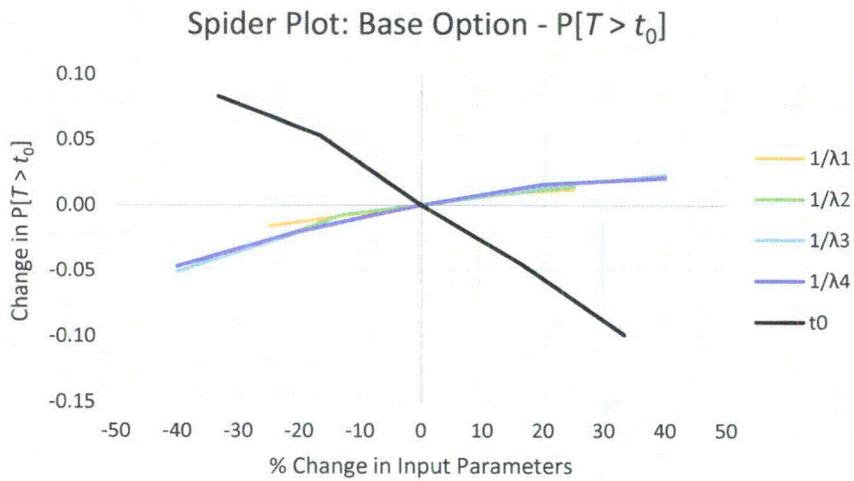
A spider plot is an x - y graph, in which the x -axis depicts changes in the input parameters and the y -axis captures corresponding changes in the model's output measure. Like a tornado diagram, a spider plot involves multiple input parameters and a single output variable. The output variable is typically expressed in its natural units. For example, we express changes in $\mathbb{E}[T]$ in months and we express changes in $\mathbb{P}\{T > t_0\}$ as a unitless value between 0 and 1, where the changes are relative to estimates under the nominal value of the parameters. In order to allow the x -axis to simultaneously represent multiple input parameters, which are on different scales with different units, there are two possibilities. One possibility is to express percentage changes in the input parameters from their nominal values. The second possibility is to express changes as multiples of the standard deviation of the input parameters, when those input parameters are governed by probability distributions. In either case, the magnitude we vary the parameters is determined by the reasonable and commensurate ranges we have specified in step 4 of the analysis, e.g., in Table 1. In the former case, if the nominal value of the input parameter is zero, then a second x -axis must be added.

A tornado diagram can include a larger number of input variables than a spider plot. A spider plot allows displaying about seven input parameters before it becomes cluttered. If the output variable is monotonic (increasing or decreasing) in an input parameter then we only need to estimate the model's output at the lower bound, nominal value, and upper bound of the input parameter. A spider plot requires estimating the model's output at enough values of each input parameter that a seemingly continuous plot of (x, y) pairs can be formed. A spider plot contains more information than a tornado diagram. The tornado diagram's endpoints denote the endpoints of the spider plot, but the spider plot also specifies changes in the output at intermediate values, as does a sensitivity plot. Again like a sensitivity plot, we can assess whether changes in the output are linear or nonlinear with respect to changes in the input. Spider plots can contain point estimates or 95%, say, confidence intervals on those changes. (In the latter case, we may need to reduce the number of input parameters simultaneously displayed.)

Figure 13 displays two spider plots for our example for $\mathbb{E}[T]$ and $\mathbb{P}\{T > t_0\}$ (y -axis) for the base-option model as a function of percentage changes in the input parameters (x -axis). Panel (a) shows a spider plot for $\mathbb{E}[T]$ while panel (b) shows the spider plot for $\mathbb{P}\{T > t_0\}$. Figure 14 displays spider plots for the PM option for our example, and Figure 15 displays spider plots for $\Delta\mathbb{E}[T]$ and $\Delta\mathbb{P}\{T > t_0\}$. Note that we choose not to include confidence limits for each parameter displayed in the graph because of the clutter they induce. Also note that the range of the x -axis is determined by the nominal values and the lower and upper bounds specified in Table 1. Importantly, the input parameters are *not* each varied the same percentage. Rather, the limits are those specified in Table 1. Qualitatively, the figures are similar to the tornado diagrams as to the most sensitive input parameters. However, Figures 13-15 are more insightful as to the rate of change and any associated nonlinearities in the change.

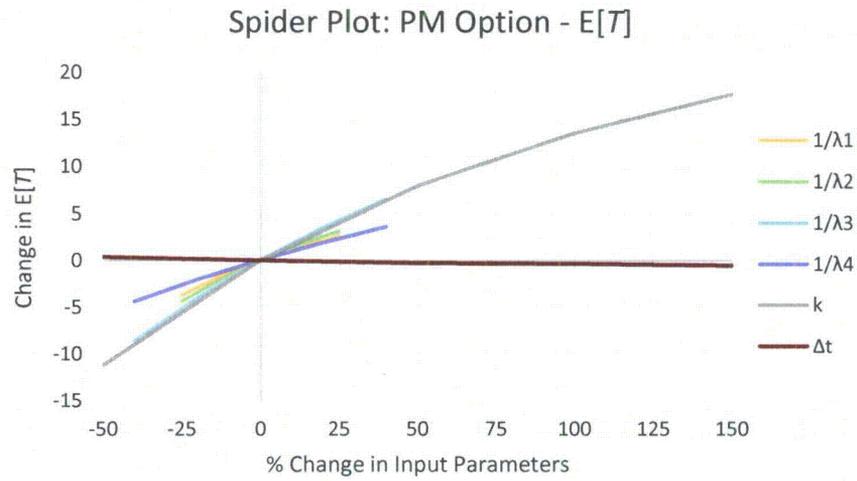


(a) $E[T]$

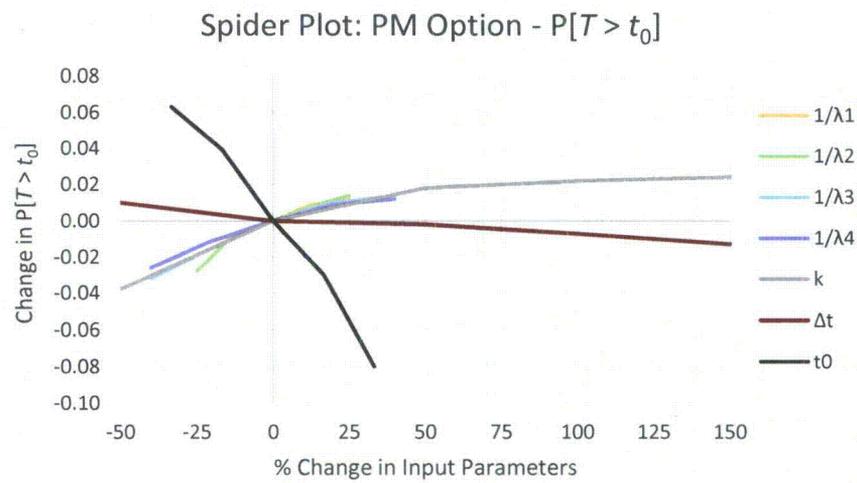


(b) $P\{T > t_0\}$

Figure 13: The figure depicts two spider plots for the base option in our example. The plot in panel (a) shows $E[T]$ (y -axis) as a function of percentage changes in the input parameters (x -axis). The plot in panel (b) is identical to the one in panel (a) except that the y -axis is $P\{T > t_0\}$.

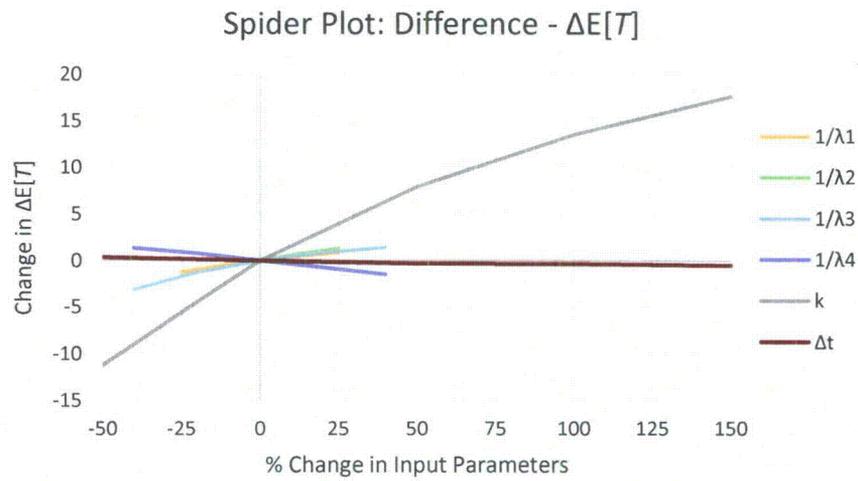


(a) $E[T]$

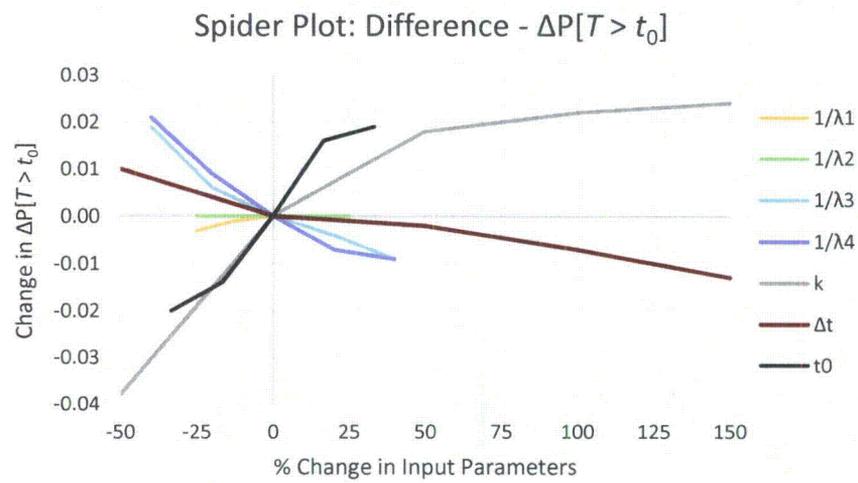


(b) $P\{T > t_0\}$

Figure 14: The figure reads as Figure 13 except that it is for the PM option in our example.



(a) $\Delta E[T]$



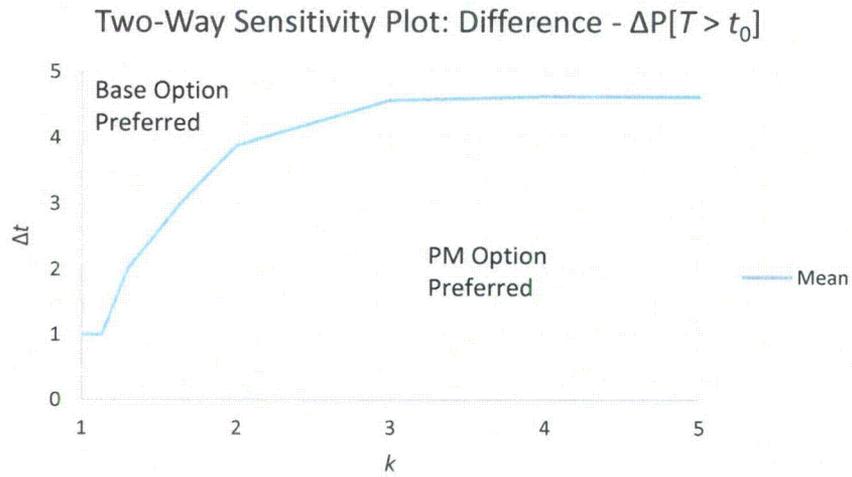
(b) $\Delta P\{T > t_0\}$

Figure 15: The figure reads as Figure 13 except that it is for the differences in performance for our example.

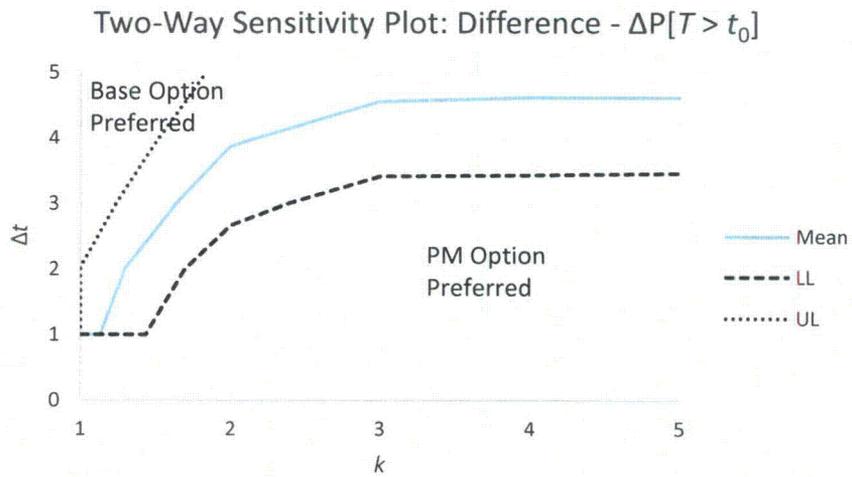
Step 9: Two-way Sensitivity Analysis

Two-way sensitivity graphs allow for visualizing the interaction of two or more input variables. While such analysis can be more difficult to perform, it can provide valuable insight. For our example, Figure 16 depicts the effect of simultaneous changes in the duration of PM (Δt) and the factor by which the PM reduces the failure rate of component 3 (k) on $\Delta\mathbb{P}\{T > t_0\}$. Panel (a) contains only the point estimate, and panel (b) contains both the point estimate and the confidence limits, allowing us to see the indifference zone where neither option is statistically better than the other. Figure 17 is similar to Figure 16, except the parameters of interest are t_0 and k .

Two-way sensitivity analyses can be extended to include more than two decision alternatives, and in such cases the plots typically partition the space into three or more regions in which each alternative is preferred. It is also possible to form a three-dimensional plot of an output variable (e.g., the difference in system reliability $\Delta\mathbb{P}\{T > t_0\}$) as a function of two input variables (e.g., Δt and k), although we do not pursue that here.

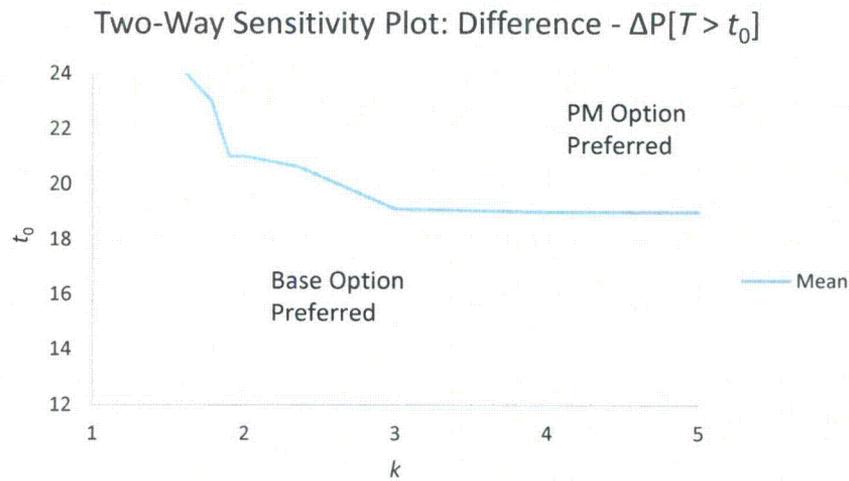


(a) Point Estimate

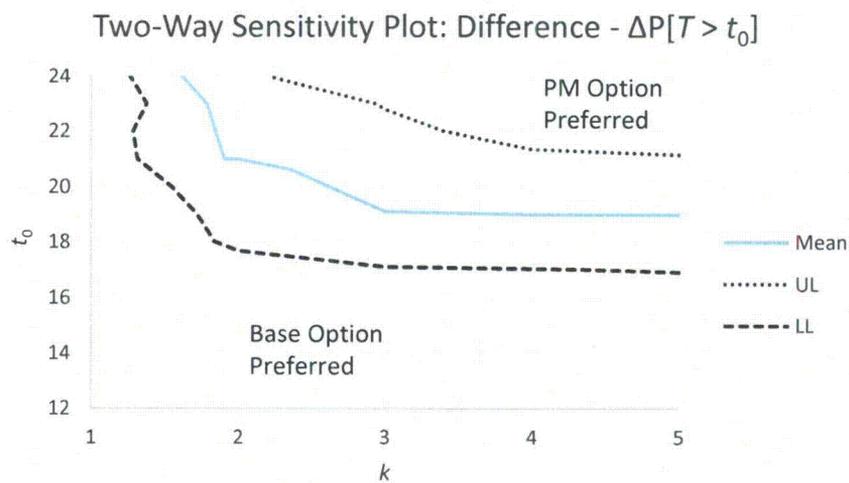


(b) Point Estimate and Confidence Limits

Figure 16: The figure depicts a two-way sensitivity plot for the input parameters governing the duration of PM, Δt , and the factor by which the failure rate of component 3 is reduced, k . When Δt is small and k is large, the PM option is preferred, and when Δt is large and k is small the base option is preferred. The figure quantifies this notion with the two-dimensional analog of a threshold analysis.



(a) Point Estimate



(b) Point Estimate and Confidence Limits

Figure 17: The figure depicts a two-way sensitivity plot for the input parameters governing the minimum time the system must be operational, t_0 , and the factor by which the failure rate of component 3 is reduced, k . When t_0 is small and k is small, the base option is preferred, and when t_0 is large and k is large the PM option is preferred.

Step 10: Metamodels & Design of Experiments

The possible pitfalls of changing only one input parameter at a time are well documented in the literature (see, e.g., [8, 10]) and include the fact that interaction effects between input parameters are lost. Graphical sensitivity analyses become more difficult when moving past a one- or two-dimensional analysis, but we can form a *metamodel* (which is also called a *response surface*, an *emulator*, or a *surrogate model*) and carry out an experimental design to fit that metamodel.

Recall from step 1 that we use y to denote the simulation model's output and we use $x = (x_1, \dots, x_n)$ to denote the simulation model's input. For simplicity we focus on a single output measure. Among the simplest metamodels typically postulated are polynomial regression models of low degree; e.g.,

$$y = \beta_0 + \sum_{k=1}^n \beta_k x_k + \sum_{k=1}^n \sum_{k'=k+1}^n \beta_{k,k'} x_k x_{k'} + \epsilon. \quad (3)$$

To fit the parameters $\beta_0, \beta_1, \dots, \beta_n$, and $\beta_{1,2}, \dots, \beta_{1,n}, \dots, \beta_{n-1,n}$, we use an experimental design to specify M , say, input parameter vectors (x_1^i, \dots, x_n^i) , $i = 1, \dots, M$, coupled with the corresponding estimated simulation output y^i . The corresponding error terms, ϵ^i , are assumed to be independent and normally distributed with mean zero, at least in the simplest approach. So far, we have emphasized the importance of using common random numbers in carrying out our analyses. However, the assumption that the error terms ϵ^i are independent requires that we draw independent Monte Carlo samples at each design point. When estimating a difference, we still use common random numbers for the base and PM options at that design point.

We could add higher-order cross terms to equation (3). This can improve the quality of the fit, but we need to take care that we have an adequate number of observations relative to the larger number of model parameters so the model is not over-fit. Perhaps more importantly, a thorough understanding of a higher-degree polynomial regression model can be challenging.

Table 1 specifies seven input parameters for our example, but only five of those input parameters matter for the base option. (The PM parameters of Δt and k are not relevant for the base option.) In this case, we can seek to explain system reliability $y = \mathbb{P}\{T > t_0\}$ as a relatively simple function of $\lambda_1^{-1}, \lambda_2^{-1}, \lambda_3^{-1}, \lambda_4^{-1}$, and t_0 . A full factorial design with two levels in this case would involve $2^5 = 32$ combinations of these values placed at their lower and upper bounds from Table 1. When we also include the nominal case for the values of the parameters we have $3^5 = 243$ combinations. If we instead have seven input parameters for the PM option, these values become $2^7 = 128$ and $3^7 = 2187$. Note that the preceding values represent the number of "design points" in a specific experimental design. In order to estimate higher-order effects and interaction terms, multiple replications are typically run at each design point. So for our example, at each design point, we could estimate $y = \mathbb{P}\{T > t_0\}$ using a sample size of $N = 1000$, and we could replicate that point estimate $N_r = 3$ times.

For our example, we present the results of a regression metamodel, where the performance measure of interest is the difference in reliability, $\Delta \mathbb{P}\{T > t_0\}$, where again, positive values favor

the PM option. We use a 3^7 full factorial design, where the three levels are the minimum, nominal, and maximum values in Table 1. At each design point, we perform $N_r = 3$ independent replications of the simulation using a sample size of $N = 1000$ for each replicate.

Table 4: Experimental design parameters for the replicated 3^7 factorial design and overall model fit statistics. The F -Statistic measures whether any of the input variables in any combination with one another have a statistically significant effect on the response ($\Delta\mathbb{P}\{T > t_0\}$). The adjusted R^2 value assesses the overall goodness-of-fit of the model to the simulation output.

# of Design Points	2,187
# of Replications Per Design Point:	3
Total Sample Size:	6,561
Residual Standard Error:	0.01295
Residual Degrees of Freedom:	6,532
Adjusted R^2 Value:	0.8895
F -Statistic:	1,886
Degrees of Freedom 1:	28
Degrees of Freedom 2:	6,532
p -value:	<2.20E-16

From the information in Table 4, we can see that based on the adjusted R^2 value of 0.8895, we have a good (not excellent) fit to the simulation output. An excellent fit is categorized by an adjusted R^2 value of at least 0.90. As we indicate above, in a 3^7 full factorial experimental design, there are 2,187 design points; i.e., 2,187 unique combinations of input parameters. We replicate these design points three times, for a total size of 6,561. Each of these 6,561 estimates of $\Delta\mathbb{P}\{T > t_0\}$ is based on a sample size of $N = 1000$. The F -Statistic and p -value are used to test the hypothesis that all of the coefficients β_k and $\beta_{k,k'}$, with the exception of the intercept β_0 , are zero. If this is the case, none of the input parameters (i.e., “factors” in the terminology of regression and experimental design) or interactions among these parameters are significant in estimating the response variable, $\Delta\mathbb{P}\{T > t_0\}$. The p -value measures the statistical significance of the result. For the F -Test, we see that the p -value is less than 2.2×10^{-16} , which is much less than the standard significance level of 0.05. So for this F -Test we can conclude that at least one coefficient in our regression model is significantly different from zero, and hence is a significant factor in estimating $\Delta\mathbb{P}\{T > t_0\}$. This, coupled with a reasonably good adjusted R^2 value of 0.8895 suggests that we have a relatively good fit to the simulation output and the fit parameters, other than the intercept, play a significant role in estimating $\Delta\mathbb{P}\{T > t_0\}$.

The next step in the analysis is to examine which regression coefficients, β_k and $\beta_{k,k'}$, are statistically significant in our model. This is a notion of attribution in that we are attempting to attribute a change in the response variable to changes in the input variable and characterize the strength of the relationship. Table 5 presents the estimates for the coefficients in the regression model (3) as well as their standard errors, and the associated p -values for determining the significance levels of

individual parameters.

Table 5: Results of fitting linear regression model (3) for $\Delta\mathbb{P}\{T > t_0\}$. We exclude all terms higher than second order terms as equation (3) indicates. Using the p -value we can determine which effects and two-way interactions have a significant effect in estimating $\Delta\mathbb{P}\{T > t_0\}$.

Coefficients	Parameters	Coefficient Estimates	Standard Error	t-value	p-value	Significant at $\alpha = 0.05$
β_0	Intercept	-4.374E-02	8.909E-03	-4.910	9.34E-07	Yes
β_1	λ_1^{-1}	-4.420E-06	3.132E-05	-0.141	8.88E-01	No
β_2	λ_2^{-1}	-4.166E-05	3.132E-05	-1.330	1.84E-01	No
β_3	λ_3^{-1}	2.448E-04	8.680E-05	2.820	4.82E-03	Yes
β_4	λ_4^{-1}	4.089E-04	8.680E-05	4.711	2.52E-06	Yes
β_5	k	1.480E-02	9.005E-04	16.434	2.00E-16	Yes
β_6	Δt	-2.160E-02	1.801E-03	-11.993	2.00E-16	Yes
β_7	t_0	2.959E-03	2.816E-04	10.507	2.00E-16	Yes
$\beta_{1,2}$	$\lambda_1^{-1} \cdot \lambda_2^{-1}$	7.682E-09	9.591E-08	0.080	9.36E-01	No
$\beta_{1,3}$	$\lambda_1^{-1} \cdot \lambda_3^{-1}$	-3.916E-07	2.398E-07	-1.633	1.02E-01	No
$\beta_{1,4}$	$\lambda_1^{-1} \cdot \lambda_4^{-1}$	-3.837E-07	2.398E-07	-1.600	1.10E-01	No
$\beta_{1,5}$	$\lambda_1^{-1} \cdot k$	1.009E-05	2.398E-06	4.206	2.63E-05	Yes
$\beta_{1,6}$	$\lambda_1^{-1} \cdot \Delta t$	-6.564E-06	4.796E-06	-1.369	1.71E-01	No
$\beta_{1,7}$	$\lambda_1^{-1} \cdot t_0$	1.901E-06	7.993E-07	2.378	1.74E-02	Yes
$\beta_{2,3}$	$\lambda_2^{-1} \cdot \lambda_3^{-1}$	-4.407E-07	2.398E-07	-1.838	6.61E-02	No
$\beta_{2,4}$	$\lambda_2^{-1} \cdot \lambda_4^{-1}$	-1.680E-08	2.398E-07	-0.070	9.44E-01	No
$\beta_{2,5}$	$\lambda_2^{-1} \cdot k$	1.061E-05	2.398E-06	4.427	9.73E-06	Yes
$\beta_{2,6}$	$\lambda_2^{-1} \cdot \Delta t$	-5.576E-06	4.796E-06	-1.163	2.45E-01	No
$\beta_{2,7}$	$\lambda_2^{-1} \cdot t_0$	3.070E-06	7.993E-07	3.842	1.23E-04	Yes
$\beta_{3,4}$	$\lambda_3^{-1} \cdot \lambda_4^{-1}$	1.319E-05	5.994E-07	21.998	2.00E-16	Yes
$\beta_{3,5}$	$\lambda_3^{-1} \cdot k$	-2.303E-04	5.994E-06	-38.416	2.00E-16	Yes
$\beta_{3,6}$	$\lambda_3^{-1} \cdot \Delta t$	-8.428E-05	1.199E-05	-7.030	2.28E-12	Yes
$\beta_{3,7}$	$\lambda_3^{-1} \cdot t_0$	-3.768E-05	1.998E-06	-18.858	2.00E-16	Yes
$\beta_{4,5}$	$\lambda_4^{-1} \cdot k$	-2.378E-04	5.994E-06	-39.675	2.00E-16	Yes
$\beta_{4,6}$	$\lambda_4^{-1} \cdot \Delta t$	2.797E-04	1.199E-05	23.329	2.00E-16	Yes
$\beta_{4,7}$	$\lambda_4^{-1} \cdot t_0$	-5.333E-05	1.998E-06	-26.691	2.00E-16	Yes
$\beta_{5,6}$	$k \cdot \Delta t$	-1.725E-03	1.199E-04	-14.390	2.00E-16	Yes
$\beta_{5,7}$	$k \cdot t_0$	1.183E-03	1.998E-05	59.200	2.00E-16	Yes
$\beta_{6,7}$	$\Delta t \cdot t_0$	3.536E-04	3.996E-05	8.847	2.00E-16	Yes

Table 5 provides several insights, and can be viewed as “typical” regression output. In the first two columns of the table, we list all of the coefficients in the model, their corresponding input parameters, and interactions among the input parameters. For example, β_0 is the coefficient representing the intercept, β_1 represents the coefficient of λ_1^{-1} , and $\beta_{5,7}$ represents the interaction between k and t_0 . The third column presents point estimates of each of the regression coefficients and the fourth column presents the standard error associated with these coefficients. The ratio of

the estimate to the standard error is the t -value for the t -test, which tests the hypothesis that each individual parameter takes value zero so that rejecting the null hypothesis indicates the parameter is significant. The p -values for the t -tests for each of these terms (column 6) can be interpreted in same manner as the p -value for the F -test we describe above, and can be used to determine the statistical significance of each term in the regression model individually, whereas the F -test determines the significance of the parameters as a group.

The positive signs on the coefficients for k and t_0 are consistent with the sensitivity plots in Figures 3 and 4 and the spider plot in Figure 15 and, of course, with intuition. Similarly, the negative coefficient for Δt is consistent with intuition and Figure 15: As the time required to carryout PM grows, the benefit of the PM option drops. The signs and magnitude of other coefficients are more subtle. The positive coefficient for λ_3^{-1} is counterintuitive: As the reliability of component 3 grows, the benefit from PM should shrink, not grow. However, examining the sign and relative magnitude of the coefficients for λ_3^{-1} and $\lambda_3^{-1} \cdot k$ —and knowing the nominal value of k is 2—we see that as λ_3^{-1} grows, the regression estimate of $\Delta\mathbb{P}\{T > t_0\}$ indeed shrinks. This holds except for values of $k \approx 1$, on the boundary of the experimental design, where the quality of the regression fit is likely poorer.

We can see from the information in Table 5, that several of the two-factor interactions terms are significant, including all interaction terms involving k and t_0 , indicating that these parameters have a significant effect on the response variable $\Delta\mathbb{P}\{T > t_0\}$. This is again consistent with what we learned from the tornado diagram in Figure 9 and the spider plot of Figure 15. In addition, we see that the interaction term $k \cdot t_0$ has the greatest t -statistic among all terms, and we can conclude that it is one of the most significant contributors to the estimate of $\Delta\mathbb{P}\{T > t_0\}$. The fact that this nonlinearity is important, and that the sign of $k \cdot t_0$'s coefficient is positive, is not surprising given the two-way sensitivity plot in Figure 17 for k and t_0 .

To illustrate the value of this regression output, we demonstrate how to use this regression equation to predict the value of $\Delta\mathbb{P}\{T > t_0\}$, without the need to rerun the simulation model. This is especially important for large-scale stochastic simulation models for which it may take several days or even weeks to run a designed experiment and collect the type of output we collected for this illustrative example. If the statistical experiment is planned well, the regression metamodel can be used to predict performance measures without the need for rerunning the simulation model. However, we note that using this approach, we should not use values of the input parameters outside the bounds of those used in the experimental design, in our case the minimum parameter values from Table 1. And, as we have already seen, near the boundary of the design, the regression fit may degrade. In addition, we should examine the goodness-of-fit statistics we describe above to ensure the statistical model is adequate before relying on its predictive power. Table 6 applies our regression metamodel to the nominal values for all parameters, and forms an estimate of $\Delta\mathbb{P}\{T > t_0\}$ without the need to run the simulation model. Table 7 presents the results of simply using the simulation model to estimate $\Delta\mathbb{P}\{T > t_0\}$ and its associated error, and we can compare these estimates to the value obtained by using the regression metamodel to determine the validity

of metamodel.

Table 6: An example of applying the results of the regression model to the nominal values of the input parameters in order to predict $\Delta\mathbb{P}\{T > t_0\}$. Note that using this method, we no longer need to run the simulation model to predict $\Delta\mathbb{P}\{T > t_0\}$ as a function of any combination of input parameters. The adjusted R^2 value from Table 4 is 0.8895, and in practice this value is acceptable, although 0.90 is typically considered the threshold for an excellent fit.

Coefficients	Coefficient Estimates	Parameters	Parameter Values	Contribution
β_0	-4.374E-02	Intercept	None	-0.0437
β_1	-4.420E-06	λ_1^{-1}	200	None
β_2	-4.166E-05	λ_2^{-1}	200	None
β_3	2.448E-04	λ_3^{-1}	50	0.0122
β_4	4.089E-04	λ_4^{-1}	50	0.0204
β_5	1.480E-02	k	2	0.0296
β_6	-2.160E-02	Δt	1	-0.0216
β_7	2.959E-03	t_0	18	0.0533
$\beta_{1,2}$	7.682E-09	$\lambda_1^{-1} \cdot \lambda_2^{-1}$	40000	None
$\beta_{1,3}$	-3.916E-07	$\lambda_1^{-1} \cdot \lambda_3^{-1}$	10000	None
$\beta_{1,4}$	-3.837E-07	$\lambda_1^{-1} \cdot \lambda_4^{-1}$	10000	None
$\beta_{1,5}$	1.009E-05	$\lambda_1^{-1} \cdot k$	400	0.0040
$\beta_{1,6}$	-6.564E-06	$\lambda_1^{-1} \cdot \Delta t$	200	None
$\beta_{1,7}$	1.901E-06	$\lambda_1^{-1} \cdot t_0$	3600	0.0068
$\beta_{2,3}$	-4.407E-07	$\lambda_2^{-1} \cdot \lambda_3^{-1}$	10000	None
$\beta_{2,4}$	-1.680E-08	$\lambda_2^{-1} \cdot \lambda_4^{-1}$	10000	None
$\beta_{2,5}$	1.061E-05	$\lambda_2^{-1} \cdot k$	400	0.0042
$\beta_{2,6}$	-5.576E-06	$\lambda_2^{-1} \cdot \Delta t$	200	None
$\beta_{2,7}$	3.070E-06	$\lambda_2^{-1} \cdot t_0$	3600	0.0111
$\beta_{3,4}$	1.319E-05	$\lambda_3^{-1} \cdot \lambda_4^{-1}$	2500	0.0330
$\beta_{3,5}$	-2.303E-04	$\lambda_3^{-1} \cdot k$	100	-0.0230
$\beta_{3,6}$	-8.428E-05	$\lambda_3^{-1} \cdot \Delta t$	50	-0.0042
$\beta_{3,7}$	-3.768E-05	$\lambda_3^{-1} \cdot t_0$	900	-0.0339
$\beta_{4,5}$	-2.378E-04	$\lambda_4^{-1} \cdot k$	100	-0.0238
$\beta_{4,6}$	2.797E-04	$\lambda_4^{-1} \cdot \Delta t$	50	0.0140
$\beta_{4,7}$	-5.333E-05	$\lambda_4^{-1} \cdot t_0$	900	-0.0480
$\beta_{5,6}$	-1.725E-03	$k \cdot \Delta t$	2	-0.0035
$\beta_{5,7}$	1.183E-03	$k \cdot t_0$	36	0.0426
$\beta_{6,7}$	3.536E-04	$\Delta t \cdot t_0$	18	0.0064
Estimate of $\Delta\mathbb{P}\{T > t_0\}$				0.03591

Table 7: Results for $\Delta\mathbb{P}\{T > t_0\}$ from running the simulation model with all input parameters at nominal levels with sample size $N = 1000$.

$\Delta\mathbb{P}\{T > t_0\}$	0.0330
95% CI Halfwidth	0.0149
95% CI Lower Limit	0.0181
95% CI Upper Limit	0.0479

In Table 6 we again provide the estimates of the coefficients and the parameters and interactions they represent. The fourth column of this table contains the parameter values for each of the associated coefficients for the nominal case, with the exception of the intercept which is not directly linked to any parameter or interaction. The first seven values in this column match the nominal parameter values given in Table 1. The interaction terms are simply the products of these input parameter values. For example, the nominal value of $\Delta t = 1$, and the nominal value of $k = 2$, and thus the parameter value for the interaction $\Delta t \cdot k = 2$, as shown in the table. As shown in regression model (3), an estimate of $\Delta\mathbb{P}\{T > t_0\}$ can be formed by computing the product of the parameter (or interaction term) values and the coefficient, and summing those values along with the value of the intercept. The final column in Table 6 is the product of the coefficient and parameter value. Summing all the values in this column provides us with an estimate of $\Delta\mathbb{P}\{T > t_0\} = 0.03591$ when all parameters are at their nominal levels.

It is useful to compare this estimate with a point estimate and associated 95% confidence limits of $\Delta\mathbb{P}\{T > t_0\}$ using the simulation model. Table 7 presents results from the simulation model, and we see that the estimate of $\Delta\mathbb{P}\{T > t_0\}$ is $0.0330 \pm 0.0149 = (0.0181, 0.0479)$. We can see that our regression metamodel estimate of 0.0359 is within the 95% confidence limits, and is different from the simulation point estimate of 0.0330 by less than 10%. This suggests that our regression metamodel can be used in lieu of running the simulation under appropriate circumstances.

In addition to predicting the values of performance measures, we can also use the results of the designed experiment to construct two-way interaction plots that describe how a given response changes as a function of two input parameters. Figures 18-21 show two-way interaction plots for pairs of input parameters, where the response variable is again $\Delta\mathbb{P}\{T > t_0\}$. For example, in Figure 18, we see how $\Delta\mathbb{P}\{T > t_0\}$ changes when all input parameters are held constant except for k and λ_3^{-1} . First, we see that when $k = 1$, using the point estimates, we prefer the base option regardless of the value of λ_3^{-1} . However, for values of k greater than one (namely 3 and 5), we prefer the PM option regardless of the value of λ_3^{-1} . When λ_3^{-1} is at its minimum value of 30, changes in the repair factor k have a more significant effect on $\Delta\mathbb{P}\{T > t_0\}$ than when λ_3^{-1} is at the nominal or maximum levels. Figure 19 shows similar results for k and t_0 . The fact that $\Delta\mathbb{P}\{T > t_0\}$ grows with k and t_0 is as expected, as is the amplification of the effect of growing k for larger values of t_0 . Figures 20 and 21 depict analogous results for the respective pairs $(k, \Delta t)$ and $(t_0, \Delta t)$.

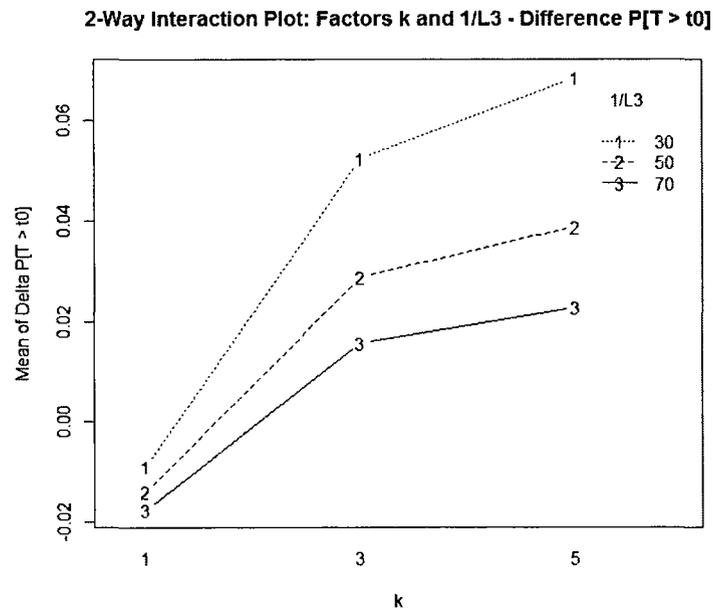


Figure 18: The figure is a two-way interaction plot for k and λ_3^{-1} , where the response variable is $\Delta P\{T > t_0\}$.

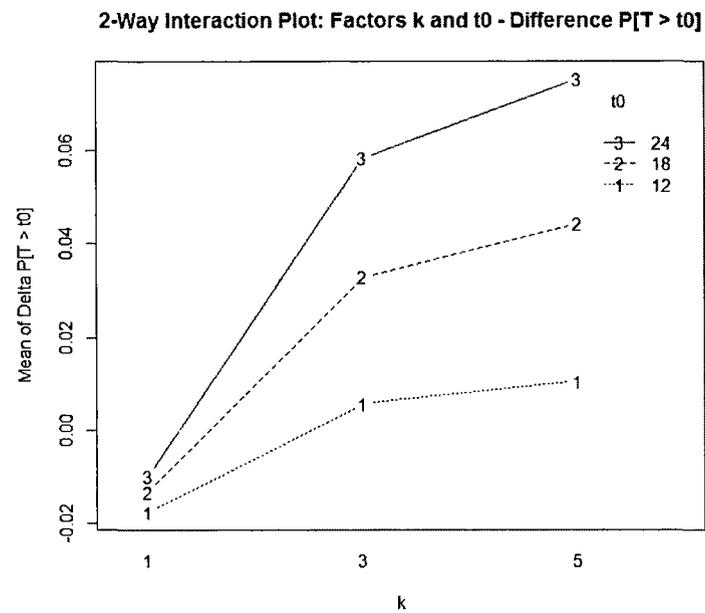


Figure 19: The figure is a two-way interaction plot for k and t_0 , where the response variable is $\Delta P\{T > t_0\}$.

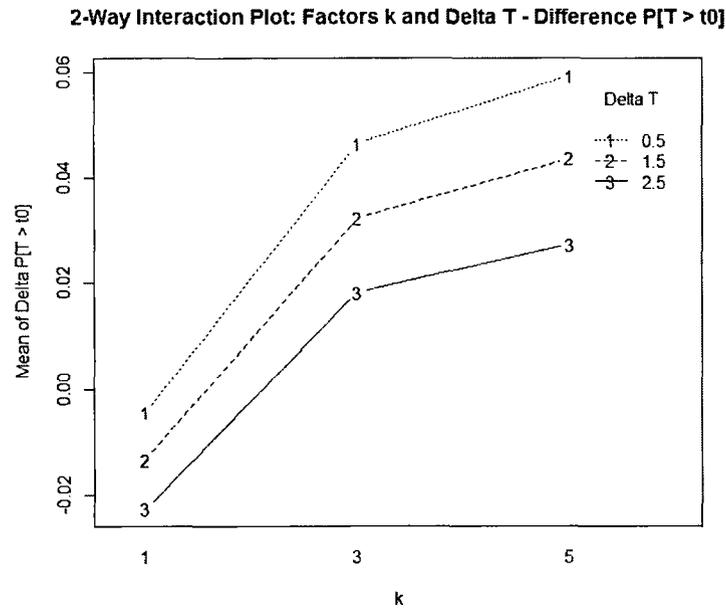


Figure 20: The figure is a two-way interaction plot for k and Δt , where the response variable is $\Delta P\{T > t_0\}$.

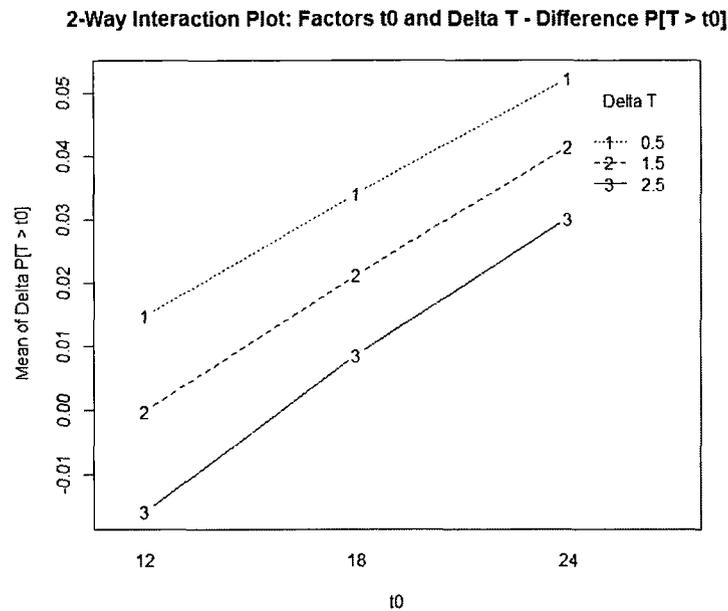


Figure 21: The figure is a two-way interaction plot for t_0 and Δt , where the response variable is $\Delta P\{T > t_0\}$.

Running full factorial designs, as the number of input parameters grows large, and the underlying simulation model is computationally expensive, quickly becomes intractable. The way forward is to employ fractional experimental designs and/or to attempt to reduce the dimension of the input vector. Fractional factorial designs use fewer design points, and like the analysis we give above, disregard higher order interaction terms in favor of estimating main effects and two-way interactions. There is a large literature on this topic, and it is not our goal here to review this in detail. See, for example, the survey in [9] and references cited therein.

4 Further Discussion

Implicit in much of our discussion in steps 5-9 is the notion of *threshold analysis*. For our example, the PM option is preferred under the nominal values of the input parameters. Understanding how much an input parameter would need to change in order to change that assessment has been important in our discussions of one- and two-parameter sensitivity plots, tornado diagrams, UQ plots, and spider plots. This notion is even embedded in our definition of the output performance measure $\Delta\mathbb{P}\{T > t_0\} \equiv \mathbb{P}\{T_{PM} > t_0\} - \mathbb{P}\{T_{base} > t_0\}$. Strictly speaking, the notion of a threshold value applies when estimates of the output variables are precise. When they contain sampling error, or they are uncertain because of uncertainties in the input parameters, a more nuanced analysis is needed. For example, in a sensitivity plot for $\Delta\mathbb{P}\{T > t_0\}$ as a function of k , we examine whether 95% confidence intervals include zero to understand whether the PM option is preferred, the base option is preferred, or whether, based on sampling error, we cannot assess which is preferable. This third characterization is made if the confidence interval contains zero. In that case, we are in an *indifference zone* in which we cannot assess whether the PM or base option is preferred. When we place a prior distribution on k , we can obtain a probability distribution governing the random variables $\Delta\mathbb{P}\{T > t_0 | k\}$, and $\Delta\mathbb{E}[T | k]$, and we can assess the *probability* that one of these outputs is positive (favoring the PM option) or negative (favoring the base option).

In some cases, as we range an input parameter, the preference for one option over an alternative does not change. In this case we have a *dominance* relationship. As Figure 3 illustrates, we prefer the PM option over the base option for all values of the input parameter t_0 of interest. It is important to note that we may have considerable variability in an output measure, but if we have a dominance relationship then this variability is of secondary interest. Of primary interest is whether the decision we would make changes.

Perhaps the foremost caveat when performing a one-way sensitivity analysis of a trusted model is to assess whether it makes sense to vary the input parameters one at a time. If two or more input parameters depend on an unstated auxiliary factor, this may not be valid. For example, it may be that components 1 and 2 in our example are identical but we are unsure of the associated failure rate. In this case, we should have $\lambda_1 = \lambda_2$, i.e., we should replace the two input parameters λ_1 and λ_2 with a single parameter. In other cases, the dependency between two parameters is not so simple. For example, if λ_1 and λ_2 are random variables they may have a dependent joint

probability distribution in which the correlation is positive (but not perfect). In this case, we could view that correlation coefficient between λ_1 and λ_2 as an input parameter to be varied or we could form a UQ plot and to characterize $\Delta\mathbb{P}\{T > t_0 | (\lambda_1, \lambda_2)\}$.

Another caveat in our one-at-a-time sensitivity analysis concerns the notion that all input parameters take their nominal values except for one. This can mask the effect of “cross terms.” The level of one input variable departing from its nominal value may amplify the effect of changes in another input variable. The purpose of the metamodel analysis in step 10 is to unmask precisely such interactions.

Whether done by a formal expert elicitation or an informal scheme, the nominal values of the parameters and their ranges are typically based on expert opinion and hence subject to well-known biases related to anchoring, over confidence, etc. Particularly relevant for GSI-191 analysis are difficulties in assessing rare-event probabilities. For example, see the discussions in Tversky and Kahneman [21] and O’Hagan et al. [15], and also see Kynn [11].

Model uncertainty is an often neglected part of sensitivity analysis. A simple form of model uncertainty for our example concerns the distributional assumption on the four-tuple of failure times (T_1, \dots, T_4) . We have assumed these four failure times to be independent and to have exponential distributions. Different distributional assumptions, e.g., a dependent joint distribution in which each component is a Weibull random variable might provide a higher fidelity model. These distinctions can arise because of important differences in assumptions made on the underlying physical model governing component failure. Hypothesizing competing models for an underlying phenomenon and understanding the domain of applicability of such models is, of course, central to scientific investigation.

5 Conclusions and Some Emerging Tools for Sensitivity Analysis

In this report, we have proposed a 10-step sensitivity analysis procedure that we see as practical for large-scale stochastic computer simulation models. And, we have illustrated these ideas on a simple example of a simulation model for system reliability. None of the steps we propose are new. Rather, we rely on the literatures from decision analysis, econometrics, statistics, and simulation to guide what we have proposed.

Tornado diagrams provide a simple means for visualizing the influence of a significant number of input parameters on an output variable and for understanding to which input variables the output variable is most sensitive. Effective use of tornado diagrams requires the analyst to specify reasonable and commensurate ranges for a collection of input parameters. Both sensitivity plots and spider plots complement tornado diagrams in that they more easily: (i) depict the nonlinear response of an output variable to changes in an input parameter, and (ii) depict the sampling-based error associated with estimating an output measure. We have advocated careful distinction of Monte Carlo sampling-based errors from uncertainties in input parameters. We model the latter type of uncertainty by placing a (possibly joint) probability distribution on the input parameters,

and in this setting we seek to understand the resulting probability distribution on the output by propagating the uncertainty through the nonlinear function represented by the simulation model. We discuss how to propagate uncertainty for univariate and multivariate distributions on input parameters. Finally, we describe regression metamodels, and associated experimental design, for understanding sensitivities and interactions between input parameters.

A number of important themes repeat throughout our recommendations. These have included the use of common random numbers in order to reduce variability and smooth output analysis. We have also focused on assessing differences in input parameters that make a difference in decisions or qualitative characterizations of the system at hand. The relevant ideas we have discussed in this regard include threshold analyses, indifference zones, and establishing dominance relations. Sensitivity analysis simplifies significantly when using deterministic simulation models. However, our simulations are stochastic and hence proper characterization of both sampling error and uncertainties on input parameters has been a pervasive theme in our presentation.

Our discussion is by no means comprehensive for sensitivity analysis of computer simulation models. Alternatives include computing derivatives, which is often termed *local sensitivity analysis*; see, e.g., Sobol [19]. Specifically, with $f(x_1, x_2, \dots, x_n)$ denoting a single output measure from our simulation model, we could estimate the gradient

$$\nabla_x f(x_1, \dots, x_n) = \left(\frac{\partial f}{\partial x_1}, \dots, \frac{\partial f}{\partial x_n} \right).$$

Local sensitivity analysis is of particular interest when attempting to optimize f , but optimization over the inputs is not our focus here. More importantly, if we simply report estimates of the partial derivatives $\frac{\partial f}{\partial x_i}$, $i = 1, \dots, n$, this can mislead with respect to what input parameters are most important because: (i) a per unit change in the temperature of water at a sump pump may not be commensurate with a per gram/fuel-assembly change in debris mass having penetrated the strainer; and, (ii) even if we compute $\frac{\partial f}{\partial x_i} \Delta x_i$ for commensurate values of Δx_i , a linear approximation may be poor over the range of parameters of interest.

It is for the reasons just discussed that we advocate the *global sensitivity analysis* that we have proposed in steps 4-10. Here, the notion of “global” is specified by the analyst via ranges associated with the input parameters (as we have done in Table 1) rather than rates of change at a single point. These ranges play a central role in sensitivity plots, tornado diagrams, spider plots, and the experimental designs associated with regression metamodels. (Even though we term these global, it is important to recognize that all but the regression metamodel involve changing one parameter at a time.) Such analyses need not associate a probability distribution with the input parameters. However, in our view it is preferable when such probability distributions can be specified because we can make use of them in UQ plots as well as our other sensitivity analyses. In such cases the specific endpoints of the ranges become less important.

We have recommended using tornado diagrams as an initial tool for assessing the most important input parameters, and using sensitivity plots, UQ plots, spider plots, and metamodels to enable a richer exploration of model sensitivity. It is possible to employ more sophisticated statistical

schemes for screening factors using metamodels [25], including sequential bifurcation screening [24]. However, even when such schemes are advocated, it is acknowledged that such approaches have yet to see significant application in practice [9]. Originally developed for interpolation in geostatistical and spatial sampling, Kriging (see, e.g., [5, 17, 18]) has seen widespread successful application in the context of deterministic simulation models as an alternative to regression metamodels. More recently, Kriging metamodels have begun to see application to stochastic simulation models; see, e.g., [1, 7, 2]. While these approaches are a promising alternative to regression metamodels, there are a number of outstanding research issues that remain to be solved [9].

References

- [1] Ankenman, B., B. L. Nelson, and J. Staum (2008). Stochastic Kriging for simulation metamodeling. In S. J. Mason, R. R. Hill, L. Moench, and O. Rose (Eds.), *Proceedings of the 2008 Winter Simulation Conference*, pp. 362–370.
- [2] Beers, W. V. and J. P. C. Kleijnen (2003). Kriging for interpolation in random simulation. *Journal of the Operational Research Society* 54, 255–262.
- [3] Clemen, R. T. and R. Reilly (2001). *Making Hard Decisions with Decision Tools*. Duxbury, Pacific Grove, CA.
- [4] Commission, N. R. (2011). Regulatory Guide 1.174: An Approach for Using Probabilistic Risk Assessment In Risk-Informed Decisions On Plant-Specific Changes to the Licensing Basis, Revision 2, Nuclear Regulatory Commission, Washington, DC.
- [5] Cressie, N. A. C. (1993). *Statistics for Spatial Data*. Wiley, New York.
- [6] Eschenbach, T. G. (1992). Spiderplots versus tornado diagrams for sensitivity analysis. *Interfaces* 22, 40–46.
- [7] Gramacy, R. B. and H. K. H. Lee (2008). Bayesian treed Gaussian process models with an application to computer modeling. *Journal of the American Statistical Association* 103, 1119–1130.
- [8] Kleijnen, J. P. C. (1995). Verification and validation of simulation models. *European Journal of Operational Research* 82, 145–162.
- [9] Kleijnen, J. P. C. (2011). Sensitivity analysis of simulation models. In *Wiley Encyclopedia of Operations Research and Management Science*. Wiley, New York.
- [10] Kleijnen, J. P. C. and W. V. Groenendaal (1992). *Simulation: A Statistical Perspective*. Wiley, Chichester.
- [11] Kynn, M. (2008). The heuristics and biases bias in expert elicitation. *Journal of the Royal Statistical Society: Series A* 171, 239–264.
- [12] Letellier, B., T. Sande, and G. Zigler (2013, November). South Texas Project Risk-Informed GSI-191 Evaluation, Volume 3, CASA Grande Analysis. Technical report, STP-RIGSI191-V03, Revision 2.
- [13] Morton, D. P., J. Tejada, and A. Zolan (2013, September). South Texas Project Risk-Informed GSI-191 Evaluation: Stratified Sampling in Monte Carlo Simulation: Motivation, Design, and Sampling Error. Technical report, STP-RIGSI191-ARAI.03, The University of Texas at Austin.

- [14] Ogden, N., D. P. Morton, and J. Tejada (2013, June). South Texas Project Risk-Informed GSI-191 Evaluation: Filtration as a Function of Debris Mass on the Strainer: Fitting a Parametric Physics-Based Model. Technical report, SSTP-RIGSI191-V03.06, The University of Texas at Austin.
- [15] O'Hagan, A., C. E. Buck, A. Daneshkhah, J. Eiser, P. Garthwaite, D. Jenkinson, J. Oakley, and T. Rakow (2006). *Uncertain Judgements: Eliciting Expert Probabilities*. Wiley, Chichester.
- [16] Pan, Y.-A., E. Popova, and D. P. Morton (2013, January). South Texas Project Risk-Informed GSI-191 Evaluation, Volume 3, Modeling and Sampling LOCA Frequency and Break Size. Technical report, STP-RIGSI191-V03.02, Revision 4, The University of Texas at Austin.
- [17] Sacks, J., W. J. Welch, T. Mitchell, and H. Wynn (1989). Design and analysis of computer experiments. *Statistical Science* 4, 409–435.
- [18] Santner, T. J., B. J. Williams, and W. I. Notz (2003). *The Design and Analysis of Computer Experiments*. Springer-Verlag, New York.
- [19] Sobol, I. M. (2001). Global sensitivity indices for nonlinear mathematical models and their Monte Carlo estimates. *Mathematics and Computers in Simulation* 55, 271–280.
- [20] Tregoning, R., P. Scott, and A. Csontos (2008, April). Estimating Loss-of-Coolant Accident (LOCA) Frequencies Through the Elicitation Process: Main Report (NUREG-1829). NUREG 1829, NRC, Washington, DC.
- [21] Tversky, A. and D. Kahneman (1981). Rational choice and the framing of decisions. *Science* 211, 453–458.
- [22] Wakefield, D. and D. Johnson (2013, January). South Texas Project Risk-Informed GSI-191 Evaluation, Volume 2, Probabilistic Risk Analysis: Determination of Change in Core Damage Frequency and Large Early Release Frequency Due to GSI-191 Issues. Technical report, STP-RIGSI191-VO2, Revision 0, ABSG Consulting Inc.
- [23] WCAP-16793-NP (2011, January). Evaluation of Long-Term Cooling Considering Particulate, Fibrous and Chemical Debris in the Recirculating Fluid, Revision 2.
- [24] Xu, J., F. Yang, and H. Wan (2007). Controlled sequential bifurcation for software reliability study. In S. G. Henderson, B. Biller, M.-H. Hsieh, J. Shortle, J. D. Tew, and R. R. Barton (Eds.), *Proceedings of the 2007 Winter Simulation Conference*, pp. 281–288.
- [25] Yu, H.-F. (2007). Designing a screening experiment with a reciprocal Weibull degradation rate. *Computers and Industrial Engineering* 52, 175–191.

A Appendix: A Sensitivity Analysis for STP GSI-191

In this appendix we apply the proposed framework to analyze the sensitivity of estimates of a risk measure to changes in input parameters of the CASA Grande simulation model, using STP data. The CASA Grande simulation model has the characteristics we describe in the abstract and in Section 1, and the framework we describe in this report was designed with large-scale stochastic simulation models like CASA Grande in mind.

In what follows, we briefly review the sampling scheme within CASA Grande, and we describe the loose coupling between CASA Grande and the PRA model. We describe how we estimate risk in terms of the contribution to core damage frequency (CDF) from GSI-191, in units of events per calendar year (CY), using estimates of the conditional failure probabilities that CASA Grande provides. That is, our risk measure is the change in core damage frequency (Δ CDF) relative to a base CDF due to non-GSI-191 issues. We present the results of 22 *scenarios*, where each scenario specifies the values of the input parameters to CASA Grande and where one of these scenarios contains nominal values for the parameters. This presentation includes a tornado diagram representing changes in all parameters we consider, and further includes a sensitivity plot for one of the key inputs.

A.1 Step 1: Define the Model

We refer to Volume 3 [12] for a discussion of the CASA Grande simulation model. One important aspect of this simulation for the purpose of our analysis here is the fact that a stratified sampling estimator is employed, in which the stratification is on the initiating frequency. The probability distribution governing the initiating frequency is consistent with percentiles from NUREG-1829 [20] as we describe in [16]. This stratified sampling estimator can be thought of as an “outer loop” of replications when running the simulation model, which we refer to as “frequency replications.” This outer loop facilitates preservation of the probability distribution for initiating frequency in the sense of the uncertainty quantification plots described in Step 7, and the stratified estimator further reduces variance versus a naïve Monte Carlo estimator.

Within each frequency replication, i.i.d. replications are performed in order to estimate conditional failure probabilities for each mode of failure (sump and boron fiber limit) and break size (small, medium, and large), conditioned on the pump state as well as the initiating frequency. A stratification with 15 cells is used for the stratified estimator with respect to the initiating frequency, and importantly, the sampling in distinct cells of the strata is done independently, unless specified otherwise. A sample size within each cell of the stratification is selected, as well as the boundaries of each cell of the strata, as indicated in Table 8. See [13] for background on the stratified sampling estimator. The right-most column in Table 8 is based on optimization model (10) in [13].

Table 8: Stratification of initiating frequency in terms of quantiles of its distribution function F . The probability mass for each cell is indicated, as is the sample size devoted to i.i.d. replications within each cell.

Frequency Replication	Cell Lower Limit	Cell Upper Limit	Probability Mass	Number of Stat. Replications
1	$F^{-1}(0.000)$	$F^{-1}(0.045)$	0.045	11
2	$F^{-1}(0.045)$	$F^{-1}(0.115)$	0.070	12
3	$F^{-1}(0.115)$	$F^{-1}(0.195)$	0.080	11
4	$F^{-1}(0.195)$	$F^{-1}(0.260)$	0.065	9
5	$F^{-1}(0.260)$	$F^{-1}(0.295)$	0.035	7
6	$F^{-1}(0.295)$	$F^{-1}(0.365)$	0.070	11
7	$F^{-1}(0.365)$	$F^{-1}(0.435)$	0.070	8
8	$F^{-1}(0.435)$	$F^{-1}(0.510)$	0.075	23
9	$F^{-1}(0.510)$	$F^{-1}(0.620)$	0.110	45
10	$F^{-1}(0.620)$	$F^{-1}(0.685)$	0.065	18
11	$F^{-1}(0.685)$	$F^{-1}(0.720)$	0.035	13
12	$F^{-1}(0.720)$	$F^{-1}(0.830)$	0.110	51
13	$F^{-1}(0.830)$	$F^{-1}(0.955)$	0.125	50
14	$F^{-1}(0.955)$	$F^{-1}(0.990)$	0.035	28
15	$F^{-1}(0.990)$	$F^{-1}(1.000)$	0.010	11

A.2 Step 2: Select Outputs of Interest

The change in core damage frequency (Δ CDF), when accounting for GSI-191 processes, is selected as the output of interest for this sensitivity study.

A.2.1 Core Damage Frequency

The method for estimating Δ CDF combines estimates from the CASA Grande simulation model with coefficients, as we explain here, from STP's PRA [22]. The CASA Grande simulation model is used to estimate the conditional probabilities of a sump failure and a boron fiber limit failure at various break sizes (small, medium, and large), when we condition on the initiating frequency of a LOCA and the pump state. From the PRA, we can use a base CDF from non-GSI-191 events, as well as the core damage frequencies associated with a sump or boron fiber limit failure, further conditioned on each permutation of pump state and break size. This is formalized as follows.

Indices and Sets:

$i = 1, \dots, F$	index for cells stratifying frequency replications
$j = 1, \dots, M_i$	index for statistical replications
$k = 1, \dots, N$	index for set of pump states

Events:

SL	small LOCA
ML	medium LOCA
LL	large LOCA
PS_k	pumps in state k
\mathcal{F}_i	initiating frequency in cell i
S	sump failure
\mathcal{B}	boron fiber limit
CD	core damage

Parameters:

f_{SL}	frequency (events/CY) of a Small LOCA
f_{ML}	frequency (events/CY) of a Medium LOCA
f_{LL}	frequency (events/CY) of a Large LOCA
$P(PS_k)$	probability mass of PS_k
$P(\mathcal{F}_i)$	probability mass of \mathcal{F}_i
$\hat{P}(S LOCA, \mathcal{F}_i, PS_k)$	estimate of probability of S given $LOCA = SL, ML, or LL, \mathcal{F}_i, PS_k$
$\hat{P}(\mathcal{B} LOCA, \mathcal{F}_i, PS_k)$	estimate of probability of \mathcal{B} given $LOCA = SL, ML, or LL, \mathcal{F}_i, PS_k$
R_{BASE}	non-GSI-191 core damage frequency (events/CY)
\hat{R}_{CD}	estimate of core damage frequency (events/CY)

The three frequencies, f_{SL} , f_{ML} , and f_{LL} , are taken from the right-most column of Table 4-1 from Volume 2 [22]. In the sensitivity analysis computations that follow, we use $F = 15$ frequency replications, and for the i -th frequency replication cell, we use M_i statistical replications with the values for M_i given in the right-most column of Table 8. As discussed in Volumes 2 and 3 [22, 12], in general we would consider a total of $N = 64$ pump states, although a reduced number of bounding pump states are used in actual computation. These 64 pump states include the mostly likely ‘‘Pump State 1,’’ which has all pumps on all three trains available. In the results we present here, we *only* consider Pump State 1, which has a probability mass of 0.935 when we consider all 64 pump states. In terms of our notation this means we have $N = 1$ and $P(PS_1) = 1$, effectively eliminating the sum over k . If we were to compute $P(PS_k)$ more generally, we would do so by normalizing the pump state frequencies in the left-hand column of Table 9-1 in Volume 2 [22] or equivalently the same frequencies in Table 2.2.11 in Volume 3 [12]. In our computations we also take $R_{BASE} = 0$ so that \hat{R}_{CD} estimates ΔCDF . That said, we develop the formulas that follow for general values of F , M_i , N , and R_{BASE} .

Estimating CDF

The estimate for CDF is calculated by summing the probability of each pump state–initiating frequency pair, and multiplying each term by the corresponding PRA frequencies coupled with the conditional failure probabilities estimated by CASA Grande. The formula for the estimator is as follows:

$$\hat{R}_{CD} = R_{BASE} + \sum_{i=1}^F \sum_{k=1}^N P(\mathcal{F}_i)P(PS_k) \cdot \quad (4a)$$

$$\left[f_{SL} \cdot \hat{P}(S|SL, \mathcal{F}_i, PS_k) + f_{SL} \cdot \hat{P}(B|SL, \mathcal{F}_i, PS_k) \right. \quad (4b)$$

$$+ f_{ML} \cdot \hat{P}(S|ML, \mathcal{F}_i, PS_k) + f_{ML} \cdot \hat{P}(B|ML, \mathcal{F}_i, PS_k) \quad (4c)$$

$$\left. + f_{LL} \cdot \hat{P}(S|LL, \mathcal{F}_i, PS_k) + f_{LL} \cdot \hat{P}(B|LL, \mathcal{F}_i, PS_k) \right]. \quad (4d)$$

Each of the six probability estimates, e.g., $\hat{P}(S|LL, \mathcal{F}_i, PS_k)$, is formed via a sample mean of i.i.d. observations, e.g., $\hat{P}^j(S|LL, \mathcal{F}_i, PS_k)$, $j = 1, \dots, M_i$, within the CASA Grande simulation. That is,

$$\hat{P}(S|LL, \mathcal{F}_i, PS_k) = \frac{1}{M_i} \sum_{j=1}^{M_i} \hat{P}^j(S|LL, \mathcal{F}_i, PS_k). \quad (5)$$

In this way, equation (5), and its five analogs (e.g., for $\hat{P}(S|ML, \mathcal{F}_i, PS_k)$), are substituted for the corresponding terms in equation (4) to form the estimator \hat{R}_{CD} .

Estimating the Variance of the CDF Estimator

We must estimate the variance of the estimator \hat{R}_{CD} in order to quantify its sampling error. There are a total of $6 \cdot F \cdot N + 1$ terms in equation (4) defining \hat{R}_{CD} , and in order to estimate the variance, we must clarify which of these pairs of terms are independent and which are dependent. First, we assume the terms $P(\mathcal{F}_i)$ and $P(PS_k)$, as well as the frequencies from the PRA such as R_{BASE} and f_{LL} , are deterministic. Dependency, or the lack thereof, between pairs of estimators like $\hat{P}(S|SL, \mathcal{F}_i, PS_k)$ and $\hat{P}(B|SL, \mathcal{F}_i, PS_k)$ depend on how the simulation is performed. The terms across distinct frequency replications and pump states are independent because independent Monte Carlo samples are drawn within each pump state–initiating frequency pair; however, the six terms within each pump state–initiating frequency pair are dependent. Thus, with $V(\cdot)$ and $COV(\cdot)$ denoting the sample variance and sample covariance operators, we have the following equation for $V(\hat{R}_{CD})$, which has 15 sample covariance terms because we have six pump state–initiating frequency pairs:

$$V \left[\hat{R}_{CD} \right] = \sum_{i=1}^F \sum_{k=1}^N [P(PS_k)]^2 \cdot [P(\mathcal{F}_i)]^2 \cdot \quad (6a)$$

$$\left\{ f_{SL}^2 \cdot V \left[\hat{P}(S|SL, \mathcal{F}_i, PS_k) \right] + f_{SL}^2 \cdot V \left[\hat{P}(B|SL, \mathcal{F}_i, PS_k) \right] \right. \quad (6b)$$

$$+ f_{ML}^2 \cdot V \left[\hat{P}(S|ML, \mathcal{F}_i, PS_k) \right] + f_{ML}^2 \cdot V \left[\hat{P}(B|ML, \mathcal{F}_i, PS_k) \right] \quad (6c)$$

$$+ f_{LL}^2 \cdot V \left[\hat{P}(S|LL, \mathcal{F}_i, PS_k) \right] + f_{LL}^2 \cdot V \left[\hat{P}(B|LL, \mathcal{F}_i, PS_k) \right] \quad (6d)$$

$$+ 2 \cdot f_{SL} \cdot f_{ML} \cdot COV \left(\hat{P}(S|SL, \mathcal{F}_i, PS_k), \hat{P}(S|ML, \mathcal{F}_i, PS_k) \right) \quad (6e)$$

$$+ 2 \cdot f_{SL} \cdot f_{LL} \cdot COV \left(\hat{P}(S|SL, \mathcal{F}_i, PS_k), \hat{P}(S|LL, \mathcal{F}_i, PS_k) \right) \quad (6f)$$

$$+ 2 \cdot f_{SL} \cdot f_{SL} \cdot COV \left(\hat{P}(S|SL, \mathcal{F}_i, PS_k), \hat{P}(B|SL, \mathcal{F}_i, PS_k) \right) \quad (6g)$$

$$+ 2 \cdot f_{SL} \cdot f_{ML} \cdot COV \left(\hat{P}(S|SL, \mathcal{F}_i, PS_k), \hat{P}(B|ML, \mathcal{F}_i, PS_k) \right) \quad (6h)$$

$$+ 2 \cdot f_{SL} \cdot f_{LL} \cdot COV \left(\hat{P}(S|SL, \mathcal{F}_i, PS_k), \hat{P}(B|LL, \mathcal{F}_i, PS_k) \right) \quad (6i)$$

$$+ 2 \cdot f_{ML} \cdot f_{LL} \cdot COV \left(\hat{P}(S|ML, \mathcal{F}_i, PS_k), \hat{P}(S|LL, \mathcal{F}_i, PS_k) \right) \quad (6j)$$

$$+ 2 \cdot f_{ML} \cdot f_{SL} \cdot COV \left(\hat{P}(S|ML, \mathcal{F}_i, PS_k), \hat{P}(B|SL, \mathcal{F}_i, PS_k) \right) \quad (6k)$$

$$+ 2 \cdot f_{ML} \cdot f_{ML} \cdot COV \left(\hat{P}(S|ML, \mathcal{F}_i, PS_k), \hat{P}(B|ML, \mathcal{F}_i, PS_k) \right) \quad (6l)$$

$$+ 2 \cdot f_{ML} \cdot f_{LL} \cdot COV \left(\hat{P}(S|ML, \mathcal{F}_i, PS_k), \hat{P}(B|LL, \mathcal{F}_i, PS_k) \right) \quad (6m)$$

$$+ 2 \cdot f_{LL} \cdot f_{SL} \cdot COV \left(\hat{P}(S|LL, \mathcal{F}_i, PS_k), \hat{P}(B|SL, \mathcal{F}_i, PS_k) \right) \quad (6n)$$

$$+ 2 \cdot f_{LL} \cdot f_{ML} \cdot COV \left(\hat{P}(S|LL, \mathcal{F}_i, PS_k), \hat{P}(B|ML, \mathcal{F}_i, PS_k) \right) \quad (6o)$$

$$+ 2 \cdot f_{LL} \cdot f_{LL} \cdot COV \left(\hat{P}(S|LL, \mathcal{F}_i, PS_k), \hat{P}(B|LL, \mathcal{F}_i, PS_k) \right) \quad (6p)$$

$$+ 2 \cdot f_{SL} \cdot f_{ML} \cdot COV \left(\hat{P}(B|SL, \mathcal{F}_i, PS_k), \hat{P}(B|ML, \mathcal{F}_i, PS_k) \right) \quad (6q)$$

$$+ 2 \cdot f_{SL} \cdot f_{LL} \cdot COV \left(\hat{P}(B|SL, \mathcal{F}_i, PS_k), \hat{P}(B|LL, \mathcal{F}_i, PS_k) \right) \quad (6r)$$

$$+ 2 \cdot f_{ML} \cdot f_{LL} \cdot COV \left(\hat{P}(B|ML, \mathcal{F}_i, PS_k), \hat{P}(B|LL, \mathcal{F}_i, PS_k) \right) \left. \right\}. \quad (6s)$$

To illustrate computation of the sample variance terms, $V(\cdot)$, and sample covariance terms, $COV(\cdot)$, in equation (6), we give the formulas for the first sample variance term from (6b) and the first sample covariance term from (6e):

$$V \left[\hat{P}(S|SL, \mathcal{F}_i, PS_k) \right] = \frac{1}{M_i} \frac{1}{M_i - 1} \sum_{j=1}^{M_i} \left[\hat{P}^j(S|SL, \mathcal{F}_i, PS_k) - \hat{P}(S|SL, \mathcal{F}_i, PS_k) \right]^2 \quad (7)$$

and

$$COV(\hat{P}(S|SL, \mathcal{F}_i, PS_k), \hat{P}(S|ML, \mathcal{F}_i, PS_k)) = \quad (8a)$$

$$\frac{1}{M_i} \frac{1}{M_i - 1} \sum_{j=1}^{M_i} \left[\hat{P}^j(S|SL, \mathcal{F}_i, PS_k) - \hat{P}(S|SL, \mathcal{F}_i, PS_k) \right] \cdot \left[\hat{P}^j(S|ML, \mathcal{F}_i, PS_k) - \hat{P}(S|ML, \mathcal{F}_i, PS_k) \right]. \quad (8b)$$

Further Remarks on Estimating Δ CDF

For this sensitivity analysis study, we estimate \hat{R}_{CD} conditional on being in the pump state in which all three pumps are operating on all three trains; i.e., the most likely pump state called ‘‘Pump State 1.’’ This eliminates the sum across pump states in the estimators given above and, because we are computing a conditional probability, has the effect of setting the probability mass associated with ‘‘Pump State 1’’ equal to 1. In addition we take $R_{BASE} = 0$ so that \hat{R}_{CD} estimates Δ CDF rather than CDF.

In what follows, we are interested in differences in \hat{R}_{CD} under pairs of scenarios, i.e., under two sets of input parameters to CASA Grande. Specifically, we have \hat{R}_{CD}^0 under the nominal settings of the parameters, \hat{R}'_{CD} under perturbed settings of the parameters, and our interest lies in the estimator $\Delta\hat{R}_{CD} = \hat{R}'_{CD} - \hat{R}_{CD}^0$. When computing this difference, we use common random numbers across the two scenarios to reduce the variance of $\Delta\hat{R}_{CD}$, which is computed using a straightforward variant of equation (6) in which the sample variance and sample covariance terms have terms like $\hat{P}^j(S|SL, \mathcal{F}_i, PS_k)$ and $\hat{P}(S|SL, \mathcal{F}_i, PS_k)$ replaced by $\Delta\hat{P}^j(S|SL, \mathcal{F}_i, PS_k)$ and $\Delta\hat{P}(S|SL, \mathcal{F}_i, PS_k)$, respectively.

Sometimes it is convenient to report and display the ratio of these frequencies estimates, rather than their difference; i.e., we report

$$\frac{\hat{R}_{CD}^1}{\hat{R}_{CD}^0}, \quad (9)$$

and term this the ratio of risk. We again use common random numbers when computing this estimator, and the sample variance of this is estimated via

$$V\left(\frac{\hat{R}_{CD}^1}{\hat{R}_{CD}^0}\right) = \frac{1}{[\hat{R}_{CD}^0]^2} \left[V(\hat{R}_{CD}^1) - 2\left(\frac{\hat{R}_{CD}^1}{\hat{R}_{CD}^0}\right) COV(\hat{R}_{CD}^1, \hat{R}_{CD}^0) + \left(\frac{\hat{R}_{CD}^1}{\hat{R}_{CD}^0}\right)^2 V(\hat{R}_{CD}^0) \right]. \quad (10)$$

A.3 Step 3: Select Inputs of Interest

The following input parameters of interest were selected, via multiple discussions of the STP Technical Team, from a larger collection of candidate parameters. The selection was based on: (i) the uncertainty associated with estimates of the values of the parameters, and (ii) the perceived likelihood that bias would, based on the team’s deliberations, have the largest effect on the estimates of risk, either in the increasing or decreasing direction.

1. Amount of Latent Fiber in the Pool; 4 levels
2. Boron Fiber Limit in the Core; 4 levels
3. Debris Transport Fractions Inside the Zone of Influence; 3 levels
4. Chemical Precipitation Temperature; 2 levels
5. Total Failure Fractions for Debris Outside the Zone of Influence (Unqualified Coatings); 2 levels
6. Chemical Bump-Up Factor; 2 levels
7. Fiber Penetration Function; 2 levels
8. Size of Zone of Influence; 2 levels
9. Time to Turn Off One Spray Pump; 2 levels
10. Time to Hot Leg Injection; 2 levels
11. Strainer Buckling Limit; 2 levels
12. Water Volume in the Pool; 3 levels
13. Debris Densities; 2 levels
14. Time-Dependent Temperature Profiles; 2 levels
15. Spray Transport Fractions for Debris Outside the Zone of Influence (Unqualified Coatings); 2 levels

A short description of the parameters of interest is provided in the following. See also Sections 2 and 5 of Volume 3 [12] for further discussion.

Amount of Latent Fiber in Pool There is an amount of existing dust and dirt in the containment, which is based on plant measurement. The latent fiber is assumed to be in the pool at the start of recirculation. This latent debris is therefore available immediately upon start of recirculation, uniformly mixed in the containment pool. During fill up, this latent debris is also available to penetrate the sump screen.

Boron Fiber Limit The boron fiber limit refers to the assumed success criterion, or threshold of concern where boron precipitation would be assumed to occur for cold leg breaks. The fiber limit comes from the testing performed by the vendor that shows no pressure drop occurs with full chemical effects. The assumption is that all fiber that penetrates through the sump screen is deposited uniformly on the core.

Debris Transport Fractions in ZOI This refers to the three-zone ZOI debris size distribution.

Each different type of insulation has a characteristic ZOI which is divided in three sections to take into account the type of damage (debris size distribution) within each zone.

Chemical Precipitation Temperature CASA Grande assumes that, once a “thin bed” of fiber is formed on the strainer, the chemical precipitation bump up factors are applied when the pool temperature reaches the precipitation temperature, defined in input.

Total Failure Fraction for Debris Outside the ZOI CASA Grande uses a table of total failure fractions that are applied to the transport logic trees. The fraction of each type (fiber, paint and coatings, and so forth) that passes through areas to the pool are used to understand what is in the pool as a function of time during recirculation. The total failure fraction multiplies the total inventory of unqualified coatings.

Chemical Bump Up Factor The chemical bump up factor is used as a multiplier on the conventional head loss calculated in CASA Grande. The multiplier is applied if a thin bed is formed and the pool temperature is at or below the precipitation temperature.

Fiber Penetration Function The amount of fiber that bypasses the ECCS sump screen (as a fraction) is correlated to the arrival time and the amount of fiber on the screen. The coefficients of the correlation define the fractional penetration amounts.

Size of ZOI The zone of influence (ZOI) is defined as a direct function (multiplier) of break size (and nominal pipe diameter). For example, for NUKON fiber, the ZOI (for STP) is 17 times the break diameter. The ZOI is assumed to be spherical unless it is associated with less than a full (double-ended) break in which case it is hemispherical. Otherwise, it is truncated by any concrete walls within the ZOI.

Time to Turn Off One Spray Pump If three spray pumps start, then by procedure one is secured. The time to secure the pump is governed by the operator acting on the conditional action step in the procedure.

Time to Hot Leg Injection Similar to the spray pump turn off time, the time to switch one or more trains to hot leg injection operation is governed by procedure.

Strainer Buckling Limit The strainer buckling limit is the differential pressure across the ECCS strainer at which the strainer is assumed to fail mechanically. This limit is based on engineering calculations that incorporate a factor of safety.

Water Volume in the Pool Depending on the break size, the amount of water that is in the pool, as opposed to held up in the RCS and other areas in containment, is variable. Smaller breaks tend to result in less pool volume than larger breaks.

Debris Densities The debris density depends on the amount and type of debris that arrives in the pool. These densities are used in head loss correlations to calculate, for example, debris volume.

Time Dependent Temperature Profiles The temperature of the water in the sump affects air release and vaporization during recirculation. The time-dependent temperature profile comes from the coupled RELAP5-3D and MELCOR simulations depending on break size.

Spray Transport Fractions for Debris Outside the ZOI CASA Grande uses a table of failure fractions that are applied to the transport logic trees. The fraction of each type (fiber, paint and coatings, and so forth) that passes through areas to the pool are used to understand what is in the pool as a function of time during recirculation. The spray transport fraction is the fraction of failed coatings that wash to the pool during spray operation.

The first two inputs, latent fiber and boron fiber limit, have four levels, including the nominal case. Items 3 and 12, debris transport within the ZOI and water volume, have three levels. And, all other of the other input parameters have two levels, the nominal case and a perturbation in a single direction. Thus, the number of runs needed to conduct one-at-a-time sensitivity analysis is: $2 \cdot (4 - 1) + 2 \cdot (3 - 1) + 11 \cdot (2 - 1) + 1 = 22$. The number of runs needed to conduct a single replicate full factorial design would be $4^2 \cdot 3^2 \cdot 2^{11} = 294,912$. We conduct the former, but we do not attempt the latter here.

A.4 Step 4: Choose Nominal Values and Ranges for Inputs

The nominal value for an input parameter is sometimes based on the STP Technical Team's best point estimate for that input. However, we sometimes instead select an appropriately conservative nominal value, as is the case for the strainer buckling limit, as we mention above. When selecting ranges for the parameters, sometimes we both increase and decrease a parameter from its nominal value, but other times we only change the parameter in a single direction. We can make the latter choice because we wish to limit changes to directions that we know will increase risk or because the nominal value is already seen as being conservative. Here, we list the 22 scenarios we use for sensitivity analysis.

Scenario 0: Nominal-value Case

All inputs have a nominal value. Those nominal values are as follows:

1. The amount of latent fiber in the pool is 12.5 ft^3 .
2. The boron fiber limit in the core is $7.5 \text{ g}/FA$.
3. The debris transport fractions for debris generated inside the zone of influence are given in Table 9.

Table 9: Nominal debris transport fractions for debris generated inside the zone of influence.

Debris Transport Model / Debris Type		LDFG Fines	LDFG Small	LDFG Large	Microtherm Fines	Qual Coat Fines	Crud Fines
Blowdown	Upper	0.70	0.60	0.22	0.70	0.70	0.70
Blowdown	Lower	0.30	0.25	0.00	0.30	0.30	0.30
Washdown	Inside	0.53	0.27	0.00	0.53	0.53	0.53
Washdown	Annulus	0.47	0.19	0.00	0.47	0.47	0.47
Washdown	BC Inside	0.00	0.27	0.00	0.00	0.00	0.00
Washdown	BC Annulus	0.00	0.00	0.00	0.00	0.00	0.00
Pool Fill	Sump	0.02	0.00	0.00	0.02	0.02	0.02
Pool Fill	Inactive	0.05	0.00	0.00	0.05	0.05	0.05
Recirculation	Lower	1.00	0.64	0.00	1.00	1.00	1.00
Recirculation	Inside	1.00	0.64	0.00	1.00	1.00	1.00
Recirculation	Annulus	1.00	0.58	0.00	1.00	1.00	1.00
Erosion	Spray	0.00	0.01	0.01	0.00	0.00	0.00
Erosion	Pool	0.00	0.07	0.07	0.00	0.00	0.00

4. The chemical precipitation temperature is 140°F.
5. The total failure fractions for debris generated outside the zone of influence (unqualified coatings) are given in row 1 of Table 10.

Table 10: Nominal debris failure fractions for debris generated outside the zone of influence (unqualified coatings).

Debris Transport Model / Debris Type	Epoxy Fines	Epoxy Fine Chips	Epoxy Small Chips	Epoxy Large Chips	Epoxy Curls	Alkyd	Baked Enamel	IOZ Fines
Total Failure Fraction	1.00	1.00	1.00	1.00	1.00	1.00	1.00	1.00
Upper Containment	0.15	0.15	0.15	0.15	0.15	0.54	0.00	0.83
Lower Containment	0.02	0.02	0.02	0.02	0.02	0.46	1.00	0.17
Reactor Cavity	0.83	0.83	0.83	0.83	0.83	0.00	0.00	0.00
Prior to Securing Sprays	0.06	0.06	0.06	0.06	0.06	0.06	0.00	0.06
Recirculation Lower Containment	1.00	0.41	0.00	0.00	1.00	1.00	1.00	1.00
Recirculation Reactor Cavity	0.00	0.00	0.00	0.00	0.00	0.00	0.00	0.00

6. The chemical bump-up factors as a function of break size are:

Small Breaks: Truncated Exponential Distribution

Mean = 1.25

Minimum = 1

Maximum = 15.3

Medium Breaks: Truncated Exponential Distribution

Mean = 1.50

Minimum = 1

Maximum = 18.2

Large Breaks: Truncated Exponential Distribution

Mean = 2.00
Minimum = 1
Maximum = 24.0

7. The fiber penetration function parameters are:

Fraction of Sheddable Debris: Uniform Distribution

Min = 0.00956

Max = 0.02720

Shedding Rate (1/min): Uniform Distribution

Min = 0.008236

Max = 0.054600

Efficiency Per Gram of Debris: Uniform Distribution

Min = 0.000339

Max = 0.003723

Fit Cut Point (g): Uniform Distribution

Min = 790

Max = 880

Initial Efficiency: Uniform Distribution

Min = 0.656

Max = 0.706

Exponential Rate Constant (1/g): Continuous Empirical Distribution Parameters:

0.0011254; 0.10

0.0013078; 0.45

0.0317870; 0.10

8. The size of zones of influence (R/D) as a function of break size are:

NUKON: 17.0

NUKON 2: 17.0

Microtherm: 28.6

RMI: 1.0

Lead: 1.0

Thermal Wrap: 17.0

IOZ: 1.0

Alkyd: 1.0

9. The times to turn off one spray pump (minutes) as a function of break size are:

Small Breaks: 0.0

Medium Breaks: Normal Distribution

Mean = 20.0

Standard Deviation = 5.0

Large Breaks: Normal Distribution

Mean = 20.0

Standard Deviation = 5.0

10. The times to hot leg injection (minutes) as a function of break size are:

Small Breaks: Uniform Distribution

Min = 345

Max = 360

Medium Breaks: Uniform Distribution

Min = 345

Max = 360

Large Breaks: Uniform Distribution

Min = 345

Max = 360

11. The strainer buckling limit is 9.35 *ft* H₂O.

12. The water volumes in the pool (ft³) as a function of break size are:

Small Breaks: Uniform Distribution

Min = 43,464

Max = 61,993

Medium Breaks: Uniform Distribution

Min = 39,533

Max = 69,444

Large Breaks: Uniform Distribution

Min = 45,201

Max = 69,263

13. The debris densities (*lb_m/ft³*) are:

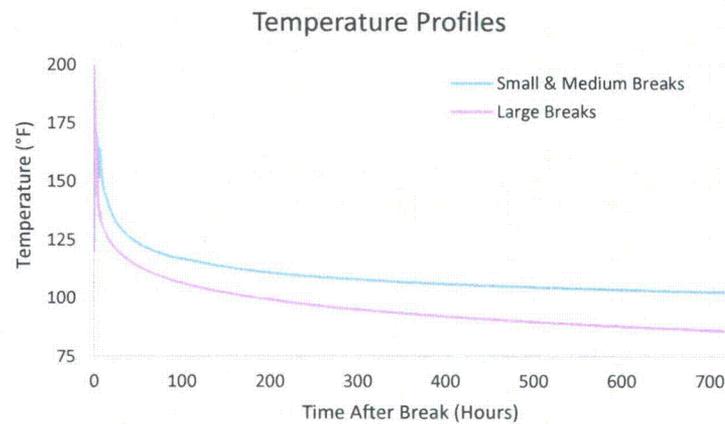
LDFG Fines: 2.4

LDFG Small: 2.4

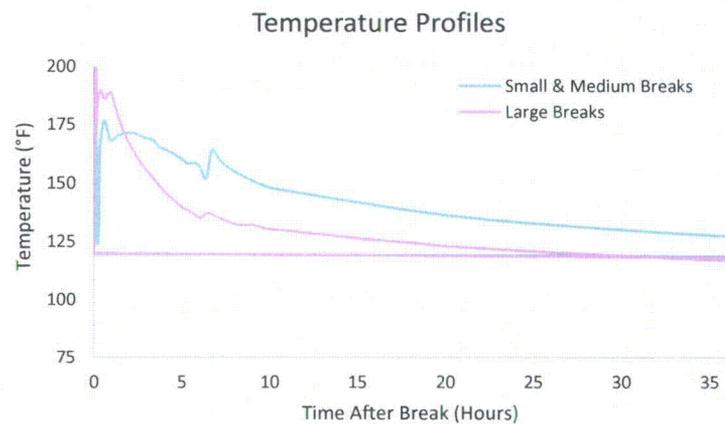
LDFG Large: 2.4

Microtherm Filaments: 2.4

14. The temperature profiles (°F) as a function of break size are given in Figure 22.



(a) Full 700 Hour Profile



(b) 36 Hour Profile Seen By CASA Grande

Figure 22: Temperature profiles (°F) for small and large breaks. Panel (a) shows the full 700 hour temperature profile, while panel (b) shows only the first 36 hours, which is the standard run length for CASA Grande scenarios.

15. The spray transport fractions for debris generated outside the zone of influence (unqualified coatings) are given in the fifth row of Table 10.

We use an upper limit of 15 g/FA for the boron fiber limit in Scenario 5 because WCAP-16793 [23] established a boron fiber limit of 15 g/FA as the maximum value for the STP fuel design based on cooling. The reason we decrease below that value in the nominal case, and further in Scenario 4, is to understand the sensitivity to this value since it is not the value for core cooling but rather the value we use for boric acid precipitation failure. At 15 g/FA , there is effectively no resistance

to flow as measured in WCAP-16793. In contrast to the situation for the boron fiber limit, for the strainer buckling limit, the nominal value is conservative, containing a significant safety margin. Hence, we do not make this limit even weaker in our sensitivity analysis, and we only consider an increase in the limit in Scenario 16.

Scenario 1: Decrease Latent Fiber

The amount of latent fiber in the pool is changed to 6.25 ft³, whereas the nominal value is 12.5 ft³.

Scenario 2: Increase Latent Fiber I

The amount of latent fiber in the pool is changed to 25.0 ft³, whereas the nominal value is 12.5 ft³.

Scenario 3: Increase Latent Fiber II

The amount of latent fiber in the pool is changed to 50.0 ft³, whereas the nominal value is 12.5 ft³.

Scenario 4: Decrease Boron Fiber Limit

The boron fiber limit in the core is changed to 4.0 *g/FA*, whereas the nominal value is 7.5 *g/FA*.

Scenario 5: Increase Boron Fiber Limit I

The boron fiber limit in the core is changed to 15.0 *g/FA*, whereas the nominal value is 7.5 *g/FA*.

Scenario 6: Increase Boron Fiber Limit II

The boron fiber limit in the core is changed to 50.0 *g/FA*, whereas the nominal value is 7.5 *g/FA*.

Scenario 7: Increase Debris Transport Inside the Zone of Influence

The debris transport fractions for this scenario are given in Table 11. Note that the only increased debris transport fractions are the blowdown and washdown transport fractions for LDFG fines and small.

Table 11: Increased debris transport fractions for debris generated inside the zone of influence.

Debris Transport Model / Debris Type		LDFG Fines	LDFG Small	LDFG Large	Microtherm Fines	Qual Coat Fines	Crud Fines
Blowdown	Upper	1.00	1.00	0.22	0.70	0.70	0.70
Blowdown	Lower	1.00	1.00	0.00	0.30	0.30	0.30
Washdown	Inside	1.00	1.00	0.00	0.53	0.53	0.53
Washdown	Annulus	1.00	1.00	0.00	0.47	0.47	0.47
Washdown	BC Inside	1.00	1.00	0.00	0.00	0.00	0.00
Washdown	BC Annulus	0.00	0.00	0.00	0.00	0.00	0.00
Pool Fill	Sump	0.02	0.00	0.00	0.02	0.02	0.02
Pool Fill	Inactive	0.05	0.00	0.00	0.05	0.05	0.05
Recirculation	Lower	1.00	0.64	0.00	1.00	1.00	1.00
Recirculation	Inside	1.00	0.64	0.00	1.00	1.00	1.00
Recirculation	Annulus	1.00	0.58	0.00	1.00	1.00	1.00
Erosion	Spray	0.00	0.01	0.01	0.00	0.00	0.00
Erosion	Pool	0.00	0.07	0.07	0.00	0.00	0.00

Scenario 8: Decrease Debris Transport Inside the Zone of Influence

The debris transport fractions for this scenario are given in Table 12. Note that the only decreased debris transport fractions are the blowdown and washdown transport fraction for LDFG fines and small.

Table 12: Decreased debris transport fractions for debris generated inside the zone of influence.

Debris Transport Model / Debris Type		LDFG Fines	LDFG Small	LDFG Large	Microtherm Fines	Qual Coat Fines	Crud Fines
Blowdown	Upper	0.60	0.51	0.22	0.70	0.70	0.70
Blowdown	Lower	0.26	0.21	0.00	0.30	0.30	0.30
Washdown	Inside	0.45	0.22	0.00	0.53	0.53	0.53
Washdown	Annulus	0.40	0.16	0.00	0.47	0.47	0.47
Washdown	BC Inside	0.00	0.23	0.00	0.00	0.00	0.00
Washdown	BC Annulus	0.00	0.00	0.00	0.00	0.00	0.00
Pool Fill	Sump	0.02	0.00	0.00	0.02	0.02	0.02
Pool Fill	Inactive	0.05	0.00	0.00	0.05	0.05	0.05
Recirculation	Lower	1.00	0.64	0.00	1.00	1.00	1.00
Recirculation	Inside	1.00	0.64	0.00	1.00	1.00	1.00
Recirculation	Annulus	1.00	0.58	0.00	1.00	1.00	1.00
Erosion	Spray	0.00	0.01	0.01	0.00	0.00	0.00
Erosion	Pool	0.00	0.07	0.07	0.00	0.00	0.00

Scenario 9: Increase Chemical Precipitation Temperature

The chemical precipitation temperature is changed to 160°F, whereas the nominal value is 140°F.

Scenario 10: Decrease Total Failure Fractions for Debris Outside the Zone of Influence (Unqualified Coatings)

Table 13: Decreased total failure fractions for debris generated outside the zone of influence (unqualified coatings).

Debris Transport Model / Debris Type	Epoxy Fines	Epoxy Fine Chips	Epoxy Small Chips	Epoxy Large Chips	Epoxy Curls	Alkyd	Baked Enamel	IOZ Fines
Total Failure Fraction	0.80	0.80	0.80	0.80	0.80	0.43	0.43	0.92
Upper Containment	0.15	0.15	0.15	0.15	0.15	0.54	0.00	0.83
Lower Containment	0.02	0.02	0.02	0.02	0.02	0.46	1.00	0.17
Reactor Cavity	0.83	0.83	0.83	0.83	0.83	0.00	0.00	0.00
Prior to Securing Sprays	0.06	0.06	0.06	0.06	0.06	0.06	0.00	0.06
Recirculation Lower Containment	1.00	0.41	0.00	0.00	1.00	1.00	1.00	1.00
Recirculation Reactor Cavity	0.00	0.00	0.00	0.00	0.00	0.00	0.00	0.00

Scenario 11: Increase Chemical Bump-Up Factor

The chemical bump-up factors as a function of break size are changed as follows:

Small Breaks: Truncated Exponential Distribution

Mean = 1.875

Minimum = 1

Maximum = 30.0

Medium Breaks: Truncated Exponential Distribution

Mean = 2.25

Minimum = 1

Maximum = 30.0

Large Breaks: Truncated Exponential Distribution

Mean = 3.00

Minimum = 1

Maximum = 30.0

Scenario 12: Increase Fiber Penetration (Lower Envelope)

The fiber penetration function parameters are no longer sampled from distributions. Instead, they are now constants with the following values:

Fraction of Sheddable Debris: 0.0196

Shedding Rate (1/min): 0.0538

Efficiency Per Gram of Debris: 0.0003391

Fit Cut Point (g): 880

Initial Efficiency: 0.656

Exponential Rate Constant (1/g): 0.0013

Scenario 13: Decrease Size of Zone of Influence (ZOI)

The size of zones of influence (R/D) as a function of break size are changed as follows:

NUKON: 12.75
NUKON 2: 12.75
Microtherm: 21.45
RMI: 0.75
Lead: 0.75
Thermal Wrap: 12.75
IOZ: 0.75
Alkyd: 0.75

Scenario 14: Increase Time to Turn Off One Spray Pump

The times to turn off one spray pump (minutes) as a function of break size are changed as follows:

Small Breaks: 0.0
Medium Breaks: Normal Distribution
Mean = 1440.0
Standard Deviation = 5.0
Large Breaks: Normal Distribution
Mean = 1440.0
Standard Deviation = 5.0

Scenario 15: Increase Time to Hot Leg Injection

The times to hot leg injection (minutes) as a function of break size are changed as follows:

Small Breaks: 450
Medium Breaks: 450
Large Breaks: 450

Scenario 16: Increase Strainer Buckling Limit

The strainer buckling limit is changed to 10.30 *ft* H₂O, whereas the nominal value is 9.35 *ft* H₂O.

Scenario 17: Decrease Water Volume

The water volumes in the pool (ft^3) as a function of break size are changed as follows:

Small Breaks: Uniform Distribution

Min = 39,191

Max = 56,720

Medium Breaks: Uniform Distribution

Min = 34,084

Max = 63,995

Large Breaks: Uniform Distribution

Min = 39,478

Max = 63,540

Scenario 18: Increase Water Volume

The water volumes in the pool (ft^3) as a function of break size are changed as follows:

Small Breaks: Uniform Distribution

Min = 48,737

Max = 67,266

Medium Breaks: Uniform Distribution

Min = 44,982

Max = 74,893

Large Breaks: Uniform Distribution

Min = 50,924

Max = 74,986

Scenario 19: Increase Debris Densities

The debris densities (lb_m/ft^3) are:

LDFG Fines: 3.0

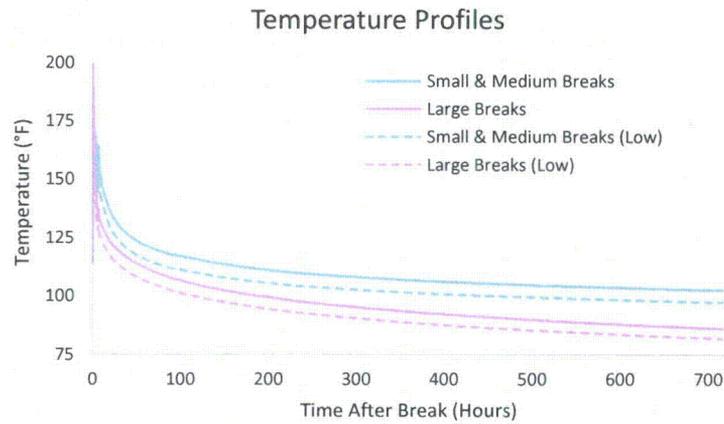
LDFG Small: 3.0

LDFG Large: 3.0

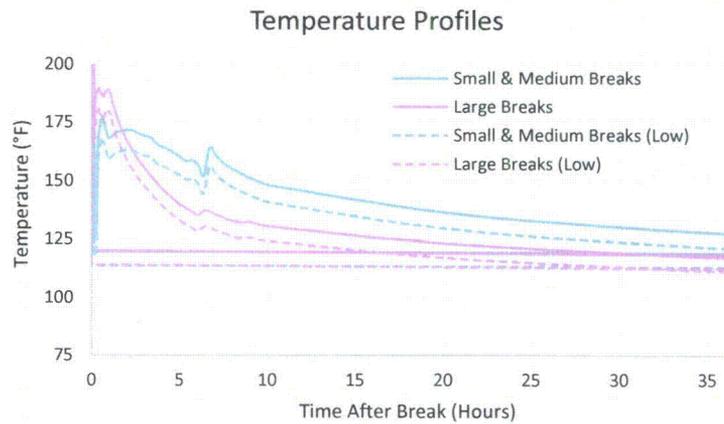
Microtherm Filaments: 3.0

Scenario 20: Decrease Time-Dependent Temperature Profiles

The modified temperature profiles ($^{\circ}\text{F}$) as a function of break size are given in Figure 23.



(a) Full 700 Hour Profile



(b) 36 Hour Profile Seen By CASA Grande

Figure 23: Temperature profiles (°F) for small and large breaks. Panel (a) shows the full 700 hour temperature profile, while panel (b) shows only the first 36 hours, which is the standard run length for CASA Grande scenarios.

Scenario 21: Increase Spray Transport Fraction for Debris Outside the Zone of Influence (Unqualified Coatings)

Table 14: Increased spray transport fractions for debris generated outside the zone of influence (unqualified coatings).

Debris Transport Model / Debris Type	Epoxy Fines	Epoxy Fine Chips	Epoxy Small Chips	Epoxy Large Chips	Epoxy Curls	Alkyd	Baked Enamel	IOZ Fines
Total Failure Fraction	1.00	1.00	1.00	1.00	1.00	1.00	1.00	1.00
Upper Containment	0.15	0.15	0.15	0.15	0.15	0.54	0.00	0.83
Lower Containment	0.02	0.02	0.02	0.02	0.02	0.46	1.00	0.17
Reactor Cavity	0.83	0.83	0.83	0.83	0.83	0.00	0.00	0.00
Prior to Securing Sprays	0.12	0.12	0.12	0.12	0.12	0.12	0.00	0.12
Recirculation Lower Containment	1.00	0.41	0.00	0.00	1.00	1.00	1.00	1.00
Recirculation Reactor Cavity	0.00	0.00	0.00	0.00	0.00	0.00	0.00	0.00

A.5 Step 5: Estimating Model Outputs under Nominal Values of Input Parameters

Table 15 presents the results from running CASA Grande with all parameters set at their nominal values (Scenario 0), using the formula for \hat{R}_{CD} from equation (4), along with estimates of sampling error. We see the point estimate of risk in terms of Δ CDF (events/CY) is 1.817E-08, with lower and upper 95% confidence limits of 1.626E-08 and 2.009E-08, respectively. If we take 1.00E-06 as a threshold of interest then our estimate of \hat{R}_{CD} is not close to this threshold when all input parameters are set to their nominal values.

Table 15: Results for Scenario 0 with all input parameters set to their nominal values. The first column is \hat{R}_{CD} in units of events/CY while the remaining columns characterize the sampling error.

Mean Risk	95% CI Half-Width	95% CI Lower Limit	95% CI Upper Limit	CI HW % of Mean
1.817E-08	1.914E-09	1.626E-08	2.009E-08	10.53%

A.6 Step 6: One-Way Sensitivity Analysis: Sensitivity Plots and Tornado Diagrams

In this step, we present results associated with running all 22 scenarios both in tabular form and using a tornado diagram, and we further present a one-way sensitivity plot. We begin with numerical results in tabular form for both the absolute risk (again, conditional on being in the state with all pumps working in all three trains) and for the difference in Δ CDF with respect to a perturbation of the input parameters relative to the nominal parameter values. Then, we present a tornado diagram corresponding to changing the 15 inputs as we detail in Section A.4. Finally, we present a one-way sensitivity plot for the boron fiber limit, which, after examining the tornado plot and tables of results, appears to be the input parameter to which our estimate of Δ CDF is most sensitive.

Tables of Results

Table 16 presents the numerical results for each of the 22 scenarios. In this table, we present our estimate of the Δ CDF (Mean Risk) associated with each scenario, and we provide 95% confidence interval (CI) limits associated with this estimate. We also present the ratio of the 95% CI half-width to the mean as a percentage.

Table 16: Δ CDF estimates, and sampling error, for all scenarios. The first two columns provide the scenario number and the parameter being changed; see Section A.4. The third column reports how we anticipate the Δ CDF will change, and the remaining columns read in the same manner as in Table 15.

#	Sensitivity Measure	Expected Direction	Mean Risk	95% CI Half-Width	95% CI LL	95% CI UL	CI HW % of Mean
0	Baseline	None	1.817E-08	1.914E-09	1.626E-08	2.009E-08	10.53%
1	Latent Fiber Low (6.25 ft ³)	Decrease	1.905E-08	1.928E-09	1.712E-08	2.098E-08	10.12%
2	Latent Fiber High (25 ft ³)	Increase	1.669E-08	1.770E-09	1.492E-08	1.846E-08	10.61%
3	Latent Fiber Very High (50 ft ³)	Increase	3.394E-08	1.447E-08	1.947E-08	4.840E-08	42.63%
4	Boron Fuel Limit (4.0 g/FA)	Increase	1.690E-06	1.146E-06	5.445E-07	2.836E-06	67.79%
5	Boron Fuel Limit (50 g/FA)	Decrease	1.308E-08	1.412E-09	1.167E-08	1.449E-08	10.80%
6	Boron Fuel Limit (15 g/FA)	Decrease	1.329E-08	1.415E-09	1.188E-08	1.471E-08	10.65%
7	Debris Transport Inside ZOI High	Increase	7.896E-08	2.250E-08	5.645E-08	1.015E-07	28.50%
8	Debris Transport Inside ZOI Low	Decrease	1.241E-08	1.493E-09	1.092E-08	1.390E-08	12.03%
9	Chemical Temp High	Increase	1.905E-08	1.937E-09	1.712E-08	2.099E-08	10.17%
10	Total Failure % Outside ZOI Low (80%)	Decrease	1.770E-08	1.878E-09	1.582E-08	1.958E-08	10.61%
11	Bump Factor High	Increase	2.287E-08	2.024E-09	2.085E-08	2.490E-08	8.85%
12	Penetration Low Envelope	Increase	1.552E-07	1.696E-08	1.382E-07	1.721E-07	10.93%
13	ZOI Size Small	Decrease	6.795E-09	8.275E-10	5.967E-09	7.622E-09	12.18%
14	Turn Off 1 Spray Longer	Decrease	1.569E-08	1.763E-09	1.393E-08	1.745E-08	11.23%
15	Hot Leg Injection Longer	Increase	1.962E-08	1.954E-09	1.766E-08	2.157E-08	9.96%
16	Strainer Limit Higher	Decrease	1.639E-08	1.801E-09	1.459E-08	1.819E-08	10.99%
17	Water Volume Low	Increase	2.001E-08	2.027E-09	1.798E-08	2.203E-08	10.13%
18	Water Volume High	Decrease	1.655E-08	1.776E-09	1.477E-08	1.833E-08	10.73%
19	Debris Density High	Increase	2.567E-08	2.353E-09	2.331E-08	2.802E-08	9.17%
20	Temperature Profiles Low	Increase	1.963E-08	1.991E-09	1.764E-08	2.162E-08	10.14%
21	Spray Transport % Outside ZOI High (12%)	Increase	1.798E-08	1.914E-09	1.606E-08	1.989E-08	10.65%

Table 17 focuses on the differences and the ratios of the Δ CDF under the nominal parameter values and under the perturbed parameter values; i.e., we report $\hat{R}'_{CD}/\hat{R}^0_{CD}$ in the third column (Ratio) and $\Delta\hat{R}_{CD} = \hat{R}'_{CD} - \hat{R}^0_{CD}$ in the fourth column (Mean Diff), where \hat{R}^0_{CD} is the point estimate of Δ CDF under the nominal scenario and \hat{R}'_{CD} is that under the perturbation scenarios.

Table 17: Δ CDF estimates for all scenarios in comparison with the nominal case. This comparison is performed via the ratio and the difference. The CI statements are for the difference, and the final column indicates whether the difference is statistically significant at a 95% confidence level.

#	Sensitivity Measure	Ratio	Mean Diff	95% CI Half-Width	95% CI LL	95% CI UL	Sig Diff?
0	Baseline	1.00	0.00E+00	0.00E+00	0.00E+00	0.00E+00	No
1	Latent Fiber Low (6.25 ft ³)	1.05	8.76E-10	5.37E-10	3.39E-10	1.41E-09	Yes
2	Latent Fiber High (25 ft ³)	0.92	-1.49E-09	8.00E-10	-2.29E-09	-6.87E-10	Yes
3	Latent Fiber Very High (50 ft ³)	1.87	1.58E-08	1.45E-08	1.27E-09	3.02E-08	Yes
4	Boron Fuel Limit (4.0 g/FA)	93.01	1.67E-06	1.15E-06	5.24E-07	2.82E-06	Yes
5	Boron Fuel Limit (50 g/FA)	0.72	-5.10E-09	1.09E-09	-6.18E-09	-4.01E-09	Yes
6	Boron Fuel Limit (15 g/FA)	0.73	-4.88E-09	1.08E-09	-5.96E-09	-3.80E-09	Yes
7	Debris Transport Inside ZOI High	4.34	6.08E-08	2.22E-08	3.86E-08	8.30E-08	Yes
8	Debris Transport Inside ZOI Low	0.68	-5.76E-09	1.05E-09	-6.81E-09	-4.72E-09	Yes
9	Chemical Temp High	1.05	8.78E-10	4.22E-10	4.56E-10	1.30E-09	Yes
10	Total Failure % Outside ZOI Low (80%)	0.97	-4.73E-10	3.07E-10	-7.80E-10	-1.66E-10	Yes
11	Bump Factor High	1.26	4.70E-09	9.52E-10	3.75E-09	5.65E-09	Yes
12	Penetration Low Envelope	8.54	1.37E-07	1.69E-08	1.20E-07	1.54E-07	Yes
13	ZOI Size Small	0.37	-1.14E-08	1.52E-09	-1.29E-08	-9.86E-09	Yes
14	Turn Off 1 Spray Longer	0.86	-2.49E-09	7.02E-10	-3.19E-09	-1.78E-09	Yes
15	Hot Leg Injection Longer	1.08	1.44E-09	2.46E-09	-1.02E-09	3.90E-09	No
16	Strainer Limit Higher	0.90	-1.78E-09	6.57E-10	-2.44E-09	-1.13E-09	Yes
17	Water Volume Low	1.10	1.83E-09	5.45E-10	1.29E-09	2.38E-09	Yes
18	Water Volume High	0.91	-1.62E-09	6.87E-10	-2.31E-09	-9.38E-10	Yes
19	Debris Density High	1.41	7.49E-09	1.36E-09	6.14E-09	8.85E-09	Yes
20	Temperature Profiles Low	1.08	1.46E-09	5.51E-10	9.05E-10	2.01E-09	Yes
21	Spray Transport % Outside ZOI High (12%)	0.99	-1.96E-10	2.08E-10	-4.04E-10	1.25E-11	No

Tornado Diagram and Analysis

Because the CD frequencies we estimate are so small, it is useful to present a tornado diagram and one-way sensitivity plot for the *ratios* on a logarithmic scale; see also our discussion surrounding Table 17. Figure 24 is a tornado diagram for the 15 input parameters we varied for this sensitivity study. Because we report results for the ratio $\hat{R}'_{CD}/\hat{R}^0_{CD}$, if the ratio has value 10, it means that the point estimate of the Δ CDF under the perturbed scenario is 10 times greater than that under the nominal scenario. The CI bounds for the risk ratios are calculated using equation (10). In what follows we examine six factors to which the estimate of Δ CDF seems to have the greatest sensitivity. Changes in the other input parameters lead to more modest changes in the Δ CDF estimate, with percentage differences of less than 30%.

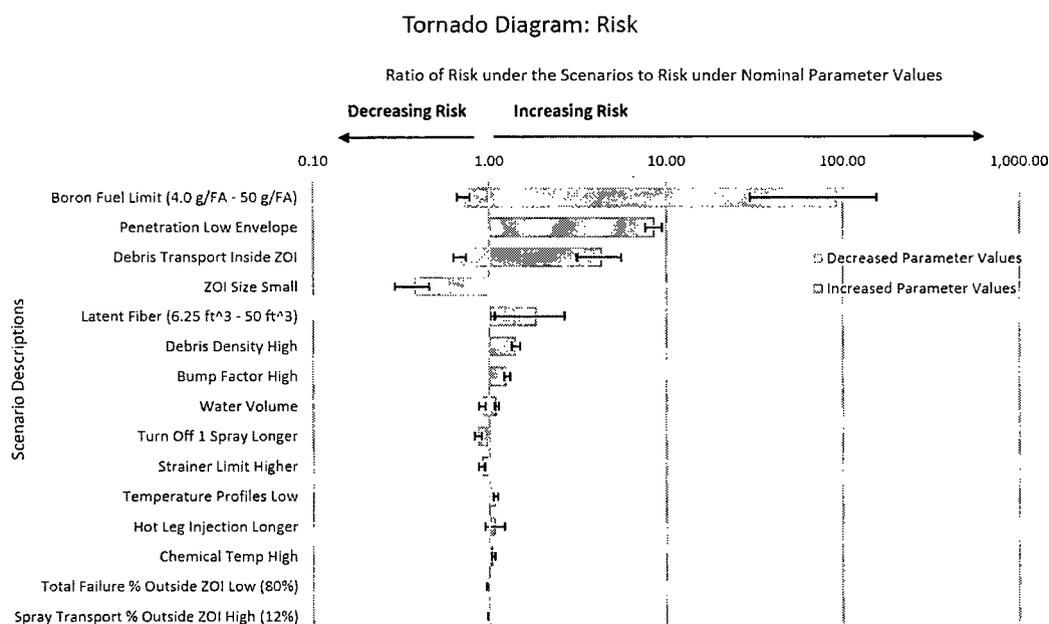


Figure 24: Tornado diagram in log space for ratios of the Δ CDF estimates (risk); i.e., we plot $\hat{R}'_{CD}/\hat{R}^0_{CD}$, along with the corresponding confidence intervals for each endpoint of the horizontal bars. Values of the ratio that exceed one correspond to an increase in risk relative to the nominal case. The scenario numbers in the first column of Tables 16 and 17 map the brief scenario descriptions here to the richer scenario descriptions in Section A.4.

We see from the tornado diagram in Figure 24 that the boron fiber limit appears to be the factor to which our estimate of Δ CDF is most sensitive. Increasing the limit from its nominal value of 7.5 g/FA should decrease the Δ CDF, and decreasing the limit should have the opposite effect. This holds because under a larger limit, more fiber can penetrate the strainer without the simulation model declaring a failure. Increasing the limit from 7.5 g/FA to 15.0 g/FA decreases Δ CDF by about 27%. Increasing the value further to 50.0 g/FA leads to little further decrease in Δ CDF. However, decreasing the value from 7.5 g/FA to 4.0 g/FA increases the point estimate of Δ CDF to 1.69E-06, larger than the nominal point estimate by a factor of 93.

The tornado diagram suggests the next perturbation to which the estimate of Δ CDF is most sensitive involves changing the filtration function to its lower envelope using the estimates provided in [14] and reported in Section A.4. The filtration function affects how much fiber penetrates the strainer. Modifying the function so that less mass is filtered means that more mass penetrates, and hence, we anticipate this will increase Δ CDF. At this lower envelope, the Δ CDF estimate increases by a factor of 8.5 to 1.55E-07.

The transport matrix for debris inside the ZOI governs the amount of each type of debris

transported to the sump. When this matrix has smaller transport fractions, we would expect the estimated Δ CDF to decrease because less debris reaches the strainer, and larger transport fractions should have the opposite effect. Under the perturbation to smaller transport fractions specified in Section A.4, the point estimate of Δ CDF decreases by about 32% to 1.24E-08, and with more debris transported to the strainer the Δ CDF estimate grows by a factor of 4.34 to 7.9E-08.

Next, we examine the effect of the size of the ZOI. We regard our nominal estimates of the ZOI size as conservative (larger ZOI than expected), and so we examine the result of reducing the size of the ZOI. A smaller ZOI means less debris will be generated, which should reduce Δ CDF. Reducing the size of the ZOI as specified in Section A.4, decreases Δ CDF by about 63% to 6.8E-09.

We now examine the effect of latent fiber in the sump. We anticipate that increasing the amount of latent fiber in the sump will increase Δ CDF as more fiber reaches the strainer and can penetrate to the core. As the tornado diagram and Table 17 indicate, increasing the amount of latent fiber from 12.5 ft³ to 50.0 ft³ leads to an 87% increase in Δ CDF. However, more modest changes in latent fiber produce counterintuitive results, as shown in Table 17. A decrease in the amount of latent fiber from 12.5 ft³ to 6.25 ft³ leads to a 5% increase in the Δ CDF estimate, and an increase in the amount of latent fiber from 12.5 ft³ to 25.0 ft³ leads to a 8% reduction in the Δ CDF estimate. The reason for these counterintuitive results is as follows. CASA Grande assumes that some fraction of latent fiber is deposited on the screen when the simulation model is initialized. This latent fiber is *not* eligible to penetrate the screen, although it is eligible to penetrate by shedding. Of course, in reality some of this fiber will penetrate the screen, and hence the STP Technical Team may suggest a minor modification to CASA Grande in this vein. Increasing the debris densities for low-density fiberglass and Microtherm filaments leads to a 41% increase in the Δ CDF estimate to a value of 2.6E-08.

Even though the change is small in magnitude, we close this section by discussing a counterintuitive result. Increasing the spray transport fraction for debris outside the ZOI (unqualified coatings failure) counterintuitively results in effectively no change or a slight reduction in debris bed head loss and consequently very little change to Δ CDF. This result is caused by a reduction in the overall (composite) surface-area-to-volume ratio (S_v) of the debris bed when spray transport applied to failed coatings is increased as a single parameter in Scenario 21. The effect is caused by competing ratios of constituents in the weighted average S_v . Specifically, enamel coatings have a large inventory and a small diameter, so the constituent S_v for enamel is large, but enamel coatings were assigned a spray transport fraction of zero. As quantities of other unqualified coating types increase with increasing spray transport fraction, the relative proportion of enamel decreases, resulting in a lower aggregate S_v . The effect is observed regardless of the weighting scheme chosen for S_v , and both the magnitude and direction of the effect depends on the relative inventories and particle diameters that are specified for the coatings debris types. In treatment of head loss through porous media, the parameter S_v represents the total surface area inside of the bed that can induce drag on the internal flow. Addition of any material inside of the same bed thickness should both increase S_v and decrease porosity. The unusual dependence of the composite S_v on relative debris

quantities and characteristics suggests that traditional use of a particulate-weighted bed property is not appropriate. If a composite parameter is needed, total available drag area should be averaged over the spatial dimensions of the bed and not over aggregate properties of the debris elements themselves.

One-Way Sensitivity Plot and Analysis

Given the significant effect of the boron fiber limit on the Δ CDF estimate, we explore this sensitivity further via a one-way sensitivity plot. Table 18 contains the results of running the simulation with boron fiber limit values of 4.0, 4.5, 5.0, 5.5, 6.0, 6.5, 7.5, and 8.5 (g/FA). Figure 25 is a one-way sensitivity plot of the Δ CDF estimate versus boron fiber limit over this range. As with the tornado diagram, we present the ratio of the Δ CDF estimate for each of these values to the Δ CDF estimate at the nominal value of 7.5 g/FA , and we present these ratios on a log scale. The CI bounds for the risk ratios are calculated using equation (10). We employ common random numbers in the simulation runs across these different fiber limit values.

Table 18: Δ CDF (Mean Risk) as a function of the boron fiber limit.

Boron Fiber Limit (g/FA)	Mean Risk	95% CI HW	Ratio
4.0	1.690E-06	1.146E-06	93.01
4.5	5.860E-07	8.359E-07	32.24
5.0	1.059E-07	5.789E-08	5.83
5.5	6.242E-08	3.961E-08	3.43
6.0	3.699E-08	2.038E-08	2.04
6.5	2.050E-08	1.999E-09	1.13
7.0	1.931E-08	1.950E-09	1.06
7.5	1.817E-08	1.914E-09	1.00
8.0	1.700E-08	1.790E-09	0.94
8.5	1.658E-08	1.729E-09	0.91

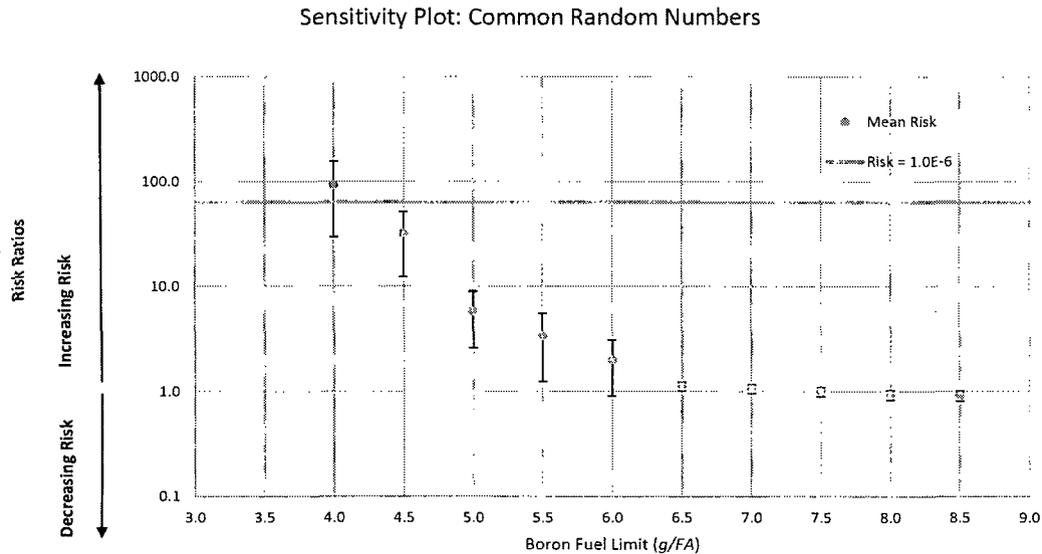


Figure 25: Sensitivity plot for boron fiber limit (g/FA).

From Figure 25 we see there is little change in the ΔCDF estimate as the fiber limit ranges from 6.5 g/FA to 8.5 g/FA . However, the ΔCDF estimate grows quickly as we decrease the fiber limit from 6.5 g/FA .

Analysis of Amount of Fiber Penetration Using Perturbed Filtration Function

In addition to examining the ΔCDF estimate associated with each of the scenarios described above, another performance measure of interest is the amount of fiber penetrating the core (g/FA) for different scenarios. In particular, it is interesting to compare the average amount of fiber penetrating the core using the nominal filtration function (scenario 0), and using the lower envelope of the filtration function (scenario 12). In Table 19, we present the results of a statistical analysis on fiber penetration for these two cases. When using the nominal filtration function, the average amount of fiber penetrating the strainer in CASA Grande is 0.318 g/FA , and when using the lower envelope of the filtration function, this same value is 0.648 g/FA . We see that approximately twice as much fiber penetrates when using the lower envelope filtration function. The far right column of Table 19 presents statistical information about the difference between these two scenarios in terms of fiber penetration. We can see the 95% confidence interval on the mean difference does not include zero, which indicates the difference is statistically significant, and of course, twice as much fiber penetrating the strainer is also significant from a practical perspective.

Table 19: Statistical analysis of fiber penetration under the nominal settings of the parameters and when we use the lower envelope of the filtration function.

Measure/Case	Nominal	Lower Envelope	Difference
Mean	0.318	0.648	0.330
Variance	0.063	0.231	0.289
Standard Deviation	0.251	0.481	0.538
Number of Observations	308	308	308
Confidence Level	0.95	0.95	0.95
CI Half-Width	0.028	0.054	0.060
CI Lower Limit	0.290	0.595	0.270
CI Upper Limit	0.346	0.702	0.390
p-value	-	-	3.673E-23
Significant Difference?	-	-	Yes

Summary

This appendix has focused on identifying the input parameters to which the performance measure of Δ CDF (change in core damage frequency due to GSI-191 issues) is most sensitive. In general, we estimate Δ CDF by coupling conditional failure probabilities, as estimated by the CASA Grande simulation model, with: (i) the frequency of small, medium, and large LOCA events, and (ii) the probability mass function governing the plant having access to a set of ECCS pumps. In the analysis we presented here, we have assumed that the most likely pump-state case, in which the plant has access to all pumps, occurs with probability one.

For this sensitivity analysis, the STP Technical Team selected a total of 15 input parameters to the CASA Grande simulation model. (We note that some “parameters” actually correspond to a collection of parameters; e.g., we simultaneously change a set of debris transport fractions.) Nominal values for these parameters correspond to the analysis performed in Volumes 2 and 3 [22, 12]. Along with this nominal scenario, 21 further scenarios corresponded to changing the values of these 15 parameters, one at a time. Some parameters were changed in only one direction, and other parameters were both increased and decreased. With the ranges for these parameters in hand, we constructed a tornado diagram characterizing the sensitivity of Δ CDF to changes in the input parameters. Key to our analysis is that the perturbations to these 15 input parameters are commensurate, meaning that they represent changes to the nominal case that have comparable likelihood, as judged by the STP Technical Team.

Our Δ CDF estimate is most sensitive to three parameters that concern: (i) how much debris is required to trigger an in-vessel failure (boron fiber limit), (ii) the fraction of debris that penetrates the sump strainer (fiber penetration function), and (iii) the fraction of debris of different types that is transported from different locations during different operational phases (debris transport fractions in ZOI). The effect of the boron fiber limit exceeds that of the next most sensitive parameter by an order of magnitude, and so we examined Δ CDF versus the boron fiber limit in further detail via a

one-way sensitivity plot. The growth in ΔCDF is modest as we decrease the boron fiber limit from 7.5 grams per fuel assembly (g/FA) to 6.5 g/FA , but then we see sharp growth in ΔCDF as we further decrease this limit.

The appendix of this report applies the initial steps of the sensitivity analysis procedure we propose. Additional analysis will be carried out. We will seek to understand, conditional upon a sump or boron fiber limit failure occurring, which weld locations are most likely to have experienced a break. We will form a spider plot (step 8) for the three or four most sensitive parameters. We will construct a meta-model of the type indicated in step 10 of our framework. And, we intend to include further pump states, beyond the most likely state considered here.

Attachment 9
Acronyms and Definitions

Definitions and Acronyms

ARL	Alden Research Laboratory	EOP	Emergency Operating Procedure(s)
BA	Boric Acid	EPRI	Electric Power Research Institute
BAP	Boric Acid Precipitation	ESF	Engineered Safety Feature
BC	Branch Connection	FA	Fuel Assembly(s)
BEP	Best Efficiency Point	FHB	Fuel Handling Building
B-F	Bimetallic Welds	GDC	General Design Criterion(ia)
B-J	Single Metal Welds	GL	Generic Letter
BWR	Boiling Water Reactor	GSI	Generic Safety Issue
CAD	Computer Aided Design	HHSI	High Head Safety Injection (ECCS Subsystem)
CASA	Containment Accident Stochastic Analysis	HLB	Hot Leg Break
CCDF	Complementary Cumulative Distribution Function or Conditional Core Damage Frequency	HTVL	High Temperature Vertical Loop
CCW	Component Cooling Water	HLSO	Hot Leg Switchover
CDF	Core Damage Frequency	ID	Inside Diameter
CET	Core Exit Thermocouple(s)	IGSCC	Intergranular Stress Corrosion Cracking
CHLE	Corrosion/Head Loss Experiments	ISI	In-Service Inspection
CHRS	Containment Heat Removal System	LAR	License Amendment Request
CLB	Cold Leg Break or Current Licensing Basis	LBB	Leak Before Break
CRMP	Configuration Risk Management Program	LBLOCA	Large Break Loss of Coolant Accident
CS	Containment Spray	LDFG	Low Density Fiberglass
CSHL	Clean Strainer Head Loss	LERF	Large Early Release Frequency
CSS	Containment Spray System (same as CS)	LHS	Latin Hypercube Sampling
CVCS	Chemical Volume Control System	LHSI	Low Head Safety Injection (ECCS Subsystem)
DBA	Design Basis Accident	LOCA	Loss of Coolant Accident
DBD	Design Basis Document	LOOP/LOSP	Loss of Off Site Power
D&C	Design and Construction Defects	MAAP	Modular Accident Analysis Program
DEGB	Double Ended Guillotine Break	MAB/MEAB	Mechanical Auxiliary Building or Mechanical Electrical Auxiliary Building
DID	Defense in Depth	MBLOCA	Medium Break Loss of Coolant Accident
DM	Degradation Mechanism	NIST	National Institute of Standards and Technology
ECC	Emergency Core Cooling (same as ECCS)	NLHS	Non-uniform Latin Hypercube Sampling
ECCS	Emergency Core Cooling System	NPSH	Net Positive Suction Head, (NPSHA – available, NPSHR – required)
ECWS	Essential Cooling Water System (also ECW)	NRC	Nuclear Regulatory Commission
EOF	Emergency Operations Facility		

Definitions and Acronyms

NSSS	Nuclear Steam Supply System	STPNOC	STP Nuclear Operating Company
OBE	Operating Basis Earthquake	TAMU	Texas A&M University
OD	Outer Diameter	TF	Thermal Fatigue
PCI	Performance Contracting, Inc.	TGSCC	Transgranular Stress Corrosion Cracking
PCT	Peak Clad Temperature	TS	Technical Specification(s)
PDF	Probability Density Function	TSB	Technical Specification Bases
PRA	Probabilistic Risk Assessment	TSC	Technical Support Center
PWR	Pressurized Water Reactor	TSP	Trisodium Phosphate
PWROG	Pressurized Water Reactor Owner's Group	UFSAR	Updated Final Safety Analysis Report
PWSCC	Primary Water Stress Corrosion Cracking	UNM	University of New Mexico
QDPS	Qualified Display Processing System	USI	Unresolved Safety Issue
RAI	Request for Additional Information	UT	University of Texas (Austin)
RCB	Reactor Containment Building	V&V	Verification and Validation
RCFC	Reactor Containment Fan Cooler	VF	Vibration Fatigue
RCS	Reactor Coolant System	WCAP	Westinghouse Commercial Atomic Power
RG	Regulatory Guide	ZOI	Zone of Influence
RHR	Residual Heat Removal		
RI-ISI	Risk-Informed In-Service Inspection		
RMI	Reflective Metal Insulation		
RMTS	Risk Managed Technical Specifications		
RVWL	Reactor Vessel Water Level		
RWST	Refueling Water Storage Tank		
SBLOCA	Small Break Loss of Coolant Accident		
SC	Stress Corrosion		
SI/SIS	Safety Injection, Safety Injection System (same as ECCS)		
SIR	Safety Injection and Recirculation		
SRM	Staff Requirements Memorandum		
SSE	Safe Shutdown Earthquake		
STP	South Texas Project		
STPEGS	South Texas Project Electric Generating Station		